# THE ACTIVITY OF QH II 66 AND IT'S ANALOGS IN MEDULLOBLASTOMA, MELANOMA AND NON-SMALL CELL LUNG CANCER CELL LINES.

by

Taukir Ahmed

A Dissertation Submitted in

Partial Fulfillment of the

Requirements for the Degree of

Doctor of Philosophy

in Chemistry

at

The University of Wisconsin-Milwaukee

May 2022

ABSTRACT

THE ACTIVITY OF QH II 66 AND IT'S ANALOGS IN MEDULLOBLASTOMA, MELANOMA AND NON-SMALL CELL LUNG CANCER CELL LINES.

by

Taukir Ahmed

The University of Wisconsin-Milwaukee, 2022
Under the Supervision of Professor James M. Cook

$GABA_AR$s (gamma-aminobutyric acid type A receptors) are transmembrane pentameric ligand-gated chloride ion channels that respond to GABA, the central nervous system's principal inhibitory neurotransmitter (CNS). The benzodiazepines (BZDs) bind between the $GABA_AR$ α+γ2-subunits at their extracellular interface. The binding of ligands to distinct subunits of $GABA_A$ receptors, notably the $\alpha_{1\text{-}6}\beta_{2/3}\gamma_2$ ion channels, can have a wide range of effects on brain activities. The sedative, ataxic, amnesic, anticonvulsant, and addictive actions of $GABA_AR$s' α1-subtype selective ion channels should be avoided, except for the anticonvulsant and anxiolytic effects, while creating ligands for this BZ allosteric modulatory site. Many studies have linked the α2/3-containing GABAARs to anxiolytic, anticonvulsant, and antinociceptive properties. Muscle relaxation may be mediated by interaction of α3 subtypes at higher doses. $GABA_AR$s that include the α5 subtype are known to play a role in cognition, learning, and memory. GABA activity disruption at α5 $GABA_AR$ subtypes plays a role in the pathophysiology of CNS illnesses such

schizophrenia, major depressive disorder (MDD), bipolar disorder, and some anxiety disorders such as OCD.

Medulloblastoma is the most common pediatric brain tumor. There are four subgroups of medulloblastoma: WNT, SHH, Group 3 and Group 4. Group 3 has the highest morbidity rate, relapse and metastasis rate. The standard treatment of medulloblastoma includes surgical removal of the tumor followed by radiation and chemotherapy which cause unwanted side effects such hearing impairment, permanent damage to the endocrine system and neurocognitive functions and secondary tumors. Better treatments of medulloblastoma are needed. In group 3 medulloblastoma tumors they show a high expression of GABRA5 receptors, which is the α5 subunit of ligand gated ionotropic γ-aminobutyric acid type A receptors. In recent times, there is a lot of evidence published on the role of ion channel activity on brain cancer progression. Collaborating with Dr. Sengupta's research group at Emory University it was shown that by using positive allosteric modulators of GABRA5 such as benzodiazepines like KRM-II-08 and QH-II-66 the cell viability of group 3 medulloblastoma can be impaired in vivo and in vitro with better specificity and potency than the standard of care treatments in the clinic. In this research several analogues of KRM-II-08 were designed, synthesized, and assayed and the most potent analogue binds with native tumor receptors with $EC_{50}$ and $IC_{50}$ values of ~0.8 micromolar. As a result of this binding, there is a 2 x $10^9$ ions.sec$^{-1}$ chloride flux which morphologically evokes mitochondrial membrane depolarization, nuclei distention, and cellular blebbing. This is correlated with the localization of pro-apoptotic Bcl-2-associated death promoter (BAD) protein. Thus, this potent, non-toxic benzodiazepine may serve as an efficient anti-cancer drug for group 3 type medulloblastoma. This study was published in 2019.

Melanoma is the deadliest form of skin cancer. More than 100,000 people are expected to be diagnosed in the USA in 2021. Current treatment with radiotherapy and immune checkpoint inhibitors does not show significant improvement in patients. Therapy combined with QH-II-66, radiation, and an immune checkpoint inhibitor shows improved results in controlling the metastasis by lowering the mass of the tumor. By gene expression analysis it was seen that these cancer cells show high expression of GABAA receptors, includes α5 GABAA subunits. Electrophysiology shows these receptors are functional. This sensitization to melanoma cells is benzodiazepine exclusive and does not impair normal cells. In a syngeneic mouse model of melanoma QH-II-66 showed increase in the depolarization in mitochondria which initiates programmed cell death of cancer cells. Combined therapy with QH II 66 and radiation show even better results. Lymphocyte and CD8+T cell counts were also increased after the treatment. Large-scale synthesis here was developed for QH II 66. It was important to point out the related benzodiazepine was either very weak or not active at all in these cancers. Thus, this potent, non-toxic benzodiazepine may serve as an efficient anti-cancer drug for melanoma. This study produced one publication in 2021 and two patent application submission in 2022.

After these studies a large scale synthesis was required. An efficient large scale synthetic route was developed for KRM II 08 and QH II 66. In the new route there was a 40% overall yield for QH II 66 and a 35% overall yield for KRM II 08. It was achieved by purification of steps by a crystallization process. This synthetic route helped reduce the time and money, as well as made the procedure more efficient to synthesize these two compounds. More than 30 grams of each of these two compounds were synthesized during this study.

These two-lead compounds were also tested in H1792 lung cancer cell lines. Both compounds were active in H1792 lung cancer cell lines. At least 20 analogues were synthesized and analyzed on H1792 cancer cell lines in collaboration of Dr. Krummel's and Dr. Sengupta's lab at University of Cincinnati. A new novel compound TA II 73 was discovered during this process which was two times more efficacious than the previous lead compound QH II 66 in H1792 non-small cell lung cancer cell lines, melanoma cell lines and glioblastoma cell lines. This TA II 73 developed a whole new series of anticancer benzodiazepines which have a 2'$CH_3$ in the pendent phenyl ring. TA II 73 is non sedative on the rotorod assay at 40 mg/Kg dose. During this process the synthetic route for TA II 73 was also improved. Experiment also showed that it is also active in LN 18 cell line which was derived from glioblastoma cancer patients.

There are important consequences of the development of the anticancer drugs contained in a privileged benzodiazepine skeleton. QH II 66, KRM II 08, TA II 73 and many other anticancer drugs have gone through the blood brain barrier in 20 to 30 minutes, as opposed to many anticancer drugs which do not have to be injected directly into the brain. While QH II 66 and analogs greatly enhance the anticancer activity of radiation and/or immune checkpoint inhibitor when they are given together, the combination of all three is even more potent, synergistically in mouse cancer models. In addition, these anticancer compounds are non-toxic for normal cells.

Furthermore, the anxiolytic activity and slight sedative activity of these agents will be important to patients who are undergoing dual or combination therapy because some stress will be decreased. It is felt, especially in combination therapy, anticancer drugs developed here will have clinical significance.

*TO*

***my mother Mrs. Momotaz Begum****,*

*my father late Md. Monirul Islam,*

*my wife Fathiya N. Jahan*

*and my sister Mowmita Ahmed.*

# TABLE OF CONTENTS

# LIST OF FIGURES

# LIST OF SCHEMES

# LIST OF TABLES

# LIST OF ABBREVIATION

| | |
|---|---|
| ACh | acetylcholine |
| AHR | airway hyperresponsiveness |
| AP-4 | 4-Aminopyridine |
| ASM | airway smooth muscle |
| BALF | bronchoalveolar lavage fluid |
| BBB | blood-brain-barrier |
| BQL | below the quantification limit |
| BZD | benzodiazepine |
| BzR | benzodiazepine receptor |
| CFA | complete Freund's adjuvant |
| CDAP | chlordiazepoxide |
| CINP | Chemotherapy-induced neuropathic pain |
| CMC | carboxymethyl cellulose |
| CNS | central nervous system |
| COPD | chronic obstructive pulmonary disease |
| CRS | chronic restraint stress |
| DI | diazepam-insensitive |
| DLM | dog liver microsomes |
| DNP-KLH | dinitrophenyl hapten-keyhole limpet hemocyanin |
| DS | diazepam-sensitive |
| ETSP | Epilepsy Therapy Screening Program |
| FDA | Food and Drug Administration |

| | |
|---|---|
| FST | forced swim test |
| GABA | gamma-aminobutyric acid |
| $GABA_AR$ | gamma-aminobutyric acid type A receptors |
| $GABA_BR$ | gamma-aminobutyric acid type B receptors |
| GINA | Global Initiative for Asthma |
| hERG | human Ether-à-go-go-Related Gene |
| HEK | human embryonic kidney cells |
| HDM | house dust mite |
| HLM | human liver microsomes |
| HPLC | high-performance liquid chromatography |
| ICSS | ICSS |
| IMDZ | imidazodiazepine |
| IgG | immunoglobulin G |
| IP | intraperitoneal |
| IV | intravenously |
| KA | kainic acid |
| KOR | kappa opioid receptors |
| LABA | long-acting $\beta_2$ agonist |
| LR | Lawesson's reagent |
| LTG | lamotrigine |
| MAM | methylazoxymethanol acetate |
| MCh | methacholine |
| MDD | major depressive disorder |

| | |
|---|---|
| MED | minimal effective dose |
| MES | maximal electroshock |
| MLM | mouse liver microsomes |
| MOE | Molecular Operating Environment |
| MPE | maximum possible effect |
| MRM | multiple reaction monitoring |
| MTD | minimal toxic dose |
| mTLE | mesial temporal lobe epilepsy |
| MW | molecular weight |
| NAM | negative allosteric modulator |
| NIMH | National Institute of Mental Health |
| NO | nitric oxide |
| NMDA | *N*-methyl-D-aspartate |
| Ova s/c | ovalbumin sensitized challenged |
| PAM | positive allosteric modulator |
| PBR | peripheral benzodiazepine receptor |
| PCLS | precision-cut lung slice |
| PCP | phencyclidine |
| PDSP | Psychoactive Drug Screening Program |
| PEG | polyethylene glycol |
| PFC | mouse prefrontal cortex |
| PI | protective indices |
| PK | pharmacokinetics |

| | |
|---|---|
| PPI | prepulse inhibition |
| PTZ | pentylenetetrazole |
| PWT | paw withdrawal threshold |
| PO | oral administration |
| RLM | rat liver microsomes |
| SABA | short-acting $\beta_2$ agonist |
| SAR | structure-activity relationship |
| scMET | subcutaneous pentylenetetrazole |
| SE | severe epilepsy |
| SEM | standard error of the mean |
| SLA | spontaneous locomotor activity |
| SNL | sciatic nerve ligation |
| SSRI | selective serotonin reuptake inhibitors |
| sRaw | specific airway resistance |
| SST | somatostatin |
| TLC | thin-layer chromatography |
| TLE | temporal lobe epilepsy |
| TPE | time of peak effect |
| TSPO | translocator protein |
| UCMS | unpredictable chronic mild stress |

# ACKNOWLEDGEMENT

First of all, I would like to thank my supervisor, Professor Dr. James M. Cook, for giving me the opportunity to work in the cancer projects. His generous personal and professional support, and his exceptional advice helped me a lot in my research as well as in the writing of my thesis. In addition, I am grateful to him for his continued encouragement to complete my PhD in synthetic medicinal Chemistry over the years on this wonderful journey. I would also like to thank the members of my doctoral committee, Professors Dr. Schwabacher, Dr. Pacheco Dr. Peng and Dr. Arnold for their excellent lectures in the field of chemistry, helpful suggestions, and insightful discussions.

I would like to thank to our numerous collaborators, and it was a great experience working with them. I want to thank Dr. Arnold at UW-Milwaukee and his group members specially to Nick Zahn and Michelle Meyer to collaborate on rotorod study and cytotoxicity assay. My sincere gratitude is with the research group of Dr. Soma Sengupta and Dr. Daniel Krummel and her group members Dr. Laura Kallay, Aniruddha Karve and Donatien Kamdem Toukam for conducting numerous assays on different types of cancer cell lines for last few years which we very crucial for my Ph.D. thesis.

I am grateful to the past and present members of the Cook Group. It is a great pleasure to be a part of this outstanding group. I want to express my sincere gratitude to Dr. Kashi Reddy Methuku who trained me for setting up a reaction for the first time and to Dr. Michael Rajesh for helping on the cytotoxicity assays. I want to thank Dr. Lalit Golani for his training on molecular modelling by using different type of modelling software. I would like to thank Dr. V.V.N. Phani Babu Tiruveedhula and Dr. Tofique Rahman for their wonderful companionship, support, discussion,

and advice after many hours of work in the lab. I want to convey my special thanks to Dr. Zubair Ahmed Khan for his excellent ideas. I really enjoyed working with my current group members Prithu Mondal, Kamal Prasad Pandey, Sepideh Rezvanian, Yeunus Mian and Dishary Sharmin.

I would like to acknowledge the financial and academic support of the UW-Milwaukee Department of Chemistry and the UW-Milwaukee Graduate School. I express my sincere gratitude to Dr. Frank H Holger for his superb support of NMR, and to Mr. Neal Korfhage for the design and manufacture of highly specialized glassware. I am grateful to and appreciate Dr. Anna Benko for her excellent expertise and support over the past five years in supporting mass spectrometry. I would also like to thank Dr. Shama Mirza for his help with the mass spectrometry analysis. I would also like to thank Mr. Kevin Blackburn, Ms. Elise D. Nicks, Ms. Wendy Grober, Ms. Shelley Hagen, Ms. Mary Eckert and Ms. Goldie Gibbs for being there for me whenever help was required.

Finally, I want to express endless respect to my Mother Mrs. Momtaz Begum, whose endless struggle after my father Md. Monirul Islam's death gave me the privilege to continue my study since my childhood. I also want to thank my wife Fathiya N Jahan who was with me during the last seven years and was the best companion for me during ups and downs in Ph.D work to keep me motivated all time. Without these two ladies I may not have enough courage and mental strength to carry on the Ph.D. work.

# Chapter 1 Introduction

## 1. 1 The GABAA receptors

Gamma (γ)-amino butyric acid (GABA) is the chief inhibitory neurotransmitter in the central nervous system (CNS) in the mammalian brain. GABA works by inhibiting excess neuronal activity.[1] The inhibitory effect of GABA initiates by binding to GABA receptors. GABA receptors have two major classes: $GABA_A$ receptors ($GABA_AR$) and $GABA_B$ receptors ($GABA_BR$). The $GABA_A$-rho receptors, usually known as $GABA_C$ receptors, are now considered as a subclass of $GABA_A$ receptors because the composition of ρ (rho) subunits is associated with $GABA_AR$. We are not discussing $GABA_C$ receptors in this thesis.[2] The $GABA_ARs$ are made up of fast-acting transmembrane ligand-gated chloride ion channels. During activation, $GABA_AR$ goes through a conformational change in the ion channel which permits chloride ions to pass through the pentameric channel. This creats a hyperpolarization of the gradient and reduces neuronal transmission.[3] On the other side the slow-acting $GABA_BR$ are members of the G-protein coupled receptor class. $GABA_BR$ are associated in the mediation of the activity of potassium and calcium channels.[4] After accumulation of evidence it has been shown that a change in the proper function of $GABA_AR$ is linked to a number of disorders in the CNS, such as schizophrenia,[5] major depressive disorder (MDD),[6] anxiety,[7] epilepsy[8] as well as neuropathic pain.[9]

To study the connection between the activity of $GABA_AR$ and different CNS disorders, a large amount of research has been carried out to learn about the structures and activities of $GABA_ARs$. The princople reason for different pharmacological effects is the presence of multiple variations of the specific combination of $GABA_AR$ subunits.[10] There are 19 subunit isoforms (α1-6, β1-3, γ1-3, δ, ε, π, θ, ρ1-3) in humans.[11] The combination of α, β and γ subunits (α1-6β1-3γ2)

in a stoichiometric ratio of 2:2:1 is the minimal requirement of the most common and well researched $GABA_AR$.[2] A fully functional allosteric effect of benzodiazepines at the α and γ interface always requires this combination.

Wisden et al.[12] proved the presence of $GABA_AR$ in the CNS of rodents, as well as the distribution of different combinations of $GABA_AR$ by immunocytochemistry studies. Studies have been showed that α1 β1-3 and γ2 have high expression throughout the brain synaptically, as well as extrasynaptically.[13] In the rat brain α1β2γ2 is the most prevalent combination and the highest abundance of $GABA_AR$ which are at least 60 % of total $GABA_AR$.[13-15] The α2 and α3 containing $GABA_ARs$ are second in abundance and are approximately 20-30 % of $GABA_AR$ in rat brain.[13-15] The α5 containing $GABA_ARs$ are mostly found in the cortex, and the hippocampus. They make up about 5 % of the total $GABA_AR$. In comparison to other subtype combinations in rat brain this number is very low.[13-16] But, $GABA_ARs$ are not localized to the CNS; a significant amount of studies indicates that $GABA_AR$ also can be found in other tissues outside of brain including the organs such as the lungs, stomach, heart sinus node, intestines, etc. [1]

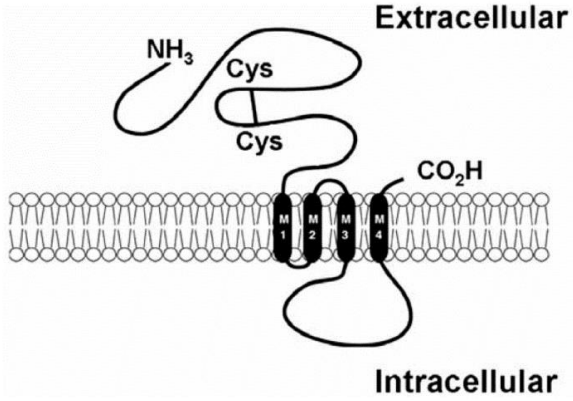


**Figure 1. A topology for GABAAR subunits that has been proposed. The N-terminal end in the extracellular domain is designated the N-terminal end, and M1-M4 are transmembrane sections. (Figure modified from Burt, et al. [17] and Clayton, et al.)[18]**

The molecular mass of $GABA_AR$ subunits is approximately ~50 kD, and the structure of the receptor proteins show high homology. Every subunit is made up of four transmembrane domains M1-M4, attached in the lipid bilayer of its neuron. Both the C- and N- terminals, of the subunit are located in the extracellular domain, which contains a potential glycosylation site and a "cys-loop" formed by a disulfide bond at the N-terminal end. The large intracellular area can be found in between domain 3 and 4. They are responsible for the modification of $GABA_AR$ at possible phosphorylation sites (Figure 1). A circular formation can be found within the five monomeric subunits in the hetero- or homo- pentameric chloride ion channel (**Figure 2**).[17-19]

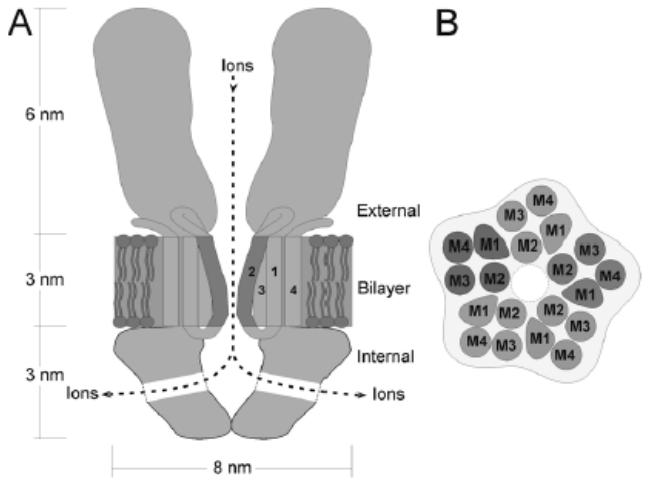


**Figure 2. In longitudinal vision (A) and cross-sectional view (B), schematic representations of GABAA; the ligand-gated chlorine ion channel, is shown (B). The M1-M4 transmembrane domains are represented by the numbers 1-4. Within the lipid bilayer membrane, the domain M2 domain is responsible for the majority of the pore lining. (Figure modified from Keramidas et al.[19] and Clayton et al.)[18]**

It has been well documented in addition to the two binding sites for GABA, $GABA_ARs$ contain multiple binding sites for other psychoactive compounds which includes benzodiazepines, barbiturates, anesthetics, neurosteroids, ethanol, etc., at the synapse and inside the channel as well.[1-2, 10, 14, 18] The view from the extracellular region of the clockwise-arranged αβαβγ subunits illustrates the binding sites of $GABA_AR$ (**Figure 3**). There are two interfaces of the $\alpha^-\beta^+$ subunits where GABA binds on the other hand the benzodiazepines bind at the interface of the $\gamma^-\alpha^+$

subunits.[1-2, 7, 18] Seighert, Ernst, Cook et al.discovered that at the interface of the proteins $\beta^{-}\alpha^{+}$ is also a binding site termed the PQ site and CGS 9895 was a receptor ligand. [18, 20-21] Very recently Knutson et al, have published an article in which he peoved that this receptor can also be alpha 6 subtype selective.[22-24] Drugs such as barbiturates[1-2, 15] and ethanol,[25-26] can also bind in the interior portion of the ion channel, which enhances the response of GABA and opens the chloride ion pore directly to a degree, which results in the addiction potential or even death.[1-2, 10, 14-17] Hence allosteric modulators of GABAR are much safer such as benzodiazepine receptor ligands.

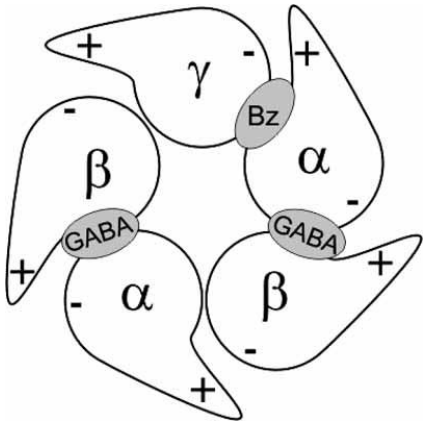


**Figure 3. As seen from the synaptic cleft, the arrangement of the α1β3γ2 GABAAR subtypes. GABA binding sites are found at the interfaces between the α+ and β- subunits, while BZD binding sites are found at the interface between the α+ and γ- subunits. Each subunit's loop C is represented by the +. (Figure modified from Clayton, et al.[18] and Ernst, et al.)[27]**

## 1. 2 Benzodiazepines (BZD)

Benzodiazepines (BZDs) are a class of psychoactive drugs. They were first discovered in 1955 by Leo Sternbach. Diazepam is one of the first and most precribed BZD drugs. It was marketed as Valium in 1963 and today.[28] BZDs show potent activity, low toxicity[29], minimal drug-drug interactions in the liver,[30] rapid penetration across the blood-brain barrier (BBB), rapid absorption from the gastrointestinal tract, and ready distribution in the brain.[31-33] This is why BZDs have been among the first choices for more than 50 years for the treatment of neumerous CNS disorders such

as anxiety, seizures, and insomnisia.[28, 34] Typical BZDs contains a core structure of a benzene ring fused with a seven-membered diazepine ring and a C-5 pendant phenyl C ring (Figure 4).[35]

Classical 1,4-benzodiazepines such as diazepam (Figure 4) and alprazolam exhibit potent affinity to Bz/$GABA_AR$ non-selectively at the benzodiazepine binding site (BzR), at the interface of the $\gamma^-$ $\alpha^+$ subunits.[1-2, 7, 18] That is why the α and γ subunits are just as crucial as the β subunits for the occurance of the pharmacological effects of BZDs.[36] It has been documented that BZDs interact with $\alpha_{1\text{-}3,5}\beta_{2/3}\gamma_2$ $GABA_AR$ subtypes, but show fewer pharmacological effects at $\gamma_{1,3}$ subtypes.[37] In additon to this the major diazepam-sensitive (DS) $GABA_AR$ subtypes are accompanied by two other subtypes, the α4- and α6-containing diazepam insensitive (DI) $GABA_AR$, which are less abundant in the brain,[38] in comparison to the DS $GABA_AR$ subtypes. Studies have shown that the binding pocket of diazepam-insensitive (DI) subtypes is unable to tolerate the pendent phenyl C ring of BZD ligands, such as the 1,4-benzodiazepine diazepam and the imidazodiazepine (IMDZ) midazolam (Figure 4).[39-40] Although, drugs like the antagonists flumazenil (Figure 4), which does not contain the pendent phenyl C ring, can bind to all 6 major subtypes at DS, as well as DI sites,[11] it can antagonize the effect at all 6 major subtypes.

Without the presence of GABA, a BZD itself can not modulate $GABA_AR$ directly.[41] After a BZD binds to the $GABA_AR$ ion channel, the affinity of GABA to $GABA_AR$ becomes tighter, which leads to a much higher frequency of the chloride ion channel opening and increased hyperpolarization of the membrane potential.[42] This leads to increased inhibition of neuronal firing, which is the reason for the series of pharmacological properties; for example, anxiolytic, ataxic, amnesic, and sedative effects, as well as anticonvulsant effects, etc as mentioned. Some of these virtues permit the in vivo use of BZDs for treatment of CNS disorders, which includes GAD,

SAD, PTSD, status epilepticus, and panic disorders. Although BZDs have a lot of advantages, they also exhibit many adverse effects. The reasons

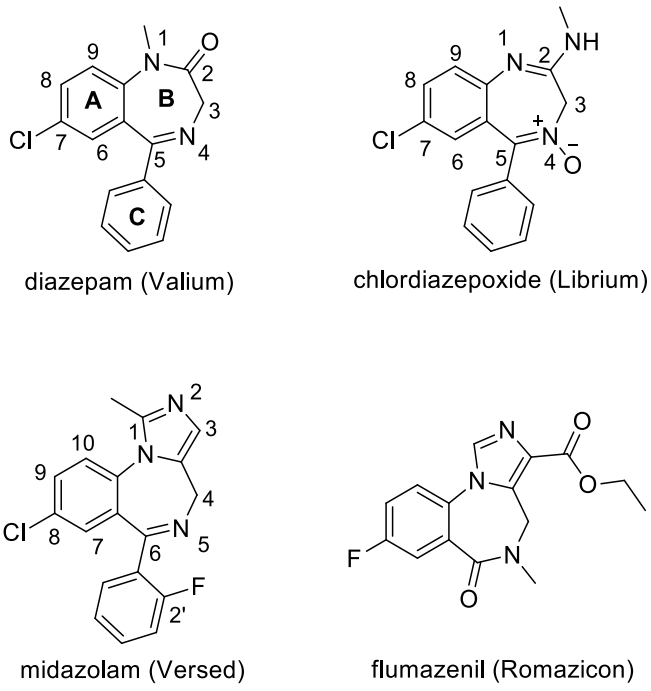


**Figure 4. Diazepam, chlordiazepoxide, imidazodiazepine (IMDZ), midazolam, and flumazenil are some of the most prevalent BZDs. Both BZDs and IMDZs have their atoms labeled. Flumazenil can bind to both the DS and DI sites, whereas diazepam, chlordiazepoxide, and midazolam can only bind to the DS sites.**

are the concurrent non-selective binding and efficacy at many of the $GABA_ARs$.[2, 28] Some common side effects of BZDs are sedation, ataxia, amnesia, addiction, fatigue, dependence, withdraw issues, muscle-relaxation, and tolerance to the antinociceptive and anticonvulsant effects.[43-45] There is a large medical need for improved BZDs which could carry the desired pharmacological properties. They need to be safe enough so that the unwanted side effects can be avoided for better treatment of a series of CNS disorders.

## 1. 3 Modulation of BZDs on the Pharmacological Effects of $GABA_AR$

There are a significant amount of studies, which have been done on $GABA_ARs$. The evidences from these studies have confirmed the pharmacological effects of the $GABA_ARs$ mostly rely on

modulation of receptor subtypes, principally due to the differences of the $\alpha_x$ subunits. \Mohler, Sieghart,

**Table 1-1 The impact of GABAA α1-6β1-3γ2 receptor subtypes on the CNS. [18, 46-58], presented at the University of the West Indies' Mona Symposium (2014).[59] Mckernan et al. had already reported a part of this (ACNP). Pharmacologists collaborated with the Milwaukee group to define the red pharmacology. Cook et al. presented at the ASPECT meeting on April 9th, 2019 in Orlando, FL.**

| Subtype | Associated effect |
|---|---|
| α1 | Anxiolytic, sedation, anterograde amnesia, ataxia, some anticonvulsant action, addiction, dependance, as well as involved in the development of tolerance and muscle relaxation |
| α2 | **Anxiolytic, anticonvulsant action, antihyperalgesic effects.** |
| α3 | Some **anxiolytic action**, some **antinociceptive effects**, anticonvulsant actions at higher doses, some muscle relaxation at higher doses. |
| α4 | Diazepam-insensitive (DI) site, important in lung disorders in the periphery. |
| α5 | Cognition, learning, temporal, and spatial memory (may be memory component of anxiety), schizophrenia, depression and in the periphery asthma. |
| α6 | Diazepam-insensitive (DI) site, important in Tic disorders, Tourette's syndrome, migraine, trigeminal orofacial pain and perhaps schizophrenia. |

McKernan, Sigel, Seeburg, Squires, and Haefely worked for several years to determine the structures and the corresponding effects for each subunit. They have achieved this by employing receptor binding, pharmacology and a molecular genetic models, that specific mutations for a specific α subunit can modify activity. This required the exchange of the histidine amino acid (AA) by an arginine AA in the α1 subunit (α1His101Arg),[46] α2His101Arg, α3His126Arg,[47] and

α5His105Arg.[48] Rodents were used in these models. These rodents contained the specific mutations, on the basis of which they were treated with diazepam. If there was a change in behavioral response (or lack thereof), it was assumed to be mediated by the mutated subunits in comparison with the wild-type animals.[46-48] The pharmacological effects of various subtypes are shown in Table 1. This table is a summary of much early work by Mohler, Rudolph, McKernan, Sieghart, Siegel et al. and in red is this activity was determined by the Milwaukee group in collaboration with pharmacologists.

The α1-containing $GABA_A$Rs are assumed to be responsible, as mentioned for the anxiolytic effects, sedative effects, anterograde amnesia, ataxia, development of tolerance, addiction, dependence, and some anticonvulsant action as well as some muscle relaxation.[46, 50] The α2-containing $GABA_A$Rs contribute in large part to the anxiolytic, antinociceptive and some anticonvulsant effects.[47, 51] Some hypnotic effects and some muscle relaxation may occur at higher doses. Most of the antihyperalgesic effects of the γ2 subtype originate from the $GABA_A$R found in the spinal cord. It was confirmed by a triple-point mutation study and other work by Zeilhofer, Cook et al. Where Hz-166 was used as the ligand.[49, 55] The α3- $GABA_A$Rs exhibit anxiolytic-like effects, anticonvulsant action, antinociceptive effects and muscle relaxation at higher doses.[47, 51-53] The α5-$GABA_A$Rs play role in cognition, memory, and spatial learning and are likely to be an important component in the memory component of anxiety.[48, 54] However α5β3γ2 ion channels are involved in asthma, MDD and schizophrenia. The α4- and α6- $GABA_A$R are diazepam insensitive (DI) subtypes because they lack, as mentioned, sufficient space in the binding pocket for the pendant C ring of BZDs, specifically for 1,4-benzodiazepines and IMDZ. Consequently, there is no ataxic nor sedative CNS side effects is related to these two subtypes.[39-40] Some recent studies have indicated that α5- and α4-containing $GABA_A$Rs can be found in the peripheral

nervous system (PNS), especially in lungs,[56-58] which give rise to one more possible treatment for asthma by using α5 selective BZDs. Recently, Knutson et al. have published evidence that the α6 Bz/GABAergic subtypes, at the PQ site, are associated with migraine, trigeminal pain, Tic diseases such as Tourette's syndrome, OCD and schizophrenia.[22-24]

In addition to receptor subtype variety, chloride ion influx plays the critical role in the pharmacological effects of $GABA_A$Rs in the CNS which results from allosteric modulation of GABA receptors. BZDs like diazepam act to the ion channel's GABAAR BZD allosteric site and lock it into an agonist conformation. The orthosteric binding of GABA to the ion channel is increased as a result of this action. When the receptor binds to GABA, it alters the conformation within the membrane, increasing the frequency with which the chloride ion channel opens. The membrane potential progressively decreases as a result of this effect (**Figure 5**). Neuronal transmission is further inhibited by this hyperpolarization, resulting in sedative, anxiolytic, hypnotic, amnesic, and anticonvulsant actions in the CNS, as well as muscle relaxant effects. In the absence of GABA, BzR ligands are unable to activate the intrinsic chloride ion channel; but, as allosteric modulators, they can mediate ion influx and vary the complex's opening frequency. [60-62] There are three types of BZDs that can interact with GABAA/BzRs: agonists, inverse agonists, and antagonists. BZD agonists, also known as positive allosteric modulators (PAM), are substances that increase chloride ion inflow and increase GABA's effects. It should be emphasized that unlike other agonists, BZD PAMs do not bind to the GABA binding site. Inverse agonists, also known as negative allosteric modulators (NAM), bind to the BZD site and have the opposite effect, lowering GABA-induced chloride ion influx. Depolarization of the membrane occurs as a result, decreasing the likelihood of neuronal firing activity. In addition to full agonists and inverse agonists, partial agonists and partial inverse agonists[10] are substances that elicit varying efficacy

in the range of maximum augmentation or reduction as a partial effect. The third kind of BZDs (antagonists)[2] have no pharmacological effect because they neither increase nor inhibit GABA function. However, because these antagonists have a higher binding affinity for BzR sites than other BZD ligands, they impede the interaction of PAMs and NAMs at the BzR site.[18] As a result, antagonists like flumazenil, βCCt, and 3PBC are widely employed to reverse the effects of a BZD-mediated response due to their capacity to occupy the BzR site and inhibit the binding of other BZDs. Flumazenil has been used as an antidote to reverse BZD overdose for more than 40 years. [63]

The notion of GABAAR subtype diversity and BZD allosteric modulation is critical for comprehending GABAAR's complex pharmacological effects, as well as a guide for future ligand

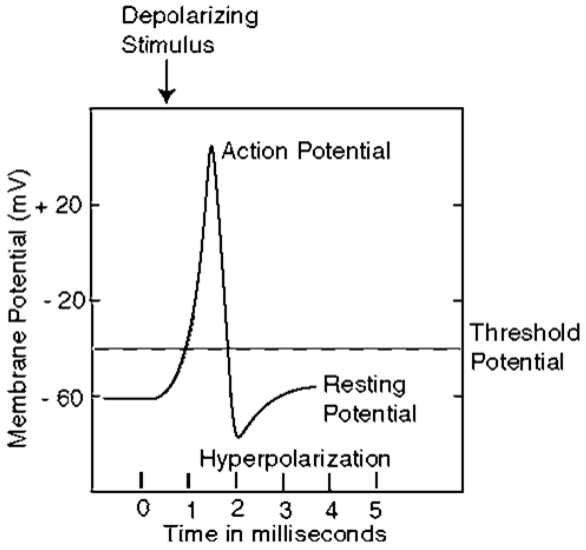


**Figure 5. When a depolarizing stimulus originates a nerve signal, the membrane potential changes with time. A potential that is hyperpolarized is one that is further away from the threshold potential. (Modified from a figure in Terry Clayton's Ph.D. thesis) [64]**

design for the treatment of many CNS illnesses. For example, hypnotic and sedative drugs can be made from ligands that are α1 subtype selective agonists. However α1 subtype selective

antagonists, on the other hand, are effective in reversing the hypnotic, ataxic, amnesic, or sedative effects of clinical BZDs, as well as the respiratory depression. Most importantly, ligands with α2/3/5 or α2/3 subtype selective agonist or partial agonist activity and devoid of α1 subtype PAM effects can elicit desirable effects in the treatment of anxiety disorders, convulsions, diabetic neuropathy, neuropathic pain, inflammatory pain, complex regional pain disorders, fibromyalgia, and panic disorders, among other conditions, with little or no sedative effects from α1 subtypes. In addition, α5 subtype specific inverse agonists have been demonstrated to improve learning and memory deficiencies without inducing undesired inverse agonist effects (anxiety, convulsions) at the α1 subtype. As a result, the varying potency at distinct subtypes can be used to create a unique spectrum of pharmacological effects.

## 1. 4 Molecular Modeling – Pharmacophore Model

Despite the fact that BZDs have a number of therapeutically important CNS pharmacological effects, multiple attempts to crystallize the transmembrane protein GABAAR, particularly the most critical recombinants of α1-6β1-3γ2, have failed until 2019, which impeded had further development and creation of novel BZDs. As a result, before electron microscopy helped to solve the structure of the α1β3γ2 ion channel last year, fragment-based molecular modeling and structure-activity relationship (SAR) studies were thought to be the best two methods for investigating the overall effects of BZDs, as well as developing new drugs with greater selectivity to treat specific diseases.

The Unified Pharmacophore/Receptor Model has been created [18, 65-67] in Milwaukee[67] during the last three decades, based on in vitro binding affinities at BzR subtypes of more than 150 BZD ligands, including all three types: agonists, inverse agonists, and antagonists.[18, 65-67] $GABA_AR$ subtype selective ligands from 15 structural families, including BZDs, [68-69] beta-carbolines, [70-72]

triazolopyrimidines, [73] pyridodiindoles, [74-75] imidazopyridines[76], and pyrazoloquinolines. To produce the estimated binding pockets, [77] ligands were overlayed on a planar template ligand (diindole template) to predict the BZD binding site. Over fifty rigid ligands were synthesized to arrive at the first pharmacophore receptor models.

The locations and descriptors of the two-dimensional representation of the full pharmacophore model are shown in Figure 6. H1 (Y210), H2 (H102), A2 (T142), and L1 were employed as anchor points in the model, with H1 and H2 representing two hydrogen bond donor sites on the protein, A2 representing one hydrogen bond acceptor site crucial for inverse agonist action in vivo, and L1 representing a lipophilic pocket. There are three additional lipophilic areas (L2, L3, and LDi) where van der Waals interactions, as well as p –π and π-π stacking mediate interactions between the ligand and the protein. Furthermore, three negative steric repulsive areas (S1, S2, and S3) that reflect the proteins themselves have been postulated. The extracellular domain lies in the LDi area between indole carbon atoms 5 and 6. [18, 65-66]

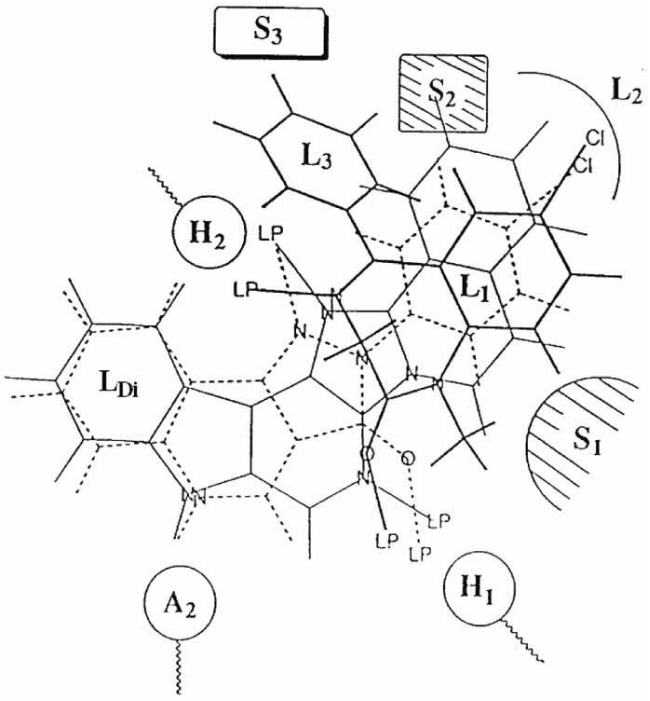

**Figure 6. GABAAR BzR displays the descriptors and regions of the Milwaukee-Unified Pharmacophore/Receptor Model for BZD. Within the unified pharmacophore/receptor model for the BzR, pyrazolo[3,4-c]quinolin-3-one CGS-9896 is depicted as a dotted line, a key diazadiindole is depicted as a thin line, and diazepam is depicted as a thick line. H1 and H2 refer to the BzR's hydrogen bond donor sites, whereas A2 refers to a hydrogen bond acceptor site that may be required for significant inverse agonist action in vivo. The four lipophilic zones are represented by L1, L2, L3, and LDi, whereas the negative steric repulsion regions are represented by S1, S2, and S3. The lone pair of electrons on the nitrogen (N) or oxygen (O) atoms of the ligands is referred to as LP. (Modified from Clayton et al) [18]**

Several major patterns were provided to explain the association between subtype selectivity and ligand structure (Figure 7) based on the ligand docking studies at the BzR using the pharmacophore model, which were incredibly useful for future ligand design and modification.[18]

- In the region L2, there is a minor difference in the induced volumes of the α1 and α2 subtypes.
- The included volume revealed that the binding pockets of the α2 and α3-containing $GABA_AR$ subtypes are extremely similar in size, lipophilicity, and shape.
- A comparison of the induced volumes of the α4 and α6 subtypes revealed that the 4 subtype's volume is smaller than the α6 subtype's, particularly in the L2 and LDi regions.
- The L3 lipophilic pocket is essentially non-existent in the α4 and α6 subtypes, as evidenced by the overlap of the included volume of the α1 subtypes vs the α4 and α6 subtypes.Because they lack the binding pocket for the pendant phenyl ring found in most BZDs and IMDZs, these two subtypes are diazepam insensitive DI sites in comparison to other DS subtypes.
- In the α5 subtypes, the volume of the L2 area is slightly bigger than in the α1 subtypes, as well as the α2 and α3 subtypes. This is a key trait for α5 subtype selectivity with reduced binding at the α1 subtype. For example, switching from a chlorine atom (diazepam) to an ethinyl group (QH-II-66) at the C (7) position (Figure 8),[65, 78] changed

the binding affinity ratio of α5 over α1 subtypes from 1.27 to 11.22, significantly increasing the selectivity of the α5 subtype in comparison to the binding affinity of the α1 subtype at the same time and resulting in QH-II-66, a potential anticancer drug. QH II 66 is less sedating than diazepam, but it just as potent as an anxiolytic.

Furthermore, a recent study by Mohler et al. found that the coupling of α1 to α5 subtypes resulted in the development of resistance to the anticonvulsant effects of BZDs.[79] As a result of the strategy of limiting binding affinities and efficacy at both α1 and α5 subtypes, a series of compounds with anticonvulsant and antinociceptive action with no evidence for the development of tolerance were developed, similar to the results proposed by Mohler [80-82] in the field of anticonvulsant medicines. **Remember that clinical BZDs are effective against status epilepticus in humans for around 3 days, but α2/α3 subtype specific ligands in animal models appear to be devoid of tolerance development in convulsions and discomfort (Cook, et al ASPECT talk, April 9th, 2019, Orlando, FL)**

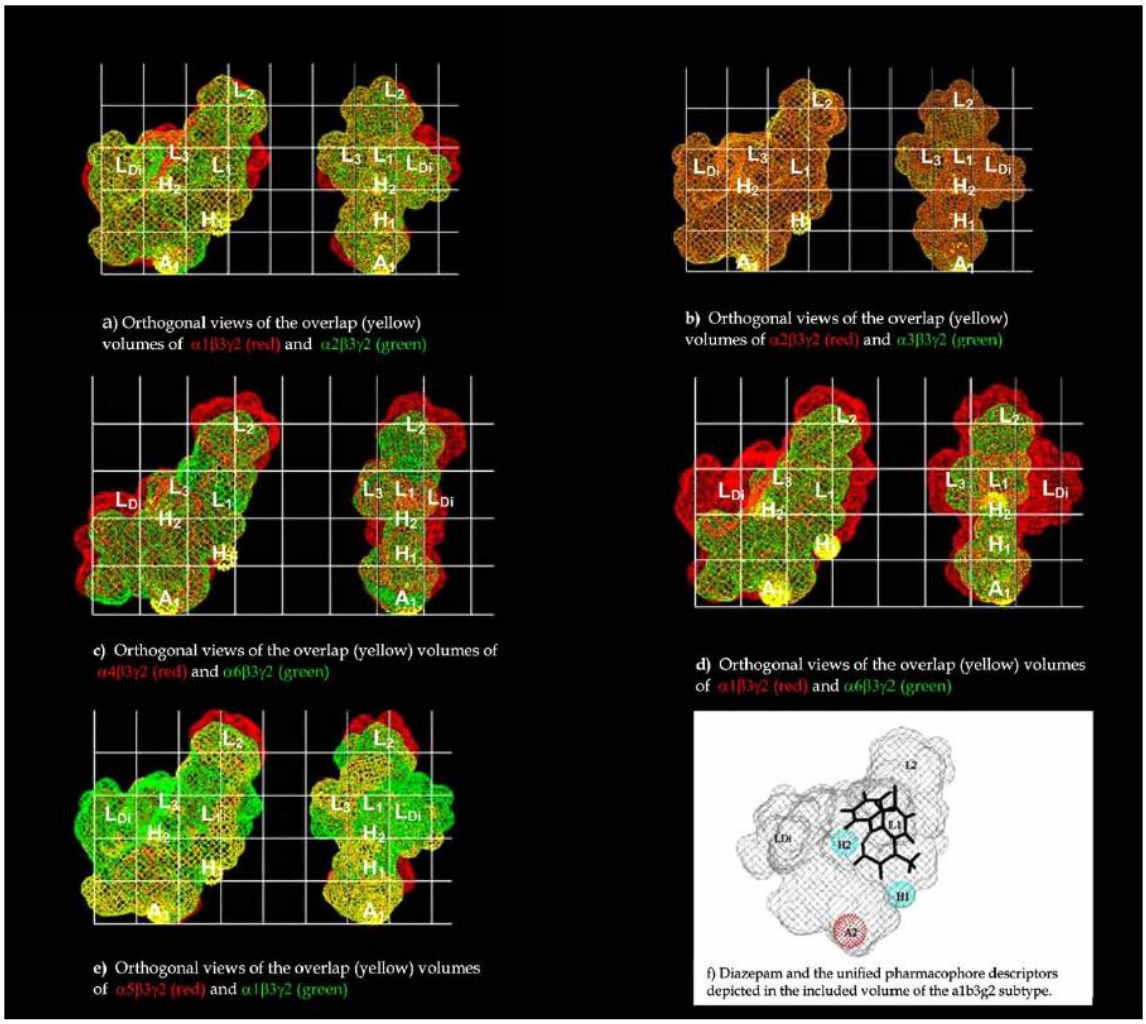


**Figure 7. Images of overlap between induced volumes produced from receptor subtype specific ligands: a) α1 and α2 subtypes; b) α2 and α3 subtypes; c) α4 and α6 subtypes; d) α1 and α6 subtypes; e) α1 and α5 subtypes; f) diazepam and the unified pharmacophore model descriptions in the contained volume of the α1 subtype Each grid measures 4 Å in width and height, and the yellow color denotes overlapping induced volumes. [67] (Modified from a figure in Clayton et al.)**

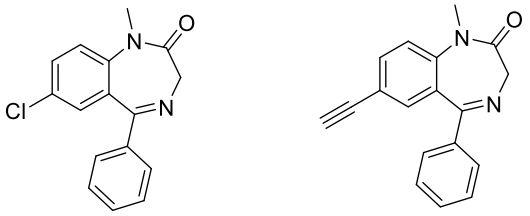


Bz/GABA$_A$ receptor binding data ($K_i$ = nM)

| | α1 | α2 | α3 | α5 | α1/α5 | Change in Selectivity |
|---|---|---|---|---|---|---|
| diazepam | 14 | 20 | 15 | 11 | 1.27 | 8.83 |
| QH-II-066 | 76.3 | 42.1 | 47.4 | 6.8 | 11.22 | |

**Figure 8. Bz/GABAAR binding data of diazepam and QH-II-066 in vitro. (Modified from a Figure in M. Poe and T. Clayton's Ph. D. theses)** [65, 78]

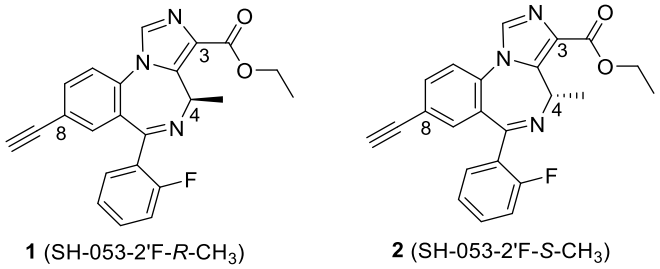


**Figure 9. IMDZ ligands 1 and 2 have enantiotropic chiral imidazodiazepine (IMDZ) structures.**

Clayton, et al. (2015) provided an improved pharmacophore model and homology model for α5 GABAAR subtypes during the last few years.[67] In addition to the binding affinities and updated compound library, the chiral methyl enantiomers at the C(4) position from the IMDZ class were identified as a new lipophilic region L4: the α5 subtype-selective ligand SH-053-2'F-R-CH3 **(1)** and its enantiomer the α2/α3/α5 subtype-selective ligand SH-053-2'F-S-CH3 **(2)**,[83] see Figure 9. According to current research, the novel binding pocket (L4) was only found in the α5 subtype and not in the α2 or α3 subtypes. Both enantiomers (R and S) can fit into the α5 subtype's binding

pocket (see included volume). However, the R-isomer **(1)**'s pendant phenyl ring did not fit into the binding pockets of the α2 or α3 subtypes. This phenyl group protruded beyond the included

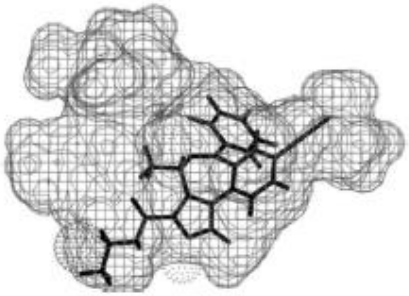

SH-053-2′F-S-$CH_3$ **2** fits the pharmacophore in the included volume of the alpha 2 subtype

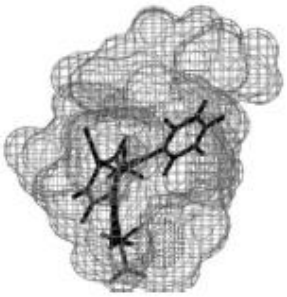

The left image of figure rotated 90°. It can be clearly seen that **2** fits within the included volume

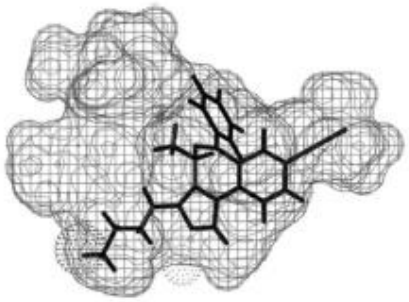

SH-053-2′F-R-$CH_3$ **1** does not fit the pharmacophore in the included volume of the alpha 2 subtype

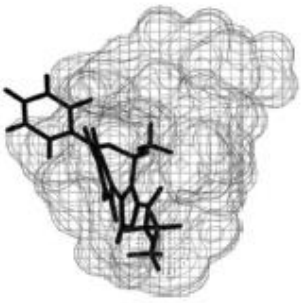

The left image of figure rotated 90°. It can be clearly seen that the conformation of **1** is such that the pendant 6-phenyl sticks outside the included volume

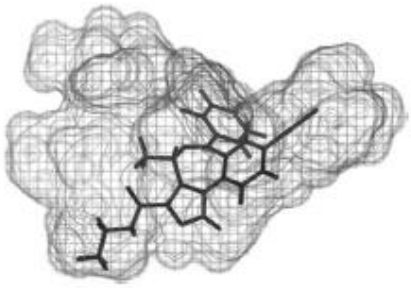

SH-053-2′F-S-$CH_3$ **2** fits the pharmacophore in the included volume of the alpha 5 subtype

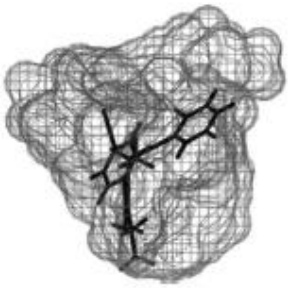

The left image of figure rotated 90°. It can be clearly seen that **2** fits within the included volume

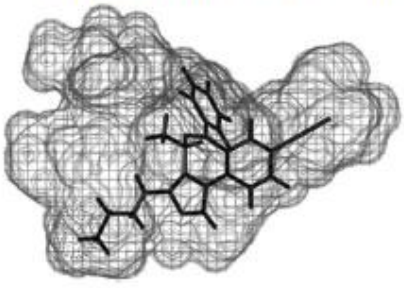

SH-053-2′F-R-$CH_3$ **1** fits the pharmacophore in the included volume of the alpha 5 subtype

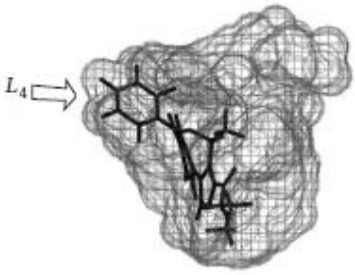


The left image of figure rotated 90°. It can be clearly seen that **1** fits within the included volume

**Figure 10. In the α5 and α2 pharmacophore/receptor models, ligand occupancy of SH-053-2'F-R-$CH_3$ (1) and SH-053-2'F-S-$CH_3$ (2) was observed. (Adapted and reprinted from Clayton et al.) [67] However ligand R-CH3 does not bind to the α1, α2 and α3 subtypes.**

volume, rendering the R-CH3 isomer ineffective at binding to at α2 and α3 subtypes. (Figure 10). The S-isomer **(2)**, on the other hand, was easily accommodated in all three subunits (α2, α3, and α5), because the α2 and α3 subunits are comparable in shape and size. The results of the pharmacophore model's are compatible with the efficacy data of the 2/3/5 subtype-selective ligand when combined with efficacy data of the S-ligand(2).[67]

# Chapter 2 Cancers

## 2. 1 Medulloblastoma

The central nervous system (CNS) is made up of the brain and spinal column. Vital functions such as thought, speech, body strength, etc are controlled by the central nervous system.

A brain tumor starts when normal and healthy cells in the brain became altered and start growing out of control, creating a tumor mass. A tumor can be either cancerous or benign. A cancerous tumor can be malignant, which means it can grow and spread to different parts of the body. A benign tumor is one that can grow but does not spread to other organs.

Medulloblastoma is one type of brain tumor. Medulloblastoma starts in cells in the cerebellum,[83] which is located at the back of the brain. It controls body movement as well as coordination.

Medulloblastomas are usually rapidly growing tumors that spread through the cerebrospinal fluid and frequently metastasize to different locations along with the surface of the brain and spinal cord. Metastasis like these, which spreads down to the cauda equina at the end of the spinal cord, is called "drop metastasis"

Each year between 250 and 500 children are diagnosed with medulloblastoma. About 18% to 20% of all childhood brain tumors cases are medulloblastoma, which makes it the most common cancerous brain tumor among children. Medulloblastomas occur mostly in children who are younger than 16 years old. In all diagnosed cases more than 70% are younger than 10 years. The chance of getting medulloblastoma becomes lower after the age of 9 years.

Medulloblastoma can also be found in adults, but it is not as common as it is in children. About 33% of medulloblastoma cases in the United States occur in adults which are between the ages of 20 to 44.

The survival rate indicates what percent of children live after the tumor is found. The survival rate of children with medulloblastoma relies on different factors, such as the risk level for this disease as well as the age of the child when he or she was diagnosed. Children who are younger than 3-years old may have a lower survival rate, may be because the disease is usually more aggressive in this age group.

Overall, the survival rate for medulloblastoma patients in which the tumor has not spread is about 70% to 80%. The survival rate in the case in which the tumor has spread to the spinal cord is lower, about 60%.

It is important to consider that statistics on the survival rates for children with medulloblastoma are estimated. The estimates were calculated from annual data based on the number of children with this type of tumor in the United States. Also, this data is measured every 5 years.

Doctors are still doing research to understand the causes of most childhood tumors, medulloblastoma is one in them. The factors listed below are linked with a higher risk of medulloblastoma:

- **Gender.** Medulloblastoma is less common in girls than in boys.
- **Age.** Medulloblastoma occurs most often in the first 8 years of life, with about 50% of cases occurring in children who are less than 6 years old.

- **Genetics. G**enetic conditions are listed below, which can be linked with a higher risk of developing medulloblastoma:
    - Nevoid basal cell carcinoma syndrome (NBCCS)
    - Turcot syndrome (a subtype of familial adenomatous polyposis (FAP) or Lynch syndrome)
    - *BRCA1* gene mutations

The following symptoms or signs are common in children with medulloblastoma. These alterations are not always present in children with medulloblastoma. A symptom could also be caused by a medical issue other than a brain tumor.

- Headaches
- Morning vomiting that worsens over time
- Clumsiness
- Problems with handwriting and other motor skills that worsen over time
- Problems with vision or an eye turning inwards

If medulloblastoma spreads to the spinal cord, it may cause the following symptoms:

- Back pain
- Inability to control the bowels and bladder
- Difficulty walking

### 2. 1. 1 Types of Medulloblastoma

Current morphological (histopathological) classification schemes for medulloblastoma include varieties such as desmoplastic/nodular, MBEN (medulloblastoma with extensive nodularity), classic medulloblastoma, large cell, and anaplastic medulloblastoma. Various groups have begun to sub-classify medulloblastoma based on changes in the transcriptome84 as a result of recent advances in the ability to monitor transcription across the genome in the context of a single experiment. This transcriptional approach to tumor sub-classification has also been applied to a variety of non-medulloblastoma histologies 85, 86, 87, 88, 89, 90, with the underlying assumption that tumors with similar transcriptomes will behave biologically similarly, allowing a transcriptionally driven classification to serve as a guide for successful anti-neoplastic therapy.

The number of medulloblastoma 'subgroups' identified within medulloblastoma patient cohorts is mostly determined by the number of individual tumors within each cohort, with bigger cohorts revealing greater layers of hierarchical complexity.[84, 91, 92, 93] Scientists from several laboratories published article on this topic agreed that there were four primary transcriptional subgroups of medulloblastoma, with many of these subgroups showing a subsequent level of hierarchical structure that will be designated the subtypes of the subgroups, based on the published literature and some unpublished data presented at a recent consensus conference in Boston, Massachusetts (**Fig. 11**). The exact number of subtypes for each subgroup is unknown at this time, however each subgroup is expected to have multiple subtypes.

WNT, SHH, Group 3, and Group 4 are the names of the four main subgroups of medulloblastoma (**Fig. 12**). The signaling pathways Wnt and Shh (Sonic Hedgehog) were called after those thought to be important in the pathophysiology of that subtype. Because the biology

of the remaining two subgroups is less well understood, the decision was to keep generic names for the time being until the underlying biology driving these subgroups could be properly defined. There is evidence for subtypes within subgroups, especially in Group 3, as indicated by the fact that by using the clustering method, a small number of "intermediate" tumors were classified into Group 3 or Group 4 among Non-WNT, Non-SHH cancers.

While the subsets of the subgroups are obvious, they are not well described at this time, thus until more characterization from several centers and on much larger cohorts were available the consensus was to designate them with Greek letters (α, β, γ etc.). (**Fig. 11**). The four principal subgroups of medulloblastoma were named as follows: WNT, SHH, Group 3, and Group 4 (**Fig. 12**). The Wnt and Shh (Sonic Hedgehog) were named for the signaling pathways thought to play prominent roles in the pathogenesis of that subgroup. Because the biology of the remaining two subgroups is less well understood, the decision was to keep generic names for the time being until the underlying biology driving these subgroups could be properly There is evidence for subtypes within subgroups, particularly in Group 3, as evidenced by the fact that among Non-WNT, Non-SHH tumors, a tiny number of "intermediate" tumors may be classified to Group 3 or Group 4 based on the clustering technique used. Particularly for Group 3, there is evidence for the existence of subtypes within the subgroups, which is also identified by the fact that among Non-WNT, Non-SHH tumors, there may be a small fraction of “intermediate” tumors that would be classified to Group 3 or Group 4 according to the clustering algorithm applied.[91] While the subsets of the subgroups appear obvious, they are not well characterized at this time, so the consensus was to name them using Greek letters (α, β, γ, etc.) until additional characterization from multiple centers, on much larger cohorts, became available. (**Fig. 11).** Since the four groups

was proposed and were clearly different in terms of demographics, histology, DNA copy-number aberrations, and

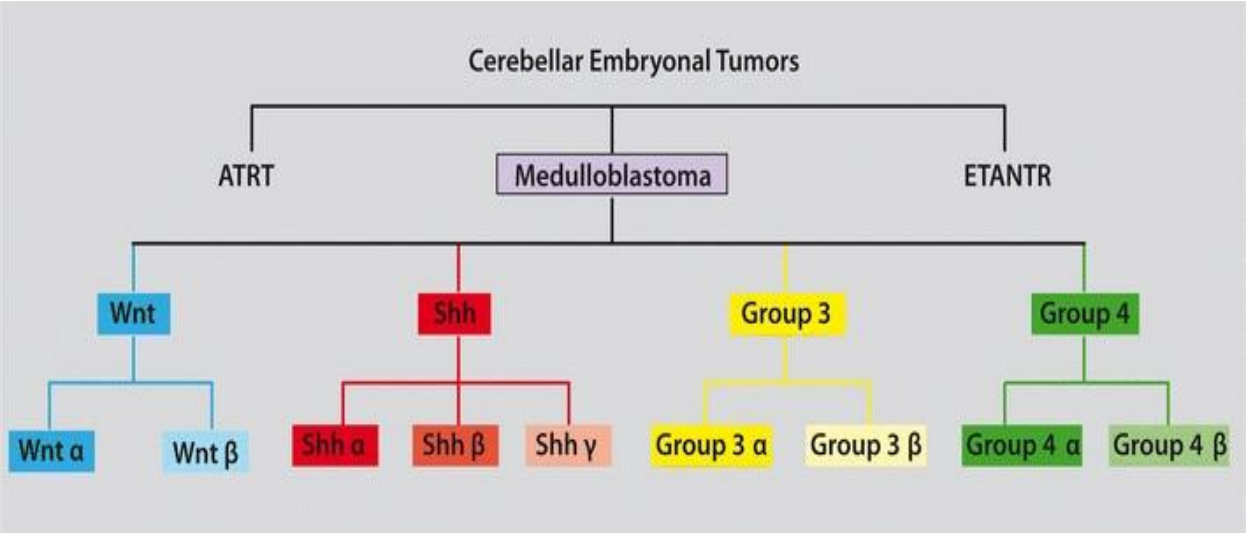


**Figure 11. Dendrogram depicting the classification of embryonal tumors of the cerebellum. Medulloblastomas should be differentiated from the less common ATRTs and ETANTRs of the cerebellum. Under the current consensus classification of medulloblastoma four principal subgroups are identified: Wnt, Shh, Group 3, and Group 4. The evidence suggests that each of the four principal subgroups will likely have distinct 'subsets' that are biologically and clinically homogeneous as compared to other subsets from within the same subgroup. As the nature and number of subsets for each subgroup are currently unknown, the consensus classification suggests that each subset be named using a Greek letter (α, β, γ, etc.) until such time as they are sufficiently characterized to be named based on their molecular etiology.**

clinical outcome as which is also nicely summarized in a meta-analysis paper.[93] The authors consider it very helpful to begin using these subgroups in the clinic. More specifically, subgrouping according to molecule will not only help to detect target cohorts for certain drugs (e.g., SHH inhibitors), but also significantly help to the outcome prediction by the time of diagnosis[93], even more than any of the currently used clinical markers such as patient age, metastatic stage at diagnosis, level of resection, and histological subtype according to the WHO classification[94]. Although it is evident that few tumors will either be positive for more than one marker or negative for all markers[92], it is good that using two markers that are supposed to use the

same subgroup (such as SFRP1 and GAB1 for SHH tumors) resulted in a very high overlap in a study which was published in the same issue.[96]. In the following, the distinctive characteristics of these four core subgroups are shown in more detail.

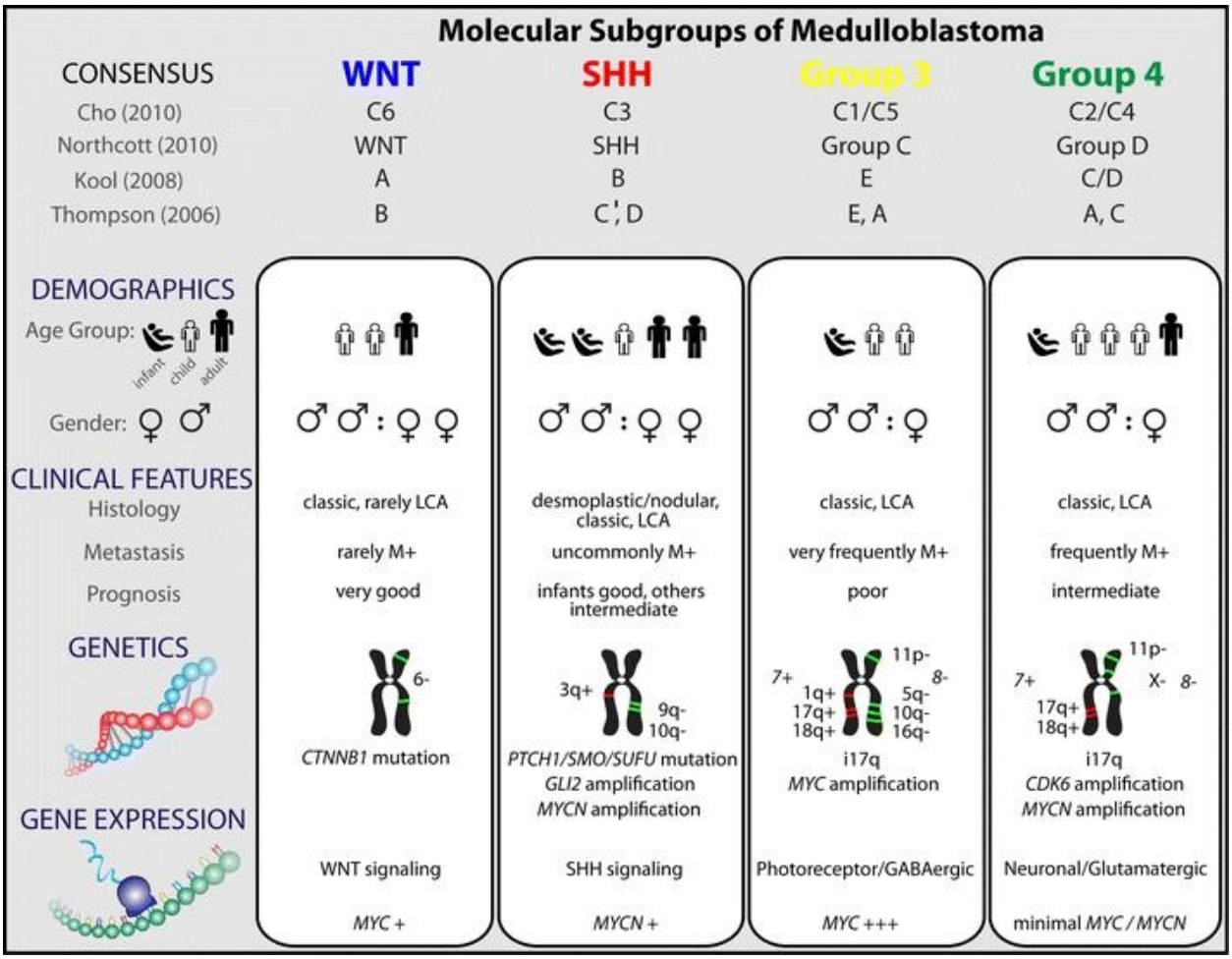


**Figure 12. Comparison of the various subgroups of medulloblastoma including their affiliations with previously published papers on medulloblastoma molecular subgrouping.**

### 2. 1. 1. 1 WNT subgroup

The Wnt subgroup is the most well-known of the medulloblastoma subgroups due to its excellent long-term prognosis in comparison to other subgroups.[95] Long-term survival rates for Wnt

medulloblastoma patients are projected to approach 90%, with those who die succumbing to therapy-related problems or secondary neoplasms rather than recurrent Wnt medulloblastoma.[96]

Turcot syndrome is caused by germline mutations in the Wnt pathway inhibitor APC, which leads to a medulloblastoma propensity. In addition, sporadic medulloblastomas have been shown to have somatic mutations in the CTNNB1 gene, which codes for β-catenin.[97, 98] These extensive germline and somatic genetic data strongly suggests that canonical Wnt signaling has an etiological role in the pathogenesis of this group of tumors, leading to the identification of 'Wnt subgroup medulloblastomas.

To date, almost all Wnt medulloblastomas investigated show a typical histology. CTNNB1 mutations, nuclear immunohistochemistry staining for -catenin, and monosomy six are all common features of Wnt medulloblastomas (deletion of one copy of chromosome 6 in the tumor). It's uncertain which of these markers is a gold standard for diagnosing Wnt medulloblastoma, as there have been reports of medulloblastomas with a clear Wnt transcriptional signature but no monosomy six.[92] The scenario is further complicated by the recent revelation of a single medulloblastoma with mutations in both CTNNB1 and PTCH.[99] Indeed, over-representation of Wnt pathway genes has been seen in Shh and Group 3 medulloblastomas, while the relevance of this finding is unknown.[92] Although medulloblastomas with giant cell/anaplastic histology have been observed in the Wnt subgroup, they appear to have the same good prognosis as the Wnt subgroup. [96] Which of the effects of monosomy 6, nuclear staining for -catenin, mutation of CTNNB1, immunohistochemical staining for DKK192, 100, or a transcriptional signature that clusters with other 'Wnt' tumors should be used as a gold standard for the diagnosis of Wnt medulloblastoma needs to be confirmed in larger cohorts of well-characterized medulloblastomas.

Even though men are more prone to develop medulloblastoma, Wnt medulloblastomas have a male to female ratio of roughly 1:1. Wnt medulloblastomas can afflict persons of any age, however they are more prevalent in adults. Apart than monosomy six, the genome of Wnt medulloblastomas has few additional areas of genetic amplification or deletion.[92] Wnt medulloblastomas are thought to emerge from the cerebellum's lower rhombic lip, according to a mouse model recently published.[101] This mouse model will surely aid in the preclinical testing of new medications. Because most patients with Wnt medulloblastoma live, it's probable that they're being overtreated with existing medicines, which are extremely morbid, and a clinical study of therapeutic de-escalation in this patient cohort is now being discussed.

#### 2. 1. 1. 2 Sonic Hedgehog Subgroup (SHH)

The Sonic Hedgehog signaling system, which is expected to induce tumor initiation in many, if not all, instances, is called after the Shh group of medulloblastomas. Gorlin syndrome is caused by germline mutations in the Shh receptor PTCH, which involves a tendency to medulloblastoma.[102,103] Individuals with germline mutations in the Shh inhibitor SUFU, infantile medulloblastoma, are prone to medulloblastoma.[104, 105, 106, 107] In sporadic medulloblastoma, somatic mutations of PTCH, SMO, and SUFU, as well as amplifications of GLI1 and GLI2, have been found.[107, 108, 109] The current suggestion to legally designate them 'Sonic Hedgehog' subgroup medulloblastomas is based on genetic findings suggesting Shh signaling in the genesis of this group of tumors.

Transcriptional profiling has mainly identified sonic hedgehog subgroup medulloblastomas.[85, 91, 92, 110,111, 112] Immunohistochemical staining for SFRP182, [112, 113], or GAB1.[115] have also been used to detect Shh medulloblastomas. Because the PTCH gene is situated on chromosome 9q22,

deletion of chromosome 9q seems to be confined to Shh medulloblastomas.[92] The Shh subgroup of tumors[115] has the majority of documented mice models of medulloblastoma. Human Shh medulloblastoma has a strangely dichotomous temporal incidence, in that it is quite common in both newborns (0–3 years) and adults (>16 years), but significantly less common in children (3–16 years). The extent to which adult Shh medulloblastomas resemble child Shh medulloblastomas will be determined through large-scale tumor studies. Females predominate in Shh medulloblastoma, according to some recent studies[92] but not others[85]. The gender ratio in all published research is roughly 1:1. The Shh subgroup includes the majority, if not all, nodular/desmoplastic medulloblastomas. However, because up to 50% of Shh subgroup medulloblastomas are not nodular/desmoplastic, this is not a useful marker for the subgroup. Shh medulloblastomas have a prognosis similar to Group 4 medulloblastomas, although it's somewhere in between Wnt medulloblastomas (excellent) and Group 3 medulloblastomas (bad). Small compounds targeting smoothened (SMO) have recently been shown to be very effective, if briefly, against Shh medulloblastoma, highlighting the critical need to discover effective and feasible markers for Shh medulloblastoma.[116, 117, 118]

#### 2. 1. 1. 3 Group 3

Although they cover the bulk of LCA cancers, Group 3 tumors are usually 'classic' medulloblastomas. A transcriptional profile that clusters with other Group 3 cancers is the current gold standard for diagnosing a Group 3 tumor.[90, 91, 93] NPR3 immunohistochemistry positive has been proposed as a Group 3 marker.[92] While Shh subgroup cancers have high levels of MYCN expression, Wnt subgroup and Group 3 tumors have high levels of MYC expression, Group 4 tumors have low levels of both MYC and MYCN expression, with the exception of a

few cases of MYCN amplification.[91, 92, 115]. As a result, one group has proposed that Group 3 cancers be dubbed the MYC group.115 MYC amplification (but not MYCN amplification) appears to be nearly exclusively restricted to Group 3.[90, 91,92] The medulloblastoma oncogene OTX2 appears to be exclusive to Group 3 and Group 4 tumors in terms of amplification and overexpression.[92, 119, 120, 121] Group 3 cancers overexpress numerous genes first discovered for their function in retinal development, while the relevance of these genes in Group 3 tumor pathogenesis is still unknown.

Malignancies in Group 3 are far more likely than cancers in Group 4 to gain chromosome 1q and/or lose chromosomes 5q and 10q. Males are more likely than females to have Group 3 tumors, which are present in newborns and children but nearly never in adults. LCA histology is common in Group 3 tumors, and they are commonly metastatic.[92] Indeed, it has been argued that earlier identification of metastatic status as a risk factor for poor prognosis in medulloblastoma was really identifying a subset of individuals who were enriched for Group 3.[92] Group 3, in which one subset (Group 3) comprises all patients with MYC amplifications and assumes that most of the high risk of recurrence and mortality is associated with a Group 3 diagnosis, has the greatest evidence for a clear'subset of a subgroup' in medulloblastoma to date. Group 3 patients, on the other hand, did not have MYC amplifications and had the same clinical result as Group 4 patients.[90] This interesting result will need to be confirmed in further cohorts, as well as the creation of therapeutically useful indicators for identifying Group 3 and Group 3 patients. Despite the fact that Group 3 tumors are more similar to Group 4 cancers than Shh or Wnt tumors, the demographic, clinical, transcriptional, and genetic distinctions between Group 3 and Group 4 show that they are separate entities.[91, 92] The poor prognosis of Group 3 patients clearly shows that the medulloblastoma community has to focus more on this subgroup in order to create useful

biomarkers, understand the underlying etiology, and establish realistic mice models to produce better therapies.

#### 2. 1. 1. 4 Group 4

A 7-year-old kid with a characteristic histology medulloblastoma with an isochromosome 17q is the prototype medulloblastoma. Because the molecular etiology of Group 4 tumors is still unknown, the current standard nomenclature has been given the generic designation 'Group 4' awaiting further research. Group 4 medulloblastomas are now distinguished by a transcriptional profile that clusters with another Group 4 medulloblastomas. KCNA1 has been proposed as an immunohistochemical marker for Group 4 cancers, however more research is needed.90,92 Although isochromosome 17q is found in 26% of Group 3 tumors, it is significantly more prevalent in Group 4 tumors, where it is the most common cytogenetic alteration (66%) as described in Kool et almeta-analysis .'s of all published data sets in this issue of the journal.[92, 122] Isolated 17p deletion is also present in Group 3 and 4 tumors, but nearly never in Wnt or Shh subgroup medulloblastomas. The deletion of the X chromosome, which is present in 80 percent of females with Group 4 medulloblastoma, is the only other significant cytogenetic abnormality among Group 4 tumors. Given the high male:female ratio in Group 4 patients, the high prevalence of X chromosome deletion in females with medulloblastomas is particularly concerning (2:1). Multiple studies have found that genes involved in neural differentiation and development are overrepresented in Group 4 tumors, albeit neither the genetic basis nor the clinical significance of this has been determined.[90, 91, 92] Group 4 patients, like those with Shh malignancies, have an intermediate prognosis. Although Group 4 tumors account for more than 30% of all

medulloblastomas, we know the least about their molecular pathophysiology, and no mice models of Group 4 tumors have been identified.

### 2. 1. 2 Interaction of benzodiazepines with α5-GABAA receptors

Several tumor models were used to do an intratumor microdose efficacy study. In the study several benzodiazepaines were used which can enhance the action of GABA at α5-GABAA receptors.

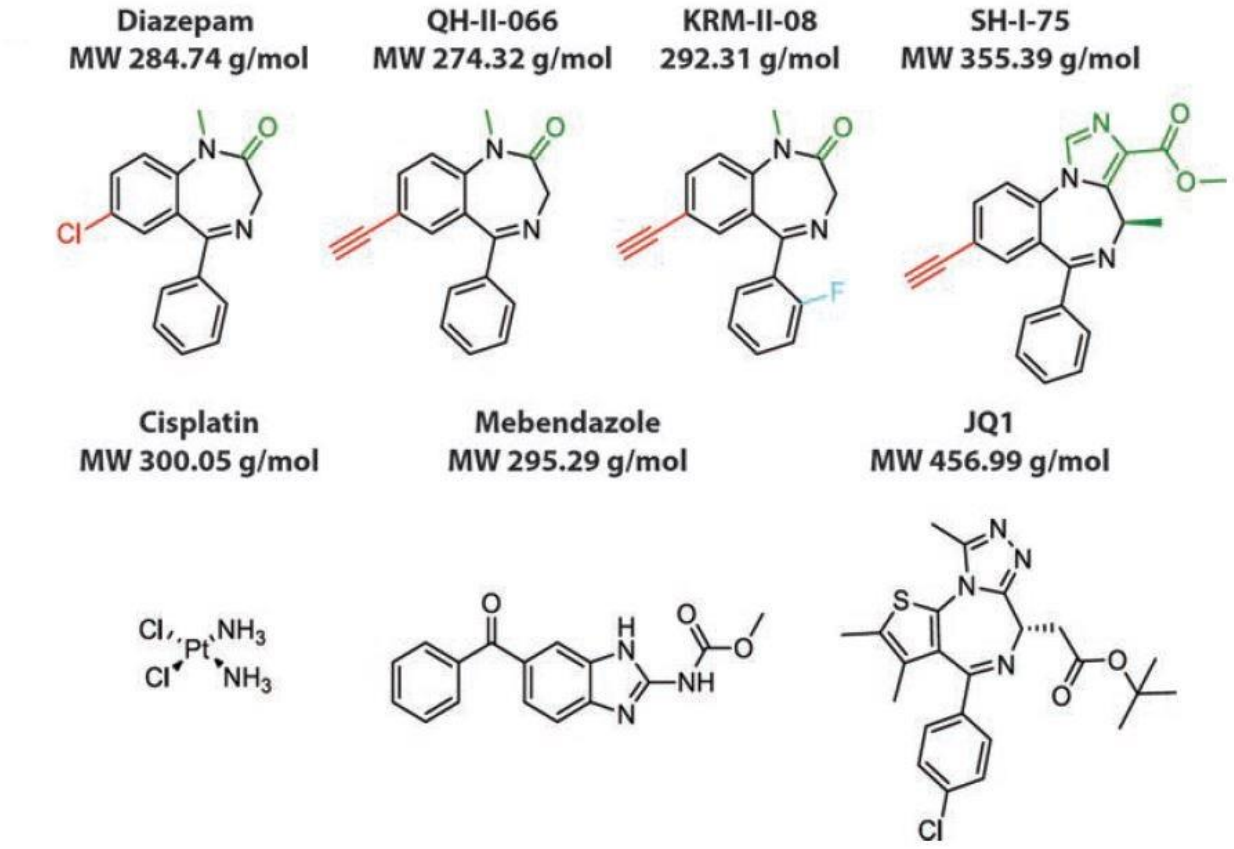


**Figure 13. Chemical structures of compounds. The study employed structurally related benzodiazepines shown in the upper line. The compounds are made up of the basic benzodiazepine chemical structure; benzene and diazepine ring fusion, and color-coded structural changes. Chemical structures of the study's standard-of-care therapy substances shown in the lower line. JQ1 has a structural resemblance to the benzodiazepine SH-I-75.**

In these agents cisplatin, mebendazole and the bromodomain JQ1 were included. Medulloblatoma tumor cell lines were used to create a nude mouse flank xenograft. D425 and D283 tumor cell xenografts express a high degree of α5-GABAA receptors. Results found from microdevice

technology indicates D425 and D283 tumor cell flank xenografts were more sensitive than DAOY tumor cell flank xenografts to the benzodiazepine derivatives. KRM-II-08 (**19**) sensitizes most, which is a positive allosteric modulator of α5-GABAA receptors. In the same model two other compounds SH-I-75 and QH-II-66 (**8**) also sensitized D425 and D283 tumor cell flank xenografts. The difference between KRM-II-08 (**19**) and QH-II-66 (**8**) is KRM-II-08 (**19**) contains a fluorine atom at the 2' position while QH-II-66 bears a hydrogen atom at the 2' position. KRM-II-08 (**19**) and QH-II-66 (**8**) have similar structures, and both are benzodiazepines.

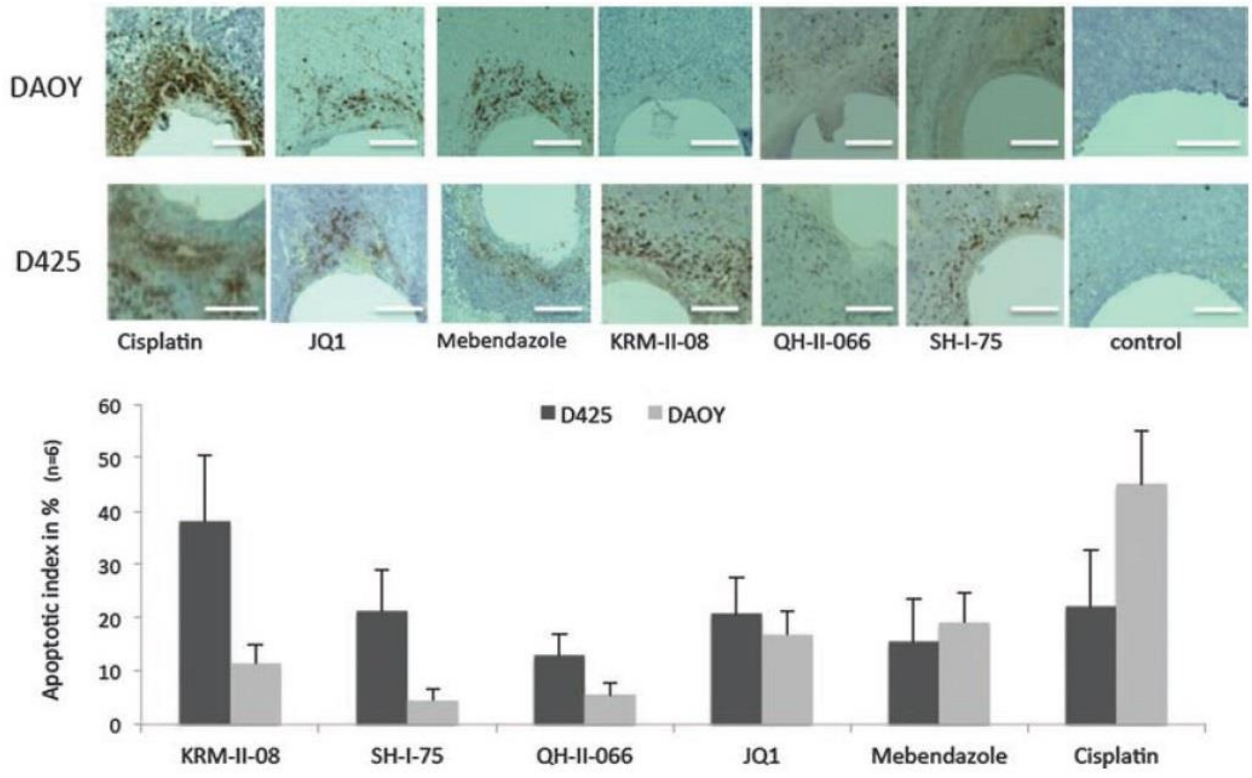


**Figure 14. Effect of compounds in a microdevice on flank tumors. Representative photos of D425 and DAOY tumor slices excised 24 hours following exposure to a microdose of each medication from the device, revealing discrete areas of apoptosis as measured by cleaved-caspase-3 expression (brown). 250 µm scale bars. For human D425 and DAOY tumors subjected to KRM-II-08, SH-I-75, QH-II-066, JQ1, mebendazole, and cisplatin, the apoptotic index (percent apoptotic cells/all cells in drug-affected tissue region) was calculated (all 35 percent drug in PEG1450). Please give (p 0_01) averages from 6 geographically different reservoirs from at least 3 tumors.**

Exposure to KRM-II-08 (**19**) leads to apoptosis in 38% of exposed cells (apoptotic index, AI) within 24 hours in this model, compared with 21% for SH-I-75 and 13% for QH-II-066 (**8**) **(Fig.**

**14).** KRM-II-08 (**19**) is also significantly more potent than all other standard-of-care treatments tested in this tumor **(Fig. 14).** Another $\alpha$5-GABAA receptor expressing tumor model, D283, also shows significantly higher local apoptosis induction in response to benzodiazepine derivatives KRM-II-08 (**19**) (AI = 32%) and QH-II-066 (**8**) (AI = 30%) treatment, as compared to other standard-of-care treatments tested. Interestingly, cisplatin,4JQ1,[10] and mebendazole11 exhibited a greater effect on the non-$\alpha$5-GABAA receptor expressing tumor cell line DAOY (**Fig. 14**).

MALDI mass spectrometry imaging analyses[134,135] was performed on cross-sectioned mouse frozen flank tissue to demonstrate local drug distribution of compounds released from the microdevice. Shown in **Figure 15** is a 2-dimensional MALDI mass spectrometry images displaying the distribution of KRM-II-08 (**19**) (Fig. 15(A)), QH-II-066 (**8**) (Fig. 15(B)), and JQ1 (Fig. 15(C)) with relative intensities. The high mass accuracy measurement achieved by the FTICR analyzer (better than 1 ppm) enabled confirmation of the release of each compound from the microdevice. For JQ1, only ions from the fragmentation of the parent molecule were detected during the MALDI MSI analysis. The high laser intensity (i.e., 35%) may be responsible for an in-source fragmentation of the drug.

Based on the correlation with a hematoxylin and eosin (H/E) stained serial section, all the compounds were released into the tumor tissue at maximum diffusion distances of 560 μm for JQ1 and greater than 1150 $\mu$m for KRM-II-08 (**19**) and QH-II-066 (**8**) (**Fig. 15**). This area of exposure is approximately congruent with the regions of apoptosis induction that are observed in **Figure 14**, implying that the presence of the drug leads to apoptosis.

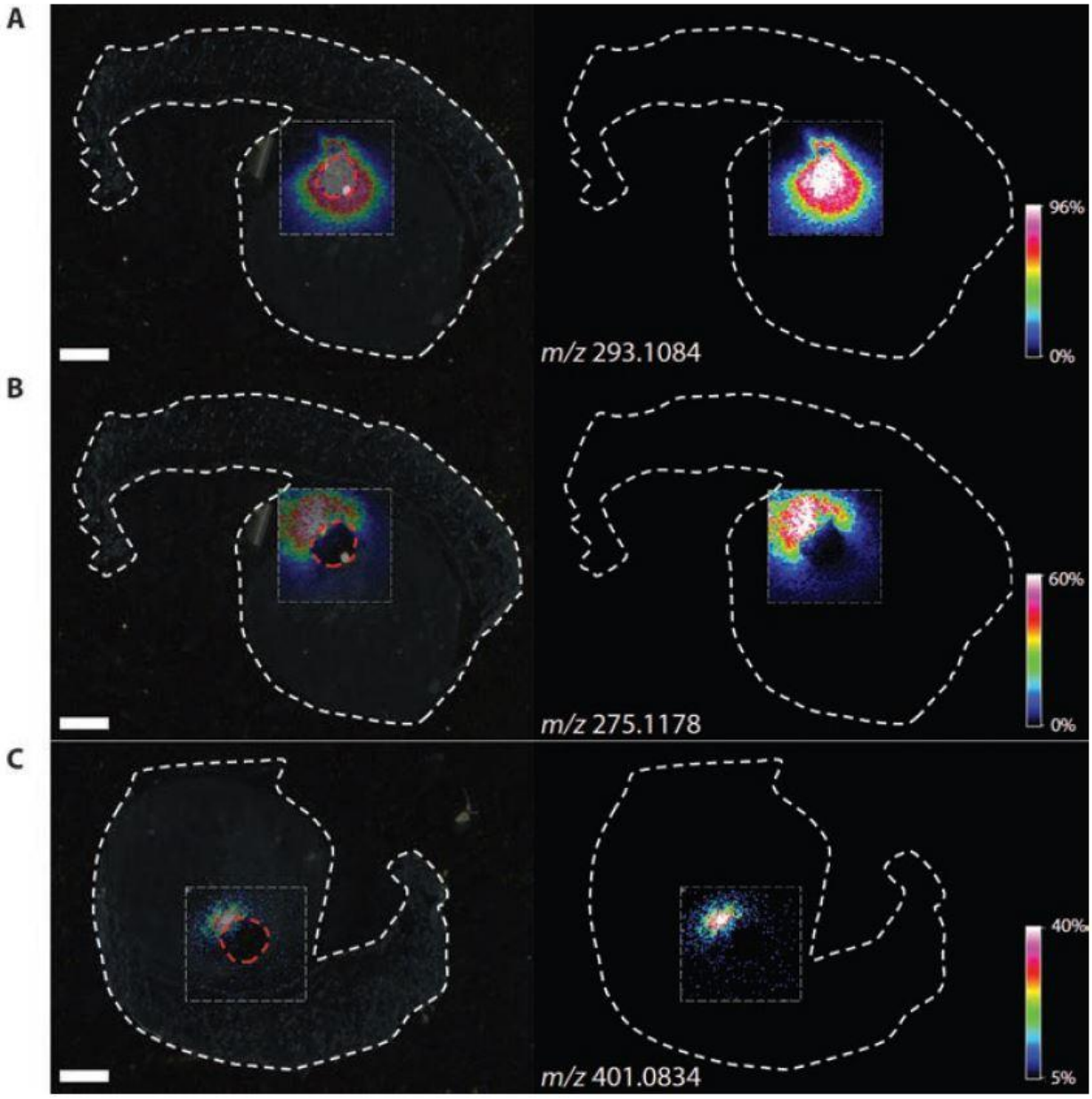


**Figure 15. Molecular imaging of chemical distribution using MALDI FTICR mass spectrometry. Laser desorption/ionization with matrix assistance Mass spectrometric imaging (MSI) of the distribution of three drugs in sections of a mouse flank tumor with an implanted device using Fourier-transform ion cyclotron resonance (MALDI FTICR) (A) KRM-II-08 (m/z 293.1084); (B) QH-II-066 (m/z 275.1178); and (C) a fragment of JQ1 (m/z 401.0834). The left and right panels, respectively, show scanned images of tissue sections overlaid with MALDI FTICR MSI data and MALDI FTICR MSI data alone. The device's location in each part is shown with red dotted lines. The images were taken at a spatial resolution of 30 meters. 1000-meter scale bars**

QH-II-066 (**8**) and KRM-II-008 (**19**) are α5GABA$_A$R positive allosteric modulators that decreased the expression of HOXA5, a homeobox transcription factor that controls p53 expression, showed

in a cell viability assay.[1] The research group of Dr. Soma Sengupta studied 763 primary medulloblastoma patient tumors to better understand the role of α5-$GABA_AR$ in group 3 cell viability.

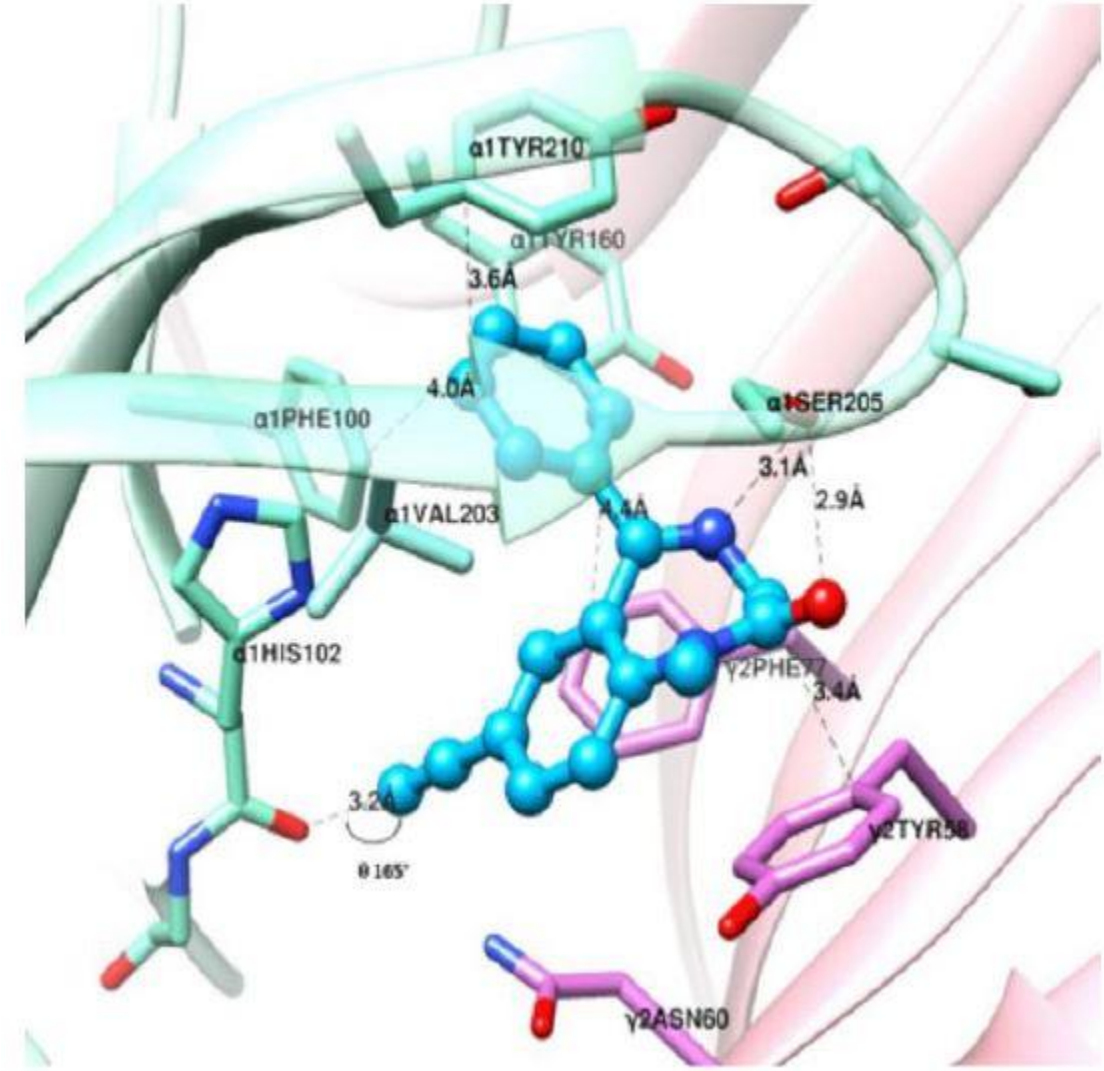


**Figure 16. QH-II-066 at $\alpha^+ \gamma^-$ Interface of $GABA_AA$ Receptor in the α1β3γ2 em cryostructure (Nature 2019)**

### 2. 1. 2. 1 QH-II-066 at $\alpha^+ \gamma^-$ Interface of GABAA Receptor

Cryo-ER structures were used to explain the three most significant interactions of (QH-II-066. **8**), which allow them to function as a PAM. But with less sedation than diazepam. (Cook et al, US Patent 2006)

- With α1 Ser205, the bifurcated hydrogen bonding was 3.1A for the N atom in the seven-member ring and 2.9A for the oxygen atom.
- The interaction created by QH-II-066 (**8**) with the α1His102 via halogen bonding with the backbone carbonyl was less than the halogen bond formed by diazepam with α1His102 via halogen bonding with the backbone carbonyl.
- The pi-pi stacking with α1Tyr210 and α1Phe100.

In the DZP bound cryo-ER structure (6HUP), the distance between the chlorine atom and the carbonyl oxygen was 3.2A, while in the case of QH-II-066 it was 3.8A for the ethinyl function. (6HUO). In both cyro-ER structures, the σ-hole angle is 165. QH- II-066's bifurcated hydrogen bond with α1Ser205 is shorter than the one produced by bound DZP. The shorter hydrogen bond and bifurcated hydrogen bond interaction of α1β3γ2 are consistent with the same sedative effect as diazepam, but it is much less. (US Patent, Cook et al, 2006)

#### 2. 1. 2. 2 KRM-II-008 at the $\alpha^{+}\gamma^{-}$ Interface of the GABAA Receptor

Here The most critical hydrogen bonding bifurcation is:

- With α1Ser205, the N atom in the seven-member ring was 2.2A, and the oxygen atom was 2.5A.
- The pi-pi stacking with α1Tyr210 and α1Phe100.

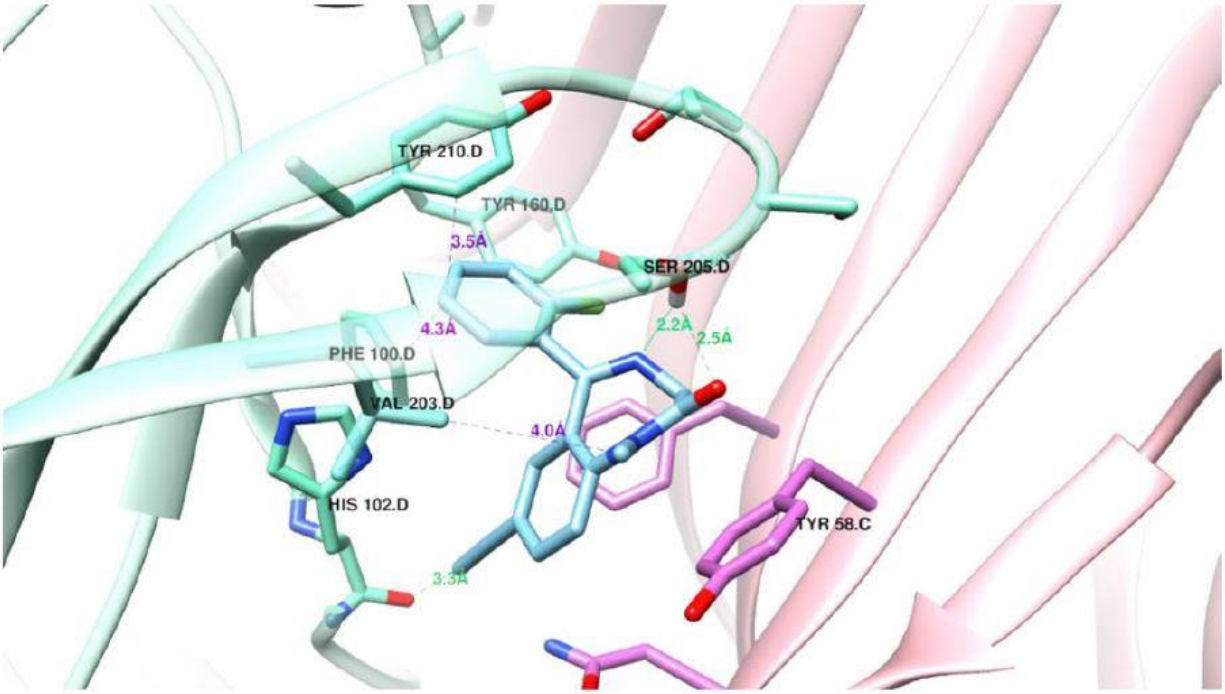


**Figure 17. KRM II 08 (19) at the $\alpha^+ \gamma^-$ Interface of GABAA Receptor**

QH- II-066 (**8**)'s bifurcated hydrogen bond with α1Ser205 is longer than the one produced by bound KRM-II-008 (**19**). Because KRM-II-008 **(19)**'s bifurcated hydrogen bond is shorter than QH-II-066 (**8**), it has a stronger affinity for the α1β3γ2 em cryostructure than QH-II-066 (**8**).

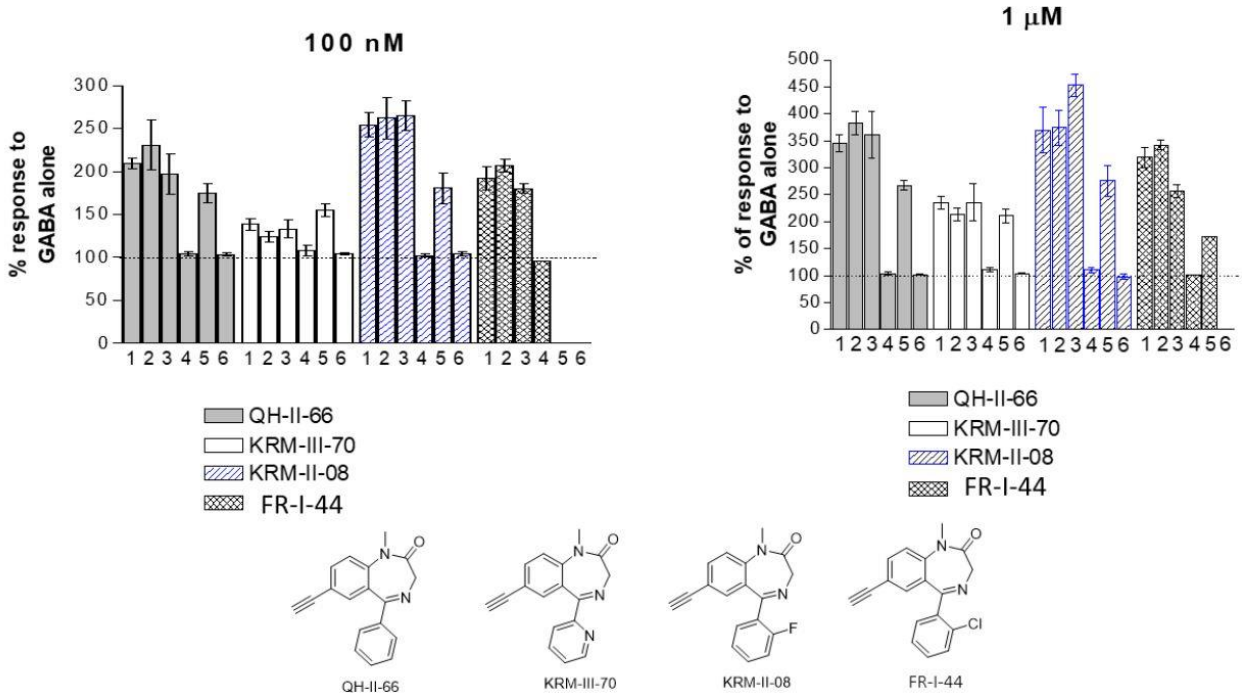

**Figure 18. The effectiveness of potentiation of ligands expressed in HEK cells, α1-6,β3γ2 GABA ion channels, with EC3 GABA with Janet Fisher (USC).**

### 2. 1. 2. 3 Cytotoxicity Study with De. Arnold et al.

The cytotoxicity experiment was done in both human embryonic kidney cells (HEK293T) and human liver cancer cell lines (HEPG2) to examine the toxicity of all analogs at the cellular level for the selection of safe lead compounds. The findings are shown in the figure 19 below.

Ligands were cultured for 48 hours with HEK293T and HEPG2 cells, respectively, before cell viability was determined using a Cell-Titer Glo (Promega). DMSO was utilized as a negative control, while 3-dibutylamino-1-(4-hexylphenyl)-propan-1-one was used as a positive control (150 mM in DMSO final concentration used as a positive control). Three independent quadruplet experiments were used to determine the data. The $LD_{50}$ values of each substance in HEK293 and HEPG2 cell lines were provided in the last two columns, respectively. The $LD_{50}$ values indicate that most of the chemicals are non-toxic.

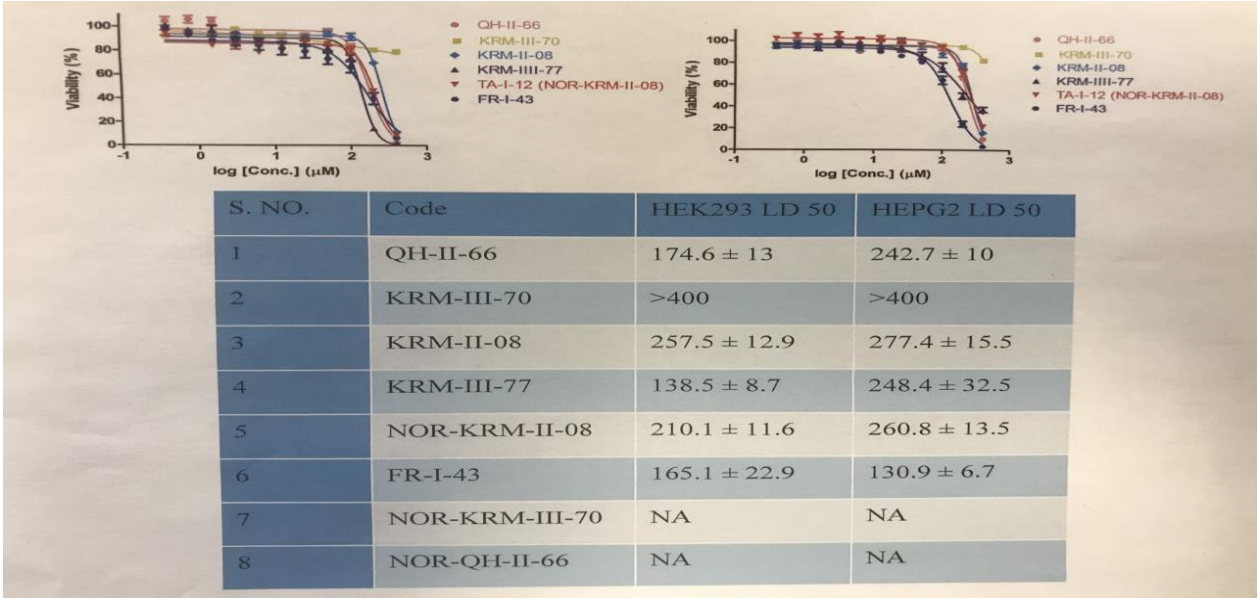


| S. NO. | Code | HEK293 LD 50 | HEPG2 LD 50 |
|---|---|---|---|
| 1 | QH-II-66 | 174.6 ± 13 | 242.7 ± 10 |
| 2 | KRM-III-70 | >400 | >400 |
| 3 | KRM-II-08 | 257.5 ± 12.9 | 277.4 ± 15.5 |
| 4 | KRM-III-77 | 138.5 ± 8.7 | 248.4 ± 32.5 |
| 5 | NOR-KRM-II-08 | 210.1 ± 11.6 | 260.8 ± 13.5 |
| 6 | FR-I-43 | 165.1 ± 22.9 | 130.9 ± 6.7 |
| 7 | NOR-KRM-III-70 | NA | NA |
| 8 | NOR-QH-II-66 | NA | NA |

**Figure 19.Cytotoxicity data of synthesized QH II 66 analogs in HEK293T and HEPG2 cells.**

The $LD_{50}$ values for most of the compounds in HEPG2 cell lines were greater than 200 μM, indicating that they are safe and non-cytotoxic. The $LD_{50}$ value of QH-II-66 and KRM-II-08 are also greater than 100 μM, indicating that they are safe to use. For safety reasons, the chemical concentration in the clinical trial will be substantially lower than 100 μM. Toxicology assays for ADME must be performed with GMP material for further research. Due to the presence of more metabolic enzymes in the liver than in the kidney, the $LD_{50}$ value of the same drug is usually higher in the liver HEPG2 cell lines than in the kidney HEK293 cell lines.

### 2. 1. 3 Modulating native $GABA_A$ receptors in medulloblastoma with α5 subtype preferring positive allosteric benzodiazepine-derivatives induces cell death.

Group 3 tumors contain a high expression of *GABRA5,* which codes for the α5-subunit of the ligand-gated ionotropic γ-aminobutyric acid type A neurotransmitter receptor ($GABA_AR$).[132] $GABA_ARs$ are fundamental in determining excitation/inhibition balance in the central nervous system. As an ionotropic receptor regulating chloride-ion flux, $GABA_ARs$ predominantly function to hyperpolarize neural cells following binding of the ligand, γ-aminobutyric acid (GABA), thereby decreasing the likelihood of generating an action potential. $GABA_AR$ is a pentameric complex, usually consisting of two α, two β, and single γ subunits topologically arranged as α-β-γ-α-β (**Fig. 18**). There are nineteen genes that encode subunits of $GABA_ARs$, including of six α (*GABRA1-6*), three β (*GABRB1-3*), and three γ (*GABRG1-3*) subunits.[142, 143] Given the critical role of $GABA_AR$ in brain function, $GABA_ARs$ have been an important therapeutic target since the clinical introduction of benzodiazepines Librium and Valium (or diazepam) in the 1960s.[144, 145] Benzodiazepines bind at the γ-α interface of a $GABA_AR$ (**Fig. 18**) and are positive allosteric modulators, acting to increase the effectiveness of GABA and thus chloride-anion flux. FDA

approved benzodiazepines consist most commonly of fusion of diazepine and benzene rings (1,4-benzodiazepine) and a phenol ring (5-phenyl-1H-benzo[e]) (**Fig. 18**). Changes to the chemical structure of a benzodiazepine can alter its selectivity for a $GABA_AR$ subtype. For example, Cook and colleagues introduced an ethinyl bond to the diazepine ring of 1,4-benzodiazepine at C-7, in place of a chlorine atom in diazepam (**Fig. 18**) and reported increased selectivity for the α5 containing $GABA_AR$.[146, 147]

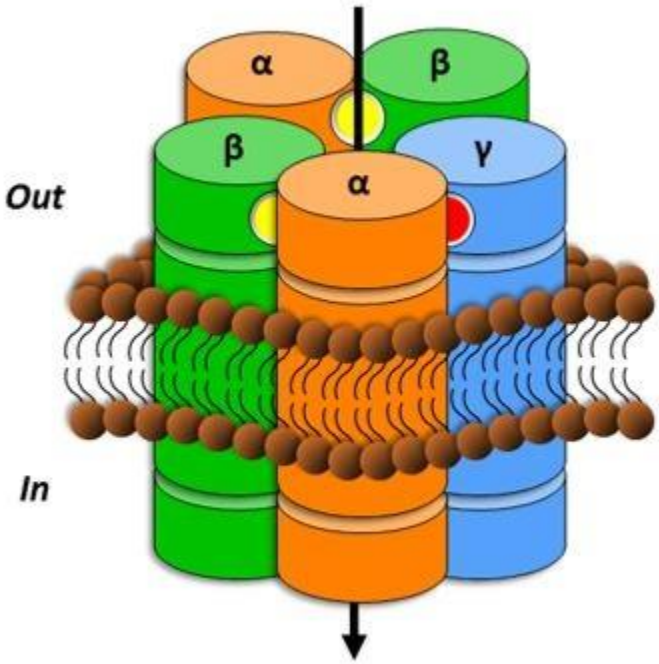


**Figure 20. Cartoon of a $GABA_A$ receptor ($GABA_AR$) with an αβαβγ subunit stoichiometry. $GABA_AR$ consists of five subunit transmembrane segments (each subunit has four transmembrane helices), represented as cylinders, and extra/intra-cellular domains. The five subunits create the chloride-anion conduction pore. Inter-subunit binding sites for γ-aminobutyric acid (GABA) and benzodiazepine are shown as yellow and red spheres, respectively.**

In the investigation of $GABA_AR$ in group 3 with Dr. Sengupta and Dr. Krummel, we showed that the *GABRA5* protein product (or α5-subunit) was present in-patient derived group 3 cell lines and tumor tissue and contributed to assembly of a functional $GABA_AR$.[148] Drugs that inhibited $GABA_AR$ did not impair cancer cell growth significantly. Paradoxically, the

benzodiazepine diazepam did impair growth of group 3 cells *in vitro* but only weakly. This suggested that benzodiazepines might impair cell viability by perturbation of cell ion homeostasis, possibly leading to osmotic stress and inducing cell death.[149] Still, diazepam had an $IC_{50}$ of only ~10 μM and it is a non-selective benzodiazepine. Given that group 3 patient tumors exhibit high expression of α5-$GABA_AR$, an α5-$GABA_AR$ selective benzodiazepine was tested, and it was observed to exhibit an order of magnitude more potent $IC_{50.}$ [148] Further, potency of the α5-$GABA_AR$ selective benzodiazepines tested in an intracranial xenograft mouse model was greater than the standard-of-care chemotherapeutic agent cisplatin,[150] as well as agents proposed as potential

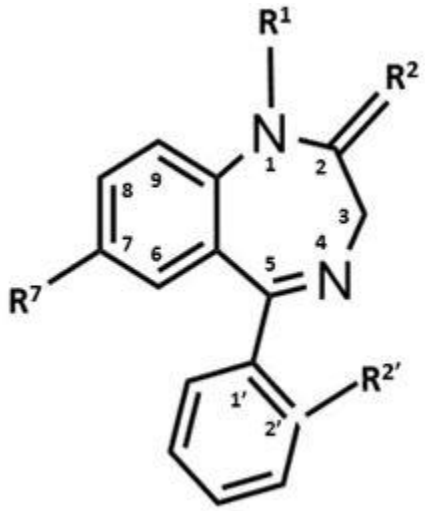


**Figure 21. Common core structure of a 'benzodiazepine' (1,4-benzodiazepine and 5-phenyl ring systems.) Indicated are sites frequently modified in a benzodiazepine ($R^1$, $R^2$, $R^{2'}$, $R^7$), which may impart a degree of $GABA_AR$ subtype-selectivity. Introduction of an additional ethinyl group at $R^7$ imparts the benzodiazepine with α5-$GABA_AR$ selectivity[146, 147].**

therapeutics for medulloblastoma, including bromo-domain inhibitor JQ1[151] and the anthelmintic drug mebendazole.[152] Mechanistically, the α5-$GABA_AR$ selective benzodiazepine assayed (termed 'QH-II-066') caused cell cycle arrest and its effectiveness in inducing apoptosis was abrogated by loss in expression of HOXA5, a homeobox transcription factor that regulates p53 expression.[148]

Further, QH-II-066 was capable of sensitizing group 3 cells to radiation and cisplatin in a p53-dependent manner.[148] Thus, p53 appears important in the response of group 3 cells to $GABA_AR$ mediated chloride-anion flux.

The following is a broad analysis of $GABA_AR$ and *MYC* expression in 763 primary medulloblastoma patient tumors, detailed characterization of $GABA_AR$ in a patient derived cell line, identification of chemical features critical to α5-$GABA_AR$ selective benzodiazepine potency and examination of how such α5-$GABA_AR$ selective benzodiazepines may impair viability of group 3 cells. It was found that group 3 tumors share high subgroup-specific and correlative expression of specific $GABA_AR$ subtypes. Group 3 cells have functional $GABA_ARs$ that are druggable using α5-$GABA_AR$ preferring benzodiazepines. The chloride flux in this tumor cells is efflux mechanism and cause severe stress and effects apoptosis. The binding of one such potent and non-toxic α5-$GABA_AR$ selective benzodiazepine (KRM-II-08, **19**) to the native α5-$GABA_AR$ in these cells enhances a chloride-anion flux that rapidly induces mitochondrial fragmentation and its membrane depolarization, as well as upregulates expression of *TP53* and activates apoptosis, without arresting the cell cycle. Benzodiazepines are psychoactive $GABA_AR$ modulators that are non-toxic, cross the blood-brain barrier, and clinically used widely. Either alone or in conjunction with other therapeutic modalities, the benzodiazepine KRM-II-08 (**19**) may serve as a non-toxic therapeutic for treating medulloblastoma. The ligands QH II 66 (**8**) and KRM II 08 do exhibit some sedation, but not nearly as much as diazepam (Cook et al, Us Patent 2006). Moreover, in treating patients with brain tumors drug that is also anxiolytic and slightly sedating is considered a plus in this treatment paradigm.

#### 2. 1. 3. 1 $GABA_AR$ subunit and MYC gene expression in primary medulloblastomas

The *GABAR* and *MYC* expression was analyzed across all four subgroups (WNT, SHH, group 3 and group 4) in 763 resected primary medulloblastoma tumors[137] (**Fig. 20; Fig. 23**). This analysis by Dr. Sengupta reveals that:

- All subgroups have a shared high expression of select *GABR* genes.
- There is subgroup-specific high expression of some *GABR* genes, and some subgroups have *GABR* expression that is specific to only a subset of patients within the subgroup.
- There is a positive correlation in expression of *GABRA5* and *MYC* in a subset of group 3 and WNT tumors.

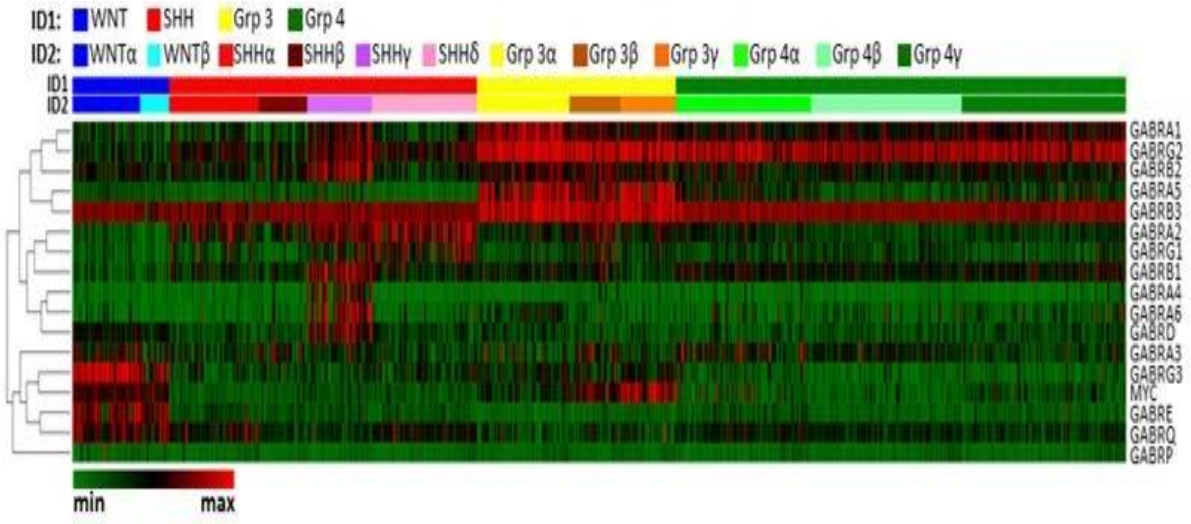


**Figure 22. Supervised heatmap clustering analysis across molecular subgroups WNT, SHH, group 3, and group 4 using z-score scaling, 1-Pearson correlation distance, and average clustering. The relationship between genes is indicated by the dendrogram (left). Shown bottom, left is a color palette where color scaling indicates low (green) to high (red) expression. ID1 are the subgroups: WNT, blue; SHH, red; group 3, yellow; group 4, green; and ID2 are within individual subgroups: WNT: α, blue; β, cyan; SHH: α, red; β, brown; γ, purple; δ, pink; group 3: α, yellow; β, brown; γ, orange; group 4: α, neon green; β, mint green; γ, green).**

*GABRB3* expression is high across all four subgroups, with subtle differences in the degree of expression across subgroups (**Fig. 20 and 22**). Expression is also high for *GABRG2*, but there is greater variability in the degree of expression between subgroups. Group 3 and group 4 have highest expression of *GABRG2* reported by Dr. Sengupta and Dr. Krummel.

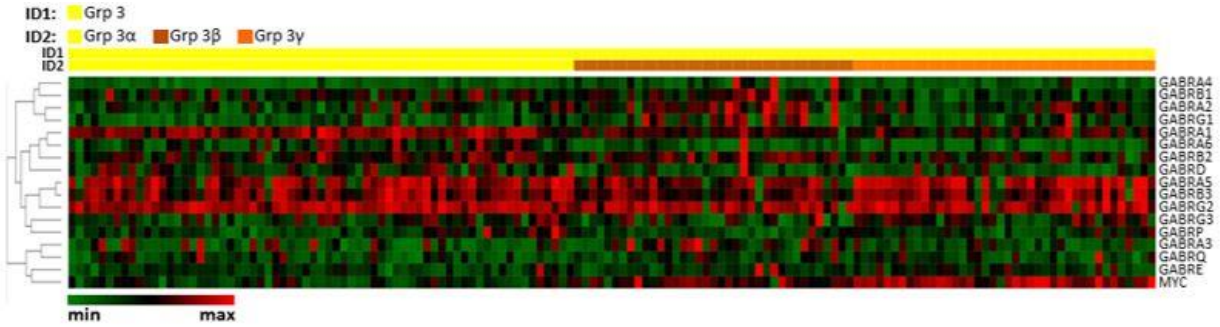


**Figure 23. Supervised heatmap clustering analysis of the molecular subgroup group 3 using z-score scaling, 1-Pearson correlation distance, and complete clustering. Shown bottom, left is a color palette where color scaling indicates low (green) to high (red) expression. ID1: group 3, yellow; ID2 within group 3: α, yellow; β, brown; γ, orange.**

*GABR* expression between subgroups and within some subgroups is variable: (*i*) WNT subgroup subtypes (α and β) have high expression of *GABRG3* and *GABRE*; (*ii*) SHHγ subtype has high expression of several *GABR* genes that distinguish it from SHHα, SHHβ, SHHδ, while all SHH subgroup patients have high expression of *GABRA2* and *GABRG1*. Medulloblastoma patients with poorest prognosis are those in the group 3 subtype. Group 3 patients have high *GABRA5* expression (**Fig. 21**), as reported previously but based now on analysis of a significantly larger dataset. *GABRA5* expression is consistently highest in the group 3γ subtype, which carries the poorest prognosis.

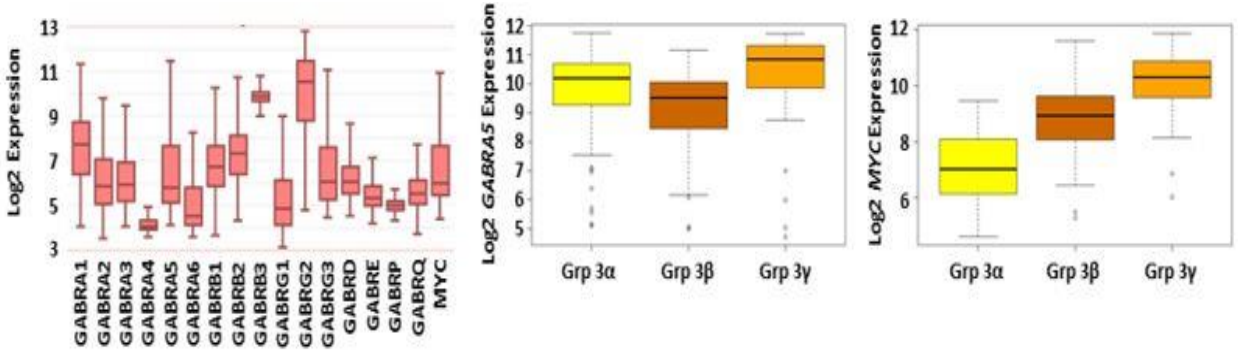


**Figure 24. Boxplots of *GABR* and *MYC* gene expression across all four molecular subgroups (left) and separately *GABRA5* (middle) and *MYC* (right) gene expression of the group 3 subgroup.Supervised heatmaps and boxplots show expression differences for both *GABRA*5 and *MYC* within the group 3 and WNT subgroups. The correlation between *MYC* and *GABRA5* is not overall statistically significant in group 3 ($p$ = 0.202). However, there is a significant positive correlation in expression between *GABRA5* and *MYC* in the group 3α subtype ($p$ = 0.006), where it was reported that *MYC* loss is more frequent [135], but not in group 3β ($p$ = 0.336).**

**Group 3γ has the highest level of *MYC* expression.[137] A significant positive correlation (*p* = 0.634) in expression between *MYC* and *GABRA5* in the group 3γ subtype was not found. As well as the group 3γ, the WNT subgroup of patients have high *MYC* expression (Figure. 20). There is a significant positive correlation**

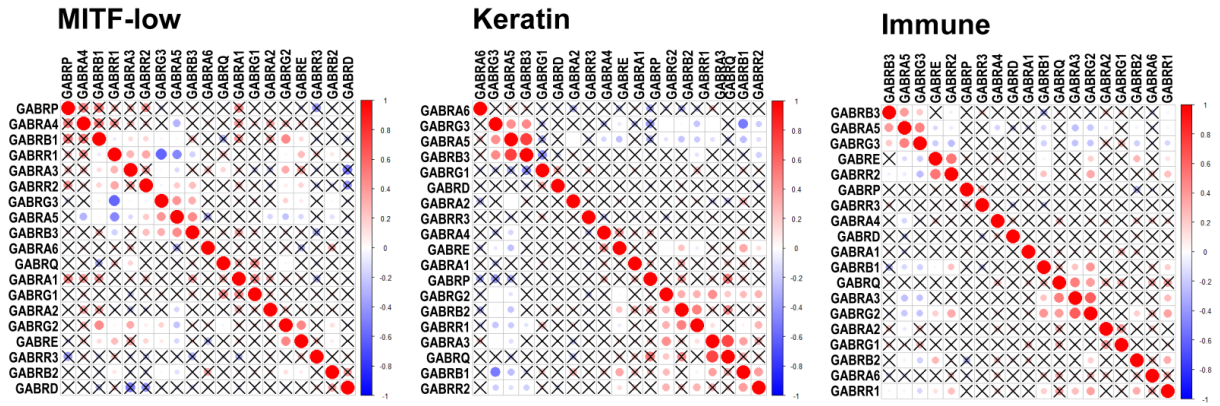


**Figure 25.GABA$_A$ receptor subunit (*GABR*) correlation in gene expression in stages 3 and 4 cutaneous melanoma patients. Correlograms of *GABR* gene expression by molecular subgroup: MITF-low, Keratin, and Immune. Positive correlation values are indicated in red and negative values in blue. Correlation values not marked by an "X" are not statistically significant, using a correlation test at *p*-value < 0.01. Correlation analyses among the *GABR* genes were performed using Spearman's correlation. Correlograms were used to summarize the correlations using the 'corrplot' R package.**

of *MYC* and *GABRA5* ($p < 0.001$) in the WNT subgroup (**Fig. 23**), but *GABRA5* expression is significantly lower than in group 3 tumors.

### 2. 1. 3. 2 GABR expression in group 3 tumors and D283 cells is consistent with assembly of a α5-GABR$_A$R

Benzodiazepines bind at the γ-α interface of a GABA$_A$R. A pentameric GABA$_A$R that is sensitive to modulation by a benzodiazepine would require α, β and γ subunits (**Fig. 19**). To identify the probable composition of a GABA$_A$R in medulloblastoma patient tumors that would be sensitive to benzodiazepine modulation, the correlation in the expression of GABA$_A$R subunits in

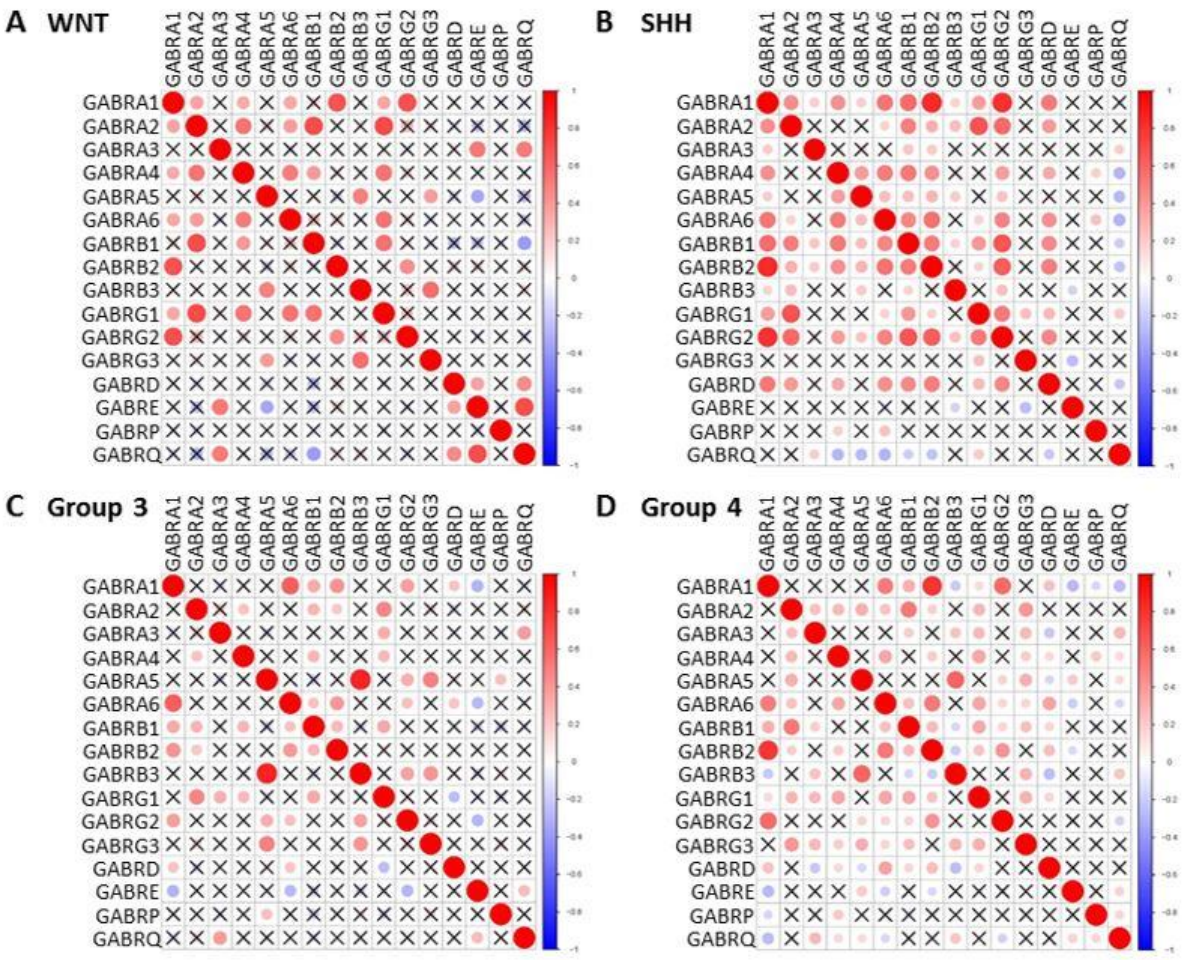


**Figure 26. GABA$_A$ receptor subunit (*GABR*) correlation in gene expression in 763 medulloblastoma tumors. Correlogram of *GABR* gene expression by subgroup: (A) WNT, (B) SHH, (C) group 3, and (D) group 4. Positive correlation values are indicated in red and negative values in blue. Correlation values not marked by an "X" are statistically significant, using a correlation test at p-value <0.01.**

all four subgroups of medulloblastoma using the 763 primary tumor normalized dataset were examined[137] (**Fig. 24**). Using a Spearman's correlation test (where $p < 0.01$) it was found that:

- There was a positive correlation in all four subgroups in expression of *GABR* genes that may form a functional GABA$_A$R sensitive to benzodiazepine modulation.
- Group 3 has a particularly high and correlative expression that includes *GABRA5*. In the WNT, SHH, and group 4 subgroups there is a shared correlation in expression of two groups of genes that suggest assembly of a functional GABA$_A$R and its composition.

The *GABR* gene groups in WNT, SHH, and group 4 are:

(1) *GABRA1*, *GABRB2*, and *GABRG2,* which code for α1, β2, and γ2 subunits, respectively; and

(2) *GABRA2*, *GABRB1*, and *GABRG1*, which code for α2, β1, and γ1 subunits, respectively.

In group 3 there is a set of *GABR* genes that exhibit high expression and have a significant correlation in expression of *GABRA5*, *GABRB3,* and *GABRG2 or GABRAG3,* which code for α5, β3, γ2 and γ3 subunits, respectively.

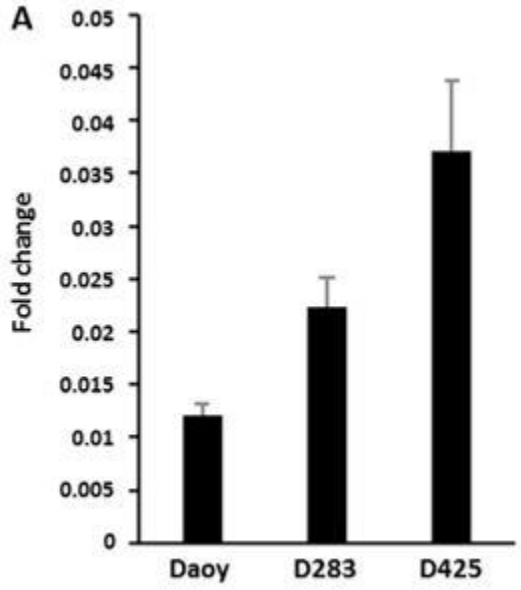


**Figure 27. *GABR* and *MYC* gene expression in medulloblastoma cell lines. qRT-PCR of *N-MYC* in patient derived medulloblastoma cell lines Daoy, D283, and D425. Values in all panels are presented as the mean and standard deviation of three experiments.**

To investigate how benzodiazepines may impair group 3 cell viability requires use of a cell line(s) that reflects the molecular profile of group 3 patient tumors (**Fig. 21**). As noted, a significant difference in expression between group 3 subtypes and other medulloblastoma subgroups is the degree of *GABRA5* expression. Further, group 3 tumors typically have low *N-MYC* and high *C-MYC* or *MYC* expression [137]. We therefore analyzed expression by qRT-PCR of patient derived

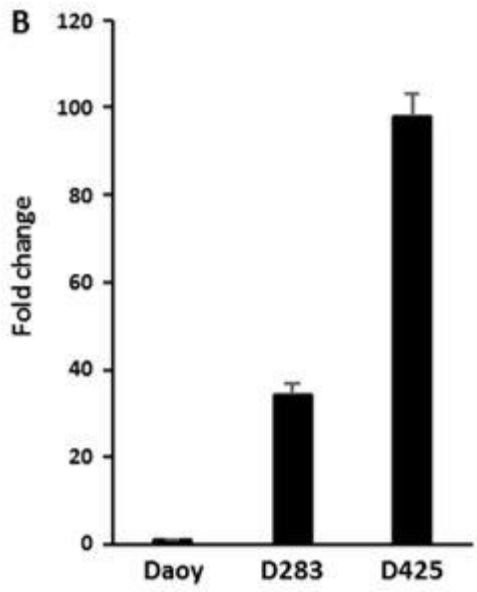


**Figure 28. *GABR* and *MYC* gene expression in medulloblastoma cell lines. qRT-PCR of *C-MYC* in Daoy, D283, and D425. Values in all panels are presented as the mean and standard deviation of three experiments.**

cell lines Daoy, D283 and D425 for *N/C-MYC* and *GABRA5*. Daoy is reported as SHH subgroup derived, [155, 156] while D283 and D425 cell lines are both reported as group 3 patient derived cell lines.[155- 159] Quantitative RT-PCR analysis reveals that Daoy, D283, and D425 have a low and similar degree of expression of *N-MYC* (**Fig. 25**). Daoy has no significant expression of *C-MYC*. In contrast, D283 and D425 cell lines have high *C-MYC* expression (**Fig. 33**), as is characteristic of some WNT and group 3 patient tumors (**Fig. 23**). As noted, group 3 tumors have high correlative expression of *GABRA5*, *GABRB3*, and *GABRG2*, genes which cluster on chromosome/locus 15q12. In addition, group 3α patient tumors have high *GABRA1* expression. The D283 cell line has very high *GABRA5* expression, relative to other *GABRA* genes, and higher *GABRB3* and *GABRG2* than other *GABRB* and *GABRG* genes, respectively (**Fig. 27**). There is a consistency in expression between group 3 patient tumors and the D283 cell line. Most likely, the D283 cell line is representative of group 3β or

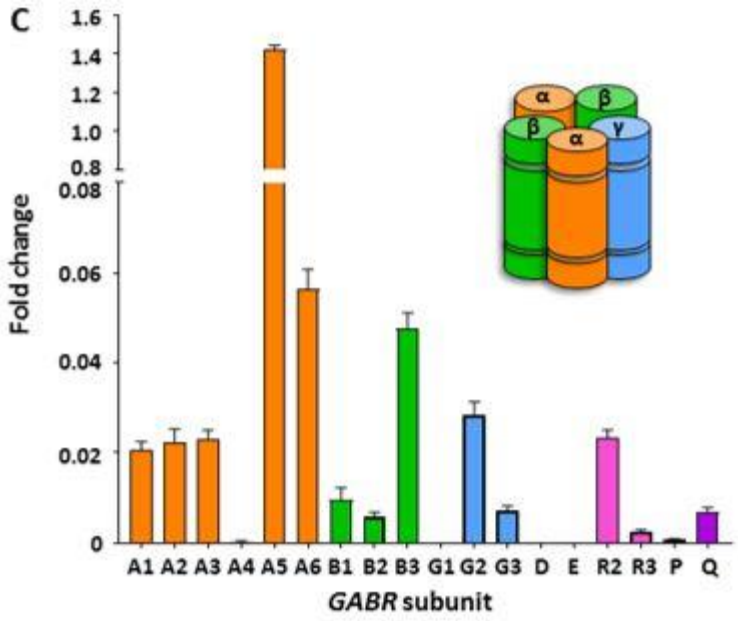


**Figure 29. qRT-PCR of *GABR* expression in D283. Data are represented as a fold-change value with respect to expression of the housekeeping gene *TBP*, TATA Box binding protein. Values in all panels are presented as the mean and standard deviation of three experiments.**

3γ, given the lower *GABRA1* expression detected by qRT-PCR in this cell line, which is more reflective of group 3α as reported by Sengupta and Krummel et al.

### 2. 1. 3. 3 D283 cells have a functional α5-GABR$_A$R

Gene expression alone does not indicate that D283 cells have a functional GABA$_A$R. Immuno-staining for the *GABRA5* protein product (the α5-subunit) shows diffuse staining that appears localized to the plasma membrane (**Fig. 28**). However, to establish that D283 cells express functional GABA$_A$Rs, whole-cell path clamp recordings of single D283 cells were obtained. If functional GABA$_A$Rs were expressed on the cell surface, then its agonist GABA should elicit a concentration-dependent chloride-anion flux. For D283 cells the average maximal current, $EC_{50}$, and Hill slope of GABA responses in D283 cells was -480 ± 120 pA, 1.26 ± 0.05 μM, and 1.37 ±

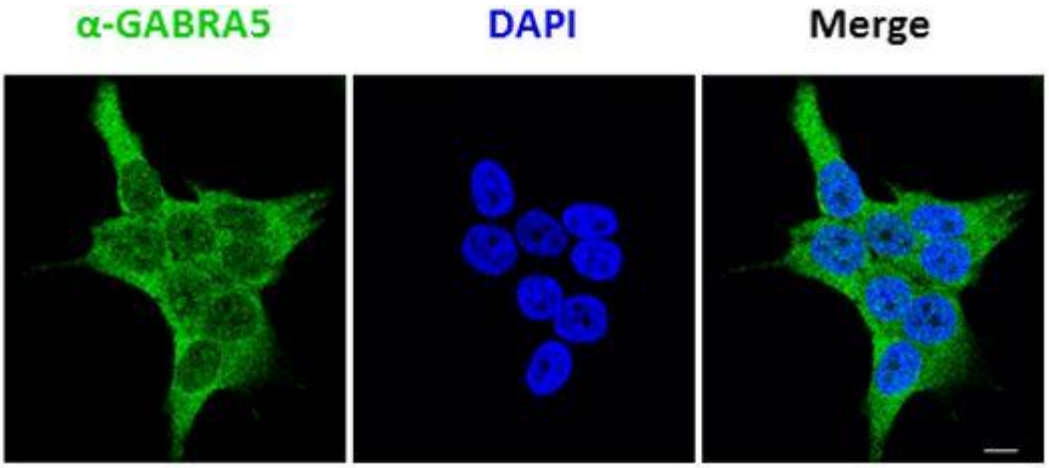


**Figure 30 A functional α5-GABA$_A$ receptor in D283 cells. The *GABRA5* protein product (or α5 subunit) localizes to the cell membrane in patient derived medulloblastoma cell line D283 with diffuse staining over the plasma membrane, as visualized by immunofluorescence microscopy using an antibody specific to the α5 subunit (green). Nucleus of cells is stained with 4′,6-diamidino-2-phenylindole (DAPI). Scale bar, 10 microns.**

0.07 respectively (where n=8) (**Fig. 29**) demonstrating a concentration-dependent chloride-anion flux commensurate with GABA concentration. The electrophysiology recordings also provide insight into the GABA$_A$R subtype, the chloride-anion flux rate, and number of functional receptors per D283 cell. The low GABA $EC_{50}$ of the native GABA-sensitive receptor in D283 cells is consistent with the expression of a $\alpha_5\beta_3\gamma_2$ or $\gamma_3$-like GABA$_A$R, and this is supported by the qRT-PCR analysis of D283 cells (**Fig. 27**), as well as *GABR* expression in group 3 patient tumors. The basal chloride-anion efflux rate is ~2 x $10^9$ ions per second, which is consistent with the rate of recombinantly expressed GABA$_A$R. We estimate that there are 1000 functional native α5-GABA$_A$Rs per D283 cell.

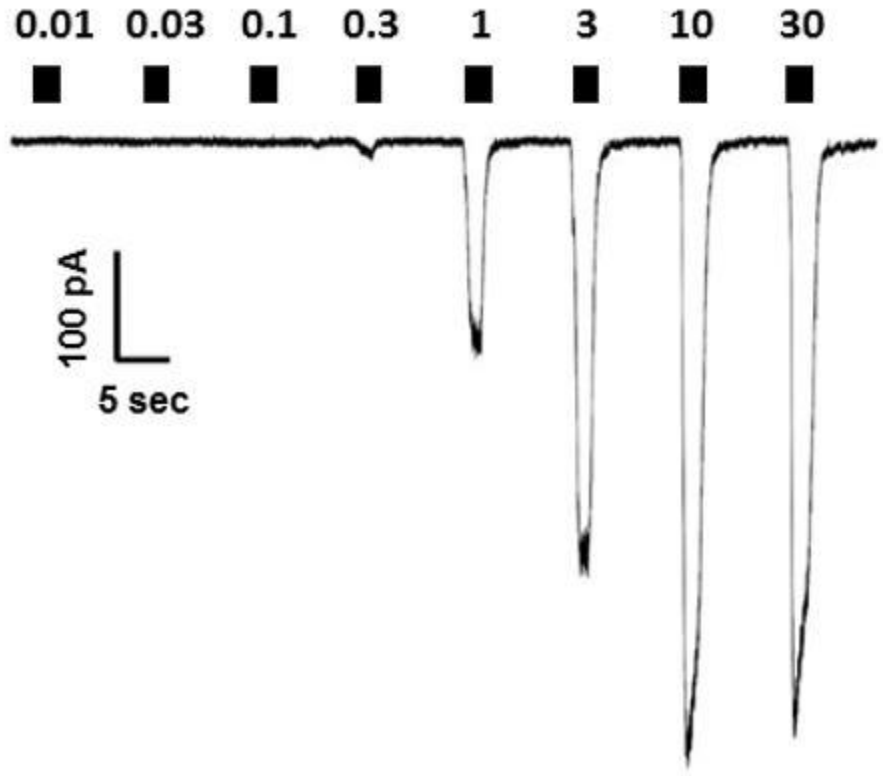


**Figure 31.Representative current trace from a whole-cell patch clamp electrophysiology recording of a D283 cell, clamped at -60 mV. Filled boxes above the current trace denote the period of γ-aminobutyric acid (GABA) exposure (2 seconds) and are labeled with the concentration applied (0.01 – 30 μM).**

### 2. 1. 3. 4 Benzodiazepines are potent modulators of the native α5-GABA$_A$R

Using a cell proliferation assay and the D283 cell line, the benzodiazepine variants to

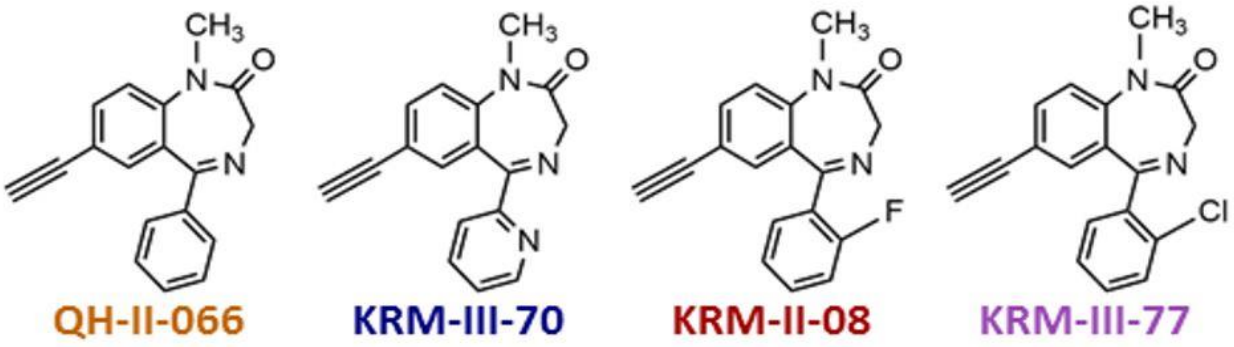


**Figure 32. Chemical structures of α5-selective benzodiazepines (Bz) tested.**

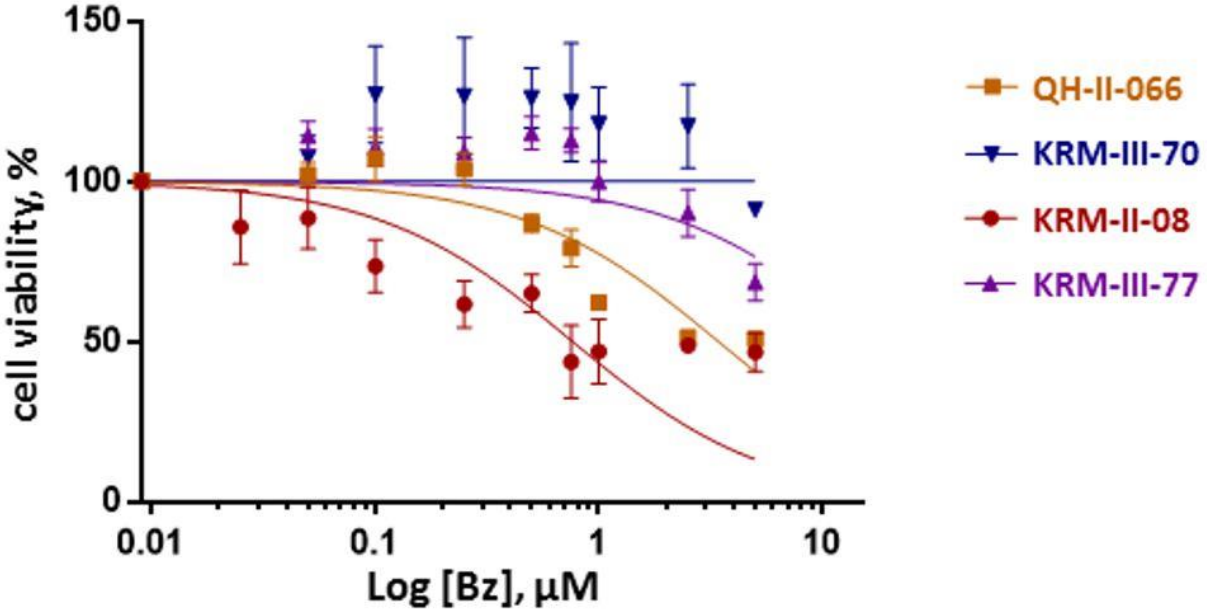


**Figure 33. Dose-response curves from MTS cell proliferation assay at 48 hours presented as semi-log plots.**

identify aspects of the chemical structure that might be critical to potency were screened. All benzodiazepines examined were synthesized to be α5-$GABA_AR$ selective and differed chemically at R1' of the 1,4-benzodiazepine ring system or the endocyclic 2' or exocyclic $R^{2'}$ of the phenyl ring (**Fig. 30 - 35**).

| Bz | $IC_{50}$ (µM) |
|---|---|
| QH-II-066 | 3.4 ± 0.3 |
| KRM-III-70 | - |
| KRM-II-08 | 0.8 ± 0.1 |
| KRM-III-77 | 16.3 ± 3.4 |

**Figure 34. Derived $IC_{50}$ values for tested benzodiazepines.**

The most potent benzodiazepines that emerged from this analysis are compounds with a hydrogen at R1' and no modification at the endocyclic 2' or exocyclic $R^{2'}$ (NOR-QH-II-066) or fluoride at

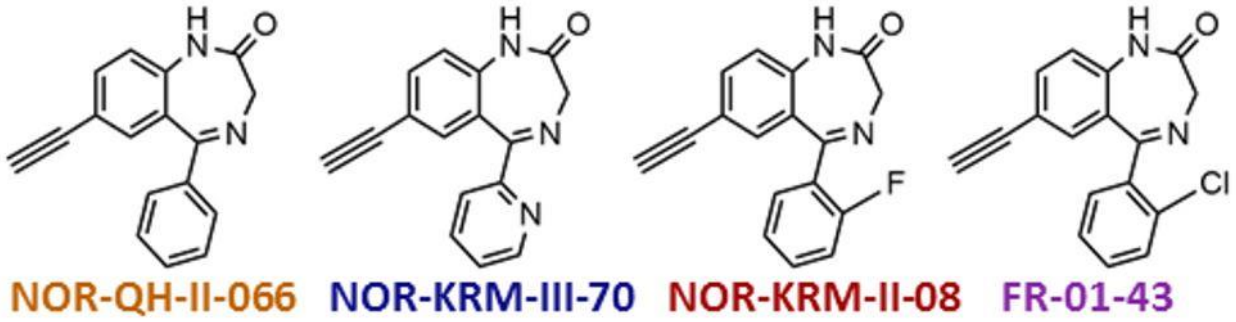


**Figure 35. Chemical structures of NOR variations of α5-selective benzodiazepines (Bz) tested.**

the exocyclic $R^{2'}$ (KRM-II-08 and NOR-KRM-II-08). Benzodiazepines with a larger halide (e.g., chloride) at exocyclic $R^{2'}$ (KRM-III-77 and FR-01-43) are significantly poorer ligands for the

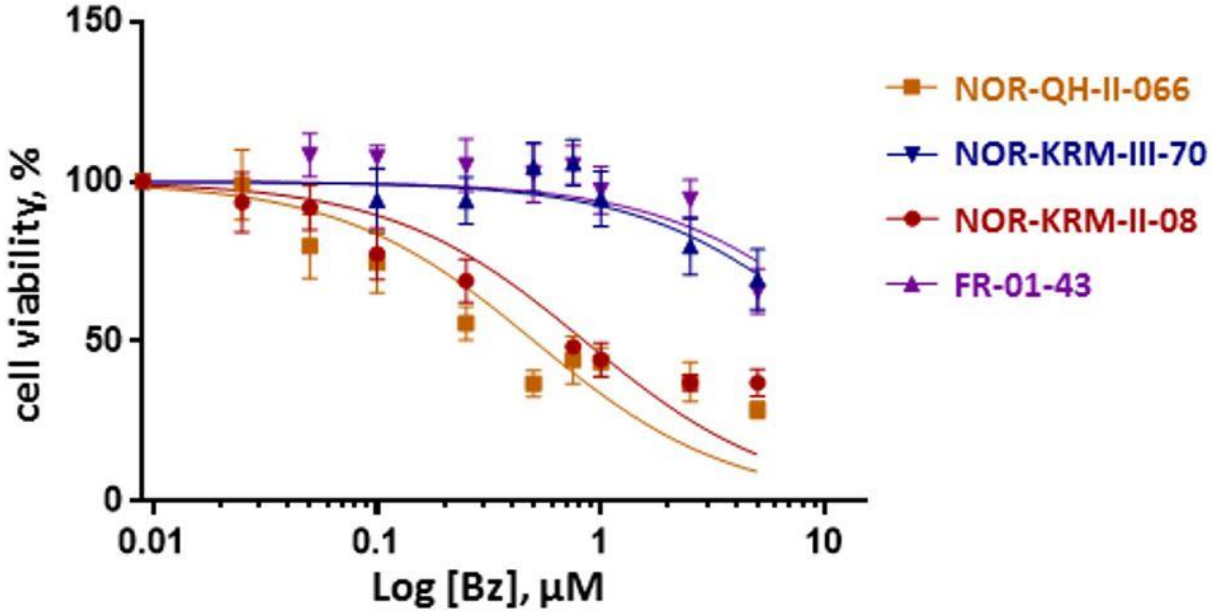


**Figure 36. Dose-response curves from MTS cell proliferation assay at 48 hours presented as semi-log plots.**

native D283 α5-$GABA_AR$. The 2'-F at the exocyclic $R^{2'}$ on KRM-II-08 may form a better three-centered hydrogen bond in the α5-$GABA_AR$ binding site, which is consistent with *in silico* modeling studies.[161, 162] **It was also noted, surprisingly, an apparent increase in cell growth for**

**benzodiazepine KRM-III-70, which has an exocyclic nitrogen at $R^{2'}$**. This benzodiazepine may bind to an alternative or secondary target to elicit such an effect. A possible secondary target is the peripheral

| Bz | $IC_{50}$ (μM) |
|---|---|
| NOR-QH-II-066 | 0.51 ± 0.06 |
| NOR-KRM-III-70 | 12.16 ± 1.85 |
| NOR-KRM-II-08 | 0.85 ± 0.09 |
| FR-01-43 | 14.97 ± 2.54 |

**Figure 37. Derived $IC_{50}$ values for NOR variations of tested benzodiazepines.**

benzodiazepine channel TSPO, which could enhance mitochondrial function and cell proliferation.

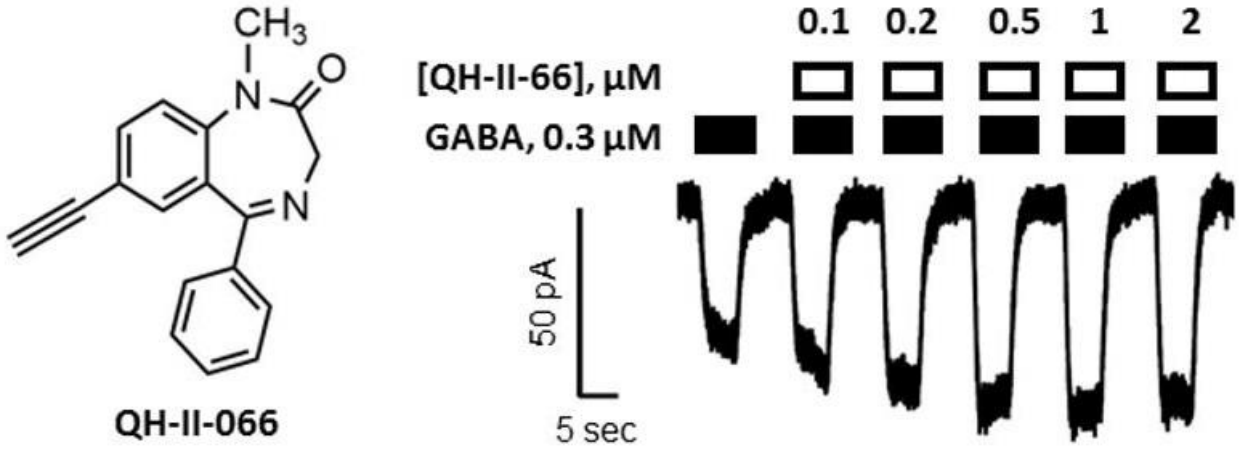


**Figure 38. Whole-cell patch clamp recordings from D283 cells. Patient derived medulloblastoma cell line D283, clamped at -60 mV, responses to GABA by α5-selective benzodiazepines QH-II-066. Filled boxes above current trace denote duration of GABA application. Open boxes denote the period of benzodiazepine exposure and are labeled with the concentration applied.**

### 2. 1. 3. 5 Benzodiazepines enhances a significant chloride-anion eflux in tumors.

We elected to pursue for greater in vivo, etc analysis the benzodiazepines QH-II-066 (**8**) and KRM-II-08 (**19**), which have $IC_{50}$ values of 3.4 ± 0.3 and 0.8 ± 0.1 μM, respectively on D283 cells,

determined using a cells viability assay (**Fig. 16, 19**). Whole-cell patch clamp recordings were obtained of the effect of these two benzodiazepines on $GABA_AR$ function on D283 cells (**Fig. 37; Fig. 38**). QH-II-066 (**8**) and KRM-II-08 (**19**) both

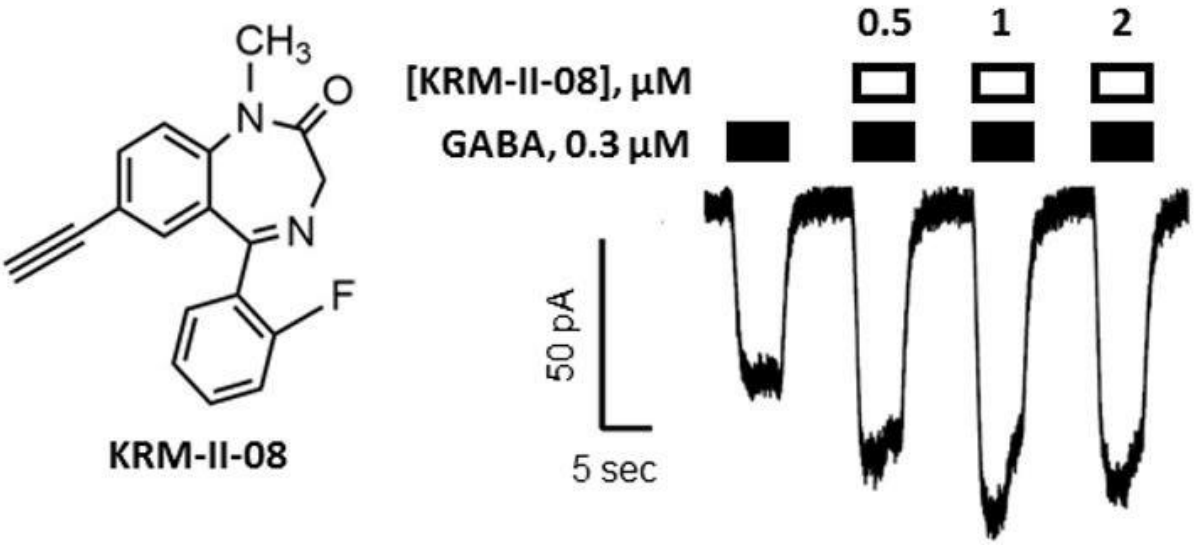


**Figure 39. Whole-cell patch clamp recordings from D283 cells. Patient derived medulloblastoma cell line D283, clamped at -60 mV, responses to GABA by α5-selective benzodiazepines KRM-II-08. Filled boxes above current trace denote duration of GABA application. Open boxes denote the period of benzodiazepine exposure and are labeled with the concentration applied.**

enhanced $EC_{10}$ responses in a concentration-dependent manner: $PC_{50}$: 43 ± 7 vs 61 ± 9, Hill slope 2.7 ± 5 vs 2.9 ± 5 and $PC_{50}$ 0.13 ± 0.09 vs 0.14 ± 0.07 µM, respectively. The high apparent affinity for GABA in D283 cells is consistent with the presence of functional α5-containing $GABA_ARs$ in D283 cells. The $EC_{50}$ values for benzodiazepines QH-II-066 (**8**) and KRM-II-08 (**19**) are remarkably similar in all the assays performed, $p > 0.05$ Student's *t*-test, in contrast to their $IC_{50}$ values (**Fig. 38**). In all cases, the modulation peaks below 2 µM and has a maximum effect of ~50%.

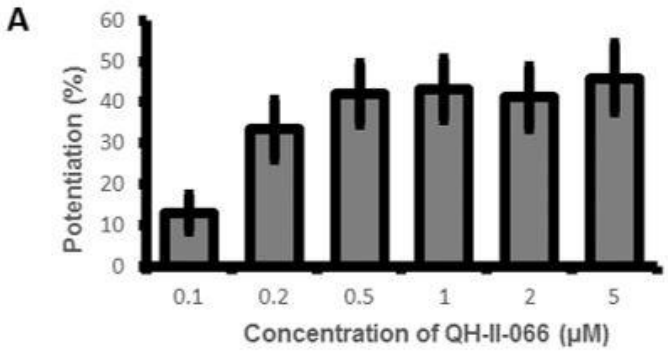


**Potentiation (%) by QH-II-066**

| | 0.1 μM | 0.2 μM | 0.5 μM | 1 μM | 2 μM | 5 μM |
|---|---|---|---|---|---|---|
| Avg | 12.96 | 33.36 | 42.12 | 43.12 | 41.19 | 45.83 |
| SEM | 4.61 | 7.29 | 7.53 | 7.45 | 7.56 | 8.42 |
| Stdev | 16.63 | 26.29 | 28.18 | 27.87 | 28.30 | 31.50 |
| n | 13 | 13 | 14 | 14 | 14 | 14 |

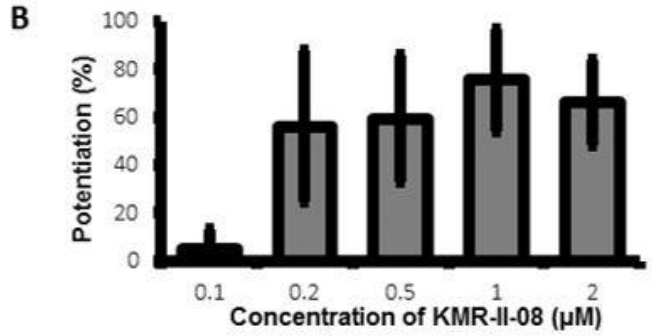


**Potentiation (%) by KMR-II-08**

| | 0.1 μM | 0.2 μM | 0.5 μM | 1 μM | 2 μM |
|---|---|---|---|---|---|
| Avg | 4.90 | 56.06 | 59.42 | 75.71 | 66.32 |
| SEM | 8.32 | 31.58 | 26.73 | 21.41 | 17.97 |
| Stdev | 20.38 | 63.16 | 70.72 | 42.83 | 35.95 |
| n | 6 | 4 | 7 | 4 | 4 |

**Figure 40. Data of whole-cell patch clamp recordings from D283 cells. Patient derived medulloblastoma cell line D283, clamped at -60 mV, responses to GABA by α5-selective benzodiazepines QH-II-066 (A) and KRM-II-08 (B). Both QH-II-066 and KRM-II-08 (Bz) show enhanced submaximal ($EC_5$-$EC_{10}$) responses in a concentration-dependent manner. The effects of QH-II-066 (8) and KRM-II-08 (19) were not significantly different from one another ($p > 0.05$, Student's t-test). Whole-cell patch-clamp recordings were performed on D283 using methods like those previously described [127].**

Given the more potent $IC_{50}$ of KRM-II-08 and its potential for future therapeutic use, we assessed its hepatocyte toxicity profile to establish if it were safe at the concentration at which it shows efficacy. The median lethal doses ($LD_{50}$ values) for KRM-II-08 (**19**) as well as the NOR variant (NOR-KRM-II-08, **21**) are greater than 200 and 100 μM, respectively, when tested using two different cell lines (HEPG2 and HEK293) (**Fig. 39**). KRM-II-08 (**19**) as well as the NOR variant are safe and non-toxic until the concentration is less than or equal to 100 μM. A concentration significantly higher than the $IC_{50}$ and $EC_{50}$ values for these benzodiazepines they were used to treat tumors.

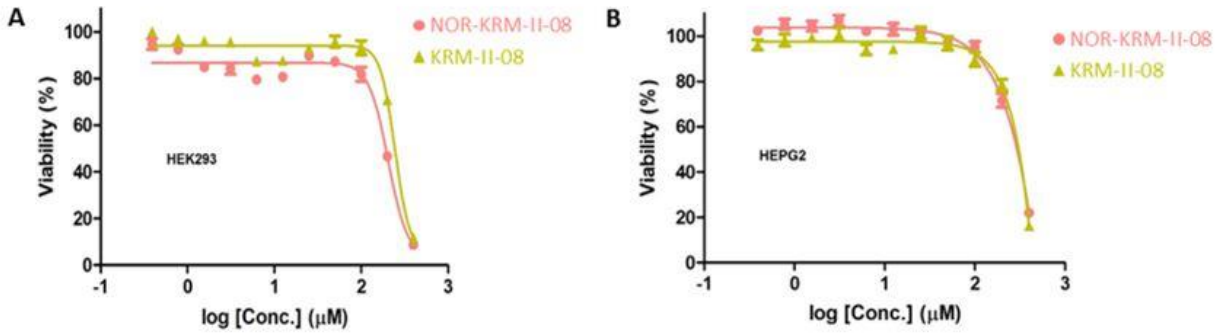


**Figure 41. Cytotoxicity assay of benzodiazepines. (A) Measurement of cytotoxicity of KRM-II-08 and the NOR variant using HEK293 (A) and HEPG2 (B) cell lines. In both the cell lines the LD50 values for KRM-II-08 and the NOR variant are greater than 200 µM. Hence, KRM-II-08 is safe and non-toxic until the concentration is less than or equal to 200 µM. TA-I-12: In HEPG2 cell lines, the LD50 value is greater than 200 µM. In HEK293 cell lines, the LD50 value is greater than 100 µM. Hence, NOR compound is safe and non-toxic until the concentration is less than or equal to 100 µM. This is much higher than any therapeutic dose.**

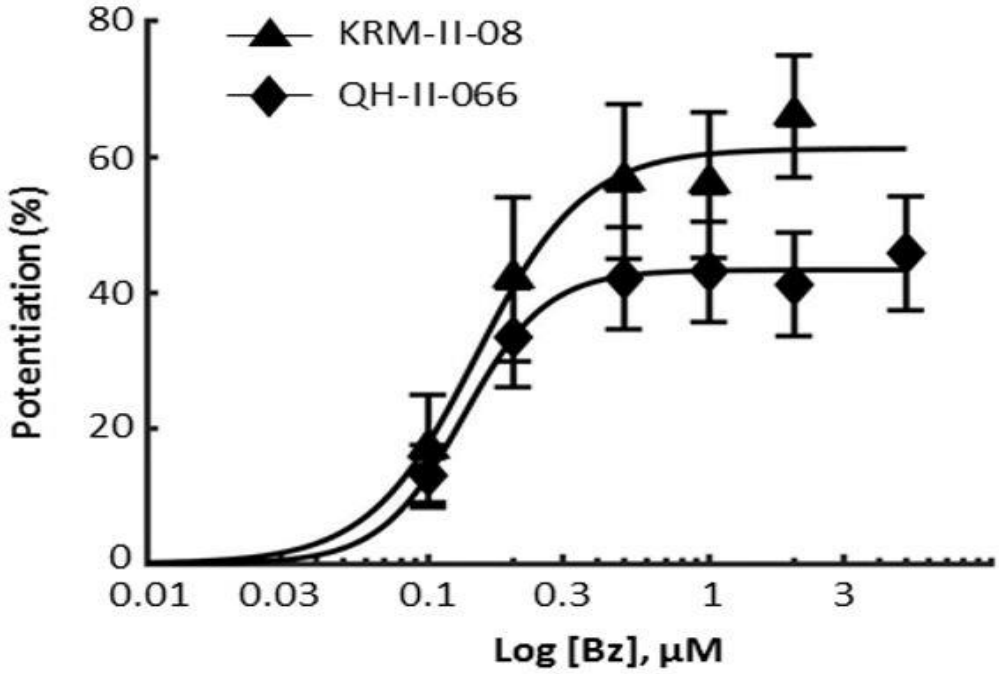


**Figure 42. Both QH-II-066 and KRM-II-08 (Bz) show enhanced GABA potentiation submaximal ($EC_5$-$EC_{10}$) responses in a concentration-dependent manner: $PC_{50}$: 43 ± 7 vs 61 ± 9, Hill slope 2.7 ± 5 versus 2.9 ± 5 and $PC_{50}$ 0.13 ± 0.09 versus 0.14 ± 0.07 µM, respectively. The effects of QH-II-066 and KRM-II-08 were not significantly different from one another ($p > 0.05$, Student's t-test).**

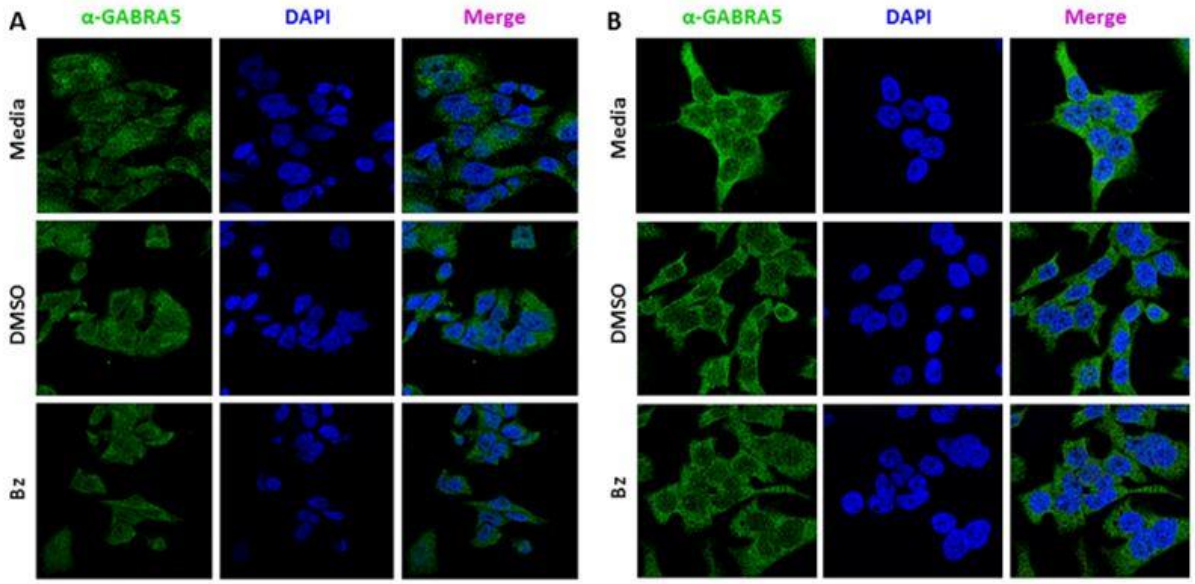


**Figure 43. Assessment of change in native $GABA_AR$ in D283 cells over time following exposure to KRM-II-08. D283 cells were untreated, treated with DMSO, or treated with KRM-II-08 (Bz) for 6 (A) and 24 (B) hours and then stained for imaging. There is no detectable change in degree or localization of staining for protein product of *GABRA5* (green).**

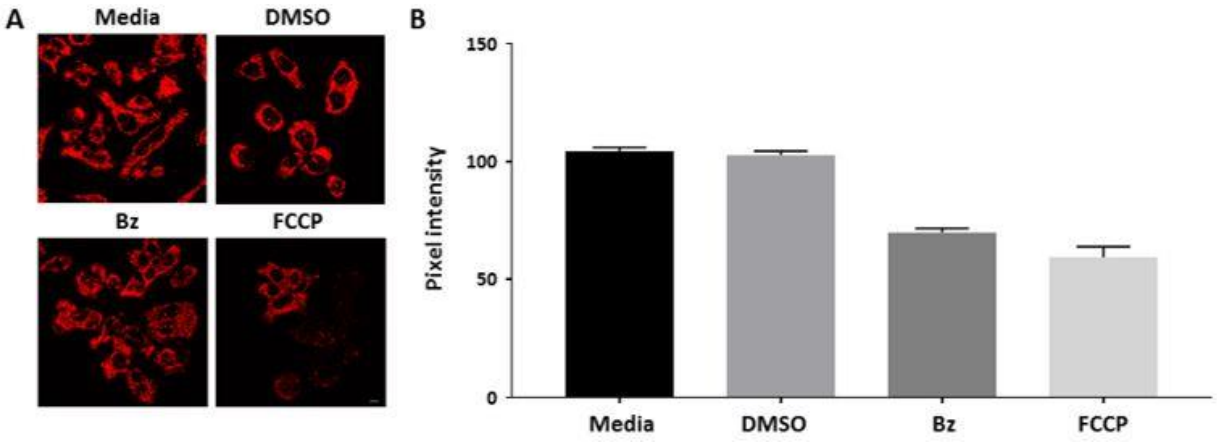


**Figure 44. Mitochondrial fission and depolarization induced by benzodiazepine target. (A) Flourescence microscopy imaging of live D283 cells following a 10-minute incubation with dimethyl sulfoxide (DMSO; 0.125%), carbonyl cyanide 4-trifluoromethoxy) phenylhydrazone (FCCP, 20 µM), or KRM-II-08 (Bz) (0.8 µM). Media alone had no DMSO. Peak: $\lambda_{ex}$, 549 nm; $\lambda_{em}$, 575 nm. (B) Quantitation of the positively charged red-orange dye tetramethylrhodamine ethyl ester (TMRE) after a 10-minute incubation of DMSO, FCCP, or KRM-II-08 (Bz). Media alone had no DMSO. TMRE staining was quantified with the Leica Application Suite X (LAS X) software platform. Data are presented as standard deviation from mean of thirty or more cells (media, n=30; DMSO, n=43; KRM, n=39; FCCP, n=35). Scale bar in panel (A) image is 10 microns.**

### 2. 1. 3. 6 Benzodiazepine induces early changes in mitochondrial structure-function.

Since one expected that the binding of a benzodiazepine target to the native $GABA_AR$ in group 3 medulloblastoma cells might alter ionic flux rapidly assuming exogenous GABA is ≥ 0.3 μM,

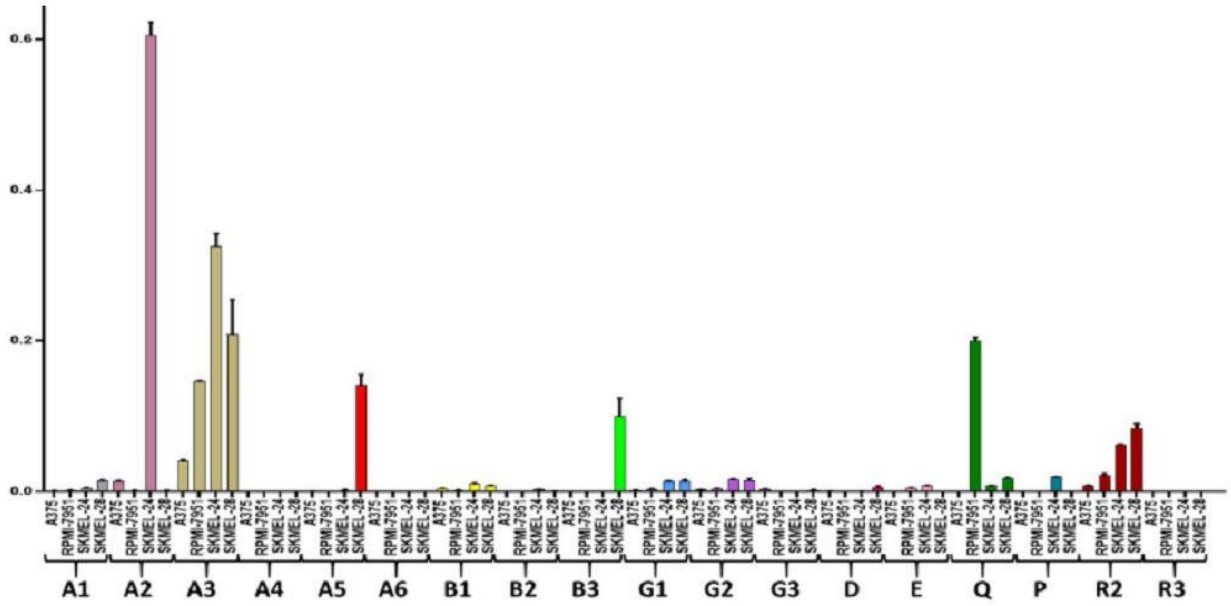


**Figure 45. RT-PCR of human metastatic melanoma lines for *GABR* genes.**

early changes were examined both to the mitochondria and the mitochondrial membrane potential. The staining for $GABA_AR$ at the plasma membrane remains similar and constant in DMSO and KRM-II-08 treated cells, as well as untreated cells over 48 hours (**Fig. 41)**, suggesting that the receptor remains intact and possibly then functional. We also examined changes in mitochondrial morphology using the cationic stain tetramethylrhodamine ethyl ether (TMRE), which is taken-up by functioning mitochondria. We observe that at ten minutes following benzodiazepine exposure, the mitochondria have fragmented or undergone fission but continue to take-up TMRE **(Fig. 42A**). Fission of the mitochondria is not observed in the DMSO control but is when a protonophore, carbonyl cyanide-4-(triflouromethoxy)phenylhydrazone (or FCCP) is added to the cells. FCCP disrupts mitochondrial ATP synthesis.[163, 164]

FCCP depolarizes mitochondria or causes loss of ΔΨm. [164] FCCP is therefore commonly used as a positive control for monitoring a change in mitochondria membrane potential, as it causes reduced TMRE staining. We quantified the degree of TMRE staining of thirty or more cells in all

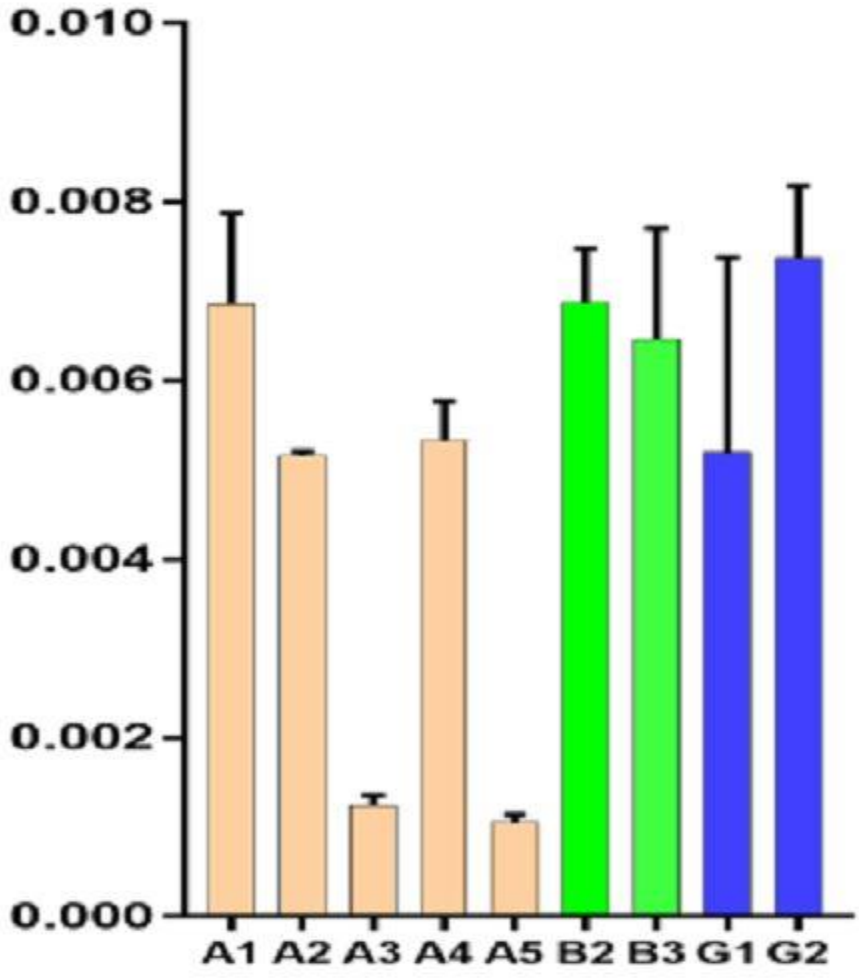


**Figure 46. RT-PCR of murine cell line B16F10-GP for select *GABR* genes. Total RNA was extracted from cells (RNeasy Mini Kit, Qiagen), converted into cDNA by PCR (Cloned AMV First-strand Synthesis Kit, Invitrogen), analyzed using SYBR dye (SYBR Green PCR Master Mix, Applied Biosystems). Primers used were as detailed in Kallay et al. [162].**

treated groups (media only, n=30; DMSO alone, n=43; KRM-II-08 treated, n=39; and FCCP treated, n=35) (**Fig. 42B**). KRM-II-08 caused a depolarization of mitochondrial membrane potential to D283 cells within 10 minutes of exposure. DMSO does not cause a change in mitochondrial membrane polarization.

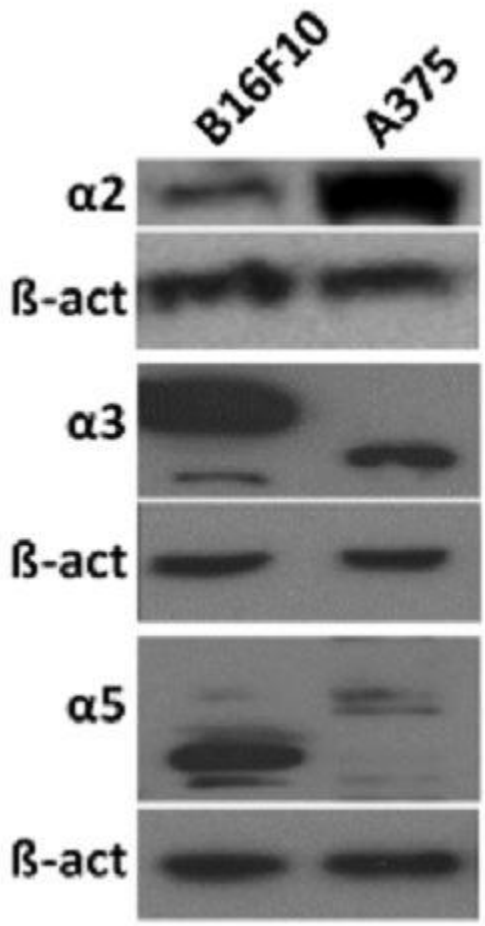


**Figure 47. Western blots of cell lines B16F10-GP and A375.**

There is observed, as noted above, a chloride-anion eflux in D283 cells that is commensurate with benzodiazepine target administration. This flux then mediates depolarization of the mitochondrial membrane. Also present in the outer mitochondrial membrane is the peripheral benzodiazepine metabotropic receptor TSPO to which the benzodiazepine diazepam has reported to bind and whose activity can reduce mitochondrial membrane potential.[165, 166] We therefore tested if the TSPO agonist emapunil influences viability of Daoy and D283 cell lines to **determine if the observed potency of KRM-II-08 was a consequence of its binding to TSPO (Fig. 47).**

**Emapunil does not impair viability of either Daoy or D283 cells. This observation supports the contention that the**

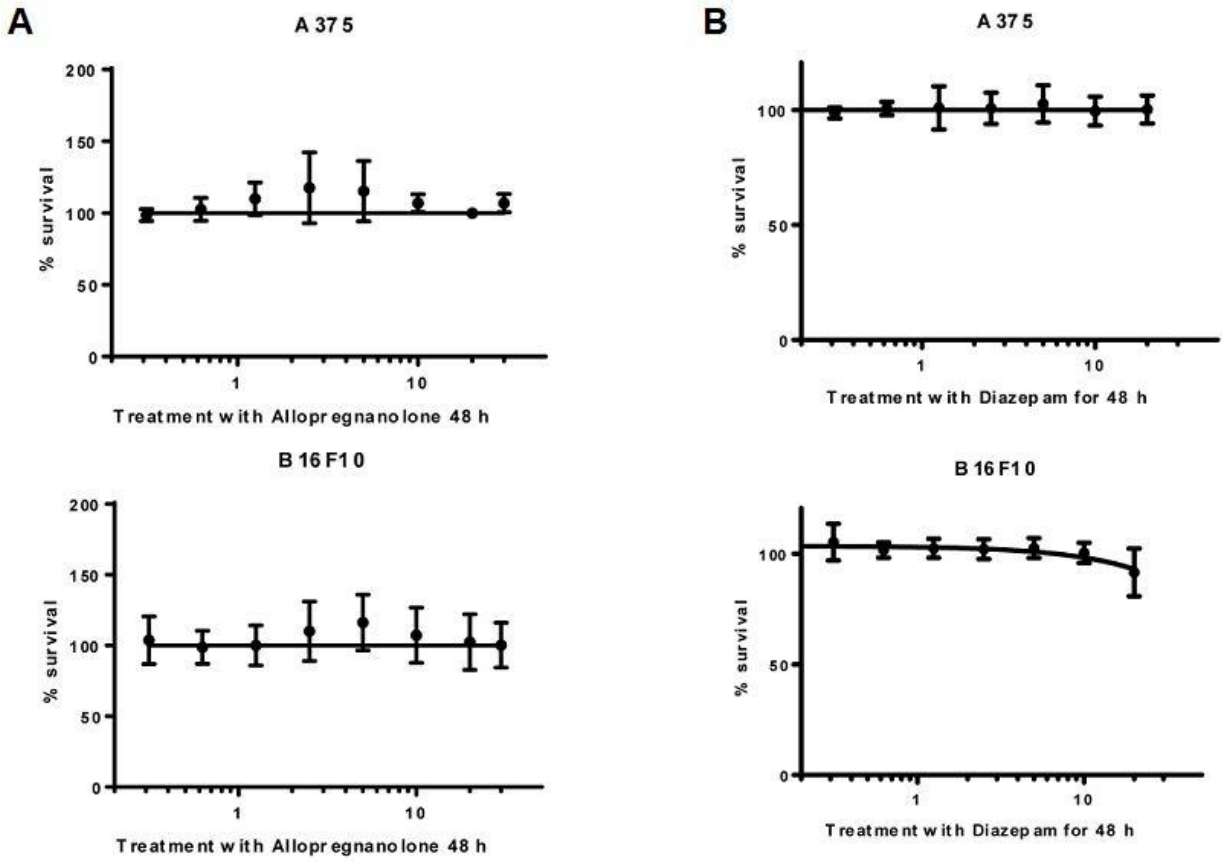


**Figure 48. Effect of $GABA_A$ receptor positive allosteric modulators on viability of human metastatic melanoma cell line A375 and murine line B16F10. (A) MTS assay of cell lines A375 (top) and B16F10-GP (bottom) treated with allopregnanolone for 48 h. (B) MTS assay of cell lines A375 (top) and B16F10-GP (bottom) treated with diazepam for 48 h. Methods used were as detailed in Methods section of text; dose-response curve error bars are ± standard error of the mean.**

**primary and effective binding site of KRM-II-08 that induces apoptosis is not TSPO, but the $GABA_AR$.**

| | | | | | | | | | | |
|---|---|---|---|---|---|---|---|---|---|---|
| 24 hours | | | | | | | | | | |
| | 0 uM | 0.001 uM | 0.005 uM | 0.01 uM | 0.1 uM | 0.25 uM | 0.5 uM | 1 uM | 5 uM | 10 uM |
| D425 | 0.635958 | 1.089945 | 0.879021 | 1.264235 | 1.078416 | 0.971513 | 1.196077 | 1.023491 | 1.067237 | 0.898072 |
| | 0.836882 | 1.003872 | 0.919883 | 0.894704 | 1.071298 | 0.954253 | 1.014776 | 1.011363 | 1.042226 | 0.925426 |
| | 0.726099 | 0.878634 | 0.817826 | 0.81848 | 0.917387 | 0.853126 | 0.915103 | 0.946958 | 0.907385 | 0.818054 |
| DAOY | 0.229591 | 0.334401 | 0.350007 | 0.354972 | 0.347152 | 0.35729 | 0.337904 | 0.351486 | 0.338566 | 0.236435 |
| | 0.231598 | 0.370285 | 0.333499 | 0.321891 | 0.343269 | 0.344033 | 0.313529 | 0.334964 | 0.326327 | 0.20914 |
| | 0.223466 | 0.350331 | 0.307379 | 0.302256 | 0.317886 | 0.329083 | 0.318565 | 0.315925 | 0.284288 | 0.205419 |
| | | | | | | | | | | |
| 48 hours | | | | | | | | | | |
| | 0 uM | 0.001 uM | 0.005 uM | 0.01 uM | 0.1 uM | 0.25 uM | 0.5 uM | 1 uM | 5 uM | 10 uM |
| D425 | 0.966358 | 1.718359 | 1.762605 | 1.622537 | 1.519529 | 1.328353 | 1.490564 | 1.538633 | 1.446277 | 0.882807 |
| | 0.868259 | 1.01366 | 1.01528 | 1.052033 | 1.142959 | 1.089493 | 1.173447 | 1.096473 | 1.207792 | 0.791286 |
| | 1.017032 | 1.053547 | 1.120952 | 0.987312 | 1.080568 | 1.191473 | 1.234102 | 1.169289 | 1.269107 | 0.842516 |
| DAOY | 0.21478 | 0.502489 | 0.463778 | 0.496715 | 0.542546 | 0.508249 | 0.503271 | 0.52495 | 0.464344 | 0.222386 |
| | 0.183241 | 0.446577 | 0.479389 | 0.441762 | 0.47371 | 0.484035 | 0.500567 | 0.515595 | 0.424958 | 0.209861 |
| | 0.232681 | 0.503429 | 0.510201 | 0.516524 | 0.497429 | 0.513919 | 0.527963 | 0.507376 | 0.477231 | 0.218317 |

**Figure 49. Examination of the effect of emapunil on medulloblastoma cells.**

### 2. 1. 3. 7 Contribution of p53 in response to the benzodiazepine anticancer targets.

Previously it was demonstrated that antitumor benzodiazepines were capable of impairing cell viability of group 3 cells including of the cell line D425, which has a *TP53* exon 4 single-nucleotide polymorphism (R72P), which has been reported to impact the apoptotic response to some types of stress.[167] Since the D425 response to the benzodiazepine's tested was not impacted by the *TP53* polymorphism, this supports p53 not being critical to the cell death response. However, this point mutation may not impair all functions of p53 and the apoptotic response of some types of stress are not impacted.[168] It was also previously observed that anticancer benzodiazepines were capable of sensitizing group 3 cells to either radiation or a chemotherapeutic intervention and this phenomenon was abrogated by a p53 knockdown[148], which supports the role of p53 in the apoptotic response mediated by these benzodiazepines targets. To

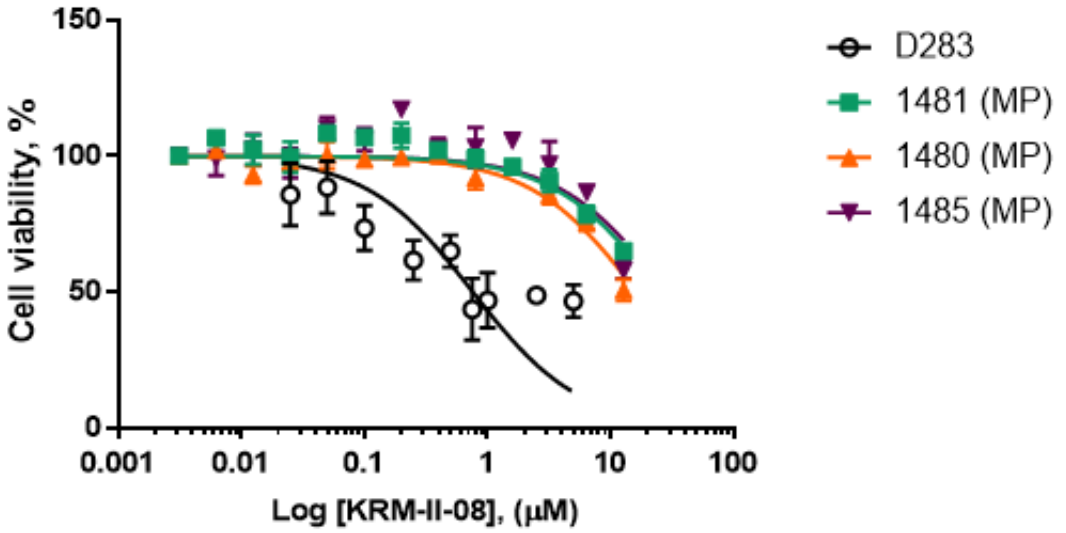


**Figure 50. Response of mouse MYC-driven/dominant-negative p53 cell line to KRM-II-08. Mouse MYC-driven MB with a dominant-negative p53 missense mutation in the DNA-binding domain [2] does not respond to KRM-II-08 *in vitro*. Tumor cells from three samples (MP) were treated with drug for 48 hours and viability was assessed.**

further establish the possible importance and role of p53 in responding to anticancer benzodiazepine mediated stress and apoptosis, we have tested the efficacy of KRM-II-08 (**19**) was tested to impair viability of cells originating from the mouse *MYC*-driven tumor generated from CD133+ cells in the postnatal cerebellum by overexpression of *MYC* and dominant-negative p53 (DNp53) (termed MP tumors), which have a missense mutation that impairs the proteins DNA-binding domain.[169] Tumors of this mouse model resemble human *MYC*-driven medulloblastoma molecularly and the analysis of microarray data from this tumor indicates a high gene expression of *GABRA5* (**Fig. 48**). We observed that the MP tumors have a KRM-II-08 $IC_{50}$ > 16 μM (**Fig. 48**), as compared to KRM-II-08 $IC_{50}$ in D283 cells of 0.8 μM (**Fig. 32**). This is consistent with the transcriptional function of p53 having a role in the stress--mediated response to the anticancer benzodiazepine, but possibly that is the DNA-binding domain's function (i.e., gene expression) alone is not critical to inducing apoptosis.

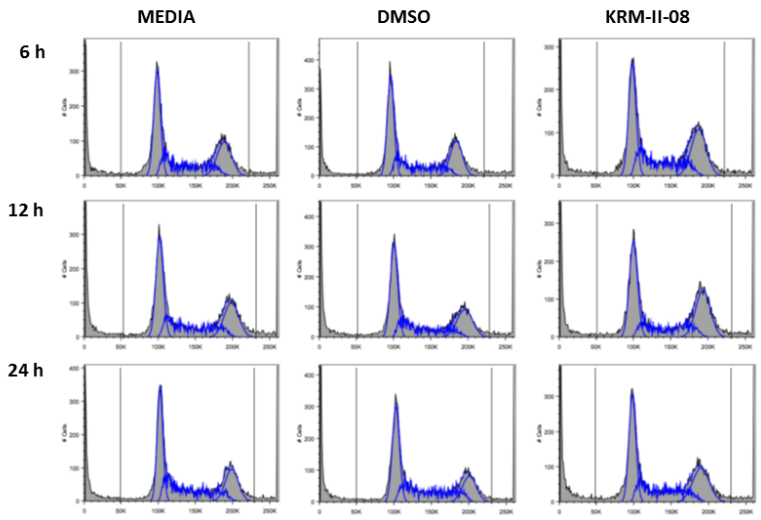


| Condition/Time | % G1 | % S | % G2 |
|---|---|---|---|
| Media/6 h | 37.1 | 30.1 | 25.4 |
| DMSO/6 h | 38.7 | 28.6 | 25.1 |
| KRM-II-08/6 h | 33.9 | 30.9 | 28.9 |
| Media/12 h | 37.5 | 29.7 | 26.1 |
| DMSO/12 h | 39.7 | 28.5 | 25.6 |
| KRM-II-08/12 h | 36.8 | 24.1 | 32.3 |
| Media/24 h | 35.2 | 36 | 22.9 |
| DMSO/24 h | 38.3 | 35.6 | 20.4 |
| KRM-II-08/24 h | 35.4 | 29 | 26.9 |

**Figure 51. KRM-II-08 does not alter the cell cycle. Shown is fluorescence-activated cell sorting or FACS data of D283 cells untreated or media control (left three panels), treated with DMSO (middle three panels), or α5-selective benzodiazepine KRM-II-08 (right three panels) at 6, 12, and 24 hours. Table contains peak values at G1, S, and G2 phases of the cell cycle for the three experimental groups.**

Previously it was observed that a less potent benzodiazepine studied here (see QH-II-066 (**8**), $IC_{50}$ 3.4 μM) (**Fig. 32**), caused cell cycle arrest. We therefore repeated an analysis on the cell cycle of D283 cells of the more potent benzodiazepine KRM-II-08 ($IC_{50}$ 0.8 μM). Surprisingly, KRM-II-08 does not arrest the cell cycle of D283 cells at either 24 or 48 hours following its incubation with D283 cells (**Fig. 49**). This suggests that the less potent benzodiazepine tested earlier may have a secondary or 'off-target' effect in group 3 medulloblastoma cells that contributes to this cell cycle death phenomenon. However, arresting the cell cycle is not critical to benzodiazepine-mediated apoptosis.

Since p53 appears to play a critical role in the cells stress response to benzodiazepine target mediated chloride-anion flux and its DNA-binding domain contributes to this role, the impact of the benzodiazepine KRM-II-08 on expression of genes that participate in the PTEN-p53-AKT-MDM2 signaling axis was examined, [170-172] specifically: PI3K molecules (Class I regulatory and

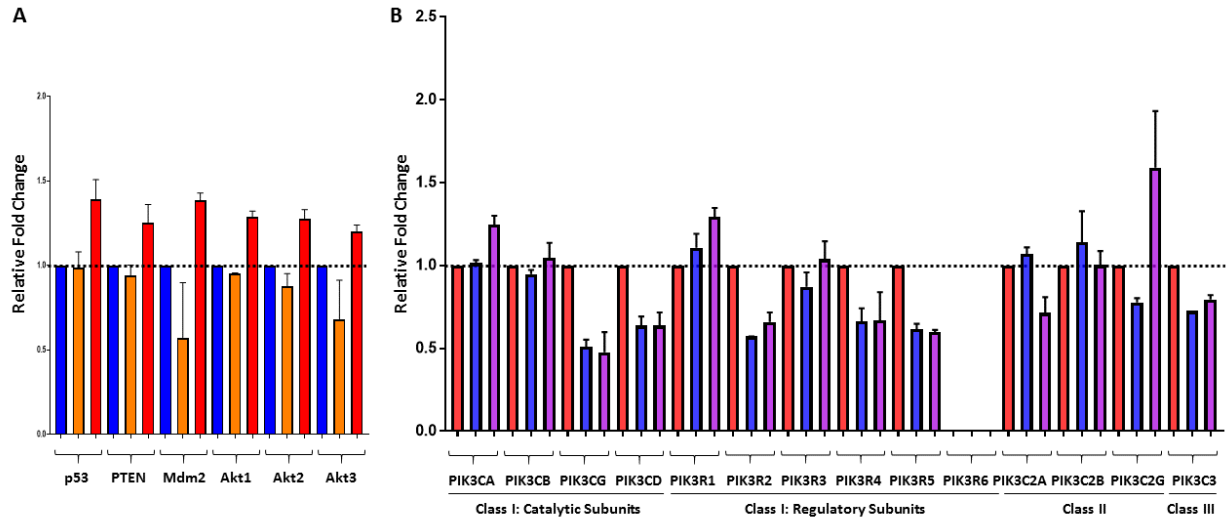


**Figure 52. Quantitative RT-PCR of gene expression in D283 cells following KRM-II-08 exposure. (A) *TP53*, *PTEN*, *MDM2* and *AKT1-3* expression in D283 cells exposed to media (blue column), DMSO (orange column), or KRM-II-08 (red column). (B) *PI3K* subunit expression in D283 cells exposed to media (red column), DMSO (blue column, or KRM-II-08 (purple column).**

catalytic subunits, Class II, and Class III); serine/threonine kinases *AKT1*, *AKT2*, and *AKT3*; *PTEN*, the phosphatase which negatively regulates the PI3K/Akt signaling pathway, stabilizes p53, and whose expression is regulated by p53; and *MDM2*, which codes for the E3 ubiquitin ligase that functions as a negative regulator of p53 (**Fig. 50**). The changes were examined in the expression of these genes as well as *TP53* in D283 cells at 6- and 24-hours post-incubation with KRM-II-08. *MDM2*, *PTEN*, *AKT1-3*, as well as *TP53* are all upregulated in the KRM-II-08 treated cells. This effect is anticancer benzodiazepine-specific, since the DMSO control shows no change in *TP53* and *PTEN* levels while *MDM2 and AKT1-3* expression are down-regulated in DMSO treated cells (**Fig. 50**). Of the *PI3K* genes, only the Class I catalytic and regulatory subunits PI3CA and PIK3R1, respectively, are significantly upregulated. Although *MDM2*, *PTEN*, and *AKT* expression is upregulated in KRM-II-08 (**19**) treated cells, protein levels are unchanged. Only p53

protein levels increased significantly at the 24-hour time point in the D283 cells treated with KRM-II-08 (**19**) and in both nuclear

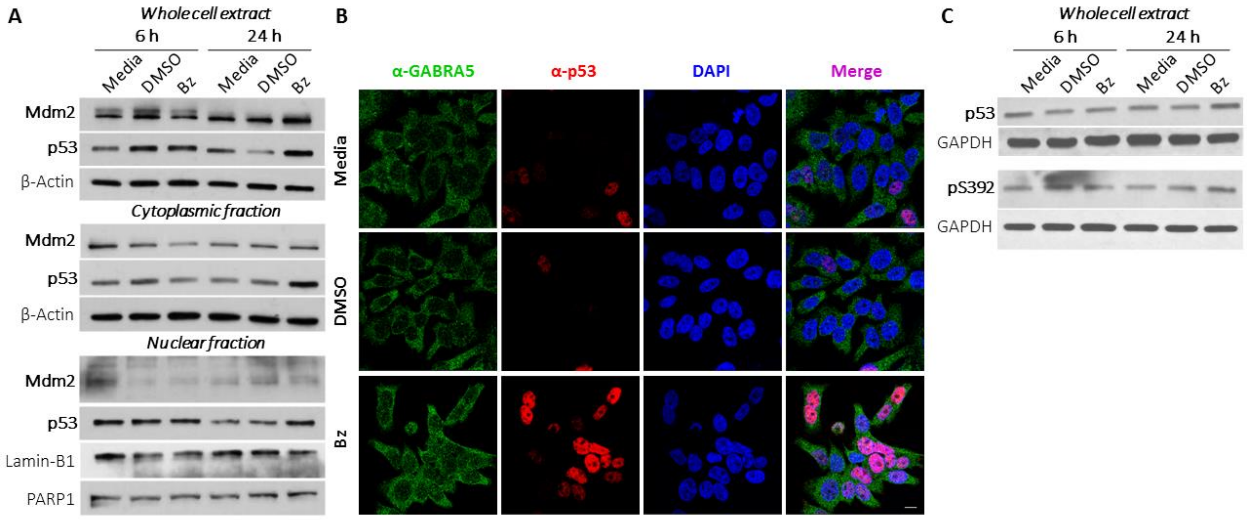


**Figure 53. Contribution of p53 to response of α5-selective benzodiazepine KRM-II-08. (A) Immunoflourescence microscopy imaging of D283 cells at 24 hours following incubation with media alone, DMSO, or KRM-II-08 (Bz, 0.8 μM). Cells were stained using antibodies specific to α5 (green) and p53 (red). Nucleus of cells were stained with 4′,6-diamidino-2-phenylindole (DAPI). Scale bar in bottom, right image is 10 microns. (B) Western blot of Mdm2 and p53 at 6- and 24-hours post-incubation with KRM-II-08. Western blots of whole cell (top), cytoplasmic (middle), and nuclear (bottom) extracts. Loading controls for blots are beta-actin, Lamin-B1, and/or PARP1. (C) Western blot of p53 using antibody that recognize the protein regardless of post-translational modification and specific to phosphorylation of p53 Serine392 (pS392). GAPDH is the loading control. (D) Dose-response curve of mouse *MYC*-driven medulloblastoma cells with a p53 dominant-negative missense mutation following incubation with KRM-II-08. Tumor cells were treated with varying concentrations of KRM-II-08 for 48 hours and viability of cells was then assessed.**

and cytoplasmic fractions (**Fig. 51A**). As well as observing an increase in p53 levels by Western blot, we observed an increase in p53 levels by immunofluorescence with the most intense staining in the nucleus (**Fig. 51B**).

### 2. 1. 3. 8 Activation of cell death

As reported above, there are very early changes observed in mitochondrial structure and function. These early changes, including a change in mitochondrial transmembrane potential, may function to

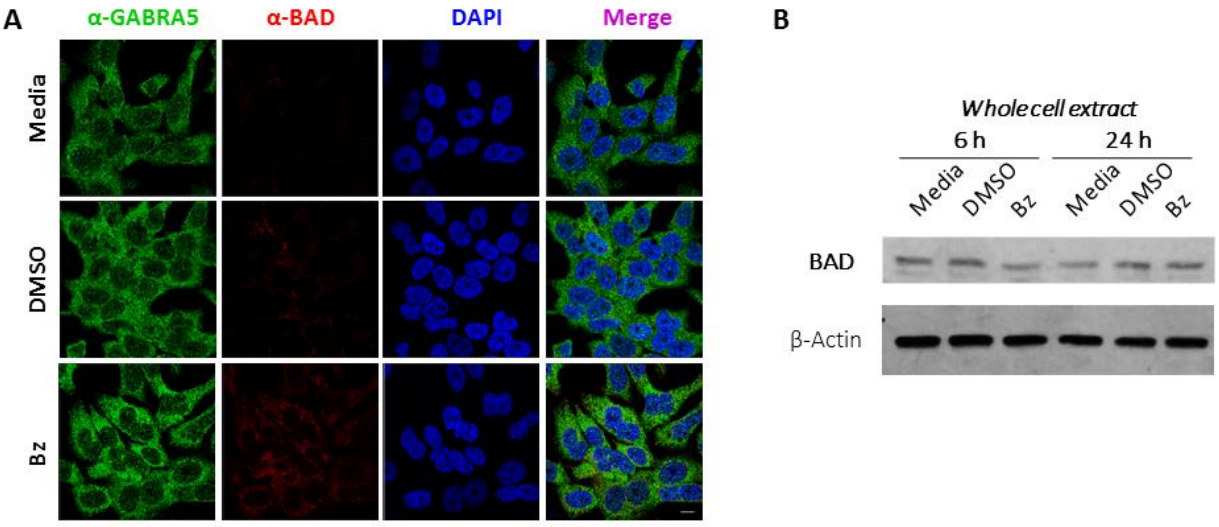


**Figure 54. Activation of the instrinsic pathway of apoptosis. (A) Immunoflourescence microscopy imaging of D283 cells at 24 hours following incubation with media alone, DMSO, or KRM-II-08 (Bz, 0.8 μM). Cells were stained using antibodies specific to α5 (green) and the protein BAD (red). Nucleus of cells were stained with 4′,6-diamidino-2-phenylindole (DAPI). Scale bar in bottom, right image is 10 microns. (B) Western blot of protein BAD at 6- and 24-hours post-incubation with KRM-II-08 (Bz). Loading control for blot is beta-actin.**

precipitate events that result in D283 cell death. However, cell death is not immediate and may require the transcriptional activity of p53, as noted above, as well as its migration to the cytoplasm. We initially examined whether D283 cells underwent senescence. Analysis of senescence-associated beta-galactosidase of DMSO alone and KRM-II-08 (**19**) treated that in 48 hours at most ~12% of the cells may be undergoing senescence (**Fig. 53**), which does not account for the loss in cell viability observed in our cell viability assays using KRM-II-08 (**19**) reported earlier (**Fig. 32**). Subsequently utilized an immune-blotting approach was utilized to identify a change in levels and/or post-translation modification of proteins that have a role in apoptosis in D283 cells incubated with DMSO alone or KRM-II-08. The only significant change observed was of the degree of post-translation modification of p53, and phosphorylation of residue Serine392 (pS392)

(**Fig. 53**). It was confirmed by Western blot that p53 was modified at S392 (**Fig. 52**). We also probed for other

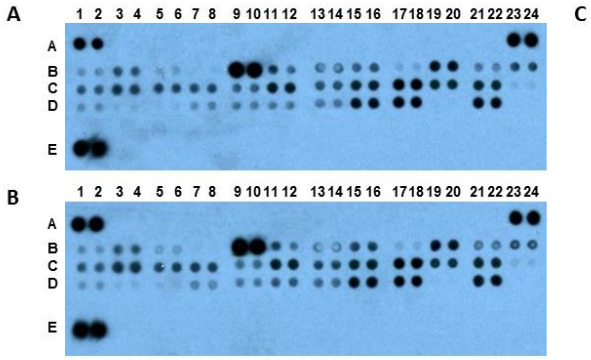


C

| Coordinate | Target/Control | Coodinate | Target/Control |
|---|---|---|---|
| A1, A2 | Reference Spots | C13, C14 | HO-2/HMOX2 |
| A23, A24 | Reference Spots | C15, C16 | HSP27 |
| B1, B2 | Bad | C17, C18 | HSP60 |
| B3, B4 | Bax | C19, C20 | HSP70 |
| B5, B6 | Bcl-2 | C21, C22 | HTRA2/Omi |
| B7, B8 | Bcl-x | C23, C24 | Livin |
| B9, B10 | Pro-Caspase-3 | D1, D2 | PON2 |
| B11, B12 | Cleaved Caspase-3 | D3, D4 | p21/CIP1/CDKN1A |
| B13, B14 | Catalase | D5, D6 | p27/Kip1 |
| B15, B16 | cIAP-1 | D7, D8 | Phospho-p53 (S15) |
| B17, B18 | cIAP-2 | D9, D10 | Phospho-p53 (S46) |
| B19, B20 | Claspin | D11, D12 | Phospho-p53 (S392) |
| B21, B22 | Clusterin | D13, D14 | Phospho-Rad17 (S635) |
| B23, B24 | Cytochrome c | D15, D16 | SMAC/Diablo |
| C1, C2 | TRAIL R1/DR4 | D17, D18 | Survivin |
| C3, C4 | TRAIL R2/DR5 | D19, D20 | TNF RI/TNFRSF1A |
| C5, C6 | FADD | D21, D22 | XIAP |
| C7, C8 | Fas/TNFRSF6/CD95 | D23, D24 | PBS (Negative Control) |
| C9, C10 | HIF-1α | E1, E2 | Reference Spots |
| C11, C12 | HO-1/HMOX1/HSP32 | | |

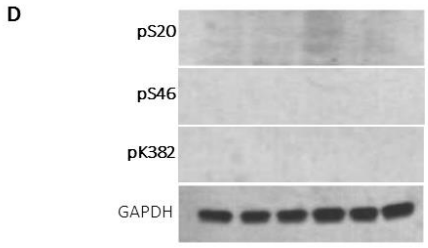


**Figure 55. Apoptosis proteome profiler array assay. (A) Raw data from two independent experiments (A and B panels) of D283 cells treated with DMSO or 0.7 µM KRM-II-08 for 24 hours. 300 micrograms of protein was used per assay. Arrays were incubated at 4˚C overnight. (C) Guide to wells labeled in panels "A" and "B".**

important p53 phosphorylated residues (S20, S46, or K382) (**Fig. 53**). Only p392 was observed and not only in the anticancer benzodiazepine target treated cells, but also in control cells (DMSO alone and media or untreated). The pS392 appears to be a constitutively active modification of p53 in D283 cells.

This was, therefore, examined by immunofluorescence for KRM-II-08 treated D283 cells for a change in amount and/or localization of pro-apoptotic Bcl-2 family members Bax, Puma, Bcl-2, Bcl-xL, and BAD.[173] Only the BAD protein exhibits a change in intensity detected by immunoflourescence in the KRM-II-08 treated D283 cells (**Fig. 52A**). There is a slight increase in

BAD levels between 6 and 24 hours (**Fig. 52B**). It has been reported that BAD and p53 do complex at mitochondria to induce apoptosis. [174, 175]

## 2. 1. 4 MATERIALS AND METHODS

### 2. 1. 4. 1 Gene expression analysis

Normalized gene expression data for sixteen *GABR* genes and *MYC* from 763 primary resected medulloblastoma specimens was used[137]. Samples were classified into four medulloblastoma subgroups and further into twelve subtypes: two WNT subgroups [α (n=49), β (n= 21)], four SHH subgroups [α (n= 65), β (n= 35), γ (n= 47), δ (n= 76)], three group 3 subgroups (α (n= 67), β (n= 37), γ (n= 40)] and three group 4 subgroups [α (n=98), β (n = 109), γ (n = 119)]. Heatmaps for analysis of expression across all four subgroups and among group 3 subtypes were generated using Morpheus (https://software.broadinstitute.org/morpheus). Boxplots for expression analysis were created in R. Correlation analyses among the *GABR* genes were performed using Spearman's correlation and the *p*-values of the correlation test are reported in legends to Figures. Correlograms were used to summarize the correlations using the 'corrplot' R package.

### 2. 1. 4. 2 Human medulloblastoma cell lines

Daoy and D283 cell lines were purchased from the American Type Culture Collection (ATCC), while D425 was obtained through a material transfer agreement between Emory and Duke University. Daoy is a human medulloblastoma derived cell line representative of the SHH subgroup.[155,156] D283 is a human medulloblastoma derived cell line that is *TP53*-wildtype and

representative of group 3.[157] D425 is a human medulloblastoma derived cell line that is *TP53*-mutated and representative of group 3.[158,159]

### 2. 1. 4. 3 Cell proliferation assay

The D283 cells (75 µL; 7500 cells) were added per well of a Falcon® 96 well flat bottom TC-treated polystyrene cell culture plate (Corning) in pentaplicates and incubated at 37°C (5% $CO_2$) for 4-5 hours. Dulbecco modified eagle's medium (DMEM) (1X) (Thermo Fisher Scientific), lacking phenol-red and penicillin/streptomycin but with 20% FBS and 4 mM L-glutamine, was used for plating. Benzodiazepines were suspended at room temperature in DMSO (0.125%) to prepare a 40 mM stock solution of drug. Benzodiazepines were further diluted in DMSO (0.125%) to a 4 mM working stock to use for drug dilution in DMEM. Drug was added to prepare final concentrations (0.05, 0.1, 0.25, 0.5, 0.75, 1.0, 2.5, and 5.0 µM in 0.125% DMSO). After a 48-hour incubation of drug with cells or DMSO alone as control at 37°C (5% $CO_2$), 20 µL of CellTiter 96® AQueous One Solution Cell Proliferation Assay (MTS) (Promega) was added per well and plate was then incubated for 1 hour at 37°C (5% $CO_2$). Cell absorbance (490 nm) was recorded using a Synergy H1 microplate reader (BioTek). To obtain an experimental reading, media alone control (the average reading of wells containing only media) was subtracted from DMSO (0.125%) control and drug treated values. Drug treated values were then divided by DMSO control values to normalize data. Inhibitor concentration at half-maximal binding ($IC_{50}$) values and dose response drug curves were obtained using the '[Inhibitor] versus normalized response' nonlinear regression function in Prism 7 software (GraphPad).

#### 2. 1. 4. 4 Electrophysiology

D283 cells were maintained at 37°C in 5% $CO_2$ in DMEM: F12 (1:1), GlutaMax, 10% FBS, with 1% penicillin/ streptomycin (DMEM+). Cells were grown on poly-D-lysine-coated glass coverslips (VWR). Patch-clamp experiments were performed on cells at 24-72 hours post-plating. All experiments were performed at 22°C and across multiple days to control for cell health and expression efficiency. All reagents used in electrophysiology experiments were purchased from Sigma, unless otherwise noted.

Whole-cell patch-clamp recordings were performed on D283 using methods like those previously described.[160] Patch pipettes were fabricated from thin-walled borosilicate glass (TW150F-4, World Precision Instruments, Inc.) using a horizontal puller (P-97, Sutter Instruments, Inc.) to give a resistance of 2-8 MΩ when filled with intracellular solution (120 mM KCl, 2 mM $MgCl_2$, 10 mM EGTA, and 10 mM HEPES, adjusted to pH 7.2 with NaOH, 315 mOsm). Extracellular solution contained 161 mM NaCl, 3 mM KCl, 1 mM $MgCl_2$, 1.5 mM $CaCl_2$, 10 mM HEPES, and 6 mM D-glucose, adjusted to pH 7.4 with NaOH (320-330 mOsm). A rapid solution changer (RSC-160, BioLogic Science Instruments) connected to a 10-channel infusion pump (KD Scientific Inc.) was used to deliver GABA and benzodiazepine solutions. The rapid solution changer was controlled by protocols written in pClamp 9 (Molecular Devices, LLC). Whole-cell currents were recorded at -60 mV, filtered at 100 Hz, and sampled at 200 Hz with a MultiClamp 700B amplifier and DigiData 1322A digitizer (Molecular Devices, LLC).

GABA concentration-response assays were performed by exposing each whole-cell patch to increasing concentrations of GABA (0.01, 0.03, 0.01, 0.3, 1, 3, 10, and 30 μM) for 2 seconds, with an 8 second washout between concentrations. Recordings were baseline corrected and analyzed in MATLAB (MathWorks, Inc.). Peak currents (*I*) were measured from GABA exposures

and fitted using least-squares nonlinear regression analysis based on the Hill equation: $I = I_{max} *[A]^{nH}/(EC_{50}^{nH} + [A]^{nH})$, where $I$ is current peak amplitude, $I_{max}$ is maximum current amplitude, $EC_{50}$ is the GABA concentration producing the half-maximal response, $A$ is agonist concentration, and $nH$ is the Hill coefficient. GABA concentration-response assays were individually fitted to the Hill equation for each whole-cell recording. The maximum peak current, $EC_{50}$, and Hill coefficient were estimated based on averaged values for the receptor and are reported as mean ± standard error of the mean (SEM).

$GABA_AR$ α5-selective benzodiazepine concentration response relationships were constructed for QH-II-66 (0.1 – 2 μM) and KRM-II-08 (0.1 – 5 μM). For each D283 cell, the reference $EC_{10}$ GABA response was established (C) before determining the peak response to co-application of benzodiazepine and GABA $EC_{10}$ (M). Percent potentiation (P) was calculated using the equation P=100x(M-C)/C. Potentiation was fitted using least-squares nonlinear regression analysis based on the equation: $P = P_{max} *[Bz]^{nH}/(PC_{50}^{nH} + [Bz]^{nH})$, where $P$ is potentiation, $P_{max}$ is maximum potentiation, $PC_{50}$ is the benzodiazepine concentration producing the half-maximal effect, $Bz$ is the benzodiazepine concentration, and $nH$ is the Hill coefficient. Concentration-Potentiation relationships were individually fitted to the Hill equation for each whole-cell recording. The maximum potentiation, $PC_{50}$, and Hill coefficient were estimated based on averaged values for the receptor and are reported as mean ± standard error of the mean (SEM).

#### 2. 1. 4. 5 Determining mitochondria structure and membrane potential

Mitochondrial membrane potential was measured in live D283 cells using the TMRE (tetramethylrhodamine, ethyl ester) Mitochondrial Membrane Potential Assay Kit (Abcam). Briefly, D283 cells were plated on poly-D-lysine–coated glass coverslips and allowed to adhere

overnight. Cells were treated with either 0.7 μM KRM-II-08, DMSO, 20 μM FCCP (carbonyl cyaninde 4-(trifluoromethoxy) phenylhydrazone) or fresh media. After 10 minutes at 37°C (5% $CO_2$) treatment media was removed and replaced with 50 nM TMRE in cell culture media and incubated for 20 minutes at 37°C (5% $CO_2$). Cells were then rinsed with PBS and TMRE fluorescence was immediately visualized with a Leica SP8 confocal microscope. Fluorescence intensity was quantified with the Leica Application Suite X (LAS X) software platform (Leica Microsystems, Wetzlar, Germany).

#### 2. 1. 4. 6 Quantitative real time PCR

Total RNA was extracted from cells using the RNeasy Mini Kit (Qiagen) and converted into cDNA with the Cloned AMV First-strand Synthesis Kit (Invitrogen) and a 7500 Fast Real Time PCR system (Applied Biosystem). RNA expression was analyzed using a SYBR dye based approach (SYBR Green PCR Master Mix, Applied Biosystems) in 96-well plates (Applied Biosystems). Each well contained 20 μL, consisting of 8 μL SYBR Green PCR Master Mix, 4 μL primers, and 4 μL cDNA. TBP primers were used for normalization.

#### 2. 1. 4. 7 Microscopy

Preparation of cells for fluorescence microscopy was carried out at room temperature. Cells were plated on poly-D-lysine coated glass coverslips and treated for the indicated times. Cells were fixed in 4% (w/v) paraformaldehyde (Electron Microscopy Sciences, EMS) for 1 hour, washed in PBS (6X, 5 minutes each time), incubated 1 hour in blocking buffer (PBS, 0.8% Triton X-100, 10% normal goat serum), and then kept overnight in blocking buffer with antibody (anti-GABRA5 (Aviva Systems Biology Corp.); anti-BAD (Santa Cruz Biotechnology); TP53 (Cell Signaling

Technology), or anti-Bcl-xL (Santa Cruz Biotechnology). Cells were washed in PBS (6X, 5 minutes each time) before addition of fluorescent goat anti-rabbit and goat anti-mouse secondary antibodies (Alexa Ig488 [green] or Alexa Ig555 [red], Invitrogen) for 60 minutes. Cells were washed in PBS (6X, 5 minutes each time) and coverslips were mounted on slides using Immuno Mount DAPI and DABCO Mounting Media (EMS). Fluorescence was visualized with a Leica SP8 confocal microscope and images prepared using the Leica Application Suite X (LAS X) software platform (Leica Microsystems).

#### 2. 1. 4. 8 Western blot analysis

Cells for Western blots of whole cell extract were washed with ice-cold PBS twice and centrifuged at 1200 rpm for 5 minutes. After washing, cells were lysed with ice-cold phosphate buffered RIPA with glycerol (2X) (20 mM sodium phosphate, 300 mM NaCl, 2% Triton X-100, 1% Sodium deoxycholate, 0.2% SDS, and 10% Glycerol) (Boston BioProducts) with added phosphatase inhibitors (Halt™ Phosphatase Inhibitor Cocktail, Thermo-Scientific), protease inhibitor cocktail (Sigma-Aldrich) and supplemented with 1 mM EDTA and 1 mM phenylmethylsulfonyl fluoride (Sigma-Aldrich). Cells were then vortexed 5 seconds every 5 minutes for a total of 15 minutes. After lysing, the cells were centrifuged (11000 rpm, 10 minutes) to separate remaining cell debris. Cells for preparation of nuclear and cytoplasmic extract fractions were prepared using the NE-PER Nuclear Cytoplasmic Extraction Reagent kit (Thermo-Scientific) per manufacturer's instructions. The treated cells were also washed with ice-cold PBS twice and centrifuged at 1200 rpm for 5 minutes prior to lysis with the extraction kit.

The Pierce BCA Protein Assay (Thermo-Scientific) was used to quantify the amount of protein in lysates prior to Western Blot analysis. The proteins (20 µg whole cell and 15 µg

cytoplasmic and nuclear fractions) were resolved by polyacrylamide/SDS gel electrophoresis using 10% pre-cast gels (Bio-Rad). Running conditions were set to 120 V for 2 hours. For most Westerns, proteins were transferred (130 V, 50 minutes) to 0.45 µM PVDF membranes. However, to detect BAD and Caspase-9 antibodies, proteins were transferred (130 V, 50 minutes) to a 0.45 µM nitrocellulose membrane. Membranes were blocked for 1 hour in PBS containing 0.1% Tween 20 and either 5% non-fat dry milk or 5% BSA. Membranes were incubated overnight with primary antibody (anti-p53, anti-PTEN, anti-Caspase-9, anti-GAPDH, anti-β-actin, Lamin B1, PARP, Cell Signaling Technologies; anti-MDM2, Abcam). Additionally, Abcam's p53 Antibody Sampler Panel (S20, S46, S392, phospho-p53 (K382), and p53 (DO)), was used. After primary antibody incubation, membranes were washed 3X for 10 minutes each time with 0.1% PBST or 0.1% TBST (for phospho-p53 antibodies). Membranes were incubated in appropriate horseradish peroxidase-conjugated secondary antibodies: anti-rabbit or anti-mouse (GE Healthcare). Membranes were washed again (3X, 10 minutes each) with 0.1% PBST or 0.1% TBST. Proteins were visualized using either ECL Western Blotting Detection Reagent (Amersham) or SuperSignal™ West Pico PLUS Chemiluminescent Substrate (Thermo Scientific) and X-ray film.

## 2. 2 Melanoma

The incidence of melanoma continues to rise, and advanced/metastatic disease confers a poor prognosis.[190] Approximately 50% of melanomas harbor somatic B-raf (*BRAF*) mutations, most

commonly V600E (80%) or V600K (14%),[191-193] which sensitizes them to treatment with BRAF or BRAF/MEK inhibitor combinations. The first generation of a clinically active BRAF-inhibitor (vemurafenib) produced high systemic objective response rates.[194] Subsequent development of the next-generation combination therapies with BRAF/MEK-inhibitors, such as dabrafenib and trametinib, further improved progression-free survival.[195-197] However, most patients acquire resistance to these therapies through several genetic or adaptive mechanisms or to a lesser extent, experience intrinsic resistance.[198-203] More recently, a combination of immune checkpoint inhibitors targeting programmed cell death-1 (PD-1) and cytotoxic T-lymphocyte-associated protein 4 (CTLA-4) (nivolumab and ipilimumab) produced an overall response rate of ~60% and durable responses in a portion of patients, including in patients with melanoma brain metastases.[204-208] These therapies work independently from the *BRAF* mutational status. **However, most metastatic melanoma patients do not experience durable responses to ICI. While significant progress has been made, novel therapeutic strategies to treat BRAF/MEK inhibitor or ICI resistant disease are desperately needed.** Furthermore, there are unique clinical challenges, such as the presence of melanoma brain metastases, which are associated with significant morbidity and mortality, and the brain may represent a therapeutic sanctuary site because of the blood-brain barrier. Target that penetrates the BBB would be a key advantage in treatments.

Gene expression analysis by The Cancer Genome Atlas (TCGA) of melanoma patient tumors revealed that *GABR* genes, which code for subunits of the Type A γ-aminobutyric acid (GABA) neurotransmitter receptor (GABAAR), are among those most highly expressed.[209] Soma et al. conducted a more extensive analysis of *GABR* expression in metastatic melanoma tumors as well as characterization of melanoma cells for intrinsic GABAAR activity. It was found that

melanoma patient expression of *GABR* genes varied with the molecular subgroups of melanoma defined by TCGA, including the MITF-low and Keratin groups, and that melanoma cells express functional GABAARs, as assessed by whole cell patch-clamp electrophysiology experiments. Furthermore, it was found by Dasgupta et al. that enhanced GABAAR mediated membrane permeability to anions with GABAAR subtype selective benzodiazepines results in depolarized mitochondria in melanoma cells and impaired melanoma cell viability *in vitro*. In a syngeneic melanoma mouse model, the anticancer benzodiazepine alone promotes reduction in tumor growth and when combined with radiation and/or the programmed death ligand immune checkpoint inhibitor (α-PD-L1), greatly potentiated effectiveness. The target benzodiazepine with radiation promotes both ipsilateral and an abscopal antitumor activity associated with increased tumor infiltration with antigen-specific polyfunctional CD8 T-cells. The study identified a potential novel anti-tumor strategy combining radiation and/or immune checkpoint inhibitors with modulation of GABAARs in melanoma using a subtype preferring anticancer benzodiazepine.

## 2. 2. 1 RESULTS

### 2. 2. 1. 1 $GABA_AR$ subunit expression in metastatic melanoma patient tumors.

Type A γ-aminobutyric acid (GABA) neurotransmitter receptors (GABAARs) form pentameric chloride anion channels, composed mostly of two α, two β, and γ subunits encoded by *GABR* genes *GABRA* (1 to 6), *GABRB* (1 to 3), and *GABRG* (1 to 3), respectively[210,211] (**Figure 54**). We conducted a comprehensive analysis of *GABR* expression in stage III/IV melanoma patients in the TCGA dataset of cutaneous melanoma[209] (**Figure 55**). This analysis reveals that in the

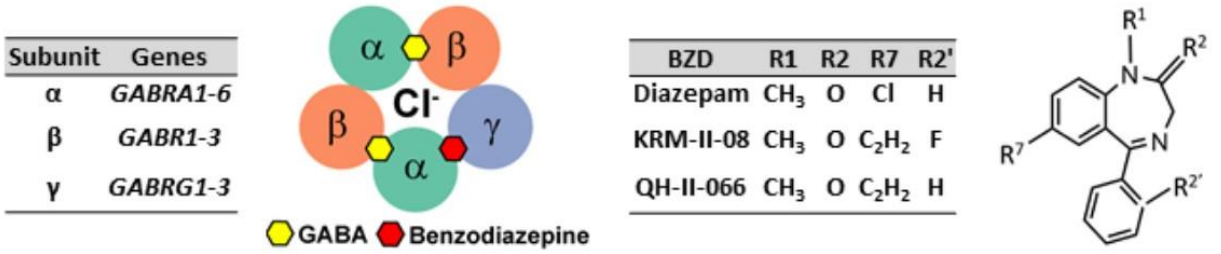


**Figure 56. Type A GABA neurotransmitter receptors (GABAARs) are composed primarily of two α, two β, and γ subunits encoded by *GABR* genes *GABRA (1* to *6)*, *GABRB (1* to *3)*, and *GABRG (1* to *3)*, respectively. GABAAR consists of five subunit transmembrane segments which create the chloride anion (Cl-) conduction pore. Inter-subunit binding sites for GABA (yellow hexagon) and benzodiazepine (red hexagon) are shown, recognizing the αβαβγ subunit stoichiometry. Benzodiazepine and GABA bind at α/γ and α/β interfaces, respectively. Benzodiazepines have a common core structure. Shown are sites frequently modified (R1, R2, R2′, R7), which may impart a GABAAR subtype-preference. GABAAR subtype preferring benzodiazepines (BZD) KRM-II-08 and QH-II-066 differ from diazepam by having an R7 acetylene group.**

'MITF-low' subgroup patients, there is notable expression of *GABRA3, GABRB1,* and *GABRG2.* In contrast, 'Keratin' subgroup patients exhibit a greater enhanced expression of *GABRA5, GABRB3,* and *GABRG3.* 'Immune' subgroup patients similarly exhibit *GABR* expression, but not of a clear subset of *GABR* genes. A pairwise correlation analysis of the *GABR* expression patient data in the three TCGA proposed melanoma subgroups suggests there is a correlated expression in MITF-low and Keratin subgroups that may yield GABAARs composed of α3β1γ2 and α5β3γ3, respectively (**Figure 56**).

*GABR* expression measured by bulk-RNA sequencing in the TCGA study[209] may be reflective of transcripts from non-tumor as well as tumor cells. To confirm expression of *GABR* genes in melanoma cells, Sengupta et al. performed RT-PCR analysis for *GABR* expression in four patient derived melanoma cell lines (A375, RPMI-7951, SKMEL-24, SKMEL-28). All cell lines tested

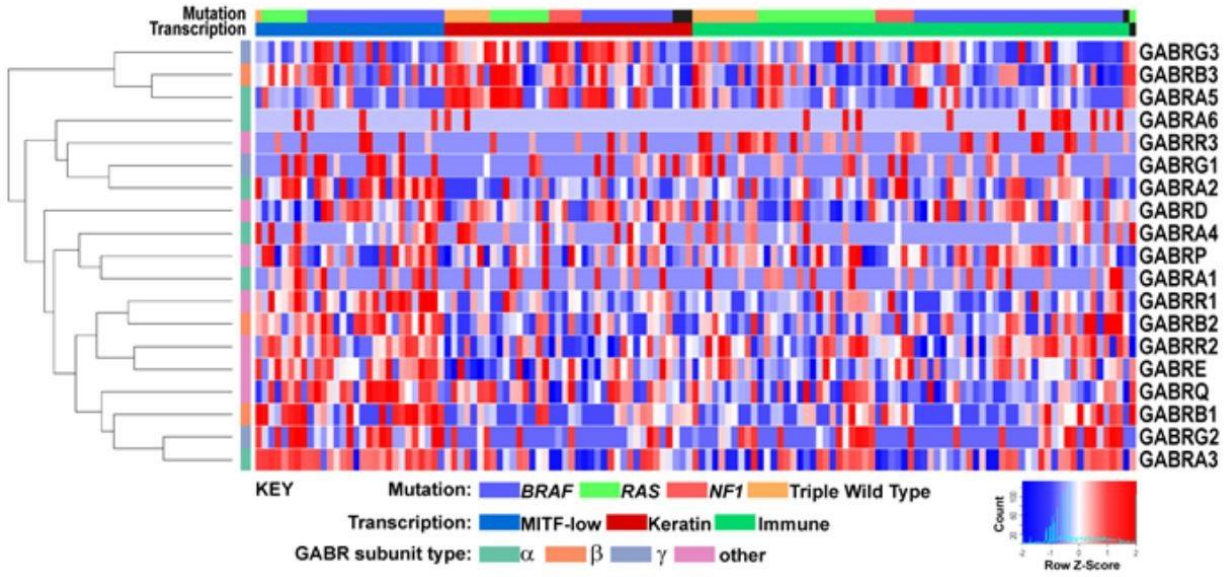


**Figure 57. Normalized gene expression data for *GABR* genes from stage III/IV melanoma specimens. Samples were classified into three melanoma molecular subgroups. Heatmap for analysis of expression across subgroups was generated using Morpheus (https://software.broadinstitute.org/morpheus).**

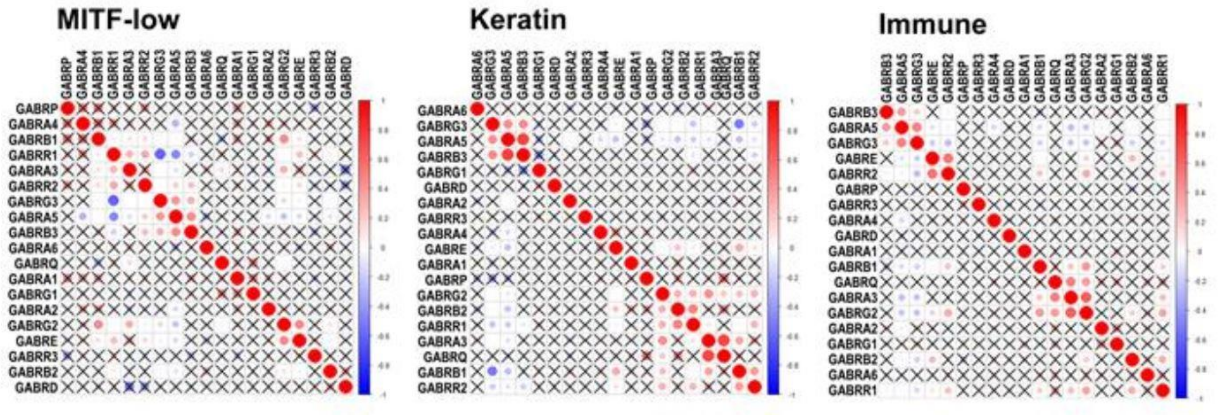


**Figure 58. GABAA receptor subunit (*GABR*) correlation in gene expression in stages 3 and 4 cutaneous melanoma patients. Correlograms of *GABR* gene expression by molecular subgroup: MITF-low, Keratin, and Immune. Positive correlation values are indicated in red and negative values in blue. Correlation values not marked by an "X" are not statistically significant, using a correlation test at *p*-value < 0.01. Correlation analyses among the *GABR* genes were performed using Spearman's correlation. Correlograms were used to summarize the correlations using the 'corrplot' R package.**

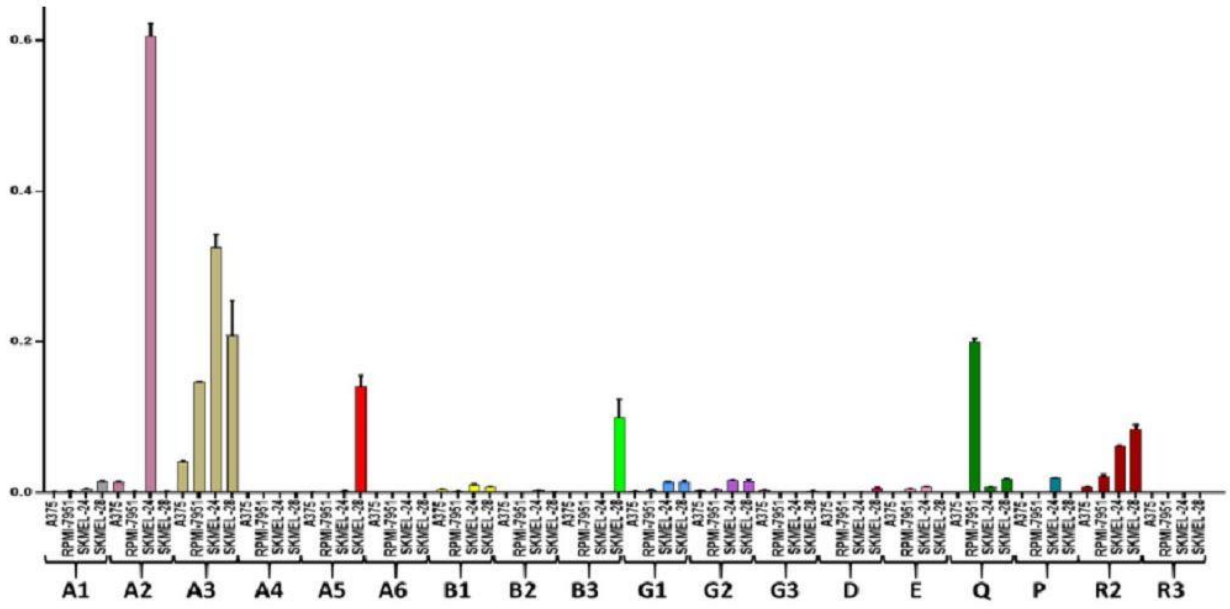


**Figure 59. RT-PCR of human metastatic melanoma lines for *GABR* genes (Key: *GABRA1-6,* A1-A6; *GABRB1-3,* B1-B3; *GABRG1-3,* G1-G3; *GABRD,* D; *GABRE,* E; *GABRQ,* Q; *GABRP,* P; *GABRR2,* R2; *GABRR3,* R3). Bar graphs show means ± standard error of the mean.**

express to a varying degree *GABRA3*, while SKMEL-24 and SKMEL-28 have uniquely high *GABRA2* and *GABRA5* expression, respectively (**Figure 57 and 58**). There is significantly less expression of *GABRB1-3* and *GABRG1-3* in these human melanoma cell lines, compared to *GABRA1-6* levels. Western blotting of human melanoma cell line A375 and murine line B16F10-GP for subunits α2, α3 and α5 protein abundance is concordant with RT-PCR results (**Figure 59**).

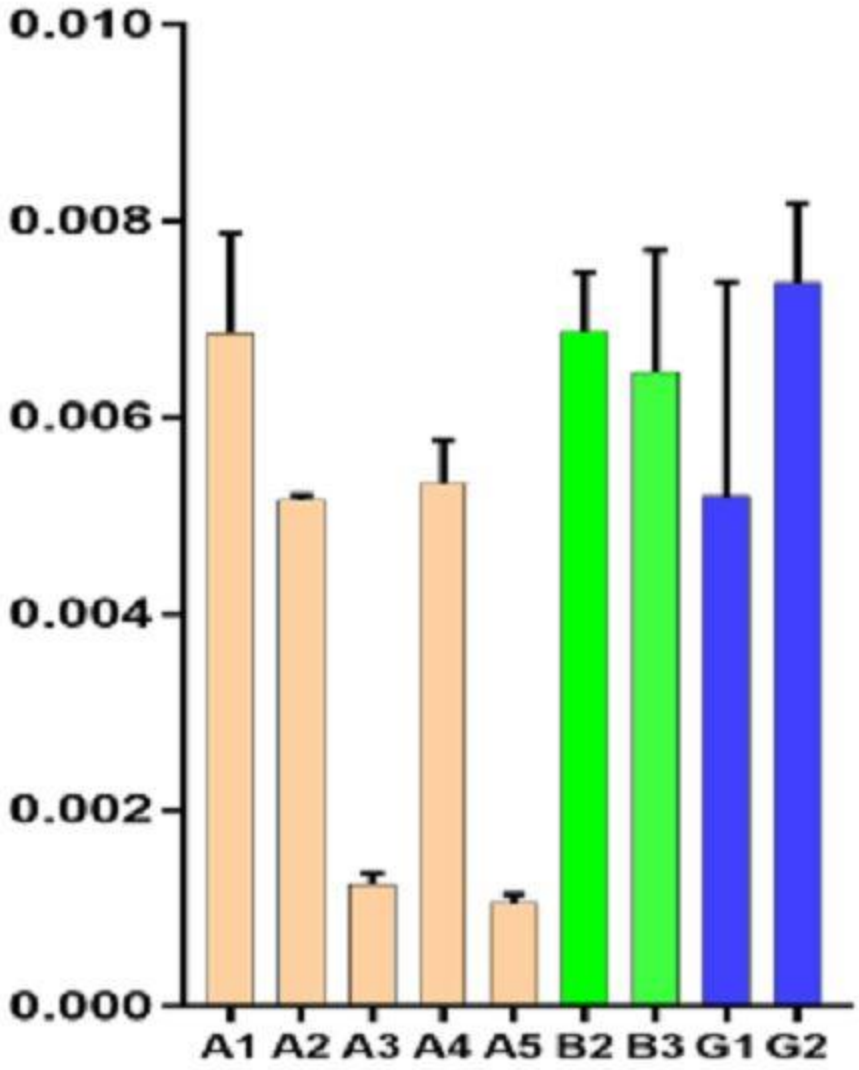


**Figure 60. RT-PCR of murine cell line B16F10-GP for select *GABR* genes (Key: *GABRA1-5,* A1-A5; *GABRB2-3,* B2-B3; *GABRG1-2,* G1-G2). Total RNA was extracted from cells (RNeasy Mini Kit, Qiagen), converted into cDNA by PCR (Cloned AMV First-strand Synthesis Kit, Invitrogen), and analyzed using SYBR dye (SYBR Green PCR Master Mix, Applied Biosystems). Primers used were as detailed in Kallay et al. (30). Bar graphs show means ± standard error of the mean.**

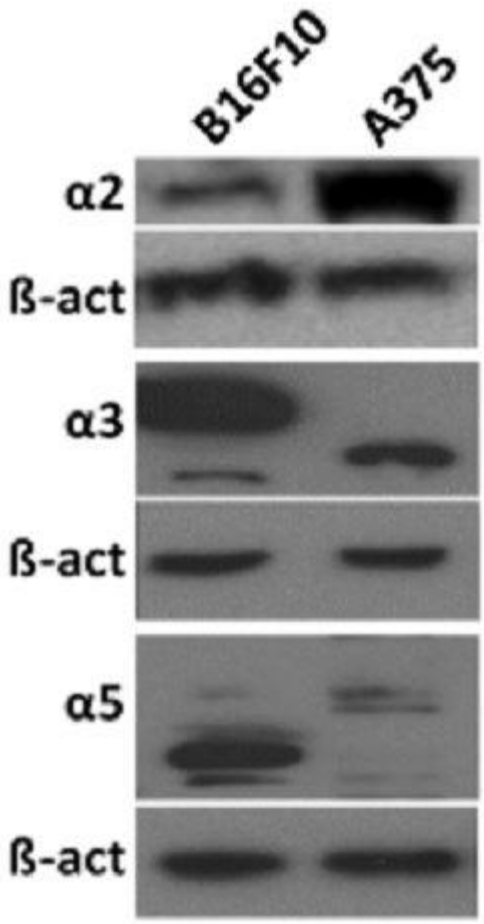


**Figure 61. Western blots of cell lines B16F10-GP and A375. Whole-cell extracts were prepared as described[30]. Cells were washed 2x with ice cold PBS and scraped into RIPA buffer (Boston BioProducts), 10 mM NaF, 1 mM sodium orthovanadate with complete protease inhibitor cocktail (ROCHE). Lysate was then incubated on ice for 30 min, centrifuged, and supernatant protein concentrations determined using the BCA kit (Pierce). Cell lysates (10-30 µg) were prepared in Laemmli sample buffer (Bio-Rad), reducing agent (Bolt), heated 5 min at 100°C and cooled on ice. Proteins were subjected to SDS-PAGE on a 10% precast gradient gel (BioRad) and transferred to PVDF membrane (Amersham). After transfer, membranes were blocked in 5% Nonfat Dry Milk in 1x PBST (Cell Signaling) for 1 h and incubated for 16 h at 4°C with primary antibody: p53 (1:1000, Cell Signaling Technology), GABRA2 (1:1000, Aviva), GABRA3 (1:1000, Sigma-Aldrich), GABRA5 (1:1000, Aviva), and β-actin (1:1000, Cell Signaling Technology) in 5% milk in PBST. Immunodetection was performed with anti-rabbit horseradish-peroxidaseconjugated secondary antibody (1:10000, Cell Signaling Technology) or anti-mouse horseradish–conjugated secondary antibody (1:10000, GE Healthcare limited), and visualized with Chemoluminiscent HRP Antibody Detection Reagent (Thermo Scientific, SuperSignal West Femto Maximum Sensitivity Substrate).**

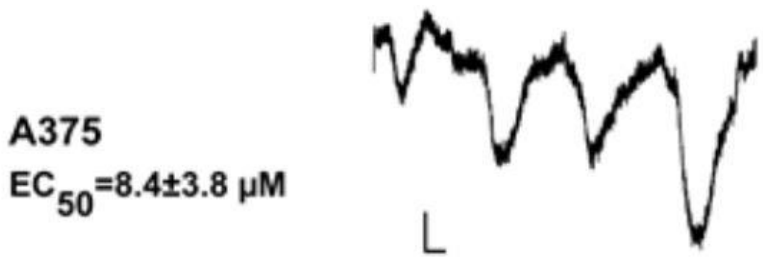


**Figure 62. Representative whole-cell patch clamp electrophysiology recordings of transmembrane anion flow in A375 cell lines in response to GABA at 1, 3, 10, and 30 µM GABA. Horizontal calibration bars represent 2 seconds, and the vertical bars represent 500 pA; sweeps are ensemble recordings from 8 electrodes.**

### 2. 2. 1. 2 Melanoma cells possess functional $GABA_AR$s.

GABAAR is a chloride anion channel that changes the transmembrane potential of cells, either depolarizing or hyperpolarizing depending upon the activity of other membrane transport proteins as described earlier.[21,22] To validate that expression of GABAAR subunits in melanoma cell lines leads to assembly of a functional receptor, we utilized whole cell patch-clamping of human (A375) and murine (B16F10-GP) melanoma lines was emplyed to detect electrophysiological currents. Both cell lines exhibited a response to the neurotransmitter GABA, the GABAAR endogenous ligand (**Figure 60; Table 1**). Compared to A375, B16F10-GP cells exhibited a larger maximal response to and a greater affinity for GABA.

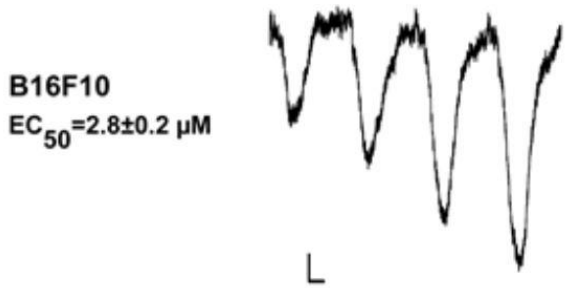


**Figure 63. Representative whole-cell patch clamp electrophysiology recordings of transmembrane anion flow in B16F10-GP cell lines in response to GABA at 1, 3, 10, and 30 µM GABA. Horizontal calibration bars represent 2 seconds, and the vertical bars represent 500 pA; sweeps are ensemble recordings from 8 electrodes.**

**Table 2-1 Summary of electrophysiology derived values for GABA ± anticancer benzodiazepines on human metastatic melanoma cell line A375 and murine line B16F10-GP.**

| **B16F10-GP cells** | | | | | |
|---|---|---|---|---|---|
| **Condition** | **$EC_{50}$ (μM)** | **$n_H$** | **$I_{max}$ (pA)** | **$P_{max}$ (%)** | **N** |
| GABA | 2.8 ± 0.2 | 1.3 ± 0.6 | -430 ± 70 | - | 6 |
| KRM-II-08 + 1 μM GABA | 0.2 ± 0.1 | 1.3 ± 0.2 | - | 86 ± 4 | 4 |
| QH-II-066 + 1 μM GABA | 0.16 ± 0.09 | 1.0 ± 0.3 | - | 52 ± 6 | 5 |
| **A375 cells** | | | | | |
| **Condition** | **$EC_{50}$ (μM)** | **$n_H$** | **$I_{max}$ (pA)** | **$P_{max}$ (%)** | **N** |
| GABA | 8.4 ± 3.8 | 1.1 ± 0.3 | -230 ± 41 | - | 8 |
| KRM-II-08 + 1 μM GABA | 1.7 ± 0.2 | 0.7 ± 0.2 | - | 77 ± 2 | 6 |
| QH-II-066 + 1 μM GABA | 0.9 ± 0.4 | 0.5 ± 0.1 | - | 105 ± 5 | 5 |

**Where: EC50, concentration of compound producing half or 50% of the maximum response; *n*H, Hill coefficient; Imax, maximal current observed; Pmax, maximal percent potentiation; N, number of independent measurements. Values are means ± standard error of the mean for the indicated number (N) of cells.**

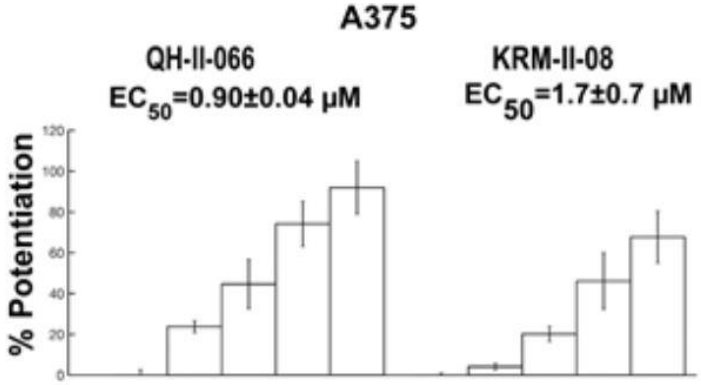


**Figure 64. Potentiation of GABA responses in A375 cells in response to benzodiazepines (QH-II-066 and KRM-II-08). The GABA concentration was 1 μM. The benzodiazepine concentrations were 0, 0.3, 1, 3 and 10 μM.**

Benzodiazepines bind at the α-ɣ interface of a GABAAR (**Figure 54**). A fully functional benzodiazepine binding site requires assembly of a GABAAR with a canonical αβαβɣ subunit stoichiometry as mentioned previously.[23,24]

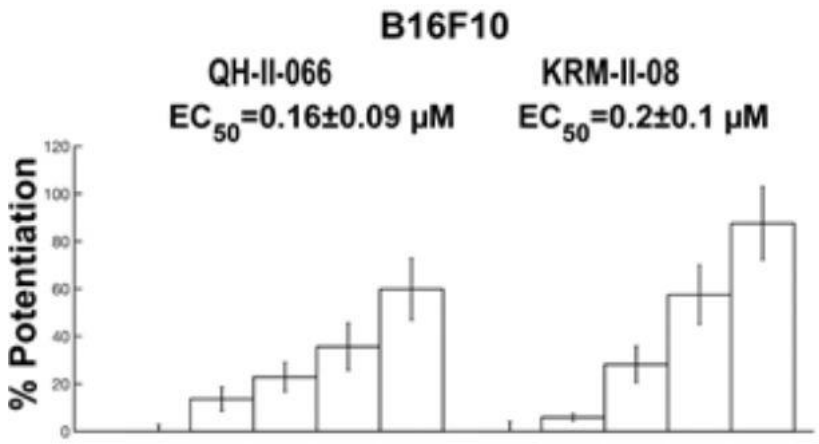


**Figure 65. Potentiation of GABA responses in B16F10 cells in response to benzodiazepines (QH-II-066 and KRM-II-08). The GABA concentration was 1 µM. The benzodiazepine concentrations were 0, 0.3, 1, 3 and 10 µM.**

Benzodiazepine binding increases the probability of the channel opening in the presence of GABA, thus increasing the flow of anions crossing the membrane or holds the channel open longer. Since benzodiazepines interact with the GABAAR at a site different than GABA, one tested the effect of benzodiazepines on the current of A375 and B16F10-GP cells. We tested two benzodiazepines (QH-II-066 and KRM-II-08) that were originally designed as anxiolytics were tested, to observe if an enhanced current was elicited, as expected if a GABAAR has an αβαβɣ subunit stoichiometry. QH-II-066 and KRM-II-08 possess the privileged structure of diazepam, but with less sedative and ataxic effects than diazepam and Librium.[214-216] which was achieved by a subtle alteration of their chemical structure (**Figure 54**) that increased preference for specific GABAAR subtypes, as opposed to diazepam.

It was found that QH-II-066 and KRM-II-08 enhanced the effect of GABA in a dose dependent manner in A375 and B16F10-GP cells (**Figure 62 and 63; Table 1**). The electrophysiology results also indicate that both QH-II-066 and KRM-II-08 act as $GABA_AR$ positive allosteric modulators, increasing membrane anion permeability. Further, the micromolar GABA EC50 values obtained by electrophysiology indicate that the receptors in the melanoma cells studied are more likely to

be ‘synaptic’ isoforms (α1, 2 or 3 containing) and not GABA supersensitive ‘extra synaptic’ isoforms (or α4 or 5 containing), consistent overall with RT-PCR and Western blots of cell lines A375 and B16F10-GP.

### 2. 2. 1. 3 Benzodiazepine QH II 66 (8) depolarizes melanoma cell membrane potential and impairs viability.

In our studies of the effect of the benzodiazepine QH II 66 (**8**) on medulloblastoma cells it was shown that changes that followed the benzodiazepine-mediated increase in membrane anion permeability included, depolarization of the mitochondrial transmembrane potential.[217,219] ultimately resulting in apoptosis via the intrinsic mitochondria-mediated pathway. Thus, one tested if QH II 66 elicited a similar response in A375 and B16F10-GP cells. To test if the melanoma cell membrane potential was changed the cationic stain tetramethylrhodamine ethyl ether (TMRE) and fluorescence microscopy imaging of live cells was employed. TMRE is taken-up by functioning mitochondria and exhibits reduced staining if the mitochondrial transmembrane is depolarized. We find at 10 minutes after exposure to QH-II-066 (**8**) that mitochondrial membranes of A375 and B16F10-GP cells are depolarized (**Figure 64**). This is consistent with a flow of chloride anions out of the melanoma cell, which was established to be the case in medulloblastoma cells.[219] Previously, in the studies of medulloblastoma cancer cells which have intrinsic GABAAR activity, it was found that sustained incubation of medulloblastoma cells with the benzodiazepines QH-II-066 or KRM-II-08 can impair their viability in culture.[217-219]

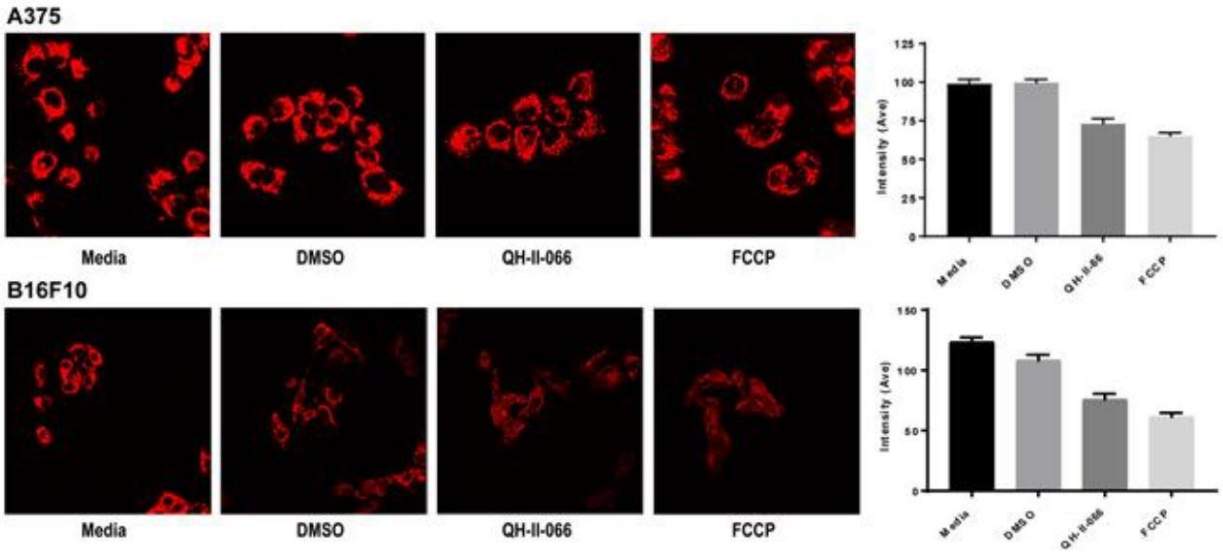


**Figure 66. Mechanism of benzodiazepine impairment of metastatic melanoma cell line A375 and murine line B16F10. Study of mitochondria transmembrane potential in A375 (upper panel) and B16F10-GP (lower panel) cells. Mitochondrial membrane potential was measured using the TMRE Mitochondrial Membrane Potential Assay Kit (Abcam). A375 or B16F10-GP cells were treated with drug (2 µM QH-II-066) or control solutions (10 min, 37°C), 50 nM TMRE added (20 min, 37°C), and TMRE fluorescence visualized (Leica SP8) and quantified (LAS X platform, Leica). DMSO concentration is equivalent to DMSO concentration in QH-II-066, 0.125%. Standard error of the mean (where: A375: n=28 (media), 32 (dimethyl sulfoxide, DMSO), 30 (QH-II-066), 28 (FCCP); B16F10: n=24 (media), n=13 (DMSO), n=26 (QH-II-066), n=27 (FCCP).**

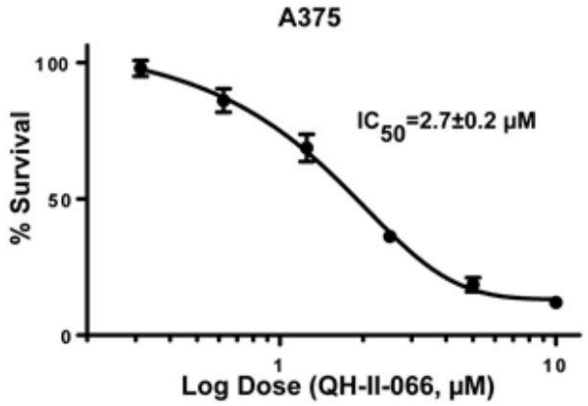


**Figure 67. *In vitro* MTS assay of A375 cells in response to QH-II-066 have IC50 = 2.7 ± 0.2 µM and IC50 = 8.2 ± 0.9 µM, respectively.**

In medulloblastoma cells these anticancer benzodiazepines were more than 10-fold effective in impairing cell viability than diazepam[217].

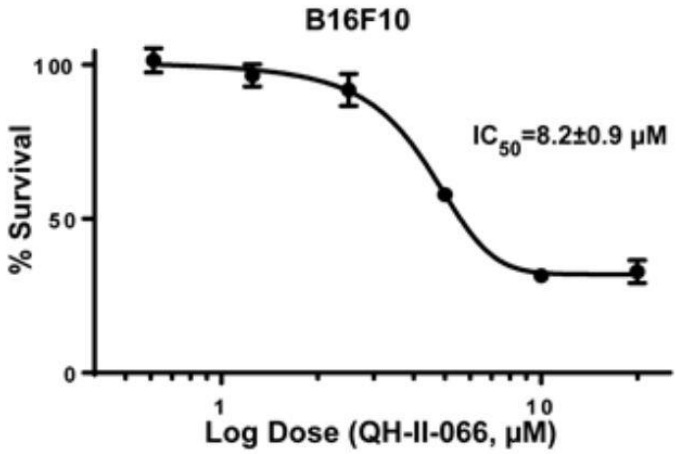


**Figure 68.** ***In vitro*** **MTS assay of B16F10-GP cells in response to QH-II-066 have IC50 = 2.7 ± 0.2 µM and IC50 = 8.2 ± 0.9 µM, respectively.**

We therefore examined if these benzodiazepines as well as diazepam impacted the viability of melanoma cells. To determine their effect on melanoma cell survival, we treated A375 and B16F10-GP cell lines in culture with QH-II-066 (**8**), KRM-II-08 (**19**), or diazepam over 48 hours. We observed a dose-dependent reduction in cell viability in both cell lines with QH-II-066 (**8**) or KRM-II- 08 (**19**) (**Figure 65 and 66**). In contrast, diazepam had no effect on the viability of either A375 or B16F10-GP cells (**Figure 67A**).

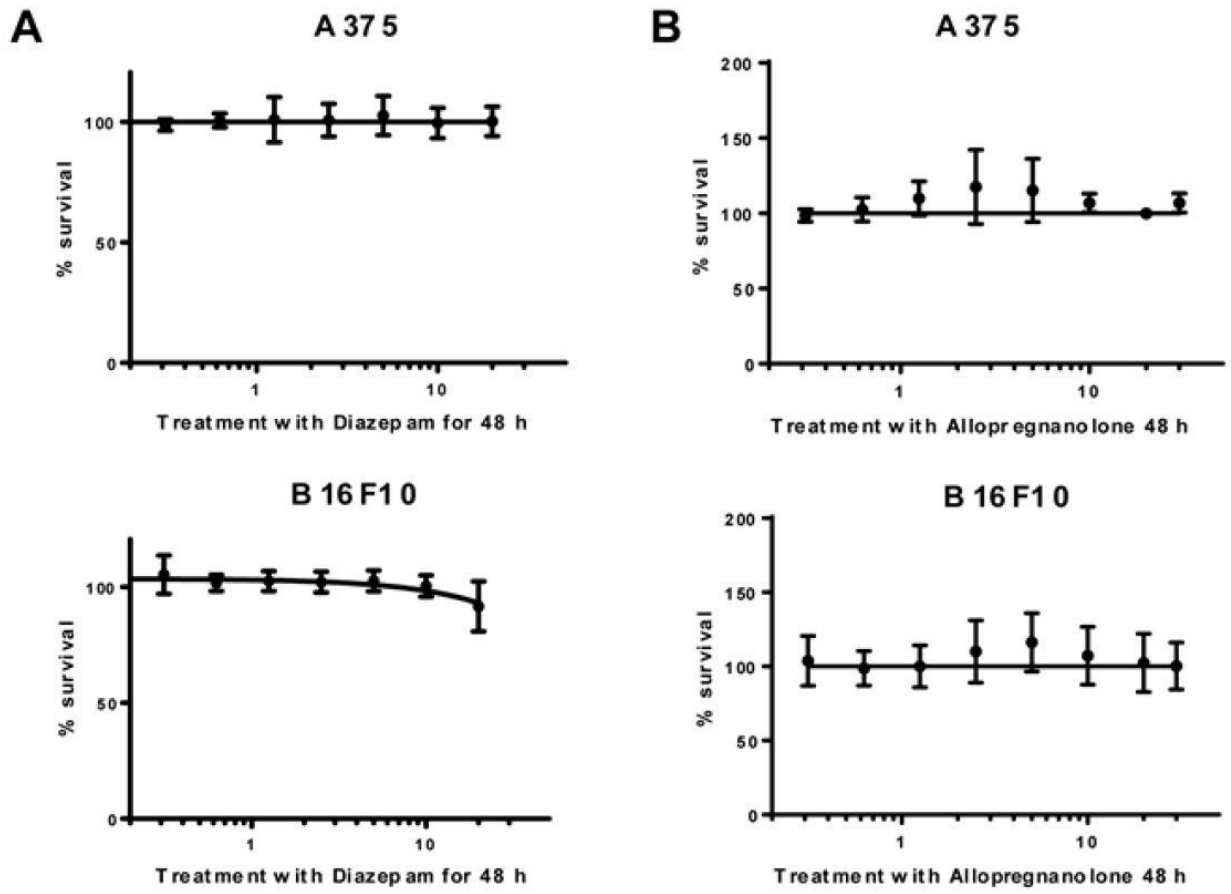


**Figure 69. Effect of GABAA receptor positive allosteric modulators on viability of human metastatic melanoma line A375 and murine line B16F10. (A) MTS assay of cell lines A375 (top) and B16F10-GP (bottom) treated with allopregnanolone for 48 h. (B) MTS assay of cell lines A375 (top) and B16F10-GP (bottom) treated with diazepam for 48 h. Methods used were as detailed in Methods section of text; dose-response curve error bars are ± standard error of the mean.**

Similar IC50 values were obtained for additional human metastatic melanoma lines treated with QH-II-066 (**8**) and KRM-II-08 (**19**) (**Table 2**). Cell lines which appeared to show no response to the

**Table 2-2 Effect of benzodiazepines on viability of human and mouse melanoma cell lines.**

| | | | $IC_{50}$ Benzodiazepine | |
|---|---|---|---|---|
| **Cell line** | | **p53** | **KRM-II-08** | **QH-II-066** |
| B16F10-GP (*Mm*) | | | 6.1 ± 0.5 μM | 8.2 ± 0.9 μM |
| A375 (*Hs*) | Skin; epithelial morphology; malignant melanoma | WT | 1.33 ± 0.08 μM | 2.7 ± 0.2 μM |
| MeWo (*Hs*) | Derived from lymph node; malignant melanoma; fibroblast morphology | E258K/Q317 | Minimal sensitivity at 5 μM | Minimal sensitivity at 5 μM |
| SK-MEL-2 (*Hs*) | skin: derived from metastasis on skin of thigh; polygonal morphology | G245S | 1.84 ± 1.2 μM | 1.52 ± 0.63 μM |
| SK-MEL-5 (*Hs*) | Skin, derived from metastatic axillary node; | WT | 2.15 ± 0.95 μM | 1.78 ± 0.89 μM |
| SK-MEL-28 (*Hs*) | Polygonal morphology; melanoma | L145R | No sensitivity at 10 μM | No sensitivity at 10 μM |

benzodiazepines were those where *TP53* was mutated, which is consistent with a role of p53 signaling in the response of cells to the benzodiazepines, as noted in previous medulloblastoma studies.[217,219]

To determine whether the effect on cell survival was benzodiazepine-specific, we tested the effect of allopregnanolone on cell viability. Allopregnanolone is also a positive allosteric modulator of GABAAR like benzodiazepines, but a non-benzodiazepine neurosteroid that does not bind at the canonical high affinity benzodiazepine binding site located at the α-γ interface. Allopregnanolone does not impair the viability of A375 or B16F10-GP lines (**Figure 67B**), suggesting that the effect on melanoma cell survival is anticancer benzodiazepine-specific or at

least specific to the more selective benzodiazepine-derivatives tested (QH-II-066 and KRM-II-088).

### 2. 2. 1. 4 The lead ligands alone promote reduction in tumor growth.

The IC50 values in melanoma cells with benzodiazepines QH-II-066 and KRM-II-08 are an order of magnitude higher than in medulloblastoma cells, ~6 μM vs. ~0.6 μM, respectively.

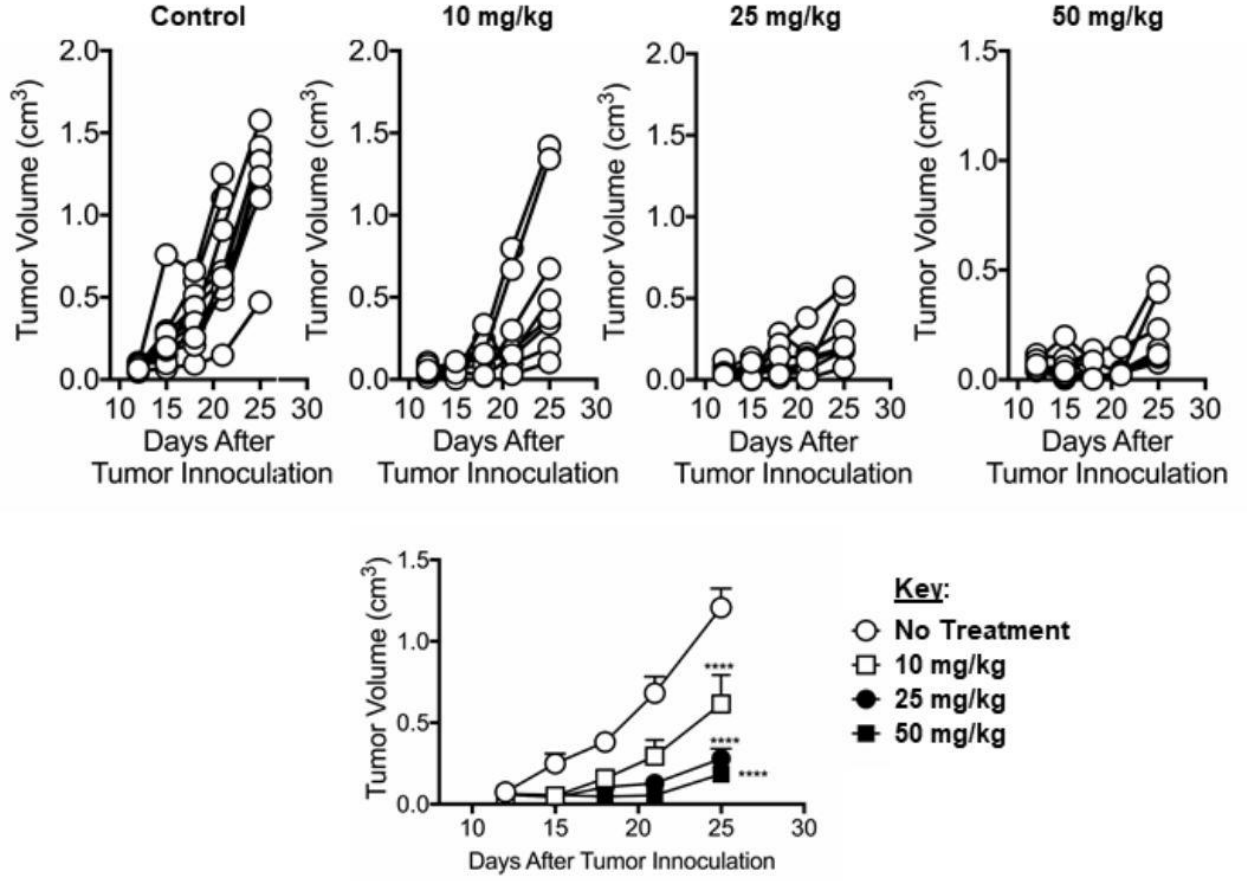


**Figure 70. The dose-dependent reduction in B16F10-GP tumor growth. Mice were implanted in left and right flanks with B16F10-GP tumor cells. Mice received QH-II-066 i.p. at three different doses (10, 25, and 50 mg/kg) from Day 10 daily for 7 days. Tumor measurements were taken with at least 4-5 mice per group (*$p$<0.05; **$p$<0.01; ***$p$<0.001; ****$p$<0.0001). Each line in the top panel represents a tumor. Methods used were as detailed in Methods section of the text.**

Since it was observed that melanoma cell viability *in vitro* was impaired by QH-II-066 and KRM-II-08 (albeit with a modest IC50), one investigated if the benzodiazepines had anti-tumor activity

in the B16F10-GP syngeneic melanoma murine model. The QH-II-066 was used for *in vivo* testing given that this compound has previously been tested in primates as an anxiolytic without any adverse effects or toxicity,[31] while KRM-II-08 has not been similarly tested. In addition, QH-II-066 is more soluble which makes it more experimentally tractable for detailed study. Employing QH-II-066, one observed a dose-dependent reduction in B16F10-GP tumor growth at three dosage points (10, 25, and 50 mg/kg) (**Figure 68**). There was a negligible difference between doses of 25 and 50 mg/kg, indicating that a lower dose of the benzodiazepine is sufficient for anti-tumor activity in an otherwise aggressive melanoma model.

#### 2. 2. 1. 5 Anti-cancer Benzodiazepine anti-tumor activity was potentiated in combination with either radiotherapy or α-PD-L1 checkpoint therapy.

Radiotherapy remains a standard-of-care for most cancers. In the earlier study on medulloblastoma, it was found that QH-II-66 (**8**) was capable of sensitizing cells in culture to radiation. This phenomenon was not tested in an animal model. It was reasoned that a benzodiazepine might be beneficial in an *in vivo* model in conjunction with radiation and that this should be explored in an immunocompetent model more reflective of the tumor microenvironment, given that varied immune cells may also possess GABAARs and contribute to increased effectiveness of the drug. We elected to use the B16F10-GP syngeneic melanoma murine model to assess whether QH-II-066 (**8**) potentiates radiation to control both ipsilateral and contralateral tumor volume. Further, we chose to use a dose of 10 mg/kg of QH-II-066 (**8**), which by itself had little direct anti-tumor activity relative to the higher doses tested. Using this dose the objective was to assess for real synergy, rather than treatment additivity with radiation. We implanted B16F10-GP melanoma cells in both the right and left flanks of C57BL/6 mice (**Figure 69**). A single dose of radiation (either 10 or 5 Gy) was delivered to the right flank

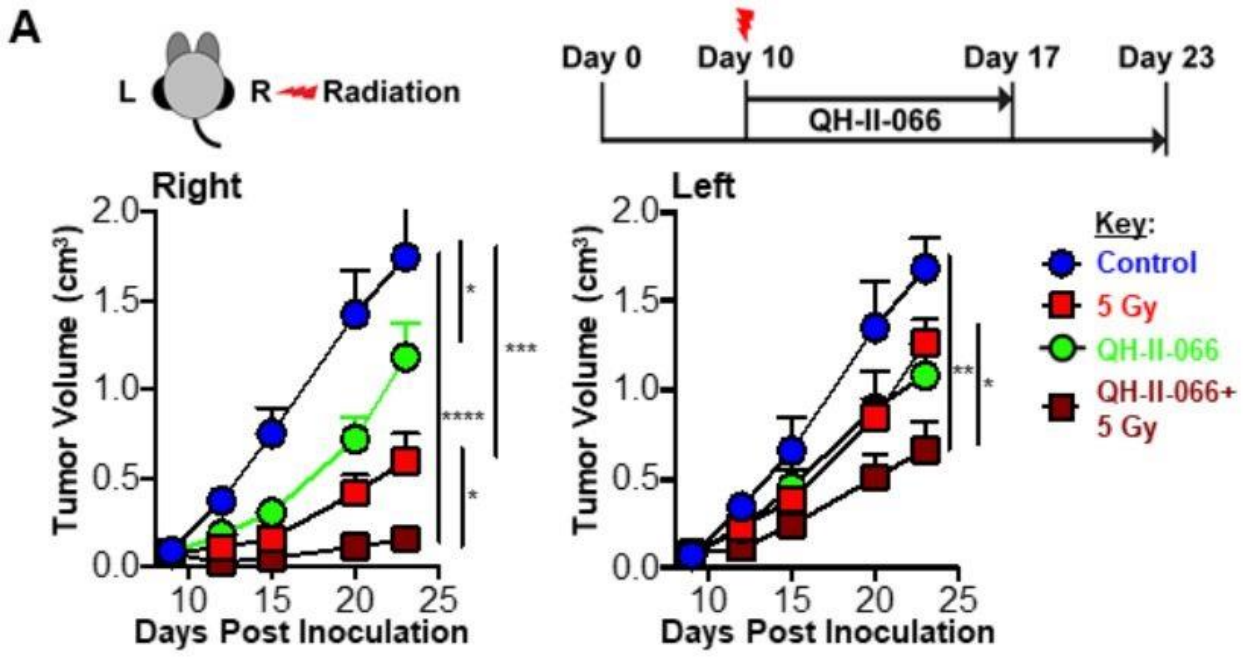


**Figure 71. Top, Schematic showing showing the tumor, benzodiazepine, and radiation strategy. Mice were implanted in left (L) and right (R) flanks with B16F10-GP tumor cells. Mice received either: (*i*) vehicle alone. control; (*ii*) radiation alone (5 Gy, right flank only); (*iii*) QH-II-066 beginning Day 10; (*iv*) radiation (5 Gy, right flank only) on Day 10 (in the morning), followed by QH-II-066 (in the evening. Bottom, Effect of combination of QH-II-066 and 5 Gy radiation on tumor growth kinetics. Tumor measurements were taken with at least 4-5 mice per group and results are a combination of two experiments. In groups receiving QH-II- 066, 10 mg/kg was injected i.p. daily for 7 days. (**p*<0.05; ***p*<0.01; ****p*<0.001; *****p*<0.0001).**

only on Day 10 after tumor implantation, when tumors are palpable. Tumor growth was then measured for the following experimental groups: (*i*) vehicle alone control; (*ii*) QH-II-066 alone at 10 mg/kg, injected i.p. every day for seven days beginning on Day 10; (*iii*) a single dose of radiation (10 or 5 Gy), delivered on Day 10; (*iv*) 10 or 5 Gy (in the morning) on Day 10, followed by QH-II-066 (10 mg/kg, in the evening), then injected i.p. every day for seven days. We find that combination of radiation and QH-II-066 resulted in significantly reduced ipsilateral and

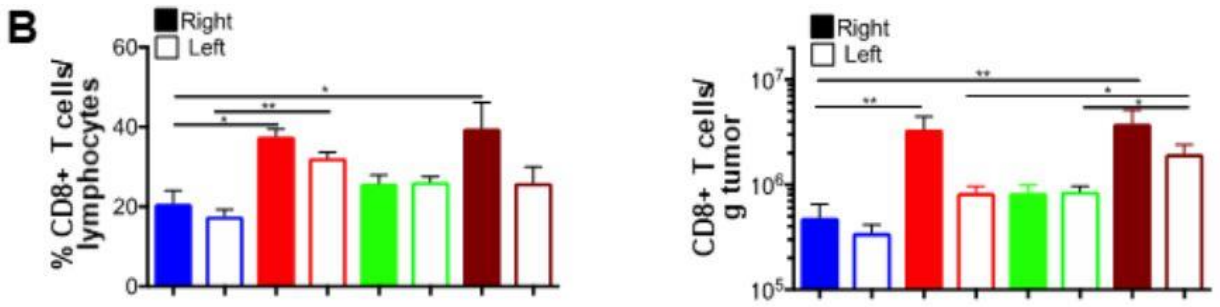


**Figure 72. Percent CD8 of total lymphocytes and number of CD8 T cells per gram of tumor. TILs were isolated at day 7-8 after radiation as described in materials and methods and stained with indicated antibodies. Error bars are representation of SEM.**

contralateral tumor volume, when compared to either monotherapy (benzodiazepine or radiation alone) or the control (**Figure 69; Figure 70**). These effects were consistent at both tested radiation doses (10 or 5 Gy). Together, these results indicated a synergistic anti-tumor response of QH-II-66 (**8**) plus radiation and a potent out of field abscopal effect of this combination in an otherwise highly treatment resistant tumor model. The transcriptomes of the tumors treated with QH-II-066 (**8**) was sequenced and with radiation, and then QH-II-066 (**8**), plus radiation, as well as the control. In comparison to the control, one identified: 42 differentially expressed (FDR < 0.1) genes in QH-II-066 (**8**) treated tumors; 1564 differentially expressed genes in the radiation treated tumors; and 587 differentially expressed genes in QH-II-066 (**8**) plus radiation treated tumors (**Table 2**). An enrichment analyses of gene expression for all Kyoto Encyclopedia of Genes and Genome (KEGG) pathways and transcription factor targets (Table S3) revealed statistically significant up-regulation in all three treatment groups in comparison to control of genes with roles in the cytokine: cytokine receptor interaction pathway, whereas target genes of the p63, a member of the p53 family of transcription factors, were upregulated in the radiation and QH-II-066 (**8**) plus radiation

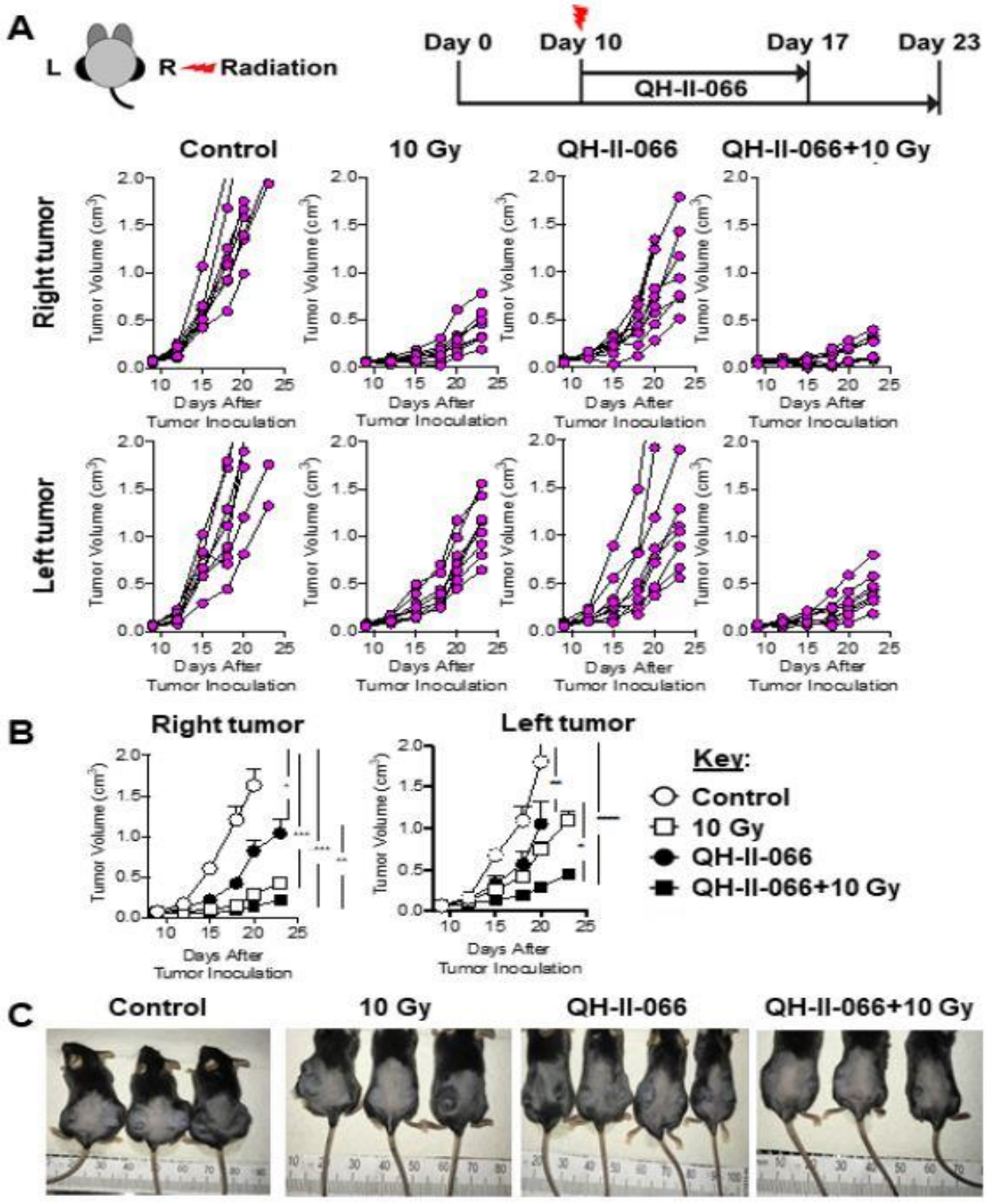


**Figure 73. QH-II-66 and 10 Gy radiation in B16F10-GP melanoma mouse model. (A) Top, Schematic showing the tumor, benzodiazepine, and radiation strategy. Mice were implanted in left (L) and right (R) flanks with B16F10-GP tumor cells (0.5 million cells in 25% matrigel). At Day 10, mice received either: (*i*) vehicle alone**

**control; (*ii*) radiation alone (10 Gy, right flank only); (*iii*) QH-II-066 beginning Day 10; (*iv*) radiation (10 Gy, right flank only) on Day 10 (in the morning), followed by QH-II-066 (in the evening). Bottom, Effect of combination of QH-II-066 and 10 Gy radiation on tumor growth kinetics. Each line represents a mouse. (B) Mean tumor growth of mice in (A). Tumor measurements were taken with at least 4-5 mice per group and results are the combination of two experiments. (*$p$<0.05; **$p$<0.01; ***$p$<0.001; ****$p$<0.0001). In groups receiving QH-II-066, 10 mg/kg was injected i.p. daily for 7 days. (C) Photographs of mice from four treatment groups at the conclusion of the experiment. Note left and right flanks.**

treated tumors. Increased expression of *TP63* has been associated with the genotoxic treatment of melanoma cell lines, and in our results

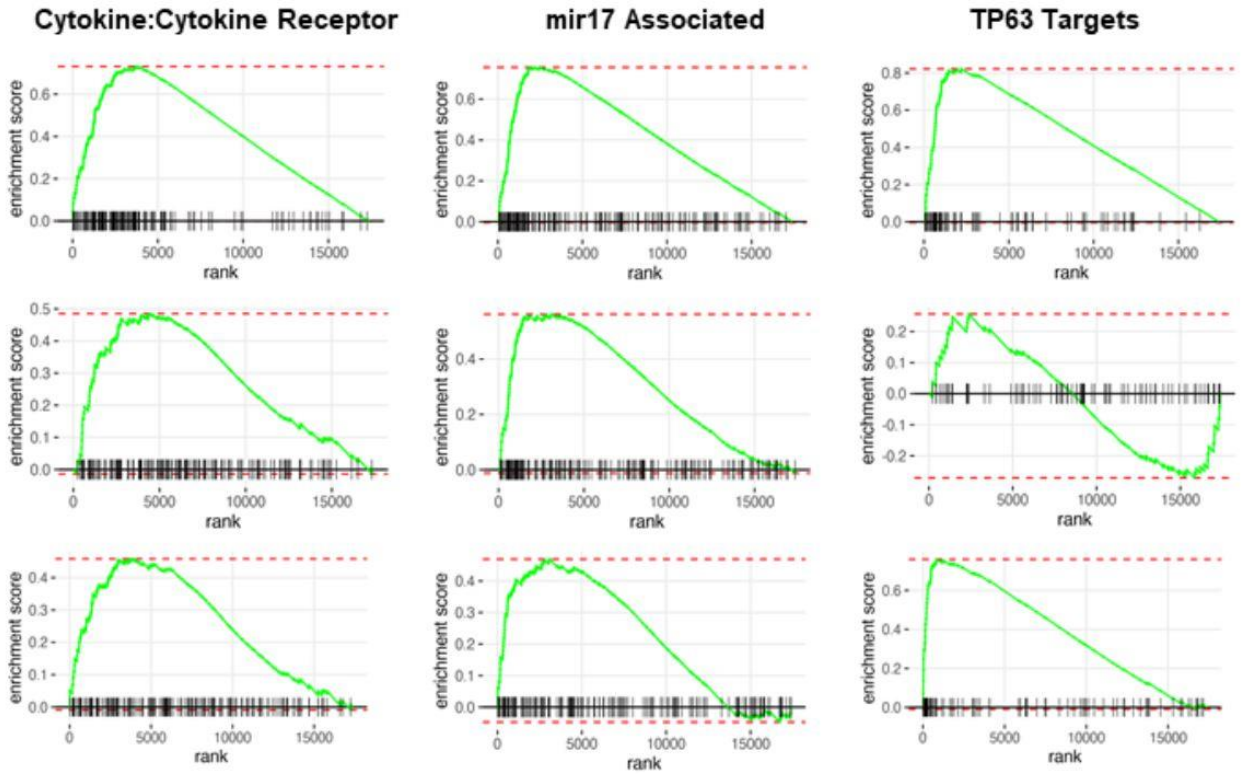


**Figure 74. GSEA plots of differentially expressed genes. Gene Set Enrichment Analysis (GSEA) plots of differentially expressed genes for Cytokine:Cytokine receptor interaction pathway (left), GSE32533_WT_VS_MIR17 (middle), and TP63 (right) for the three treatment groups: 5 Gy vs Control (top row), 5 Gy+QH-II-066 vs Control (middle row), QH-II-066 vs Control (bottom row).**

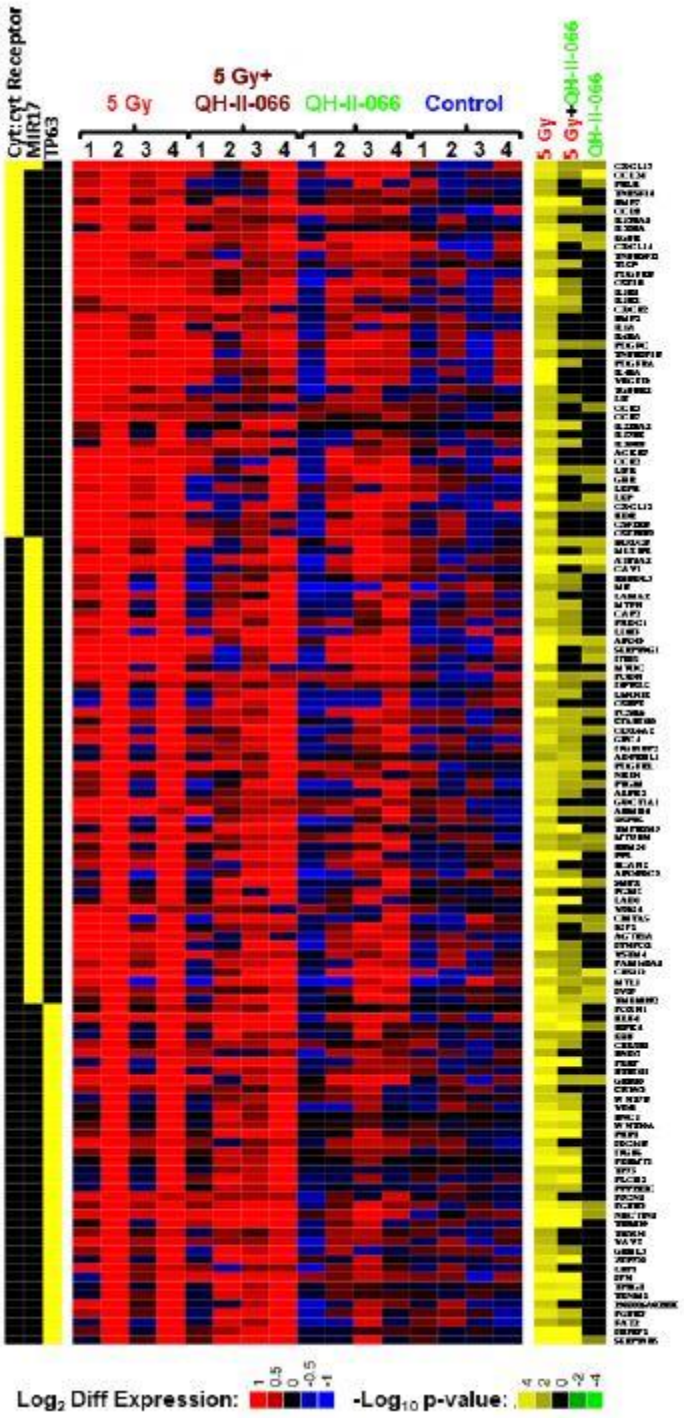


**Figure 75. Differential gene expression in mouse tumors treated with benzodiazepine and/or radiation. Expression levels of differentially expressed genes in enriched immunity-related KEGG pathway (cyt:cyt Receptor is abbreviation for cytokine:cytokine receptor), p63 target genes, and enhanced expression of genes associated with overexpression of the microRNA mir-17, identified by enrichment analysis of the ImmuneSigDB compendium of transcriptional immune signatures.[50,54-55] Genes in the enriched gene sets were considered to be differentially expressed if edgeR FDR < 0.05 in any one of the 3 comparisons. Left, heatmap indicates the membership of each gene (rows) in the enriched gene sets (columns). Middle, heatmap displays the expression levels of the genes in individual samples (columns) in terms of log2 counts per million (LCPM)56.**

**Each LCPM has been normalized by subtracting the gene-specific average LCPM of the untreated samples. Right, heatmap displays the statistical significance and the direction of the change in each of the comparisons made (5 Gy vs Control; 5 Gy+QH-II-066 vs Control; QH-II-066 vs Control) (columns), each vs control. The statistical significance is expressed in log10(p-value) when expression ratio was less than 1 (down-regulation) and -log10(p-value) when expression ratio was greater than 1 (up-regulation) resulting in negative numbers for downregulation and positive for upregulation.**

the enrichment of p63 targets was corroborated by the increased expression of *TP63* in the radiation and QH-II-066 (**8**) plus radiation treated tumors (> 100-fold increase, FDR < 0.0002 in both comparisons), but not in the QH-II-066 (**8**) alone treated tumors (FDR > 0.7). We also conducted an enrichment analysis of the ImmuneSigDB compendium of transcriptional immune signatures. This analysis identified the enhanced expression of genes associated with overexpression of the microRNA mir-17, whose expression has also been shown to be enhanced by p6336. Having observed that QH-II-066 (**8**) could sensitize a melanoma tumor to radiation and that expression of genes with roles in the cytokine: cytokine receptor interaction pathway was enhanced, one set out

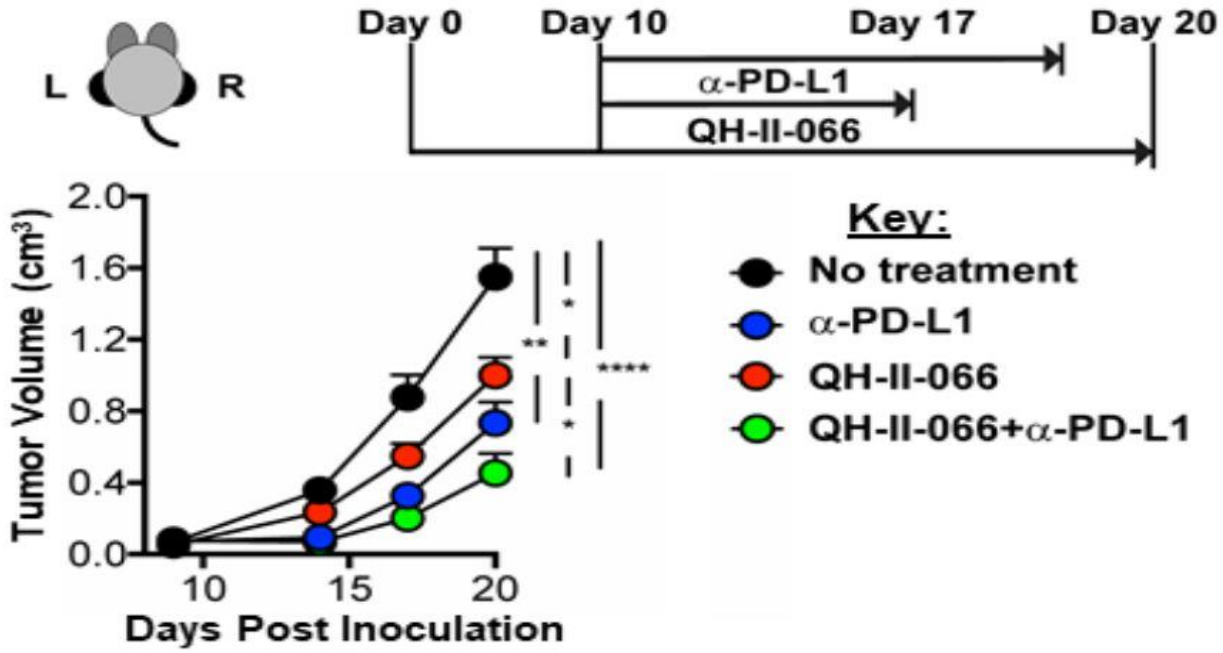

**Figure 76. QH-II-66 (an anxiolytic and slightly sedative benzodiazepam) potentiates immune checkpoint inhibitor. Top, Schematic showing the therapeutic strategy. Mice were implanted in the left (L) and right (R) flanks with B16F10-GP tumor cells (Day 0). Day 10, mice received either: (*i*) vehicle alone control; (*ii*) QH-II-066; (*iii*) α- PD-L1; (*iv*) QH-II-066 and α-PD-L1. Bottom, Effect of combination of QH-II-066 and α-PD-L1 on tumor growth kinetics. In the groups receiving QH-II-066, 10 mg/kg was injected i.p. daily for 7 days. In group receiving α-PD-L1, 200 μg was injected i.p. every 3 days through end of the experiment. Tumor measurements were taken with at least five mice per group (*$p$<0.05; **$p$<0.01; ***$p$<0.001; ****$p$<0.0001).**

to examine if potentiation could be extended to an immune checkpoint inhibitor. Immune checkpoint inhibitors have shown some degree of success in treatment of metastatic melanoma, but most patients with advanced disease exhibit poor and variable response to immunotherapy.[15-19] We elected to examine if QH-II-066 (**8**) could potentiate the programmed death ligand 1 immune checkpoint inhibitor (α-PD-L1). One implanted B16F10- GP melanoma cells in both the right and left flanks of C57BL/6 mice. Then one injected i.p. on Day 10 in both the right and left flanks: (*i*) QH-II-066 (10 mg/kg), then every day for seven days; (*ii*) α-PDL1 (200 μg), then every third day thereafter; (*iii*) QH-II-066 (**8**) (10 mg/kg) and α-PD-L1 (200 μg) at time and frequency detailed for monotherapy treatment groups (**Figure 73**). It was found that monotherapy treatment with QH-II-066 (**8**) or α-PD-L1 resulted in comparable reductions in tumor volume. The most significant reduction in tumor volume is observed with the dual therapy consisting of QH-II-066 (**8**) and α-PD-L1 (**Figure 73**). Similar to what was observed for radiation, QH-II-066 (**8**) and α-PD-L1 exhibited a synergistic anti-tumor response.

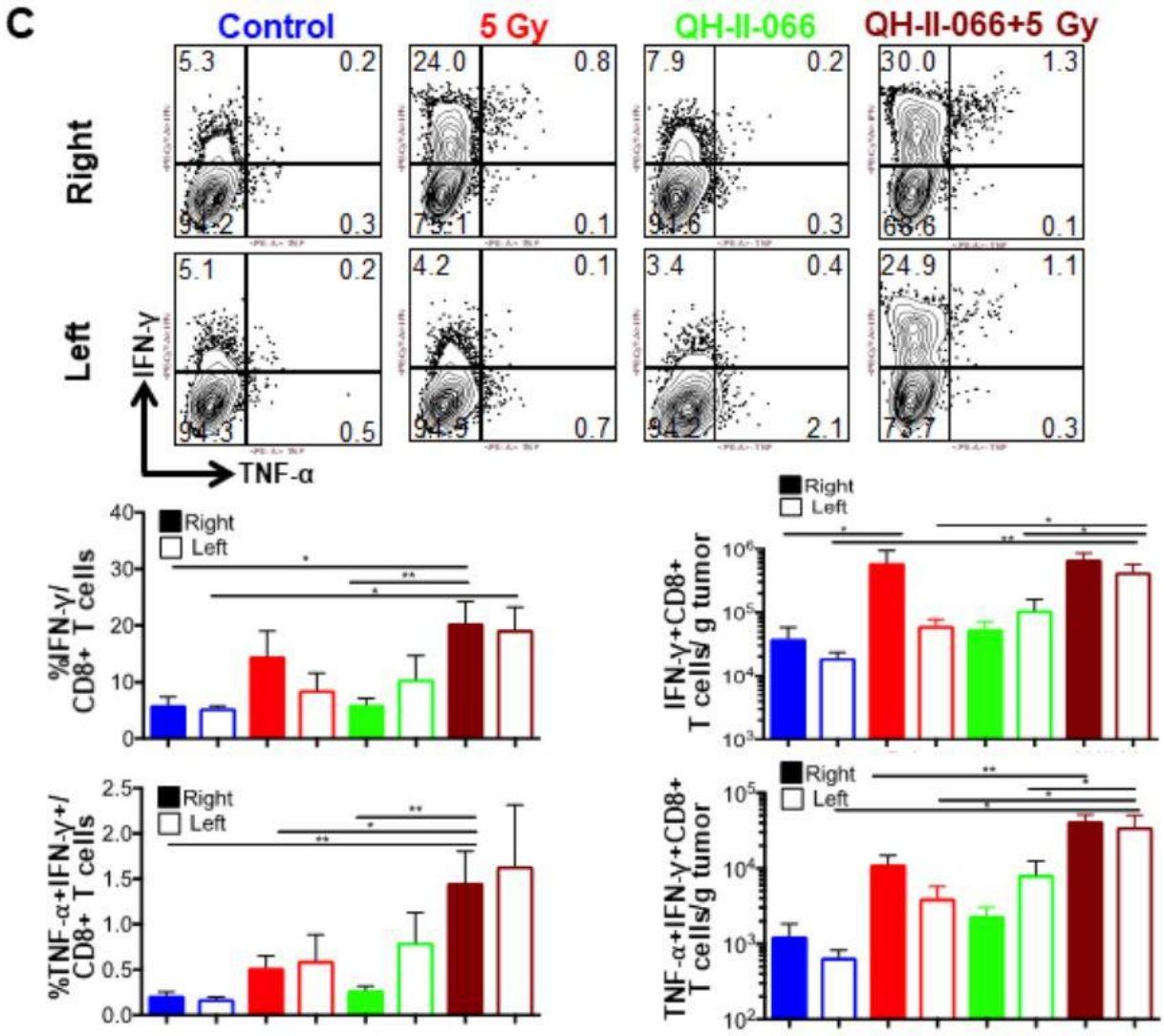


**Figure 77. Top, Representative flow showing percent IFN-γ and TNF-α in total CD8+ T cells after TILs were stimulated with peptide, as described in materials and methods. IFN-γ and TNF-α were stained with appropriate antibodies by intracellular staining. Middle, Graph showing percent IFN-γ+CD8+ of total CD8+ T cells and number of IFN-γ+CD8 T+ cells per gram of tumor. Bottom, Graph showing percent TNF-α +CD8+ of total CD8+ T cells and number of TNF-α +CD8 T+ cells per gram of tumor.**

### 2. 2. 1. 6 Combined QH-II-66 (8), α-PD-L1, and radiotherapy results in significant tumor regression. We reasoned that having observed potentiation of radiation and α-PD-L1 by QH-II-066

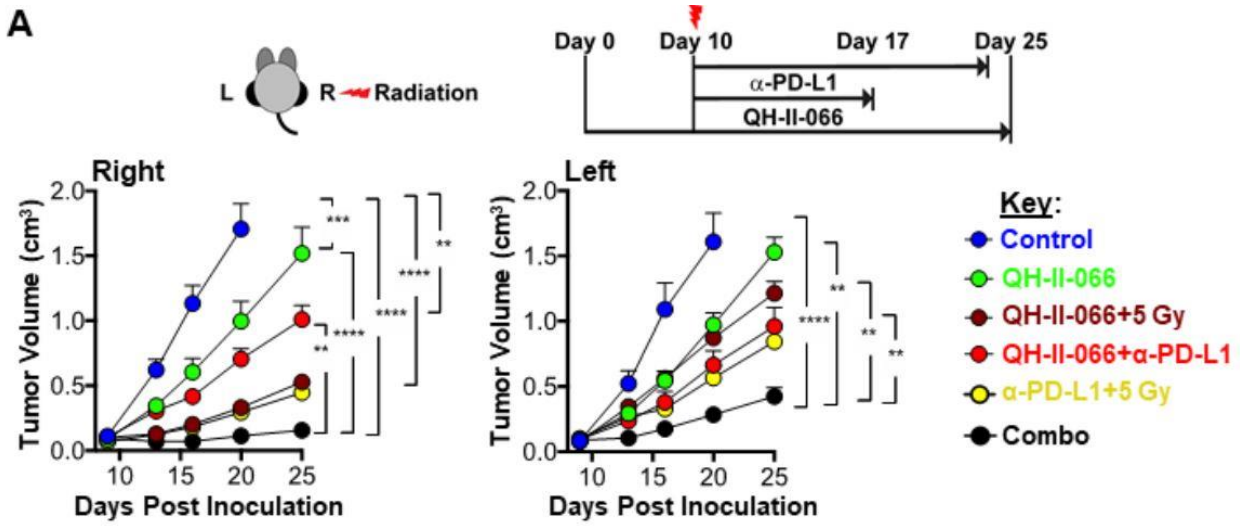


**Figure 78. Effectiveness of polytherapy with QH-II-66 on tumor volume. (A) Top, Schematic showing the therapeutic strategy. Mice were implanted in the left (L) and right (R) flanks with B16F10-GP tumor cells (Day 0). Day 10, mice received either: (*i*) vehicle alone; (*ii*) QH-II- 066; (*iii*) radiation (5 Gy, right flank only) on Day 10 (in the morning), followed by QH-II-066 (in the evening); (iv) QH-II-066 and α-PD-L1, beginning on day 10; radiation (5 Gy, right flank only) on Day 10 (in the morning), followed by α-PD-L1 (in the evening). In groups receiving QH-II-066, 10 mg/kg was injected i.p. daily for 7 days. In group receiving α-PD-L1, 200 μg was injected i.p. every 3 days through the end of experiment or maximum of 5 injections. Bottom, Effect of combination of dual and triple therapy on tumor growth kinetics. Tumor measurements were taken with at least 4-5 mice per group (**p*<0.05; ***p*<0.01; ****p*<0.001; *****p*<0.0001). For kinetics of tumor volume, tumors were measured at Indicated time points and experiment were done twice. The data is a combination of both experiments. Vehicle alone control, n=9; QH-II-066, n=10; QH-II-066/5 Gy n=10; QH-II-066/α-PD-L1, n=10; 5 Gy/α-PD-L1, n=10; Combo, n=10.**

individually, there might be a more significant tumor response if one administered a 'combo' consisting of radiation (5 Gy), α-PD-L1, plus QH-II-066. As before, we implanted B16F10-GP melanoma cells in both the right and left flanks of C57BL/6 mice **(Figure 75)**. One tested the following experimental groups: (*i*) vehicle alone control; (*ii*) QH-II-066 alone (10 mg/kg); (*iii*) a

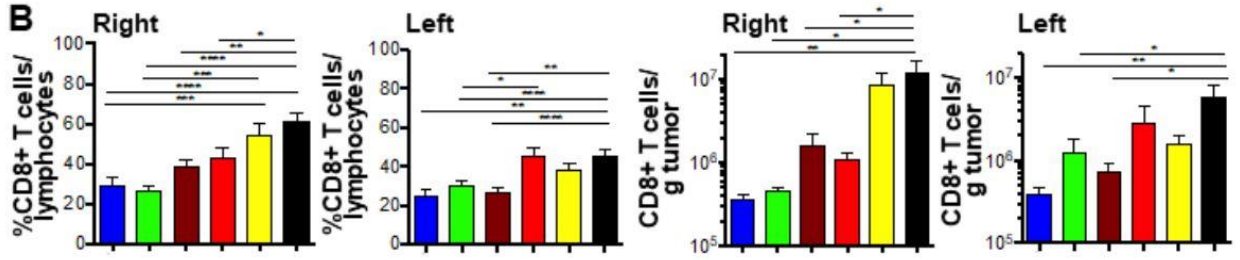


**Figure 79. Percent CD8 of total lymphocytes and number of CD8 T cells per gram of tumor in right and left tumors. TILs were isolated at day 7-8 after radiation as described in materials and methods and stained with indicated antibodies. Error bars are a representation of SEM.**

single morning dose of radiation (5 Gy) delivered to the right flank, followed by an evening dose of QH-II-066 (10 mg/kg); (*iv*) α-PD-L1 plus QH-II-066; (*v*) a single morning dose of radiation (5 Gy) delivered to the right flank, followed by an evening dose of α-PD-L1; (*vi*) a triple or combo therapy, consisting of a single morning dose of radiation (5 Gy) delivered to the right flank, followed by evening doses of α-PD-L1 plus QH-II-066. After initial i.p. injection of QH-II-066 on Day 10, QH-II-066 was injected i.p. every day for seven days, while α-PD-L1 was injected i.p. every third day thereafter.

The dual treatments of QH-II-66 plus radiation or QH-II-66 plus α-PD-L1 were better than radiation or α-PD-L1 alone (**Figure 75**), as reported above. Further, right flank tumors which received radiation exhibited greater reduction in tumor growth in treatments including radiation than the left flank tumors, as expected based on above. There is again a pronounced abscopal effect for left non-irradiated flank tumors, as noted above. But clearly, the most significant ipsilateral and abscopal effect is seen in the combo treatment group, complete tumor regression in some animals (**Figure 75**). **QH-II-066 plus radiation, plus α-PD-L1 treatment have a synergistic anti-tumor response, as well as a potent abscopal effect in combination.**

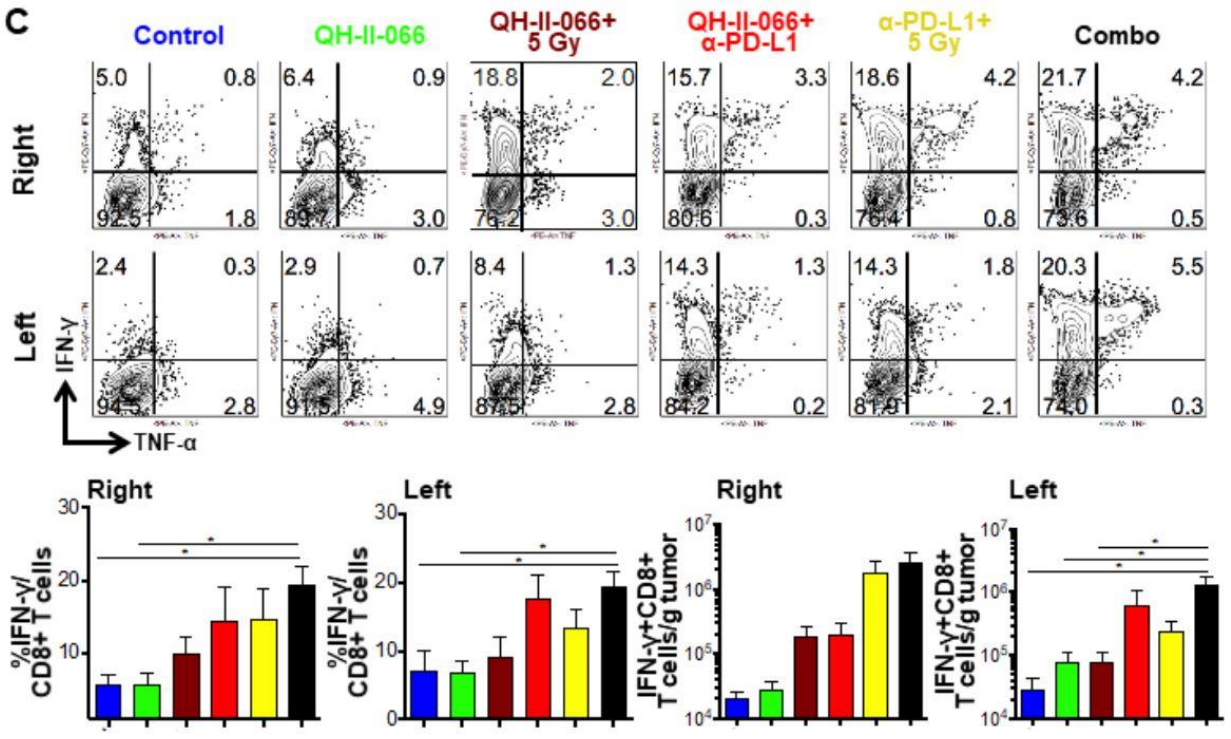


**Figure 80. Top and Middle, Representative flow showing percent IFN-γ and TNF-α in total CD8+ T cells after TILs were stimulated with peptide as described in materials and methods. IFN-γ and TNF-α were stained with appropriate antibodies by intracellular staining. Bottom, Graph summarizing the percent IFN-γ+CD8+ of total CD8+ T cells and number of IFN-γ+CD8 T+ cells per gram of tumor.**

### 2. 2. 1. 7 Immunophenotyping treated tumors.

To determine whether the apparent synergistic effect of benzodiazepine QH-II-066 plus radiation (10 or 5 Gy) and/or α-PD-L1 was mediated by an enhanced immune response, one performed immunophenotyping of bilateral tumors (**Figure 70 and 74; Figure 76 and 77); Figures 78, 79 and 80**). Compared to the control, QH-II-066 and radiation (5 or 10 Gy) monotherapies resulted in significantly increased numbers of tumor-infiltrating lymphocytes (TILs) in both ipsilateral and contralateral tumors. The dual therapy of QH-II-066 and radiation (5 or 10 Gy) results in a particularly pronounced increase in numbers of TILs in contralateral tumors, as compared to

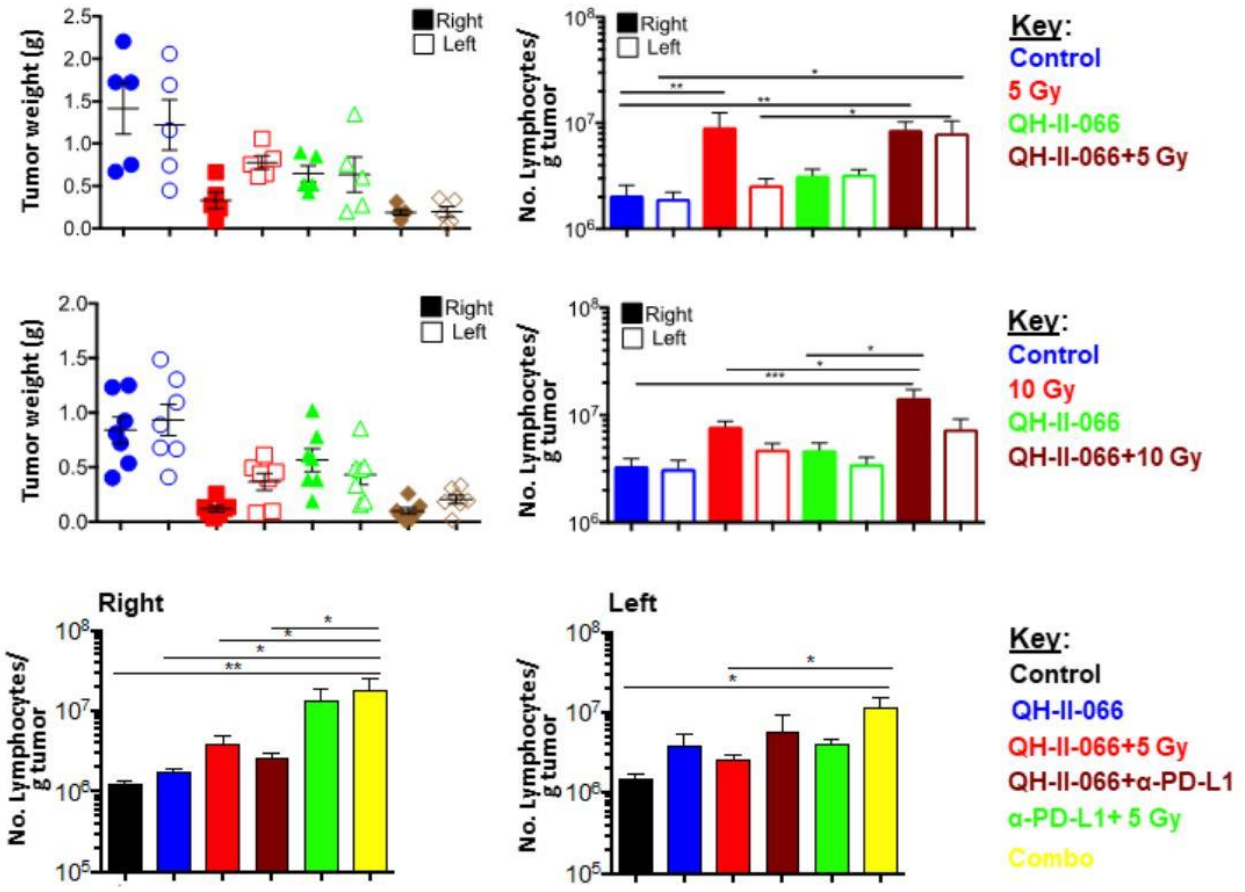


**Figure 81. Tumor Weights and total number of lymphocytes per tumor with different treatments. Tumor weight and total lymphocyte numbers per gram of tumor on the right and the left sides for monotherapy, dual, and combo therapies, as indicated. Mice were sacrificed and tumors excised at the end of the experiment, 8 days after radiation treatment. Cells were isolated as described in Materials and Methods. The cells were counted using count bright absolute counting beads and analyzed on BD FACSCanto II.**

either radiation or QH-II-066 monotherapies. This effect appears most pronounced at the lower radiation dose (5 Gy) administered. Compared to the control, monotherapy, and dual therapy, the combo therapy resulted in significantly increased numbers of TILs in both ipsilateral and contralateral tumors.

The total number of CD8+ T cells increased with radiation (10 or 5 Gy) in the ipsilateral tumor, as compared to the contralateral tumor. When QH-II-066 was

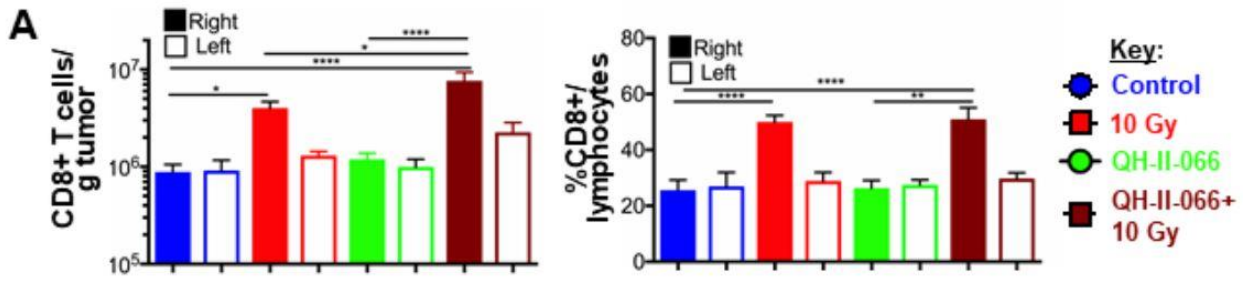


**Figure 82. Immune response to benzodiazepine and 10 Gy radiation. (A) Graphs showing number of CD8+ T cells per gram of tumor and percent CD8 T cells of total lymphocytes. (*$p$<0.05; **$p$<0.01; ***$p$<0.001; ****$p$<0.0001).**

combined with radiation, there was a comparable increase in the total number of CD8+ T cells in both ipsilateral and contralateral tumors. While the number of CD8+ T cells increase in number in this treatment group, the overall portion of lymphocytes that are CD8+ T cells does not show a significant increase, indicating that QH-II-066 may elicit an infiltration of other immune cells into the tumor. While the total number of CD8+ T cells increased with radiation (10 or 5 Gy) alone and the dual combination of QH-II-066 plus radiation or α-PD-L1 in the ipsilateral tumor, GP33-antigen specific CD8+ cells significantly increased in both ipsilateral and contralateral tumors only in the dual or combo therapy groups, indicating a potent tumor-specific immune response (**Figure 81**). **This is extremely important in terms of potential treatment of patients.**

Examination of the polyfunctionality of the CD8+ T cells reveals that the frequency of interferon-γ (IFN-ɣ) and IFN-ɣ/tumor necrosis factor-α (IFN-ɣ/TNF-α) producing CD8+ T cells were most significantly increased in both ipsilateral and contralateral tumors treated with dual and combo therapies (**Figure 70C; Figure 80**), indicating an increase in antigen-specific, polyfunctional effector T cells. QH-II-066 has a significant effect on the numbers and frequency of IFN-ɣ and IFN-ɣ/TNF-α producing CD8+ T cells on contralateral tumors treated with radiation (5 or 10 Gy). Together, these results indicate that QH-II-066 has direct anti-tumor activity, while

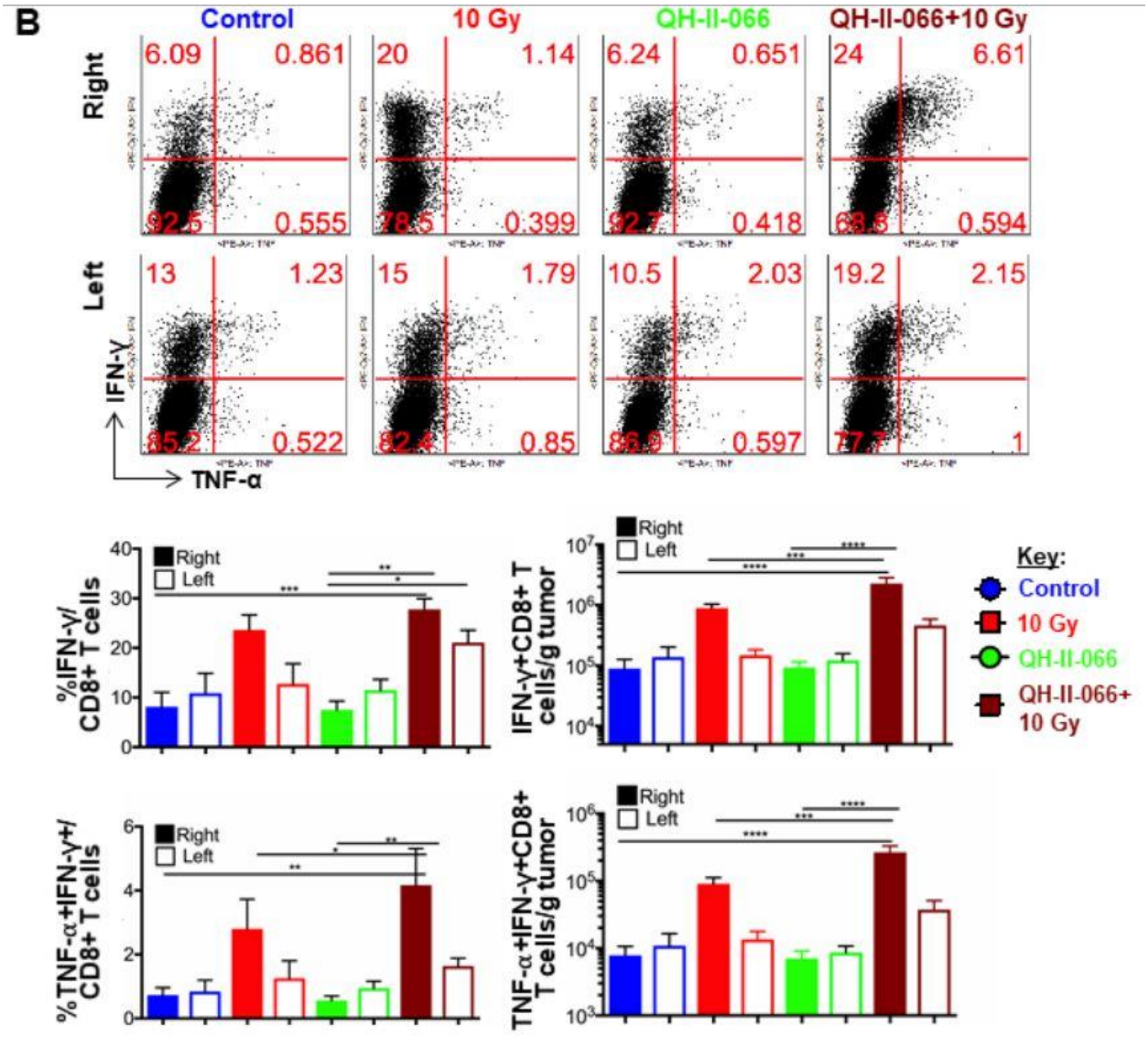


**Figure 83. Immune response to QH-II-66 and 10 Gy radiation. Representative flow plots showing percent TNF-*α*+ and IFN-γ+ CD8+ T cells. The cells were stimulated with GP33-41 peptide as described in the Methods section of the text. The graphs summarize the results of the flow plots and show number per gram of tumor. The graphs are a mean from 8-10 mice from two experiments. (**p*<0.05; ***p*<0.01; ****p*<0.001; *****p*<0.0001). Methods used were as detailed in the Methods section of text.**

a **dual or triple combination with QH-II-066 has synergy with ipsilateral and abscopal anti-tumor activity mediated by an increase in antigen-specific effector CD8+ T cells.**

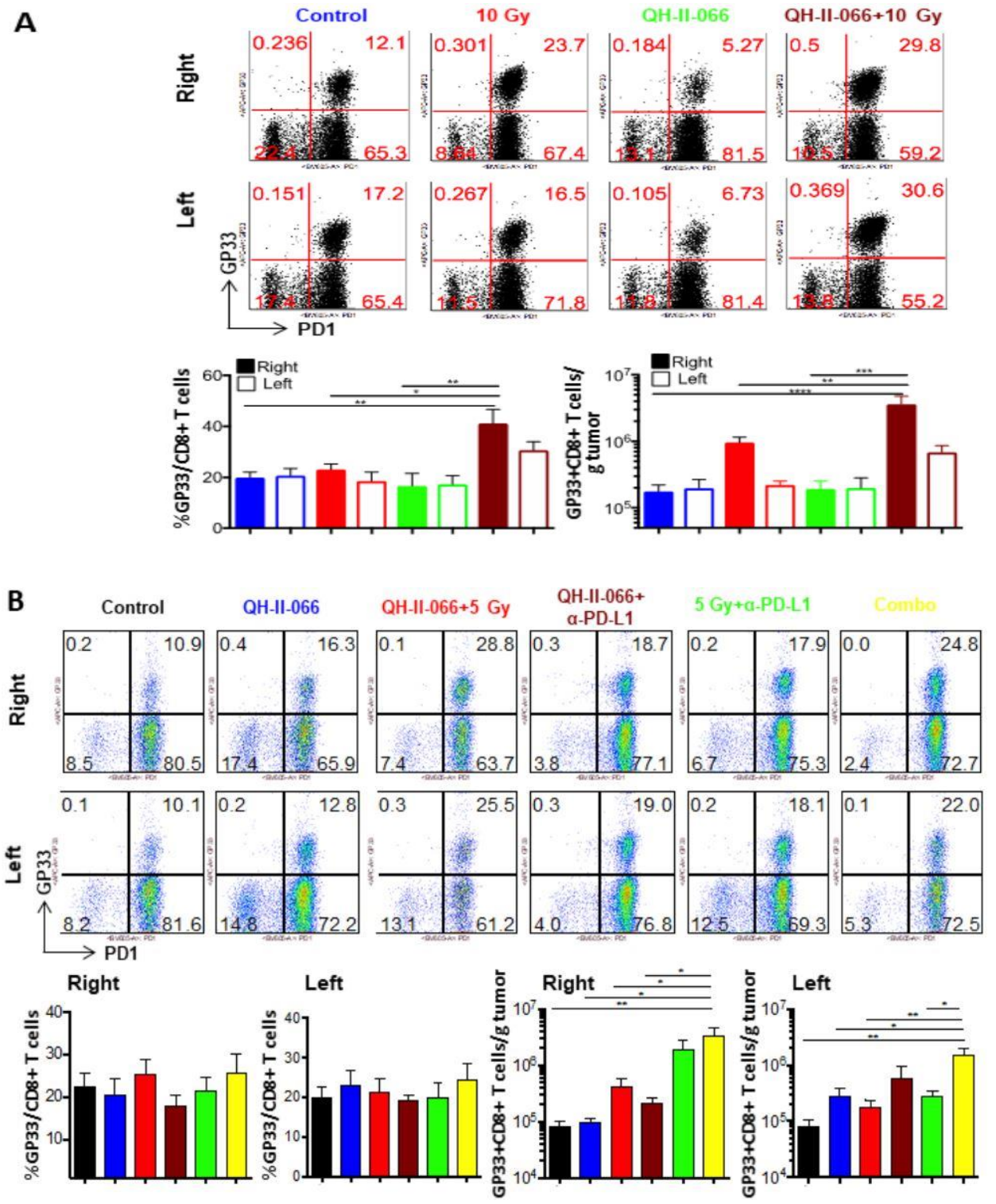


**Figure 84. Increase in antigen specific CD8 T cells by QH-II-66 and 10 Gy radiation. (A & B) Representative flow plots showing percent GP33+PD1+ CD8+ T cells among CD8+ T cells. The graphs summarize the results of the flow plots and show the number of GP33+CD8+ T cells per gram of tumor. The graphs are mean from 8-10 mice from two experiments. (*$p$<0.05; **$p$<0.01; ***$p$<0.001). Methods used were as detailed in the Methods section of text.**

### 2. 2. 2 Discussion

Here, it is shown that melanoma cell lines, both human and murine, express functional $GABA_AR$s that are activated by the ligand/agonist GABA, and this is enhanced by specific anticancer benzodiazepines, positive allosteric modulators of the ion channel. These observations are consistent with the GABAAR in melanoma cells forming a hetero-pentameric structure with a canonical αβαβɣ subunit stoichiometry. It is shown that the benzodiazepine QH-II-066 (**8**) is capable of directly impairing the viability of melanoma cells *in vitro*, while reducing tumor volume in a syngeneic melanoma model, even at a benzodiazepine dose comparable to that administered for adult human patients for a wide range of clinical conditions, including anxiety. We also find that QH-II-066 (**8**) potentiates radiation, even at a sub-optimal dose, and also the immune checkpoint inhibitor α-PD-L1, to enhance both ipsilateral and distant abscopal anti-tumor responses. The response is associated with enhanced tumor infiltration of CD8+ T cells that produce IFN-γ and TNF-α. There is also enhanced expression of genes with roles in cytokine:cytokine receptor activity, transcription factors in the p53 pathway (notably p63), and genes concordant with microRNA mir-17 overexpression. At this point in time, a more detailed understanding of the underlying molecular mechanism of beneficial anticancer benzodiazepine mediated potentiation of radiotherapy and immune checkpoint inhibition in melanoma tumor cells is necessary, but QH-II-66 (**8**) mediated enhancement in expression of cytokine:cytokine receptor activity may be pivotal.

From the findings reported here and elsewhere, we hypothesize that a benzodiazepine may contribute to regression of melanoma tumors by direct and indirect mechanisms. In the ‘direct’ contribution to tumor control, QH-II-66 (**8**) enhanced membrane anion permeability in melanoma tumor cells, which depolarizes their mitochondria, as we observed in cell culture

experiments, and thereby elicits an apoptotic response. Depolarization of mitochondria may result in an opening of the permeability transition pore, commensurate with dysregulation of $Ca^{2+}$ homeostasis; defective respiration, commensurate with depletion of ATP; increase in reactive oxygen and nitrogen species; and cytochrome *c* release.[222] In the studies of medulloblastoma cell response to QH-II-66, it was found that the intrinsic mitochondrial mediated apoptotic pathway is activated.[219] As noted, perturbation in ion homeostasis may also underly the enhanced expression of genes involved in the p53 pathway signaling and cytokine:cytokine receptor activity and signaling which we find in the treated tumors. We find enhanced expression of p63 target genes in all treatment groups in comparison to the control. **Increased p63 expression after genotoxic treatment of melanoma cells has been observed and shown to interfere with p53 mediated apoptosis by the mechanism that involves mitochondrial translocation[32]**. The increase of p63 expression was comparable in both radiation and combined QH-II-066 plus radiation treated samples, but it is plausible that depolarization of mitochondria by QH-II-066 interferes with the anti-apoptotic function of the p63 protein**. Interestingly, breast cancer tumors exhibit enriched IFN-γ signaling that is associated with enhanced p63 expression[223], highlighting an important connection between p63 and immune signaling.** Further, p63 has been reported to suppress both tumorigenesis and metastatic spread in a murine model by mediating down-regulation of the microRNA processing enzyme Dicer as well as the 'oncomiRNA' miR-130b.[35] The observation that there is enhanced expression of genes associated with overexpression of the microRNA mir-17 is intriguing, as *MIR17* expression has also been shown to be enhanced by p63. **It may be that p63 enhanced expression in melanoma cells regresses the tumors in part by controlling Dicer and miRNA activity.**

In the ‘indirect’ mechanism to tumor control, the benzodiazepine QH-II-066 may enhance CD8+ T cell infiltrate into the melanoma tumor milieu to contribute to potentiating the response to radiation and immune checkpoint inhibition. As noted, QH-II-066 has a small effect on cell viability *in vitro*, as assessed by its micromolar IC50, while *in vivo,* when administered in combination with radiation and/or an immune checkpoint inhibitor, or even on its own at a higher dose, regresses the melanoma tumors. This observation suggests that the benzodiazepine at a lower dose is acting as a ‘sensitizer’ and at a higher dose (25 mg/kg once daily) is acting through another mechanism, perhaps by positively modulating GABAAR receptors on CD8+ T cells[37]. Indeed, GABAARs have been reported to be expressed in CD8+ T cells (as well as in neutrophils, monocytes, CD3+ and CD4+ T cells) and GABAergic signaling has been observed to contribute to responses to intracellular pathogens[227] and autoimmune diseases[228]. However, it remains unclear whether GABAAR may mediate directly in enhancing T cell infiltration into the tumor and/or whether the receptor can modulate co-inhibitory checkpoints. **It can not be overlooked that QH-II-66 (8), KRM-II-08 (19) and their analogs go through BBB in 20 to 30 minutes in contrast to other anticancer agents. Moreover, the anxiolytic and slight sedative activity (Cook et al, US Patent 2006) would be a positive effect to patients undergoing radiation therapy or any anticancer treatment.**

The results of this study suggest that use of QH-II-66 (**8**) or analogs to modulate GABAAR as a ‘sensitizer’ of melanoma tumors to radiation and/or an immune checkpoint inhibitor is a future avenue to explore clinically. Repurposing of a benzodiazepine in such therapeutic combinations have the potential to improve outcomes for patients in a rapidly translatable and cost-effective manner. QH-II-066 (**8**) exhibits anxiolytic activity and has been shown to be safely administered in non-human primates and has a penetrance through the blood-brain barrier

equivalent to diazepam.[216,220,230,231] Hence, while additional preclinical evaluation is necessary, this study suggests that clinical investigation of QH-II-66 (**8**) or analog-based combination therapies are warranted. Examination of QH-II-066 (**8**) to amplify immune checkpoint inhibition is an important finding here. Finally, QH-II-066 (**8**) may be particularly effective in tackling the challenging melanoma metastatic lesions that form throughout the body, including to the brain in ~50% of these patients, as well as and obviously serving to remedy the anxiety that such patients experience.

### 2. 2. 3 Materials and Methods by Dr. Kallay, Kamdem, Dr. Krummel and Dr. Sengupta (University of Cincinnati).

#### 2. 2. 3. 1 Cell lines.

Human melanoma cell line A375 and murine line B16F10 were purchased from American Type Culture Collection (ATCC, Manassas, VA). The B16F10 line was transduced according to manufacturer instructions (Clontech) with lentiviral vector expressing Lymphocytic choriomeningitis (LCMV) Glycoprotein (GP). The genome was engineered to express GP protein together with green fluorescent protein (GFP). This engineered line is referred to as B16F10-GP throughout the text. The cell lines were tested for pathogen contamination to ensure an absence of all major viruses and mycoplasmas, according to past instructions.

#### 2. 2. 3. 2 Electrophysiology.

Electrophysiology recordings utilized methods like those described in the past publications.[30,43] Intracellular saline solution contained 145 mM CsCl, 2 mM CaCl2, 2 mM MgCl2, 10 mM EGTA and 10 mM HEPES. Extracellular saline solution contained 140 mM NaCl, 5mM KCl, 2 mM CaCl2, 1 mM MgCl2, 10 mM HEPES and 10 mM D-glucose. Both salines were adjusted to pH 7.4 (320-330 mOsm) and 0.2 μm filter sterilized. A375 and B16F10-GP cells were dissociated

with detachin (Genlantis, San Diego, CA), resuspended in extracellular saline (2.5x106 cells/mL) and agitated prior to loading on to 384-well fluxion ensemble plates. $GABA^{17}$ concentration response relationships were constructed by measuring responses to 0.03, 0.1, 0.3, 1, 3, 10 and 30 μM GABA. Benzodiazepine concentration-potentiation relationships were constructed by measuring responses to 1 μM GABA in the absence and presence of 0.03, 0.1, 0.3, 1, 3, and 10 μM of QH-II-066 or KRM-II-08. Cells were patched using an Ionflux Mercury microfluidic automated patch clamp system (Fluxion Biosciences, Alameda, CA). Up to 1,280 cells were patched at -60 mV using an automated suction protocol, followed by superfusion with ligand and drug combinations. Current data was recorded at 10 kHz and stored for offline analysis with bespoke MatLab scripts.

#### 2. 2. 3. 3 Cell viability.

The A375 and B16F10-GP cells were cultured in DMEM (Corning CellGro) containing 10% FBS (GIBCO), L-glutamine 1x (GIBCO), and penicillin-streptomycin solution 1x (GIBCO). Cells were used in early passage (fewer than 25 passages after resuscitation) and were negative for Mycoplasma. For cell viability dose-response assays, cells (1500 for B16F10-GP; 2000 for A375) were seeded (75 μL per well) in a 96-well flat bottom cell culture plate (Falcon) and incubated at 37°C (5% $CO_2$) for 16 hours in HEPES and phenol-red-free 1X Dulbecco modified eagle's medium (DMEM, Gibco) with L-glutamine and sodium pyruvate, penicillin-streptomycin, and 10% FBS. Benzodiazepines were synthesized as described[214-216], kept lyophilized at room temperature, and suspended prior to use in dimethyl sulfoxide (DMSO; 0.125%) to prepare a 40 mM stock solution. Drug was added to plated cells in 25 μL aliquots to prepare final concentrations in pentaplicates (0.3125, 0.625, 1.25, 2.5, 5.0, 10, 20, and 30.0 μM). After a 24- or 48-hour incubation of drug with cells or a DMSO vehicle control at 37°C (5% $CO_2$), 20 μL CellTiter 96®

AQueous One Solution (Promega) was added per well, after which the plate was incubated 1 hour at 37°C, and absorbance (490 nm) was measured to quantify cell viability. To calculate % cell viability, media control (average reading of wells containing only media) was subtracted from DMSO control and drug-treated values. Drug-treated values were normalized by dividing by mean DMSO absorbance values and converting to percent. IC50 values were obtained using GraphPad Prism 7 (GraphPad Software Inc., La Jolla, CA). All graphs were produced in GraphPad Prism 7.

#### 2. 2. 3. 4 Mouse experiments at the University of Cincinnati.

The B16F10-GP cell line was grown in Dulbecco's Modified Eagle's medium (DMEM) supplemented with 10% Fetal Bovine Serum, 100 U/mL penicillin and 100 µg/mL streptomycin, with 2 mM glutamine. Cells were cultured at 37ºC with 5% $CO_2$. The B16F10-GP melanoma cells (5 x 105) were implanted in matrigel (25%) on the right and left flank of 6–8-week-old female C57BL/6 mice (Jackson Laboratories, Bar Harbor, ME). Mice were used in accordance with the Emory University Institutional Animal Care and Use Committee guidelines. After the tumors were palpable (10 days), mice were irradiated on the right side with a Superflab bolus (0.5 cm tissue equivalent material) placed over the tumor, and thereafter tumor measurements taken as indicated. Measurements of the left tumor are indicative of an abscopal response. Irradiation was done using an X-RAD 320 irradiation unit; a self-contained X-ray system for delivering a precise radiation dosage. The shielded cabinet includes an Adjustable Specimen Shelf, Sample Viewing Window and Beam Hardening Filter Holder. The light beam (< 8 mm2) was focussed on the tumor (right flank only) and mice were irradiated while under anesthesia. Tumor diameters were measured using calipers. Tumor volume was calculated using the formula for an ellipse (i.e. 4/3π.(l.w.h), where l, w, h are three radii of the tumor taken perpendicullar to each other).

Treatment of mice with α-PD-L1 or QH-II-066 occurred after 10 days tumor inoculation, as detailed in legends of relevant Figures. The α-PD-L1 antibody (200 µg; clone 10F9.G2) was in phosphate buffer saline (500 µL) and injected i.p. every third day per the protocol, as antibody levels decrease and need to be maintained at a constant level. QH-II-066 was dissolved in 1% DMSO and 0.5% Tween-20 as well as water, and injected i.p. at the indicated doses daily for a week. Control mice in the experiments were injected i.p. with vehicle for a week.

#### 2. 2. 3. 5 Tumor infiltrating lymphocytes (TILs) isolation and flow cytometry.

For flow cytometric analysis, tumors were harvested 7-8 days after radiation. Single cell suspensions of tumors were prepared by mincing the tumors with scissors and digesting them with collagenase IV (150 U/mL) and DNAse (20 µg/mL) for one hour under shaking. The cells were centrifuged and suspended in 195% RPMI. The cell suspension was layered on top of histopaque (Sigma). After centrifugation, the TILs were collected at the interphase and stained with markers of interest. All samples were run on LSRII (BD) or BD FACSCanto and analyzed using FlowJo software. For intracellular cytokine analysis, TILs were isolated from the tumor and stimulated for 6 hours in the presence of brefeldin and myostatin with a LCMV specific glycoprotein peptide GP33-41 and stained with antibodies of interest and analyzed by flow cytometry.

#### 2. 2. 3. 6 RNA-seq and data analysis.

Tumors were excised from mice, immediately snap frozen in liquid nitrogen, and then stored at -80°C. RNA was extracted (Qiagen, AllPrep FFPE kit), quantified, and then quality measured using the DV200 score (fraction of RNA fragments whose length is > 200 nucleotides). The samples used met the following requirements: ≥750 ng RNA, a preferred concentration 10 ng/µL, DV200 > 0.3). Samples (n=4 per treatment group) were processed and

sequenced at the Broad Institute by the Transcriptome Capture method using Illumina HiSeq2500. Sequence reads were aligned to the reference mouse genome (mm10) using the STAR aligner[233], reads aligning to each known gene were counted using featureCounts.[45] The differential expression analysis between different sample types was performed based on the negative-binomial statistical model of read counts as implemented in the edgeR Bioconductor package46 and p-values were adjusted using False Discovery Rates (FDR).[236] The enrichment KEGG pathways[237], transcription factor targets[238], and ImmuneSigDB gene sets[239] were identified using the gene set enrichment analysis[240] as implemented in the FGSEA R package[241] with 100,000 random permutations. Results were visualized using the ComplexHeatmap package. [242]

## 2. 3 Activity of analogs and metabolites of QH II 66 in H1792 lung cancer cell lines.

Some anticancer benzodiazepine-target analogues and metabolites were synthesized and tested in H1792 cell lines. H1792 cell lines are related to non-small cell lung cancer such as adenocarcinoma. These types of lung cancers are among the most aggressive type of lung cancers and lead to many patient fatalities.

### 2. 3. 1 Direct analogue of QH II 66

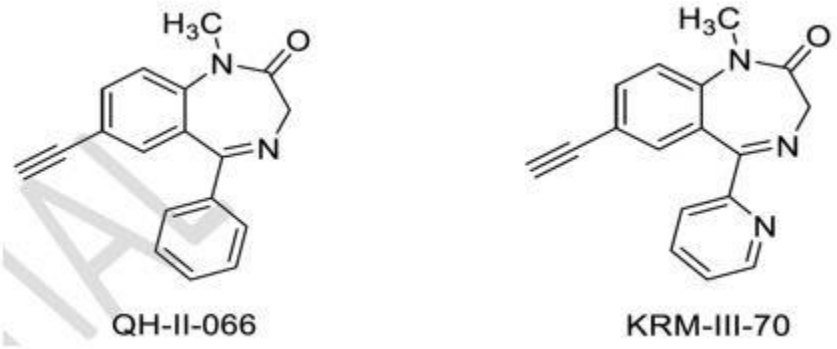


**Figure 85. Structures of QH II 66 and KRM III 70**

QH II 66 and KRM III 70 were tested in the cell viability assay on the H1792 cell line. The $IC_{50}$ of QH II 66 was between 5.523 μM to 6.563 μM. The average $IC_{50}$ was 6.027 μM. **(Figure 86)** On the other hand KRM III 70 showed an $IC_{50}$ value 4.474 μM to 6.107 μM. The average $IC_{50}$ value was 5.240 μM. **(Figure 87)** Based on this data KRM III 70 shows better results in comparison with QH II 66. KRM III 70 has a nitrogen at the 2' position of the C-5 pendant phenyl ring, whereas QH II 66 has a 2'H at this position.

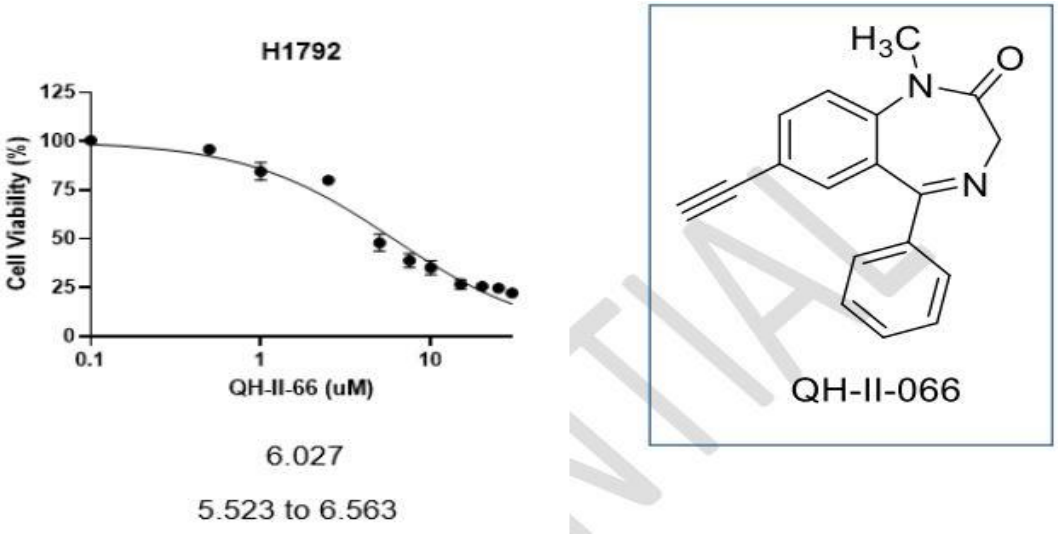


**Figure 86. Cell viability assay for QH II 66 in the H1792 lung cancer cell line. Data unit is μM.**

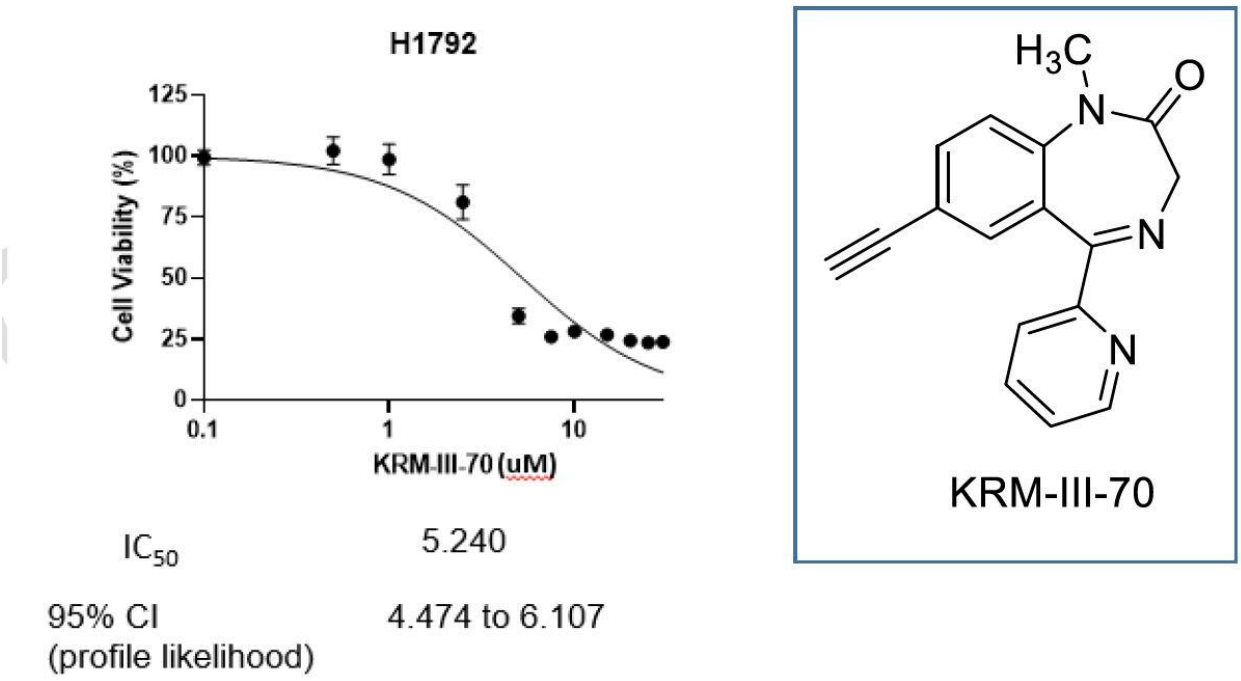


**Figure 87. Cell viability assay for KRM III 70 in H1792 lung cancer cell line. Data unit is µM.**

### 2. 3. 2 Deuterated analogues of QH II 66

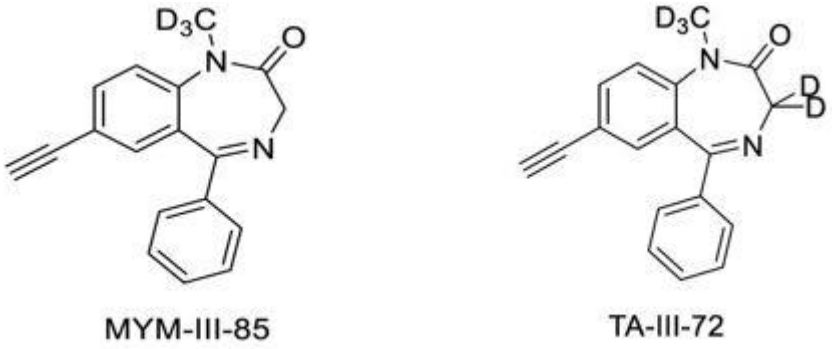


Two deuterium compounds, **TA III 72** and **MYM III 85** were synthesized and analyzed in the lung cancer cell viability assay. TA III 72 has 5 deuterium atoms and MYM III 85 has three deuterium atoms as N-$CD_3$. The C-D bonds are nine times stronger than a C-H bond. After analysis on the lung cancer cells the $IC_{50}$ value for **TA III 72** was in the range from 5.069 µM to 6.483 µM. The average $IC_{50}$ was 5.741 µM and was close to the $IC_{50}$ obtained for QH II 66 and KRM III 70 (**Figure 85**). The $IC_{50}$ value for **MYM III 85** range from 5.903 µM to 7.460 µM and the average

was 6.644 μM which indicates this compound is also active against metastasis in the H1792 lung cancer cell line. (**Figure 86**)

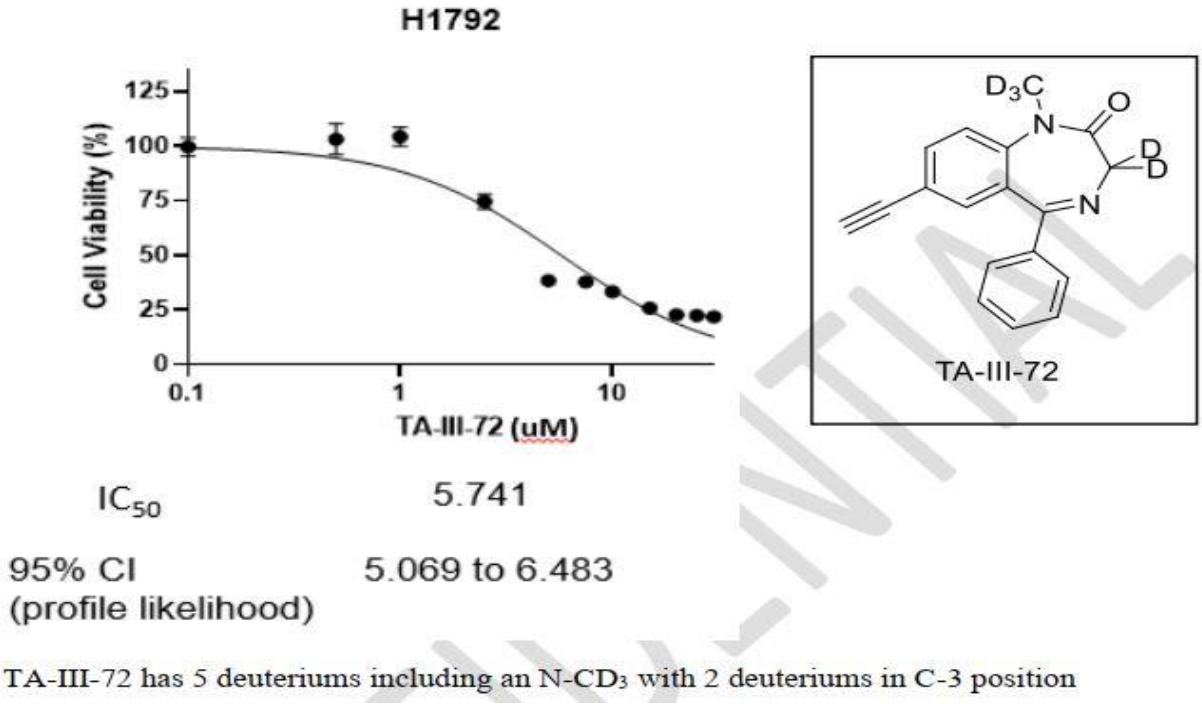


**Figure 88. Cell viability assay for TA III 72 in the H1792 cell line. Data unit is μM.**

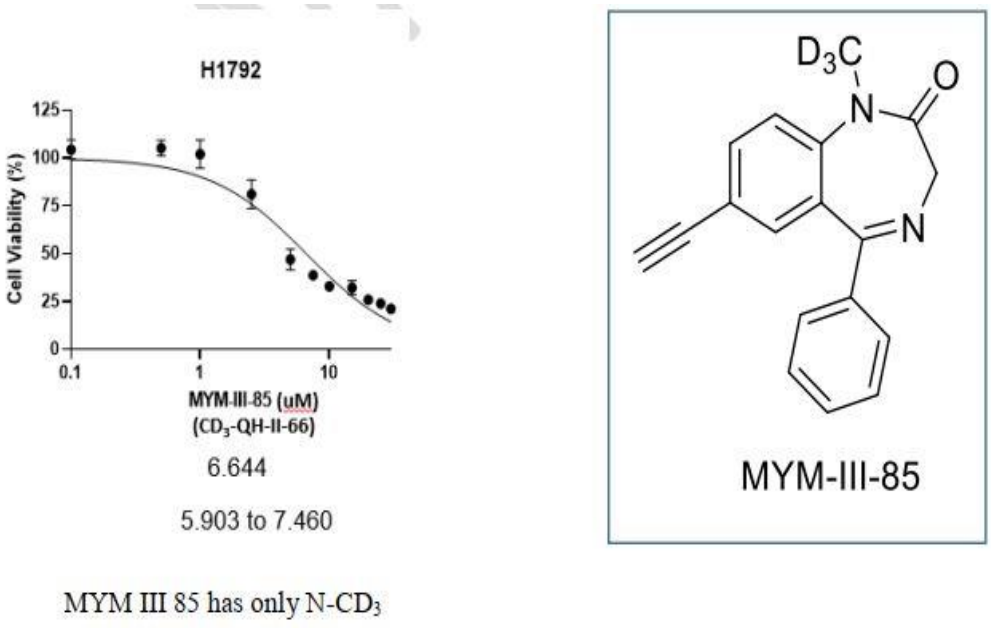


**Figure 89. Cell viability assay for MYM III 85 in the H1792 cell line. Data unit is μM.**

### 2. 3. 3 Metabolites of QH II 66 analogs.

Benzodiazepines are normally metabolized at two different sites. If it is a N-CH3 benzodiazepine it become a desmethyl benzodiazepine by N-desmethylation of the N-CH3 group. In the next step this desmethyl intermediate can be converted to a 3-hydroxy desmethylbenzodiazepine metabolite. They can also form 3-hydroxy intermediates and then undergo desmethylation. Even if the chiral 3-hydroxy metabolite is formed it racemizes very readily. Four of the QH II 66 analog metabolites were assayed to observe their activity in H1792 lung cancer cell lines.

**MYM I 43** was tested in the cell viability assay on the H1792 cell line. The $IC_{50}$ of **MYM I 43** was in between 63.19 μM to 179.3 μM. The average $IC_{50}$ was 95.70 μM. **(Figure 90)**

**MYM IV 95** was tested in the cell viability assay on the H1792 cell line. The $IC_{50}$ of **MYM IV 95** was in between 391.8 μM to 2643 μM. The average $IC_{50}$ was 694.9 μM. **(Figure 91)**

**MYM V 17** was tested in the cell viability assay on the H1792 cell line. The $IC_{50}$ of **MYM V 17** was in between 18.01 μM to 22.97 μM. The average $IC_{50}$ was 20.32 μM. **(Figure 92)**

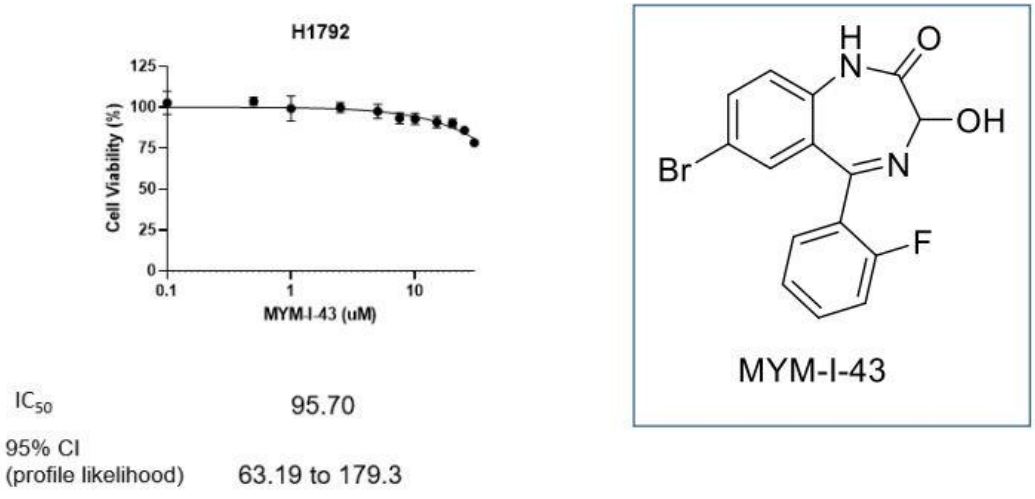


**Figure 90. Cell viability assay for MYM I 43 in H1792 cell line. Data unit is μM.**

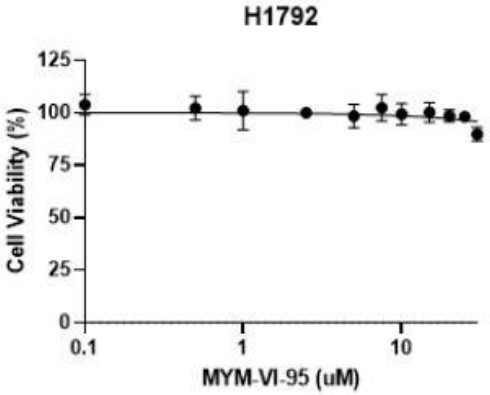


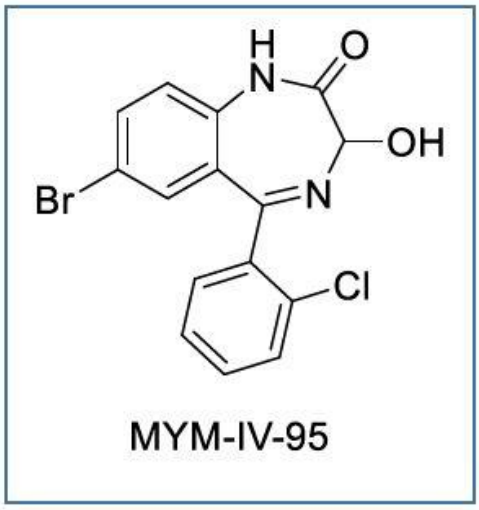


| | |
|---|---|
| $IC_{50}$ | 694.9 |
| 95% CI (profile likelihood) | 391.8 to 2643 |

**Figure 91. Cell viability assay for MYM IV 95 in H1792 cell line. Data unit is µM.**

**MYM I 59** was tested in the cell viability assay on the H1792 cell line. The $IC_{50}$ of **MYM I 59** was infinity which means this compound is inactive against this type of cancer. **(Figure 93)**

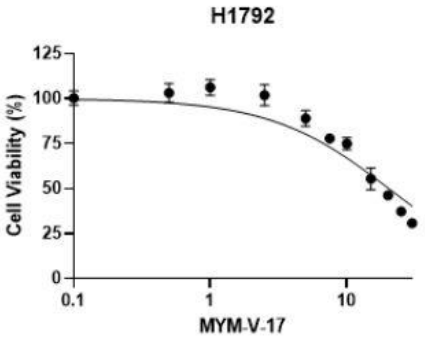


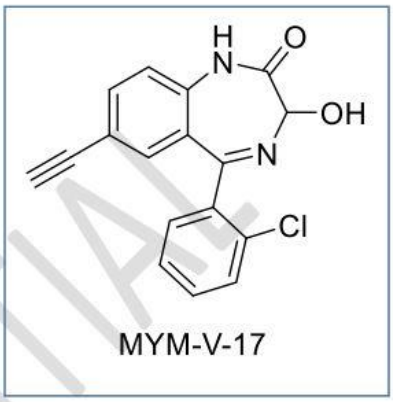


| | |
|---|---|
| | 20.32 |
| | 18.01 to 22.97 |

**Figure 92. Cell viability assay for MYM V 17 in the H1792 in the cell line. Data unit is µM.**

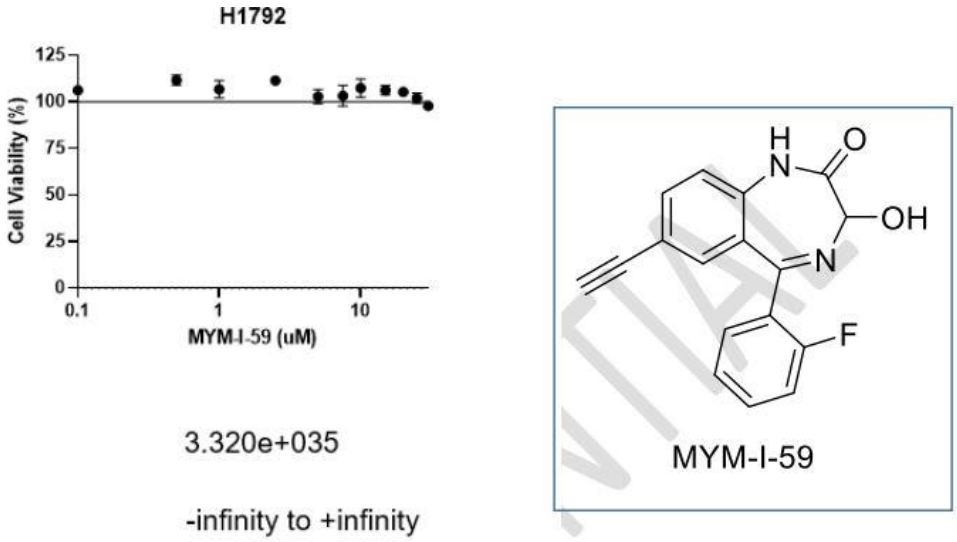


**Figure 93. Cell viability assay for MYM 1 59 in the H1792 cell line. Data unit is µM.**

**TA III 70** was tested in the cell viability assay on the H1792 cell line. The $IC_{50}$ of **TA III 70** was in between 100.3 µM to 212771 µM. The average $IC_{50}$ was 660.2 µM. **(Figure 94)**

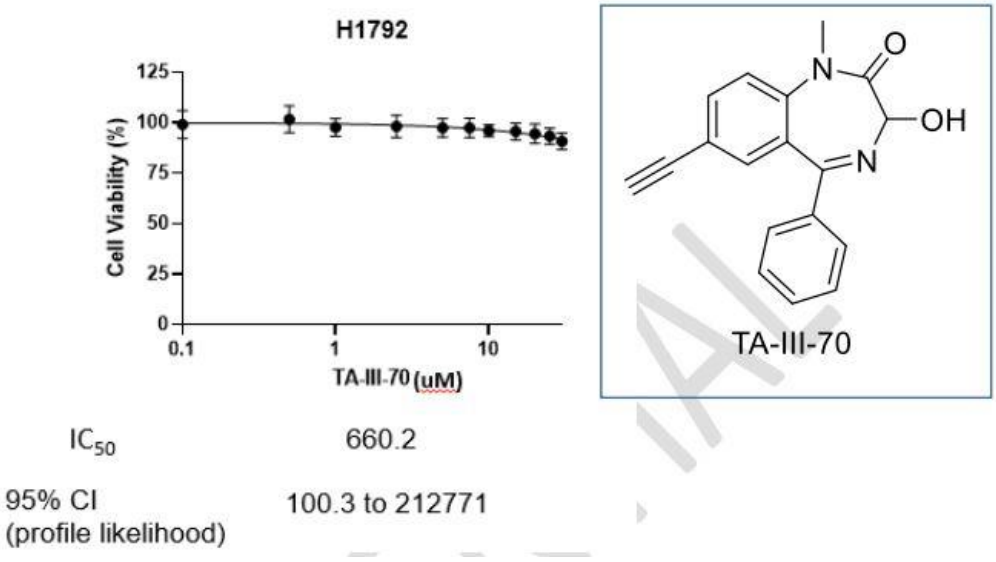


**Figure 94. Cell viability assay for TA III 70 in the H1792 cell line. Data unit is µM.**

A difference between the activity of these compounds or duration of action might be realized in vivo in rodents. Since these are in vitro screens the similar activity of QH-II-66, KRM-II-08, TA-III-72 and MYM-III-85 are expected.

### 2. 3. 4 Thio analogues of QH II 66.

Two thio analogues TA III 50 and TA III 52 of QH-II-66 were synthesized and tested on H1792 the lung cancer cell lines. TA II 52 contains a 2'H substituent and TA III 50 bears a 2'F group. The $IC_{50}$ value range of TA III 50 was from 35.9 μM to 48.9 μM over three trials. (**Figure 95**)

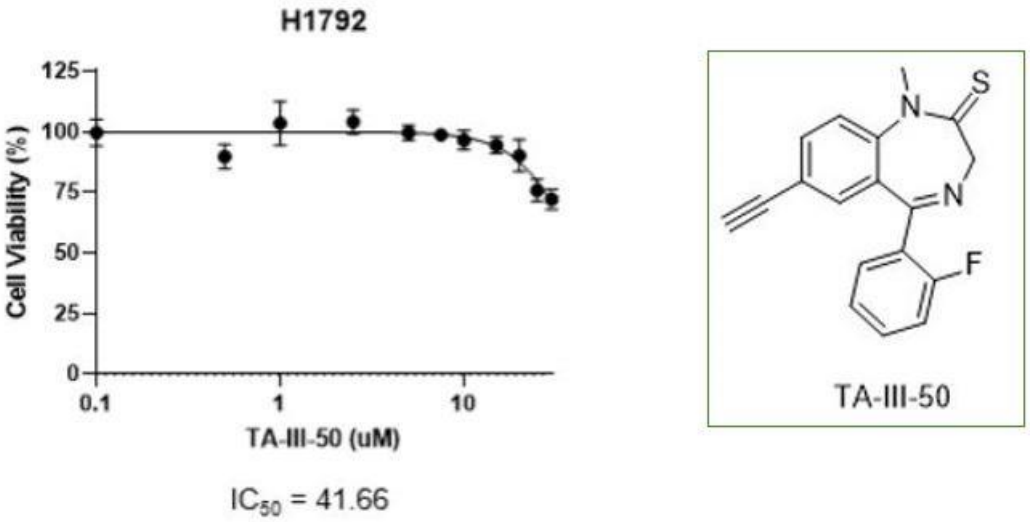


**Figure 95. Cell viability assay for TA 1II 50 on the H1792 cell line. Data unit is μM.**

For TA III 52 the $IC_{50}$ value ranges from 28.7 μM to 38.2 μM over three trials. (**Figure 96**).

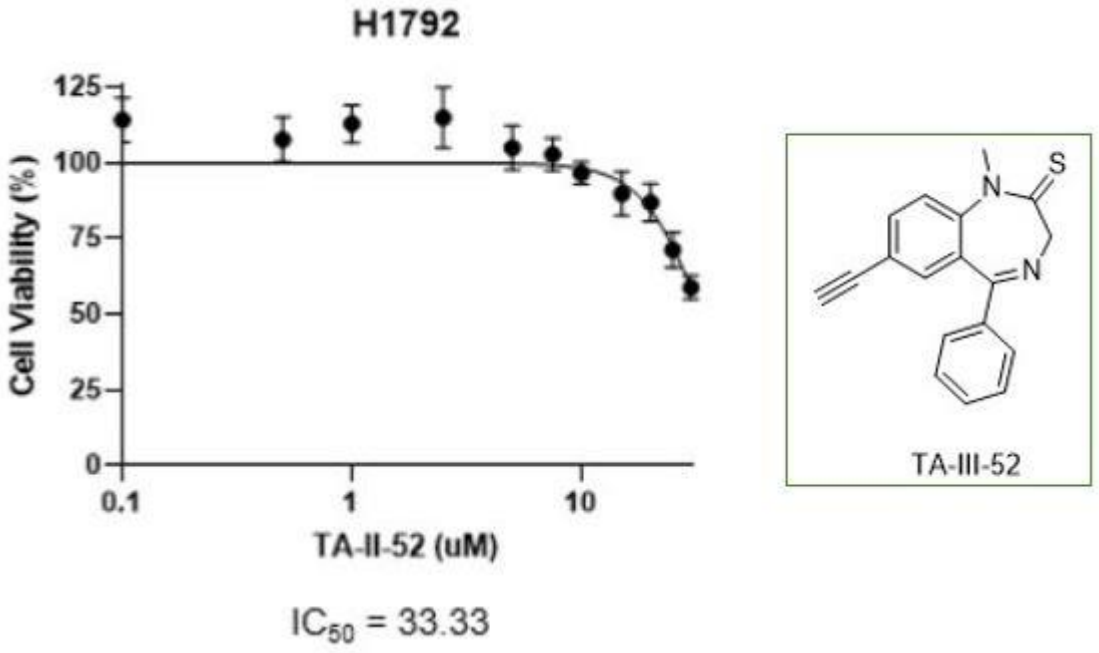


**Figure 96. Cell viability assay for TA 1II 52 on the H1792 cell line. Data unit is µM.**

## 2. 3. 5 Bis-ethnyl and Bis-bromo analogues of QH II 66.

Two other analogues TA III 56 and TA III 62 of QH-II-66 were synthesized and tested in H1792 cell lines. TA III 56 contains two bromine atoms at the C-5 and C-7 positions. The corresponding TA III 62 bears two acetylene groups at the C-5 and C-7 positions. The $IC_{50}$ value range of TA III 56 was from 36.1 µM to 43.0 µM over three trials. (**Figure 97**) The $IC_{50}$ value range of TA III 62 was from 144.3 µM to 297.2 µM over three trials. (**Figure 98**)

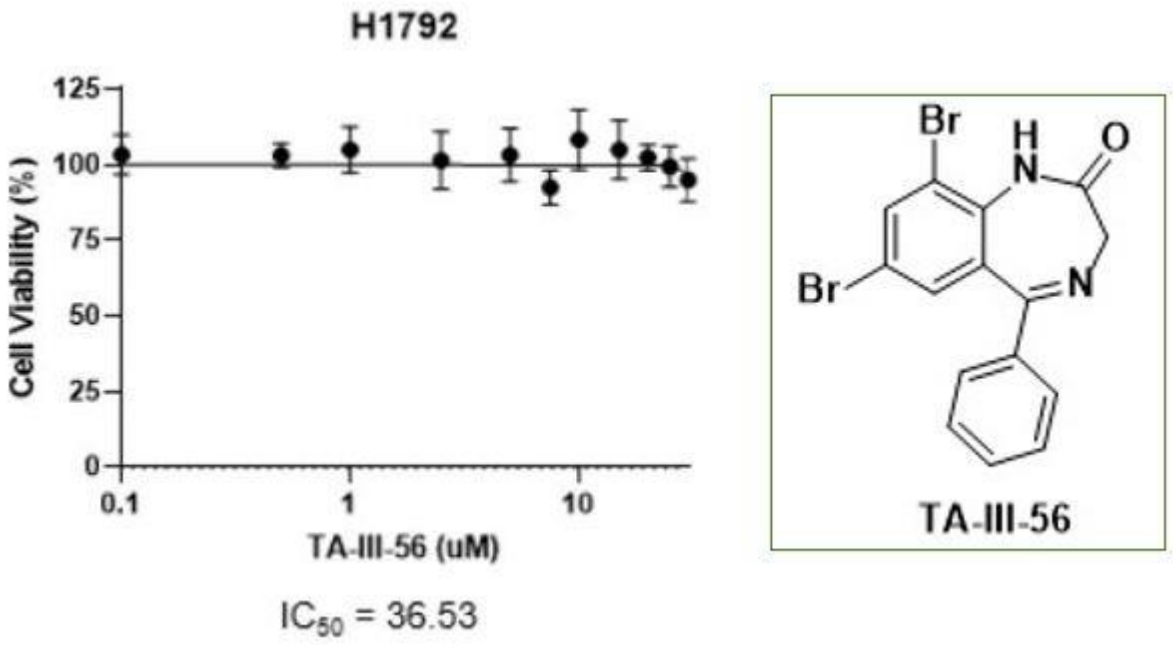


**Figure 97. Cell viability assay for TA 1II 56 on the H1792 cell line. Data unit is µM.**

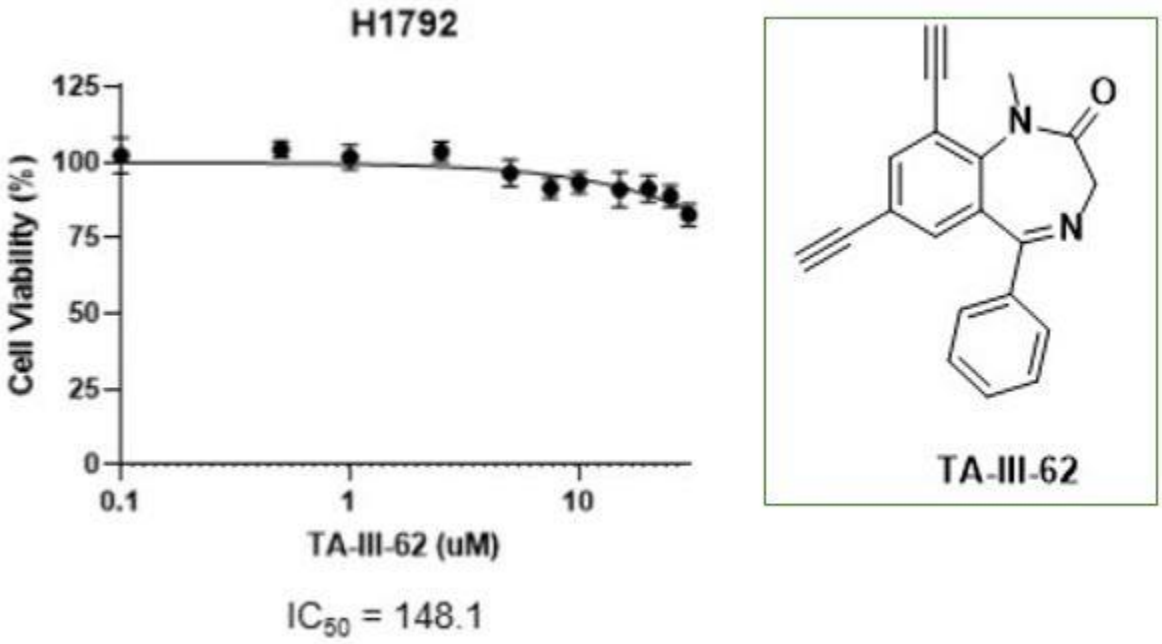


**Figure 98. Cell viability assay for TA 1II 62 in the H1792 cell line.**

## 2. 4 Chemistry

### 2. 4. 1 Synthesis of QH II 66

The ethinyl benzodiazepine QH II 66 (**8**) is the lead compound in this research. This compound showed very good activity in lung cancer H1792 cell lines, medulloblastoma G3 D283 cell lines and two melanoma cell lines A375 and B16F10. After obtaining excellent data on different cancer cell lines, it was decided to develop a synthetic route to synthesize QH II 66 (**8**) on large scale.

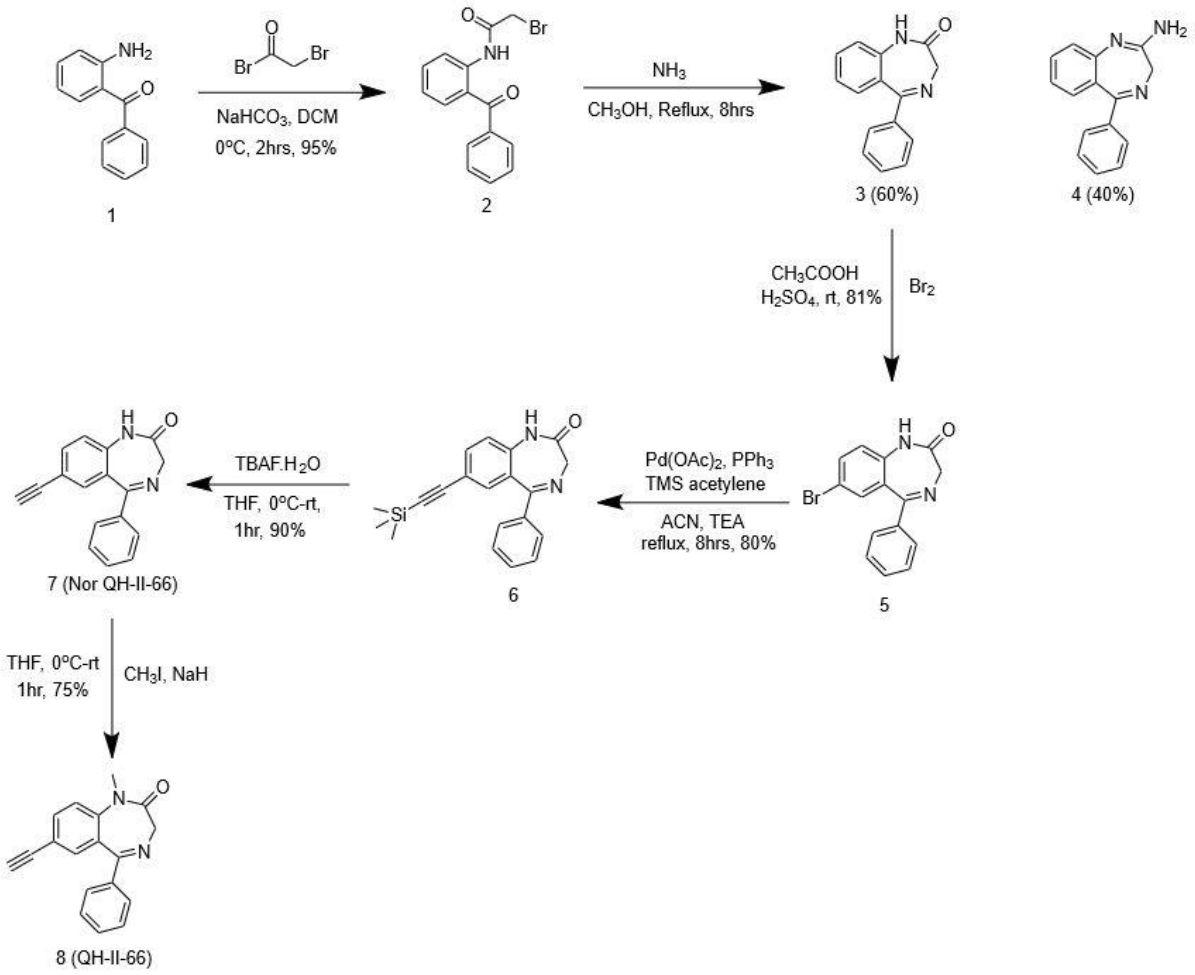


**Scheme 1. Initial synthetic route for QH II 66 (8)**

QH II 66 (8) previously synthesized by the Milwaukee group was a six-step process. The 2-amino benzophenone (1) was used as the starting material. An amide coupling reaction was carried out

by using bromoacetyl bromide in the presence of solid sodium bicarbonate in DCM at 0$^{o}$C to room temperature. In the second step the so formed amide was cyclized by stirring in a saturated solution of ammonia in methanol. This step required at least 8 hours at reflux. In the third step the cyclized product was brominated by using bromine in the presence of acetic acid and concentrated sulfuric acid. In the fourth step a Heck-type coupling reaction was performed to replace the bromine atom by an ethinyl trimethyl silyl group. For this reaction palladium acetate and triphenyl phosphine were used as the catalyst. The silyl group was removed by using tetrabutylammonium fluoride in THF. In the final step the N-methylation was done by treatment of N-H amide with methyl iodide and sodium hydride was used as the base to provide QH II 66 (**8**).

In this method there were several problems.

1. In the second step a saturated ammonia solution in methanol was employed. The ammonia does an $Sn^2$ reaction with the terminal bromine to furnish a terminal amine. This amine then attacks the carbonyl group to initiate the cyclization to provide the desired imine. To make a saturated solution of ammonia in methanol one needed a continuous flow of ammonia into the dry methanol. The temperature during this process must be at zero degrees Celsius. When dissolving ammonia in methanol on large scale it was very difficult to control the concentration. If the saturated solution of ammonia in methanol was too concentrated the desired product formed an imidate impurity. This makes the purification of the benzodiazepine more difficult for the $R_f$ values were very similar.

2. In the third step the bromination at the 7 position was executed by using bromine. Acetic acid and concentrated sulfuric acid were also used. The problem with this reagent is the toxicity of the bromine was an undesirable trait for this reagent.

3. In the fourth step a Heck-type coupling reaction was carried out to replace the bromine at the 7 position by a trimethyl silyl acetylene function. In this process palladiam aceteate and triphenyl phosphine were used. Triphenyl phosphine is air sensitive; it forms triphenyl phosphine oxide in the presence of oxygen in the air. Because of this problem, degassing is required for this process. Another problem was the $R_f$ value of the TMS protected benzodiazepine was very close to the 7-bromo starting material (5) which made the purification very difficult on chromatography. The crystallization of most intermediates must be achieved.

4. In the final step the N-methylation was done by using methyl iodide in the presence of sodium hydride in THF. Sodium hydride acts a base. This base is strong. It can not only remove the N-H proton but also abstract the proton from the C-3 position of the reactant. This provides another impurity in the reaction mixture which must be removed.

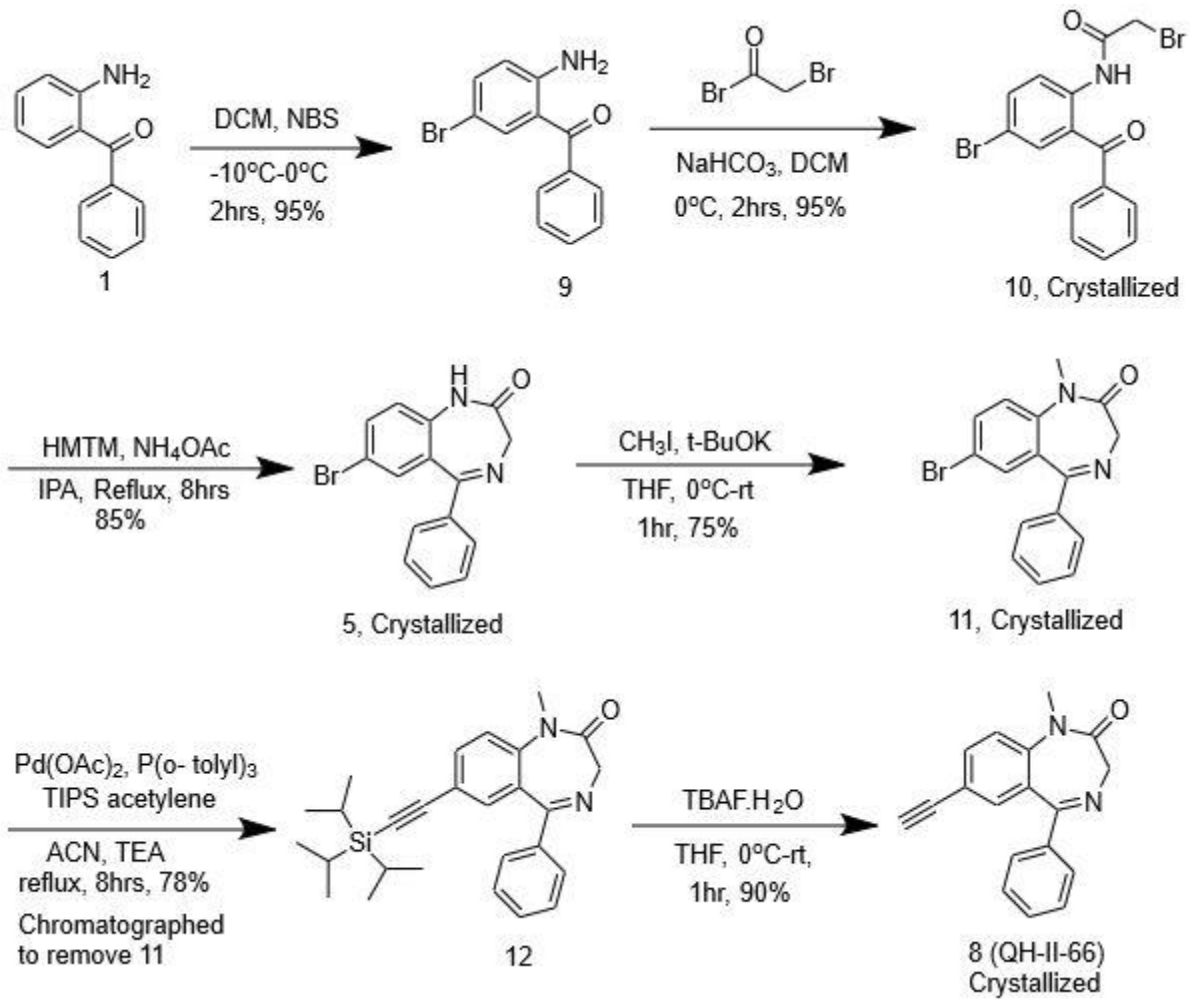


**Scheme 2. Improved synthetic route to make QH II 66.**

To solve the above-mentioned problems the synthetic route was redesigned. The redesigned synthetic route contained six steps. (See **Scheme 2)**

- In the first step 2-aminobenzophenone was brominated at the para position and it was done by treatment with N-bromosuccinamide. The reaction was done in DCM at -10$^{o}$C to 0$^{o}$C and stirred for 2 hours. The product was purified by crystallization in 5:95 ethyl acetate: hexanes. The best percent yield of this reaction process was 95%. The other 5% was the dibrominated impurity. The use of N-Bromosuccinamide solved the difficulties using bromine.

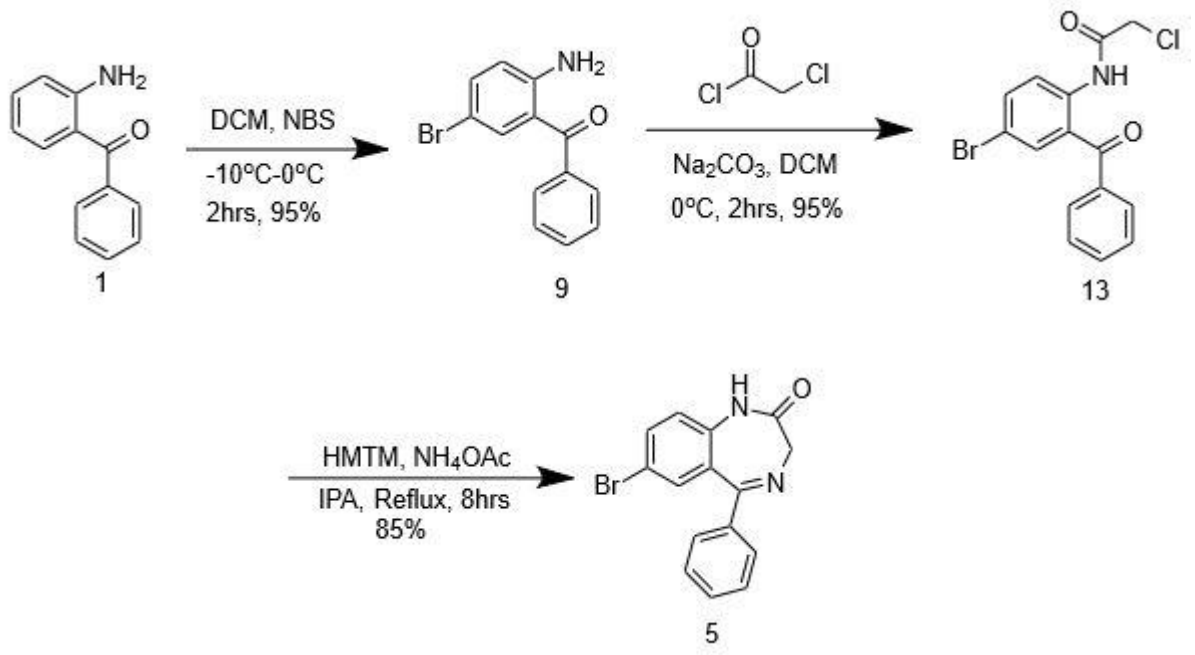


**Scheme 3. Improved cyclization route**

- In the second step the amide coupling was done by using bromoacetyl bromide in the presence of sodium bicarbonate. This reaction was done in DCM at $0^{o}$C to room temperature. Chloroacetyl chloride works as well as bromoacetyl bromide and was much cheaper. The product was purified by crystallization using (10: 90) ethyl acetate: hexanes to give a 95% yield.

- In the third step the cyclization was done by replacing ammonia with hexamethylenetetramine (HMTM) developed by Dan Knutson in the presence of ammonium acetate. The reaction was done in isopropyl alcohol by heating to reflux for 6 hours. The reaction is known as the Delapine reaction. This approach solved the imidate byproduct issue faced in the previous route. There was only one product formed. The benzodiazepine was purified by crystallization with 30:70 ethyl acetate: hexanes. The yield of pure benzodiazepine was 85%.

- The N-methylation was done in the fourth step of this route. There are two reasons to do it at the fourth step. The first one is the Heck-type coupling provides a lot of impurities if there is an N-H group present. If the N-H group is protected, the Heck-type coupling process proceeds well, which makes the purification very easy. The second reason is if this step is done after the installation of the acetylene function the base can abstract the acetylene proton which can generate one more impurity. In previous routes sodium hydride was used which was causing problems by producing more than two unnecessary byproducts. This problem was solved by using potassium tert-butoxide, a more hindered base than sodium hydride and one in which it was easier to control. This approach provided 75% yield of the desired N-methyl amide.
- In the fifth step the Heck-type coupling was done. Using ortho tolyl phosphine as the ligand solved the problem of forming triphenylphosphine oxide byproduct due to the presence of air. Ortho tolyl phosphine does not become oxidized by oxygen from the air, so degassing was not required in this stage. This was discovered by Greg Fu and the ortho tolyl ligand has a bigger bite angle. The TIPS acetylene function was used to form a greater $R_f$ difference between the starting material and desired product. The TIPS group was also easier on chromatography to remove which reduced byproducts. The percent yield of this stage was 78%.
- In the final step the TIPS group was removed by using tetrabutyl ammonium fluoride (TBAF) in THF at -20$^{o}$C to room temperature. This step takes about 1 hour with stirring. QH-II-66 was crystallized from isopropanol in 90% yield.

### 2. 4. 2 Synthesis of NOR QH II 66

Analogous to QH II 66, Nor QH II 66 also showed very good anticancer activity. It exhibited the most potent IC50 value in the medulloblastoma G3 cancer cell line. This compound was able to penetrate the blood brain barrier within 30 minutes of IP administration as is QH-II-66. Nor QH II 66 was synthesized by following the steps in the Scheme below. The largest scale executed was 50g scale and the overall yield was 70%.

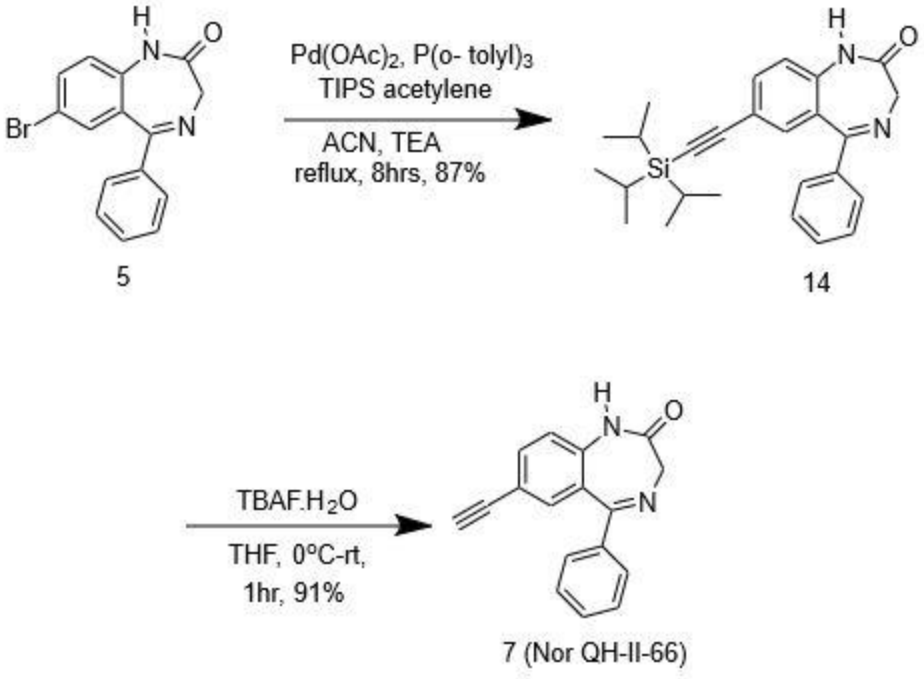


**Scheme 4. Synthetic route to synthesis of Nor-QH II 66**

### 2. 4. 3 Synthesis of KRM II 08 and TA I 12

KRM II 08 is the 2'F analog of QH-II-66. This compound showed very good activity in medulloblastoma G3 cancer cell lines. It induced a 38% apoptosis rate. TA I 12 is the 2'F analog of Nor QH II 66, TA I 12 is also known as Nor KRM II 08.

The starting material for KRM II 08 was 2-amino 5-bromo 2'fluoro benzophenone. The synthesis

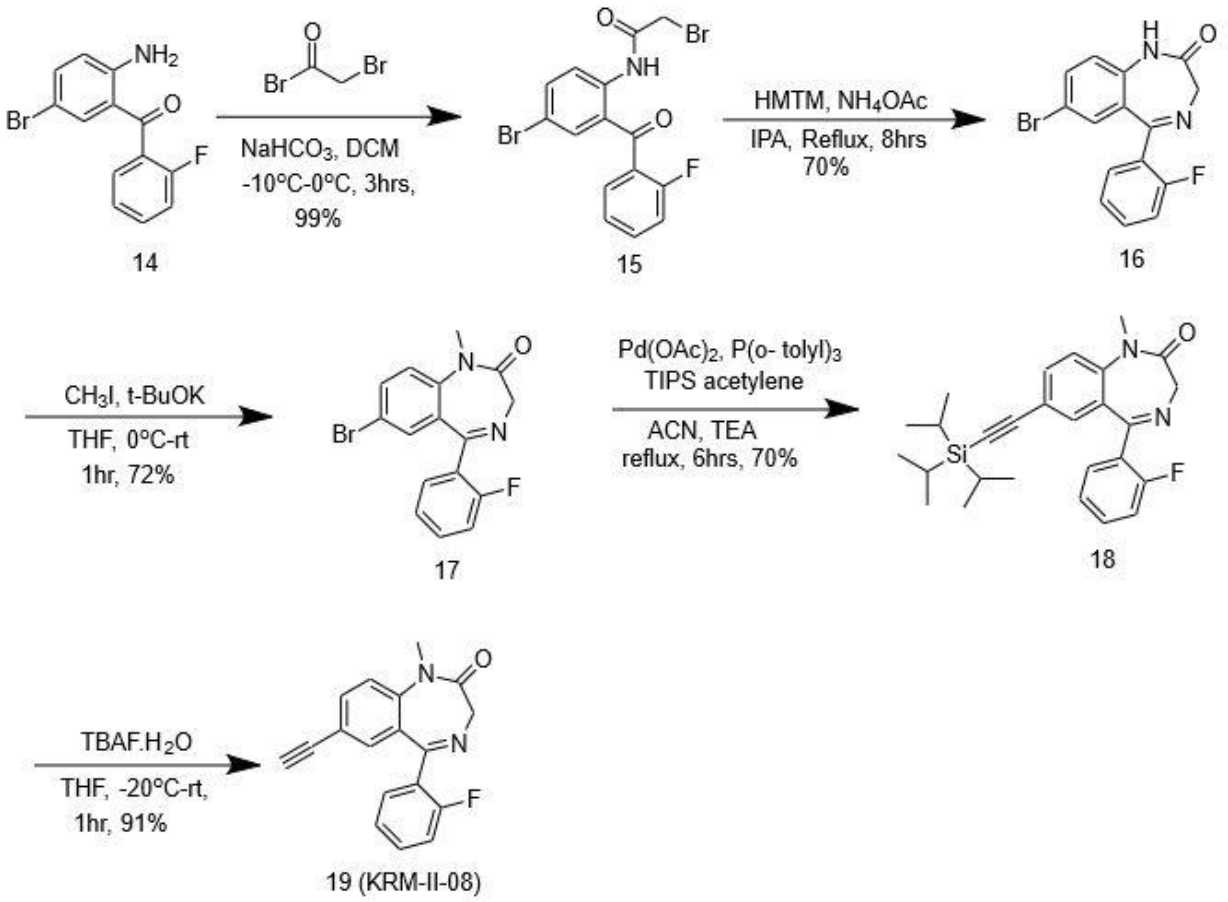


**Scheme 5. Synthetic route to synthesis of KRM II 08**

Was similar to the route to QH II 66. It is illustrated in Scheme 5. The largest scale was done on 50g, of starting material 2-amino 5-bromo 2'fluoro benzophenone.

TA I 12 (Nor KRM-II-08) was also synthesized via the same route as nor QH-II-66. The largest scale in that case was 20 grams starting from the compound 9. (**Scheme 6**)

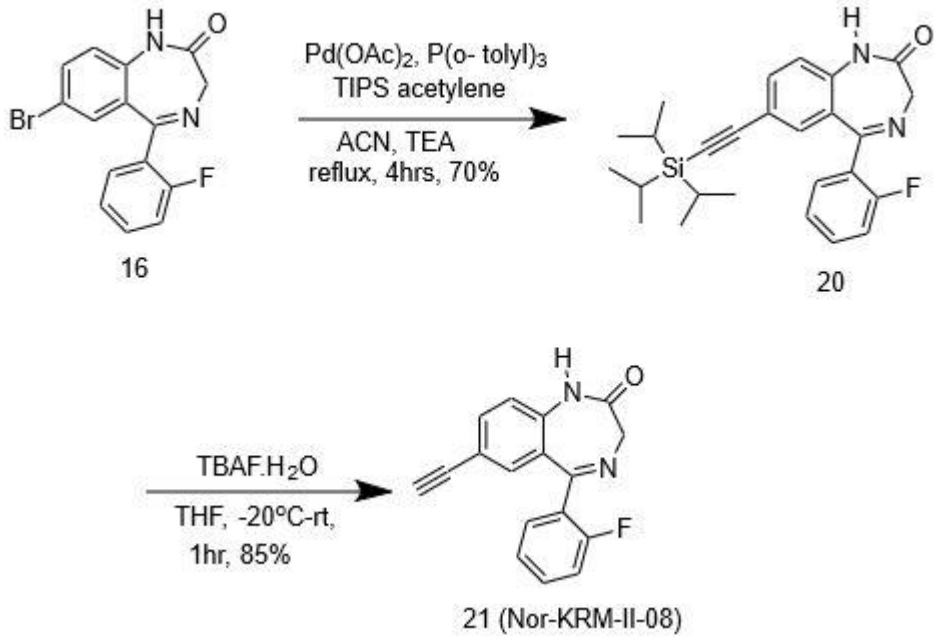


**Scheme 6. Synthetic route to synthesize Nor KRM II 08.**

### 2. 4. 4 The synthesis of deuterated analogues of QH II 66

#### 2. 4. 4. 1 Synthesis of the N-$CD_3$ analogs of QH II 66 and KRM-II-08.

Two N-$CD_3$ compounds were synthesized designated TA I 16 and MYM III 85. The TA I 16 can be synthesized from Nor KRM II 08 by treating the amide with deuterated methyl iodide in the presence of potassium tert-butoxide in THF at $0^oC$ to room temperature. MYM III 85 can be synthesized from nor QH II 66 via a similar route. The final products can be purified by column chromatography with ethyl acetate-hexanes (20:80).

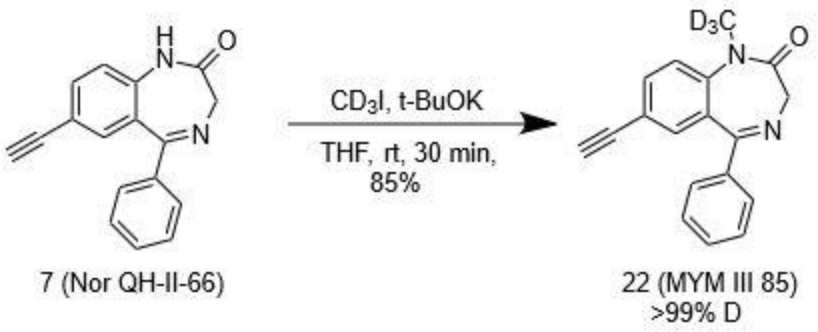


**Scheme 7. Synthetic route to synthesize MYM III 85.**

### 2. 4. 4. 2 Synthesis of D2 QH II 66

To synthesize D2 QH II 66 one needed to exchange the hydrogen atoms at the C-3 position of QH II 66. To do this one needed a sufficiently strong base and a deuterated solvent. The procedure was as follows:

- Dissolved 50mg of QH II 66 in 1mL of D4-methanol
- Add 1equivalent of base
- Stir for 1 hour at room temperature
- Filter the ppt by using a PTFE filter
- Evaporate the D4-Methanol on a rotary evaporator under reduced pressure. Take the 1H NMR to confirm the exchange of three hydrogen atoms with deuterium. One deuterium from the acetylene and two from the C3 position.
- Dissolve the solid in regular methanol and evaporate the solvent for 5-6 times to regenerate the acetylene hydrogen atom.


**Scheme 8. Synthetic route to synthesize D2 QH II 66 (<86% D).**

D4-methanol was used as a solvent. In the first attempt $K_2CO_3$ was used as a base, but there was no deuterium exchange observed. For the next trial potassium tert-butoxide was employed. In this attempt 86% deuterium was present at the C3 position. Many attempts were made to increase the percent deuterium exchange by changing the bases and reaction temperatures, but there were no improvements. We concluded that if heat is applied the deuteriums after work up become exchanged with hydrogen. Without heat one cannot regenerate back the acetylene hydrogen. 95+% deuterium was required to do most in vivo assay.

### 2. 4. 4. 3 Synthesis of D5-QH II 66.

After several unsuccessful attempts to synthesize at least 95% deuterated D2 QH II 66 we decided to see what we observed in the case of deuteration of D3- MYM III 85. This compound contains an N-$CD_3$ moiety. We followed the exact procedure for synthesis of D2-QH II 66 for the deuteration of MYM III 85, but the results were the same as observed in the case of D2 QH II 66. Potassium tert-butoxide was used as the base and D4-methanol was used as the solvent.

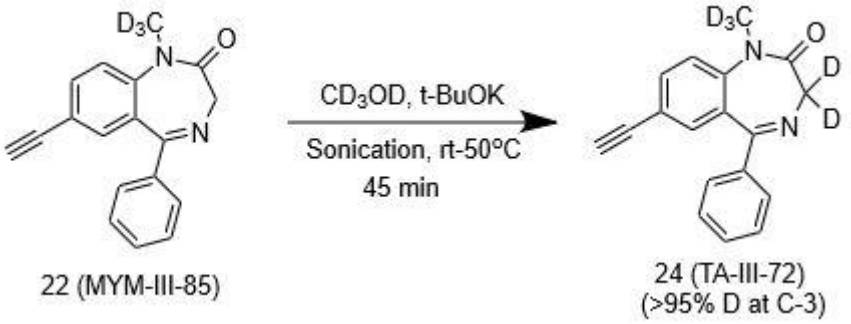


**Scheme 9. Successful synthetic route to >95% D5 QH II 66**

After this result of 86% incorporation the synthetic procedure was altered slightly. The MYM III 85 was dissolved in D4-methanol and 1.1 equivalents of potassium tert-butoxide was added. The mixture was sonicated at 50$^{o}$C for one hour. Then 4mL of DI water was added to the mixture at room temperature. This solution was extracted with ethyl acetate and the solvent was removed under an argon flow. After this a 96% deuterium exchange at the C-3 position of MYM III 85 was observed and gave this 95%+ D5 QH II 66, which was assigned code number of TA III 72. (D5-QH-II-66)

### 2. 4. 4. 3. 1 Stability of the deuteriums in TA III 72 at different pH values.

Several different pH conditions were employed to observe the stability of the deuterium atoms in TA III 72. The stability was tested at pH 4, 7.4 and 8 at room temperature and at 37$^{o}$C. There were no significant changes observed in the percentage of deuterium atoms neither at the acetylene position nor at the C-3 position. Observing this result, it was concluded that TA III 72 was stable enough in the human body that one could conduct the in vitro and in vivo anticancer assays and use it to treat cancer patients.

| D5 QH II 66 | Integration |
|---|---|
| C3 H1 | 0.05 |
| C3 H2 | 0.06 |
| Acetylene H | 0.94 |

**Table 2-3 Integration of H atom at normal temperature of QH II 66**

| Sample | C3 H1 | C3 H2 | Acetylene H |
|---|---|---|---|
| 1 hr | 0.06 | 0.07 | .92 |
| 2 hr | 0.06 | 0.07 | 0.91 |
| 4 hr | 0.07 | 0.08 | 0.90 |
| 24 Hr | 0.07 | 0.08 | 0.90 |

**Table 2-4 At pH 7.4 RT, No change at all.**

| Sample | C3 H1 | C3 H2 | Acetylene |
|---|---|---|---|
| 1 hr | 0.06 | 0.06 | 0.93 |
| 2 hr | 0.06 | 0.07 | 0.92 |
| 4 hr | 0.07 | 0.08 | 0.92 |
| 24 hrs | 0.07 | 0.08 | 0.91 |

**Table 2-5 At pH 7.4 37C, No change at all.**

| Sample | C3 H1 | C3 H2 | Acetylene H |
|---|---|---|---|
| 1 hr | 0.09 | 0.11 | 0.89 |
| 2 hr | 0.09 | 0.11 | 0.88 |
| 4 hr | 0.10 | 0.11 | 0.90 |
| 24 Hr | 0.09 | 0.10 | 0.91 |

**Table 2-6 At pH 8.0 RT, No significant change.**

| Sample | C3 H1 | C3 H2 | Acetylene |
|---|---|---|---|
| 1 hr | 0.06 | 0.06 | 0.93 |
| 2 hr | 0.06 | 0.07 | 0.92 |
| 4 hr | 0.07 | 0.08 | 0.92 |
| 24 hrs | 0.07 | 0.08 | 0.91 |

**Table 2-7 At pH 8.0 37ºC, No significant change.**

| Sample | C3 H1 | C3 H2 | Acetylene H |
|---|---|---|---|
| 1 hr | 0.09 | 0.10 | 0.91 |
| 2 hr | 0.09 | 0.11 | 0.91 |
| 4 hr | 0.09 | 0.11 | 0.90 |
| 24 Hr | 0.10 | 0.12 | 0.91 |

**Table 2-8 At pH 4.0 RT, No significant change.**

| Sample | C3 H1 | C3 H2 | Acetylene |
|---|---|---|---|
| 1 hr | 0.09 | 0.09 | 0.89 |
| 2 hr | 0.10 | 0.11 | 0.88 |
| 4 hr | 0.10 | 0.11 | 0.91 |
| 24 hrs | 0.10 | 0.12 | 0.91 |

**Table 2-9 At pH 4.0 37°C, No significant change.**

### 2. 4. 4. 3. 2 Solubility comparison of TA I 16 with other N-substituted QH II 66 analogs inD4-methanol.

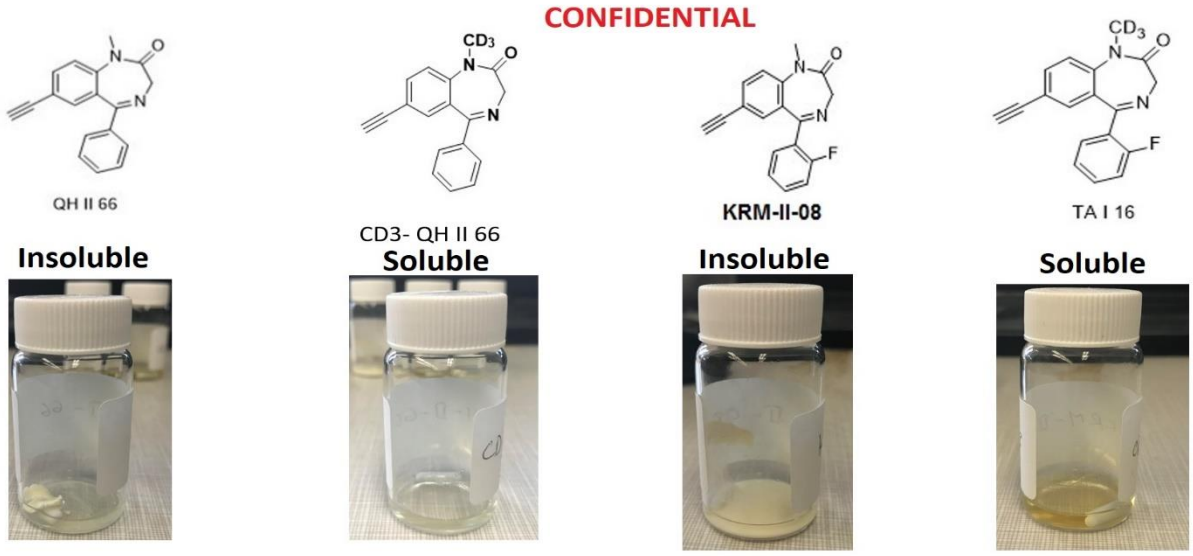


**Figure 99. Solubility of N-$CD_3$ and N-$CH_3$ analogs of KRM II 08 and QH II 66**

One observed an anomaly during deuteration of N-CH3 and N-CD3 analogs of QH II 66. The deuterium incorporation at the C-3 position in case of N-CD3 analogs was better than N-CH3 analogs. It was proposed a theory that the reason for this was due to the presence of unreacted potassium tert-butoxide present during the work up. To prove this theory, we designed an experiment wherein we stirred different N-CH3 and N-CD3 analogs in the absence of any base in D4-methanol at room temperature for 24 hours. After the experiment we observed the N-CD3 analogs had much better solubility in D4-methanol without the base at room temperature than the N-CH3 analogs in D4-methanol. We checked the 1H NMR to see any changes at the C-3 position of all the analogs. We did not observe any hydrogen replaced with deuterium. This indicates that a base is required to install deuterium at the C-3 position of a QH II 66 analog whether it is an N-CH3 or N-CD3 analog.

But this observation does not provide the reason for having better deuterium exchange in the case of N-CD3 analogs.

However, from the **Figure 99** in the previous page it is clear $CD_3$-QH-II-66 and $CD_3$-KRM-II-08 (TA-I-16) are more soluble in D4-methanol than the two N-$CH_3$ analogs. One point is that in the N-$CH_3$ analogs immediately after the deuteration the percent deuteration is around 95%. It is only in refluxing in H4-methanol wherein the percent deuteration drops to 86% while trying to remove the ethinyl-D bond. Perhaps it is harder to dissolve the N-$CH_3$ analogs, so it takes more heat and time to remove the ethinyl C-D bond than in $CD_3$-analogs, hence the percent incorporation at the C-3 remains at >95% deuterium in the N-$CD_3$ analogs.

### 2. 4. 5 Synthesis of thio analogues of QH II 66.

The thio analogs of QH II 66 (TA III 50) and KRM-II-08 (TA-III-52) were synthesized from the KRM II 08 by using Lawesson's reagents in THF by refluxing them for an hour respectively. The

TA III 52 was synthesized from the QH II 66 via a similar route as stated. The percent yield of both processes was approximately 50% in both cases.

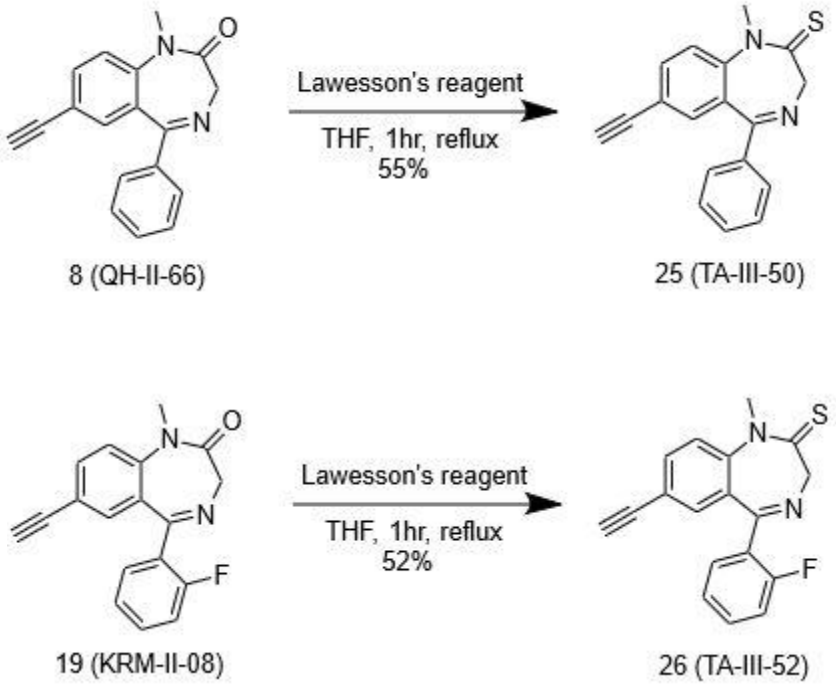


**Scheme 10. Synthetic route to sulfur analogs TA III 50 and TA III 52**

## 2. 4. 6 Synthesis of 7,9- disubstituted analogues of QH II 66

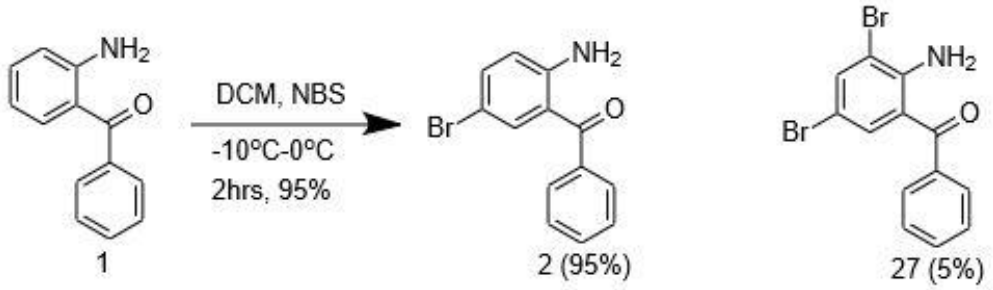

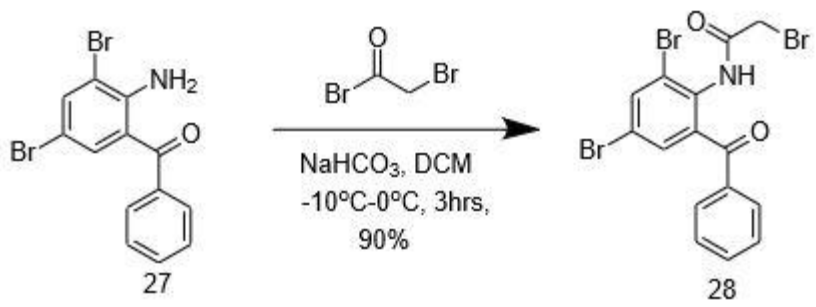


**Scheme 11.Synthetic route to TA III 62 (part 1)**

During the purification stage of the bromination of 2-aminobenzophenone by using N-bromosuccinamide it was observed that there was a dibrominated byproduct which was removed by ethyl acetate-hexanes 10:90. It was decided to make a diacetylated analog of QH II 66 to see if it can fit in the binding pocket in the H1792 cancer cell lines. One followed a similar route employed for the synthesis of QH II 66 to synthesize the diacetylated analog of QH II 66. The code number for this analog is TA III 62.

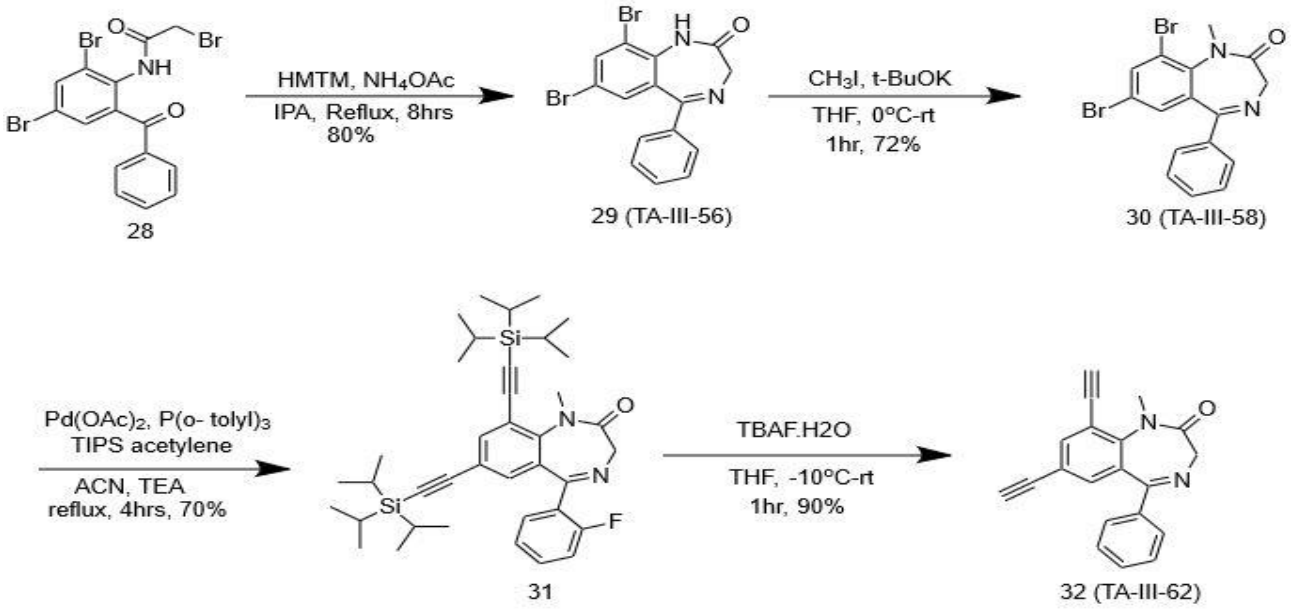


**Scheme 12. Synthetic route to synthesize TA III 62 (part 2)**

## 2. 5 Experimental

### 2. 5. 1 (2-Amino-5-bromophenyl) (phenyl)methanone (9)

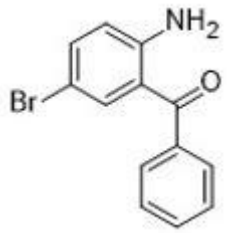


To a solution of 2-aminobenzophenone **1** (50 g, 253.5 mmol) in DCM (600 mL), which was stirred at -10°C for 10 min, NBS (47.4 g, 266.2 mmol) was added in portions. The mixture was stirred for 2 hours at 0°C. After the reaction progress was completed (TLC), the mixture was diluted with $H_2O$ (300 mL), extracted with DCM (300 mL), washed with brine (100 mL), and dried ($Na_2SO_4$). It was concentrated under reduced pressure. The crude bromide compound was purified by crystallization from EtOAc and hexanes (10:90) to give (2-amino-5 bromophenyl)(phenyl)methanone **9** (66 g, 94.29% yield) as a yellow solid.

$^1$H NMR (500 MHz, $CDCl_3$): δ 7.66-7.64 (m, 2H, 2 x ArH), 7.60-7.57 (m, 2H, 2 x ArH), 7.52-7.49 (m, 2H, 2xArH), 7.38 (dd, 1H, J=8.5, 2.0Hz,H-4), 6.67(d, 1H, J=8.5Hz, H-3), 6.11 (br s, 2H, $NH_2$). 13C NMR (500 MHz, $CDCl_3$): 198.2, 149.4, 139.5, 134.4, 133.4, 131.7, 129.3, 128.5, 120.3, 119.2, 118.8. $R_f$ = 0.4 at 1:9 (silicagel, ethylacetate/Hexanes) The spectral properties of **2** were identical to those in the published reports.

**2. 5. 2 N-(4-Methyl-2-(1- phenylethenyl) phenyl)propanamide (10)**


To a mixture of **(2-amino-5-bromophenyl)(phenyl) methanone** (**9**, 60 g, 217.29 mmol), sodium bicarbonate (36.50 g, 434.58 mmol), and DCM (600 mL), bromoacetyl bromide (24.61 mL, 282.48 mmol) was added dropwise over a 60 minutes period. The temperature was kept between -10°C – 0°C with continuous stirring. The white colored reaction mixture, which resulted, was then allowed to stir for longer than 3 h at rt. The completion of the reaction was verified by analysis by TLC (silica gel) and 50% ethyl acetate / hexanes. The reaction mixture was then slowly diluted over 30 min with water (300 mL) as carbon dioxide bubbles evolved. The biphasic mixture, which resulted, was allowed to stand for 15 min and the layers were separated. The aq layer was extracted with dichloromethane (300 mL) and the combined organic layers were washed with 5% aq sodium bicarbonate solution (300 mL) and then 10% aq sodium chloride solution (300 mL). The organic layer was dried ($Na_2SO_4$). The solvents were removed under reduced pressure and the residue was slurried with ethanol (300 mL) at 50 – 55°C for 30 min. Upon cooling to rt and after holding the temperature for 1 h, the solid, which formed, was filtered and washed with ethanol (60 mL x 3). The solid was dried under vacuum at 40°C to afford the product *N*-(4-methyl-2-(1-phenylethenyl)phenyl)propanamide **3** as an off-white solid (82.6 g, 95.5%).

$^{1}$H NMR (500 MHz, $CDCl_3$): δ11.60 (s,1H) 7.66-7.64 (m, 2H, 2 x ArH), 7.60-7.57 (m, 2H, 2 x ArH), 7.52-7.49 (m, 2H, 2xArH), 7.38 (dd, 1H, J=8.5, 2.0Hz,H-4), 6.67(d, 1H, J=8.5Hz, H-3), 4.21 (s, 2H). 13C NMR (500 MHz, $CDCl_3$): 198.2,165.21, 149.4, 139.5, 134.4, 133.4, 131.7, 129.3, 128.5, 120.3, 119.2, 118.8, 42.3 The spectral properties of **2** were identical to the published values[2].

**2. 5. 3 7-Bromo-5-phenyl-1,3-dihydro-2*H*-1,4-benzodiazepin-2-one (5).**


A mixture of ***N*-(4-Methyl-2-(1- phenylethenyl) phenyl) propanamide (10)** (70 g, 176.3 mmol), hexamethylenetetramine (HMTM, 54.38 g, 387.9 mmol), ammonium acetate (29.9 g, 387.9 mmol), and isopropanol (700 mL) was heated to reflux (82$^{o}$C). The reaction mixture was held at reflux for 6 h, at which point the reaction progress was deemed complete on analysis by TLC (silica gel and 1:1, ethyl acetate/hexanes). The reaction mixture was then cooled to 0 – 5$^{o}$C using an ice bath. The solid, which resulted, was filtered, and washed with cold isopropanol (100 mL x 2) and then water (100mL x 4). The solid was dried under vacuum at 40$^{o}$C to afford 32 g of the benzodiazepine **4** as an off-white solid. The IPA was removed from the mother liquor under reduced pressure. The solid was then extracted with ethyl acetate. The ethyl acetate was removed under reduced pressure and the residue was purified by column chromatography using 1:4 ethyl acetate/hexanes to afford 7-bromo-5-phenyl-1,3-dihydro-2*H*-1,4-benzodiazepin-2-one (5). (38.9 g, 70%)

$^1$H NMR (500 MHz, $CDCl_3$): δ9.89 (s,1H), 7.82(d, 1H) 7.66-7.64 (m, 2H, 2 x ArH), 7.60-7.57 (m, 2H, 2 x ArH), 7.52-7.49 (m, 2H, 2xArH), 7.38 (dd, 1H, J=8.5, 2.0Hz,H-4), 4.32 (s, 2H). 13C NMR (500 MHz, $CDCl_3$): 170.2,165.21, 149.4, 139.5, 134.4, 133.4, 131.7, 129.3, 128.5, 120.3, 119.2, 118.8, 56.2. $R_f$ = .4 (Silicagel, ethylacetate/Hexanes 1:2) The spectral properties of **2** was identical to the published values.[3]

**2. 5. 4 7-Bromo-1-methyl-5-phenyl-1,3-dihydro-2*H*-1,4-benzodiazepin-2-one (11)**

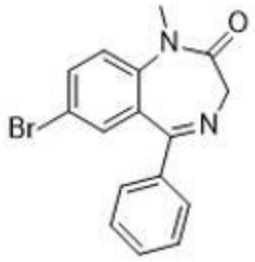


The 7-bromo-5-phenyl-1,3-dihydro-2*H*-1,4-benzodiazepin-2-one **5**, (38.0 g, 120.6 mmol) was dissolved in THF, (150 mL) and the solution was cooled to -0$^o$C using an ice bath. Then potassium tert butoxide (16.23 g, 144.7 mmol), which was dissolved in 100 mL of THF, was added dropwise by using an addition funnel. Then methyl iodide (8.26 mL, 132.7 mmoL) was added dropwise to the reaction mixture over a 5 min period, while maintaining the temperature at 0$^o$C. Upon completion of the addition, the reaction mixture was allowed to warm to rt and stir for 60 min, at which point the reaction was deemed complete on analysis by TLC (silica gel). The reaction mixture was then diluted with ethyl acetate (200 mL) and a solution of 10% aq sodium chloride (200 mL) was added. The biphasic mixture, which resulted, was allowed to stand for 15 min and the layers were separated. The aq layer was then extracted with ethyl acetate (100 mL) and the combined organic layers were washed with 10% aq sodium chloride solution (100 mL). The organic layer was dried ($Na_2SO_4$). The solvent was removed under reduced pressure. The brown solid, which was obtained, was purified by crystallization using 15:85(ethyl acetate/hexanes), to

give 7-bromo-1-methyl-5-phenyl-1,3-dihydro-2*H*-1,4-benzodiazepin-2-one **11** (29.76 g, 75%) as a brownish white solid.

$^1$H NMR (500 MHz, $CDCl_3$): 7.82(d, 1H) 7.66-7.64 (m, 2H, 2 x ArH), 7.60-7.57 (m, 2H, 2 x ArH), 7.52-7.49 (m, 2H, 2xArH), 7.38 (dd, 1H, J=8.5, 2.0Hz,H-4), 4.6 (D, 1H), 3.6(D,1H), 3.3(S,3H). 13C NMR (500 MHz, $CDCl_3$): 171.2, 168.21, 149.4, 139.5, 134.4, 133.4, 131.7, 129.3, 128.5, 120.3, 119.2, 118.8, 82.3, 79.2, 56.2, 34.2. $R_f$ = 0.5 (silica gel, ethyl acetate/hexanes 1:2) The spectral properties of **5** were identical to the published values.[3]

### 2. 5. 5 1-Methyl-5-phenyl-7-((tripropan-2-ylsilyl) ethynyl)-1,3-dihydro-2*H*-1,4-benzodiazepin-2-one. (12)

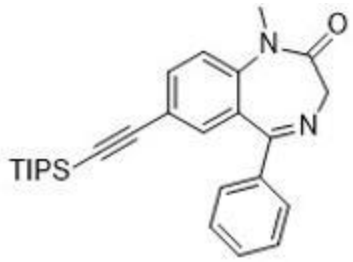


In a 500mL round bottom flask, Pd $(OAc)_2$ (955mg, 4.25 mmol) and P(o-tolyl)$_3$ (2.58gm, 8.45 mmol) was added to 50 mL of acetonitrile. The mixture was stirred until a slurry appeared, which took about 20 min. Then 7-bromo-1-methyl-5-phenyl-1,3-dihydro-2*H*-1,4-benzodiazepin-2-one **11**, (28.0 g, 85.05 mmol), triethylamine (23.63 mL, 190.34 mmol), (triisopropylylsilyl)acetylene (24.8 mL,110.57 mmol) and additional acetonitrile (250 mL) was added. The reaction mixture was then heated to reflux (75$^o$C) and held for 6 h, at which point the reaction was deemed complete on analysis by TLC (silica gel). Upon completion of the reaction progress, the mixture was cooled to rt and filtered through celite. After washing with acetonitrile (100 mL x 2), the solvents were removed under reduced pressure and the residue was dissolved in dichloromethane (400 mL). Then

5% aq sodium bicarbonate (400 mL) was added. The biphasic mixture, which resulted, was allowed to stand for 15 min and the layers were separated. The aq layer was then extracted with DCM (300 mL) and the combined organic layers were washed with 5% aq sodium bicarbonate solution (300 mL) and then 10% aq sodium chloride solution (300 mL x 3). The organic layer was dried ($Na_2SO_4$) and it was purified by flash chromatography on silica gel. This process gave a dark orange liquid that became solidified eventually on standing to give 1-methyl-5-phenyl-7-((tripropan-2-ylsilyl) ethynyl)-1,3-dihydro-2*H*-1,4-benzodiazepin-2-one, **(12)** (26g ,71% crude yield) as a waxy solid.

$^1$H NMR (300 MHz, $CDCl_3$): 7.67(d, 3H) 7.43-7.51 (m, 4H), 7.32-7.28 (d, 1H), 4.83 (D, 1H), 3.81(D,1H), 3.42(S,3H), 1.11(s,21H). 13C NMR (500 MHz, $CDCl_3$): 169.8, 168.7, 143.6, 138.0, 135.1, 133.6, 130.8, 129.7, 128.4, 121.0, 119.4, 118.8, 105.0, 92.3, 56.6, 34.8, 18.6, 11.2. $R_f$ = 0.7 (silica gel, ethyl acetate/hexanes 1:2) The spectral properties of **6** was identical to the published values.[3]

**2. 5. 6 7-ethynyl-1-methyl-5-phenyl-1,3-dihydro-2*H*-benzo[*e*][1,4]diazepin-2-one (8)**

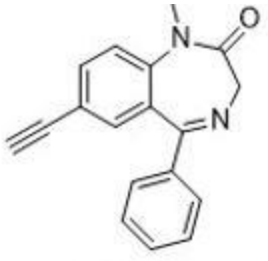


1-Methyl-5-phenyl-7-((tripropan-2-ylsilyl) ethynyl)-1,3-dihydro-2*H*-1,4-benzodiazepin-2-one **12**, (20.0 g, 60.16 mmol), water (3 mL) and tetrahydrofuran (200 mL) were cooled to -20$^o$C using a dry ice / IPA bath. Then tetrabutylammonium fluoride hydrate, [1M in THF (72.19 mL, 72.19 mmoL)] was added dropwise to the reaction mixture over a 30 min period, while maintaining the

temperature at -20 to -15$^{o}$C. Upon completion of the addition, the reaction mixture was allowed to warm to rt and stir for an additional 60 min, at which point the reaction progress was deemed complete on analysis by TLC (silica gel). The reaction mixture was then diluted with ethyl acetate (150 mL) and 10% aq sodium chloride (150 mL). The biphasic mixture, which resulted, was allowed to stand for 15 min and the layers were separated. The aq layer was then extracted with ethyl acetate (150 mL x 3) and the combined organic layers were washed with 10% aq sodium chloride solution (150 mL). The organic layer was dried ($Na_2SO_4$). The solvents were removed under reduced pressure. Then the mixture was dissolved in 300 mL of ethyl acetate and then stirred with 200gm of silica gel for 2 hours and filtered. The amount of solvent was reduced to about 40 ml under reduced pressure. Then 200mL of hexanes was added dropwise to the mixture and it was allowed to stir overnight. The solid, which formed, was filtered and the grey solid was recrystallized from 1:4 (ethyl acetate/hexanes) to get 9 gm of cream white colored QH II 66. The filtrate was concentrated under reduced pressure and after purification by column chromatography this provided more of QH II 66 (8) (1.2 g). These solids were dried under vacuum at 40$^{o}$C. (10.2 g, 80%)

$^{1}$H NMR (500 MHz, $CDCl_3$): 7.82(d, 1H) 7.66-7.64 (m, 2H, 2 x ArH), 7.60-7.57 (m, 2H, 2 x ArH), 7.52-7.49 (m, 2H, 2xArH), 7.38 (dd, 1H, J=8.5, 2.0Hz,H-4), 4.6 (d, 1H), 3.6(d,1H), 3.3(S,3H), 3.1(s,1H). 13C NMR (500 MHz, $CDCl_3$): 171.2, 168.21, 149.4, 139.5, 134.4, 133.4, 131.7, 129.3, 128.5, 120.3, 119.2, 118.8, 82.3, 79.2, 56.2, 34.2. $R_f$ = 0.4 (silicagel, ethylacetate/hexanes 1:2) HRMS (ESI/IT-TOF): *m/z* $[M + H]^+$ calcd for $C_{18}H_{14}N_2O$: 275.1179; found 275.1148. The spectral properties of **8** was identical to the published values.[154]

**2. 5. 7 5-phenyl-7-((triisopropylsilyl)ethynyl)-1,3-dihydro-2*H*-benzo[*e*] [1,4] diazepin-2-one (14)**

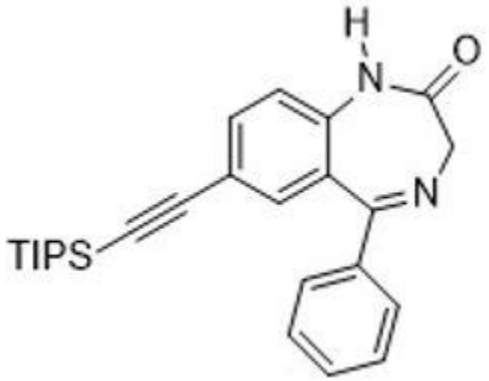


In a 500mL round bottom flask, Pd $(OAc)_2$ (955mg, 4.25 mmol) and P(o-tolyl)$_3$ (2.58gm, 8.45 mmol) was added to 50 mL of acetonitrile. The mixture was stirred until a slurry appeared, which took about 20 min. Then 7-bromo-5-phenyl-1,3-dihydro-2*H*-1,4-benzodiazepin-2-one (**5**) (28.0 g, 85.05 mmol), triethylamine (23.63 mL, 190.34 mmol), (triisopropylylsilyl)acetylene (24.8 mL,110.57 mmol) and additional acetonitrile (250 mL) was added. The reaction mixture was then heated to reflux (75$^o$C) and held for 6 h, at which point the reaction was deemed complete on analysis by TLC (silica gel). Upon completion of the reaction progress, the mixture was cooled to rt and filtered through celite. After washing with acetonitrile (100 mL x 2), the solvents were removed under reduced pressure and the residue was dissolved in dichloromethane (400 mL) and 5% aq sodium bicarbonate (400 mL) was added. The biphasic mixture, which resulted, was allowed to stand for 15 min and the layers were separated. The aq layer was then extracted with dichloromethane (300 mL) and the combined organic layers were washed with 5% aq sodium bicarbonate solution (300 mL) and then 10% aq sodium chloride solution (300 mL x 3). The organic layer was dried ($Na_2SO_4$) and it was purified by flash chromatography on silica gel. This process gave a dark orange liquid that gets solidified eventually on standing to give 1-methyl-5-

phenyl-7-((tripropan-2-ylsilyl) ethynyl)-1,3-dihydro-2*H*-1,4-benzodiazepin-2-one **14**, (32.10 g ,87% crude yield)

$^1$H NMR (300 MHz, $CDCl_3$): 7.67(d, 3H) 7.43-7.51 (m, 4H), 7.32-7.28 (d, 1H), 4.83 (D, 1H), 3.81(D,1H), 3.42(S,3H), 1.11(s,21H). 13C NMR (500 MHz, $CDCl_3$): 169.8, 168.7, 143.6, 138.0, 135.1, 133.6, 130.8, 129.7, 128.4, 121.0, 119.4, 118.8, 105.0, 92.3, 56.6, 34.8, 18.6, 11.2. $R_f$ = 0.7 (silica gel, ethyl acetate/hexanes 1:2)

**2. 5. 8 7-ethynyl-5-phenyl-1,3-dihydro-2*H*-benzo[*e*] [1,4] diazepin-2-one (7)**

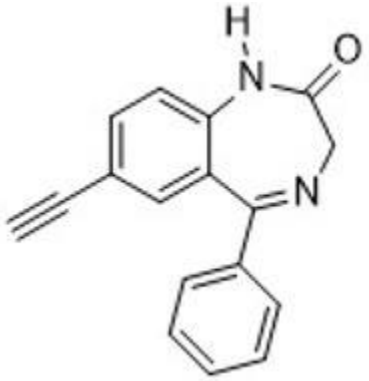


1-Methyl-5-phenyl-7-((tripropan-2-ylsilyl) ethynyl)-1,3-dihydro-2*H*-1,4-benzodiazepin-2-one **14**, (20.0 g, 60.16 mmol), water (3 mL) and tetrahydrofuran (200 mL) were cooled to -20$^o$C using a dry ice / IPA bath. Then tetrabutylammonium fluoride hydrate, [1M in THF (72.19 mL, 72.19 mmoL)] was added dropwise to the reaction mixture over a 30 min period, while maintaining the temperature at -20 to -15$^o$C. Upon completion of the addition, the reaction mixture was allowed to warm to rt and stir for an additional 60 min at which point the reaction progress was deemed complete on analysis by TLC (silica gel). The reaction mixture was then diluted with ethyl acetate (150 mL) and 10% aq sodium chloride (150 mL). The biphasic mixture, which resulted, was allowed to stand for 15 min and the layers were separated. The aq layer was then extracted with

ethyl acetate (150 mL x 3) and the combined organic layers were washed with 10% aq sodium chloride solution (150 mL). The organic layer was dried ($Na_2SO_4$). The solvents were removed under reduced pressure. Then the mixture was dissolved in 300 mL of ethyl acetate and then stirred with 200gm of silica gel for 2 hours and filtered. The amount of solvent was reduced to about 40 ml under reduced pressure. Then 200mL of hexanes was added dropwise to the mixture and it was allowed to stir overnight. The solid, which formed, was filtered and the grey solid was recrystallized from 1:4 (ethyl acetate/hexanes) to get 10.18 gm of cream white colored Nor QH II 66. The filtrate was concentrated under reduced pressure and after purification by column chromatography provided more of Nor QH II 66 (1.19 g). These solids were dried under vacuum at 40$^{o}$C. (11.37 g, 91%)

$^{1}$H NMR (500 MHz, $CDCl_3$): 7.82(d, 1H) 7.66-7.64 (m, 2H, 2 x ArH), 7.60-7.57 (m, 2H, 2 x ArH), 7.52-7.49 (m, 2H, 2xArH), 7.38 (dd, 1H, J=8.5, 2.0Hz,H-4), 4.6 (D, 1H), 3.6(D,1H), 3.3(S,3H), 3.1(s,1H). 13C NMR (500 MHz, $CDCl_3$): 171.2, 168.21, 149.4, 139.5, 134.4, 133.4, 131.7, 129.3, 128.5, 120.3, 119.2, 118.8, 82.3, 79.2, 56.2, 34.2. $R_f$ = 0.4 (silicagel, ethylacetate/hexanes 1:2) HRMS (ESI/IT-TOF): *m/z* $[M + H]^+$ calcd for C17H12N2O: 260.2890; found 260.2865. The spectral properties of **6** was identical to the published values.

**2. 5. 9 2-bromo-*N*-[4-bromo-2-(2-fluorobenzoyl)phenyl]-acetamide (15)**

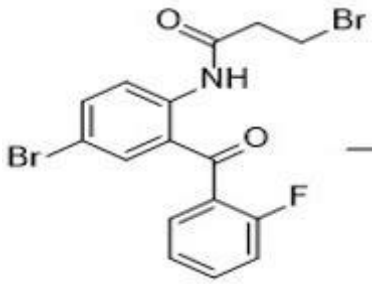

To a mixture of **(2-amino-5-bromophenyl)(2' fluorophenyl) methanone** (50 g, 169.99 mmol), sodium bicarbonate (28.56 g, 339.99 mmol), and dichloromethane (500 mL), bromoacetyl bromide (17.76 mL, 203.98 mmol) was added dropwise over a 60 min time period. The temperature was kept between -10°C – 0°C with continuous stirring. The white colored reaction mixture, which resulted, was then allowed to stir for longer than 3 h at rt. The completion of the reaction was verified by analysis by TLC (silica gel) and 50% ethyl acetate / hexanes. The reaction mixture was then slowly diluted over 30 min with water (300 mL) as carbon dioxide bubbles ocurred. The biphasic mixture, which resulted, was allowed to stand for 15 min and the layers were separated. The aq layer was extracted with dichloromethane (300 mL) and the combined organic layers were washed with 5% aq sodium bicarbonate solution (300 mL) and then 10% aq sodium chloride solution (300 mL). The organic layer was dried ($Na_2SO_4$). The solvents were removed under reduced pressure and the residue was slurried with ethanol (300 mL) at 50 – 55°C for 30 min. Upon cooling to rt and after holding the temperature for 1 h, the solid, which formed, was filtered, and washed with ethanol (60 mL x 3). The solid was dried under vacuum at 40°C to afford the product **2-bromo-*N*-[4-bromo-2-(2-fluorobenzoyl)phenyl]-acetamide (15)** as an off-white solid (67.73 g, 96%).

$^1$H NMR (500 MHz, $CDCl_3$): δ11.60 (s,1H) 7.66-7.64 (m, 2H, 2 x ArH), 7.60-7.57 (m, 2H, 2 x ArH), 7.52-7.49 (m, 2H, 2xArH), 7.38 (dd, 1H, J=8.5, 2.0Hz,H-4), 6.67(d, 1H, J=8.5Hz, H-3), 4.21 (s, 2H). 13C NMR (500 MHz, $CDCl_3$): 198.2,165.21, 149.4, 139.5, 134.4, 133.4, 131.7, 129.3, 128.5, 120.3, 119.2, 118.8, 42.3

**2. 5. 10 7-Bromo-5-(2-fluorophenyl)-1,3-dihydrobenzo[e]-1,4-diazepin-2-one (16)**

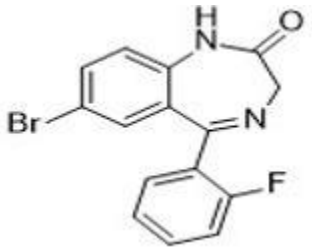


A mixture of **2-bromo-*N*-[4-bromo-2-(2-fluorobenzoyl)phenyl]-acetamide (15),** (50 g, 120.48 mmol), hexamethylenetetramine (HMTM, 35.47 g, 252.99 mmol), ammonium acetate (19.5 g, 252.99 mmol), and isopropanol (500 mL) was heated to reflux (82$^{o}$C). The reaction mixture was held at reflux for 6 h, at which point the reaction progress was deemed complete on analysis by TLC (silica gel and 1:1, ethyl acetate/hexanes). The reaction mixture was then cooled to 0 – 5$^{o}$C using an ice bath. The solid, which resulted, was filtered, and washed with cold isopropanol (100 mL x 2) and then water (100mL x 4). The solid was dried under vacuum at 40$^{o}$C to afford 32 g of the benzodiazepine **4** as an off-white solid. The IPA was removed from the mother liquor under reduced pressure. The solid was then extracted with ethyl acetate. The ethyl acetate was removed under reduced pressure and the residue was purified by column chromatograpy using 1:4 etheyl acetate/hexanes to afford **7-Bromo-5-(2-fluorophenyl)-1,3-dihydrobenzo[e]-1,4-diazepin-2-one**. (**16)** (28.1 g, 70%)

$^{1}$H NMR (500 MHz, $CDCl_3$): δ9.89 (s,1H), 7.82(d, 1H) 7.66-7.64 (m, 2H, 2 x ArH), 7.60-7.57 (m, 2H, 2 x ArH), 7.52-7.49 (m, 2H, 2xArH), 7.38 (dd, 1H, J=8.5, 2.0Hz,H-4), 4.32 (s, 2H). 13C NMR (500 MHz, $CDCl_3$): 170.2,165.21, 149.4, 139.5, 134.4, 133.4, 131.7, 129.3, 128.5, 120.3, 119.2, 118.8, 56.2. $R_f$ = .4 (silicagel, ethylacetate/hexanes 1:2)

**2. 5. 11 7-Bromo-5-(2-fluorophenyl)-1,3-dihydro-1-methyl-2H-1,4 benzodiazepin-2-one. (17)**

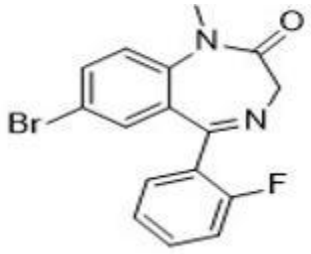


The **7-Bromo-5-(2-fluorophenyl)-1,3-dihydrobenzo[e]-1,4-diazepin-2-one (16)**. (25 g, 75.04 mmol) was dissolved in THF, (150 mL) and the solution was cooled to -0$^{o}$C using an ice bath. Then potassium tert butoxide (10.10 g, 90.00 mmol) which was dissolved in 100 mL of THF, was added dropwise by using an addition funnel. Then methyl iodide (5.14 mL, 82.54 mmoL) was added dropwise to the reaction mixture over a 5 min period, while maintaining the temperature at 0$^{o}$C. Upon completion of the addition, the reaction mixture was allowed to warm to rt and stir for 60 min, at which point the reaction was deemed complete on analysis by TLC (silica gel). The reaction mixture was then diluted with ethyl acetate (200 mL) and a solution of 10% aq sodium chloride (200 mL) was added. The biphasic mixture, which resulted, was allowed to stand for 15 min and the layers were separated. The aq layer was then extracted with ethyl acetate (100 mL) and the combined organic layers were washed with 10% aq sodium chloride solution (100 mL). The organic layer was dried ($Na_2SO_4$). The solvent was removed under reduced pressure. The brown solid which was obtained was purified by crystallization using 15:85(ethyl acetate/hexanes), to give **7-Bromo-5-(2-fluorophenyl)-1,3-dihydro-1-methyl-2H-1,4-benzodiazepin-2-one (17)** (18.75 g, 72%) as a brownish white solid.

$^{1}$H NMR (500 MHz, $CDCl_3$): 7.82(d, 1H) 7.66-7.64 (m, 2H, 2 x ArH), 7.60-7.57 (m, 2H, 2 x ArH), 7.52-7.49 (m, 2H, 2xArH), 7.38 (dd, 1H, J=8.5, 2.0Hz,H-4), 4.6 (D, 1H), 3.6(D,1H), 3.3(S,3H).

13C NMR (500 MHz, $CDCl_3$): 171.2, 168.21, 149.4, 139.5, 134.4, 133.4, 131.7, 129.3, 128.5, 120.3, 119.2, 118.8, 82.3, 79.2, 56.2, 34.2. $R_f$ = 0.5 (silica gel, ethyl acetate/hexanes 1:2)

**2. 5. 12 1-methyl-5-(2-fluorophenyl)-7-((tripropan-2-ylsilyl) ethynyl)-1,3-dihydro-2*H*-1,4-benzodiazepin-2-one. (18)**

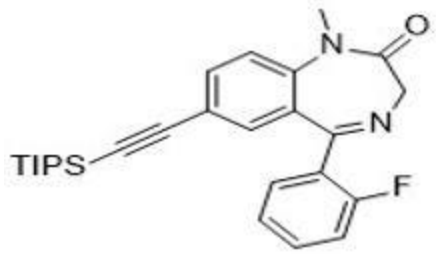


In a 500mL round bottom flask, $Pd(OAc)_2$ (615mg, 2.74 mmol) and P(o-tolyl)$_3$ (1.66 gm, 5.47 mmol) was added to 50 mL of acetonitrile. The mixture was stirred until a slurry appeared, which took about 20 min. Then **7-Bromo-5-(2-fluorophenyl)-1,3-dihydro-1-methyl-2H-1,4 benzodiazepin-2-one**, **(17)** (18 g, 51.84 mmol), triethylamine (15.26 mL, 109.46 mmol), (triisopropylylsilyl)acetylene (18.4 mL,82.01 mmol) and additional acetonitrile (200 mL) was added. The reaction mixture was then heated to reflux (75$^o$C) and held for 6 h, at which point the reaction was deemed complete on analysis by TLC (Silica gel). Upon completion of the reaction progress, the mixture was cooled to rt and filtered through celite. After washing with acetonitrile (100 mL x 2), the solvents were removed under reduced pressure and the residue was dissolved in dichloromethane (400 mL) and 5% aq sodium bicarbonate (400 mL) was added. The biphasic mixture, which resulted, was allowed to stand for 15 min and the layers were separated. The aq layer was then extracted with dichloromethane (300 mL) and the combined organic layers were washed with 5% aq sodium bicarbonate solution (300 mL) and then 10% aq sodium chloride solution (300 mL x 3). The organic layer was dried ($Na_2SO_4$) and it was purified by flash

chromatography on silica gel. This process gave a dark orange liquid that gets solidified eventually on standing to give **1-methyl-5-(2-fluorophenyl)-7-((tripropan-2-ylsilyl) ethynyl)-1,3-dihydro-2*H*-1,4-benzodiazepin-2-one**, (**18**) (16.28g ,70% crude yield) as waxy solid.

$^1$H NMR (300 MHz, $CDCl_3$): 7.67(d, 3H) 7.43-7.51 (m, 4H), 7.32-7.28 (d, 1H), 4.83 (D, 1H), 3.81(D,1H), 3.42(S,3H), 1.11(s,21H). 13C NMR (500 MHz, $CDCl_3$): 169.8, 168.7, 143.6, 138.0, 135.1, 133.6, 130.8, 129.7, 128.4, 121.0, 119.4, 118.8, 105.0, 92.3, 56.6, 34.8, 18.6, 11.2. $R_f$ = 0.7 (silica gel, ethyl acetate/hexanes 1:2)

### 2. 5. 13 7-ethynyl-5-(2-fluorophenyl)-1,3-dihydro-1-methyl-2*H*-1,4-Benzodiazepin-2-one (KRM II 08) (19)

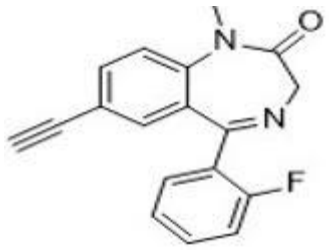


**1-methyl-5-(2-fluorophenyl)-7-((tripropan-2-ylsilyl) ethynyl)-1,3-dihydro-2*H*-1,4-benzodiazepin-2-one**, **(18)** (16.0 g, 35.66 mmol), water (3 mL) and tetrahydrofuran (200 mL) were cooled to -20$^o$C using a dry ice / IPA bath. Then tetrabutylammonium fluoride hydrate, [1M in THF (42.79 mL, 42.79 mmoL)] was added dropwise to the reaction mixture over a 30 min period, while maintaining the temperature at -20 to -15$^o$C. Upon completion of the addition, the reaction mixture was allowed to warm to rt and stir for an additional 60 min, at which point the reaction progress was deemed complete on analysis by TLC (silica gel). The reaction mixture was then diluted with ethyl acetate (150 mL) and 10% aq sodium chloride (150 mL) solution. The biphasic mixture, which resulted, was allowed to stand for 15 min and the layers were separated.

The aq layer was then extracted with ethyl acetate (150 mL x 3) and the combined organic layers were washed with 10% aq sodium chloride solution (150 mL). The organic layer was dried ($Na_2SO_4$). The solvents were removed under reduced pressure. Then the mixture was dissolved in 300 mL of ethyl acetate and then stirred with 200gm of silica gel for 2 hours and filtered. The amount of solvent was reduced to about 40 ml under reduced pressure. Then 200mL of hexanes was added dropwise to the mixture and it was allowed to stir overnight. The solid, which formed, was filtered and the grey solid was recrystallized from 1:4 (ethyl acetate/hexanes) to get 9.20 gm of cream white colored KRM II 08. The filtrate was concentrated under reduced pressure and after purification by column chromatography provided more of KRM II 08 (1.22 g). These solids were dried under vacuum at 40$^oC$. (10.42 g, 91%)

$^1H$ NMR (500 MHz, $CDCl_3$): 7.82(d, 1H) 7.66-7.64 (m, 2H, 2 x ArH), 7.60-7.57 (m, 2H, 2 x ArH), 7.52-7.49 (m, 2H, 2xArH), 7.38 (dd, 1H, J=8.5, 2.0Hz,H-4), 4.6 (D, 1H), 3.6(D,1H), 3.3(S,3H), 3.1(s,1H). 13C NMR (500 MHz, $CDCl_3$): 171.2, 168.21, 149.4, 139.5, 134.4, 133.4, 131.7, 129.3, 128.5, 120.3, 119.2, 118.8, 82.3, 79.2, 56.2, 34.2. $R_f$ = 0.4 (silicagel, ethylacetate/hexanes 1:2) HRMS (ESI/IT-TOF): *m/z* $[M + H]^+$ calcd for C18H13FN2O: 292.3112; found 292.3098.

**2. 5. 14 1-methyl-5-(2-fluorophenyl)-7-((tripropan-2-ylsilyl) ethynyl)-1,3-dihydro-2*H*-1,4-benzodiazepin-2-one. (20)**

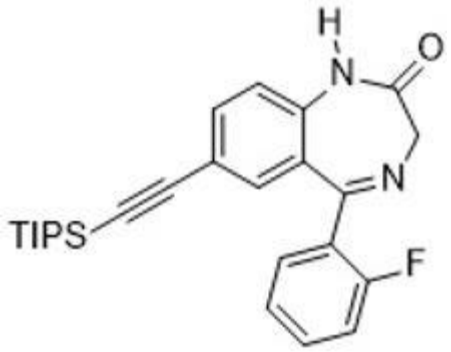

In a 500mL round bottom flask, $Pd(OAc)_2$ (955mg, 4.25 mmol) and $P(o\text{-}tolyl)_3$ (2.58gm, 8.45 mmol) was added to 50 mL of acetonitrile. The mixture was stirred until a slurry appeared, which took about 20 min. Then **7-Bromo-5-(2-fluorophenyl)-1,3-dihydrobenzo[e]-1,4-diazepin-2-one (16),** (28.0 g, 85.05 mmol), triethylamine (23.63 mL, 190.34 mmol), (triisopropylylsilyl)acetylene (24.8 mL,110.57 mmol) and additional acetonitrile (250 mL) was added. The reaction mixture was then heated to reflux (75$^o$C) and held for 6 h, at which point the reaction was deemed complete on analysis by TLC (Silica gel). Upon completion of the reaction progress, the mixture was cooled to rt and filtered through celite. After washing with acetonitrile (100 mL x 2), the solvents were removed under reduced pressure and the residue was dissolved in dichloromethane (400 mL) and 5% aq sodium bicarbonate (400 mL) was added. The biphasic mixture, which resulted, was allowed to stand for 15 min and the layers were separated. The aq layer was then extracted with dichloromethane (300 mL) and the combined organic layers were washed with 5% aq sodium bicarbonate solution (300 mL) and then 10% aq sodium chloride solution (300 mL x 3). The organic layer was dried ($Na_2SO_4$) and it was purified by flash chromatography on silica gel. This process gave a dark orange liquid that gets solidified eventually on standing to give **5-(2-fluorophenyl)-7-((tripropan-2-ylsilyl) ethynyl)-1,3-dihydro-2*H*-1,4-benzodiazepin-2-one** (**20**,) (25.54g ,70% crude yield)

$^1$H NMR (300 MHz, $CDCl_3$): 7.67(d, 3H) 7.43-7.51 (m, 4H), 7.32-7.28 (d, 1H), 4.83 (D, 1H), 3.81(D,1H), 3.42(S,3H), 1.11(s,21H). 13C NMR (500 MHz, $CDCl_3$): 169.8, 168.7, 143.6, 138.0, 135.1, 133.6, 130.8, 129.7, 128.4, 121.0, 119.4, 118.8, 105.0, 92.3, 56.6, 34.8, 18.6, 11.2. $R_f$ = 0.7 (silica gel, ethyl acetate/hexanes 1:2) The spectral properties of **20** was identical to the published values.

**2. 5. 15 7-Ethynyl-5-(2-fluorophenyl)-1,3-dihydro-2*H*-1,4-benzodiazepin-2-one (21)**

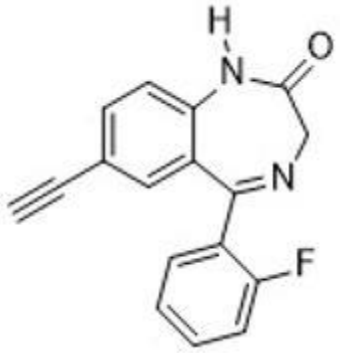


5-(2-fluorophenyl)-7-((tripropan-2-ylsilyl) ethynyl)-1,3-dihydro-2*H*-1,4-benzodiazepin-2-one (20) , (20.0 g, 60.16 mmol), water (3 mL) and tetrahydrofuran (200 mL) was cooled to -20$^{o}$C using a dry ice / IPA bath. Then tetrabutylammonium fluoride hydrate, [1M in THF (72.19 mL, 72.19 mmoL)] was added dropwise to the reaction mixture over a 30 min period, while maintaining the temperature at -20 to -15$^{o}$C. Upon completion of the addition, the reaction mixture was allowed to warm to rt and stir for an additional 60 min at which point the reaction progress was deemed complete on analysis by TLC (silica gel). The reaction mixture was then diluted with ethyl acetate (150 mL) and 10% aq sodium chloride (150 mL). The biphasic mixture, which resulted, was allowed to stand for 15 min and the layers were separated. The aq layer was then extracted with ethyl acetate (150 mL x 3) and the combined organic layers were washed with 10% aq sodium chloride solution (150 mL). The organic layer was dried ($Na_2SO_4$). The solvents were removed under reduced pressure. Then the mixture was dissolved in 300 mL of ethyl acetate and then stirred with 200gm of silica gel for 2 hours and filtered. The amount of solvent was reduced to about 40 ml under reduced pressure. Then 200mL of hexanes was added dropwise to the mixture and it was allowed to stir overnight. The solid, which formed, was filtered and the grey solid was recrystallized from 1:4 (ethyl acetate/hexanes) to get 9.00 gm of cream white colored Nor KRM II

08 (TA I 12) **(21)**. The filtrate was concentrated under reduced pressure and after purification by column chromatography provided more of TA I 12 (**21**) (1.89 g). These solids were dried under vacuum at 40$^{o}$C. (10.89 g, 85%)

$^{1}$H NMR (500 MHz, $CDCl_3$): 7.82(d, 1H) 7.66-7.64 (m, 2H, 2 x ArH), 7.60-7.57 (m, 2H, 2 x ArH), 7.52-7.49 (m, 2H, 2xArH), 7.38 (dd, 1H, J=8.5, 2.0Hz,H-4), 4.6 (D, 1H), 3.6(D,1H), 3.3(S,3H), 3.1(s,1H). 13C NMR (500 MHz, $CDCl_3$): 171.2, 168.21, 149.4, 139.5, 134.4, 133.4, 131.7, 129.3, 128.5, 120.3, 119.2, 118.8, 82.3, 79.2, 56.2, 34.2. $R_f$ = 0.4 (silicagel, ethylacetate/hexanes 1:2) HRMS (ESI/IT-TOF): *m/z* $[M + H]^+$ calcd for $C_{17}H_{11}FN_2O$: 278.2779; found 278.2768.

**2. 5. 16 7-ethynyl-1-(methyl-*d*$_3$)-5-phenyl-1,3-dihydro-2*H*-benzo[*e*][1,4]diazepin-2-one. (22)**

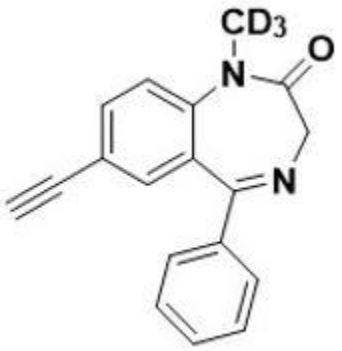


The 5-phenyl-7-((ethynyl)-1,3-dihydro-2*H*-1,4-benzodiazepin-2-one (**7**), (4.0 g, 15.34 mmol) was dissolved in THF (15 mL) and the solution was cooled to 0$^{o}$C using an ice bath. Then potassium tert butoxide (1.90 g, 16.92 mmol), which was dissolved in 20 mL of THF, was added dropwise by using an addition funnel. Then deuterated methyl iodide (1.24 mL, 19.94 mmoL) was added dropwise to the reaction mixture over a 5 min period, while maintaining the temperature at 0$^{o}$C. Upon completion of the addition, the reaction mixture was allowed to warm to rt and stirred for 60 min, at which point the reaction was deemed complete on analysis by TLC (silica gel). The

reaction mixture was then diluted with ethyl acetate (20 mL) and a solution of 10% aq sodium chloride (20 mL) was added. The biphasic mixture, which resulted, was allowed to stand for 15 min and the layers were separated. The aq layer was then extracted with ethyl acetate (20 mL) and the combined organic layers were washed with 10% aq sodium chloride solution (20 mL). The organic layer was dried ($Na_2SO_4$). The solvent was removed under reduced pressure. The brown solid, which was obtained was purified by crystallization using 15:85(ethyl acetate/hexanes), to give 7-ethynyl-1-(methyl-$d_3$)-5-phenyl-1,3-dihydro-2*H*-benzo[*e*][1,4]diazepin-2-one (**22**)(3.7 g, 86%) as a white solid.

$^1$H NMR (500 MHz, $CDCl_3$): 7.82(d, 1H) 7.66-7.64 (m, 2H, 2 x ArH), 7.60-7.57 (m, 2H, 2 x ArH), 7.52-7.49 (m, 2H, 2xArH), 7.38 (dd, 1H, J=8.5, 2.0Hz,H-4), 4.6 (D, 1H), 3.6(D,1H), 3.1(s,1H). 13C NMR (500 MHz, $CDCl_3$): 171.2, 168.21, 149.4, 139.5, 134.4, 133.4, 131.7, 129.3, 128.5, 120.3, 119.2, 118.8, 82.3, 79.2, 56.2, 34.2. $R_f$ = 0.5 (silica gel, ethyl acetate/hexanes 1:2) HRMS (ESI/IT-TOF): *m/z* [M +H] + calcd for $C_{18}H_{11}D_3N_2O$: 277.3350; found 277.3329

### 2. 5. 17 7-Ethynyl-1-(methyl-$d_3$)-5-phenyl-1,3-dihydro-2*H*-benzo[*e*] [1,4] diazepin-2-one-3,3-$d_2$ (24)

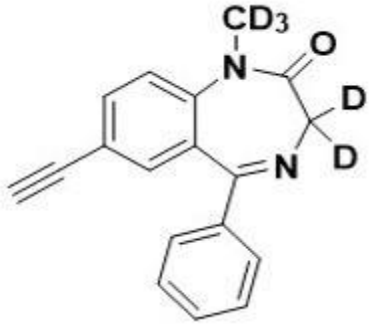


The 7-ethynyl-1-(methyl-$d_3$)-5-phenyl-1,3-dihydro-2*H*-benzo[*e*] [1,4] diazepin-2-one(22), (0.5 g, 1.8 mmol) was dissolved in d$^4$-methanol (1 mL). Then potassium tert butoxide (0.22 g, 1.9 mmol)

was added to the solution. The mixture was sonicated for 45 min starting from rt to 50C. After the reaction was completed (checked by NMR) 5 ml of de-ionized water was added and the mixture was extracted with (5ml X 2) ethyl acetate. It was dried by first with blowing argon over it and then placing it in high vacuum. This gave 1-CD3-methyl-5-phenyl-7-ethynyl-1,3-dihydro-2*d*-1,4-benzodiazepin-2-one with 97% deuteration at C-3 position via integration by NMR spectroscopy, to give 7-Ethynyl-1-(methyl-$d_3$)-5-phenyl-1,3-dihydro-2*H*-benzo[*e*] [1,4] diazepin-2-one-3,3-$d_2$ (D5 QH II 66) (**24**) (0.49 g, 97%) as a white solid.

$^1$H NMR (500 MHz, $CDCl_3$): 7.82(d, 1H) 7.66-7.64 (m, 2H, 2 x ArH), 7.60-7.57 (m, 2H, 2 x ArH), 7.52-7.49 (m, 2H, 2xArH), 7.38 (dd, 1H, J=8.5, 2.0Hz,H-4), 3.1(s,1H), . 13C NMR (500 MHz, $CDCl_3$): 171.2, 168.21, 149.4, 139.5, 134.4, 133.4, 131.7, 129.3, 128.5, 120.3, 119.2, 118.8, 82.3, 79.2, 56.2, 34.2. $R_f$ = 0.5 (silica gel, ethyl acetate/hexanes 1:2), HRMS (ESI/IT-TOF): *m/z* [M + H] + calcd for $C_{18}H_9D_5N_2O$: 279.3473; found 279.3422.

**2. 5. 18 (2-amino-3,5-dibromophenyl) (phenyl) methanone (27)**


To a solution of 2-aminobenzophenone **1** (100 g, 253.5 mmol) in DCM (600 mL), which was stirred at -10°C for 10 min, NBS (94.8 g, 532.4 mmol) was added in portions. The mixture was stirred for 2 hours at 0°C. After the reaction progress was completed, the mixture was diluted with

$H_2O$ (600 mL), extracted with DCM (600 mL), washed with brine (200 mL), dried over $Na_2SO_4$, and concentrated under reduced pressure. The crude bromide compound was purified by crystallization from ethylacetate and hexanes (10:90) to give **(2-amino-3,5-dibromophenyl) phenyl- methanone (27)** (9 g, 5% yield) as a yellow solid.

$^1$H NMR (500 MHz, $CDCl_3$): δ 7.66-7.64 (m, 2H, 2 x ArH), 7.60-7.57 (m, 2H, 2 x ArH), 7.52-7.49 (m, 2H, 2xArH), 7.38 (dd, 1H, J=8.5, 2.0Hz,H-4), 6.67(d, 1H, J=8.5Hz, H-3), 6.11 (br s, 2H, $NH_2$). 13C NMR (500 MHz, $CDCl_3$): 198.2, 149.4, 139.5, 134.4, 133.4, 131.7, 129.3, 128.5, 120.3, 119.2, 118.8. $R_f$ = 0.4 at 1:9 (silicagel, ethylacetate/Hexanes)

**2. 5. 19 *N*-(2-benzoyl-4,6-dibromophenyl)-2-bromoacetamide (28)**


To a mixture of **(2-amino-3,5-dibromophenyl) (phenyl) methanone** (**27**, 8 g, 22.53 mmol), sodium bicarbonate (3.79 g, 45.06 mmol), and dichloromethane (100 mL), bromoacetyl bromide (2.75 mL, 31.52 mmol) was added dropwise over a 60 min time period. The temperature was kept between -10°C – 0°C with continuous stirring. The white colored reaction mixture, which resulted, was then allowed to stir for longer than 3 h at rt. The completion of the reaction was verified by analysis by TLC (silica gel) and 50% ethyl acetate / hexanes. The reaction mixture was then slowly diluted over 30 min with water (30 mL) as carbon dioxide bubbles ocurred. The biphasic mixture, which resulted, was allowed to stand for 15 min and the layers were separated. The aq layer was

extracted with dichloromethane (30 mL) and the combined organic layers were washed with 5% aq sodium bicarbonate solution (30 mL) and then 10% aq sodium chloride solution (30 mL). The organic layer was dried ($Na_2SO_4$). The solvents were removed under reduced pressure and the residue was slurried with ethanol (30 mL) at 50 – 55$^oC$ for 30 min. Upon cooling to rt and after holding the temperature for 1 h, the solid, which formed, was filtered, and washed with ethanol (60 mL x 3). The solid was dried under vacuum at 40$^oC$ to afford the product *N*-(2-benzoyl-4,6-dibromophenyl)-2-bromoacetamide **28** as an off-white solid (10.24 g, 95.5%).

$^1H$ NMR (500 MHz, $CDCl_3$): δ11.60 (s,1H) 7.66-7.64 (m, 2H, 2 x ArH), 7.60-7.57 (m, 2H, 2 x ArH), 7.52-7.49 (m, 2H, 2xArH), 7.38 (dd, 1H, J=8.5, 2.0Hz,H-4), 6.67(d, 1H, J=8.5Hz, H-3), 4.21 (s, 2H). 13C NMR (500 MHz, $CDCl_3$): 198.2,165.21, 149.4, 139.5, 134.4, 133.4, 131.7, 129.3, 128.5, 120.3, 119.2, 118.8, 42.3

**2. 5. 20 (5,7-Dibromo)-5-phenyl-1,3-dihydro-2*H*-1,4-benzodiazepin-2-one 29**


A mixture of ***N*-(2-benzoyl-4,6-dibromophenyl)-2-bromoacetamide**, **28** (10 g, 21.01 mmol), hexamethylenetetramine (HMTM, 6.48 g, 46.22 mmol), ammonium acetate (3.56 g, 46.22 mmol), and isopropanol (100 mL) was heated to reflux (82$^oC$). The reaction mixture was held at reflux for 6 h, at which point the reaction progress was deemed complete on analysis by TLC (silica gel and 1:1, ethyl acetate/hexanes). The reaction mixture was then cooled to 0 – 5$^oC$ using an ice bath.

The solid, which resulted, was filtered, and washed with cold isopropanol (50 mL x 2) and then water (50mL x 4). The solid was dried under vacuum at 40$^{o}$C to afford 4.8 g of the benzodiazepine **4** as an off-white solid. The IPA was removed from the mother liquor under reduced pressure. The solid was then extracted with ethyl acetate. The ethyl acetate was removed under reduced pressure and the residue was purified by column chromatograpy using 1:4 etheyl acetate/hexanes to afford **(5,7-Dibromo)-5-phenyl-1,3-dihydro-2*H*-1,4-benzodiazepin-2-one. 29** (5.8 g, 70%)

$^{1}$H NMR (500 MHz, $CDCl_3$): δ9.89 (s,1H), 7.82(d, 1H) 7.66-7.64 (m, 2H, 2 x ArH), 7.60-7.57 (m, 2H, 2 x ArH), 7.52-7.49 (m, 2H, 2xArH), 7.38 (dd, 1H, J=8.5, 2.0Hz,H-4), 4.32 (s, 2H). 13C NMR (500 MHz, $CDCl_3$): 170.2,165.21, 149.4, 139.5, 134.4, 133.4, 131.7, 129.3, 128.5, 120.3, 119.2, 118.8, 56.2. $R_f$ = .4 (Silicagel, ethylacetate/Hexanes 1:2)

**2. 5. 21 (5, 7-Dibromo)-1-methyl-5-phenyl-1,3-dihydro-2*H*-1,4-benzodiazepin-2-one 30**

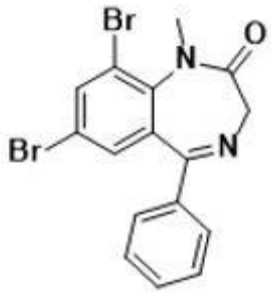


The **(5,7-Dibromo)-5-phenyl-1,3-dihydro-2*H*-1,4-benzodiazepin-2-one**, **29** (5.0 g, 12.69 mmol) was dissolved in THF, (50 mL) and the solution was cooled to -0$^{o}$C using an ice bath. Then potassium tert butoxide (1.57 g, 13.95 mmol) which was dissolved in 100 mL of THF was added dropwise by using an addition funnel. Then methyl iodide (0.87 mL, 13.95 mmoL) was added dropwise to the reaction mixture over a 5 min period, while maintaining the temperature at 0$^{o}$C. Upon completion of the addition, the reaction mixture was allowed to warm to rt and stir for 60

min, at which point the reaction was deemed complete on analysis by TLC (silica gel). The reaction mixture was then diluted with ethyl acetate (20 mL) and a solution of 10% aq sodium chloride (20 mL) was added. The biphasic mixture, which resulted, was allowed to stand for 15 min and the layers were separated. The aq layer was then extracted with ethyl acetate (50 mL) and the combined organic layers were washed with 10% aq sodium chloride solution (50 mL). The organic layer was dried ($Na_2SO_4$). The solvent was removed under reduced pressure. The brown solid which was obtained was purified by crystallization using 15:85(ethyl acetate/hexanes), to give **(5, 7-Dibromo)-1-methyl-5-phenyl-1,3-dihydro-2*H*-1,4-benzodiazepin-2-one 30** (3.88 g, 75%) as a brownish white solid.

$^1$H NMR (500 MHz, $CDCl_3$): 7.82(d, 1H) 7.66-7.64 (m, 2H, 2 x ArH), 7.60-7.57 (m, 2H, 2 x ArH), 7.52-7.49 (m, 2H, 2xArH), 7.38 (dd, 1H, J=8.5, 2.0Hz,H-4), 4.6 (D, 1H), 3.6(D,1H), 3.3(S,3H). 13C NMR (500 MHz, $CDCl_3$): 171.2, 168.21, 149.4, 139.5, 134.4, 133.4, 131.7, 129.3, 128.5, 120.3, 119.2, 118.8, 82.3, 79.2, 56.2, 34.2. $R_f$ = 0.5 (silica gel, ethyl acetate/hexanes 1:2) The spectral properties of **5** was identical to the published values.

### 2. 5. 22 1-Methyl-5-phenyl-(5.7-((ditripropan-2-ylsilyl) bisethynyl)-1,3-dihydro-2*H*-1,4-benzodiazepin-2-one

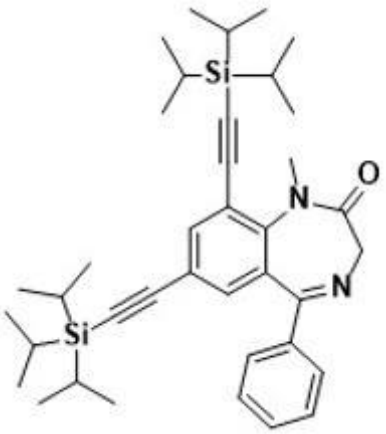

In a 500mL round bottom flask, $Pd(OAc)_2$ (213 mg, 0.95 mmol) and $P(o\text{-}tolyl)_3$ (578mg, 1.9 mmol) was added to 50 mL of acetonitrile. The mixture was stirred until a slurry appeared, which took about 20 min. Then 7-bromo-1-methyl-5-phenyl-1,3-dihydro-2*H*-1,4-benzodiazepin-2-one **29**, (3.88 g, 9.5 mmol), triethylamine (2.66 mL, 19 mmol), (triisopropylylsilyl)acetylene (6.4 mL,28.5 mmol) and additional acetonitrile (50 mL) was added. The reaction mixture was then heated to reflux (75$^oC$) and held for 6 h, at which point the reaction was deemed complete on analysis by TLC (Silica gel). Upon completion of the reaction progress, the mixture was cooled to rt and filtered through celite. After washing with acetonitrile (20 mL x 2), the solvents were removed under reduced pressure and the residue was dissolved in dichloromethane (40 mL) and 5% aq sodium bicarbonate (40 mL) was added. The biphasic mixture, which resulted, was allowed to stand for 15 min and the layers were separated. The aq layer was then extracted with dichloromethane (30 mL) and the combined organic layers were washed with 5% aq sodium bicarbonate solution (30 mL) and then 10% aq sodium chloride solution (30 mL x 3). The organic layer was dried ($Na_2SO_4$) and it was purified by flash chromatography on silica gel. This process gave a dark orange liquid that gets solidified eventually on standing to give 1-Methyl-5-phenyl-(5.7-((ditripropan-2-ylsilyl) bisethynyl)-1,3-dihydro-2*H*-1,4-benzodiazepin-2-one **31**, (4.12 g ,71% crude yield) This material was used in the next step without further purification.

$R_f$ = 0.7 (silica gel, ethyl acetate/hexanes 1:2)

**2. 5. 23 7,9-diethynyl-1-methyl-5-phenyl-1,3-dihydro-2*H*-benzo[*e*] [1,4] diazepin-2-one**

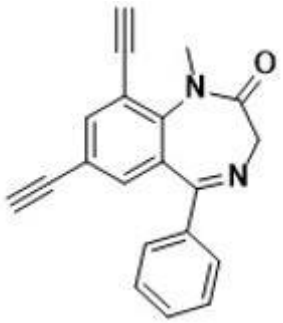


1-Methyl-5-phenyl-7-((tripropan-2-ylsilyl) ethynyl)-1,3-dihydro-2*H*-1,4-benzodiazepin-2-one **31**, (4.12 g, 6.74 mmol), water (3 mL) and tetrahydrofuran (200 mL) were cooled to -20$^{o}$C using a dry ice / IPA bath. Then tetrabutylammonium fluoride hydrate, [1M in THF (13.48 mL, 13.48 mmoL)] was added dropwise to the reaction mixture over a 30 min period, while maintaining the temperature at -20 to -15$^{o}$C. Upon completion of the addition, the reaction mixture was allowed to warm to rt and stir for an additional 60 min at which point the reaction progress was deemed complete on analysis by TLC (silica gel). The reaction mixture was then diluted with ethyl acetate (50 mL) and 10% aq sodium chloride (50 mL). The biphasic mixture, which resulted, was allowed to stand for 15 min and the layers were separated. The aq layer was then extracted with ethyl acetate (50 mL x 3) and the combined organic layers were washed with 10% aq sodium chloride solution (50 mL). The organic layer was dried ($Na_2SO_4$). The solvents were removed under reduced pressure. Then the mixture was dissolved in 30 mL of ethyl acetate and then stirred with 20gm of silica gel for 2 hours and filtered. The amount of solvent was reduced to about 40 ml under reduced pressure. Then 40mL of hexanes was added dropwise to the mixture and it was allowed to stir overnight. The solid, which formed, was filtered and the grey solid was recrystallized from 1:4 (ethyl acetate/hexanes) to get 1.3 gm of cream white colored QH II 66. The

filtrate was concentrated under reduced pressure and after purification by column chromatography provided more of QH II 66 (0.5 g). These solids were dried under vacuum at 40$^{o}$C. (1.8 g, 80%)

$^{1}$H NMR (500 MHz, $CDCl_3$): 7.82(d, 1H) 7.66-7.64 (m, 2H, 2 x ArH), 7.60-7.57 (m, 2H, 2 x ArH), 7.52-7.49 (m, 2H, 2xArH), 7.38 (dd, 1H, J=8.5, 2.0Hz,H-4), 4.6 (D, 1H), 3.6(D,1H), 3.3(S,3H), 3.1(s,1H). 13C NMR (500 MHz, $CDCl_3$): 171.2, 168.21, 149.4, 139.5, 134.4, 133.4, 131.7, 129.3, 128.5, 120.3, 119.2, 118.8, 82.3, 79.2, 56.2, 34.2. $R_f$ = 0.4 (silicagel, ethylacetate/hexanes 1:2) HRMS (ESI/IT-TOF): *m/z* $[M + H]^+$ calcd for $C_{20}H_{14}N_2O$: 298.3367; found 298.3352.

# Chapter 3 Synthesis of QH II 66 analogues

## **3. 1** Synthesis of 7-Br NOR QH II 66 analogues.

### **3. 1. 1** BISCHLER-NAPIERLSKI Approach

#### **3. 1. 1. 1** Chemistry

The plan to the targets was to start with p-bromoaniline. An amide coupling reaction would be carried out by using a Boc protected chiral or non-chiral amino acid. This reaction could be done using DCC as a coupling reagent in DCM at room temperature. In the next step deprotection of the Boc group would be done via stirring in trifluoracetic acid in DCM at room temperature. Then the amine group would be re-protected by using a ortho substituted benzoyl chloride in the presence of sodium bicarbonate in DCM at room temperature. In the next step the product would be cyclized by using polyphosphoric acid or phosphorous oxychloride and heat. After that using a copper free sonogashira coupling reaction would be used to install a silyl protected ethinyl group at the c-7 position. In the next step the silyl group would be deprotected by using the tetra butyl

ammonium fluoride (TBAF) reagent. In the final step the N-H group would be N-methylated by using methyl iodide in presence of sodium tert-butoxide to be furnished the final product. See the **scheme 13.**

The first step was done on 20-gram scale. The para bromoaniline (33) was reacted with the Boc protected glycine (34) in the presence of DCC in DCM. This reaction was started at 0oC and it was allowed to warm to room temperature. This reaction mixture was stirred for 12 hours. After the reaction was completed (TLC). The white colored urea byproduct was removed by filtration. The solvent was removed under reduced pressure and the solid was crystallized by using 20:80 (Ethyl acetate: Hexanes). After recrystallization an 80% yield of amide (35) was achieved. In the next step deprotection of the Boc group was carried out in the presence of trifluoroacetic acid in DCM at room temperature. This mixture was stirred for 12 hours.

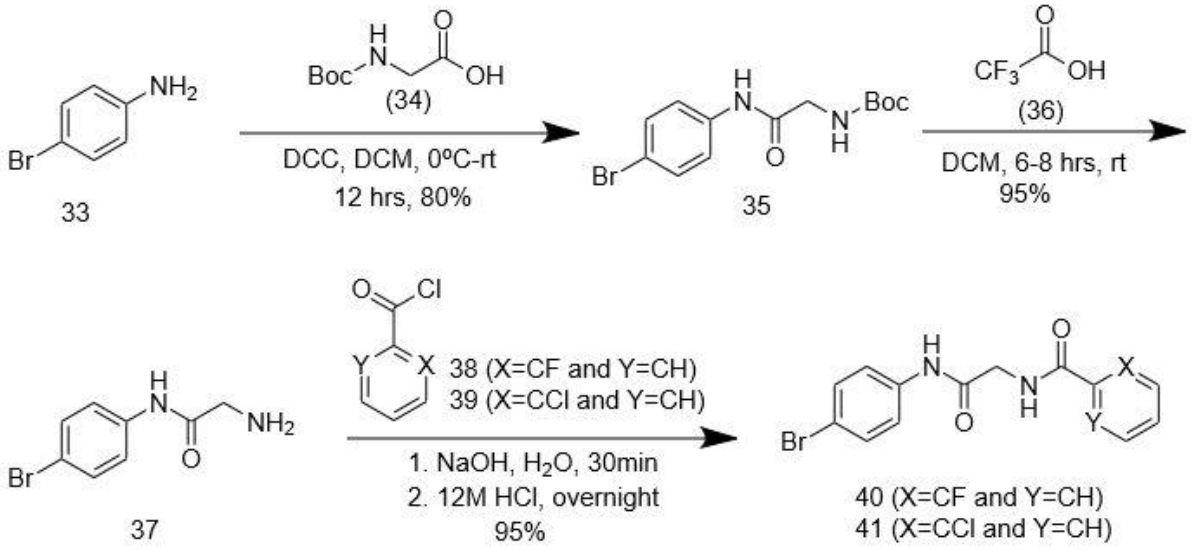


**Scheme 13. Proposed synthetic route for KRM II 08 analogues (part 1)**

After the completion of the reaction the solvent was removed under reduced pressure. The solid which remained was dissolved by using ethyl acetate and washed with sat. sodium bicarbonate

solution. The product was crystallized from 50:50 (Ethylacetate: Hexanes) to furnish 95% yield. The amine function of the product was protected by a benzoyl group. Benzoyl chloride was used to do this reaction. The reaction process was done in DCM in the presence of sodium bicarbonate at room temperature. The reaction process was completed in 30 minutes and the solid was purified by crystallization in 30:70 (Ethyl acetate: Hexanes) to give a 95% yield of the benzamide (40, 41). Cyclization of the benzamide (40) was attempted in the presence of phosphorous oxychloride and polyphosphoric acid with extreme heat. In the first approach phosphorous oxychloride was employed. This process was done in toluene, acetonitrile at reflux and with no solvent at extreme heat.

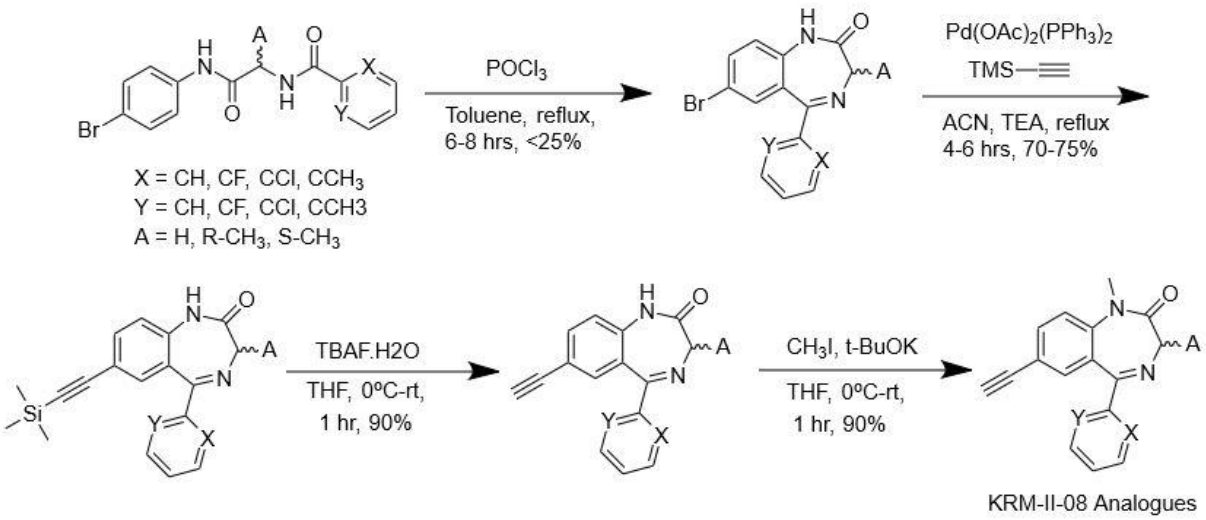


**Scheme 14. Proposed synthetic route for KRM II 08 analogues (part 2)**

**Table 3-1 Optimization of cyclization of amide 40**


| X=,Y= | SOLVENTS | Time | Reagent | Yield |
|---|---|---|---|---|
| CF,CH | None | 6-8 | POCl3 | 22% |
| CF,CH | ACN | 6-8 | POCl3 | 23% |
| CF,CH | Toluene | 6-8 | POCl3 | 27% |

The mixture was refluxed for 6-8 hours. In all the trials the percentage yield was very low, approximately 25% (See Table 2). The product was purified by column chromatography in 30:70 (Ethyl acetate : Hexanes).

The same trials were carried out in polyphosphoric acid, but there was no reaction. A few different types of substituted benzoyl chlorides were used later on but there was still no reaction in poly phosphoric acid. (**See scheme 15**)

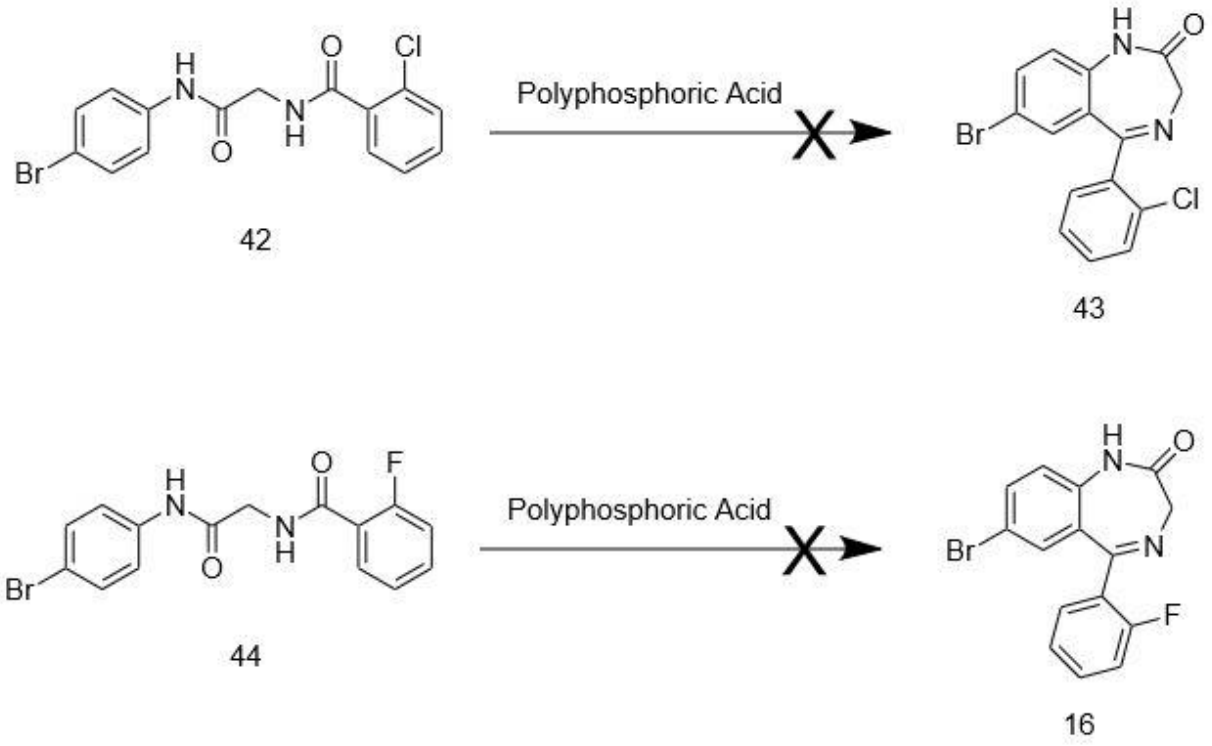


**Scheme 15. Proposed synthetic rout of 43 and 16.**

### 3. 1. 2 Gate's method to synthesize Diazepam.

Marshall Gates published a route to prepare diazepam in 1980. It was a six-step route. He started from 5-chloro isatoic anhydride (54). In the first step the N-H group was protected by converting it into an N-$CH_3$ compound. The reaction process was done in DMF, methyl iodide was used as methylating agent. In the next step a seven membered diazepine ring was synthesized from a six membered anhydride (55). Glycine was used in this step. The next step was protection of the N-H group in the seven membered diazepine ring. This step was carried out with an excess of acetic anhydride by refluxing for two- and one-half hours. The next step was to perform Grignard reaction to obtain the desired benzophenone 58. The deprotection of the amide function was done in the

next step to furnish a terminal amine function with hydroxyl amine. In the last step a cyclization was carried out in presence of sodium bisulfite. (Scheme 16)

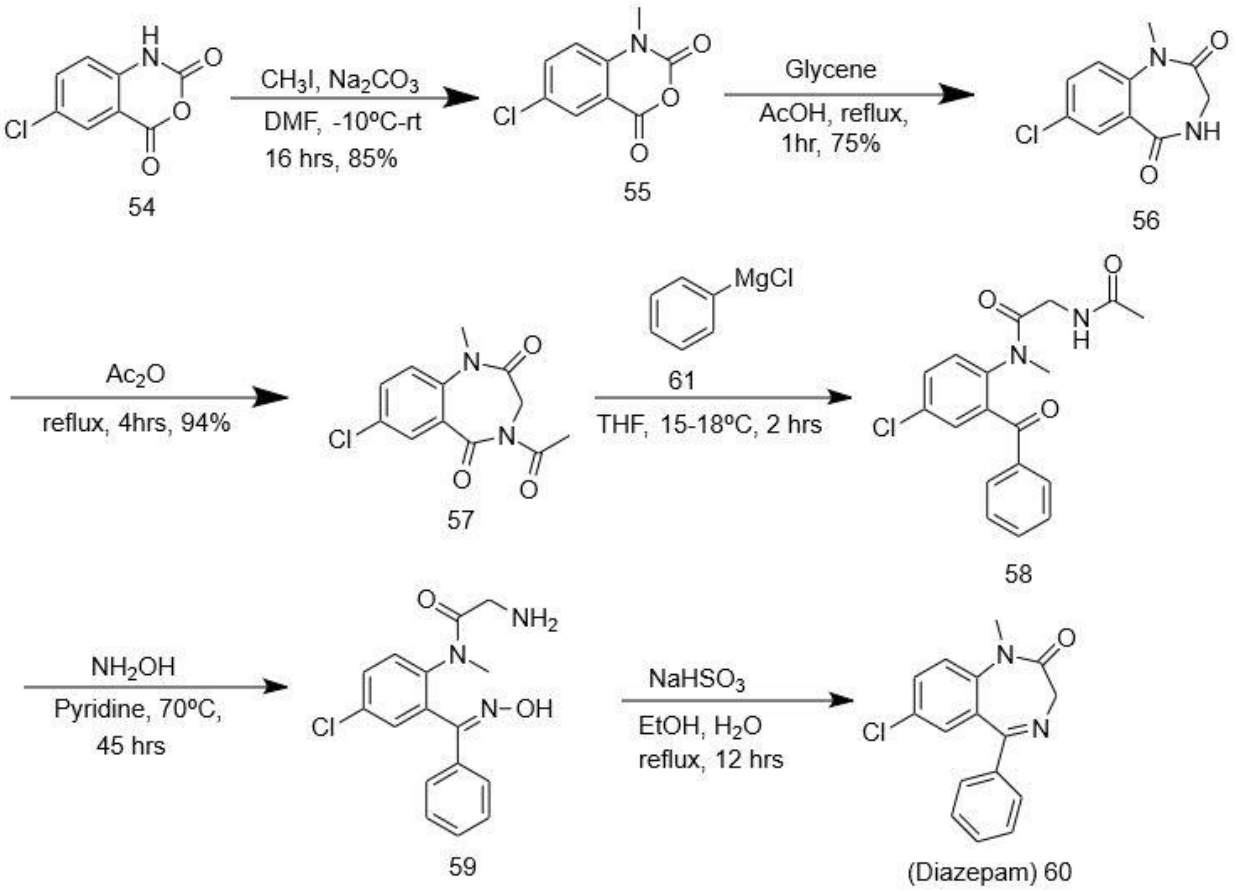


**Scheme 16. The Gate's method for the synthesis of diazepam 60.**

### 3. 1. 2. 1 Chemistry

The synthetic route presented in Scheme 16 was proposed the synthesis of TA II 73 (74), 2'$CH_3$ analog of QH II 66 which is a very important compound in the study of cancer. It was an eight-step process. The Gate's method for diazepam was adopted to prepare TA II 73 (74).

The 2-amino 5-bromo benzoic acid 45 was used as the staring material for the proposed route. In the first step 5-bromo isatoic anhydride 46 was synthesized by treating 2-amino 5-bromo benzoic acid 45 with triphosgene in THF at 70°C. The reaction mixture was allowed to stir for 2 hours.

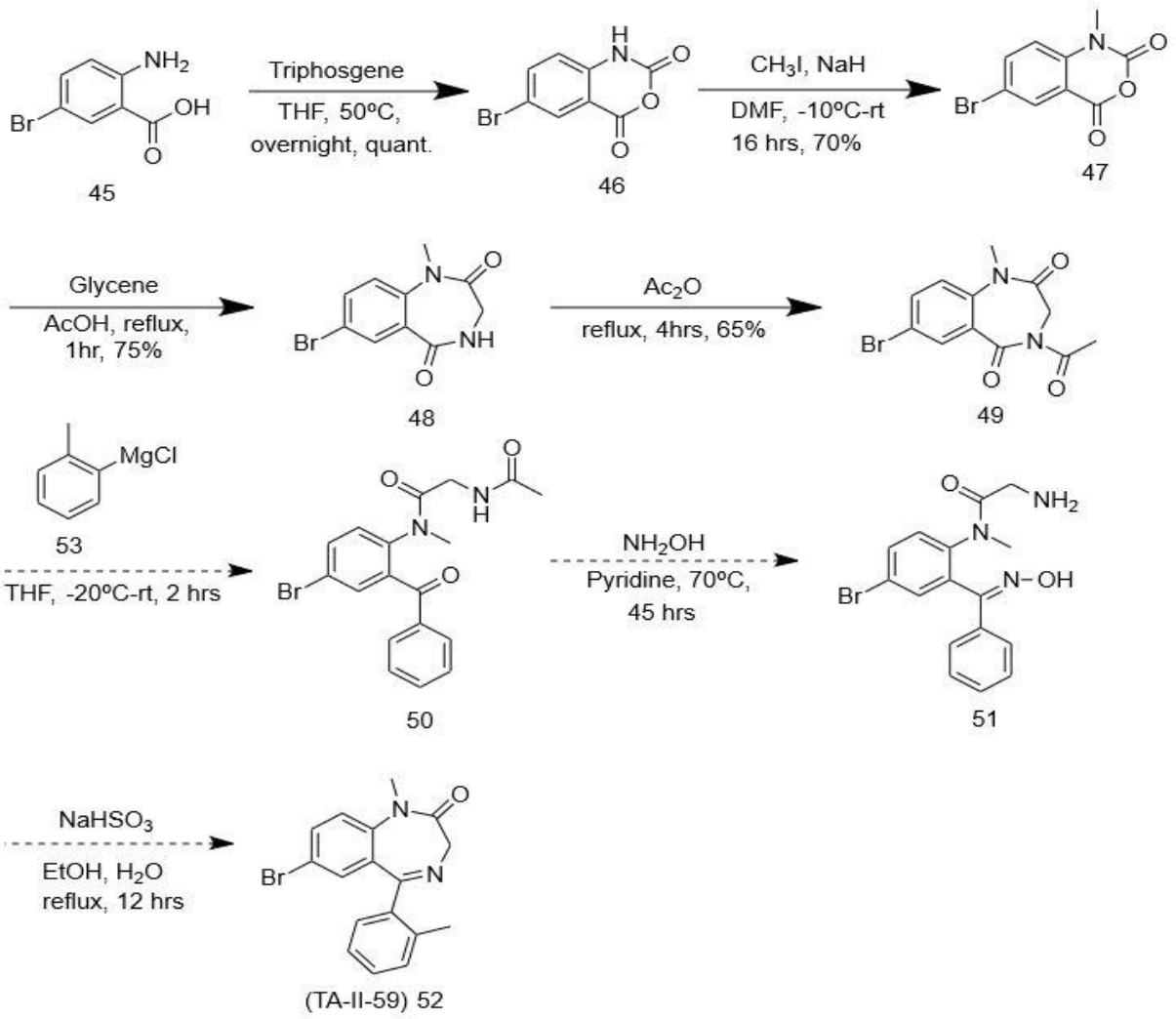


**Scheme 17. Proposed synthesis route to synthesize TA II 59, 2'$CH_3$ analog of 7-Br QH II 66.**

A saturated solution of sodium hydroxide was used to trap the unreacted phosgene gas during the reaction process in a phosgene gas trapping vessel. After complete conversion to the anhydride 46 reaction process was stopped and allowed to cool down to room temperature. The anhydride 46 precipitated as a white solid. It was separated by filtration and washed with methanol to furnish

the pure 5-bromo isatoic anhydride 46. The yield of this step was 95%. The largest scale was done on 50-gram to provide a large amount of the anhydride 46.

The methylation was done in the second step at the N-H position by using methyl iodide, sodium hydride used as the base and DMF was used as the solvent. The reaction mixture was stirred at room temperature for 16 hours. The reaction was quenched by adding water at $0^oC$ and extracted with DCM. The N-methyl amide 47 was crystallized by adding hexane dropwise at $0^oC$ to $10^oC$ to DCM solution. The percentage yield at this stage was 85%.

In the third step a ring expansion reaction was done to form the diazepine system. Acetic acid was used as the solvent. The N-methyl 5-bromo isotoic anhydride 47 was treated with glycine in acetic acid. This mixture was heated to reflux for 2.5 hours. After the reaction was completed (TLC) the hot solution was added directly to an ice-water mixture. The white precipitate which formed was filtered to furnish the diazepine 48. The yield was 65% at this stage.

The N-H group of the 7-membered diazepine ring 48 was protected by installing an acetyl group. This was done by refluxing the starting material in an excess amount of acetic anhydride for four hours. After four hours the rection mixture was allowed to cool down to room temperature. The acetamide 49 crystallized and was filtered to furnish the product. The yield was 70%.

After this step the acetyl protected 7 membered diazepine ring 49 was treated with ortho tolyl magnesium chloride in THF at room temperature analogous to the method of Gate's. At first the Grignard reagent was prepared by adding metallic magnesium to a solution of ortho tolylchloride in THF by refluxing for an hour. A solution was made of the reactant in THF, and the temperature was cooled to $-20^oC$. Then freshly prepared Grignard reagent was added dropwise for 20 minutes at a rate of 1mL per minute. After completing the addition, the temperature was increased to room temperature it was allowed to stir for an hour. After consuming all the staring material, the reaction

progress was stopped by using a saturated ammonium chloride solution. After workup with ethyl acetate a white product was collected. After characterization by 1H NMR it was confirmed that the product which formed, was not the desired benzophenone. The product was the corresponding tertiary alcohol 62.

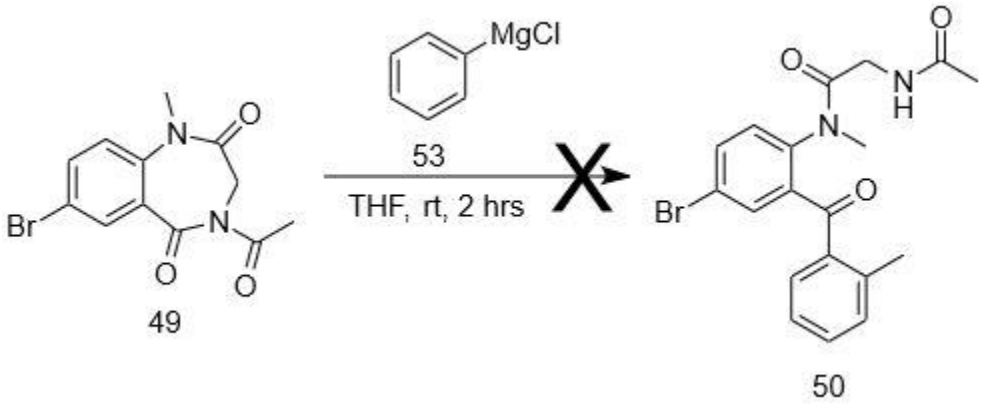


**Scheme 18. Grignard reaction of 49.**

This reaction was repeated several times, but the results were the same, and the product was always a tertiary alcohol.

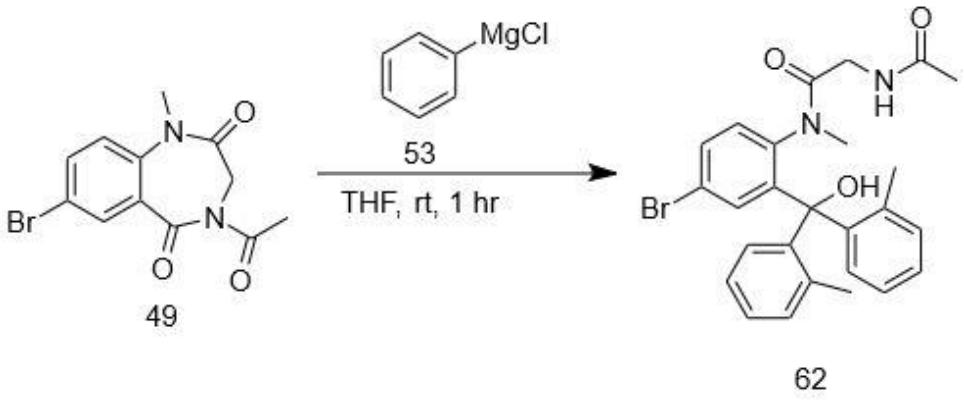


**Scheme 19. Product of Grignard reaction with 49**

After getting similar results in several trials, we decided to stop trying this route and moved forward to a different route.

## 3. 2 Synthesis of 5-bromo 2-amino benzophenone analogues.

### 3. 2. 1 Weijian Zhang's Method.

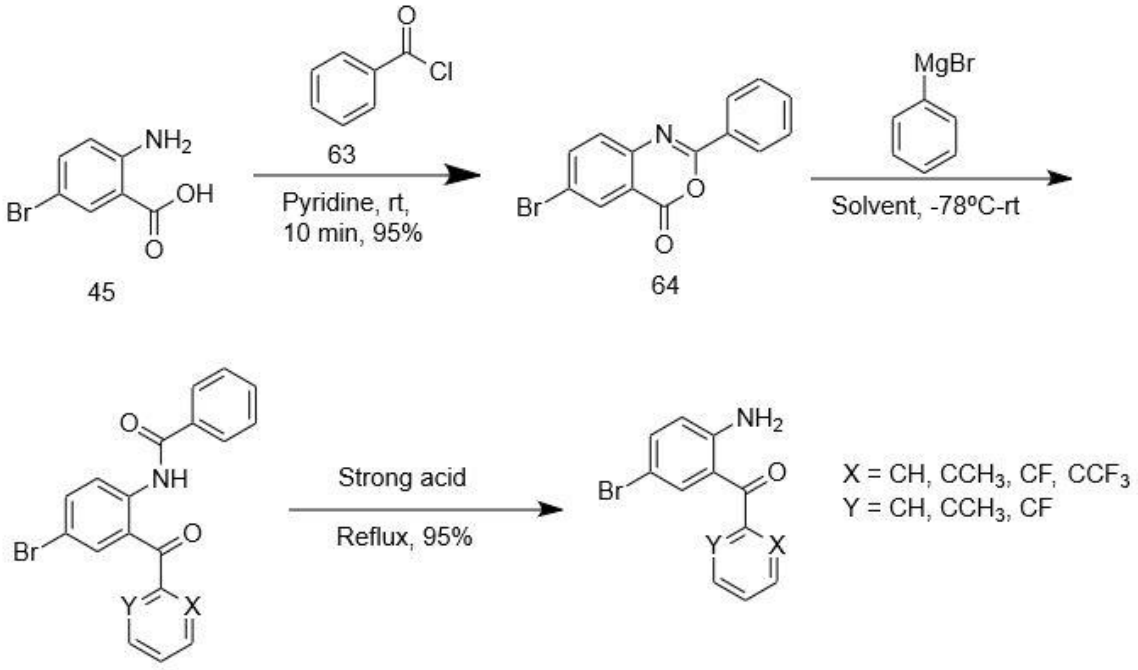


**Scheme 20. Proposed synthesis for 68 and it's analogues.**

#### 3. 2. 1. 1 Chemistry

According to the proposed route of Weijiang Zhang in Milwaukee, in the first step 6-bromo-2-phenyl-4*H*-benzo[*d*] [1,3] oxazin-4-one 64 was synthesized. 5 bromo 2 amino benzoic acid 45 and benzoyl chloride 63 were used as starting materials. This reaction was carried out in pyridine. 5 bromo 2 amino benzoic acid 45 was dissolved in pyridine. A second solution of benzoyl chloride 63 in pyridine was made and added dropwise into the first solution over 15 minutes at 0ºC. After addition of benzoyl chloride 63, the reaction process was completed within 10 minutes with

stirring. The precipitate which formed was filtered and collected. The product was washed with enough water used to remove the excess amount of pyridine several times.

In the second step the required Grignard reagent was made. To make the Grignard reagent a solution in a solution of ortho substituted bromobenzene in THF, dry Mg turnings were added. The mixture was allowed to heat to reflux until all the magnesium metal was consumed. To the other solution of 6-bromo-2-phenyl-4*H*-benzo[*d*] [1,3] oxazin-4-one 64 in THF the freshly prepared Grignard reagent was added at -20$^{o}$C over a period of 20 minutes. The reaction mixture was then allowed to stir at room temperature for an hour. The reaction was quenched by adding ammonium chloride. Ethyl acetate was used to extract the product. One of the products, the tertiary alcohol precipitated from a solution of 20% ethyl acetate in hexane. Only about 20% of desired product was collected by chromatography.

This Grignard reaction was done for four other analogs of ortho substituted bromobenzenes. On all occasions the respective tertiary alcohol was found as major product. (See Table 3)

**Table 3-2 Reaction of 64 with different Grignard reagents.**

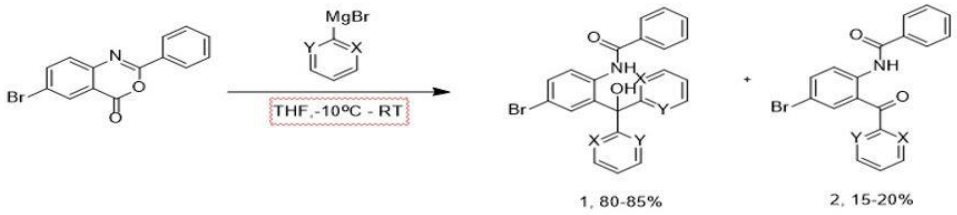


| Sl No | X | Y | Temperature | Equivalance | Duration | Product No 2 Yield |
|---|---|---|---|---|---|---|
| 1 | CF | CF | -10C-RT | 2 | 30 Min | 19% |
| 2 | CCH3 | CH | -10C-RT | 2 | 30 Min | 17% |
| 3 | CCF3 | CH | -10C-RT | 2 | 30 Min | 20% |
| 4 | CCH3 | CCH3 | -10C-RT | 2 | 30 Min | 15% |

In order to increase the amount of the desired product (*N*-(4-bromo-2-(2-methylbenzoyl) phenyl) benzamide) the Grignard reaction attempts were made to optimize the process by altering the Grignard solvent, reaction solvent, temperature, and duration. In the table 2 data is shown for the ortho tolyl ligand. The data indicated to get rid of the formation of the tertiary alcohol the Grignard reagent should be added at -40$^{o}$C and let solution slowly climb to room temperature. The yield of the desired product from this process was less than 20% but no alcohol was formed.

The similar yields were obtained for the 2'6' difluoro analogue. In this case the tertiary alcohol was not formed if the Grignard reagent was added at -40$^{o}$C but the desired product (*N*-(4-bromo-2-(2-methylbenzoyl) phenyl) benzamide) was formed in lower yield, which was less than 20%. (See table 4)

**Table 3-3 Optimization of the Grignard reaction of 64 with o-tolyl magnesium bromide**

| SL NO | X | Y | Grignard Solvent | Reaction Solvent | Equivalance | Condition | Duration | Formation of Products (1,2) |
|---|---|---|---|---|---|---|---|---|
| 1 | CCH3 | CH | DEE | THF | 2 | -40C-RT | 30 min | >80%,<15% |
| 2 | CCH3 | CH | DEE | THF | 2 | -78C-RT | 30 min | >80%, <15% |
| 3 | CCH3 | CH | DEE | THF | 2 | 0C-RT | 30 min | >80%, <15% |
| 4 | CCH3 | CH | DEE | THF | 2 | -78C-(-)40C | 2 hrs | 0%(TLC), 0% |
| 5 | CCH3 | CH | DEE | THF | 2 | -78C-0C | 30 min | >60%, <10% |
| 6 | CCH3 | CH | DEE | DCM | 2 | -40C-RT | 30 min | 0%,<20% |
| 7 | CCH3 | CH | DEE | DCM | 2 | -40C-RT | 1hr | 0%, <25% |
| 8 | CCH3 | CH | DEE | DCM | 2 | -40C-RT | 2 hrs | 0%,<25% |
| 9 | CCH3 | CH | DEE | DCM | 2 | -40C-RT | 4 hrs | 0%, <25% |
| 10 | CCH3 | CH | THF | DCM | 2 | -40C-RT | 30 min | >70%,<15% |
| 11 | CCH3 | CH | DEE | DCM | 2 | -40C-RT | 1 hr | 0%, <25% |

**Table 3-4 Optimization of the Grignard reaction of 64 with o-tolyl magnesium bromide**

| SL NO | X | Y | Grignard Solvent | Reaction Solvent | Equivalance | Condition | Duration | Formation of Products (1,2) |
|---|---|---|---|---|---|---|---|---|
| 1 | CF | CF | DEE | THF | 2 | -40C-RT | 30 min | >50%,<15% |
| 2 | CF | CF | DEE | THF | 2 | -78C-RT | 30 min | >50%, <15% |
| 3 | CF | CF | DEE | THF | 2 | 0C-RT | 30 min | >50%, <15% |
| 4 | CF | CF | DEE | THF | 2 | -78C-(-)40C | 2 hrs | 0%(TLC), 0% |
| 5 | CF | CF | DEE | THF | 2 | -78C-0C | 30 min | >30%, <5% |
| 6 | CF | CF | DEE | DCM | 2 | -40C-RT | 30 min | 0%,<10% |
| 7 | CF | CF | DEE | DCM | 2 | -40C-RT | 1hr | 0%, <15% |
| 8 | CF | CF | DEE | DCM | 2 | -40C-RT | 2 hrs | 0%,<15% |
| 9 | CF | CF | DEE | DCM | 2 | -40C-Rflx | 1 hrs | 0%, <20% |
| 10 | CF | CF | THF | DCM | 2 | -40C-RT | 30 min | >30%,<15% |
| 11 | CF | CF | DEE | DCM | 2 | -40C-Rflx | 2 hr | 0%, <20% |

In the final step of the proposed route the *N*-(4-bromo-2-(2-methylbenzoyl) phenyl) benzamide was treated with 10N hydrochloric acid to remove the benzoyl group. The reaction was unsuccessful. Later, the acid was changed to Hydrobromic acid and refluxed for 17 hours, but also in this trial the benzoyl group was not get removed.

### 3. 2. 2 Friedel crafts acylation.

#### 3. 2. 2. 1 Chemistry

##### 3. 2. 2. 1. 1 Synthesis of 2'$CH_3$ 5-Br 2-aminobenzophenone 68.

Friedel crafts acylation method was applied to synthesize the 2'$CH_3$ 5-Br 2-aminobenzophenone 68. In the first trial para bromoaniline 33 was used as the starting material. The starting material was treated with 2 equivalents of ortho tolyl benzoyl chloride 67. (See Scheme 21)

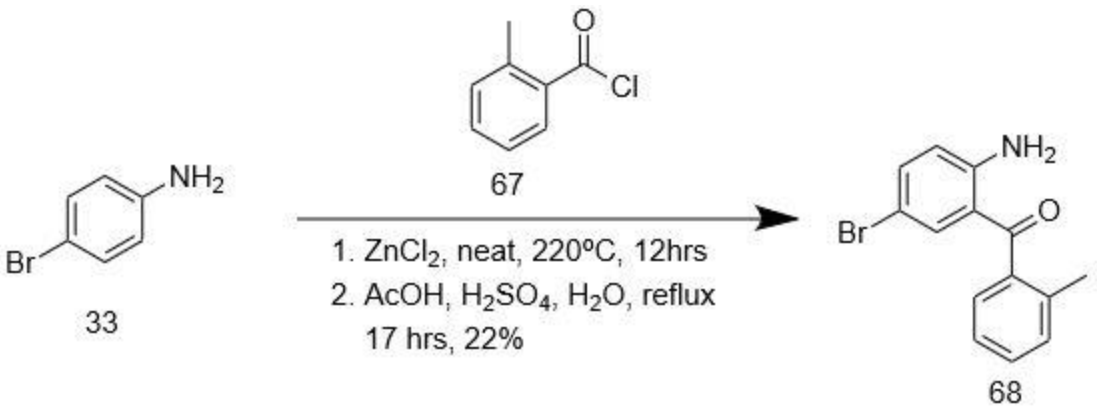


**Scheme 21. Synthetic route for 2'$CH_3$ 5-Br 2-aminobenzophenone 68.**

The reaction was done under neat conditions analogous to extensive work done by Farjana Rashid and Yeunus Mian. Zinc chloride was used as a catalyst. In the first step a mixture of para bromoaniline 33 and ortho tolyl benzoyl chloride 67 was heated until the mixture turned to a liquid phase. When the temperature reached 180°C, the zinc chloride was added under a flow of argon. Then the temperature was increased to 220°C and maintained at this temperature for 12 hours. After 12 hours the reaction was allowed to cool to room temperature. Acetic acid, sulfuric acid, and water in a ratio of 2:1.5:1 was added to the cooled mixture and temperature was raised until the mixture began to reflux. The reflux was carried on for 17 hours. After 17 hours the reaction mixture was allowed to cool to room temperature and was poured into a large amount of a mixture of ice-water. Then diethyl ether was used to extract the ketone. It was then washed with a saturated sodium chloride solution (x3). Then sodium sulfate was used to furnish a moisture free diethyl ether extract. The solvent was evaporated to get a crude mixture of 2'$CH_3$ 5-bromo 2-aminobenzophenone 68. The crude material was purified by column chromatography by using a mixture of 5:95 ethyl acetate and hexane on silica gel. This process was done on 10 gram in scale and the yield was only 22%. However, this attempt gave enough starting material of 68 to continue.

This reaction has three steps. In the first step the para bromoaniline 33 was protected by forming para bromophenyl N-benzamide 69. In the second step the Friedel Craft acylation reaction took place and formed the benzophenone 68. In the third step a mixture of acetic acid, sulfuric acid and water in a ratio of 2:1.5:1 used to deprotect the benzamide to form the 2'$CH_3$ 5-Bromo 2-Aminobenzophenone.

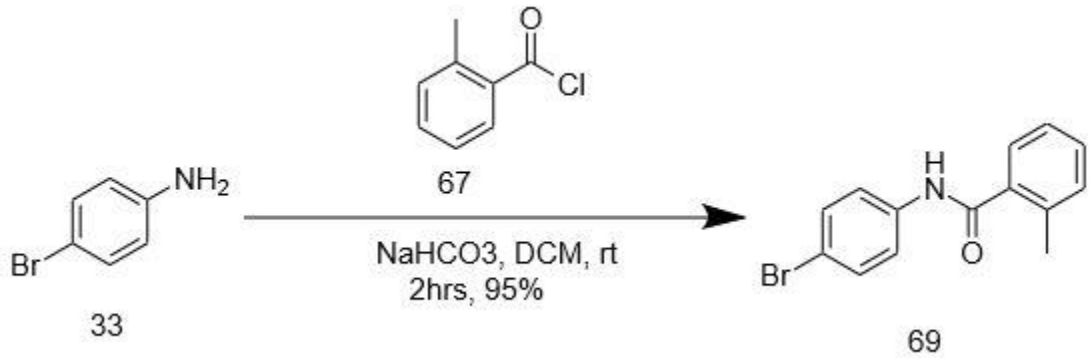


**Scheme 22. Synthesis of para bromophenyl N-benzamide 69.**

It was decided to follow these three different steps to get rid of additional impurities and improve the overall percentage yield.

N-(4-bromophenyl)-2-methylbenzamide 69 was synthesized by treating para bromoaniline 33 with ortho tolyl benzoyl chloride 67 in DCM in the presence of solid Sodium bicarbonate at room temperature. The mixture was stirred for two hours. After confirming the consumption of starting material by TLC the reaction was quenched by adding water. A white precipitate was formed and filtered out to get the purified N-(4-bromophenyl)-2-methylbenzamide 69. The amide 69 was dried under the air for 24 hours to furnish a moisture free product. This step was performed for two more times. The overall yield was 95%.

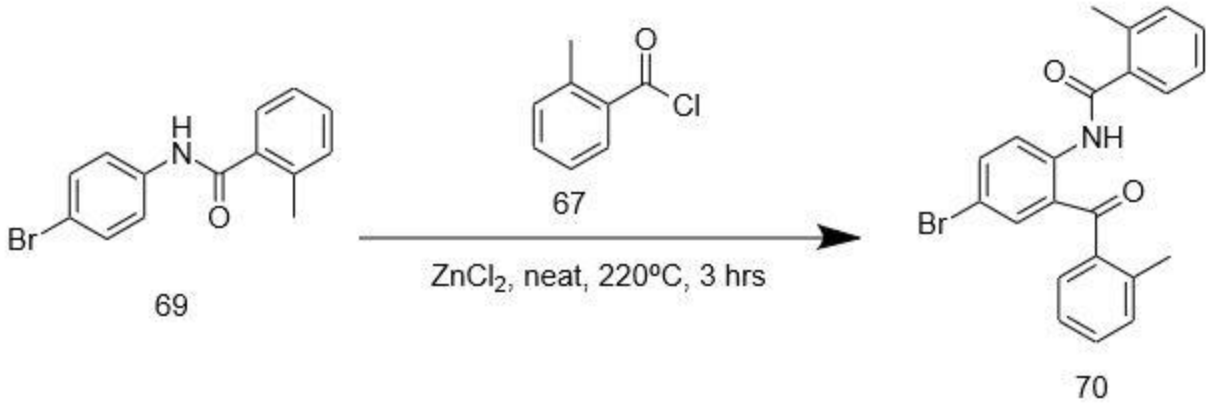


**Scheme 23. Synthetic route of N-(4-bromo-2-(2-methylbenzoyl) phenyl) benzamide 70.**

In the second step the Friedel Crafts acylation reaction was carried out. One equivalent of ortho tolyl benzoyl chloride 67 was used at this stage. The reaction was done in neat conditions. The $ZnCl_2$ was added at 180$^oC$. The mixture was heated at 220$^oC$ for 12 hours. After this the mixture was allowed to cool to room temperature. Excess water was added to the mixture and the mixture which resulted clots heated to reflux at 100$^oC$. The hot water was cooled to about 70$^oC$ and decanted. This process was done 3-5 times. This process removes the unreacted $ZnCl_2$ from the product which is not required in the final step of this process where in the benzoyl group is removed. This provides a much cleaner reaction product and is a significant progress. The product formed in this step was not purified.

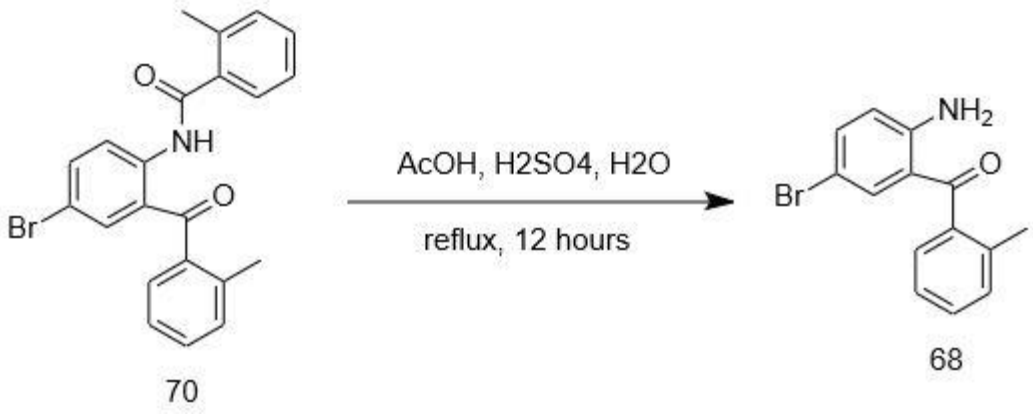


**Scheme 24. Deprotection of benzoyl group from 70 to furnish 68.**

To a mixture of acetic acid, sulfuric acid, and water in a ratio of 2:1.5:1 the crude 70 was added. This mixture was allowed to heat to reflux for 17 hours. After the reaction is done (TLC) the mixture was transferred into an ice-water mixture and extracted with diethyl ether. The extract was brought to alkaline pH by using 3M potassium hydroxide to remove the excess amount of acid from the diethyl eth mixture. The diethyl ether was removed under reduced pressure to furnish a crude mixture of the 2'$CH_3$ 5-bromo 2-bminobenzophenone 68. The product was purified by using 5:95 ratio of ethyl acetate and hexanes mixture on column chromatography.

**Figure 100. Effect of removal of $ZnCl_2$ from the reaction mixture in the second step of the synthesis of 2'$CH_3$ 5-bromo 2-bminobenzophenone 68. Left image shows the hard mass formation due to the solidification of $ZnCl_2$ after wet loading in column chromatography. Right picture shows the effect of complete removal of $ZnCl_2$ from the reaction mixture.**

This process was repeated two times as mentioned. From the benzamide step, the highest yield was 44%. The product was characterized by 1H NMR and C13 NMR. This is better yield than (<25%) yield via other methods.

### 3. 2. 2. 1. 2 Synthesis of 2'$CF_3$ 5-Br 2-aminobenzophenone and 2',6'-difluoro 5-Br 2-aminobenzophenone.

By following a similar synthetic route for the synthesis of 2'$CH_3$ 5-Br 2-aminobenzophenone 68, attempts were made to synthesize 2'$CF_3$ 5-Br 2-aminobenzophenone and 2',6'-difluoro 5-Br 2-aminobenzophenone.

After synthesizing these other benzophenones via this route, we went forward to make their 7-bromo NOR QH II 66 analogs with a trace amount of solvent remaining because in both cases it was impossible to get rid of the solvent totally. After synthesizing the analogs in both cases, we observed eight hydrogen atoms in the 1H NMR spectrum in the aromatic regions which is similar to that of 7-bromo NOR QH II 66. It was decided to take 19F NMR to confirm the presence of fluorine. KRM II 08 was used as a standard because it has a fluorine atom at the 2' position.

The 19F NMR indicated that in both fluorine cases there was an absence of fluorine atoms. The standard and the starting materials 2-trifluoromethyl benzoyl chloride and 2,6 difluoro benzoyl chloride did contain the fluorine peak in the 19F NMR spectrum at -112 ppm. By conducting the synthesis one more time it was found one was losing the fluorine atoms during the deprotection of the benzamide group due to the harsh condition. We found several published articles to support for this phenomenon.

It was decided to perform the deprotection of the benzoyl group by using hydrazine monohydrate but in both cases the reactions were unsuccessful.

### 3. 2. 2. 1. 3 Synthesis of TA II 73 (74), 2'$CH_3$ analogue of QH II 66.

After the synthesis of 2'$CH_3$ 5-Bromo 2-Aminobenzophenone 68, the synthesis TA II 73 74 was carried out by following the same route employed for the preparation of QH II 66. (See Scheme 25) The route employed consisted of five steps from the starting material 68. The largest scale was on 10-gram scale began with the 2'$CH_3$ 5-bromo 2-aminobenzophenone 68. Overall of TA II 73 (74) was 29%.

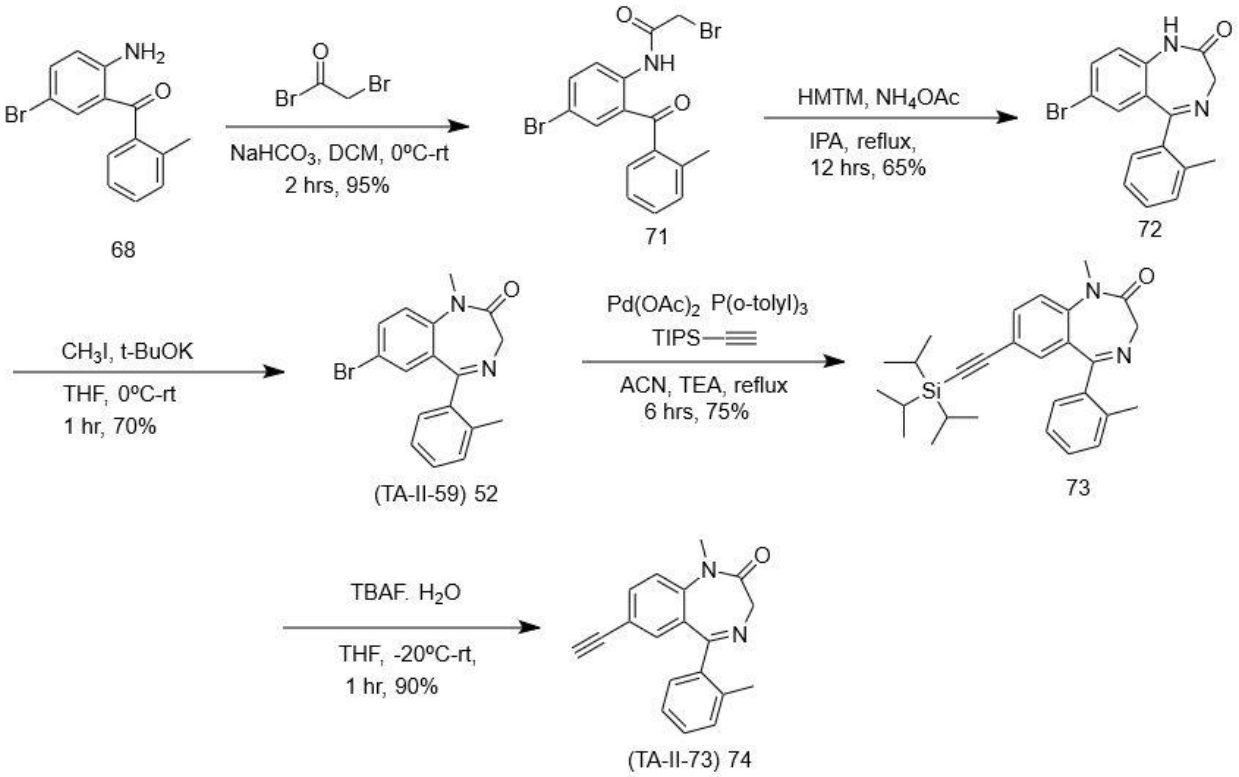


**Scheme 25. Synthetic route for TA II 73 (74).**

### 3. 2. 2. 1. 4 Synthesis of TA IV 46 (77).

The related imidazobenzodiazepine for studies of SAR TA IV 46 was synthesized from the bromide TA II 59 (72). The imidazole part was installed by executing two steps. In the first step TA II 59 (72) was treated with diethyl chlorophosphate in the presence of potassium tert-butoxide in THF. A solution of diethyl chlorophosphate in THF was added to the reaction vessel at -50$^{o}$C dropwise for 5 minutes. This was analogous to Li's, Poe's and Sharmin's procedure. Then the temperature was allowed to rise to room temperature and the mixture was allowed to stir until all the starting material 72 had been consumed. After this the mixture was cooled down to -50$^{o}$C, potassium tert butoxide and ethyl isocyanoacetate were added to the the mixture and let the temperature allowed to rise to the room temperature. This mixture was allowed to stir overnight. After completion of the reaction on confirmation by TLC (silica gel), a saturated solution of sodium bicarbonate was added to the reaction mixture.

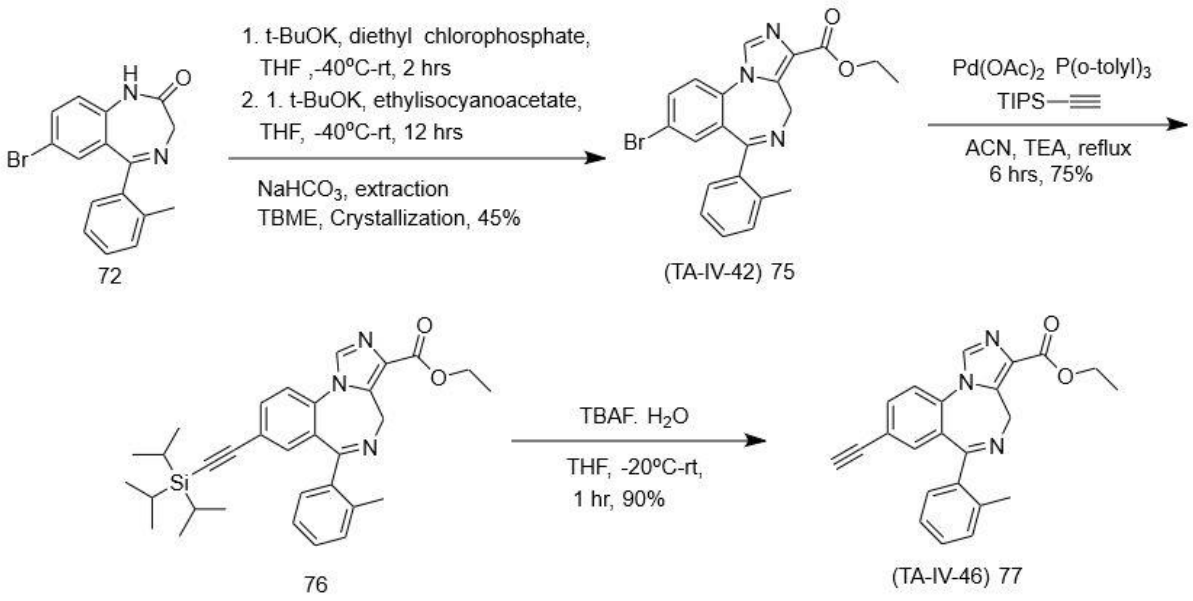


**Scheme 26. Synthetic route for TA IV 46 (77).**

Ethyl acetate was used to extract the product (TA-IV-42, 75) and it was purified by column chromatography with a 50:50 ethyl acetate and hexanes mixture.

In the next step a copper free sonogashira coupling reaction was performed to install the TIPS acetylene in the 7-Br position. In the final step the TIPS protected TA-IV-42 (76) was treated with TBAF to deprotect the TIPS group to get the final product TA-IV-46 (77). The product was purified by column chromatography with a solution of 50% ethyl acetate in hexanes. The overall yield from TA II 59 to TA-IV-46 was 30%. The largest scale from TA-II-59 was 5 grams. This material 75 and 77 was immediately sent out for PDSP, rotorod, righting reflex for the results will be important regarding SAR.

## 3. 3 Experimental

### 3. 3. 1 *tert*-butyl (2-((4-bromophenyl) amino)-2-oxoethyl) carbamate. (35)

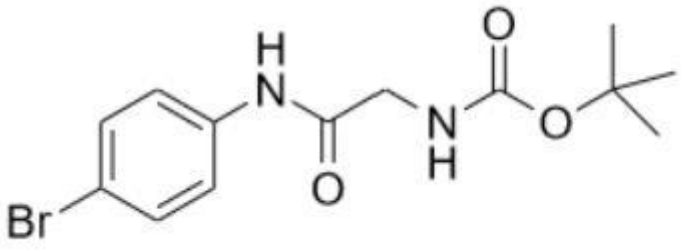


The parabromoaniline (33, 50 g, 290.0 mmol) and Boc-D-alanine (34, 84.5 g, 482.5 mmol) were dissolved in dry DCM (300 mL) and stirred at 0 oC. Then dicyclohexylcarbodiimide (DCC; 104.7 g, 507.5 mmol) was dissolved in dry DCM (150 mL) to form a homogenous solution, which was added to the former mixture dropwise over a 30 min period at 0$^{o}$C. The solution was allowed to stir for 22 h at rt. The dicyclohexyl urea byproduct which was formed was filtered off and washed with DCM until the solid was colorless. The organic layers were combined and concentrated under reduced pressure. The crude solid was dissolved in hexane at 45$^{o}$C, and the Boc analog was recrystallized when cooled down to rt after adding seed crystals. The crystals were further washed with hexane to afford the majority of Boc analog. The filtrate was combined, concentrated, and purified on a flash column chromatography (silica gel, DCM/hexane 1:1) to yield additional product (76.4 g, 80 %):

$^{1}$H NMR (300 MHz, $CDCl_3$) δ 9.41 (s, 2H), 7.58-7.61 (d, *J* = 9.0 Hz, 2H), 7.23– 7.27 (d, J = 9.0 Hz 2H), 4.15 (s, 2H), 0.74 (s, 9H), 1.45 (m, 1H); 13C NMR (300 MHz, $CDCl_3$) δ 172.73 (s),

169.03 (s), 131.75 (s), 130.16 (s), 126.66 (s), 122.75(s), 78.43 (s), 47.73 (s), 25.52 (s); This was used in the next step without further characterization.

**3. 3. 2** 2-amino-*N*-(4-bromophenyl) acetamide (37)

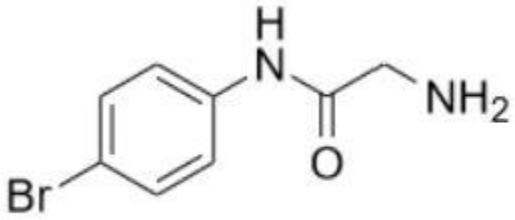


In a two neck round bottom flask the *tert*-butyl (2-((4-bromophenyl) amino)-2-oxoethyl) carbamate (35, 16.0 g, 48.6 mmol) was dissolved in dry DCM (100 mL) and stirred at 0$^{o}$C. Then trifluoroacetic acid (36; 44.6 mL, 583.2 mmol) was dissolved in dry DCM (100 mL) was added to the former solution dropwise over a 30 min period at 0$^{o}$C. An outlet pipe was added to get rid of the produced carbon dioxide. The solution was allowed to stir for 12 h at rt. After completion of the reaction confirmed by TLC the reaction was stopped. The solvent was evaporated, and the crude was extracted by using a saturated sodium bicarbonate and ethyl acetate. The organic part was washed with saturated sodium chloride. The solvent was evaporated to get the crude. The product 2-amino-*N*-(4-bromophenyl) acetamide was crystallized by using 20% ethyl acetate solution in hexanes. (10.56 g, 95 %):

1H NMR (300 MHz, CDCl3) δ 9.31 (s, 1H), 7.48-7.11 (d, *J* = 9.0 Hz, 2H), 7.22– 7.25 (d, J = 9.0 Hz 2H), 5.36 (s, 3H) 3.47 (s, 2H); 13C NMR (300 MHz, CDCl3) δ 172.23 (s), 131.55 (s, 2C), 130.35 (s, 2C), 126.86 (s), 122.75(s), 45.32 (s); This was used in the next step without further characterization.

**3. 3. 3** *N*-(2-((4-bromophenyl) amino)-2-oxoethyl)-2-fluorobenzamide (40)

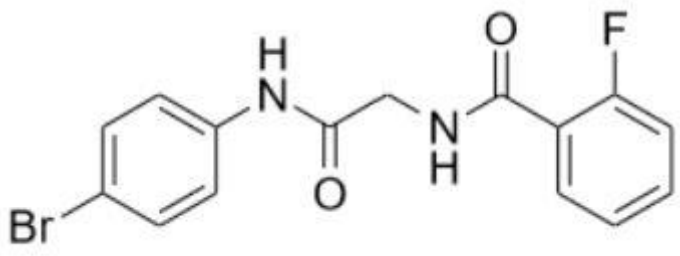


To a mixture of 2-amino-*N*-(4-bromophenyl) acetamide (5.0 g, 21.83 mmol), sodium bicarbonate (3.67 g, 43.66 mmol), and dichloromethane (60 mL), ortho fluoro benzoyl chloride (3.13 mL, 26.2 mmol) was added. The temperature was kept between -10$^{o}$C – 0$^{o}$C with continuous stirring. The white colored reaction mixture, which resulted, was then allowed to stir for longer than 2 h at rt. The completion of the reaction was verified by analysis by TLC (silica gel) and 50% ethyl acetate / hexanes. The reaction mixture was then slowly diluted over 30 min with water (100 mL) as carbon dioxide bubbles occurred. The biphasic mixture, which resulted, was allowed to stand for 15 min and the layers were separated. The aq layer was extracted with dichloromethane (50 mL) and the combined organic layers were washed with 5% aq sodium bicarbonate solution (50 mL) and then 10% aq sodium chloride solution (30 mL). The organic layer was dried ($Na_2SO_4$). The solvents were removed under reduced pressure and the residue was slurried with ethanol (30 mL) at 50 – 55$^{o}$C for 30 min. Upon cooling to rt and after holding the temperature for 1 h, the solid, which formed, was filtered, and washed with ethanol (50 mL x 3). The solid was dried under vacuum at 40$^{o}$C to afford the product *N*-(2-((4-bromophenyl) amino)-2-oxoethyl)-2-fluorobenzamide 40 as an off-white solid (7.28 g, 95%).

$^{1}$H NMR (300 MHz, $CDCl_3$) δ 9.11 (s, 2H), 7.66-7.70 (dd, 2H), 7.38-7.51 (m, 2H), 7.31-7.36 (dd,2H), 7.18-7.31 (ddd, 1H), 7.14-7.21 (ddd, 1H), 3.96 (s, 2H); $^{13}$C NMR (300 MHz, $CDCl_3$) δ

172.73 (s), 163.03 (d, J= 250Hz), 135.15 (s), 131.75 (s), 130.16 (s), 129.86(s), 126.16 (s), 122.45(s), 120.97 (s), 114.65 (s), 42.43 (s); This was used in the next step without further characterization.

**3. 3. 4** *N*-(2-((4-bromophenyl) amino)-2-oxoethyl)-2-chlorobenzamide (41)

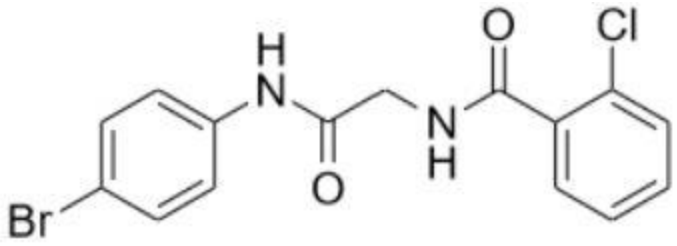


It was synthesized by following the procedure as *N*-(2-((4-bromophenyl) amino)-2-oxoethyl)-2-fluorobenzamide.

$^{1}$H NMR (300 MHz, $CDCl_3$) δ 9.41 (s, 2H), 7.58-7.61 (d, *J* = 9.0 Hz, 2H), 7.23– 7.27 (d, J = 9.0 Hz 2H), 4.15 (s, 2H), 0.74 (s, 9H), 1.45 (s, 9H); $^{13}$C NMR (300 MHz, $CDCl_3$) δ 174.23 (s) 172.73 (s), 134.85 (s), 134.46 (s), 134.36 (s), 131.75 (s), 130.16 (s), 129.56(s), 128.05 (s), 126.66 (s), 122.65(s), 42.53 (s); This was used in the next step without further characterization.

**3. 3. 5** 6-bromo-2*H*-benzo[*d*][1,3] oxazine-2,4(1*H*)-dione (46)

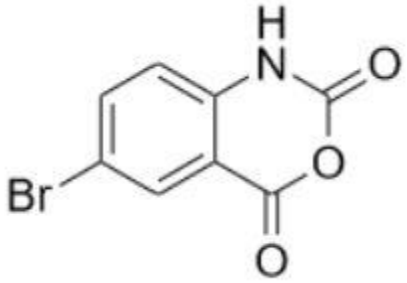


In a 1L 3-neck round bottom flask 5-bromo 2- aminobenzoic acid (50 g, 231.4 mmol) was dissolved in dry DCM (300 mL) and stirred at 0$^{o}$C. Then triphosgene (25.22 g, 85 mmol) was

added and stirred for 30 minutes to form a homogenous solution. A trap was added by using saturated sodium hydroxide to neutralize excess phosgene gas. Temperature raised to 70$^{o}$C gradually in 30 minutes. The solution was allowed to stir for 12 hrs at 70$^{o}$C. By confirming with TLC the reaction was stopped and let it cool down to room temperature. After cooling down a white precipitate was formed which is the product. The filtrate was collected and concentrated by using rotary evaporator. The crude was then first washed with 5% sodium hydroxide and later with brine. Ethyl acetate was used as the extraction solvent. The organic ethyl acetate part was concentrated and crystallized to product 6-bromo-2*H*-benzo[*d*][1,3] oxazine-2,4(1*H*)-dione by using 20% ethyl acetate in hexanes solution (55 g, 98%):

1H NMR (300 MHz, $CDCl_3$) δ 13.05 (s, 1H), 8.05-8.10 (d, 1H), 8.03-8.11 (dd, 1H), 7.31-7.38 (dd, 1H), 13C NMR (300 MHz, $CDCl_3$) δ 184.03 (s), 176.60 (s), 148.08 (s), 139.10 (s), 128.30 (s), 125.38 (s), 122.73 (s); HRMS (ESI/IT-TOF) m/z: [M + H]+ Calcd for C8H4BrNO3 242.0257; found 242.0243.

**3. 3. 6 6-bromo-1-methyl-2*H*-benzo[*d*] [1,3] oxazine-2,4(1*H*)-dione (47)**

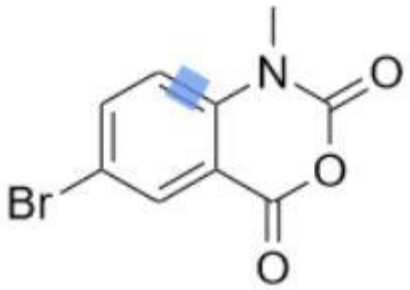


In a 1L three neck round bottom flask **6-bromo-2*H*-benzo[*d*][1,3] oxazine-2,4(1*H*)-dione** (50 g, 290.0 mmol) was dissolved in dry DMF (300 mL) and stirred at 0$^{o}$C. The flask was degassed for three times to make sure the reaction mixture remains under argon. Sodium hydride 60% dispersed in mineral oil () was added in portions. During addition the temperature kept under 0$^{o}$C. The

temperature raised to room temperature and was stirred for 16 hours. After confirming reaction completion by using TLC the reaction was stopped by adding ice water. The mixture was extracted by using ethyl acetate. The organic layer was washed with brine. The extract was concentrated by evaporating ethyl acetate. The crude was then crystallized by using 20% ethylacetate in hexanes solution gives brown solid as product **6-bromo-1-methyl-2*H*-benzo[*d*] [1,3] oxazine-2,4(1*H*)-dione**. **47** (44.5 gm, 84%)

**$^{1}$H NMR** (300 MHz, CDCl3) δ 7.85-7.93 (dd, 1H), 7.86– 7.92 (dd, 1H), 7.22-7.29 (dd, 1H), 3.45 (s, 3H); **$^{13}$C NMR** (300 MHz, CDCl3) δ 168.28 (s), 147.45 (s), 142.21 (s), 140.05 (s), 131.79 (s), 118.24(s), 116.33 (s), 113.28 (s), 33.43 (s); This was used in the next step without further characterization.

**3. 3. 7 7-bromo-1-methyl-3,4-dihydro-1*H*-benzo[*e*] [1,4] diazepine-2,5-dione (48)**

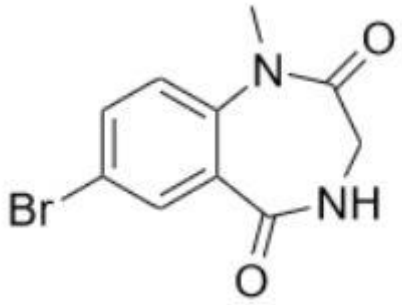


In a three neck round bottom flask **6-bromo-1-methyl-2*H*-benzo[*d*] [1,3] oxazine-2,4(1*H*)-dione (**20 g, 78.1 mmol) and glycine (8.8 g, 117.2 mmol) were dissolved in acetic acid (100 mL) and stirred at room temperature. The mixture was heated to reflux for 3 hours. After 3 hours the reaction was stopped. In a beaker filled with ice water, the hot reaction mixture was added and stirred for 30 minutes. The slurry which was produced was filtered to collect the white solid which

is the product, **7-bromo-1-methyl-3,4-dihydro-1*H*-benzo[*e*][1,4]diazepine-2,5-dione 48.** The solid was dried under air overnight to get dry product. (16.5 gm, 64%)

**$^{1}$H NMR** (300 MHz, $CDCl_3$) δ 8.11 (s, 1H), 7.78 (s, 1H), 7.68 (d, 1H), 7.11 (d, 1H), 3.85 (d, 2H), 3.41 (s, 3H); **$^{13}$C NMR** (300 MHz, $CDCl_3$) δ 169.21 (s), 167.92 (s), 135.73 (s), 133.51 (s), 128.71 (s), 123.48(s), 118.82 (s), 46.21 (s), 36.42 (s); This was used in the next step without further characterization.

### 3. 3. 8 4-acetyl-7-bromo-1-methyl-3,4-dihydro-1*H*-benzo[*e*] [1,4]diazepine-2,5-dione (49)

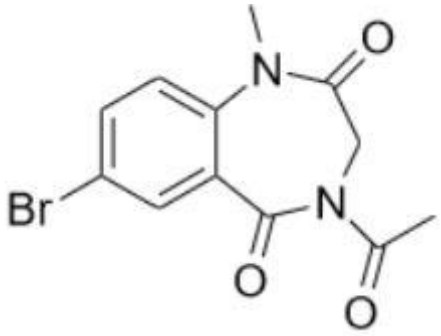


In a three neck round bottom flask 7-bromo-1-methyl-3,4-dihydro-1*H*-benzo[*e*][1,4]diazepine-2,5-dione 48 **(**15 g, 55.8 mmol) was dissolved in acetic anhydride (50 mL) and stirred at room temperature. The mixture was heated to reflux for 3 hours. After 3 hours the reaction was stopped. In a beaker filled with ice water, the hot reaction mixture was added and stirred for 30 minutes. Ethyl acetate was used to extract the product. The extract was the washed with brine. The organic part was concentrated by rotary evaporator to get the crude product. The product, **7-bromo-1-methyl-3,4-dihydro-1*H*-benzo[*e*][1,4]diazepine-2,5-dione 49** was crystallized by using a 40% ethyl acetate solution in hexanes to get it as a white solid**.** The solid was dried under air overnight to get dry product. (11.2 gm, 65%)

**$^{1}$H NMR** (300 MHz, $CDCl_3$) δ 8.11 (s, 1H), 7.78 (d, 1H), 7.21 (d, 1H), 5.71 (d, 1H), 3.76 (d, 1H), 3.47 (s, 3H), 2.73 (s, 3H); **$^{13}$C NMR** (300 MHz, $CDCl_3$) δ172.41 (s), 166.21 (s), 164.76 (s), 141.11 (s), 136.22 (s), 134.51 (s), 131.11 (s), 123.92 (s), 117.51 (s), 45.72 (s), 35.91 (s), 27.85 (s) ; This was used in the next step without further characterization.

### 3. 3. 9 6-bromo-2-methyl-4*H*-benzo[*d*] [1,3] oxazin-4-one

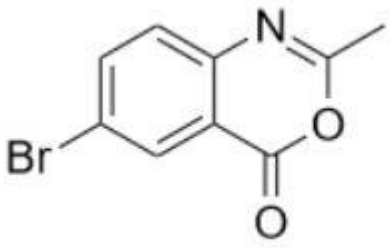


In a three neck round bottom flask 5-bromo 2- aminobenzoic acid **45 (**5 g, 23.14 mmol) was dissolved in Pyridine (50 mL) and stirred at room temperature. $NaHCO_3$ (3.88 g, 46.23 mmol) was also added to the solution. Acetyl chloride (1.98 mL, 27.77 mmol) was added dropwise to the mixture. The mixture was stirred for 10 minutes and checked by TLC. When the reaction was completed, cold water was added to mixture. The white solid which precipitated was filtered and collected which is the product **6-bromo-2-methyl-4*H*-benzo[*d*] [1,3] oxazin-4-one**. The collected solid was washed with water and dried overnight. (5.27 gm, 95%)

**1H NMR** (300 MHz, $CDCl_3$) δ 8.03-8.10 (dd, 1H), 8.05– 8.10 (dd, 1H), 7.10– 7.20 (dd, 1H) 1.77 (s, 3H); **13C NMR** (300 MHz, $CDCl_3$) δ 185.90 (s), 184.09 (s), 148.08 (s), 139.12 (s), 125.40 (s), 122.12 (s), 19.82 (s); This was used in the next step without further characterization.

### 3. 3. 10 6-bromo-2-phenyl-4*H*-benzo[*d*] [1,3] oxazin-4-one (64)

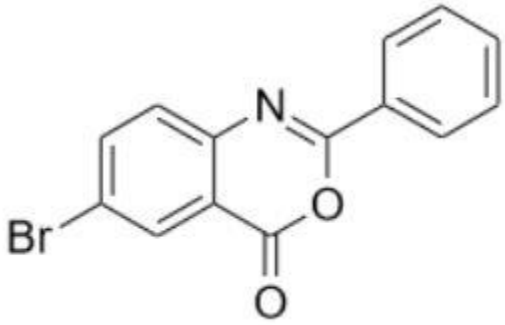


In a three neck round bottom flask 5-bromo 2- aminobenzoic acid **45 (**5 g, 23.14 mmol) was dissolved in Pyridine (50 mL) and stirred at room temperature. $NaHCO_3$ (3.88 g, 46.23 mmol) was also added to the solution. Benzoyl chloride **63** (3.22 mL, 27.77 mmol) was added dropwise to the mixture. The mixture was stirred for 10 minutes and checked by TLC. When the reaction was completed, cold water was added to mixture. The white solid which precipitated was filtered and collected which is the product **6-bromo-2-phenyl-4*H*-benzo[*d*][1,3]oxazin-4-one, 64**. The collected solid was washed with water and dried overnight. (6.64 gm, 95%)

**$^1$H NMR** (300 MHz, $CDCl_3$) δ 8.12-8.20 (dd, 1H), 8.14– 8.18 (dd, 1H), 8.06– 8.14 (dd, 2H); 7.63-7.78 (m, 1H), 7.52– 7.68 (t, 2H), 7.48– 7.55 (d, 1H) **$^{13}$C NMR** (300 MHz, $CDCl_3$) δ 189.61 (s), 184.52 (s), 148.58 (s), 142.57 (s), 139.12 (s), 129.05 (s), 126.55 (s), 126.31(s), 125.46(s). 124.38(s), 122.75(s); This was used in the next step without further characterization.

### 3. 3. 11 N-(4-bromophenyl)-2-methylbenzamide (69)

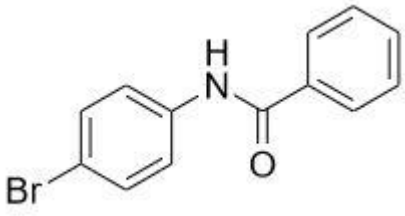


To a mixture of parabromoaniline **33** (50 g, 290.7 mmol), sodium bicarbonate (48.83 g, 581.3 mmol), and dichloromethane (500 mL), benzoyl chloride (37.15 mL, 319.77 mmol) was added dropwise. The temperature was maintained between -10ºC – 0ºC with continuous stirring. The white colored reaction mixture, which resulted, was then allowed to stir for longer than 2 h at rt. The completion of the reaction was verified by analysis by TLC (silica gel) and a solution of 50% ethyl acetate / hexanes. The reaction mixture was then slowly diluted over 30 min with water (300 mL) as carbon dioxide bubbles occurred. The biphasic mixture, which resulted, was allowed to stand for 15 min and the layers were separated. The aq layer was extracted with dichloromethane (300 mL) and the combined organic layers were washed with 5% aq sodium bicarbonate solution (300 mL) and then 10% aq sodium chloride solution (300 mL). The organic layer was dried ($Na_2SO_4$). The solvents were removed under reduced pressure and the residue was slurried with ethanol (300 mL) at 50 – 55ºC for 30 min. Upon cooling to rt and after holding the temperature for 1 h, the solid, which formed, was filtered, and washed with ethanol (60 mL x 3). The solid was dried under vacuum at 40ºC to afford the product **N-(4-bromophenyl)-2-methylbenzamide 69** as an off-white solid (80.12 g, 95%).

**$^1$H NMR** (300 MHz, $CDCl_3$) δ 10.56 (s, 1H), 7.65-7.72 (dd, 2H), 7.41– 7.51 (dd, 2H), 7.41-7.54 (tt, 1H), 7.41-7.53 (ddd, 2H), 7.30-7.37 (dd, 2H); **$^{13}$C NMR** (300 MHz, $CDCl_3$) δ 169.73 (s), 133.96 (s), 133.55 (s), 131.75 (s), 130.16 (s), 128.25 (s, 2C), 127.62 (s, 2C), 126.66 (s), 122.75 (s)

**3. 3. 12 (2-amino-5-bromophenyl) (*o*-tolyl) methanone (68)**

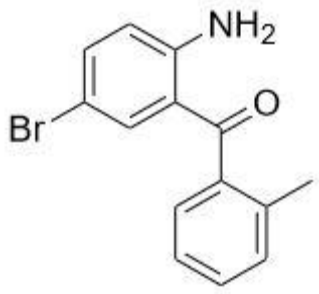


In a 500 mL 3-neck round bottom flask **N-(4-bromophenyl)-2-methylbenzamide 69** (50 gm, 172.32 mmol) was charged at room temperature. Under argon flow ortho toluoyl benzoyl chloride **69** (24.8 mL, 189.5mmol) was added. A condenser and a thermometer were added to the round bottom flask. The temperature of the mixture was raised to 180$^{o}$C. ZnCl2 was added to the hot liquid. After that the temperature was allowed to rise to 220$^{o}$C and kept the temperature at that point for 3 hours. After 3 hours the reaction mixture was cooled down to room temperature and water was added to it. The reaction mixture was refluxed for an hour and cooled down to 50$^{o}$C. The liquid was decanted. A mixture of sulfuric acid, Acetic acid and water in a ratio of 2:1.5:1 was added to the mixture and refluxed for 17 hours. After 17 hours the hot mixture was transferred to an ice-water mixture and extracted with diethyl ether. The organic part was then washed with a saturated sodium bicarbonate solution and with brine. The solvent was evaporated to get a crude mixture. The product **(2-amino-5-bromophenyl) (*o*-tolyl) methanone 68** was purified by column chromatography as yellow solid (20.7 g, 39%). A 2% ethyl acetate solution in hexanes was used.

**1H NMR** (300 MHz, $CDCl_3$) δ 8.07- 8.11 (dd, 1H), 7.96- 8.07 (ddd, 1H), 7.70-7.79 (dd, 1H), 7.61-7.75 (ddd, 1H), 7.34-7.43 (m, 2H), 6.64-6.72 (dd, 1H) 5.35 (s, 2H), 2.23 (s, 3H); **13C NMR** (300 MHz, $CDCl_3$) δ 190.64 (s), 145.46 (s), 138.47 (s), 137.96 (s), 133.16 (s), 129.35(s), 128.85 (s),

128.66 (s), 128.67 (s), 125.65 (s), 124.35 (s), 117.76 (s), 113.26 (s), 19.82 (s); **HRMS** (ESI/IT-TOF) m/z: [M + H]+ Calcd for $C_{14}H_{12}BrNO$ 290.1543; found 290.1528.

### 3. 3. 13 2-bromo-*N*-(4-bromo-2-(2-methylbenzoyl) phenyl) acetamide (71)


To a mixture of (2-amino-5-bromophenyl) (*o*-tolyl) methanone **68** (10 g, 34.46 mmol), sodium bicarbonate (5.79 g, 68.92 mmol), and dichloromethane (100 mL), bromoacetyl bromide (3.60 mL, 41.35 mmol) was added dropwise. The temperature was kept between -10ºC – 0ºC with continuous stirring. The white colored reaction mixture, which resulted, was then allowed to stir for longer than 3 h at rt. The completion of the reaction was verified by analysis by TLC (silica gel) and 50% ethyl acetate / hexanes. The reaction mixture was then slowly diluted over 30 min with water (100 mL) as carbon dioxide bubbles occurred. The biphasic mixture, which resulted, was allowed to stand for 15 min and the layers were separated. The aq layer was extracted with dichloromethane (100 mL) and the combined organic layers were washed with 5% aq sodium bicarbonate solution (100 mL) and then 10% aq sodium chloride solution (300 mL). The organic layer was dried ($Na_2SO_4$). The solvents were removed under reduced pressure and the residue was slurried with ethanol (100 mL) at 50 – 55ºC for 30 min. Upon cooling to rt and after holding the temperature for 1 h, the solid, which formed, was filtered, and washed with ethanol (60 mL x 3).

The solid was dried under vacuum at 40$^{o}$C to afford the product **2-bromo-*N*-(4-bromo-2-(2-methylbenzoyl) phenyl) acetamide** as an off-white solid (13.56 g, 95.5%).

$^{1}$H NMR (300 MHz, $CDCl_3$) δ 12.01 (s, 1H), 8.66 (d, *J* = 9.0 Hz, 1H), 7.71 (d, *J* = 9.0 Hz, 1H), 7.55 (s, 1H), 7.44 (s, 1H), 7.35 (s, 2H), 4.07 (s, 2H), 2.35 (s, 3H).**13C NMR** (300 MHz, $CDCl_3$) δ 190.64 (s), 172.73 (s), 139.27 (s), 138.47 (s), 137.96 (s), 131.86 (s), 130.16 (s), 129.35 (s), 128.66 (s), 127.56 (s), 125.65(s). 124.35(s), 122.76(s), 36.02 (s), 19.82(s); **HRMS** (ESI/IT-TOF) m/z: [M + H]+ Calcd for $C_{16}H_{13}BrNO_2$ 411.0869; found 411.0851.

### 3. 3. 14 7-bromo-5-(*o*-tolyl)-1,3-dihydro-2*H*-benzo[*e*] [1,4] diazepin-2-one (72)


A mixture of 2-bromo-*N*-(4-bromo-2-(2-methylbenzoyl) phenyl) acetamide, **71** (10 g, 24.3 mmol), hexamethylenetetramine (HMTM, 7.50 g, 53.5 mmol), ammonium acetate (4.12 g, 53.5 mmol), and isopropanol (100 mL) was heated to reflux (82$^{o}$C). The reaction mixture was held at reflux for 6 h, at which point the reaction progress was deemed complete on analysis by TLC (silica gel and 1:1, ethyl acetate/hexanes). The reaction mixture was then cooled to 0 – 5$^{o}$C using an ice bath. The solid, which resulted, was filtered, and washed with cold isopropanol (100 mL x 2) and then water (100mL x 4). The solid was dried under vacuum at 40$^{o}$C to afford 3.2 g of the benzodiazepine **72** as an off-white solid. The IPA was removed from the mother liquor under

reduced pressure. The solid was then extracted with ethyl acetate. The ethyl acetate was removed under reduced pressure and the residue was purified by column chromatograpy using 1:4 etheyl acetate/hexanes to afford 2.01 grams more of **7-bromo-5-(*o*-tolyl)-1,3-dihydro-2*H*-benzo[*e*] [1,4] diazepin-2-one 72** (5.21 g, 65%)

$^{1}$H NMR (300 MHz, $CDCl_3$) δ 11.95 (s, 1H), 8.68 (d, *J* = 9.0 Hz, 1H), 7.65 (d, *J* = 9.0 Hz, 1H), 7.45 (d, *J* = 22.1 Hz, 2H), 7.27 – 7.17 (m, 2H), 7.14 (d, *J* = 7.6 Hz, 1H), 3.65 (s, 2H), 2.23 (s, 3H). $^{13}$C NMR (75 MHz, $CDCl_3$) δ 200.64, 170.52, 139.35, 138.24, 137.51, 136.52, 136.16, 131.20, 130.77, 128.31, 125.50, 122.95, 115.09, 53.65, 19.80. **HRMS** (ESI/IT-TOF) m/z: [M + H]+ Calcd for $C_{17}H_{15}BrN_2O$ 329.1892; found 329.1922.

**3. 3. 15 7-bromo-1-methyl-5-(*o*-tolyl)-1,3-dihydro-2*H*-benzo[*e*] [1,4] diazepin-2-one (52)**


The **7-bromo-5-(*o*-tolyl)-1,3-dihydro-2*H*-benzo[*e*] [1,4]diazepin-2-one 72**, (5.0 g, 15.2 mmol) was dissolved in THF, (30 mL) and the solution was cooled to -0$^{o}$C using an ice bath. Then potassium tert butoxide (1.87 g, 16.7 mmol) which was dissolved in 30 mL of THF was added dropwise by using an addition funnel. Then methyl iodide (1.14 mL, 18.2 mmoL) was added dropwise to the reaction mixture over an 1 min period, while maintaining the temperature at 0$^{o}$C. Upon completion of the addition, the reaction mixture was allowed to warm to rt and stir for 60 min, at which point the reaction was deemed complete on analysis by TLC (silica gel). The

reaction mixture was then diluted with ethyl acetate (20 mL) and a solution of 10% aq sodium chloride (200 mL) was added. The biphasic mixture, which resulted, was allowed to stand for 15 min and the layers were separated. The aq layer was then extracted with ethyl acetate (50 mL) and the combined organic layers were washed with 10% aq sodium chloride solution (50 mL). The organic layer was dried ($Na_2SO_4$). The solvent was removed under reduced pressure. The brown solid which was obtained was purified by crystallization using 15:85(ethyl acetate/hexanes), to give **7-bromo-1-methyl-5-(*o*-tolyl)-1,3-dihydro-2*H*-benzo[*e*] [1,4] diazepin-2-one 52** (3.91 g, 75%) as a brownish white solid.

$^1$H NMR (300 MHz, $CDCl_3$) δ 7.42 (d, *J* = 6.4 Hz, 4H), 7.28 (d, *J* = 4.1 Hz, 1H), 7.17 (d, *J* = 8.1 Hz, 1H), 7.01 (d, *J* = 2.2 Hz, 1H), 4.33 (s, 2H), 3.87 (s, 3H), 2.10 (s, 3H). $^{13}$C NMR (126 MHz, $CDCl_3$) δ 169.93, 168.86, 143.10, 138.19, 134.37, 132.89, 130.73, 129.50, 128.45, 122.79, 116.82, 56.94, 34.85, 19.98.; **HRMS** (ESI/IT-TOF) m/z: [M + H] + Calcd for $C_{17}H_{15}BrN_2O$ 343.2169; found 343.2152.

### 3. 3. 16 1-methyl-5-(*o*-tolyl)-7-((triisopropylsilyl)ethynyl)-1,3-dihydro-2*H*-benzo[*e*] [1,4] diazepin-2-one (73)

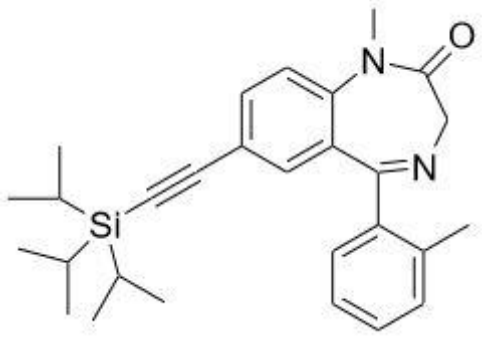


In a 500mL round bottom flask, Pd $(OAc)_2$ (112 mg, 0.5 mmol) and P(o-tolyl)$_3$ (304.37 mg, 1.0 mmol) was added to 50 mL of acetonitrile. The mixture was stirred until a slurry appeared, which

took about 20 min. Then 7-bromo-1-methyl-5-phenyl-1,3-dihydro-2*H*-1,4-benzodiazepin-2-one **52**, (3.50 g, 10.2 mmol), triethylamine (4.26 mL, 30.6 mmol), (triisopropylylsilyl)acetylene (3.43 mL,15.3 mmol) and additional acetonitrile (50 mL) was added. The reaction mixture was then heated to reflux (75$^{o}$C) and held for 6 h, at which point the reaction was deemed complete on analysis by TLC (Silica gel). Upon completion of the reaction progress, the mixture was cooled to rt and filtered through celite. After washing with acetonitrile (100 mL x 2), the solvents were removed under reduced pressure and the residue was dissolved in dichloromethane (400 mL) and 5% aq sodium bicarbonate (400 mL) was added. The biphasic mixture, which resulted, was allowed to stand for 15 min and the layers were separated. The aq layer was then extracted with dichloromethane (300 mL) and the combined organic layers were washed with 5% aq sodium bicarbonate solution (300 mL) and then 10% aq sodium chloride solution (300 mL x 3). The organic layer was dried ($Na_2SO_4$) and was evaporated under reduced pressure. This process gave a dark orange liquid that gets solidified eventually on standing to give 1-methyl-5-phenyl-7-((tripropan-2-ylsilyl) ethynyl)-1,3-dihydro-2*H*-1,4-benzodiazepin-2-one, **73** (3.4 gm ,71% crude yield). This material was used in the next step without further purification.

**3. 3. 17 7-ethynyl-1-methyl-5-(*o*-tolyl)-1,3-dihydro-2*H*-benzo[*e*] [1,4] diazepin-2-one (74)**

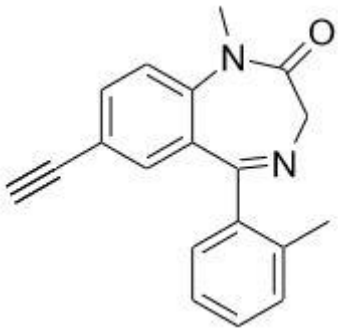

1-Methyl-5-phenyl-7-((tripropan-2-ylsilyl) ethynyl)-1,3-dihydro-2*H*-1,4-benzodiazepin-2-one **73**, (3.40 g, 7.6 mmol), water (0.5 mL) and tetrahydrofuran (30 mL) were cooled to -20$^{o}$C using a dry ice / IPA bath. Then tetrabutylammonium fluoride hydrate, [1M in THF (10.9 mL, 10.9 mmoL)] was added dropwise to the reaction mixture over a 30 min period, while maintaining the temperature at -20 to -15$^{o}$C. Upon completion of the addition, the reaction mixture was allowed to warm to rt and stir for an additional 60 min at which point the reaction progress was deemed complete on analysis by TLC (silica gel). The reaction mixture was then diluted with ethyl acetate (50 mL) and 10% aq sodium chloride (50 mL). The biphasic mixture, which resulted, was allowed to stand for 15 min and the layers were separated. The aq layer was then extracted with ethyl acetate (50 mL x 3) and the combined organic layers were washed with 10% aq sodium chloride solution (150 mL). The organic layer was dried ($Na_2SO_4$). The solvents were removed under reduced pressure. Then the mixture was dissolved in 50 mL of ethyl acetate and then stirred with 20gm of silica gel for 2 hours and filtered. The amount of solvent was reduced to about 40 ml under reduced pressure. Then 20mL of hexanes was added dropwise to the mixture and it was allowed to stir overnight. The solid, which formed, was filtered and the grey solid was recrystallized from 1:4 (ethyl acetate/hexanes) to obtain cream white colored TA II 73. (1.98 g, 90%)

$^{1}$H NMR (500 MHz, $CDCl_3$) δ 7.63 – 7.60 (m, 1H), 7.38 – 7.27 (m, 4H), 7.24 – 7.18 (m, 2H), 4.86 (t, *J* = 11.4 Hz, 1H), 3.81 (dd, *J* = 18.3, 10.8 Hz, 1H), 3.46 (s, 3H), 3.05 (s, 1H), 1.99 (d, *J* = 8.0 Hz, 3H). $^{13}$C NMR (126 MHz, $CDCl_3$) δ 171.32, 169.86, 143.10, 138.91, 136.26, 134.67, 133.12, 130.84, 130.49, 129.67, 128.39, 125.97, 121.12, 118.19, 81.95, 78.27, 56.79, 34.72, 19.94. **HRMS** (ESI/IT-TOF) m/z: [M + H] + Calcd for $C_{19}H_{16}N_2O$ 288.3420; found 288.3406.

**3. 3. 18 ethyl 8-bromo-6-(*o*-tolyl)-4*H*-benzo[*f*]imidazo[1,5-*a*] [1,4] diazepine-3-carboxylate (75)**

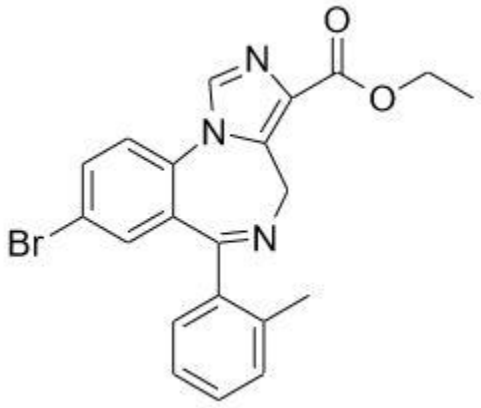


7-bromo-5-(*o*-tolyl)-1,3-dihydro-2*H*-benzo[*e*] [1,4] diazepin-2-one (**72**) (10 g, 30.3 mmol) was suspended in dry THF (150 mL) and cooled to -50 °C using a dry ice bath, after which potassium *t*-butoxide (4.1 g, 36.5 mmol) was added in one portion. The reaction mixture was stirred until it reached 0 °C and then stirred for 0.5 h at 0 °C. The mixture was then cooled to -50 °C, after which diethyl chlorophosphate (6.15 mL, 42.4 mmol) was added dropwise with an addition funnel. The dry ice bath was removed to allow the temperature to rise to 0 °C, after which it was allowed to stir for 2 h with an ice-water bath. The solution was then cooled to -78 °C with a dry-ice bath and ethyl isocyanoacetate (4.63 g, 42.4 mmol) was added, immediately followed by a second portion of potassium *t*-butoxide (4.1 g, 36.5 mmol). This solution was allowed to stir overnight during which period it was allowed to warm to rt. The reaction was completed after 14 h on analysis by TLC (silica gel, EtOAc/hexanes, 1:1). The reaction mixture was quenched by addition of a cold saturated aq solution of $NaHCO_3$ (50 mL) and extracted with EtOAc. The organic layers were combined and washed with brine (2 x 20 mL), and dried ($Na_2SO_4$). The solvent was removed under reduced pressure to obtain a dark brown solid residue. The solid was washed with $Et_2O$/EtOAc (9:1) to remove most of the impurities and the solid was further recrystallized from EtOAc and

hexane (1:4), and this was followed by washing the solid with cold $Et_2O$ to afford the majority of the pure ethyl ester **75**. The remaining filtrate was combined and purified by flash chromatography to obtain additional ethyl ester **75** (silica gel, EtOAc/ hexanes=1:1) as an off-white solid (7.22 g, 56% yield)

**$^1$H NMR** (500 MHz, $CDCl_3$): δ = 8.60 (d, *J* = 4.4 Hz, 1H), 8.11 (d, *J* = 7.9 Hz, 1H), 8.00 (s, 1H), 7.86 (td, *J* = 8.0, 1.7 Hz, 1H), 7.80 (dd, *J* = 8.6, 2.2 Hz, 1H), 7.60 (d, *J* = 2.1 Hz, 1H), 7.51 (d, *J* = 8.6 Hz, 1H), 7.41 (dd, *J* = 7.1, 5.2 Hz, 1H), 6.13 (d, *J* = 10.4 Hz, 1H), 4.51 – 4.33 (m, 2H), 4.17 (d, *J* = 11.6 Hz, 1H), 1.44 (t, *J* = 7.1 Hz, 3H); **$^{13}$C NMR** (500 MHz, $CDCl_3$): δ = 167.0, 162.9, 156.2, 148.7, 138.4, 136.9, 135.3, 135.0, 134.5, 134.4, 129.3, 128.5, 124.9, 124.3, 123.9, 120.5, 60.7, 45.0, 14.4; **HRMS** (ESI/IT-TOF): m/z $[M + H]^+$ calcd for $C_{21}H_{18}BrN_3O_2$: 424.2892; found: 424.2881.

### 3. 3. 19 ethyl 6-(*o*-tolyl)-8-((triisopropylsilyl)ethynyl)-4*H*-benzo[*f*]imidazo[1,5-*a*] [1,4] diazepine-3-carboxylate (76)

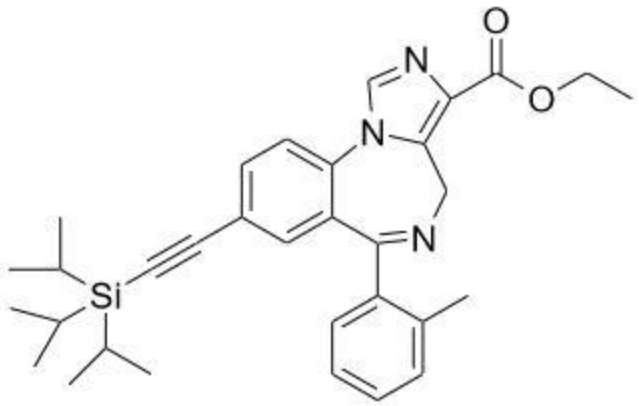


In a 500mL round bottom flask, Pd $(OAc)_2$ (132mg, 0.59 mmol) and P(o-tolyl)$_3$ (359 mg, 1.18 mmol) was added to 50 mL of acetonitrile. The mixture was stirred until a slurry appeared, which took about 20 min. Then 7-bromo-1-methyl-5-phenyl-1,3-dihydro-2*H*-1,4-benzodiazepin-2-one **5**, (5.0 g, 11.8 mmol), triethylamine (3.62 mL, 25.96 mmol), (triisopropylylsilyl)acetylene (3.44

mL,15.34 mmol) and additional acetonitrile (50 mL) was added. The reaction mixture was then heated to reflux (75$^{o}$C) and held for 6 h, at which point the reaction was deemed complete on analysis by TLC (Silica gel). Upon completion of the reaction progress, the mixture was cooled to rt and filtered through celite. After washing with acetonitrile (100 mL x 2), the solvents were removed under reduced pressure and the residue was dissolved in dichloromethane (100 mL) and 5% aq sodium bicarbonate (100 mL) was added. The biphasic mixture, which resulted, was allowed to stand for 15 min and the layers were separated. The aq layer was then extracted with dichloromethane (100 mL) and the combined organic layers were washed with 5% aq sodium bicarbonate solution (100 mL) and then 10% aq sodium chloride solution (100 mL x 3). The organic layer was dried ($Na_2SO_4$) and was evaporated under reduced pressure. This process gave a dark orange liquid that gets solidified eventually on standing to give ethyl 6-(*o*-tolyl)-8-((triisopropylsilyl)ethynyl)-4*H*-benzo[*f*]imidazo[1,5-*a*] [1,4] diazepine-3-carboxylate, **76** (4.39g ,71% crude yield). This material was used at the next step without purification.

### 3. 3. 20 ethyl 8-ethynyl-6-(*o*-tolyl)-4*H*-benzo[*f*]imidazo[1,5-*a*][1,4]diazepine-3-carboxylate (77)

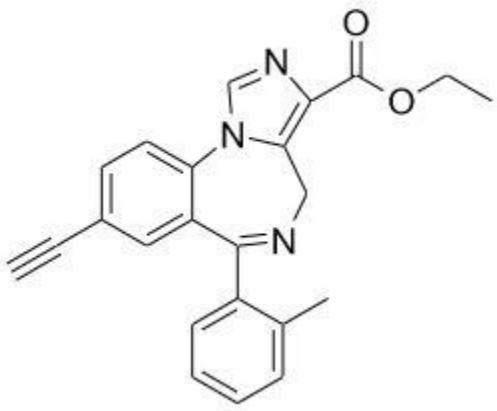


ethyl 6-(*o*-tolyl)-8-((triisopropylsilyl)ethynyl)-4*H*-benzo[*f*]imidazo[1,5-*a*] [1,4] diazepine-3-carboxylate **76**, (4.39 g, 8.35 mmol), water (0.5 mL) and tetrahydrofuran (30 mL) were cooled to

-20°C using a dry ice / IPA bath. Then tetrabutylammonium fluoride hydrate, [1M in THF (10.9 mL, 10.9 mmoL)] was added dropwise to the reaction mixture over a 30 min period, while maintaining the temperature at -20 to -15°C. Upon completion of the addition, the reaction mixture was allowed to warm to rt and stir for an additional 60 min at which point the reaction progress was deemed complete on analysis by TLC (silica gel). The reaction mixture was then diluted with ethyl acetate (50 mL) and 10% aq sodium chloride (50 mL). The biphasic mixture, which resulted, was allowed to stand for 15 min and the layers were separated. The aq layer was then extracted with ethyl acetate (50 mL x 3) and the combined organic layers were washed with 10% aq sodium chloride solution (150 mL). The organic layer was dried ($Na_2SO_4$). The solvents were removed under reduced pressure. Then the mixture was dissolved in 50 mL of ethyl acetate and then stirred with 20gm of silica gel for 2 hours and filtered. The amount of solvent was reduced to about 40 ml under reduced pressure. Then 20mL of hexanes was added dropwise to the mixture and it was allowed to stir overnight. The solid, which formed, was filtered and the grey solid was recrystallized from 1:4 (ethyl acetate/hexanes) to obtain cream white colored TA IV 46 (**77**). (2.77 g, 90%)

$^1$H NMR (500 MHz, $CDCl_3$) δ 7.97 (s, 1H), 7.74 (dd, *J* = 8.3, 1.8 Hz, 1H), 7.58 (d, *J* = 8.3 Hz, 1H), 7.37 (d, *J* = 1.8 Hz, 1H), 7.33 (dd, *J* = 14.0, 6.7 Hz, 2H), 7.26 (t, *J* = 7.2 Hz, 1H), 7.17 (d, *J* = 7.5 Hz, 1H), 6.09 (s, 1H), 4.43 (s, 2H), 4.14 (s, 1H), 3.16 (s, 1H), 1.89 (s, 3H), 1.44 (t, *J* = 7.1 Hz, 3H). $^{13}$C NMR (126 MHz, $CDCl_3$) δ 170.24, 162.82, 139.57, 138.71, 135.83, 135.28, 134.79, 134.52, 134.10, 130.90, 129.68, 129.60, 129.56, 129.47, 126.03, 122.50, 121.97, 81.36, 79.92, 60.86, 44.81, 19.83, 14.45. **HRMS** (ESI/IT-TOF) m/z: [M + H] + Calcd for $C_{23}H_{19}BN_3O_2$ 369.4145; found 369.4105.

# Chapter 4 References


1. Watanabe, M.; Maemura, K.; Kanbara, K.; Tamayama, T.; Hayasaki, H., GABA and GABA receptors in the central nervous system and other organs. In *Int. Rev. Cytol.*, Jeon, K. W., Ed. Academic Press: 2002; Vol. 213, pp 1-47.
2. Sieghart, W., Structure and pharmacology of gamma-aminobutyric acid A receptor subtypes. *Pharmacol. Rev.* **1995,** *47* (2), 181.
3. Twyman, R. E.; Rogers, C. J.; Macdonald, R. L., Differential regulation of gamma-aminobutyric acid receptor channels by diazepam and phenobarbital. *Ann. Neurol.* **1989,** *25* (3), 213-20.
4. Hyland, N. P.; Cryan, J. F., A gut feeling about gaba: focus on GABA(B) receptors. *Front. Pharmacol.* **2010,** *1*, 124-124.
5. Guidotti, A.; Auta, J.; Davis, J. M.; Dong, E.; Grayson, D. R.; Veldic, M.; Zhang, X.; Costa, E., GABAergic dysfunction in schizophrenia: new treatment strategies on the horizon. *Psychopharmacology (Berl.)* **2005,** *180* (2), 191-205.
6. Luscher, B.; Shen, Q.; Sahir, N., The GABAergic deficit hypothesis of major depressive disorder. *Mol. Psychiatry* **2011,** *16* (4), 383-406.
7. Sieghart, W.; Ernst, M., Heterogeneity of GABAA receptors: revived interest in the development of subtype-selective drugs. *Current Medicinal Chemistry - Central Nervous System Agents* **2005,** *5* (3), 217-242.
8. Bowser, D. N.; Wagner, D. A.; Czajkowski, C.; Cromer, B. A.; Parker, M. W.; Wallace, R. H.; Harkin, L. A.; Mulley, J. C.; Marini, C.; Berkovic, S. F.; Williams, D. A.; Jones, M. V.; Petrou, S., Altered kinetics and benzodiazepine sensitivity of a GABAA receptor

subunit mutation [gamma 2(R43Q)] found in human epilepsy. *Proc. Natl. Acad. Sci. U. S. A.* **2002,** *99* (23), 15170-5.

9. Munro, G.; Hansen, R. R.; Mirza, N. R., GABAA receptor modulation: Potential to deliver novel pain medicines? *Eur. J. Pharmacol.* **2013,** *716* (1), 17-23.
10. Barnard, E. A.; Skolnick, P.; Olsen, R. W.; Mohler, H.; Sieghart, W.; Biggio, G.; Braestrup, C.; Bateson, A. N.; Langer, S. Z., International Union of Pharmacology. XV. Subtypes of gamma-aminobutyric acidA receptors: classification on the basis of subunit structure and receptor function. *Pharmacol. Rev.* **1998,** *50* (2), 291-313.
11. Olsen, R. W.; Sieghart, W., GABA A receptors: subtypes provide diversity of function and pharmacology. *Neuropharmacology* **2009,** *56* (1), 141-8.
12. Wisden, W.; Laurie, D. J.; Monyer, H.; Seeburg, P. H., The distribution of 13 GABAA receptor subunit mRNAs in the rat brain. I. Telencephalon, diencephalon, mesencephalon. *J. Neurosci.* **1992,** *12* (3), 1040-62.
13. Fritschy, J. M.; Mohler, H., GABAA-receptor heterogeneity in the adult rat brain: differential regional and cellular distribution of seven major subunits. *J. Comp. Neurol.* **1995,** *359* (1), 154-94.
14. Sieghart, W.; Sperk, G., subunit composition, distribution and function of GABA-A receptor subtypes. *Curr. Top. Med. Chem.* **2002,** *2* (8), 795-816.
15. Nutt, D., GABAA receptors: subtypes, regional distribution, and function. *J. Clin. Sleep Med.* **2006,** *2* (2), S7-11.
16. Pirker, S.; Schwarzer, C.; Wieselthaler, A.; Sieghart, W.; Sperk, G., GABA(A) receptors: immunocytochemical distribution of 13 subunits in the adult rat brain. *Neuroscience* **2000,** *101* (4), 815-50.

17. Burt, D. R.; Kamatchi, G. L., GABAA receptor subtypes: from pharmacology to molecular biology. *The FASEB Journal* **1991,** *5* (14), 2916-2923.

18. Clayton, T.; Chen, J. L.; Ernst, M.; Richter, L.; Cromer, B. A.; Morton, C. J.; Ng, H.; Kaczorowski, C. C.; Helmstetter, F. J.; Furtmuller, R.; Ecker, G.; Parker, M. W.; Sieghart, W.; Cook, J. M., An updated unified pharmacophore model of the benzodiazepine binding site on gamma-aminobutyric acid(a) receptors: correlation with comparative models. *Curr. Med. Chem.* **2007,** *14* (26), 2755-75.

19. Keramidas, A.; Moorhouse, A. J.; Schofield, P. R.; Barry, P. H., Ligand-gated ion channels: mechanisms underlying ion selectivity. *Prog. Biophys. Mol. Biol.* **2004,** *86* (2), 161-204.

20. Ramerstorfer, J.; Furtmuller, R.; Sarto-Jackson, I.; Varagic, Z.; Sieghart, W.; Ernst, M., The GABAA receptor alpha+beta- interface: a novel target for subtype selective drugs. *J. Neurosci.* **2011,** *31* (3), 870-7.

21. Varagic, Z.; Ramerstorfer, J.; Huang, S.; Rallapalli, S.; Sarto-Jackson, I.; Cook, J.; Sieghart, W.; Ernst, M., Subtype selectivity of α+β- site ligands of GABAA receptors: identification of the first highly specific positive modulators at α6β2/3γ2 receptors. *Br. J. Pharmacol.* **2013,** *169* (2), 384-399.

22. Chiou, L.-C.; Tzeng, H.-R.; Fan, P.-C.; Sieghart, W.; Ernst, M.; Knutson, D. E.; Cook, J., A novel drug target for migraine: The GABAA receptor α6 subtype in trigeminal ganglia. *The FASEB Journal* **2019,** *33* (1_supplement), lb78-lb78.

23. Knutson, D. E.; Kodali, R.; Divović, B.; Treven, M.; Stephen, M. R.; Zahn, N. M.; Dobričić, V.; Huber, A. T.; Meirelles, M. A.; Verma, R. S.; Wimmer, L.; Witzigmann, C.; Arnold, L. A.; Chiou, L.-C.; Ernst, M.; Mihovilovic, M. D.; Savić, M. M.; Sieghart, W.; Cook, J. M., Design and synthesis of novel deuterated ligands functionally selective for the

γ-aminobutyric acid type a receptor (GABAAR) α6 subtype with improved metabolic stability and enhanced bioavailability. *J. Med. Chem.* **2018,** *61* (6), 2422-2446.

24. Vasović, D.; Divović, B.; Treven, M.; Knutson, D. E.; Steudle, F.; Scholze, P.; Obradović, A.; Fabjan, J.; Brković, B.; Sieghart, W.; Ernst, M.; Cook, J. M.; Savić, M. M., Trigeminal neuropathic pain development and maintenance in rats are suppressed by a positive modulator of α6 GABAA receptors. *European Journal of Pain* **2019,** *23* (5), 973-984.
25. Olsen, R. W.; Hanchar, H. J.; Meera, P.; Wallner, M., GABAA receptor subtypes: the "one glass of wine" receptors. *Alcohol* **2007,** *41* (3), 201-9.
26. Sawyer, E. K.; Moran, C.; Sirbu, M. H.; Szafir, M.; Van Linn, M.; Namjoshi, O.; Phani Babu Tiruveedhula, V. V. N.; Cook, J. M.; Platt, D. M., Little evidence of a role for the α1GABAA subunit-containing receptor in a rhesus monkey model of alcohol drinking. *Alcohol. Clin. Exp. Res.* **2014,** *38* (4), 1108-1117.
27. Ernst, M.; Brauchart, D.; Boresch, S.; Sieghart, W., Comparative modeling of GABA(A) receptors: limits, insights, future developments. *Neuroscience* **2003,** *119* (4), 933-43.
28. Haefely, W., The biological basis of benzodiazepine actions. *J. Psychoactive Drugs* **1983,** *15* (1-2), 19-39.
29. Hillestad, L.; Hansen, T.; Melsom, H.; Drivenes, A., Diazepam metabolism in normal man I. Serum concentrations and clinical effects after intravenous, intramuscular, and oral administrations. *Clin. Pharmacol. Therapeutics* **1974,** *16*, 479 - 484.
30. Stevenson, I. H.; Browning, M.; Crooks, J.; O'Malley, K., Changes in human drug metabolism after long-term exposure to hypnotics. *Br. Med. Journal* **1972,** *4*, 322 - 324.

31. Garattini, S.; Mussini, E.; Marucci, F.; Guaitani, A., Metabolic studies on benzodiazepines in various animal species. In *The Benzodiazepines*, Garattini, S.; Mussini, E.; Randall, L. O., Eds. Raven Press: New York, 1973; pp 75 - 97.

32. Rutherford, D. M.; Okoko, A.; Tyrer, P. J., Plasma concentrations of diazepam and desmethyldiazepam during chronic diazepam therapy. *Br. J. Clin. Pharmacol.* **1978,** *1978* (6).

33. Bond, A. J.; Hailey, D. M.; Lader, M. H., Plasma concentrations of benzodiazepines. *Br. J. Clin. Pharmacol.* **1977,** *4*, 51 - 56.

34. Haefely, W.; Facklam, M.; Schoch, P.; Martin, J. R.; Bonetti, E. P.; Moreau, J. L.; Jenck, F.; Richards, J. G., Partial agonists of benzodiazepine receptors for the treatment of epilepsy, sleep, and anxiety disorders. *Advances in biochemical psychopharmacology* **1992,** *47*, 379-394.

35. Moss, G. P., Nomenclature of fused and bridged fused ring systems (IUPAC Recommendations 1998). In *Pure Appl. Chem.*, 1998; Vol. 70, p 143.

36. Hadingham, K. L.; Wingrove, P. B.; Wafford, K. A.; Bain, C.; Kemp, J. A.; Palmer, K. J.; Wilson, A. W.; Wilcox, A. S.; Sikela, J. M.; Ragan, C. I.; et al., Role of the beta subunit in determining the pharmacology of human gamma-aminobutyric acid type A receptors. *Mol. Pharmacol.* **1993,** *44* (6), 1211-8.

37. Khom, S.; Baburin, I.; Timin, E. N.; Hohaus, A.; Sieghart, W.; Hering, S., Pharmacological properties of GABAA receptors containing gamma1 subunits. *Mol. Pharmacol.* **2006,** *69* (2), 640-9.

38. Bencsits, E.; Ebert, V.; Tretter, V.; Sieghart, W., A significant part of native gamma-aminobutyric AcidA receptors containing alpha4 subunits do not contain gamma or delta subunits. *J. Biol. Chem.* **1999,** *274* (28), 19613-6.

39. Yang, W.; Drewe, J. A.; Lan, N. C., Cloning and characterization of the human GABAA receptor alpha 4 subunit: identification of a unique diazepam-insensitive binding site. *Eur. J. Pharmacol.* **1995,** *291* (3), 319-25.

40. Korpi, E. R.; Seeburg, P. H., Natural mutation of GABAA receptor alpha 6 subunit alters benzodiazepine affinity but not allosteric GABA effects. *Eur. J. Pharmacol.* **1993,** *247* (1), 23-27.

41. Macdonald, R. L.; Olsen, R. W., GABAA receptor channels. *Annu. Rev. Neurosci.* **1994,** *17* (1), 569-602.

42. Study, R. E.; Barker, J. L., Diazepam and (--)-pentobarbital: fluctuation analysis reveals different mechanisms for potentiation of gamma-aminobutyric acid responses in cultured central neurons. *Proc. Natl. Acad. Sci. U. S. A.* **1981,** *78* (11), 7180-7184.

43. MacDonald, R. L., Benzodiazepine mechanisms of action. In *Antiepileptic Drugs*, Levy, R. H.; Mattson, R. H.; Meldrum, B. S.; Perucca, E., Eds. Lippincott Williams and Wilkins: Philadelphia, 2002; pp 179 - 186.

44. Killam, E. K.; Suria, A., Benzodiazepines. In *Antiepileptic Drugs: Mechanisms of Action*, Glaser, G. H.; Penry, J. K.; Woodbury, D. M., Eds. Raven Press: New York, 1980; pp 597 - 615.

45. Rogawski, M. A., Principles of antiepileptic drug action. In *Antiepileptic Drugs*, 5th ed.; Levy, R. H.; Mattson, R. H.; Meldrum, B. S.; Perucca, E., Eds. Lippincott Williams and Wilkins: Philadelphia, 2002; pp 3 - 22.

46. Rudolph, U.; Crestani, F.; Benke, D.; Brunig, I.; Benson, J. A.; Fritschy, J. M.; Martin, J. R.; Bluethmann, H.; Mohler, H., Benzodiazepine actions mediated by specific gamma-aminobutyric acid(A) receptor subtypes. *Nature* **1999,** *401* (6755), 796-800.

47. Low, K.; Crestani, F.; Keist, R.; Benke, D.; Brunig, I.; Benson, J. A.; Fritschy, J. M.; Rulicke, T.; Bluethmann, H.; Mohler, H.; Rudolph, U., Molecular and neuronal substrate for the selective attenuation of anxiety. *Science* **2000,** *290* (5489), 131-4.

48. Collinson, N.; Kuenzi, F. M.; Jarolimek, W.; Maubach, K. A.; Cothliff, R.; Sur, C.; Smith, A.; Otu, F. M.; Howell, O.; Atack, J. R.; McKernan, R. M.; Seabrook, G. R.; Dawson, G. R.; Whiting, P. J.; Rosahl, T. W., Enhanced learning and memory and altered GABAergic synaptic transmission in mice lacking the alpha 5 subunit of the GABAA receptor. *J. Neurosci.* **2002,** *22* (13), 5572-80.

49. Paul, J.; Yévenes, G. E.; Benke, D.; Di Lio, A.; Ralvenius, W. T.; Witschi, R.; Scheurer, L.; Cook, J. M.; Rudolph, U.; Fritschy, J.-M.; Zeilhofer, H. U., Antihyperalgesia by α2-GABAA receptors occurs via a genuine spinal action and does not involve supraspinal sites. *Neuropsychopharmacology : official publication of the American College of Neuropsychopharmacology* **2014,** *39* (2), 477-487.

50. McKernan, R. M.; Rosahl, T. W.; Reynolds, D. S.; Sur, C.; Wafford, K. A.; Atack, J. R.; Farrar, S.; Myers, J.; Cook, G.; Ferris, P.; Garrett, L.; Bristow, L.; Marshall, G.; Macaulay, A.; Brown, N.; Howell, O.; Moore, K. W.; Carling, R. W.; Street, L. J.; Castro, J. L.; Ragan, C. I.; Dawson, G. R.; Whiting, P. J., Sedative but not anxiolytic properties of benzodiazepines are mediated by the GABAA receptor α1 subtype. *Nat. Neurosci.* **2000,** *3*, 587.

51. Morris, H. V.; Dawson, G. R.; Reynolds, D. S.; Atack, J. R.; Stephens, D. N., Both alpha2 and alpha3 GABAA receptor subtypes mediate the anxiolytic properties of benzodiazepine site ligands in the conditioned emotional response paradigm. *Eur. J. Neurosci.* **2006,** *23* (9), 2495-504.

52. Dias, R.; Sheppard, W. F.; Fradley, R. L.; Garrett, E. M.; Stanley, J. L.; Tye, S. J.; Goodacre, S.; Lincoln, R. J.; Cook, S. M.; Conley, R.; Hallett, D.; Humphries, A. C.; Thompson, S. A.; Wafford, K. A.; Street, L. J.; Castro, J. L.; Whiting, P. J.; Rosahl, T. W.; Atack, J. R.; McKernan, R. M.; Dawson, G. R.; Reynolds, D. S., Evidence for a significant role of alpha 3-containing GABAA receptors in mediating the anxiolytic effects of benzodiazepines. *J. Neurosci.* **2005,** *25* (46), 10682-8.

53. Yee, B. K.; Keist, R.; von Boehmer, L.; Studer, R.; Benke, D.; Hagenbuch, N.; Dong, Y.; Malenka, R. C.; Fritschy, J. M.; Bluethmann, H.; Feldon, J.; Möhler, H.; Rudolph, U., A schizophrenia-related sensorimotor deficit links α3-containing GABAA receptors to a dopamine hyperfunction. *Proc. Natl. Acad. Sci. U. S. A.* **2005,** *102* (47), 17154.

54. Crestani, F.; Keist, R.; Fritschy, J. M.; Benke, D.; Vogt, K.; Prut, L.; Blüthmann, H.; Möhler, H.; Rudolph, U., Trace fear conditioning involves hippocampal alpha5 GABA(A) receptors. *Proc. Natl. Acad. Sci. U. S. A.* **2002,** *99* (13), 8980-8985.

55. Ralvenius, W. T.; Benke, D.; Acuna, M. A.; Rudolph, U.; Zeilhofer, H. U., Analgesia and unwanted benzodiazepine effects in point-mutated mice expressing only one benzodiazepine-sensitive GABAA receptor subtype. *Nature communications* **2015,** *6*, 6803.

56. Mizuta, K.; Xu, D.; Pan, Y.; Comas, G.; Sonett, J. R.; Zhang, Y.; Panettieri, R. A., Jr.; Yang, J.; Emala, C. W., Sr., GABAA receptors are expressed and facilitate relaxation in airway smooth muscle. *Am. J. Physiol. Lung Cell Mol. Physiol.* **2008,** *294* (6), L1206-16.

57. Gallos, G.; Yim, P.; Chang, S.; Zhang, Y.; Xu, D.; Cook, J. M.; Gerthoffer, W. T.; Emala, C. W., Sr., Targeting the restricted alpha-subunit repertoire of airway smooth muscle GABAA receptors augments airway smooth muscle relaxation. *Am. J. Physiol. Lung Cell Mol. Physiol.* **2012,** *302* (2), L248-56.

58. Gallos, G.; Yocum, G. T.; Siviski, M. E.; Yim, P. D.; Fu, X. W.; Poe, M. M.; Cook, J. M.; Harrison, N.; Perez-Zoghbi, J.; Emala, C. W., Sr., Selective targeting of the alpha5-subunit of GABAA receptors relaxes airway smooth muscle and inhibits cellular calcium handling. *Am. J. Physiol. Lung Cell Mol. Physiol.* **2015,** *308* (9), L931-42.

59. Cook, J. M.; Edwankar, R.; Poe, M. M.; Tiruveedhula, V. V. N. P. B.; Witzigmann, C., Synthesis of natural products and related heterocyclic compounds. Search for agents to treat neuropathic pain, epilepsy and anxiety disorders as well as simple molecules to treat TB and MRSA infections. In *Mona Symposium on Natural Products and Medicinal Chemistry*, Kingston, Jamaica, 2014.

60. Davies, M.; Bateson, A. N.; Dunn, S. M. J., Structural requirements for ligand interactions at the benzodiazepine recognition site of the GABAA receptor. *J. Neurochem.* **1998,** *70* (5), 2188-2194.

61. Dunn, S. M. J.; Davies, M.; Muntoni, A. L.; Lambert, J. J., Mutagenesis of the Rat α1 Subunit of the γ-aminobutyric acid receptor reveals the importance of residue 101 in determining the allosteric effects of benzodiazepine site ligands. *Mol. Pharmacol.* **1999,** *56* (4), 768.

62. Sigel, E.; Schaerer, M. T.; Buhr, A.; Baur, R., The benzodiazepine binding pocket of recombinant α1β2γ2 γ-aminobutyric acid receptors: relative orientation of ligands and amino acid side chains. *Mol. Pharmacol.* **1998,** *54* (6), 1097.

63. Whitwam, J. G.; Amrein, R., Pharmacology of flumazenil. *Acta Anaesthesiol. Scand. Suppl.* **1995,** *108*, 3-14.

64. Clayton, T. S. Ph.D. Thesis, Part I. Unified Pharmacophoric Protein Models of the Benzodiazepine Receptor Subtypes. Part II. Subtype Selective Ligands for a5 GABAA/Bz Receptors. University of Wisconsin-Milwaukee, 2011.

65. He, X.; Huang, Q.; Ma, C.; Yu, S.; McKernan, R.; Cook, J. M., Pharmacophore/receptor models for GABAA/BzR a2b3g2, a3b3g2 and a4b3g2 recombinant subtypes. Included volume analysis and comparison to a1b3g2, a5b3g2 and a6b3g2 subtypes. *Drug Des. Discov.* **2000,** *17*, 131 - 171.

66. Huang, Q.; He, X.; Ma, C.; Liu, R.; Yu, S.; Dayer, C. A.; Wenger, G. R.; McKernan, R.; Cook, J. M., Pharmacophore/Receptor Models for GABAA/BzR Subtypes (α1β3γ2, α5β3γ2, and α6β3γ2) via a Comprehensive Ligand-Mapping Approach. *J. Med. Chem.* **2000,** *43* (1), 71-95.

67. Clayton, T.; Poe, M. M.; Rallapalli, S.; Biawat, P.; Savic, M. M.; Rowlett, J. K.; Gallos, G.; Emala, C. W.; Kaczorowski, C. C.; Stafford, D. C.; Arnold, L. A.; Cook, J. M., A Review of the updated pharmacophore for the alpha 5 GABA(A) benzodiazepine receptor model. *Int J Med Chem* **2015,** *2015*, 430248.

68. Gu, Z. Q.; Wong, G.; Dominguez, C.; de Costa, B. R.; Rice, K. C.; Skolnick, P., Synthesis and evaluation of imidazo[1,5a][1,4]benzodiazepine esters with high affinities and

selectivities at diazepam insensitive (DI) benzodiazepine receptors. *J. Med. Chem* **1993,** *36*, 1001 - 1006.

69. Wong, G.; Koehler, K. F.; Skolnick, P.; Gu, Z. Q.; Ananthan, S.; Schonholze, P.; Hunkeler, W.; Zhang, W.; Cook, J. M., Synthetic and computer-assisted analysis of the structural requirements for selective, high affinity ligand binding to 'diazepam-insensitive' benzodiazepine receptors. *J. Med. Chem* **1993,** *36*, 1820 - 1830.
70. Lippke, K. P.; Schunack, W. G.; Wenning, W.; Muller, W. E., b-Carbolines as benzodiazepine receptor ligands. I. Synthesis and benzodiazepine receptor interactino of esters of b-carboline-3-carboxylic acid. *J. Med. Chem* **1983,** *26*, 499 - 503.
71. Haefely, W.; Martin, J. R.; Schoch, P., Novel anxiolytics that act as partial agonists at benzodiazepine receptors. *Trends Pharmacol. Sci.* **1990,** *11*, 452 - 456.
72. Hagen, T. J.; Guzman, F.; Schultz, C.; Cook, J. M., Synthesis of 3,6-disubstituted b-carbolines which possess either benzodiazepine antagonist or agonist activity. *Heterocycles* **1986,** *24*, 2845 - 855.
73. Gee, K. W.; Brinton, R. E.; Yamamura, H. I., CL-218872 antagonism of diazepam induced loss of righting reflex: Evidence for partial agonistic activity at the benzodiazepine receptor. *Life Sci.* **1983,** *32*, 1037 - 1040.
74. Allen, M. S.; Hagen, T. J.; Trudell, M. L.; Codding, P. W.; Skolnick, P.; Cook, J. M., Synthesis of novel 3-substituted b-carbolines as benzodiazepine receptor ligands: probing the benzodiazepine receptor pharmacophore. *J. Med. Chem* **1988,** *31*, 1854 - 1861.
75. Trudell, M. L.; Lifer, S. L.; Tan, Y. C.; Martin, M. J.; Deng, T.; Skolnick, P.; Cook, J. M., Synthesis of substituted 7,12-dihydropyrido[3,2-*b*:5,4-*b*'] diindoles: rigid planar

benzodiazepine receptor ligands with inverse agonist/antagonist properties. *J. Med. Chem* **1990,** *33*, 2412 - 2420.

76. Arbilla, S.; Depoortere, H.; Geroge, P.; Langer, S. Z., Pharmacological profile of the imidazopyridine zolpidem at benzodiazepine receptors and electrocorticogram in rats. *Naunym Schmiederbergs Arch. Pharmacol.* **1985,** *330*, 248 - 251.

77. Yokoyama, N.; Ritter, B.; Neubert, A. D., 2-Arylpyrazolo[4,3-*c*]quinolin-3-ones: novel agonist, partial agonist, and antagonist of benzodiazepines. *J. Med. Chem* **1982,** *25*, 337 - 339.

78. Huang, Q.; Zhang, W.; Liu, R.; McKernan, R. M.; Cook, J. M., Benzo-fused benzodiazepines employed as topological probes for the study of benzodiazepine receptor subtypes. *Med. Chem. Res.* **1996,** *6*, 384 - 391.

79. van Rijnsoever, C.; Täuber, M.; Choulli, M. K.; Keist, R.; Rudolph, U.; Mohler, H.; Fritschy, J. M.; Crestani, F., Requirement of α5GABA receptors for the development of tolerance to the sedative action of diazepam in mice. *The Journal of Neuroscience* **2004,** *24* (30), 6785.

80. Cook, J.; Huang, S.; Edwankar, R.; Namjoshi, O. A.; Wang, Z. J. Selective agents for pain suppression. Patent: US 8835424 B2. Date: Sep. 16, 2014.

81. Cook, J. M.; Huang, Q.; He, X.; Li, X.; Yu, J.; Han, D.; Lelas, S.; McElroy, J. F. Anxiolytic agents with reduced sedative and ataxic effects. Patent: US7119196 B2. Date: Oct. 10, 2006.

82. Cook, J. M.; Zhou, H.; Huang, S.; Sarma, P. V. V. S.; Zhang, C., Stereospecific anxiolytic and anticonvulsant agents with reduced muscle-relaxant, sedative-hypnotic and ataxic effects. Patent: US 7618958 B2. Date: Nov. 17, 2009.

83. *Roussel MF, Hatten ME (2011). Cerebellum development and medulloblastoma. Current Topics in Developmental Biology.* ***94****. pp. 235–82. doi:10.1016/B978-0-12-380916-2.00008-5. ISBN 9780123809162. PMC 3213765. PMID 21295689.*

84. Pomeroy SL, Tamayo P, Gaasenbeek M, Sturla LM, Angelo M, McLaughlin ME, Kim JY, Goumnerova LC, Black PM, Lau C, Allen JC, Zagzag D, Olson JM, Curran T, Wetmore C, Biegel JA, Poggio T, Mukherjee S, Rifkin R, Califano A, Stolovitzky G, Louis DN, Mesirov JP, Lander ES, Golub TR. Prediction of central nervous system embryonal tumour outcome based on gene expression. Nature. 2002;415:436–442. doi: 10.1038/415436a.

85. Bhattacharjee A, Richards WG, Staunton J, Li C, Monti S, Vasa P, Ladd C, Beheshti J, Bueno R, Gillette M, Loda M, Weber G, Mark EJ, Lander ES, Wong W, Johnson BE, Golub TR, Sugarbaker DJ, Meyerson M. Classification of human lung carcinomas by mRNA expression profiling reveals distinct adenocarcinoma subclasses. Proc Natl Acad Sci USA. 2001;98:13790–13795. doi: 10.1073/pnas.191502998.

86. Gatza ML, Lucas JE, Barry WT, Kim JW, Wang Q, Crawford MD, Datto MB, Kelley M, Mathey-Prevot B, Potti A, Nevins JR. A pathway-based classification of human breast cancer. Proc Natl Acad Sci USA. 2010;107:6994–6999. doi: 10.1073/pnas.0912708107.

87. Golub TR, Slonim DK, Tamayo P, Huard C, Gaasenbeek M, Mesirov JP, Coller H, Loh ML, Downing JR, Caligiuri MA, Bloomfield CD, Lander ES. Molecular classification of cancer: class discovery and class prediction by gene expression monitoring. Science. 1999;286:531–537. doi: 10.1126/science.286.5439.531.

88. Noushmehr H, Weisenberger DJ, Diefes K, Phillips HS, Pujara K, Berman BP, Pan F, Pelloski CE, Sulman EP, Bhat KP, Verhaak RG, Hoadley KA, Hayes DN, Perou CM, Schmidt HK, Ding L, Wilson RK, Van Den Berg D, Shen H, Bengtsson H, Neuvial P,

Cope LM, Buckley J, Herman JG, Baylin SB, Laird PW, Aldape K. Identification of a CpG island methylator phenotype that defines a distinct subgroup of glioma. Cancer Cell. 2010;17:510–522. doi: 10.1016/j.ccr.2010.03.017.

89. Stegmaier K, Ross KN, Colavito SA, O'Malley S, Stockwell BR, Golub TR. Gene expression-based high-throughput screening(GE-HTS) and application to leukemia differentiation. Nat Genet. 2004;36:257–263. doi: 10.1038/ng1305.

90. Cho YJ, Tsherniak A, Tamayo P, Santagata S, Ligon A, Greulich H, Berhoukim R, Amani V, Goumnerova L, Eberhart CG, Lau CC, Olson JM, Gilbertson RJ, Gajjar A, Delattre O, Kool M, Ligon K, Meyerson M, Mesirov JP, Pomeroy SL. Integrative genomic analysis of medulloblastoma identifies a molecular subgroup that drives poor clinical outcome. J Clin Oncol. 2011;29:1424–1430. doi: 10.1200/JCO.2010.28.5148.

91. Kool M, Koster J, Bunt J, Hasselt NE, Lakeman A, van Sluis P, Troost D, Meeteren NS, Caron HN, Cloos J, Mrsic A, Ylstra B, Grajkowska W, Hartmann W, Pietsch T, Ellison D, Clifford SC, Versteeg R. Integrated genomics identifies five medulloblastoma subtypes with distinct genetic profiles, pathway signatures and clinicopathological features. PLoS ONE. 2008;3:e3088. doi: 10.1371/journal.pone.0003088.

92. Northcott P, Korshunov A, Witt H, ***Hielscher*** T, Eberhart C, Mack S, Bouffet E, Clifford S, Hawkins C, French P, Rutka J, Pfister S, Taylor M. Medulloblastoma comprises four distinct molecular variants. J Clin Oncol. 2011;29:1408–1414. doi: 10.1200/JCO.2009.27.4324.

93. Kool M, Korshunov A, Remke M, Jones D, Schlanstein M, Northcott P, Cho Y, Schouten - van Meeteren N, van Vuurden D, Clifford S, Pietsch T, von Bueren A, Rutkowski S, McCabe M, Collins P, Bäcklund M, Haberler C, Bourdeaut F, Delattre O, Doz F, Ellison

D, Gilbertson R, Pomeroy S, Taylor M, Lichter P, Pfister S (2011) Molecular subgroups of medulloblastoma: An international meta-analysis of transcriptome, genetic aberrations, and clinical data of wnt, shh, group 3, and group 4 medulloblastomas. Acta Neuropathol (under review)

94. Louis D, Ohgaki H, Wiestler O, Cavenee W, Burger P, Jouvet A, Scheithauer B, Kleihues P. The 2007 WHO classification of tumours of the central nervous system. Acta Neuropathol. 2007;114:97–109. doi: 10.1007/s00401-007-0243-4.

95. Korshunov A, Remke M, Kool M, Hielscher T, Northcott P, Williamson D, Pfaff E, Witt H, Jones D, Ryzhova M, Cho Y, Wittmann A, Benner A, Weiss W, von Deimling A, Scheurlen W, Kulozik A, Clifford S, Collins V, Westermann F, Taylor M, Lichter P, Pfister S (2011) Biological and clinical heterogeneity of *MYCN*-amplified medulloblastoma. Acta Neuropathol. doi:10.1007/s00401-011-0918-8

96. Ellison DW, Kocak M, Dalton J, Megahed H, Lusher ME, Ryan SL, Zhao W, Nicholson SL, Taylor RE, Bailey S, Clifford SC. Definition of disease-risk stratification groups in childhood medulloblastoma using combined clinical, pathologic, and molecular variables. J Clin Oncol. 2011;29:1400–1407. doi: 10.1200/JCO.2010.30.2810.

97. Hamilton SR, Liu B, Parsons RE, Papadopoulos N, Jen J, Powell SM, Krush AJ, Berk T, Cohen Z, Tetu B, et al. The molecular basis of Turcot's syndrome. N Engl J Med. 1995;332:839–847. doi: 10.1056/NEJM199503303321302.

98. Zurawel RH, Chiappa SA, Allen C, Raffel C. Sporadic medulloblastomas contain oncogenic beta-catenin mutations. Cancer Res. 1998;58:896–899.

99. Parsons DW, Li M, Zhang X, Jones S, Leary RJ, Lin JC, Boca SM, Carter H, Samayoa J, Bettegowda C, Gallia GL, Jallo GI, Binder ZA, Nikolsky Y, Hartigan J, Smith DR, Gerhard

DS, Fults DW, VandenBerg S, Berger MS, Marie SK, Shinjo SM, Clara C, Phillips PC, Minturn JE, Biegel JA, Judkins AR, Resnick AC, Storm PB, Curran T, He Y, Rasheed BA, Friedman HS, Keir ST, McLendon R, Northcott PA, Taylor MD, Burger PC, Riggins GJ, Karchin R, Parmigiani G, Bigner DD, Yan H, Papadopoulos N, Vogelstein B, Kinzler KW, Velculescu VE. The genetic landscape of the childhood cancer medulloblastoma. Science. 2011;331:435–439. doi: 10.1126/science.1198056.

100. Thompson MC, Fuller C, Hogg TL, Dalton J, Finkelstein D, Lau CC, Chintagumpala M, Adesina A, Ashley DM, Kellie SJ, Taylor MD, Curran T, Gajjar A, Gilbertson RJ. Genomics identifies medulloblastoma subgroups that are enriched for specific genetic alterations. J Clin Oncol. 2006;24:1924–1931. doi: 10.1200/JCO.2005.04.4974.

101. Gibson P, Tong Y, Robinson G, Thompson MC, Currle DS, Eden C, Kranenburg TA, Hogg T, Poppleton H, Martin J, Finkelstein D, Pounds S, Weiss A, Patay Z, Scoggins M, Ogg R, Pei Y, Yang ZJ, Brun S, Lee Y, Zindy F, Lindsey JC, Taketo MM, Boop FA, Sanford RA, Gajjar A, Clifford SC, Roussel MF, McKinnon PJ, Gutmann DH, Ellison DW, Wechsler-Reya R, Gilbertson RJ. Subtypes of medulloblastoma have distinct developmental origins. Nature. 2010;468:1095–1099. doi: 10.1038/nature09587.

102. Bale SJ, Falk RT, Rogers GR. Patching together the genetics of Gorlin syndrome. J Cutan Med Surg. 1998;3:31–34.

103. Taylor MD, Mainprize TG, Rutka JT. Molecular insight into medulloblastoma and central nervous system primitive neuroectodermal tumor biology from hereditary syndromes: a review. Neurosurgery. 2000;47:888–901. doi: 10.1097/00006123-200010000-00020.

104. Brugieres L, Pierron G, Chompret A, Paillerets BB, Di Rocco F, Varlet P, Pierre-Kahn A, Caron O, Grill J, Delattre O. Incomplete penetrance of the predisposition to

medulloblastoma associated with germ-line SUFU mutations. J Med Genet. 2010;47:142–144. doi: 10.1136/jmg.2009.067751.

105. Pastorino L, Ghiorzo P, Nasti S, Battistuzzi L, Cusano R, Marzocchi C, Garre ML, Clementi M, Scarra GB. Identification of a SUFU germline mutation in a family with Gorlin syndrome. Am J Med Genet A. 2009;149A:1539–1543. doi: 10.1002/ajmg.a.32944.

106. Slade I, Murray A, Hanks S, Kumar A, Walker L, Hargrave D, Douglas J, Stiller C, Izatt L, Rahman N. Heterogeneity of familial medulloblastoma and contribution of germline PTCH1 and SUFU mutations to sporadic medulloblastoma. Fam Cancer. 2010;10(2):337–342. doi: 10.1007/s10689-010-9411-0.

107. Taylor MD, Liu L, Raffel C, Hui CC, Mainprize TG, Zhang X, Agatep R, Chiappa S, Gao L, Lowrance A, Hao A, Goldstein AM, Stavrou T, Scherer SW, Dura WT, Wainwright B, Squire JA, Rutka JT, Hogg D. Mutations in SUFU predispose to medulloblastoma. Nat Genet. 2002;31:306–310. doi: 10.1038/ng916.

108. Northcott P, Hielscher T, Dubuc A, Mack S, Shih D, Remke M, Al-Halabi H, Albrecht S, Jabado N, Eberhart C, Grajkowska W, Weiss W, Clifford S, Bouffet E, Rutka J, Korshunov A, Pfister S, Taylor M. Pediatric and adult sonic hedgehog medulloblastomas are clinically and molecularly distinct. Acta Neuropathol. 2011;122:231–240. doi: 10.1007/s00401-011-0846-7.

109. Northcott PA, Nakahara Y, Wu X, Feuk L, Ellison DW, Croul S, Mack S, Kongkham PN, Peacock J, Dubuc A, Ra YS, Zilberberg K, McLeod J, Scherer SW, Sunil Rao J, Eberhart CG, Grajkowska W, Gillespie Y, Lach B, Grundy R, Pollack IF, Hamilton RL, Van Meter T, Carlotti CG, Boop F, Bigner D, Gilbertson RJ, Rutka JT, Taylor MD. Multiple recurrent

genetic events converge on control of histone lysine methylation in medulloblastoma. Nat Genet. 2009; 41:465–472. doi: 10.1038/ng.336.

110. Northcott PA, Fernandez LA, Hagan JP, Ellison DW, Grajkowska W, Gillespie Y, Grundy R, Van Meter T, Rutka JT, Croce CM, Kenney AM, Taylor MD. The miR-17/92 polycistron is up-regulated in sonic hedgehog-driven medulloblastomas and induced by N-myc in sonic hedgehog-treated cerebellar neural precursors. Cancer Res. 2009; 69:3249–3255. doi: 10.1158/0008-5472.CAN-08-4710.

111. Schwalbe EC, Lindsey JC, Straughton D, Hogg TL, Cole M, Megahed H, Ryan SL, Lusher ME, Taylor MD, Gilbertson RJ, Ellison DW, Bailey S, Clifford SC. Rapid diagnosis of medulloblastoma molecular subgroups. Clin Cancer Res. 2011;17:1883–1894. doi: 10.1158/1078-0432.CCR-10-2210.

112. Thompson MC, Fuller C, Hogg TL, Dalton J, Finkelstein D, Lau CC, Chintagumpala M, Adesina A, Ashley DM, Kellie SJ, Taylor MD, Curran T, Gajjar A, Gilbertson RJ. Genomics identifies medulloblastoma subgroups that are enriched for specific genetic alterations. J Clin Oncol. 2006;24:1924–1931. doi: 10.1200/JCO.2005.04.4974.

113. Al-Halabi H, Nantel A, Klekner A, Guiot MC, Albrecht S, Hauser P, Garami M, Bognar L, Kavan P, Gerges N, Shirinian M, Roberge D, Muanza T, Jabado N. Preponderance of sonic hedgehog pathway activation characterizes adult medulloblastoma. Acta Neuropathol. 2011;121:229–239. doi: 10.1007/s00401-010-0780-0.

114. Ellison DW, Dalton J, Kocak M, Nicholson SL, Fraga C, Neale G, Kenney AM, Brat DJ, Perry A, Yong WH, Taylor RE, Bailey S, Clifford SC, Gilbertson RJ. Medulloblastoma: clinicopathological correlates of SHH, WNT, and non-SHH/WNT molecular subgroups. Acta Neuropathol. 2011;121:381–396. doi: 10.1007/s00401-011-0800-8.

115. Hatten ME, Roussel MF. Development and cancer of the cerebellum. Trends Neurosci. 2011;34(3):134–142. doi: 10.1016/j.tins.2011.01.002.

116. Buonamici S, Williams J, Morrissey M, Wang A, Guo R, Vattay A, Hsiao K, Yuan J, Green J, Ospina B, Yu Q, Ostrom L, Fordjour P, Anderson DL, Monahan JE, Kelleher JF, Peukert S, Pan S, Wu X, Maira SM, Garcia-Echeverria C, Briggs KJ, Watkins DN, Yao YM, Lengauer C, Warmuth M, Sellers WR, Dorsch M (2010) Interfering with resistance to smoothened antagonists by inhibition of the PI3K pathway in medulloblastoma. Sci Transl Med 2:51ra70

117. Rudin CM, Hann CL, Laterra J, Yauch RL, Callahan CA, Fu L, Holcomb T, Stinson J, Gould SE, Coleman B, LoRusso PM, Von Hoff DD, de Sauvage FJ, Low JA. Treatment of medulloblastoma with hedgehog pathway inhibitor GDC-0449. N Engl J Med. 2009;361:1173–1178. doi: 10.1056/NEJMoa0902903.

118. Yauch RL, Dijkgraaf GJ, Alicke B, Januario T, Ahn CP, Holcomb T, Pujara K, Stinson J, Callahan CA, Tang T, Bazan JF, Kan Z, Seshagiri S, Hann CL, Gould SE, Low JA, Rudin CM, de Sauvage FJ. Smoothened mutation confers resistance to a Hedgehog pathway inhibitor in medulloblastoma. Science. 2009;326:572–574. doi: 10.1126/science.1179386.

119. Adamson DC, Shi Q, Wortham M, Northcott PA, Di C, Duncan CG, Li J, McLendon RE, Bigner DD, Taylor MD, Yan H. OTX2 is critical for the maintenance and progression of Shh-independent medulloblastomas. Cancer Res. 2010;70:181–191. doi: 10.1158/0008-5472.CAN-09-2331.

120. de Haas T, Oussoren E, Grajkowska W, Perek-Polnik M, Popovic M, Zadravec-Zalatel L, Perera M, Corte G, Wirths O, van Sluis P, Pietsch T, Troost D, Baas F, Versteeg R, Kool M. OTX1 and OTX2 expression correlates with the clinicopathologic classification of

medulloblastomas. J Neuropathol Exp Neurol. 2006;65:1–11. doi: 10.1097/01.jnen.0000196131.72302.68.

121. Di C, Liao S, Adamson DC, Parrett TJ, Broderick DK, Shi Q, Lengauer C, Cummins JM, Velculescu VE, Fults DW, McLendon RE, Bigner DD, Yan H. Identification of OTX2 as a medulloblastoma oncogene whose product can be targeted by all-trans retinoic acid. Cancer Res. 2005;65:919–924.

122. Kool, M., Korshunov, A., Remke, M., Jones, D. T., Schlanstein, M., Northcott, P. A., Cho, Y. J., Koster, J., Schouten-van Meeteren, A., van Vuurden, D., Clifford, S. C., Pietsch, T., von Bueren, A. O., Rutkowski, S., McCabe, M., Collins, V. P., Bäcklund, M. L., Haberler, C., Bourdeaut, F., Delattre, O., … Pfister, S. M. (2012). Molecular subgroups of medulloblastoma: an international meta-analysis of transcriptome, genetic aberrations, and clinical data of WNT, SHH, Group 3, and Group 4 medulloblastomas. *Acta neuropathologica*, *123*(4), 473–484. https://doi.org/10.1007/s00401-012-0958-8

123. Sengupta, S., Pomeranz Krummel, D., Pomeroy, S. The evolution of medulloblastoma therapy to personalized medicine. F1000Research 6, 490 (2017).

124. Hargrave, D., Zacharoulis, S. Pediatric CNS tumors: current treatment and future directions. Expert Rev. Neurother. 35, 2370–2377 (2017).

125. Sturm, D., Pfister, S., Jones, D. Pediatric Gliomas: Current Concepts on Diagnosis, Biology, and Clinical Management. J. Clin. Oncol. 35, 2370–2377 (2017).

126. Marini, B., Benitez, L., Zureick, A. Blood-brain barrier-adapted precision medicine therapy for pediatric brain tumors. Transl. Res. 188, e1–27.e14 (2017).

127. Wu, L., Li, X., Janagam, D. Overcoming the blood-brain barrier in chemotherapy treatment of pediatric brain tumors. Pharm. Res. 31, 531–540 (2014).

128. Archer TC, Mahoney EL, Pomeroy SL. Medulloblastoma: Molecular Classification-Based Personal Therapeutics. Neurotherapeutics 14(2), 265-273 (2017).

129. Kuzan-Fischer CM, Guerreiro Stucklin AS, Taylor MD. Advances in Genomics Explain Medulloblastoma Behavior at the Bedside. Neurosurgery. (2017) 64(CN_suppl_1):21-26.

130. Louis DN, Perry A, Reifenberger G, von Deimling A, Figarella-Branger D, Cavenee WK, Ohgaki H, Wiestler OD, Kleihues P, Ellison DW. The 2016 World Health Organization Classification of Tumors of the Central Nervous System: a summary. Acta Neuropathol. 131(6): 803-820 (2016).

131. Schwalbe, E. C. et al. Novel molecular subgroups for clinical classification and outcome prediction in childhood medulloblastoma: a cohort study. Lancet Oncol. 18, 958–971 (2017).

132. Cho YJ, Tsherniak A, Tamayo P *et al*. Integrative genomic analysis of medulloblastoma identifies a molecular subgroup that drives poor clinical outcome. J. Clinical Oncology. 29: 1424-1430 (2011).

133. Northcott PA1, Korshunov A, Witt H, Hielscher T, Eberhart CG, Mack S, Bouffet E, Clifford SC, Hawkins CE, French P, Rutka JT, Pfister S, Taylor MD. Medulloblastoma comprises four distinct molecular variants. J Clin Oncol. 29(11):1408-14 (2011).

134. Kool M, Korshunov A, Remke M, *et al*. Molecular subgroups of medulloblastoma: an international meta-analysis of transcriptome, genetic aberrations, and clinical data of WNT, SHH, Group 3, and Group 4 medulloblastomas. Acta Neuropathol. 123(4): 473–84 (2012).

135. Northcott PA, Shih DJ, Peacock J, *et al*. Subgroup-specific structural variation across 1,000 medulloblastoma genomes. Nature. 488(7409): 49–56 (2012).

136. Pugh TJ, Weeraratne SD, Archer TC *et al.* Medulloblastoma exome sequencing uncovers subtype-specific somatic mutations within a broad landscape of genetic heterogeneity. Nature. 488: 106-110. (2012).

137. Cavalli FMG, Remke M, Rampasek L, Peacock J, et al. Intertumoral Heterogeneity within Medulloblastoma Subgroups. Cancer Cell. 31(6): 737-754 (2017).

138. Shih DJ, Northcott PA, Remke M et al. Cytogenetic prognostication within medulloblastoma subgroups. J Clin Oncol. 32(9): 886-896 (2014).

139. Martine F. Roussel, Giles W. Robinson. Role of MYC in Medulloblastoma. Cold Spring Harb Perspect Med. 3(11): a014308 (2013).

140. Gessi P53 expression predicts dismal outcome for medulloblastoma patients with metastatic disease. J Neuro-Onc (2012).

141. Northcott PA, Buchhalter I, Morrissy AS, Hovestadt V, et al. The whole-genome landscape of medulloblastoma subtypes. Nature. 547(7663): 311-317 (2017).

142. Olsen RW, Sieghart W. GABAA receptors: subtypes provide diversity of function and pharmacology. Neuropharmacology 56: 141-148. Neuropharmacology 56(1):141-8

143. Erwin Sigel, Michael E. Steinmann Structure, Function, and Modulation of GABAA Receptors. J Biological Chemistry 287, 40224-40231 (2012).

144. Sternbach LH. The benzodiazepine story. J. Med. Chem. 22(1):1-7 (1979).

145. Wick JY. The history of benzodiazepines. Consult Pharm. 28(9): 538-48 (2013).

146. Huang Q, Zhang W, Liu R, McKernan RM, and Cook JM. Benzo-fused benzodiazepines employed as topological probes for the study of benzodiazepine receptor subtypes. Medicinal Chem. Res. 6(3): 384–391 (1996).

147. Huang Q, He X, Ma C, Liu R, Yu S, Dayer CA, Wenger GR, McKernan R, Cook JM. Pharmacophore/receptor models for GABA(A)/BzR subtypes (alpha1beta3gamma2, alpha5beta3gamma2, and alpha6beta3gamma2) via a comprehensive ligand-mapping approach. J Med Chem. 43(1): 71-95. 2000.

148. S. Sengupta, S.D. Weeraratne, H. Sun, J. Phallen, S.K. Rallapalli, N. Teider, B. Kosaras, V. Amani, J. Pierre-Francois, Y. Tang, B. Nguyen, F. Yu, S. Schubert, B. Balansay, D. Mathios, M. Lechpammer, T.C. Archer, P. Tran, R.J. Reimer, J.M. Cook, M. Lim, F.E. Jensen, S.L. Pomeroy, Y.-J. Cho. α5-GABAA receptors negatively regulate MYC-amplified medulloblastoma growth. Acta Neuropathol. 127: 593-603 (2014).

149. Lambert, Hoffman, Pedersen. Acta Phys 194, 255-282 (2008).

150. Jonas O, Calligaris D, Methuku KR et al. First in vivo testing of compounds targeting Group 3 medulloblastoma using an implantable microdevice as a new paradigm for drug development. J. Biomedical Nanotechnology. 12(6): 1297-1302. (2016)

151. Bandopadhayay P1, Bergthold G, Nguyen B, Schubert S, Gholamin S, Tang Y, Bolin S, Schumacher SE, Zeid R, Masoud S, Yu F, Vue N, Gibson WJ, Paolella BR, Mitra SS, Cheshier SH, Qi J, Liu KW, Wechsler-Reya R, Weiss WA, Swartling FJ, Kieran MW, Bradner JE, Beroukhim R, Cho YJ. BET bromodomain inhibition of MYC-amplified medulloblastoma. Clin Cancer Res. 20(4):912-25. 2014.

152. Bai RY, Staedtke V, Rudin CM, Bunz F, Riggins GJ. Effective treatment of diverse medulloblastoma models with mebendazole and its impact on tumor angiogenesis. Neuro Oncol. 17(4):545-54. 2015.

153. Cook JM, Zhou H, Huang S, Sarma PVVS, Zhang C. Stereospecific Anxiolytic and Anticonvulsant Agents with Reduced Muscle-Relaxant, Sedative-Hypnotic and Ataxic Effects. 2006. Pub No. US2006/0003995A1.

154. Cook J, Huang S, Edwankar R, Namjoshi OA, Wang Z. Selective Agents for Pain Suppression. 2010. Pub. No. US2010/0317619A1.

155. P.F. Jacobsen, D.J. Jenkyn, J.M. Papadimitriou. Establishment of a human medulloblastoma cell line and its heterotransplantation into nude mice. J. Neuropathol. Exp. Neurol., 44 (1985), pp. 472-485

156. Triscott J1, Lee C, Foster C, Manoranjan B, Pambid MR, Berns R, Fotovati A, Venugopal C, O'Halloran K, Narendran A, Hawkins C, Ramaswamy V, Bouffet E, Taylor MD, Singhal A, Hukin J, Rassekh R, Yip S, Northcott P, Singh SK, Dunham C, Dunn SE. Personalizing the treatment of pediatric medulloblastoma: Polo-like kinase 1 as a molecular target in high-risk children. Cancer Res. 2013 Nov 15;73(22):6734-44.

157. H.S. Friedman, P.C. Burger, S.H. Bigner, J.Q. Trojanowski, C.J. Wikstrand, E.C. Halperin, D.D. Bigner. Establishment and characterization of the human medulloblastoma cell line and transplantable Xenograft D283 Med. J. Neuropathol. Exp. Neurol., 44 (1985), pp. 592-605,

158. S.H. Bigner, H.S. Friedman, B. Vogelstein, W.J. Oakes, D.D. Bigner. Amplification of the c-myc Gene in human medulloblastoma cell lines and xenografts. Cancer Res., 50 (1990), pp. 2347-2350

159. Weeraratne SD, Amani V, Teider N, Pierre-Francois J, Winter D, Kye MJ, Sengupta S, Archer T, Remke M, Bai AH, Warren P, Pfister SM, Steen JA, Pomeroy SL, Cho YJ.

Pleiotropic effects of miR-183~96~182 converge to regulate cell survival, proliferation, and migration in medulloblastoma. Acta Neuropathol. 2012 Apr;123(4):539-52.

160. Williams CA, Bell SV, Jenkins A. A residue in loop 9 of the beta2-subunit stabilizes the closed state of the GABAA receptor. J Biol Chem. 285(10): 7281-7287 (2010).

161. Clayton T, Chen JL, Ernst M, Richter L, Cromer BA, Morton CJ, Ng H, Kaczorowski CC, Helmstetter FJ, Furtmüller R, Ecker G, Parker MW, Sieghart W, Cook JM. An updated unified pharmacophore model of the benzodiazepine binding site on gamma-aminobutyric acid(a) receptors: correlation with comparative models. Curr Med Chem. 14(26): 2755-75 (2007)

162. Clayton T, Poe MM, Rallapalli S, Biawat P, Savić MM, Rowlett JK, Gallos G, Emala CW, Kaczorowski CC, Stafford DC, Arnold LA, Cook JM. A Review of the Updated Pharmacophore for the Alpha 5 GABA(A) Benzodiazepine Receptor Model. Int J Med Chem. 430248 (2015).

163. B Maro, M C Marty, and M Bornens. In vivo and in vitro effects of the mitochondrial uncoupler FCCP on microtubules. EMBO J. 1(11): 1347–1352 (1982).

164. Benz R, McLaughlin S. The molecular mechanism of action of the proton ionophore FCCP (carbonylcyanide p-trifluoromethoxyphenylhydrazone). Biophys J. 41(3):381-98 (1983).

165. Translocator protein as a promising target for novel anxiolytics. Costa B, Da Pozzo E, Martini C. Curr Top Med Chem. 12(4):270-85 (2012).

166. Li F, Liu J, Liu N, Kuhn LA, Garavito RM, Ferguson-Miller S. Translocator Protein 18 kDa (TSPO): An Old Protein with New Functions? Biochemistry. 55(20):2821-31 (2016).

167. Zhu F, Dollé ME, Berton TR, Kuiper RV, Capps C, Espejo A, McArthur MJ, Bedford MT, van Steeg H, de Vries A, Johnson DG. Mouse models for the p53 R72P polymorphism mimic human phenotypes. Cancer Res. 2010;70(14):5851

168. Domínguez ER, Orona J, Lin K, Pérez CJ, Benavides F, Kusewitt DF, Johnson DG. The p53 R72P polymorphism does not affect the physiological response to ionizing radiation in a mouse model. Cell Cycle. 2017;16(12):1153-1163.

169. Pei and Wechsler-Reya. An animal model of MYC-driven medulloblastoma. Cancer ell 2012.

170. Abraham AG, O'Neill E. PI3K/Akt-mediated regulation of p53 in cancer. Biochem Soc Trans. 2014; 42(4):798-803.

171. Freeman DJ, Li AG, Wei G, Li HH, Kertesz N, Lesche R, Whale AD, Martinez-Diaz H, Rozengurt N, Cardiff RD, Liu X, Wu H. PTEN tumor suppressor regulates p53 protein levels and activity through phosphatase-dependent and -independent mechanisms. Cancer Cell. 2003; 3(2):117-30.

172. Stambolic V, MacPherson D, Sas D, Lin Y, Snow B, Jang Y, Benchimol S, Mak TW. Regulation of PTEN transcription by p53. Mol Cell. 2001 Aug;8(2):317-25.

173. Jerry E. Chipuk and Douglas R. Green. How do BCL-2 proteins induce mitochondrial outer membrane permeabilization? Trends Cell Biol. 2008 Apr; 18(4): 157–164.

174. Peng Jiang, Wenjing Du, Klaus Heese, Mian Wu. The Bad Guy Cooperates with Good Cop p53: Bad Is Transcriptionally Up-Regulated by p53 and Forms a Bad/p53 Complex at the Mitochondria To Induce Apoptosis

175. Charlot JF1, Prétet JL, Haughey C, Mougin C. Mitochondrial translocation of p53 and mitochondrial membrane potential (Delta Psi m) dissipation are early events in

staurosporine-induced apoptosis of wild type and mutated p53 epithelial cells. Apoptosis. 2004 May;9(3):333-43.

176. Douglas J. Blackiston1,2, Kelly A. McLaughlin3, and Michael Levin. Bioelectric controls of cell proliferation: Ion channels, membrane voltage and the cell cycle. Cell Cycle. 2009 November 1; 8(21): 3519–3528.

177. Shan Ping Yu*, Lorella MT Canzoniero† and Dennis W Choi. Ion homeostasis and apoptosis. Current Opinion in Cell Biology 2001, 13:405–411.

178. Sakaguchi K. 1997. Phosphorylation of serine 392 stabilizes the tetramer formation of tumor suppressor protein p53. Biochemistry 36:10117–10124.

179. Expression of p53 protein phosphorylated at serine 20 and serine 392 in malignant and benign ovarian neoplasms: correlation with clinicopathological parameters of tumors. Bar JK, Słomska I, Rabczyński J, Noga L, Gryboś M. Int J Gynecol Cancer. 2009 Nov; 19(8):1322-8.

180. Matsumoto M, et al. Phosphorylation state of tumor-suppressor gene p53 product overexpressed in skin tumors. Oncol Rep. 2004;12:1039–1043.

181. Matsumoto M, et al. Prognostic significance of serine 392 phosphorylation in overexpressed p53 protein in human esophageal squamous cell carcinoma. Oncology. 2004;67:143–150.

182. Young SZ, Bordey A. GABA's control of stem and cancer cell proliferation in adult neural and peripheral niches. Physiology 24:171-185 (2009).

183. James OT, Livesey MR, Qiu J, Dando O, Bilican B, Haghi G, Rajan R, Burr K, Hardingham GE, Chandran S, Kind PC, Wyllie DJ. Ionotropic GABA and glycine receptor

subunit composition in human pluripotent stem cell-derived excitatory cortical neurones. J Physiol. 592(19):4353-63 (2014).

184. Neuroblastoma reference.

185. Smits A, Jin Z, Elsir T, Pedder H, Nistér M, Alafuzoff I, Dimberg A, Edqvist PH, Pontén F, Aronica E, Birnir B. GABA-A channel subunit expression in human glioma correlates with tumor histology and clinical outcome. PLoS One. 7(5):e37041 (2012).

186. Gumireddy K, Li A, Kossenkov AV, Sakurai M, Yan J, Li Y, Xu H, Wang J, Zhang PJ, Zhang L, Showe LC, Nishikura K, Huang Q. The mRNA-edited form of GABRA3 suppresses GABRA3-mediated Akt activation and breast cancer metastasis. Nat Commun. 7:10715 (2016).

187. Liu L, Yang C, Shen J, Huang L, Lin W, Tang H, Liang W, Shao W, Zhang H, He J. GABRA3 promotes lymphatic metastasis in lung adenocarcinoma by mediating upregulation of matrix metalloproteinases. Oncotarget. 7(22):32341-50 (2016).

188. Long M, Zhan M, Xu S, Yang R, Chen W, Zhang S, Shi Y, He Q, Mohan M, Liu Q, Wang J. miR-92b-3p acts as a tumor suppressor by targeting Gabra3 in pancreatic cancer. Mol Cancer. 16(1):167 (2017).

189. Vijay Pralhad Kale, Shantu G. Amin, Manoj K. Pandey. Targeting ion channels for cancer therapy by repurposing the approved drugs. Biochimica et Biophysica Acta 1848 (2015) 2747–2755.

190. Shonka, N., Venur, V. A. & Ahluwalia, M. S. Targeted treatment of brain metastases. *Curr. Neurol. Neurosci. Rep.* 17, 37 (2017).

191. Davies, H. et al. Mutations of the BRAF gene in human cancer. *Nature* 417, 949-954 (2002).

192. Hayward, N.K. et al. Whole-genome landscapes of major melanoma subtypes. *Nature* 545, 175-180 (2017).

193. Hodis, E., et al. A landscape of driver mutations in melanoma. *Cell* 150, 251-263 (2012).

194. McArthur, G. A. et al. Vemurafenib in metastatic melanoma patients with brain metastases: an open-label, single-arm, phase 2, multicentre study. *Ann. Oncol.* 28, 634-641 (2017).

195. Falchook, G. S. et al. Dabrafenib in patients with melanoma, untreated brain metastases, and other solid tumours: a phase 1 dose-escalation trial. *Lancet* 379, 1893-1901 (2012).

196. Long, G. V. et al. Dabrafenib in patients with Val600Glu or Val600Lys BRAF-mutant melanoma metastatic to the brain (BREAK-MB): a multicentre, open-label, phase 2 trial. *Lancet Oncol.* 13, 1087-1095 (2012).

197. Davies, M. A. et al. Dabrafenib plus trametinib in patients with BRAF(V600)-mutant melanoma brain metastases (COMBI-MB): a multicentre, multicohort, open-label, phase 2 trial. *Lancet Oncol.* 18, 863-873 (2017).

198. Hauschild, A. et al. Dabrafenib in BRAF-mutated metastatic melanoma: a multicentre, open-label, phase 3 randomised controlled trial. *Lancet* 380, 358-365 (2012).

199. Sosman, J. A. et al. Survival in BRAF V600-mutant advanced melanoma treated with vemurafenib. *N. Engl. J. Med.* 366, 707-714 (2012).

200. Turajlic, S. et al. Whole-genome sequencing reveals complex mechanisms of intrinsic resistance to BRAF inhibition. *Ann. Oncol.* 25, 959-967 (2014).

201. Long, G. V. et al. Overall survival and durable responses in patients with BRAF V600-mutant metastatic melanoma receiving Dabrafenib combined With Trametinib. *J. Clin. Oncol.* 34, 871-878 (2016).

202. Tirosh, I. et al. Dissecting the multicellular ecosystem of metastatic melanoma by single-cell RNA-seq. *Science* 352, 189-196 (2016).

203. Luke, J. J., Flaherty, K. T., Ribas, A. & Long, G. V. Targeted agents and immunotherapies: optimizing outcomes in melanoma. *Nat. Rev. Clin. Oncol.* 14, 463-482 (2017).

204. Tawbi, H. A. et al. New era in the management of melanoma brain metastases. *Am. Soc. Clin. Oncol. Educ. Book* 38, 741-750 (2018).

205. Tawbi, H. A. et al. Combined nivolumab and ipilimumab in melanoma metastatic to the brain. *N. Engl. J. Med.* 379, 722-730 (2018).

206. Postow, M. A., Sidlow, R. & Hellmann, M. D. Immune-related adverse events associated with immune checkpoint blockade. *N. Engl. J. Med.* 378, 158-168 (2018).

207. Wolchok, J. D. et al. Overall survival with combined nivolumab and ipilimumab in advanced melanoma. *N. Engl. J. Med.* 377, 1345-1356 (2017).

208. Larkin, J., Hodi, F. S. & Wolchok, J. D. Combined nivolumab and ipilimumab or monotherapy in untreated melanoma. *N. Engl. J. Med.* 373, 1270-1271 (2015).

209. Akbani, R. et al. Genomic classification of cutaneous melanoma. *Cell* 161, 1681-1696 (2015).

210. Sigel, E. & Steinmann, M.E. Structure, function, and modulation of GABAA receptors. *J. Biol. Chem.* 287, 40224–40231 (2012).

211. Sieghart, W. Allosteric modulation of GABAA receptors via multiple drug-binding sites. *Adv. Pharmacol.* 72, 53-96 (2015).

212. Clayton, T. et al. An updated unified pharmacophore model of the benzodiazepine binding site on gamma-aminobutyric acid(a) receptors: correlation with comparative models. *Curr. Med. Chem.* 14, 2755-2775 (2007). 22

213. Clayton, T. et al. A review of the updated pharmacophore for the alpha 5 gaba(a) benzodiazepine receptor model. *Int. J. Med. Chem.* 2015, 430248 (2015).

214. Huang, Q. et al. Predictive models for GABAA/benzodiazepine receptor subtypes: studies of quantitative structure – activity relationships for imidazobenzodiazepines at five recombinant GABAA/benzodiazepine receptor subtypes [αxβ3γ2 (x = 1–3, 5, and 6)] via comparative molecular field analysis. *J. Med. Chem.* 41, 4130–4142 (1998).

215. Huang, Q. et al. Pharmacophore/receptor models for GABA(A)/BzR subtypes (alpha1beta3gamma2, alpha5beta3gamma2, and alpha6beta3gamma2) via a comprehensive ligand-mapping approach. *J. Med. Chem.* 43, 71-95 (2000).

216. Cook, J. M. et al. Stereospecific anxiolytic and anticonvulsant agents with reduced muscle-relaxant, sedative-hypnotic and ataxic effects. US Patent 7119196 B2 (2006).

217. Sengupta, S. et al. alpha5-GABAA receptors negatively regulate MYC-amplified medulloblastoma growth. *Acta Neuropathol.* 127, 593-603 (2014).

218. Jonas, O. et al. First in vivo testing of compounds targeting Group 3 medulloblastoma using an implantable microdevice as a new paradigm for drug development. *J. Biomed. Nanotechnol.* 12, 1297-1302 (2016).

219. Kallay, L. et al. Modulating native GABAA receptors in medulloblastoma with positive allosteric benzodiazepine-derivatives induces cell death. *J. Neurooncol.* 142, 411-422 (2019).

220. Platt, D.M. et al. Contribution of alpha 1GABAA and alpha 5GABAA receptor subtypes to the discriminative stimulus effects of ethanol in squirrel monkeys. *J. Pharmacol. Exp. Ther.* 313, 658-667 (2005).

221. Matin, R. N. et al. p63 is an alternative p53 repressor in melanoma that confers chemoresistance and a poor prognosis. *J. Exp. Med.* 210, 581-603 (2013).

222. Wang, C., Youle, R.J. The role of mitochondria in apoptosis. *Annu. Rev. Genet.* 43, 95-118 (2009).

223. Mehta, S.Y. Regulation of the interferon-gamma (IFN-γ) pathway by p63 and Δ133p53 isoform in different breast cancer subtypes. *Oncotarget* 9, 29146-29161 (2018).

224. Su et al. TAp63 suppresses metastasis through coordinate regulation of Dicer and miRNAs. *Nature* 467, 986-990 (2010).

225. Ratovitski, E.A. Tumor protein p63/microRNA network in epithelial cancer cells. *Current Genomics* 14, 441-452 (2013).

226. Mendu, S.K. et al. Different subtypes of GABA-A receptors are expressed in human, mouse and rat T lymphocytes. *PLoS One* 7, e42959 (2012).

227. Kim, J.K. et al. GABAergic signaling linked to autophagy enhances host protection against intracellular bacterial infections. *Nat. Commun.* 9, 4184 (2018).

228. Jin, Z., Mendu, S. K. & Birnir, B. GABA is an effective immunomodulatory molecule. *Amino Acids* 45, 87-94 (2013).

229. Khan, M.K. et al. Repurposing drugs for cancer radiotherapy: early successes and emerging opportunities. *Cancer J.* 25, 106-115 (2019).

230. Friedman, H. et al. Pharmacokinetics and pharmacodynamics of oral diazepam: effect of dose, plasma concentration, and time. *Clin. Pharmacol. Ther.* 52, 139-150 (1992).

231. Berro, L.F. et al. GABAa receptor subtypes and the abuse-related effects of ethanol in rhesus monkeys: experiments with selective positive allosteric modulators. *Alcohol Clin. Exp. Res.* 43, 791-802 (2019).

232. Williams, C.A., Bell, S.V. & Jenkins, A. A residue in loop 9 of the beta2-subunit stabilizes the closed state of the GABAA receptor. *J. Biol. Chem.* 285, 7281-7287 (2010).

233. Dobin, A., Davis, C.A., Schlesinger, F., Drenkow, J., Zaleski, C. & Jha, S. STAR: ultrafast universal RNA-seq aligner. *Bioinformatics* 29, 15-21 (2013).

234. Liao, Y., Smyth, G.K. & Shi, W. FeatureCounts: an efficient general purpose program for assigning sequence reads to genomic features. *Bioinformatics* 30, 923-930 (2013).

235. Anders, S., McCarthy, D.J., Chen, Y., Okoniewski, M., Smyth, G.K., Huber, W. & Robinson, M.D. Count-based differential expression analysis of RNA sequencing data using R and Bioconductor. *Nat. Protocols* 8, 1765-1786 (2013). 23

236. Benjamini, Y. & Hochberg, Y. Controlling the false discovery rate: a practical and powerful approach to multiple testing. *J. Royal Stat. Soc. B* 57, 289-300 (1995).

237. Kanehisa, M., Furumichi, M., Tanabe, M., Sato, Y. & Morishima, K. KEGG: new perspectives on genomes, pathways, diseases and drugs. *Nucleic Acids Res.* 45, D353-D361 (2017).

238. Garcia-Alonso, L., Holland, C. H., Ibrahim, M. M., Turei, D. & Saez-Rodriguez, J. Benchmark and integration of resources for the estimation of human transcription factor activities. *Genome Res.* 29, 1363-1375 (2019).

239. Godec, J., Tan, Y., Liberzon, A., Tamayo, P., Bhattacharya. S., Butte, A.T., Mesirov, J.P., Haining, W.N. Compendium of immune signatures identifies conserved and species-specific biology in response to inflammation. *Immunity* 44, 194-206 (2016).

240. Subramanian, A. et al. Gene set enrichment analysis: a knowledge-based approach for interpreting genome-wide expression profiles. *Proc. Natl. Acad. Sci. U.S.A.* 102, 15545-15550 (2005).

241. Korotkevich, G., Sukhov, V. & Sergushichev, A. Fast gene set enrichment analysis. *bioRxiv*, 060012 (2019).

242. Gu, Z., Eils, R. & Schlesner, M. Complex heatmaps reveal patterns and correlations in multidimensional genomic data. *Bioinformatics* 32, 2847-2849 (2016).

243. Kanehisa, M., Furumichi, M., Tanabe, M., Sato, Y. & Morishima, K. KEGG: new perspectives on genomes, pathways, diseases and drugs. *Nucleic Acids Res.* 45, D353-D361 (2017).

244. Su, A.I., Wiltshire, T., Batalov, S., Lapp, H., Ching, K.A., Block, D., Zhang, J., Soden, R., Hayakawa, M., Kreiman, G., Cooke, M.P., Walker, J.R. & Hogenesch, J.B. A gene atlas of the mouse and human protein-encoding transcriptomes. *Proc. Natl. Acad. Sci. U.S.A.* 101, 6062-6067 (2004).

245. Robinson, M.D., McCarthy, D.J. & Smyth, G.K. edgeR: a Bioconductor package for differential expression analysis of digital gene expression data. *Bioinformatics* 26, 139-140 (2010).

# Chapter 5 Appendix

## 5. 1 Appendix I

### 5. 1. 1 Testing New Compounds from Dr Cook's Lab

# Testing New Compounds from Dr Cook's Lab

(Donatien Kamdem Toukam, Roman Caceres and Laura Kallay)

| Compound | Cell line tested** | ≈ $IC_{50}$* |
|---|---|---|
| QH-II-066 | LN18 | 2.8 µM |
| | H1792 | 4.5 µM |
| | B16F10 | 10.7 µM |
| NOR-QH-II-066 | LN18 | 0.69 µM |
| MYM-III-85 | LN18 | 2.2 µM |
| | H1792 | 3.3 µM |
| | U-87 MG-Luc2 | 4 µM |
| | MB002 | 2.2 µM |
| | B16F10 | 12.4 µM |
| MYM-V-17 | LN18 | 5.17 µM |
| MYM-I-43 | LN18 | ∞ |
| MYM-I-59 | LN18 | ∞ |
| MYM-IV-95 | LN18 | ∞ |

*$IC_{50}$ was determined using *CellTiter96R Aqueous One Solution Cell Proliferation Assay* kit (#G3581) from Promega.

** - **LN18**: Human Glioma cell line from ATCC# CRL-2610 (https://www.biocompare.com/20260-Miscellaneous-Human-Cell-Lines/893528-LN18/).

- **U-87 MG-Luc2**: Human Glioma cell line, from ATCC? #HTB-14-LUC2 (https://www.atcc.org/products/htb-14-luc2).

- **MB002**: Human Medulloblastoma cell line, from Expasy, Accession# CVCL_VU79, (https://web.expasy.org/cellosaurus/CVCL_VU79).

- **H1792**: Human Lung Adenocacinoma cell line from ATCC #CRL-5895 (https://www.atcc.org/search#q=h1792&sort=relevancy&numberOfResults=24).

- **B16F10**: Mouse melanoma cell line from ATCC # CRL-6475 (https://www.atcc.org/products/crl-6475).

### 5. 1. 2 Testing TA II 73

# Testing TA II 73

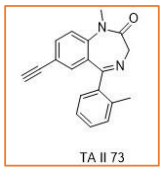


| Summary TA II 73 | |
|---|---|
| **Cell lines** | **TA II 73** |
| **A375** | 2.05 µM |
| **LN18** | 0.92 µM |
| **H1792** | 2.1 µM |

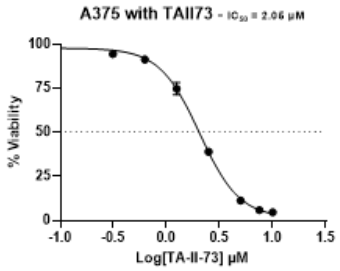


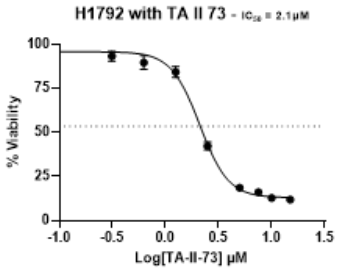


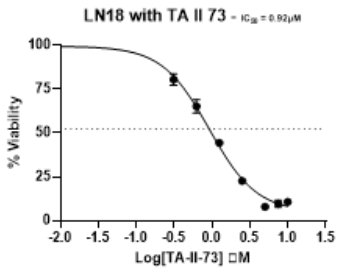


**TA II 73 on** LN18

| | | | | | | | | | | | |
|---|---|---|---|---|---|---|---|---|---|---|---|
| **DMSO** | 0.79738 | 0.71308 | 0.71678 | 0.76128 | 0.77088 | 0.08788 | 0.08188 | 0.06958 | 0.04798 | 0.07698 | **7.5** |
| **0.3125** | 0.43788 | 0.56838 | 0.59078 | 0.63608 | 0.58798 | 0.08338 | 0.07178 | 0.08438 | 0.09148 | 0.07468 | **10** |
| **0.625** | 0.42728 | 0.45918 | 0.43968 | 0.49238 | 0.54278 | 0.08268 | 0.10608 | 0.09398 | 0.11098 | 0.08668 | **15** |
| **1.25** | 0.21338 | 0.31858 | 0.31448 | 0.34768 | 0.33348 | 0.11718 | 0.10668 | 0.10358 | 0.14068 | 0.11228 | **20** |
| **2.5** | 0.11648 | 0.15718 | 0.15728 | 0.18288 | 0.23838 | 0.14598 | 0.11648 | 0.15788 | 0.07518 | 0.12578 | **25** |
| **5** | 0.04388 | 0.05778 | 0.06138 | 0.05568 | 0.08528 | 0.13098 | 0.12248 | 0.14708 | 0.10368 | 0.09418 | **30** |

**TA II 73 on H1792**

| | | | | | | | | | | | |
|---|---|---|---|---|---|---|---|---|---|---|---|
| **DMSO** | 1.58404 | 1.65584 | 1.71794 | 1.72644 | 1.77764 | 0.28504 | 0.29484 | 0.26484 | 0.25964 | 0.25844 | **7.5** |
| **0.3125** | 1.54154 | 1.52874 | 1.50564 | 1.59624 | 1.61804 | 0.21664 | 0.21494 | 0.19754 | 0.20434 | 0.24524 | **10** |
| **0.625** | 1.54914 | 1.55654 | 1.50524 | 1.57904 | 1.51644 | 0.18434 | 0.19124 | 0.21484 | 0.21114 | 0.20084 | **15** |
| **1.25** | 1.29904 | 1.43074 | 1.47874 | 1.50414 | 1.42144 | 0.20064 | 0.23784 | 0.25524 | 0.23584 | 0.20244 | **20** |
| **2.5** | 0.69724 | 0.75054 | 0.69564 | 0.70614 | 0.72114 | 0.22834 | 0.22464 | 0.22004 | 0.20404 | 0.17034 | **25** |
| **5** | 0.24154 | 0.30614 | 0.29524 | 0.31604 | 0.36194 | 0.26834 | 0.23474 | 0.25354 | 0.20394 | 0.25714 | **30** |

**TA II 73 on A375**

| | | | | | | | | | | | |
|---|---|---|---|---|---|---|---|---|---|---|---|
| **DMSO** | 1.19146 | 1.21346 | 1.18086 | 1.19776 | 1.18076 | 0.05826 | 0.07006 | 0.09006 | 0.05506 | 0.08366 | **7.5** |
| **0.3125** | 1.13266 | 1.10766 | 1.11936 | 1.14546 | 1.12706 | 0.05016 | 0.05306 | 0.07306 | 0.05046 | 0.09976 | **10** |
| **0.625** | 1.11026 | 1.08856 | 1.09196 | 1.08156 | 1.20366 | 0.08146 | 0.08386 | 0.08446 | 0.08536 | 0.10306 | **15** |
| **1.25** | 0.86086 | 0.87436 | 0.85906 | 0.95756 | 0.91066 | 0.10966 | 0.13626 | 0.12866 | 0.10386 | 0.10416 | **20** |
| **2.5** | 0.46826 | 0.46726 | 0.45916 | 0.47156 | 0.46426 | 0.13136 | 0.12406 | 0.13466 | 0.11146 | 0.11436 | **25** |
| **5** | 0.13236 | 0.13706 | 0.13556 | 0.13906 | 0.13396 | 0.13086 | 0.13496 | 0.11316 | 0.11566 | 0.14136 | **30** |

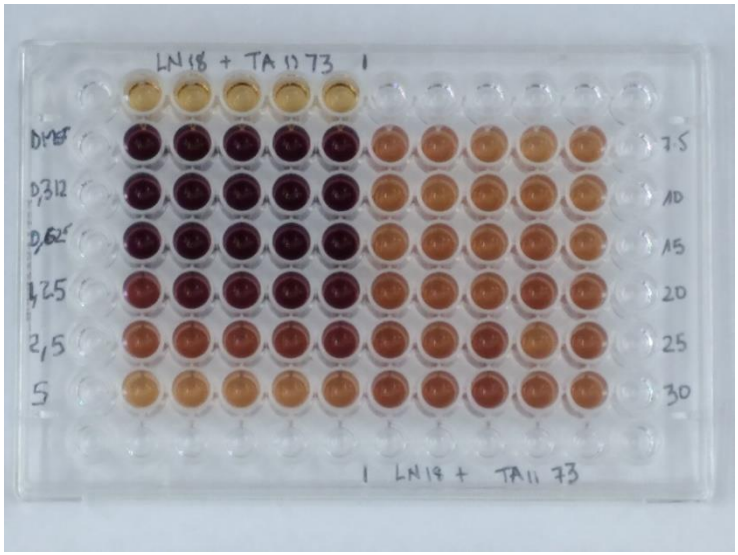


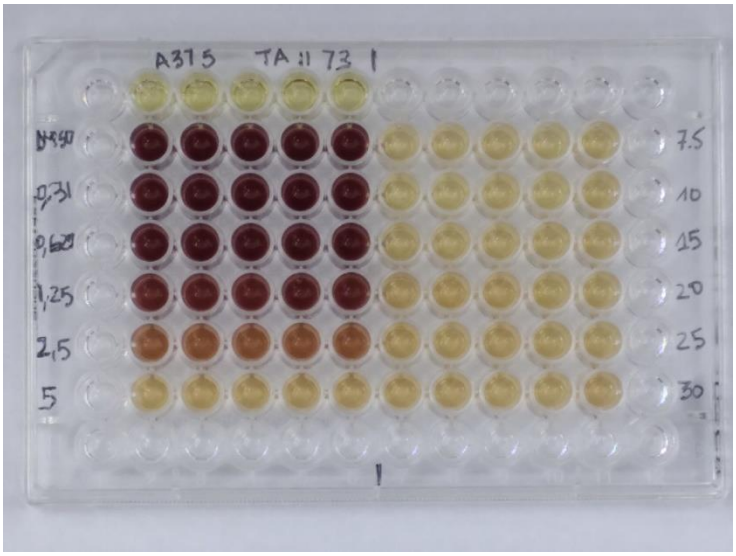

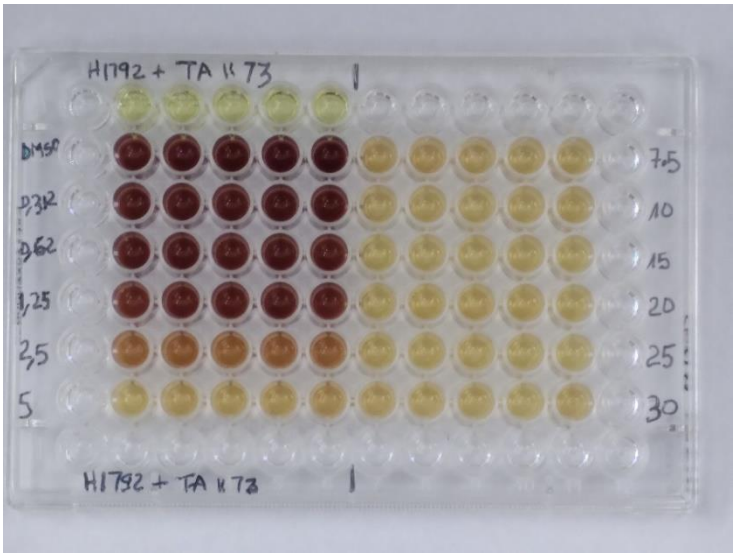
H1792 + TA II 73
DMSO
7,5
10
15
20
25
30
5
H1792 + TA II 73

## 5. 1. 3 Testing deuterated analogues of Diazepam, QH II 66 and KRM II 08

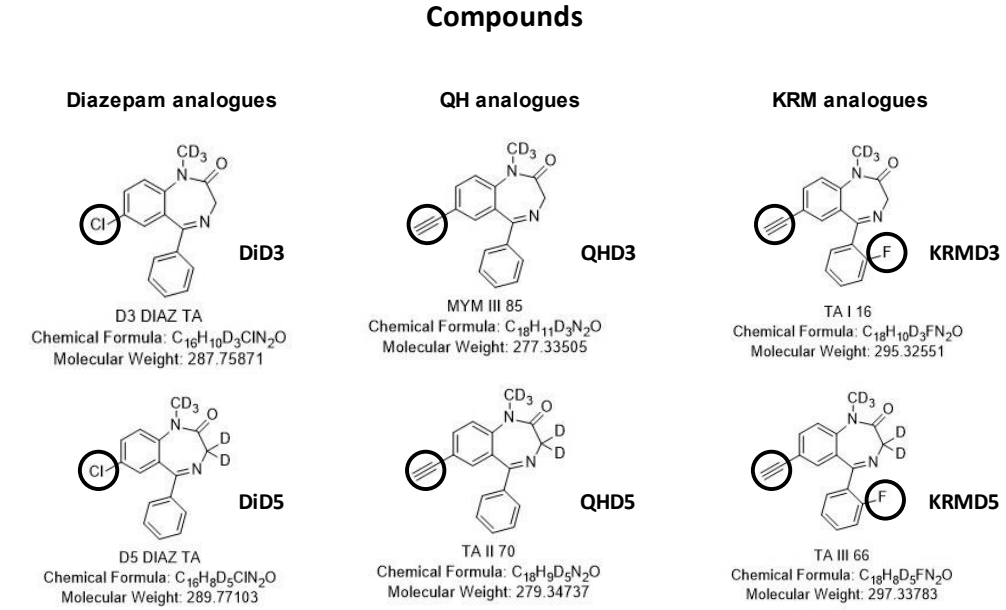


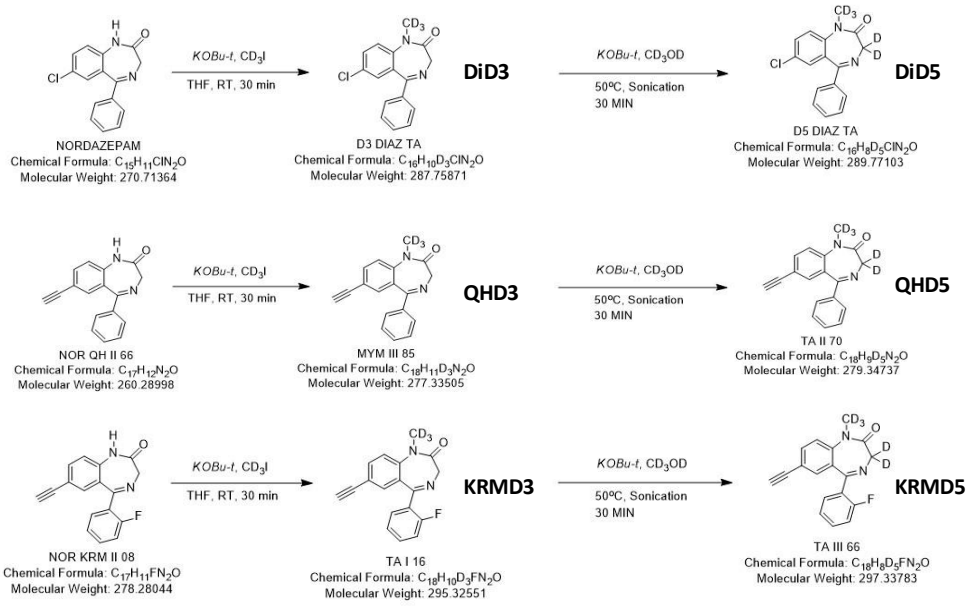

## DiD3/D5 cytotoxicity

| Cell lines | DiD3 (μM) | DiD5 (μM) |
|---|---|---|
| A375 | N/A | N/A |
| LN18 | N/A | N/A |
| H1792 | N/A | N/A |

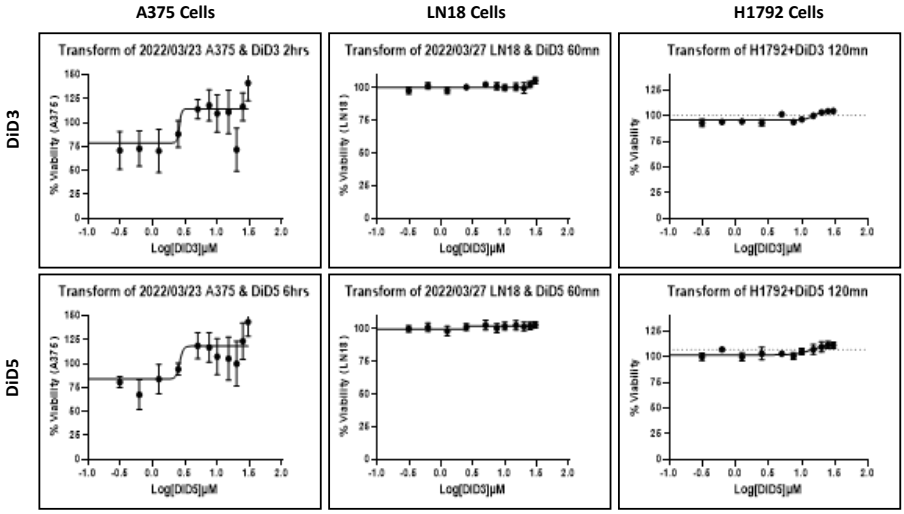


## QHD3/D5 cytotoxicity

| Cell line | QHD3 (μM) | QHD5 (μM) |
|---|---|---|
| A375 | 0.31 | 0.46 |
| LN18 | 1.81 | 2.51 |
| H1792 | 1.75 | 1.98 |

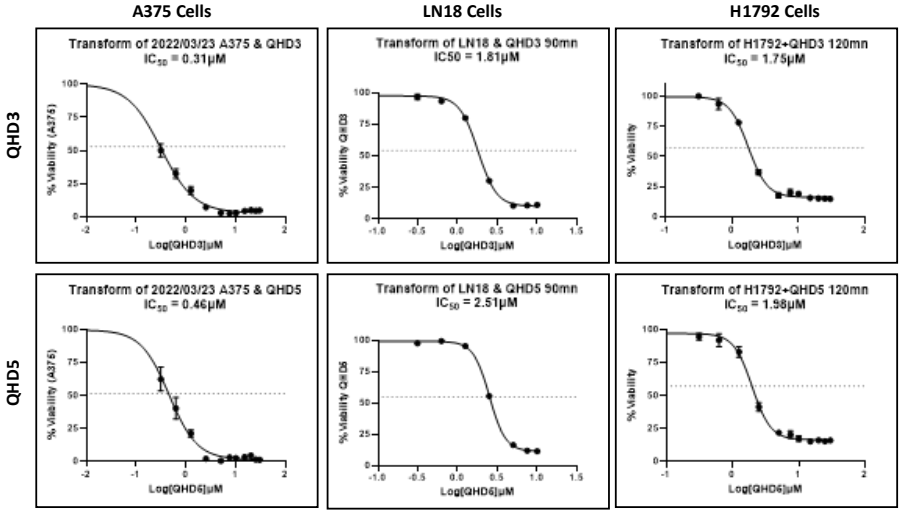

## KRMD3/D5 cytotoxicity

| Cell line | KRMD3 (μM) | KRMD5 (μM) |
|---|---|---|
| A375 | 0.35 | 0.63 |
| LN18 | 2.43 | 2.67 |
| H1792 | 2.13 | 2.52 |

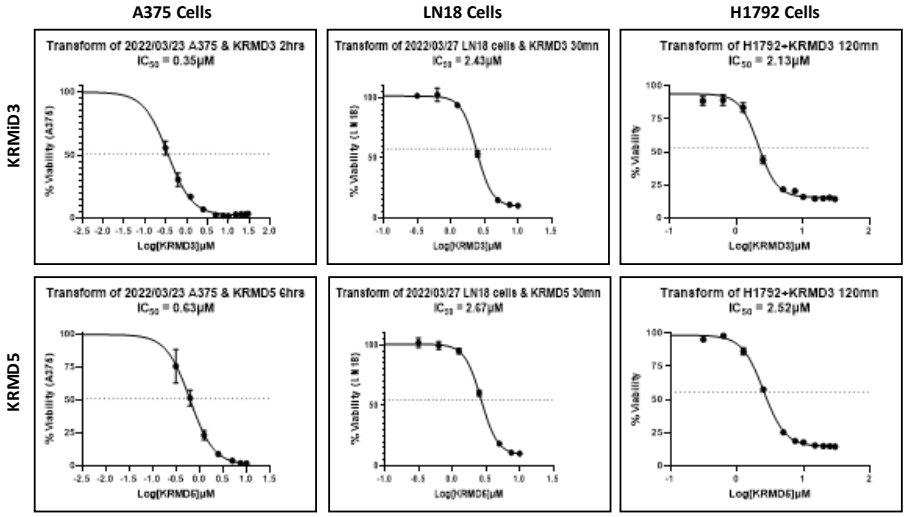


**LN18 human glioma cell line**

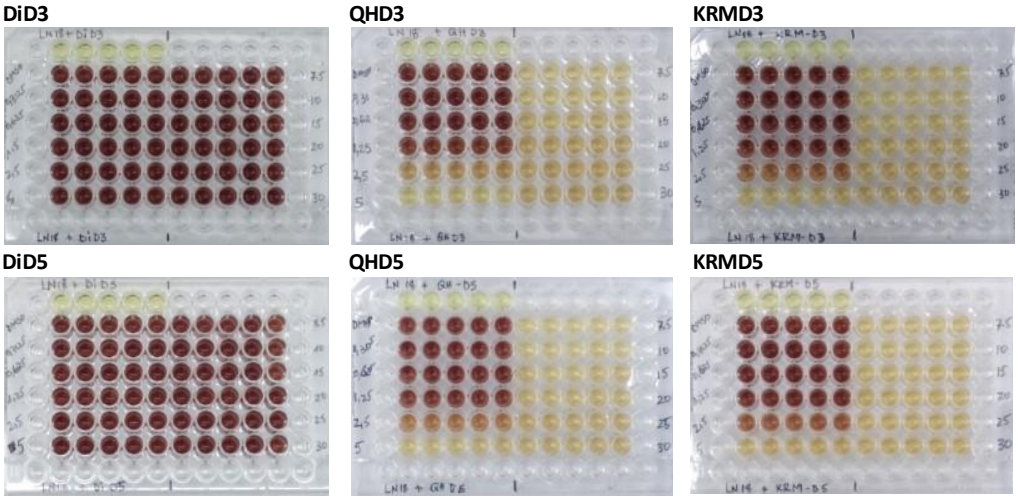

**A375 human melanoma cell line**

**DiD3**

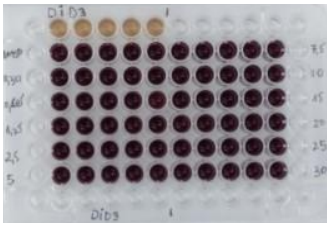

**QHD3**

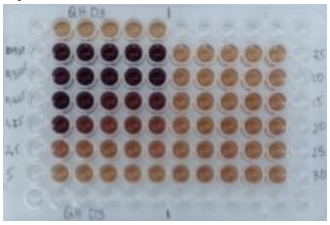

**KRMD3**

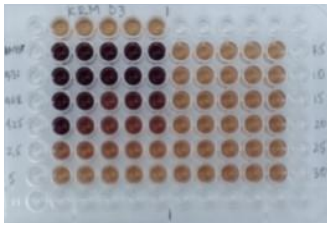

**DiD5**

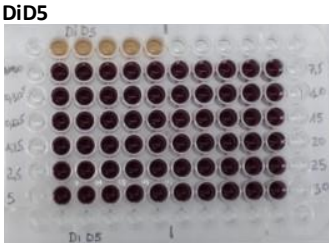

**QHD5**

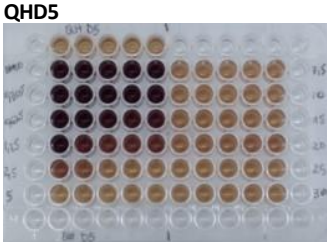

**KRMD5**

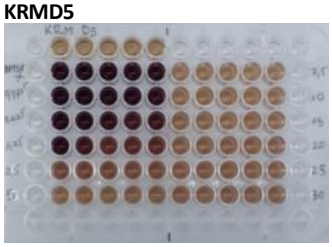

**H1792 human non -small cell lung cancer line**

**DiD3**

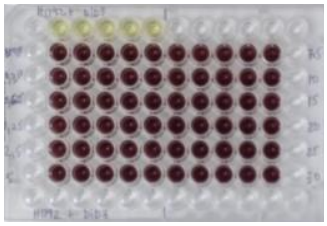

**QHD3**

**KRMD3**

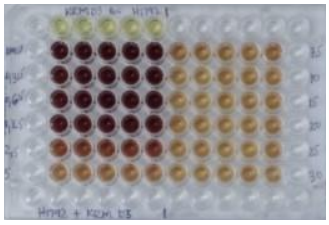

**DiD5**

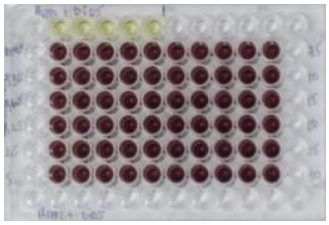

**QHD5**

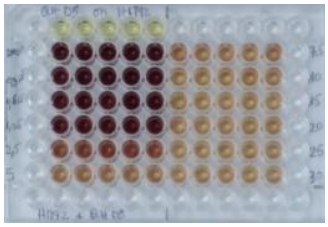

**KRMD5**

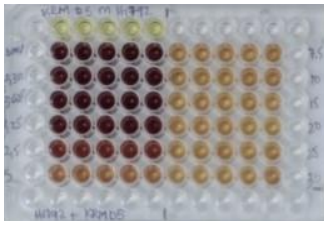

### 5. 1. 4 Cytotoxicity Methods

**1- Drug Preparation:**

Each compound powder was weighed and dissolved in DMSO to a concentration of 40mM. Dissolved compounds were stored at 4°C.

**2- Drug dilutions:**

Eleven dilutions were used with preparation protocol was as follow:

| Drug Concentration (µM) | Volume of medium | Volume of 40 mM stock | Volume of prediluted drug |
|---|---|---|---|
| 30 | 2 mL | 1.5 µL | / |
| 25 | 2 mL | 1.25 µL | / |
| 20 | 2 mL | 1.0 µL | / |
| 15 | 1 mL | / | 1mL of 30 µM |
| 10 | 1 mL | / | 1 mL of 20 µM |
| 7.5 | 1 mL | / | 1mL of 15 µM |
| 5 | 1 mL | / | 1 mL of 10 µM |
| 2.5 | 1 mL | / | 1 mL of 5 µM |
| 1.25 | 1 mL | / | 1 mL of 2.5 µM |
| 0.625 | 1 mL | / | 1 mL of 1.25 µM |
| 0.3125 | 1 mL | / | 1 mL of 0.625 µM |
| DMSO | 2 mL | / | **1.5 µL of DMSO** |
| | | | |

**3- Cell culture process:**

Prior to cell proliferation assay, optimum cell number for each cell line was determined and the cell number giving about 1.0 OD value after one hour of incubation with the CellTiter 96® AQueous One Solution Cell Proliferation Assay reagent (Promega) was choose for cell proliferation experiments.

**Day1:** Cells were trypsinized, count and diluted to:

- A375 Human melanoma cells: 30000 cells/mL (3000 cells/100 µL or 3000 cells/well)
- LN18 Human Glioma cells: 50000 cells/mL (5000 cells/100 µL or 5000 cells/well)
- H1792 Human NSCLC cells: 12000 cells/mL (1200 cells/100 µL or 1200 cells/well)

100 µL of cell suspension was added to 96 well plate: Rows B to G and columns 2 to 11 were seeded with cells, outer wells around the plate were filled with 100 µL PBS except wells A2 to A6 filled with medium without cells. Cells were then incubated 24 hours and allowed to attach.

**Day2:** Addition of drug and controls to plated cells:

- Background control: Medium in wells A2 to A6 was aspirated and replaced with 100 µL fresh medium
- Control DMSO and each drug dilution was added to 5 consecutive wells in the same raw. Medium was carefully sucked out and 100 µL of control or diluted drug added.
- After drug addition, plates were returned into incubator for 48 to 72 hours.

**Day 5 or 6:** 20 µL of CellTiter 96® AQueous One Solution Cell Proliferation Assay reagent (Promega) was added to each control or test well, incubated 1 to 2 hours, then OD was acquired at 490 nm.

**4- Data analysis:**

- The average OD from the five wells containing medium and no cells (A2 to A6) was calculated and the value subtracted from each individual OD reading.
- The OD readings for each drug dilution was normalized to DMSO control, set as 100 % cell viability / proliferation.
- Log drug concentration versus percentage viability is then plotted using GraphPad Prism.

**Summary:**

Cells were counted and dispensed in 96 well plates. Plates were incubated 24 hours for cells to attach. Drugs and DMSO were diluted to desired concentrations in phenol free medium. Medium on cells was aspirated and replaced with 100 µL of fresh phenol free medium containing drug, and the plate returned to incubator for 48 to 72 hours. The CellTiter 96® AQueous One Solution Cell Proliferation Assay (Promega) reagent was reconstituted following manufacturer's instructions. Aliquots were stored at -20° C. Reconstituted reagent was thawed, vortexed and 20 µL dispensed to each well, then the plate incubated at 37°C for 1 to 2 hours. OD at 490 nm was acquired and the readings from test wells were corrected by subtracting the average OD obtained of wells containing medium only. OD readings were then normalized to DMSO and the Log concentration versus percentage cell viability plotted using GraphPad Prism software.

## 5. 1. 5 Cytotoxicity raw data for deuterium analogues of Diazepam, QH II 66 and KRM II 08.

MTS cell proliferation Experiments in 96 wells plate format
Raw OD values at 490 nm

**LN18 Human Glioma**

LN18 Glioma cells treated with KRMD3

| | 1 | 2 | 3 | 4 | 5 | 6 | | | 7 | 8 | 9 | 10 | 11 | 12 |
|---|---|---|---|---|---|---|---|---|---|---|---|---|---|---|
| **Drug[µM]** | | | | | | | | **Drug[µM]** | | | | | | |
| **Background** | | 0.0602 | 0.0583 | 0.0598 | 0.0581 | 0.0582 | | | | | | | | |
| **DMSO** | | 0.8064 | 0.8457 | 0.8732 | 0.8449 | 0.8272 | | **7.5** | 0.1426 | 0.1488 | 0.1557 | 0.1482 | 0.139 | |
| **0.3125** | | 0.8165 | 0.8588 | 0.8966 | 0.8497 | 0.8422 | | **10** | 0.1356 | 0.1332 | 0.1351 | 0.1552 | 0.1444 | |
| **0.625** | | 0.8625 | 0.8169 | 0.8568 | 0.8661 | 0.8943 | | **15** | 0.1527 | 0.1728 | 0.1536 | 0.1811 | 0.1612 | |
| **1.25** | | 0.7507 | 0.7928 | 0.8061 | 0.8144 | 0.7953 | | **20** | 0.1702 | 0.1896 | 0.1854 | 0.1884 | 0.1792 | |
| **2.5** | | 0.4608 | 0.4578 | 0.4771 | 0.4795 | 0.501 | | **25** | 0.1959 | 0.2148 | 0.1936 | 0.1909 | 0.193 | |
| **5** | | 0.1682 | 0.172 | 0.1725 | 0.1797 | 0.1895 | | **30** | 0.1997 | 0.1925 | 0.2083 | 0.192 | 0.2046 | |
| | | | | | | | | | | | | | | |

LN18 Glioma cells treated with KRMD5

| **Drug[µM]** | 1 | 2 | 3 | 4 | 5 | 6 | | **Drug[µM]** | 7 | 8 | 9 | 10 | 11 | 12 |
|---|---|---|---|---|---|---|---|---|---|---|---|---|---|---|
| **Background** | | 0.0636 | 0.0625 | 0.0629 | 0.0609 | 0.0615 | | | | | | | | |
| **DMSO** | | 0.9827 | 1.008 | 0.987 | 0.9806 | 0.9506 | | **7.5** | 0.1636 | 0.1658 | 0.1645 | 0.1604 | 0.1659 | |
| **0.3125** | | 1.033 | 0.9972 | 1.0384 | 0.9675 | 0.8674 | | **10** | 0.1531 | 0.1444 | 0.1559 | 0.1549 | 0.1797 | |
| **0.625** | | 0.9766 | 0.9914 | 0.9992 | 0.9396 | 0.9899 | | **15** | 0.1607 | 0.1747 | 0.1718 | 0.1809 | 0.1875 | |
| **1.25** | | 0.9239 | 0.9036 | 0.9362 | 0.9258 | 0.939 | | **20** | 0.2042 | 0.1965 | 0.1906 | 0.2015 | 0.1831 | |
| **2.5** | | 0.6108 | 0.6117 | 0.5996 | 0.6281 | 0.6285 | | **25** | 0.201 | 0.198 | 0.2013 | 0.2089 | 0.2142 | |
| **5** | | 0.2096 | 0.2422 | 0.2316 | 0.2411 | 0.2372 | | **30** | 0.2053 | 0.2228 | 0.2203 | 0.2165 | 0.2085 | |
| | | | | | | | | | | | | | | |

LN18 Glioma cells treated with QHD3

| **Drug[µM]** | 1 | 2 | 3 | 4 | 5 | 6 | | **Drug[µM]** | 7 | 8 | 9 | 10 | 11 | 12 |
|---|---|---|---|---|---|---|---|---|---|---|---|---|---|---|
| **Background** | | 0.0709 | 0.0846 | 0.0707 | 0.0706 | 0.0707 | | | | | | | | |
| **DMSO** | | 1.6082 | 1.6618 | 1.6368 | 1.6542 | 1.6327 | | **7.5** | 0.2424 | 0.2274 | 0.2557 | 0.2396 | 0.2581 | |
| **0.3125** | | 1.6075 | 1.5913 | 1.5981 | 1.5591 | 1.5704 | | **10** | 0.2507 | 0.2283 | 0.2557 | 0.2504 | 0.2726 | |
| **0.625** | | 1.5703 | 1.5949 | 1.527 | 1.5249 | 1.5248 | | **15** | 0.3167 | 0.3017 | 0.3237 | 0.3283 | 0.3234 | |
| **1.25** | | 1.3003 | 1.3536 | 1.3512 | 1.3088 | 1.3208 | | **20** | 0.3775 | 0.4053 | 0.4001 | 0.4041 | 0.3953 | |
| **2.5** | | 0.5377 | 0.5457 | 0.575 | 0.5296 | 0.5568 | | **25** | 0.3771 | 0.4375 | 0.4219 | 0.4111 | 0.4094 | |
| **5** | | 0.2194 | 0.2382 | 0.2702 | 0.2421 | 0.2314 | | **30** | 0.3965 | 0.4076 | 0.4364 | 0.4041 | 0.4506 | |
| | | | | | | | | | | | | | | |

LN18 Glioma cells treated with QHD5

| **Drug[µM** | 1 | 2 | 3 | 4 | 5 | 6 | | **Drug[µM** | 7 | 8 | 9 | 10 | 11 | 12 |
|---|---|---|---|---|---|---|---|---|---|---|---|---|---|---|
| **Background** | | 0.0765 | 0.0759 | 0.074 | 0.0751 | 0.074 | | | | | | | | |
| **DMSO** | | 1.5831 | 1.5774 | 1.6277 | 1.5822 | 1.6015 | | **7.5** | 0.2358 | 0.2663 | 0.2487 | 0.2681 | 0.265 | |
| **0.3125** | | 1.5535 | 1.5763 | 1.5911 | 1.5631 | 1.5213 | | **10** | 0.2439 | 0.2492 | 0.2335 | 0.2769 | 0.2507 | |
| **0.625** | | 1.5212 | 1.5742 | 1.6468 | 1.5542 | 1.5933 | | **15** | 0.3234 | 0.2873 | 0.3119 | 0.3409 | 0.3399 | |
| **1.25** | | 1.4829 | 1.532 | 1.5499 | 1.5436 | 1.5297 | | **20** | 0.3427 | 0.3179 | 0.3323 | 0.3721 | 0.3488 | |
| **2.5** | | 0.9102 | 0.938 | 0.9306 | 0.9136 | 0.9087 | | **25** | 0.4506 | 0.4466 | 0.4126 | 0.4022 | 0.4184 | |
| **5** | | 0.3271 | 0.3194 | 0.3109 | 0.3474 | 0.3799 | | **30** | 0.3733 | 0.3958 | 0.3865 | 0.4182 | 0.4251 | |
| | | | | | | | | | | | | | | |

LN18 Glioma cells treated with DiD3

| Drug[µM | 1 | 2 | 3 | 4 | 5 | 6 | | Drug[µM | 7 | 8 | 9 | 10 | 11 | 12 |
|---|---|---|---|---|---|---|---|---|---|---|---|---|---|---|
| Background | | 0.0784 | 0.0714 | 0.0697 | 0.0717 | 0.0716 | | | | | | | | |
| DMSO | | 1.6341 | 1.6248 | 1.6534 | 1.6235 | 1.6005 | | 7.5 | 1.6419 | 1.6277 | 1.6154 | 1.6817 | 1.6693 | |
| 0.3125 | | 1.6688 | 1.5675 | 1.6119 | 1.6043 | 1.5316 | | 10 | 1.6072 | 1.6249 | 1.6168 | 1.6682 | 1.6326 | |
| 0.625 | | 1.7155 | 1.6573 | 1.6627 | 1.6383 | 1.5854 | | 15 | 1.6107 | 1.6125 | 1.635 | 1.702 | 1.6386 | |
| 1.25 | | 1.6508 | 1.6205 | 1.5942 | 1.5668 | 1.5372 | | 20 | 1.5938 | 1.5893 | 1.5814 | 1.685 | 1.6718 | |
| 2.5 | | 1.6645 | 1.6314 | 1.6569 | 1.5951 | 1.6373 | | 25 | 1.6523 | 1.6527 | 1.6528 | 1.7125 | 1.6664 | |
| 5 | | 1.6953 | 1.6614 | 1.6595 | 1.674 | 1.6572 | | 30 | 1.7017 | 1.7049 | 1.6967 | 1.7309 | 1.7416 | |
| | | | | | | | | | | | | | | |

LN18 Glioma cells treated with DiD5

| Drug[µM] | 1 | 2 | 3 | 4 | 5 | 6 | | Drug[µM] | 7 | 8 | 9 | 10 | 11 | 12 |
|---|---|---|---|---|---|---|---|---|---|---|---|---|---|---|
| Background | | 0.0741 | 0.0781 | 0.0733 | 0.0721 | 0.0764 | | | | | | | | |
| DMSO | | 1.732 | 1.7125 | 1.6139 | 1.6774 | 1.632 | | 7.5 | 1.6892 | 1.6531 | 1.6705 | 1.7373 | 1.6578 | |
| 0.3125 | | 1.7417 | 1.6445 | 1.641 | 1.6795 | 1.6614 | | 10 | 1.7341 | 1.6853 | 1.7052 | 1.7468 | 1.6558 | |
| 0.625 | | 1.6994 | 1.6902 | 1.7088 | 1.6894 | 1.6737 | | 15 | 1.7134 | 1.7117 | 1.7319 | 1.7611 | 1.6703 | |
| 1.25 | | 1.6351 | 1.6377 | 1.6673 | 1.6451 | 1.6381 | | 20 | 1.7063 | 1.6852 | 1.6635 | 1.7167 | 1.73 | |
| 2.5 | | 1.7328 | 1.6837 | 1.6935 | 1.7019 | 1.6577 | | 25 | 1.7084 | 1.7315 | 1.6695 | 1.7149 | 1.7271 | |
| 5 | | 1.7427 | 1.7427 | 1.752 | 1.6699 | 1.6871 | | 30 | 1.7338 | 1.7422 | 1.7119 | 1.7342 | 1.6908 | |
| | | | | | | | | | | | | | | |

## A375 melanoma

A375 melanoma cells treated with KRMD3

| Drug[µM] | 1 | 2 | 3 | 4 | 5 | 6 | | Drug[µM] | 7 | 8 | 9 | 10 | 11 | 12 |
|---|---|---|---|---|---|---|---|---|---|---|---|---|---|---|
| Background | | 0.1603 | 0.16 | 0.1636 | 0.1612 | 0.1651 | | | | | | | | |
| DMSO | | 1.4589 | 1.3988 | 1.2223 | 1.1161 | 1.3267 | | 7.5 | 0.1905 | 0.192 | 0.1897 | 0.1764 | 0.1904 | |
| 0.3125 | | 1.276 | 0.9274 | 0.7121 | 0.7274 | 0.6751 | | 10 | 0.1827 | 0.1841 | 0.1876 | 0.1824 | 0.1944 | |
| 0.625 | | 1.0479 | 0.6119 | 0.3703 | 0.5102 | 0.4734 | | 15 | 0.1944 | 0.2024 | 0.2031 | 0.2071 | 0.2114 | |
| 1.25 | | 0.6998 | 0.4111 | 0.3488 | 0.3412 | 0.3385 | | 20 | 0.1994 | 0.2054 | 0.1953 | 0.1936 | 0.2224 | |
| 2.5 | | 0.2611 | 0.2548 | 0.2529 | 0.242 | 0.2257 | | 25 | 0.2005 | 0.2036 | 0.1966 | 0.2002 | 0.2071 | |
| 5 | | 0.1983 | 0.1925 | 0.1986 | 0.2051 | 0.1873 | | 30 | 0.2037 | 0.2118 | 0.2148 | 0.2067 | 0.2055 | |
| | | | | | | | | | | | | | | |

A375 melanoma cells treated with KRMD5

| Drug[µM] | 1 | 2 | 3 | 4 | 5 | 6 | | Drug[µM] | 7 | 8 | 9 | 10 | 11 | 12 |
|---|---|---|---|---|---|---|---|---|---|---|---|---|---|---|
| Background | | 0.1621 | 0.1603 | 0.1596 | 0.1653 | 0.1616 | | | | | | | | |
| DMSO | | 1.3588 | 1.0497 | 0.9557 | 0.8829 | 1.0792 | | 7.5 | 0.1834 | 0.1921 | 0.1847 | 0.1754 | 0.1959 | |
| 0.3125 | | 1.3477 | 0.9508 | 0.6906 | 0.6949 | 0.6365 | | 10 | 0.1789 | 0.192 | 0.181 | 0.1812 | 0.1888 | |
| 0.625 | | 1.181 | 0.6884 | 0.5779 | 0.5047 | 0.5217 | | 15 | 0.1937 | 0.1886 | 0.1838 | 0.1908 | 0.199 | |
| 1.25 | | 0.7131 | 0.5062 | 0.3574 | 0.3637 | 0.366 | | 20 | 0.1995 | 0.1978 | 0.1975 | 0.1974 | 0.2066 | |
| 2.5 | | 0.2665 | 0.2638 | 0.2515 | 0.2437 | 0.2411 | | 25 | 0.2007 | 0.2061 | 0.2076 | 0.198 | 0.2093 | |
| 5 | | 0.1895 | 0.2097 | 0.1987 | 0.1949 | 0.2045 | | 30 | 0.2012 | 0.1976 | 0.2 | 0.201 | 0.2065 | |
| | | | | | | | | | | | | | | |

A375 melanoma cells treated with QHD3

| Drug[µM] | 1 | 2 | 3 | 4 | 5 | 6 | | Drug[µM] | 7 | 8 | 9 | 10 | 11 | 12 |
|---|---|---|---|---|---|---|---|---|---|---|---|---|---|---|
| Background | | 0.1627 | 0.1608 | 0.1608 | 0.1605 | 0.1581 | | | | | | | | |
| DMSO | | 1.4472 | 1.3275 | 1.2746 | 1.1941 | 1.4627 | | 7.5 | 0.1888 | 0.1942 | 0.1914 | 0.193 | 0.1919 | |
| 0.3125 | | 1.2325 | 0.9848 | 0.7548 | 0.7057 | 0.7397 | | 10 | 0.1999 | 0.1985 | 0.2022 | 0.1969 | 0.19 | |
| 0.625 | | 1.1549 | 0.736 | 0.546 | 0.521 | 0.5343 | | 15 | 0.2148 | 0.2195 | 0.2102 | 0.2347 | 0.2211 | |
| 1.25 | | 0.5946 | 0.4284 | 0.3509 | 0.3682 | 0.3312 | | 20 | 0.2157 | 0.2175 | 0.2301 | 0.2252 | 0.2194 | |
| 2.5 | | 0.2599 | 0.2345 | 0.2419 | 0.2521 | 0.2421 | | 25 | 0.2082 | 0.2302 | 0.2226 | 0.2126 | 0.2071 | |
| 5 | | 0.1874 | 0.1977 | 0.2061 | 0.1958 | 0.2026 | | 30 | 0.2156 | 0.2327 | 0.2311 | 0.2096 | 0.2073 | |
| | | | | | | | | | | | | | | |

A375 melanoma cells treated with QHD5

| Drug[μM] | 1 | 2 | 3 | 4 | 5 | 6 | | Drug[μM] | 7 | 8 | 9 | 10 | 11 | 12 |
|---|---|---|---|---|---|---|---|---|---|---|---|---|---|---|
| **Background** | | 0.1617 | 0.162 | 0.1619 | 0.1626 | 0.1604 | | | | | | | | |
| **DMSO** | | 1.4395 | 1.3934 | 1.1239 | 1.2814 | 1.3477 | | **7.5** | 0.1937 | 0.204 | 0.1913 | 0.1913 | 0.2018 | |
| **0.3125** | | 1.3933 | 0.9785 | 0.8254 | 0.746 | 0.6908 | | **10** | 0.1866 | 0.1923 | 0.1879 | 0.1869 | 0.2029 | |
| **0.625** | | 1.2446 | 0.7538 | 0.6135 | 0.5348 | 0.5524 | | **15** | 0.1966 | 0.2019 | 0.2035 | 0.2017 | 0.1957 | |
| **1.25** | | 0.7854 | 0.4584 | 0.3801 | 0.3838 | 0.3766 | | **20** | 0.202 | 0.2067 | 0.2091 | 0.2225 | 0.221 | |
| **2.5** | | 0.3197 | 0.2674 | 0.1878 | 0.1852 | 0.1772 | | **25** | 0.1751 | 0.1799 | 0.1769 | 0.182 | 0.1763 | |
| **5** | | 0.1678 | 0.1676 | 0.1561 | 0.1686 | 0.1655 | | **30** | 0.1679 | 0.1807 | 0.1808 | 0.1798 | 0.1698 | |
| | | | | | | | | | | | | | | |

A375 melanoma cells treated with DiD3

| Drug[μM] | 1 | 2 | 3 | 4 | 5 | 6 | | Drug[μM] | 7 | 8 | 9 | 10 | 11 | 12 |
|---|---|---|---|---|---|---|---|---|---|---|---|---|---|---|
| **Background** | | 0.1671 | 0.1762 | 0.1673 | 0.1673 | 0.1642 | | | | | | | | |
| **DMSO** | | 1.4905 | 1.2847 | 1.1689 | 1.2809 | 1.3884 | | **7.5** | 1.5367 | 1.6033 | 1.6132 | 1.6141 | 1.5896 | |
| **0.3125** | | 1.4923 | 1.2134 | 0.8119 | 0.8165 | 0.8882 | | **10** | 0.8803 | 1.1181 | 1.2936 | 1.5284 | 1.603 | |
| **0.625** | | 1.4665 | 1.1145 | 0.8685 | 0.7881 | 0.6536 | | **15** | 0.8254 | 0.916 | 1.0895 | 1.4002 | 1.7093 | |
| **1.25** | | 1.526 | 1.1974 | 0.8654 | 0.7816 | 0.828 | | **20** | 0.707 | 0.8067 | 0.8583 | 1.2451 | 1.7327 | |
| **2.5** | | 1.521 | 1.3031 | 1.1787 | 1.0639 | 1.068 | | **25** | 1.0483 | 0.9845 | 1.2005 | 1.4362 | 1.6933 | |
| **5** | | 1.5522 | 1.5416 | 1.5471 | 1.5004 | 1.5155 | | **30** | 1.6771 | 1.7467 | 1.6977 | 1.7076 | 1.7025 | |
| | | | | | | | | | | | | | | |

A375 melanoma cells treated with DiD5

| Drug[μM] | 1 | 2 | 3 | 4 | 5 | 6 | | Drug[μM] | 7 | 8 | 9 | 10 | 11 | 12 |
|---|---|---|---|---|---|---|---|---|---|---|---|---|---|---|
| **Background** | | 0.1633 | 0.1606 | 0.163 | 0.1796 | 0.1646 | | | | | | | | |
| **DMSO** | | 1.3852 | 1.292 | 1.1875 | 1.24 | 1.3567 | | **7.5** | 1.4184 | 1.3997 | 1.5117 | 1.4644 | 1.498 | |
| **0.3125** | | 1.3003 | 1.0993 | 0.9681 | 1.0317 | 0.9042 | | **10** | 0.9781 | 1.0945 | 1.2619 | 1.3906 | 1.5321 | |
| **0.625** | | 1.3709 | 0.9768 | 0.7806 | 0.8258 | 0.7827 | | **15** | 0.6942 | 0.8497 | 1.0163 | 1.3413 | 1.6095 | |
| **1.25** | | 1.3846 | 1.2416 | 0.9775 | 0.8884 | 0.8684 | | **20** | 0.8781 | 0.9012 | 0.9866 | 1.1565 | 1.6049 | |
| **2.5** | | 1.3686 | 1.2552 | 1.2023 | 1.1462 | 1.0913 | | **25** | 0.9928 | 1.0816 | 1.2005 | 1.56 | 1.6426 | |
| **5** | | 1.459 | 1.4449 | 1.5155 | 1.4882 | 1.4871 | | **30** | 1.6245 | 1.6893 | 1.6455 | 1.686 | 1.6777 | |
| | | | | | | | | | | | | | | |

## H1792 NSCLC cells

H1792 NSCLC cells treated with KRMD3

| Drug[μM] | 1 | 2 | 3 | 4 | 5 | 6 | | Drug[μM] | 7 | 8 | 9 | 10 | 11 | 12 |
|---|---|---|---|---|---|---|---|---|---|---|---|---|---|---|
| **Background** | | 0.0772 | 0.0742 | 0.0699 | 0.0689 | 0.0692 | | | | | | | | |
| **DMSO** | | 0.7967 | 0.8122 | 0.8049 | 0.8497 | 0.8459 | | **7.5** | 0.202 | 0.1903 | 0.1847 | 0.1829 | 0.2056 | |
| **0.3125** | | 0.6606 | 0.7103 | 0.7383 | 0.7128 | 0.7382 | | **10** | 0.1619 | 0.1497 | 0.1739 | 0.1716 | 0.1695 | |
| **0.625** | | 0.6504 | 0.7545 | 0.8072 | 0.7105 | 0.7698 | | **15** | 0.1483 | 0.1462 | 0.1688 | 0.169 | 0.174 | |
| **1.25** | | 0.6363 | 0.6459 | 0.6569 | 0.6967 | 0.6292 | | **20** | 0.1642 | 0.166 | 0.1612 | 0.157 | 0.175 | |
| **2.5** | | 0.322 | 0.3297 | 0.3452 | 0.3488 | 0.3771 | | **25** | 0.168 | 0.1693 | 0.152 | 0.1445 | 0.1737 | |
| **5** | | 0.2005 | 0.2091 | 0.2082 | 0.2035 | 0.2047 | | **30** | 0.1582 | 0.1603 | 0.1587 | 0.1793 | 0.1586 | |
| | | | | | | | | | | | | | | |

H1792 NSCLC cells treated with KRMD5

| Drug[μM] | 1 | 2 | 3 | 4 | 5 | 6 | | Drug[μM] | 7 | 8 | 9 | 10 | 11 | 12 |
|---|---|---|---|---|---|---|---|---|---|---|---|---|---|---|
| **Background** | | 0.0716 | 0.0757 | 0.0704 | 0.0762 | 0.0781 | | | | | | | | |
| **DMSO** | | 0.7483 | 0.8678 | 0.8438 | 0.893 | 0.7905 | | **7.5** | 0.1839 | 0.1878 | 0.1963 | 0.1812 | 0.2004 | |
| **0.3125** | | 0.6244 | 0.8344 | 0.8177 | 0.8437 | 0.782 | | **10** | 0.1775 | 0.1831 | 0.1748 | 0.1997 | 0.1916 | |
| **0.625** | | 0.7664 | 0.7675 | 0.7824 | 0.8368 | 0.8092 | | **15** | 0.1624 | 0.1802 | 0.1692 | 0.1777 | 0.1588 | |
| **1.25** | | 0.6814 | 0.6907 | 0.6825 | 0.7184 | 0.6819 | | **20** | 0.1705 | 0.1778 | 0.1741 | 0.1602 | 0.1535 | |
| **2.5** | | 0.4569 | 0.4839 | 0.4647 | 0.4824 | 0.4445 | | **25** | 0.1634 | 0.1703 | 0.1814 | 0.1652 | 0.1779 | |
| **5** | | 0.2446 | 0.2476 | 0.2301 | 0.2333 | 0.2218 | | **30** | 0.1586 | 0.1578 | 0.1723 | 0.1673 | 0.1922 | |
| | | | | | | | | | | | | | | |

H1792 NSCLC cells treated with QHD3

| Drug[μM] | 1 | 2 | 3 | 4 | 5 | 6 | | Drug[μM] | 7 | 8 | 9 | 10 | 11 | 12 |
|---|---|---|---|---|---|---|---|---|---|---|---|---|---|---|
| **Background** | | 0.0673 | 0.0681 | 0.0662 | 0.0675 | 0.0669 | | | | | | | | |
| **DMSO** | | 0.72 | 0.8107 | 0.716 | 0.7623 | 0.7237 | | **7.5** | 0.1706 | 0.1967 | 0.1833 | 0.1624 | 0.1917 | |
| **0.3125** | | 0.7658 | 0.7165 | 0.759 | 0.7096 | 0.726 | | **10** | 0.179 | 0.1807 | 0.1676 | 0.1789 | 0.176 | |
| **0.625** | | 0.6395 | 0.7232 | 0.763 | 0.6914 | 0.7948 | | **15** | 0.1551 | 0.1554 | 0.157 | 0.1698 | 0.1479 | |
| **1.25** | | 0.5535 | 0.5995 | 0.5528 | 0.6011 | 0.555 | | **20** | 0.1542 | 0.1583 | 0.154 | 0.15 | 0.1538 | |
| **2.5** | | 0.268 | 0.2739 | 0.2982 | 0.2808 | 0.2812 | | **25** | 0.1557 | 0.1494 | 0.1613 | 0.1397 | 0.163 | |
| **5** | | 0.1523 | 0.1686 | 0.1801 | 0.1681 | 0.1765 | | **30** | 0.1581 | 0.1483 | 0.1402 | 0.1502 | 0.1582 | |
| | | | | | | | | | | | | | | |

H1792 NSCLC cells treated with QHD5

| Drug[μM] | 1 | 2 | 3 | 4 | 5 | 6 | | Drug[μM] | 7 | 8 | 9 | 10 | 11 | 12 |
|---|---|---|---|---|---|---|---|---|---|---|---|---|---|---|
| **Background** | | 0.073 | 0.0746 | 0.0701 | 0.0729 | 0.0706 | | | | | | | | |
| **DMSO** | | 0.731 | 0.8279 | 0.7674 | 0.7909 | 0.7592 | | **7.5** | 0.2046 | 0.1832 | 0.1806 | 0.1717 | 0.2005 | |
| **0.3125** | | 0.6716 | 0.7648 | 0.8016 | 0.7692 | 0.7396 | | **10** | 0.1597 | 0.165 | 0.1644 | 0.1862 | 0.1782 | |
| **0.625** | | 0.6135 | 0.6869 | 0.5893 | 0.7554 | 0.7216 | | **15** | 0.1662 | 0.155 | 0.1547 | 0.1663 | 0.1582 | |
| **1.25** | | 0.6177 | 0.6326 | 0.5962 | 0.6539 | 0.5967 | | **20** | 0.1551 | 0.1545 | 0.1606 | 0.1743 | 0.1745 | |
| **2.5** | | 0.3063 | 0.326 | 0.3565 | 0.3333 | 0.2937 | | **25** | 0.1578 | 0.1544 | 0.1573 | 0.167 | 0.1644 | |
| **5** | | 0.207 | 0.2063 | 0.1955 | 0.1993 | 0.2008 | | **30** | 0.1572 | 0.1699 | 0.1652 | 0.1589 | 0.1623 | |
| | | | | | | | | | | | | | | |

H1792 NSCLC cells treated with DiD3

| Drug[μM] | 1 | 2 | 3 | 4 | 5 | 6 | | Drug[μM] | 7 | 8 | 9 | 10 | 11 | 12 |
|---|---|---|---|---|---|---|---|---|---|---|---|---|---|---|
| **Background** | | 0.0687 | 0.0676 | 0.068 | 0.0761 | 0.0688 | | | | | | | | |
| **DMSO** | | 0.7485 | 0.8095 | 0.7822 | 0.795 | 0.7505 | | **7.5** | 0.7223 | 0.7165 | 0.76 | 0.7833 | 0.7881 | |
| **0.3125** | | 0.6762 | 0.7223 | 0.7736 | 0.7857 | 0.8055 | | **10** | 0.8187 | 0.8302 | 0.8294 | 0.7985 | 0.8088 | |
| **0.625** | | 0.7581 | 0.7665 | 0.7843 | 0.8107 | 0.8529 | | **15** | 0.8376 | 0.8505 | 0.8865 | 0.8851 | 0.7846 | |
| **1.25** | | 0.7154 | 0.793 | 0.7841 | 0.8219 | 0.8329 | | **20** | 0.9454 | 0.9476 | 0.9818 | 0.899 | 0.8681 | |
| **2.5** | | 0.729 | 0.7642 | 0.8003 | 0.7501 | 0.7659 | | **25** | 0.8883 | 0.9267 | 0.9528 | 0.9249 | 0.8847 | |
| **5** | | 0.8226 | 0.9724 | 0.8958 | 0.9228 | 0.8293 | | **30** | 0.8917 | 0.9614 | 0.9321 | 0.8962 | 0.878 | |
| | | | | | | | | | | | | | | |

H1792 NSCLC cells treated with DiD5

| Drug[μM] | 1 | 2 | 3 | 4 | 5 | 6 | | Drug[μM] | 7 | 8 | 9 | 10 | 11 | 12 |
|---|---|---|---|---|---|---|---|---|---|---|---|---|---|---|
| **Background** | | 0.0714 | 0.0722 | 0.0698 | 0.069 | 0.0691 | | | | | | | | |
| **DMSO** | | 0.794 | 0.7463 | 0.7804 | 0.8099 | 0.8095 | | **7.5** | 0.7589 | 0.7879 | 0.8051 | 0.7729 | 0.7684 | |
| **0.3125** | | 0.743 | 0.7251 | 0.849 | 0.8262 | 0.7892 | | **10** | 0.8026 | 0.8467 | 0.8628 | 0.7885 | 0.8233 | |
| **0.625** | | 0.6843 | 0.8283 | 0.8383 | 0.8672 | 0.8783 | | **15** | 0.8356 | 0.9191 | 0.8799 | 0.8964 | 0.8082 | |
| **1.25** | | 0.7713 | 0.7618 | 0.7892 | 0.8555 | 0.8334 | | **20** | 0.9135 | 0.8961 | 0.8836 | 0.9783 | 0.8326 | |
| **2.5** | | 0.7539 | 0.8855 | 0.8978 | 0.8648 | 0.8889 | | **25** | 0.896 | 0.9381 | 0.9167 | 0.9148 | 0.9016 | |
| **5** | | 0.7765 | 0.8166 | 0.8155 | 0.8333 | 0.8341 | | **30** | 0.9429 | 0.9565 | 0.948 | 0.9186 | 0.8877 | |
| | | | | | | | | | | | | | | |

**5. 1. 6 MTS Analysis of metabolites of QH II 66 analogues.**

# $IC_{50}$ summary for new benzodiazepines in H1792

| Compound | $IC_{50}$ (μM) | $IC_{50}$ Range (μM) |
|---|---|---|
| QH-II-66 | 6.027 | 6.027 – 6.563 |
| MYM-III-85 | 6.644 | 5.903 – 7.460 |
| TA-III-72 | 5.741 | 5.069 – 6.483 |
| KRM-III-70 | 5.240 | 4.474 – 6.107 |
| NOR-KRM-III-70 (n = 2) | 39.93, 43.91 | 34.56 – 49.27 |
| TA-III-70 | 660.2 | 100.3 – 212,771 |
| MYM-I-43 | 95.70 | 63.19 – 179.3 |
| MYM-I-59 | 3.320e+35 | infinity - infinity |
| MYM-IV-95 | 694.9 | 391.8 - 2643 |
| MYM-V-17 | 20.32 | 18.01 – 22.97 |
| | | |

# MTS Analysis of Cook Compounds – Set 1A

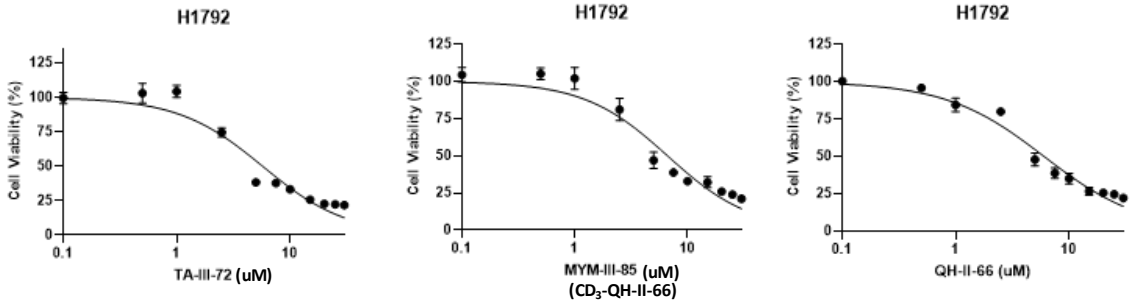


| | | | |
|---|---|---|---|
| $IC_{50}$ | 5.741 | 6.644 | 6.027 |
| 95% CI (profile likelihood) | 5.069 to 6.483 | 5.903 to 7.460 | 5.523 to 6.563 |

TA-III-72 has 5 deuteriums including an N-$CD_3$ with 2 deuteriums in C-3 position. MYM III 85 has only N -$CD_3$.

# MTS Analysis of Cook Compounds – Set 1B

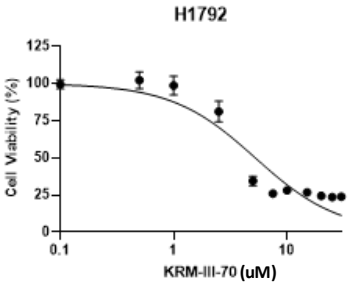


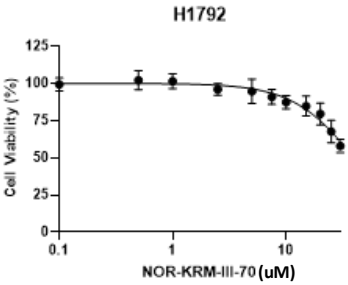


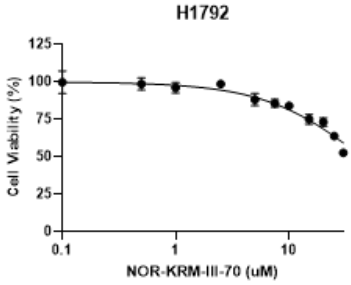


| | | | |
|---|---|---|---|
| $IC_{50}$ | 5.240 | 39.93 | 43.91 |
| 95% CI (profile likelihood) | 4.474 to 6.107 | 34.56 to 49.27 | 40.48 to 48.01 |

# MTS Analysis of Cook Compounds – Set 1B (cont.)

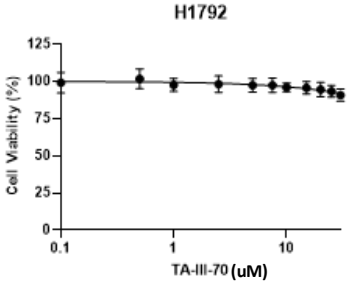


| | |
|---|---|
| $IC_{50}$ | 660.2 |
| 95% CI (profile likelihood) | 100.3 to 212771 |

# MTS Analysis of Cook Compounds – Set 2A

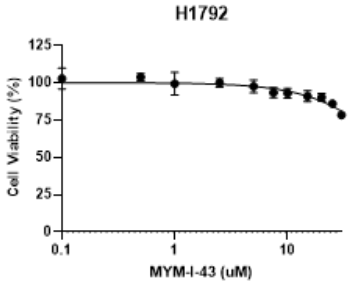


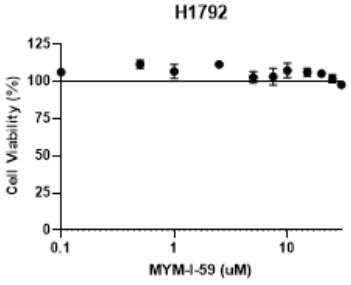


| | | |
|---|---|---|
| $IC_{50}$ | 95.70 | 3.320e+035 |
| 95% CI (profile likelihood) | 63.19 to 179.3 | -infinity to +infinity |

# MTS Analysis of Cook Compounds– Set 2B

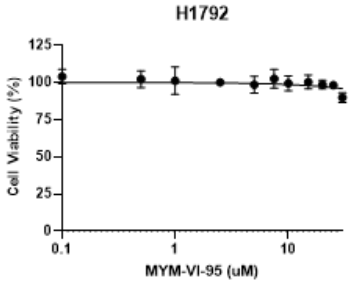


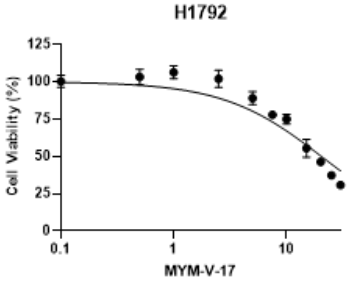


| | | |
|---|---|---|
| $IC_{50}$ | 694.9 | 20.32 |
| 95% CI (profile likelihood) | 391.8 to 2643 | 18.01 to 22.97 |

**5. 1. 7 Development of QHii066 as a Potentiator of Temozolomide in GBMs By Aniruddha S. Karve, Advisor: Pankaj B. Desai, PhD**

# Development of QHii066 as a Potentiator of Temozolomide in GBMs

Aniruddha S. Karve
Advisor: Pankaj B. Desai, PhD

# QHII066: A Novel Benzodiazepine targeting α5-GABA$_A$R

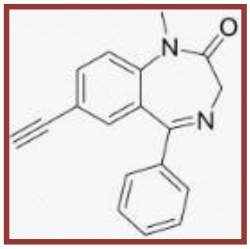

| | |
|---|---|
| **Molecular weight** | 274.3 g/mol |
| **logP (o/w)** | 2.6 |
| **pKa** | 3.9 |
| **Hydrogen Bond Donor Count** | 0 |
| **Hydrogen Bond Acceptor Count** | 2 |
| **Rotatable Bond Count** | 2 |

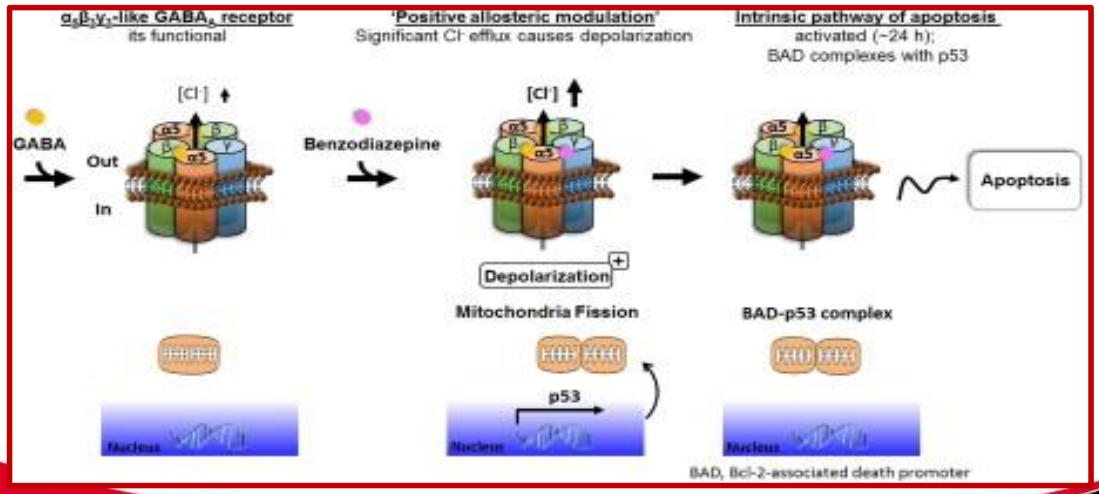


UNIVERSITY OF Cincinnati

# Formulation Development for QHi066

| **Co-solvent based injectable formulation (U.S. FDA approved for Benzodiazepines)** | **Characteristics** |
|---|---|
| Drug content (5 mg/mL) | Maximum drug solubility (10 mg/mL) |
| Propylene Glycol (40%) | Stable at room temperature up to 6 months |
| Absolute ethanol (10%) | Stable at 4° C up to at least 10 months |
| Benzoic acid (5%) | No effect on drug metabolism observed |
| Sodium Benzoate (5%) | No visible adverse effects observed in rats 12 hours after single dose iv administration |
| Benzyl alcohol (1.5%) | |
| Water for injection (q.s.) and NaOH or HCl for pH adjustment to 5.0 | |

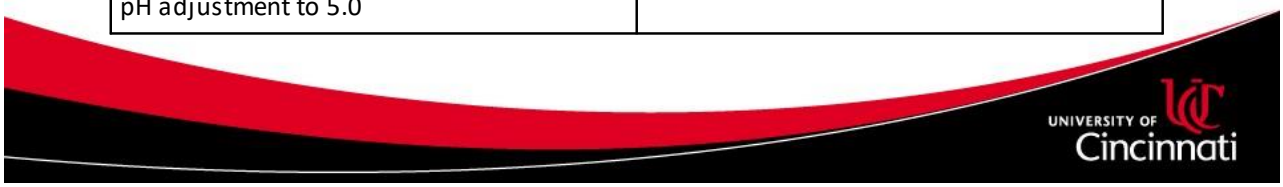

# In vitro Cytotoxicity studies of QHii066 (BT142-GFP -Luc cells)

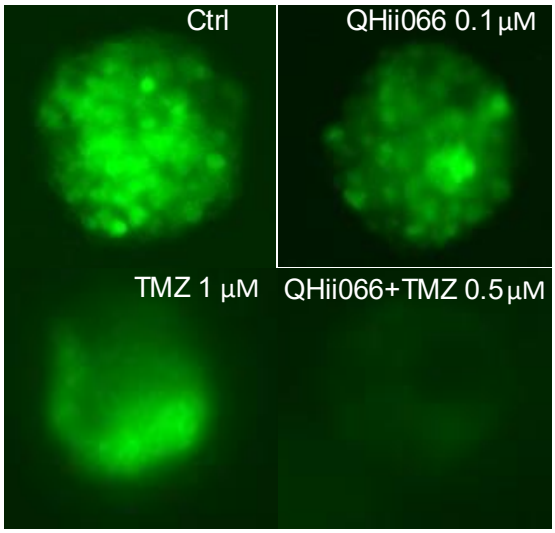


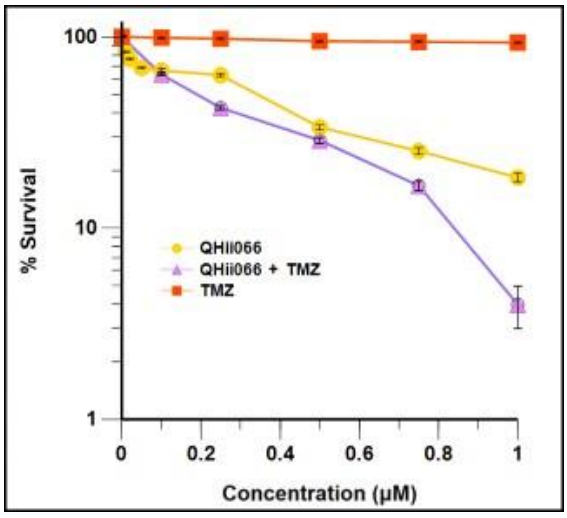


**C.I. = $IC_{50}$[QH+TMZ]/$IC_{50}$[QH] + $IC_{50}$[QH+TMZ]/$IC_{50}$[TMZ]**

Combination index: **0.235**
C.I. < 1 indicates synergy

UNIVERSITY OF Cincinnati

# In vitro Cytotoxicity studies of QHii066 (G43 cells)

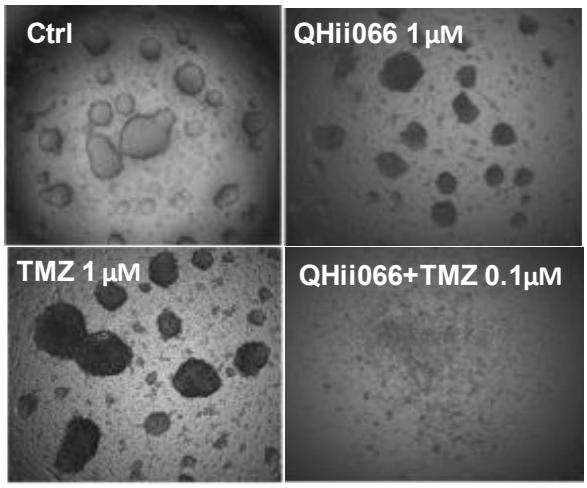


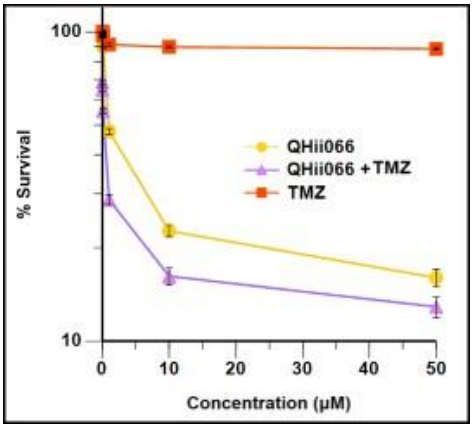


$C.I. = IC_{50}[QH+TMZ]/IC_{50}[QH] + IC_{50}[QH+TMZ]/IC_{50}[TMZ]$

Combination index: **0.02**
C.I. < 1 indicates synergy

UNIVERSITY OF Cincinnati

# Chemosensitization of a panel of GBM cells by QHii066

| Cell line | MGMT status | Recurrence status | $IC_{50}$ TMZ (μM) | $IC_{50}$ QH (μM) | $IC_{50}$ QH (0.1 μM) (non-cytotoxic concentration) + TMZ (μM) | Combination Index |
|---|---|---|---|---|---|---|
| G76 | Methylated | Recurrent | 1.31 | 0.613 | 0.103 | 0.24 |
| G75 | Methylated | Primary | 106.73 | 3.23 | 0.126 | 0.032 |
| G43 | Unmethylated | Primary | 165.43 | 6.67 | 0.360 | 0.018 |
| BT142 | Unmethylated (IDH1 mutant) | Primary | 15.33 | 0.443 | 0.190 | 0.235 |

# Mechanistic studies to Elucidate Potentiation of TMZ activity (Inhibition of efflux pumps)

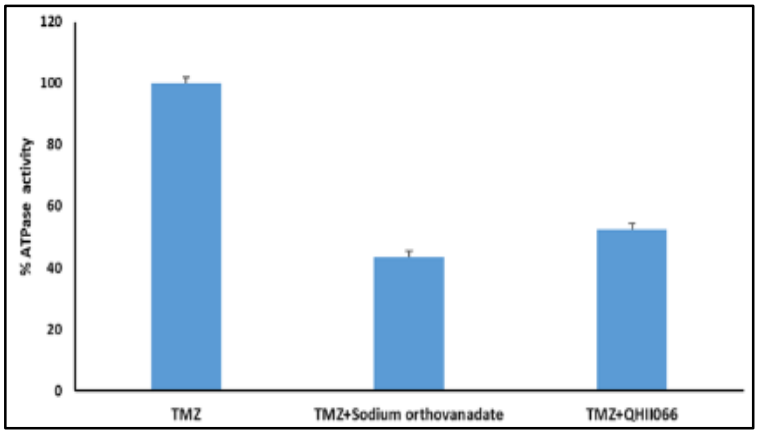


**Inhibition of ATPase activity by QHii066**

- SB-Predeasy assay for MDR1 was used to analyze effect of QHii066 on efflux of TMZ through ATPase pumps (e.g. Pgp)
- QHii066 inhibited efflux pumps at 1 µM concentration
- ATPase pump inhibition by QHii066 was comparable with that by Na-orthovanadate, a well known ATPase pump inhibitor
- Further studies are required to identify the ATPase pump inhibited by QHii066 using transformed Pgp overexpressing MDCK1 and Caco2 cell lines.

# In vitro PK studies for QHII066

Reaction mixture:
0.2 mg Human Liver microsomes
50 mM Phosphate buffer
1 mM MgCl2
0.5 mM EDTA
0.1 µM NADPH
Drug: 5 µM

Incubation times:
0, 10, 15, 30 and 60 min

Extraction solvent: Ethyl acetate

A) LC-MS/MS for **QHii066 in-vitro metabolism**

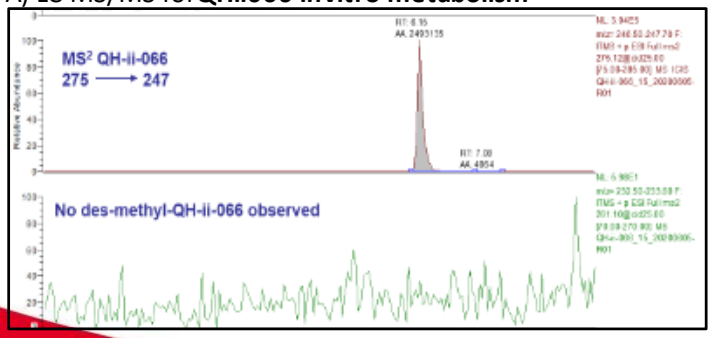


B) LC-MS/MS **for Midazolam in-vitro metabolism**

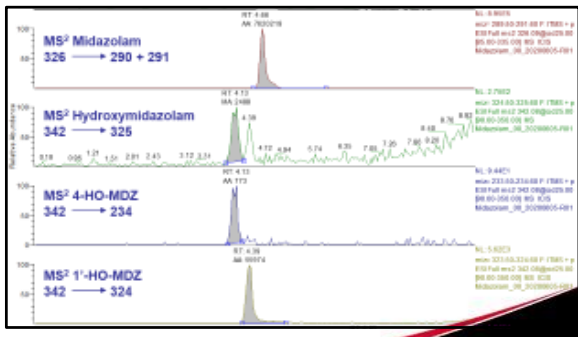


5/3/2022

UNIVERSITY OF Cincinnati

# Intracranial Microdialysis

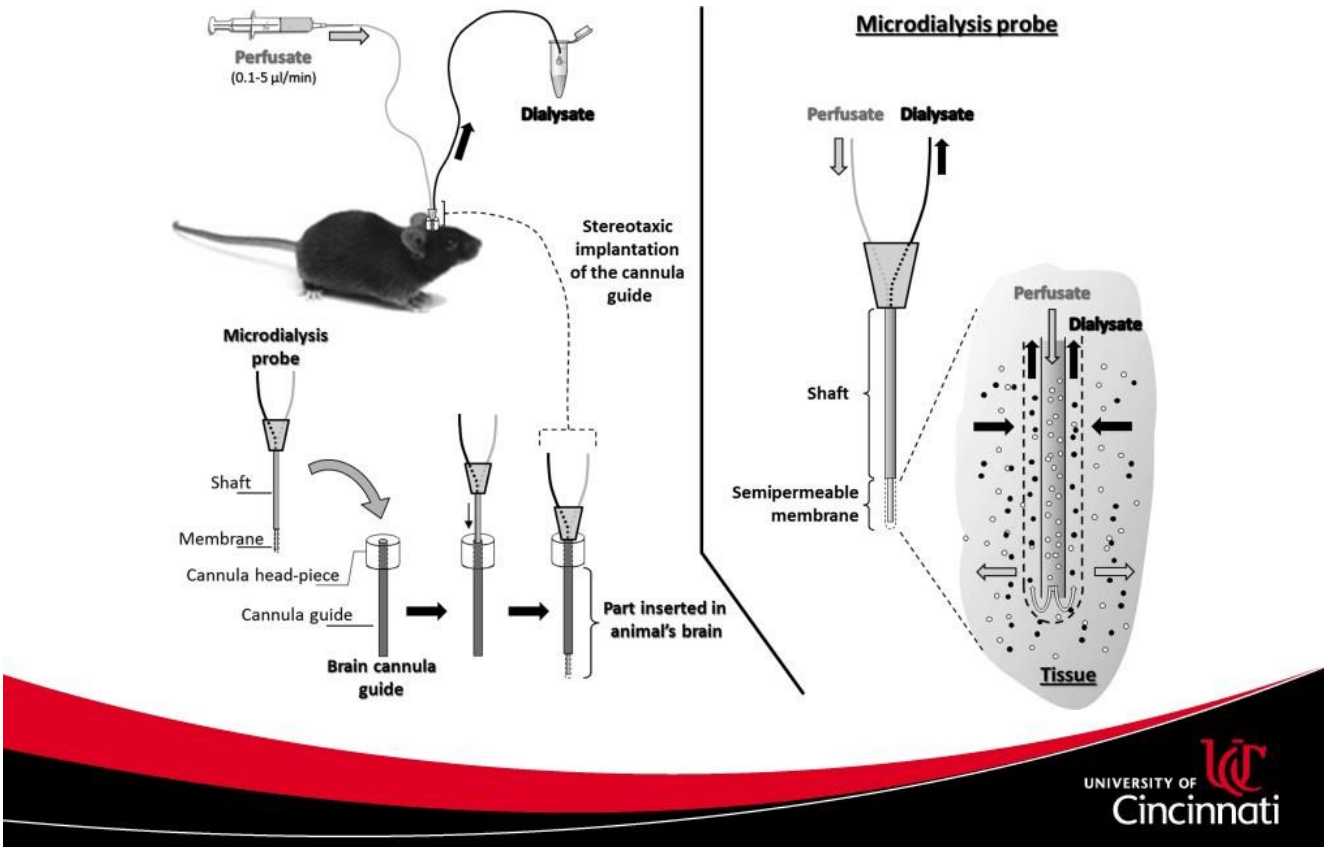

# Study Overview

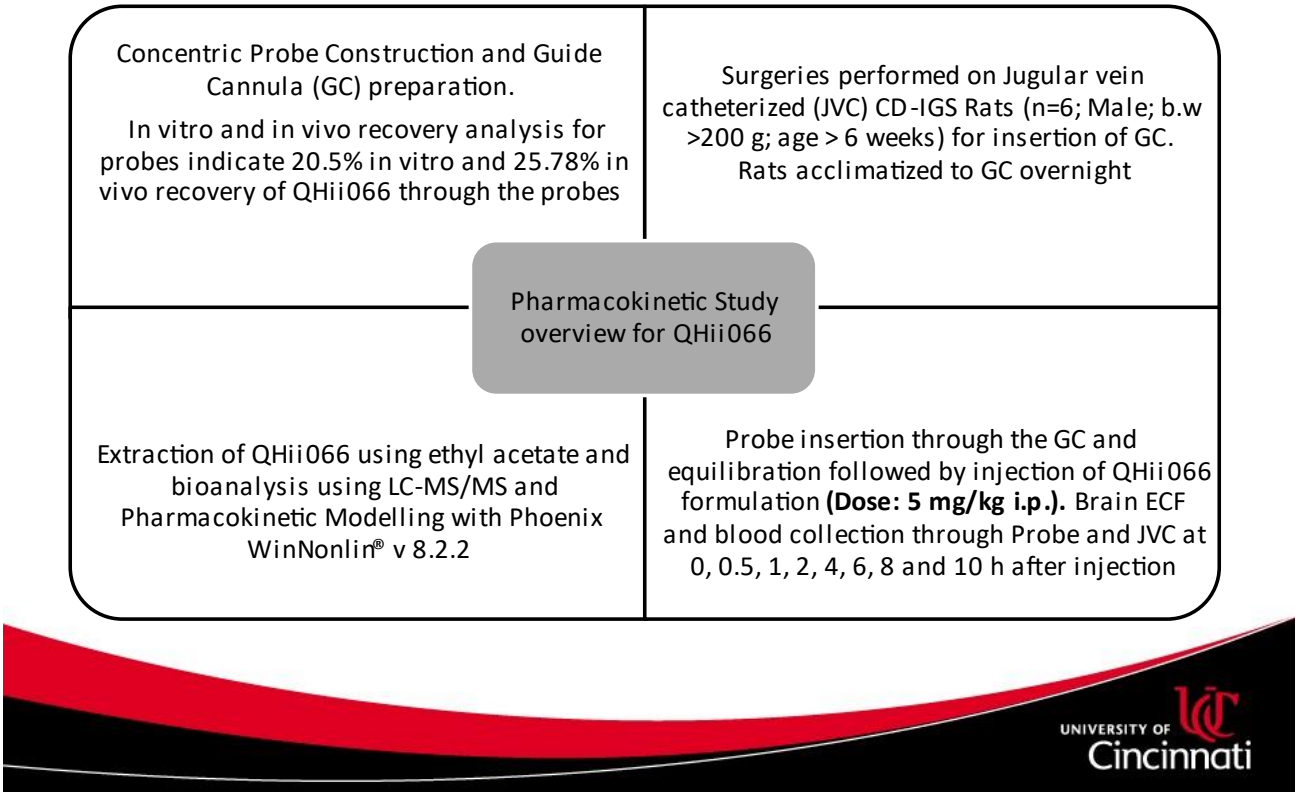

# Rat Brain ECF and Plasma PK studies for QHII066

- **QHii066 Dose: 5 mg/kg i.p.**
- **Pharmacological observations:**

Deep sedation

No visible response to toe pinch

Normal breathing and body temperatures

Slow movements after 6-8 h post administration

- **Onset of action**: ~ 0.5 h posti.p. administration
- **Duration of action:**6-8 h posti.p. administration

# PK Analysis Approach

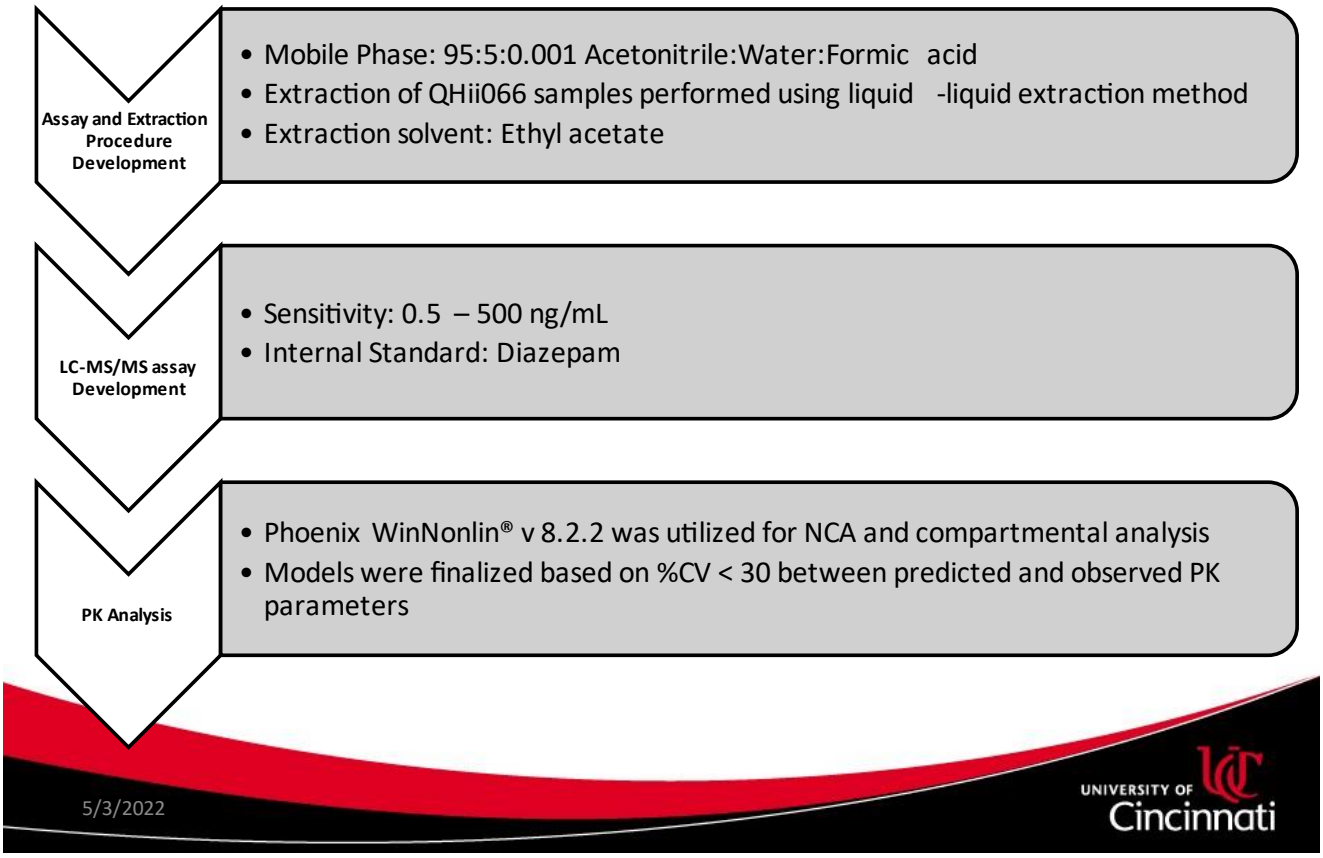

# Pharmacokinetics of QHii066 in Rat Plasma

1-compartmental PK Analysis

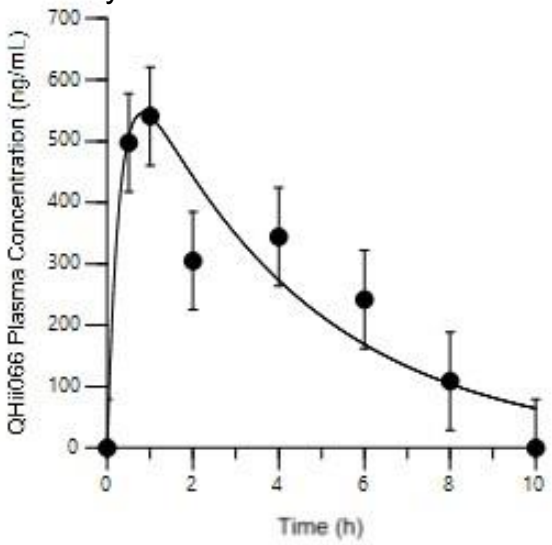


Non-compartmental PK Analysis

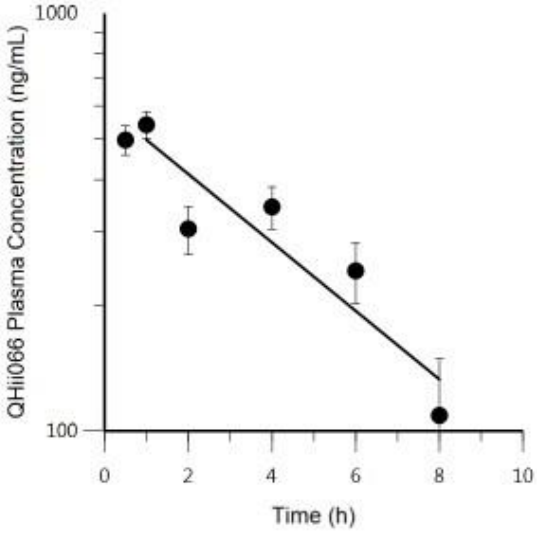

# PK Parameters of QHii066 in Rat Plasma

1-compartmental Pharmacokinetics of QHii066 in Rat Plasma

| | |
|---|---|
| V/F | 7.5 L/kg |
| K01 | 3.45 $h^{-1}$ |
| K10 | 0.241 $h^{-1}$ |
| AUC | 2768.875h*ng/mL |
| Absorptiont1/2 | 0.201h |
| Elimination t1/2 | 2.88h |
| Cl/F | 1.805L/h/kg |
| Tmax | 0.83h |
| Cmax | 545.89ng/mL |

Non-compartmental Pharmacokinetics of QHii066 in Rat Plasma

| | |
|---|---|
| V/F | 8.56L/kg |
| λz | 0.191 $h^{-1}$ |
| AUC (0-10h) | 2392.16h*ng/mL |
| Elimination t1/2 | 3.67h |
| Cl/F | 1.61L/h/kg |
| Tmax | 1.00h |
| Cmax | 541.01ng/mL |

# Pharmacokinetics of QHii066 in Rat Brain Extracellular fluid (Corrected for In vivo recovery)

1-compartmental PK Analysis

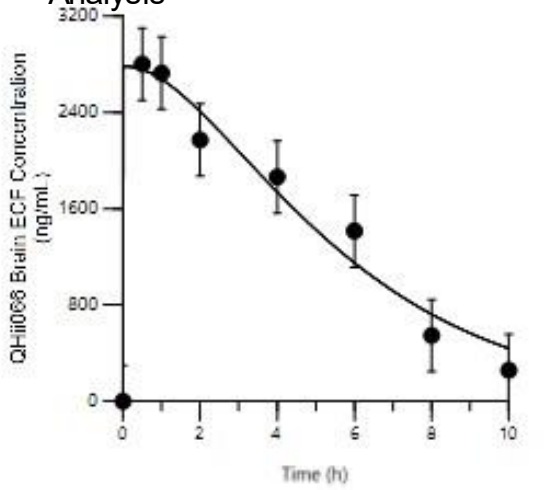


Non-compartmental PK Analysis

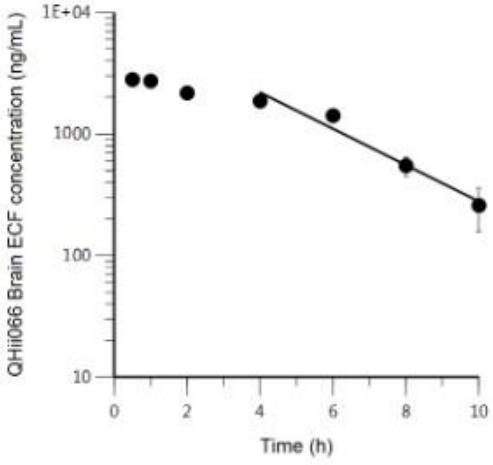

# PK Parameters of QHii066 in Rat Brain ECF

1-compartmental Pharmacokinetics of QHii066 in Rat Brain ECF

| | |
|---|---|
| Cmax | 2879ng/mL |
| Tmax | 0.5 h |
| AUC(0-10h) | 22656h*ng/mL |
| K01 | 0.335 $h^{1}$ |
| K10 | 0.331 $h^{1}$ |
| V/F | 0.67 L/kg |
| Cl/F | 0.22 L/hr/kg |
| Elimination t1/2 | 2.09 h |
| Absorption t1/2 | 2.06 h |

Non-compartmental Pharmacokinetics of QHii066 in Rat Brain ECF

| | |
|---|---|
| Cmax | 2800ng/mL |
| Tmax | 0.5 h |
| AUC(0-10h) | 14604h*ng/mL |
| AUC(0-inf) | 15352 h*ng/mL |
| V/F | 0.95 L/kg |
| Cl/F | 0.325 L/hr/kg |
| Elimination t1/2 | 2.01 h |
| λz | 0.344$h^{-1}$ |

# Brain ECF:Plasma Partitioning of QHii066

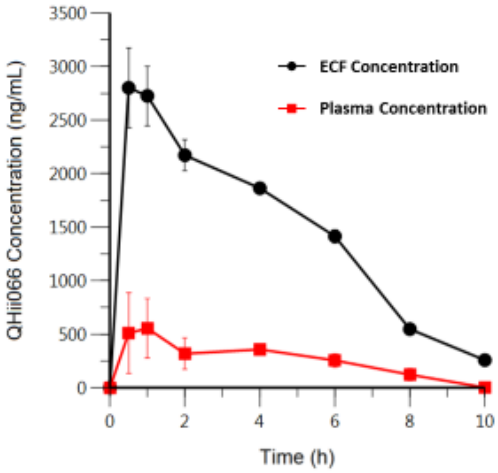


| Time (h) | Brain ECF:PlasmaRatio |
|---|---|
| 0.5 | 5.49 |
| 1 | 4.92 |
| 2 | 6.83 |
| 4 | 5.22 |
| 6 | 5.55 |
| 8 | 4.49 |

# Comparative PK of Other Benzodiazepines

Rat Brain and Plasma PK of Diazepam [1]

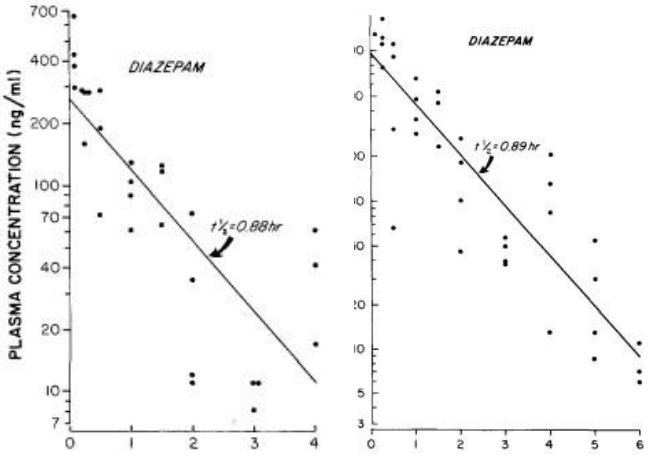


Diazepam Dose: 5 mg/kg i.p .
t1/2 = ~0.9 h

Rat Plasma PK of Midazolam [2]

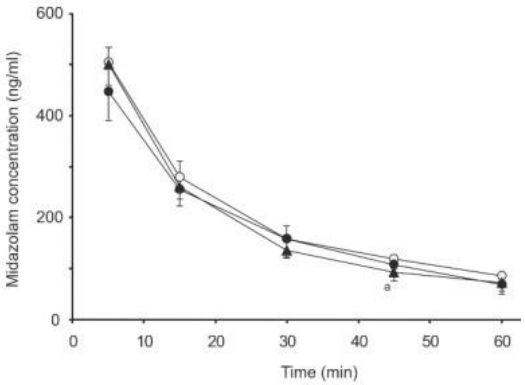


Midazolam Dose: 0.75 mg/kg i.v.
t1/2 = ~15 min

# Future Studies

- PK Studies: Protein Binding Experiments

Caco-2 cell permeability experiments

Animal experiments to determine Total Brain Concentration

- Mechanistic Studies: MGMT Methylation NGS

GABRA5 expression studies

## 5. 1. 8 Genes In Heatmap

| | genes | Cytokine.cytokine.receptor.interaction | TP63 | Radiation_vs_Untreated_log2FoldChange | Radiation_vs_Untreated_padj | QHII_vs_Untreated_log2FoldChange | QHII_vs_Untreated_padj |
|---|---|---|---|---|---|---|---|
| ENSMUSG00000004814 | Ccl24 | 1 | 0 | 3.548294193 | 0.002551078 | 3.824321839 | 0.031571673 |
| ENSMUSG00000005268 | Prlr | 1 | 0 | 2.959865947 | 0.04552787 | 3.849327512 | 0.574451203 |
| ENSMUSG00000005824 | Tnfsf14 | 1 | 0 | 1.643749172 | 0.047867046 | 0.666596253 | 0.74658225 |
| ENSMUSG00000008999 | Bmp7 | 1 | 0 | 6.8639052 | 0.000158975 | 1.74698418 | 0.740957377 |
| ENSMUSG00000009185 | Ccl8 | 1 | 0 | 1.375156483 | 0.00538401 | 0.810130665 | 0.613902131 |
| ENSMUSG00000017057 | Il13ra1 | 1 | 0 | 0.793194692 | 0.034319086 | 0.044369475 | 0.987557181 |
| ENSMUSG00000020007 | Il20ra | 1 | 0 | 6.048700666 | 0.002454351 | -0.094380019 | 1 |
| ENSMUSG00000020122 | Egfr | 1 | 0 | 3.206446051 | 8.44171E-06 | 1.141366859 | 0.446352737 |
| ENSMUSG00000021508 | Cxcl14 | 1 | 0 | 2.205415229 | 0.000836517 | 1.485213557 | 0.268408178 |
| ENSMUSG00000023078 | Cxcl13 | 1 | 0 | 3.260817943 | 0.002640159 | 1.907345607 | 0.618653562 |
| ENSMUSG00000023915 | Tnfrsf21 | 1 | 0 | 1.187055637 | 0.060159092 | 0.454936875 | 0.748232939 |
| ENSMUSG00000024379 | Tslp | 1 | 0 | 2.632825849 | 0.006068905 | 1.215496339 | 0.647795459 |
| ENSMUSG00000024620 | Pdgfrb | 1 | 0 | 0.891687542 | 0.03138916 | 0.031536253 | 0.99946126 |
| ENSMUSG00000024621 | Csf1r | 1 | 0 | 1.51635937 | 5.11361E-05 | 0.485051091 | 0.676433518 |
| ENSMUSG00000026072 | Il1r1 | 1 | 0 | 1.985242898 | 0.000144177 | 0.601226701 | 0.702257932 |
| ENSMUSG00000026073 | Il1r2 | 1 | 0 | 2.370631997 | 0.009841498 | 0.111099656 | 0.984706097 |
| ENSMUSG00000026180 | Cxcr2 | 1 | 0 | 2.569297268 | 0.049932289 | 1.469016557 | 0.734178408 |
| ENSMUSG00000027358 | Bmp2 | 1 | 0 | 1.929939781 | 0.04448678 | 0.971370484 | 0.669849823 |
| ENSMUSG00000027399 | Il1a | 1 | 0 | 1.728433942 | 0.039022305 | 0.235877121 | 0.950340468 |
| ENSMUSG00000027947 | Il6ra | 1 | 0 | 1.531930411 | 0.017257531 | 0.432766632 | 0.766884258 |
| ENSMUSG00000028019 | Pdgfc | 1 | 0 | 1.96144031 | 0.003859866 | 0.970590453 | 0.623275761 |
| ENSMUSG00000028599 | Tnfrsf1b | 1 | 0 | 0.928942705 | 0.044978636 | 0.372939759 | 0.744188347 |
| ENSMUSG00000029231 | Pdgfra | 1 | 0 | 2.588389142 | 6.81893E-08 | 0.710676758 | 0.647795459 |
| ENSMUSG00000030748 | Il4ra | 1 | 0 | 1.214904933 | 0.000219844 | 0.217686165 | 0.833517224 |
| ENSMUSG00000031380 | Vegfd | 1 | 0 | 2.832655149 | 0.000598016 | 1.229574193 | 0.657152856 |
| ENSMUSG00000032440 | Tgfbr2 | 1 | 0 | 0.680753024 | 0.028152572 | -0.044506973 | 0.97774378 |
| ENSMUSG00000034394 | Lif | 1 | 0 | 1.458808863 | 0.044985142 | 0.471382863 | 0.786714006 |
| ENSMUSG00000035448 | Ccr3 | 1 | 0 | 2.271466983 | 0.036772793 | 1.568356741 | 0.631452833 |
| ENSMUSG00000037944 | Ccr7 | 1 | 0 | 1.719088041 | 0.024796193 | 0.399782834 | 0.838697858 |
| ENSMUSG00000039760 | Il22ra2 | 1 | 0 | 6.596179235 | 0.002135483 | 0 | 1 |

| | genes | Cytokine.cytokine.receptor.interaction | TP63 | Radiation_vs_Untreated_log2FoldChange | Radiation_vs_Untreated_padj | QHII_vs_Untreated_log2FoldChange | QHII_vs_Untreated_padj |
|---|---|---|---|---|---|---|---|
| ENSMUSG00000043088 | Il17re | 1 | 0 | 2.568171149 | 0.04552787 | 0.583057684 | 0.857136323 |
| ENSMUSG00000044244 | Il20rb | 1 | 0 | 2.878955295 | 0.004515355 | 0.037612293 | 1 |
| ENSMUSG00000044337 | Ackr3 | 1 | 0 | 1.252895345 | 0.035164731 | 0.591395625 | 0.701230018 |
| ENSMUSG00000049103 | Ccr2 | 1 | 0 | 1.247155789 | 0.008892927 | 0.596067254 | 0.651832556 |
| ENSMUSG00000054263 | Lifr | 1 | 0 | 1.744655058 | 0.000239182 | 0.830215641 | 0.574451203 |
| ENSMUSG00000055737 | Ghr | 1 | 0 | 1.290037958 | 0.010764755 | 1.291699916 | 0.490248197 |
| ENSMUSG00000057722 | Lepr | 1 | 0 | 3.59944499 | 0.000675947 | 0.722443563 | 0.750330922 |
| ENSMUSG00000059201 | Lep | 1 | 0 | 3.038749581 | 0.031009532 | 3.172863193 | 0.3491081 |
| ENSMUSG00000061353 | Cxcl12 | 1 | 0 | 2.084623614 | 3.90205E-10 | 0.667040723 | 0.636697306 |
| ENSMUSG00000062960 | Kdr | 1 | 0 | 0.743869665 | 0.089426434 | 0.218970709 | 0.831092706 |
| ENSMUSG00000071713 | Csf2rb | 1 | 0 | 1.264255408 | 0.0040666 | 0.56783684 | 0.676433518 |
| ENSMUSG00000071714 | Csf2rb2 | 1 | 0 | 1.220479115 | 0.034578143 | 0.414111552 | 0.768671681 |
| ENSMUSG00000003032 | Klf4 | 0 | 1 | 2.846309153 | 5.09593E-05 | 0.823758174 | 0.647795459 |
| ENSMUSG00000005251 | Ripk4 | 0 | 1 | 7.410340918 | 0.001769584 | 3.06403167 | 0.623275761 |
| ENSMUSG00000012350 | Ehf | 0 | 1 | 4.087365974 | 0.069609143 | 1.865691527 | 0.720576226 |
| ENSMUSG00000016028 | Celsr1 | 0 | 1 | 3.446695173 | 0.003400843 | 0.28644433 | 0.91784845 |
| ENSMUSG00000017144 | Rnd3 | 0 | 1 | 1.009561035 | 0.050669479 | 0.193861481 | 0.879740653 |
| ENSMUSG00000019851 | Perp | 0 | 1 | 7.378731769 | 3.87872E-05 | 0.321544416 | 0.861549122 |
| ENSMUSG00000020042 | Btbd11 | 0 | 1 | 4.006336927 | 0.002974839 | 1.100295624 | 0.720576226 |
| ENSMUSG00000020176 | Grb10 | 0 | 1 | 1.857700176 | 0.000291413 | 1.072002297 | 0.335410006 |
| ENSMUSG00000020961 | Ston2 | 0 | 1 | 3.050704421 | 0.016532926 | 1.033386962 | 0.763284084 |
| ENSMUSG00000022382 | Wnt7b | 0 | 1 | 4.796554738 | 0.013880412 | 1.19875237 | 0.722228706 |
| ENSMUSG00000022479 | Vdr | 0 | 1 | 3.466119332 | 0.002628584 | -0.215587034 | 0.928425037 |
| ENSMUSG00000025105 | Bnc1 | 0 | 1 | 9.232690337 | 0.000799253 | 1.59587272 | 1 |
| ENSMUSG00000026167 | Wnt10a | 0 | 1 | 5.400724439 | 0.004658212 | 0.371504709 | 1 |
| ENSMUSG00000026413 | Pkp1 | 0 | 1 | 10.21850515 | 1.04647E-05 | 2.216418337 | 0.647799406 |
| ENSMUSG00000026589 | Sec16b | 0 | 1 | 2.257989566 | 0.010680613 | 1.150530776 | 0.647795459 |
| ENSMUSG00000026971 | Itgb6 | 0 | 1 | 4.988916812 | 0.001414059 | 1.694504089 | 0.652360248 |
| ENSMUSG00000027356 | Fermt1 | 0 | 1 | 9.111978136 | 0.000714318 | 3.605584171 | 0.670586273 |
| ENSMUSG00000029026 | Trp73 | 0 | 1 | 5.201340871 | 0.016355386 | -2.864985068 | 0.778089141 |

| | genes | Cytokine.cytokine.receptor.interaction | TP63 | Radiation_vs_Untreated_log2FoldChange | Radiation_vs_Untreated_padj | QHII_vs_Untreated_log2FoldChange | QHII_vs_Untreated_padj |
|---|---|---|---|---|---|---|---|
| ENSMUSG00000029055 | Plch2 | 0 | 1 | 5.476568469 | 0.003807115 | 0.255895427 | 0.998619632 |
| ENSMUSG00000029120 | Ppp2r2c | 0 | 1 | 4.621735839 | 0.028550552 | -0.488463207 | 0.982243346 |
| ENSMUSG00000029581 | Fscn1 | 0 | 1 | 1.063156504 | 0.008266135 | 0.228574504 | 0.846392578 |
| ENSMUSG00000030849 | Fgfr2 | 0 | 1 | 5.975861505 | 0.000796147 | 3.290867382 | 0.548231958 |
| ENSMUSG00000032012 | Nectin1 | 0 | 1 | 4.267556824 | 0.000112487 | 1.342376711 | 0.550353814 |
| ENSMUSG00000032013 | Trim29 | 0 | 1 | 7.985130459 | 4.26749E-05 | 0.69550018 | 0.833673904 |
| ENSMUSG00000032289 | Thsd4 | 0 | 1 | 2.409862844 | 0.071128459 | 1.178310838 | 0.720576226 |
| ENSMUSG00000033721 | Vav3 | 0 | 1 | 1.43797027 | 0.042475269 | 0.115203249 | 0.965316732 |
| ENSMUSG00000037188 | Grhl3 | 0 | 1 | 2.647459104 | 0.015670573 | 0.033382887 | 1 |
| ENSMUSG00000039238 | Zfp750 | 0 | 1 | 7.959388867 | 0.002928016 | 2.468377641 | 0.675067952 |
| ENSMUSG00000040249 | Lrp1 | 0 | 1 | 0.770175201 | 0.009540141 | 0.051636827 | 0.971865446 |
| ENSMUSG00000047281 | Sfn | 0 | 1 | 4.549928898 | 0.000274701 | 0.44502189 | 0.77597666 |
| ENSMUSG00000048399 | Tprg | 0 | 1 | 6.5417506 | 0.003427368 | 0.836217828 | 0.947893317 |
| ENSMUSG00000049336 | Tenm2 | 0 | 1 | 6.940601282 | 0.000857526 | 0.847445735 | 0.899917729 |
| ENSMUSG00000051339 | 2900026A( | 0 | 1 | 1.604940764 | 0.018032395 | 0.029842498 | 1 |
| ENSMUSG00000054252 | Fgfr3 | 0 | 1 | 3.131966868 | 0.002289168 | 0.149387417 | 0.963187105 |
| ENSMUSG00000055333 | Fat2 | 0 | 1 | 2.098292592 | 0.049526436 | 0.079625403 | 0.988780451 |
| ENSMUSG00000057719 | Sh3rf2 | 0 | 1 | 7.384122993 | 0.000391975 | 0.420740201 | 1 |
| ENSMUSG00000067006 | Serpinb5 | 0 | 1 | 10.55238268 | 8.74853E-05 | 3.831192824 | 0.646732913 |

| | Radiation_QHII_vs_Untreated_log2FoldChange | Radiation_QHII_vs_Untreated_padj | Radiation_QHII_vs_QHII_log2FoldChange | Radiation_QHII_vs_QHII_padj | Radiation_QHII_vs_Radiation_log2FoldChange | Radiation_QHII_vs_Radiation_padj |
|---|---|---|---|---|---|---|
| ENSMUSG00000004814 | 2.26116435 | 0.352438728 | -1.537385939 | 1 | -1.220494297 | 0.668621239 |
| ENSMUSG00000005268 | 1.073524536 | 0.760473829 | -2.658345415 | 1 | -1.872910482 | 0.49662579 |
| ENSMUSG00000005824 | 0.201369712 | 0.912854511 | -0.415272113 | 1 | -1.36484929 | 0.399302834 |
| ENSMUSG00000008999 | 6.479470079 | 0.002857265 | 4.781176182 | 0.027507453 | -0.276987806 | 0.96970304 |
| ENSMUSG00000009185 | 1.074068765 | 0.280286983 | 0.295298287 | 1 | -0.247429312 | 0.834924255 |
| ENSMUSG00000017057 | 0.248801941 | 0.734452385 | 0.238038043 | 1 | -0.484956627 | 0.443270545 |
| ENSMUSG00000020007 | 4.499058374 | 0.056848119 | 4.656248273 | 0.022877086 | -1.382795233 | 0.712438297 |
| ENSMUSG00000020122 | 1.634735872 | 0.080087288 | 0.539400488 | 1 | -1.486180803 | 0.296760882 |
| ENSMUSG00000021508 | 1.114856909 | 0.418975056 | -0.330621707 | 1 | -1.030472345 | 0.426486952 |
| ENSMUSG00000023078 | 2.118857596 | 0.261828244 | 0.242607531 | 1 | -1.097827585 | 0.526495635 |
| ENSMUSG00000023915 | 0.192415743 | 0.886424041 | -0.225703321 | 1 | -0.934237458 | 0.416468038 |
| ENSMUSG00000024379 | 2.245177888 | 0.06389603 | 1.063370045 | 1 | -0.314392104 | 0.909273509 |
| ENSMUSG00000024620 | 0.338781174 | 0.655228172 | 0.341983709 | 1 | -0.502342817 | 0.49334485 |
| ENSMUSG00000024621 | 0.574415724 | 0.397017313 | 0.126696665 | 1 | -0.8814656 | 0.172917065 |
| ENSMUSG00000026072 | 1.010133928 | 0.357479451 | 0.448747731 | 1 | -0.919185248 | 0.445567405 |
| ENSMUSG00000026073 | 1.684901957 | 0.060734467 | 1.605499896 | 0.135047512 | -0.608634638 | 0.749394539 |
| ENSMUSG00000026180 | 2.594930527 | 0.266023881 | 1.146293518 | 1 | 0.084846499 | 1 |
| ENSMUSG00000027358 | 1.059982997 | 0.448558788 | 0.122804191 | 1 | -0.795925682 | 0.66526418 |
| ENSMUSG00000027399 | 1.019475298 | 0.50888636 | 0.813384768 | 1 | -0.645422583 | 0.731293219 |
| ENSMUSG00000027947 | 0.753957433 | 0.457810889 | 0.359905827 | 1 | -0.707939067 | 0.581689305 |
| ENSMUSG00000028019 | 1.33179276 | 0.257419242 | 0.398956658 | 1 | -0.571771771 | 0.730834404 |
| ENSMUSG00000028599 | 0.447818864 | 0.613765246 | 0.10792457 | 1 | -0.423999508 | 0.637305124 |
| ENSMUSG00000029231 | 1.347628982 | 0.13616093 | 0.679812302 | 1 | -1.176237559 | 0.27237074 |
| ENSMUSG00000030748 | 0.299879166 | 0.686563836 | 0.113961993 | 1 | -0.859898283 | 0.082394284 |
| ENSMUSG00000031380 | 1.267733527 | 0.507242318 | 0.071495216 | 1 | -1.51050746 | 0.344439448 |
| ENSMUSG00000032440 | -0.041296695 | 0.962843689 | 0.042265727 | 1 | -0.661446777 | 0.156828295 |
| ENSMUSG00000034394 | 1.037717277 | 0.400472527 | 0.622095471 | 1 | -0.352210066 | 0.872186668 |
| ENSMUSG00000035448 | 0.795010111 | 0.874174778 | -0.713501316 | 1 | -1.397216568 | 0.444219813 |
| ENSMUSG00000037944 | 0.753253687 | 0.54467461 | 0.382475495 | 1 | -0.914060493 | 0.506856611 |
| ENSMUSG00000039760 | 6.888999358 | 0.024320261 | 6.96409912 | 0.036797118 | 0.453624121 | 0.92834049 |

| | Radiation_QHII_vs_Untreated_log2FoldChange | Radiation_QHII_vs_Untreated_padj | Radiation_QHII_vs_QHII_log2FoldChange | Radiation_QHII_vs_QHII_padj | Radiation_QHII_vs_Radiation_log2FoldChange | Radiation_QHII_vs_Radiation_padj |
|---|---|---|---|---|---|---|
| ENSMUSG00000043088 | 0.541016717 | 0.832265027 | -0.006868196 | 1 | -1.946919936 | 0.334531692 |
| ENSMUSG00000044244 | 1.526731043 | 0.075832435 | 1.53261208 | 0.232411342 | -1.248991958 | 0.525466648 |
| ENSMUSG00000044337 | 0.290725109 | 0.798051836 | -0.272761228 | 1 | -0.910056952 | 0.394716822 |
| ENSMUSG00000049103 | 0.52495957 | 0.623465151 | -0.0349283 | 1 | -0.657586662 | 0.55104014 |
| ENSMUSG00000054263 | 0.921323551 | 0.321679172 | 0.136296081 | 1 | -0.757990949 | 0.496266767 |
| ENSMUSG00000055737 | 0.203776667 | 0.880967345 | -1.024944371 | 1 | -1.019311058 | 0.32453557 |
| ENSMUSG00000057722 | 1.204868045 | 0.516482098 | 0.523691606 | 1 | -2.28184957 | 0.242631749 |
| ENSMUSG00000059201 | 0.37740559 | 0.93633692 | -2.767992521 | 0.826230966 | -2.671205329 | 0.255464542 |
| ENSMUSG00000061353 | 0.829701375 | 0.349211832 | 0.200803307 | 1 | -1.202616018 | 0.040183675 |
| ENSMUSG00000062960 | -0.000488757 | 1 | -0.182344129 | 1 | -0.689959106 | 0.312631184 |
| ENSMUSG00000071713 | 0.261167086 | 0.783267596 | -0.271317891 | 1 | -0.944487477 | 0.210540246 |
| ENSMUSG00000071714 | 0.311323266 | 0.779588611 | -0.073460466 | 1 | -0.852850231 | 0.433603253 |
| ENSMUSG00000003032 | 1.696623658 | 0.007399836 | 0.912625811 | 1 | -1.070790201 | 0.399302834 |
| ENSMUSG00000005251 | 6.426983696 | 6.37241E-05 | 3.471626337 | 0.257496234 | -0.83436111 | 0.863258207 |
| ENSMUSG00000012350 | 3.304329126 | 0.185572868 | 1.491968189 | 1 | -0.687129423 | 0.893556906 |
| ENSMUSG00000016028 | 1.81939874 | 0.219152348 | 1.570815239 | 0.731262924 | -1.515210282 | 0.512797269 |
| ENSMUSG00000017144 | 0.143416513 | 0.899468721 | -0.014830993 | 1 | -0.802604369 | 0.365073221 |
| ENSMUSG00000019851 | 6.522659262 | 4.98586E-10 | 6.247082675 | 4.51557E-09 | -0.76441502 | 0.851078923 |
| ENSMUSG00000020042 | 1.762264422 | 0.428626871 | 0.690784373 | 1 | -2.126320923 | 0.381079049 |
| ENSMUSG00000020176 | 1.285659626 | 0.141293204 | 0.247995761 | 1 | -0.516715234 | 0.707146396 |
| ENSMUSG00000020961 | 1.266942535 | 0.529617194 | 0.298749951 | 1 | -1.688742092 | 0.424125647 |
| ENSMUSG00000022382 | 3.209773189 | 0.089575431 | 2.076828681 | 1 | -1.428370039 | 0.729582023 |
| ENSMUSG00000022479 | 2.442647245 | 0.070527244 | 2.717762614 | 0.08585214 | -0.922401942 | 0.756856791 |
| ENSMUSG00000025105 | 7.76036081 | 0.001988321 | 6.274775943 | 0.010577053 | -1.271035542 | 0.788057764 |
| ENSMUSG00000026167 | 4.267910793 | 0.024291355 | 3.920400482 | 0.11068318 | -0.982590631 | 0.815141303 |
| ENSMUSG00000026413 | 8.876462828 | 1.32954E-07 | 6.720400682 | 0.000113655 | -1.249170302 | 0.759502348 |
| ENSMUSG00000026589 | 0.686179738 | 0.711889399 | -0.434011965 | 1 | -1.515530888 | 0.328735467 |
| ENSMUSG00000026971 | 3.55291644 | 0.049168281 | 1.890323425 | 1 | -1.322920943 | 0.661354113 |
| ENSMUSG00000027356 | 8.435123182 | 0.000694616 | 4.989040278 | 0.10092584 | -0.490096558 | 0.939931147 |
| ENSMUSG00000029026 | 4.165160154 | 0.061002054 | 7.014039527 | 0.005846923 | -0.894527688 | 0.85290866 |

**5. 1. 9 Cook Lab Compounds Data Summary for TA-III-50, TA-III-52, TA-III-56, TA-III-62**

Cell Viability Studies by Dr. Laura Kallay

| Compound | $IC_{50}$ range (n = 3 unless noted) |
|---|---|
| QH-II-66 | 4.0 – 6.1 μM (n = 6) |
| TA-III-50 | 35.9 – 48.9 μM |
| TA-III-52 | 28.7 – 38.2 μM |
| TA-III-56 | 36.1 – 43.0 μM |
| TA-III-62 | 144.3 – 297.2 μM |
| TI-04-74 | 43.9 – 63.2 μM |
| CD3-QH-II-66 | 5.72 μM (n = 1) |

QH-II-66

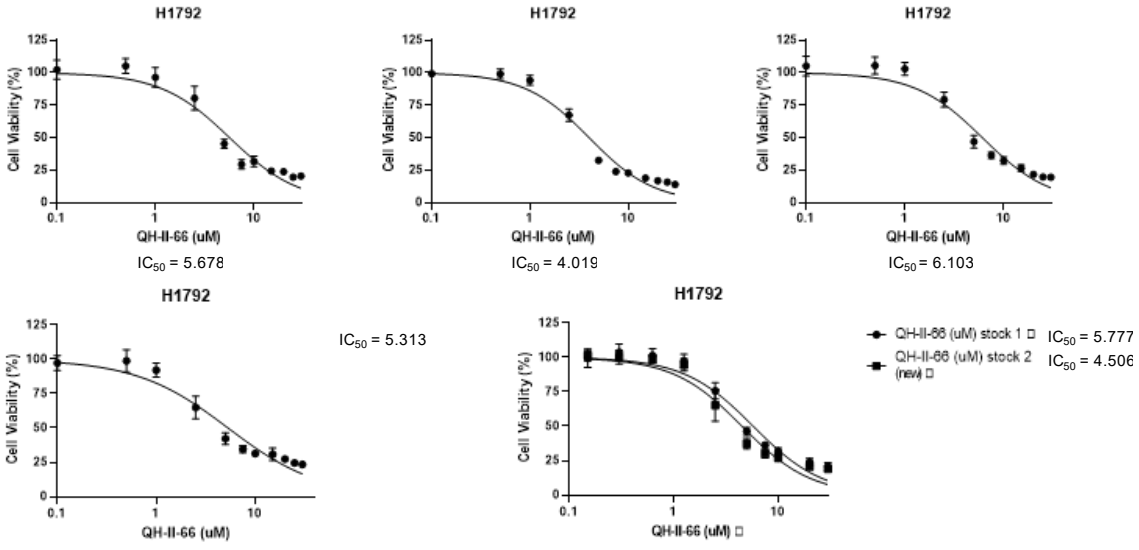

# TA-III-50

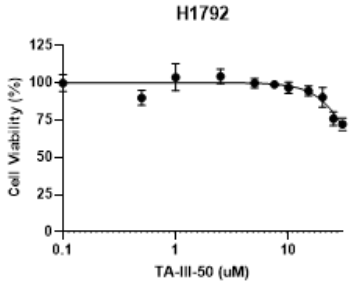


$IC_{50}$ = 41.66

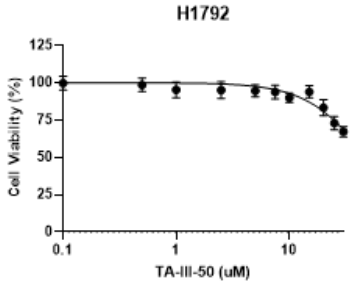


$IC_{50}$ = 48.91

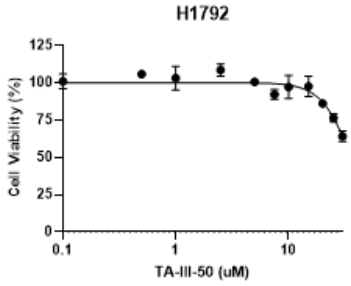


$IC_{50}$ = 35.91

# TA-III-52

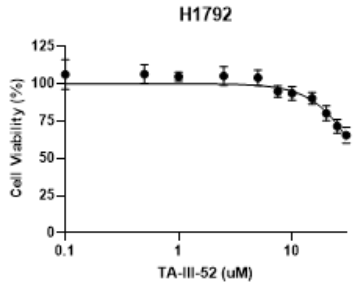


$IC_{50}$ = 38.19

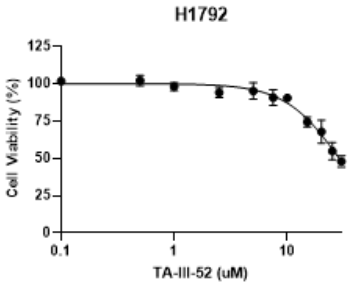


$IC_{50}$ = 28.72

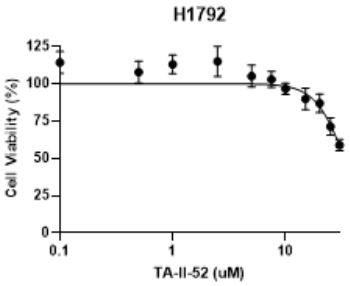


$IC_{50}$ = 33.33

# TA-III-56

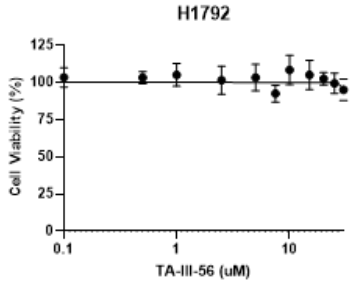


$IC_{50}$ = 36.53

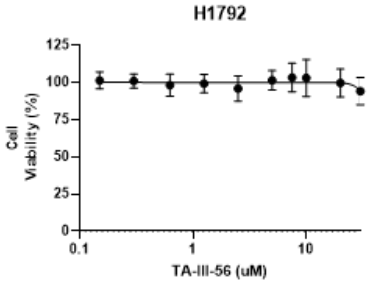


$IC_{50}$ = 43.03

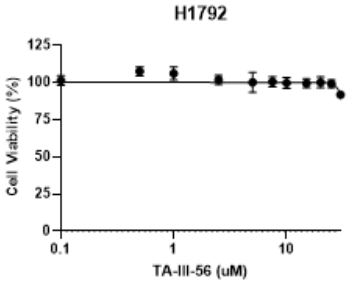


$IC_{50}$ = 36.14

# TA-III-62

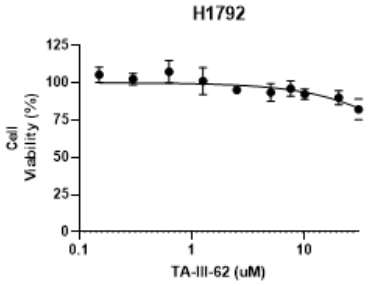


$IC_{50}$ = 144.3

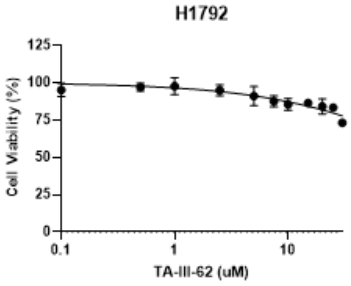


$IC_{50}$ = 240.0

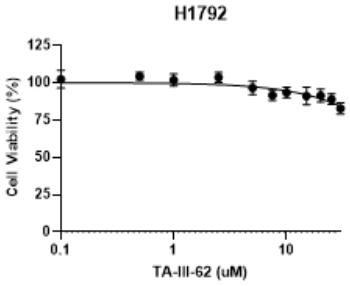


$IC_{50}$ = 148.1

# IT-04-75

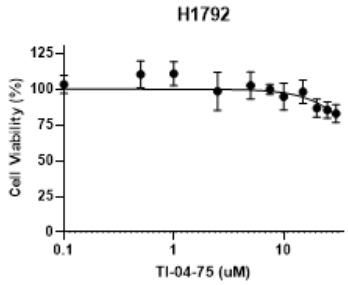


$IC_{50}$ = 63.52

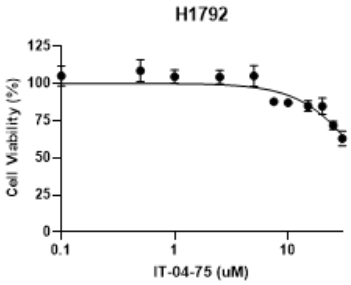


$IC_{50}$ = 43.94

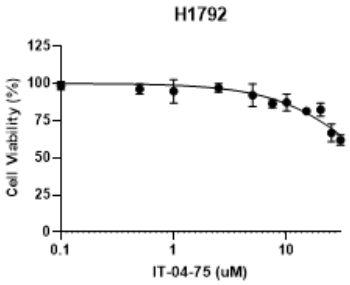


$IC_{50}$ = 53.22

# $CD_3$-QH-II-66

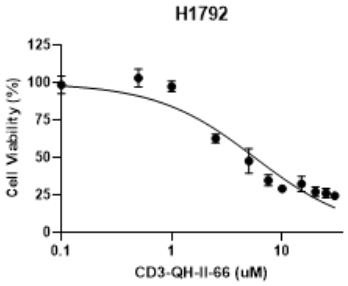


$IC_{50}$ = 5.715

Batch: MYM-III-85-1

# Assessment of new compounds in H1792 cells

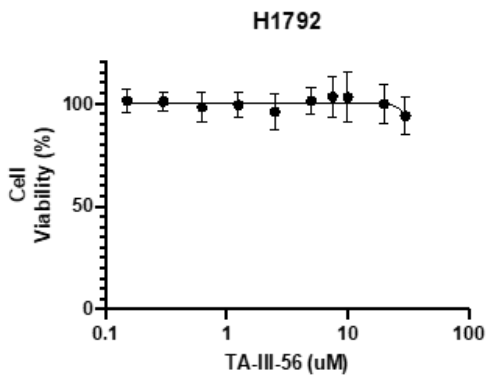


est. $IC_{50}$ = 43.03 μM

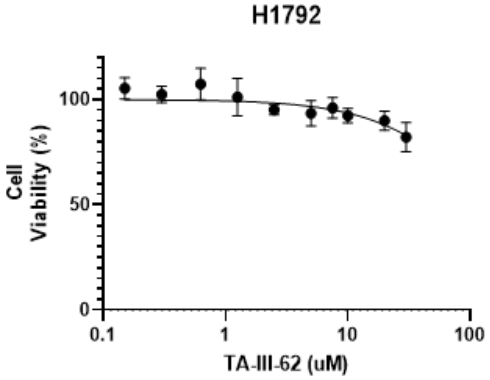


est. $IC_{50}$ = 144.3 μM

# Evaluation of new QH-II-66 stock in H1792 cells

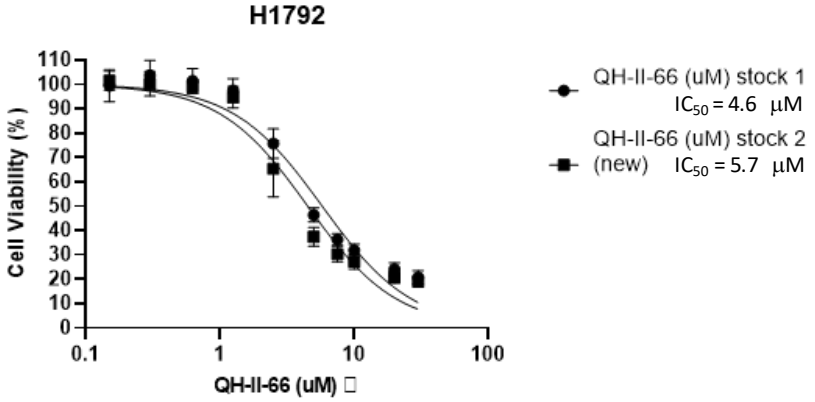

**5. 1. 10 Data of lead compounds and their metabolites on cancer cell lines.**

| MTS Assay of Cook Compounds – Set 1<br>Pilot IMF of GBM cell lines | | | |
|---|---|---|---|
| | Compound | Structure | Compounds sent by |
| 1 | QH-II-66 | 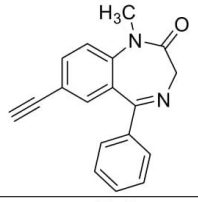 | Taukir- |
| 2 | MYM-III-85 | 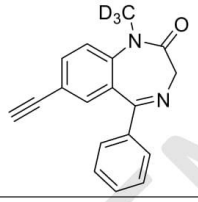 | Yeunus |
| 3 | TA-III-72 | 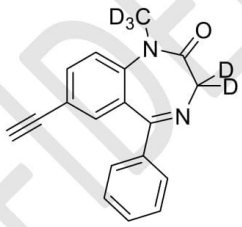 <br>TA-III-72 | Taukir |
| 5 | KRM-III-70 | 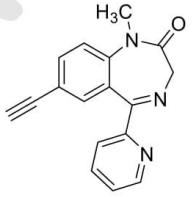 | Dishary |
| 6 | NOR-KRM-III-70 | 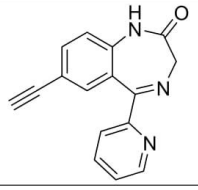 | Dishary |

| | | | |
|---|---|---|---|
| 7 | TA-III-70 | 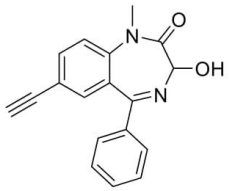 | Taukir |
| 8 | MYM-I-43 | 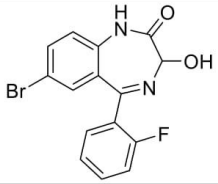 | Yeunus |
| 9 | MYM-I-59 | 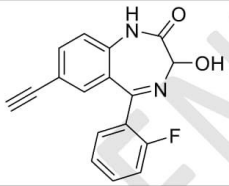 | Yeunus |
| 10 | MYM-IV-95 | 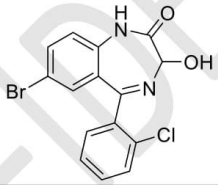 | Yeunus |
| 11 | MYM-V-17 | 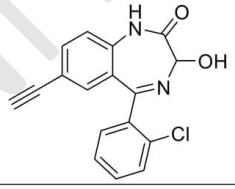 | Yeunus |

**$IC_{50}$ summary for new benzodiazepines in H1792**

| Compound | $IC_{50}$ (μM) | $IC_{50}$ Range (μM) |
|---|---|---|
| QH-II-66 | 6.027 | 6.027 – 6.563 |
| MYM-III-85 | 6.644 | 5.903 – 7.460 |
| TA-III-72 | 5.741 | 5.069 – 6.483 |
| KRM-III-70 | 5.240 | 4.474 – 6.107 |
| NOR-KRM-III-70 (n = 2) | 39.93, 43.91 | 34.56 – 49.27 |
| TA-III-70 | 660.2 | 100.3 – 212,771 |
| MYM-I-43 | 95.70 | 63.19 – 179.3 |
| MYM-I-59 | 3.320e+35 | infinity - infinity |
| MYM-IV-95 | 694.9 | 391.8 - 2643 |
| MYM-V-17 | 20.32 | 18.01 – 22.97 |

**IC50 Values of Cancer compounds on different cell lines**

| SL | Compound Code | IC50 values on different cell lines (µM) | | | |
|---|---|---|---|---|---|
| | | Lung Cancer H1792 | Medulloblastoma G3 D283 | Melanoma Cell lines | |
| | | | | A375 | B16F10 |
| | QH-II-066 | 6.027, 4-6.1 | 3.4 | 2.7 | 8.2 |
| | KRM-III-70 | 5.240 | | | |
| | KRM-II-08 | | 0.8 | | |
| | KRM-III-77 | | 16.3 | | |
| | NOR- QH-II-066 | | 0.51 | | |
| | NOR-KRM-III-70 | 34.5-49.27 | 12.46 | | |
| | NOR-KRM-II-08 | | 0.85 | | |
| | NOR-KRM-III-77 | | 14.97 | | |
| | TA-III-50 | 35.9-48.9 | | | |
| | TA-III-52 | 28.7-38.2 | | | |
| | TA-III-56 | 36.1-43.0 | | | |
| | TA-III-62 | 144.3-297.2 | | | |
| | TI-IV-04 | 43.9-63.2 | | | |
| | TA-III-70 | 660.2 | | | |
| | TA-III-72 | 5.74 | | | |
| | MYM-III-85 | 6.644 | | | |
| | MYM-I-43 | 95.7 | | | |
| | MYM-I-59 | 3.32E+35 | | | |
| | MYM-IV-95 | 694.9 | | | |
| | MYM-V-17 | 20.32 | | | |
| | SH-I-75 | | | | |
| | Diazepam | | | | |

**MTS Analysis of Cook Compounds – Set 1A**

**TA-III-72**

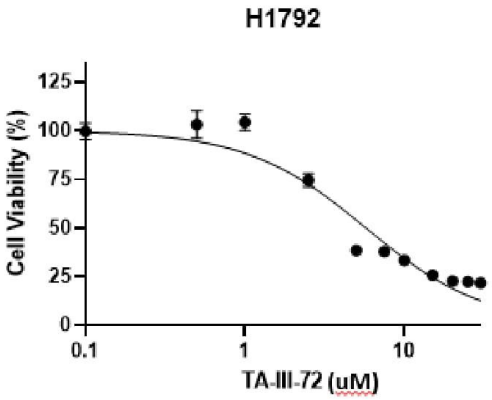


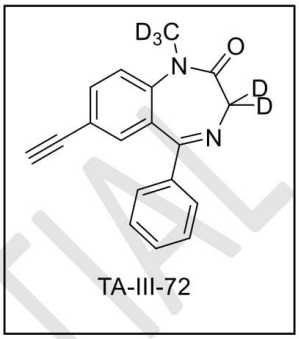


| | |
|---|---|
| $IC_{50}$ | 5.741 |
| 95% CI (profile likelihood) | 5.069 to 6.483 |

TA-III-72 has 5 deuteriums including an N-$CD_3$ with 2 deuteriums in C-3 position

**MYM-III-85**

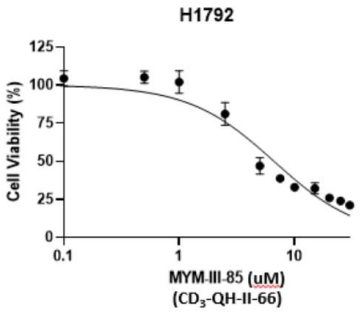


6.644

5.903 to 7.460

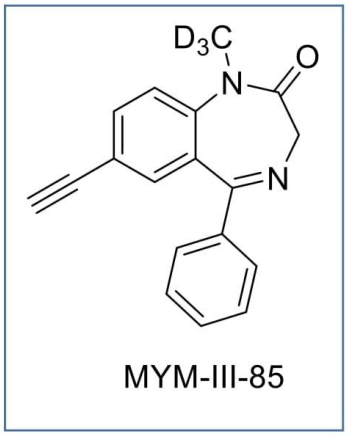


MYM III 85 has only N-$CD_3$

**QH-II-066**

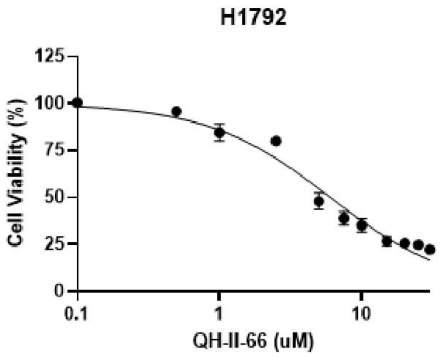


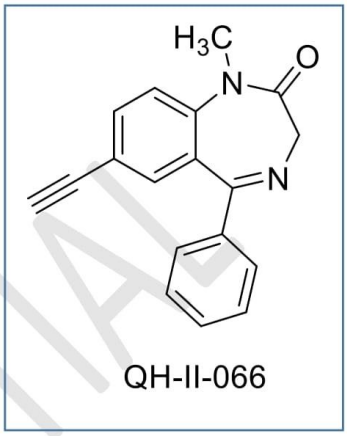


6.027

5.523 to 6.563

**KRM-III-70**

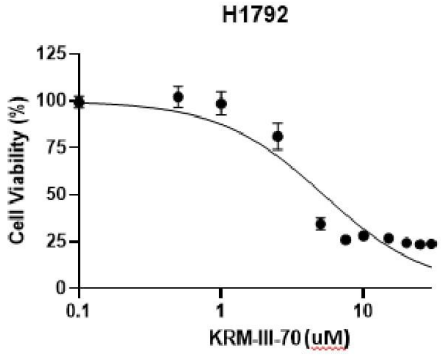


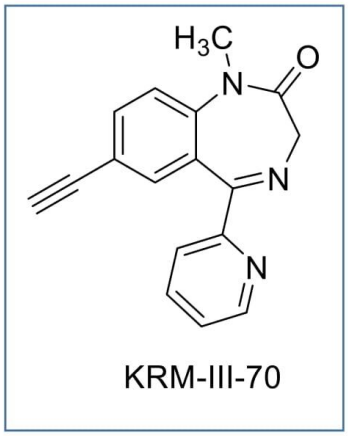


$IC_{50}$ 5.240

95% CI (profile likelihood) 4.474 to 6.107

**Nor-KRM-III-70**

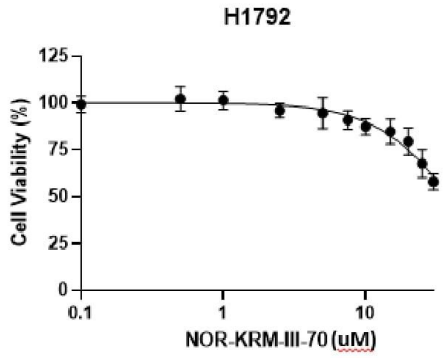


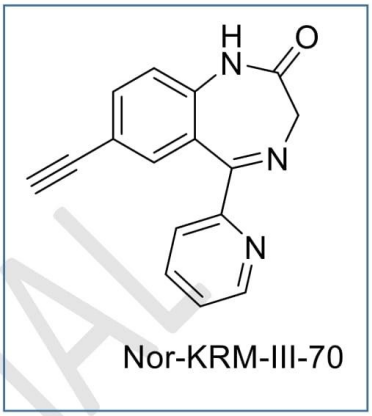


39.93

34.56 to 49.27

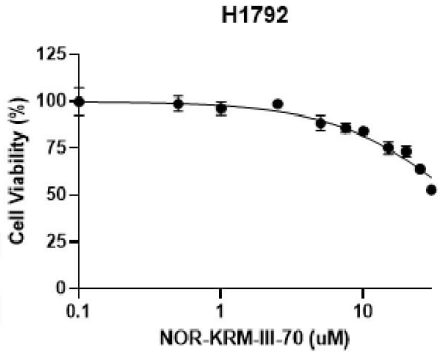


43.91

40.48 to 48.01

**TA-III-70**

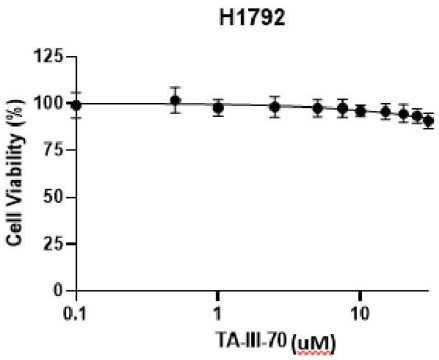


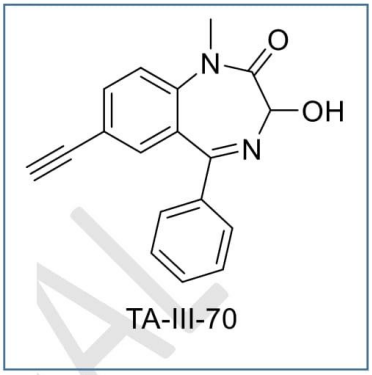


| | |
|---|---|
| $IC_{50}$ | 660.2 |
| 95% CI (profile likelihood) | 100.3 to 212771 |

**MYM-I-43**

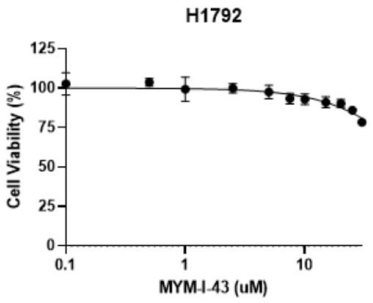


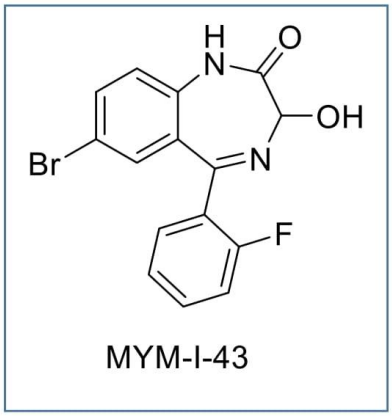


| | |
|---|---|
| $IC_{50}$ | 95.70 |
| 95% CI (profile likelihood) | 63.19 to 179.3 |

**MYM-I-59**

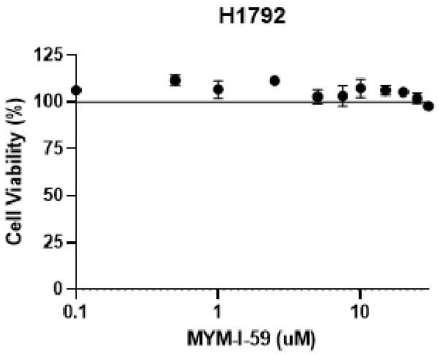


3.320e+035

-infinity to +infinity

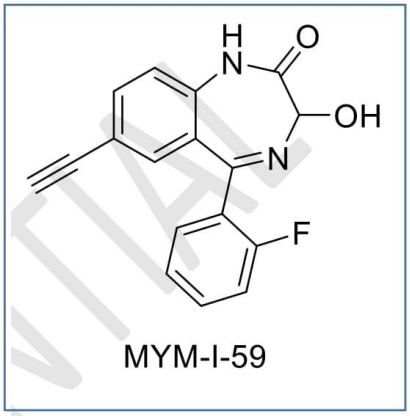


MYM-I-59

**MYM-IV-95**

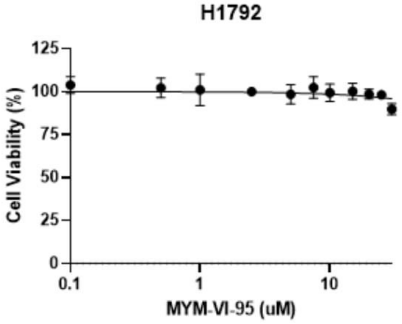


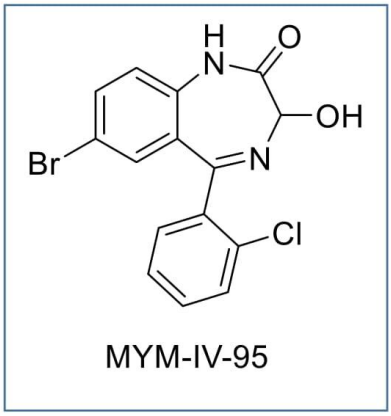


MYM-IV-95

| | |
|---|---|
| $IC_{50}$ | 694.9 |
| 95% CI (profile likelihood) | 391.8 to 2643 |

**MYM-V-17**

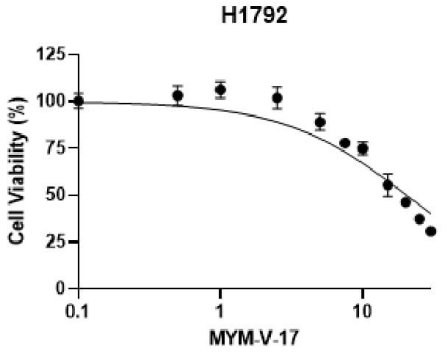


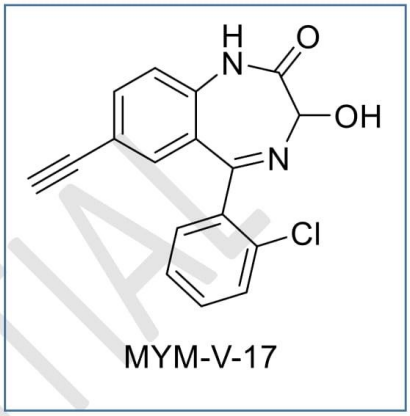


20.32

18.01 to 22.97



The IC50 values of QH-II-066 (6.027 µM) and MYM-III-85 (6.644 µM) are almost similar, TA-III-72 (5.741 µM) and KRM-III-70 (5.24 µM) also showed similar IC50 values. Among all these four compounds, KRM-III-70 showed little better activity. The structures are as follows

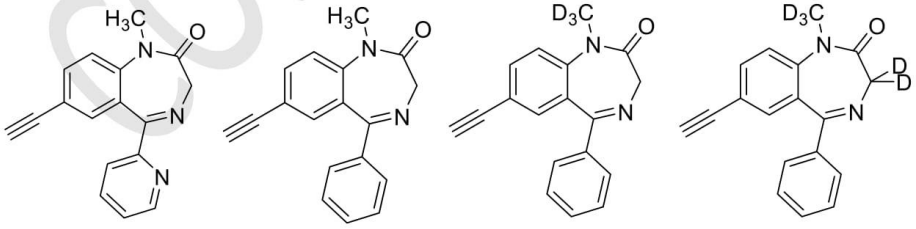

All these compounds have N-methyl group. Another compound MYM-V-17 also showed little good activity with IC50 value 20.3 µM. This compound does not have N-methyl, it has N-H. If we follow the trend and incorporate methyl group, then the N-methyl version of MYM-V-17 might be more active than any one of these compounds. The reason I am saying this because of the IC-50 values of KRM-III-70 and NOR-KRM-III-70.

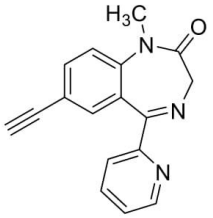


KRM-III-70

IC50 = 5.24 µM

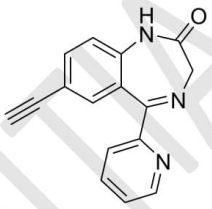


NOR-KRM-III-70

IC50 = 39.93 µM

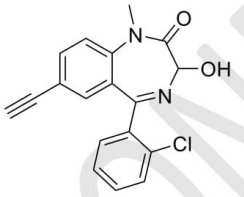


If we put N-methyl

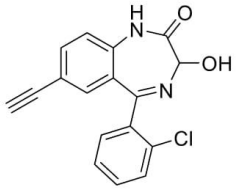


MYM-V-17

IC50= 20.32µM

Might more active compound
Than any of other active compounds

This H1792 is a lung cancer stage 4 cell line. Previously we have done cell viability assay of D283 which is medulloblastoma and A375 cell line which is malignant melanoma. QH II 66 is the only compound, we have data for all three cell lines. KRM III 70 increased metastases on D283 cell line but decreased on H1792 cell line*.

**Journal of Neuro-Oncology* (2019) 142:411–422

## 5. 2 Patent Disclosures:

### 5. 2. 1 Brain Penetrant Chemosensitizer to Treat Lung Cancer & Small brain penetrant molecule to potentiate TMZ for glioblastoma

**UWM Research Foundation** July 6, 2021

***Background Art Search REPORT***

Title: Brain Penetrant Chemosensitizer to Treat Lung Cancer & Small brain penetrant molecule to potentiate TMZ for glioblastoma

Inventor(s): James Cook, Soma Sengupta, Taukir Ahmed, Daniel Krummel, Debanjan Bhattacharya, Donatien Kamdem Toukam, Aniruddha Karve, Laura Kelly

OTT Matter: 1752 and 1753

Reviewer: Erin Puro

*This report is intended to provide information surrounding the technology and any discussion within the background art report in no way should be considered an admission that the discussed background art is prior art.*

A. SUBJECT MATTER

General Technology Description:

Non-small cell lung cancer (NSCLC) accounts for a majority (80%-85%) of lung cancer cases. The most common NSCLC histological subtype (40-50%) is lung adenocarcinoma. A great majority of NSCLC patients with advanced stage of the disease face local and/or distant recurrences, including metastasis to the brain, in the first 2 years after the completion of primary treatment. More effective therapies are needed to boost tumor control, prevent metastasis, and improve overall survival while mitigating side-effects.

We find that Type-A GABA neurotransmitter receptors (GABAARs) are expressed in not only cancers of the central nervous system, but also systemic cancers. In previous studies we reported that by activating GABAAR function and signaling with a new class of benzodiazepine analogs, tumor cells can be sensitized to radiation resulting in significant tumor regression in mouse models of medulloblastoma and melanoma (1-4). Our analysis of patient data has revealed that GABAAR expression is present in both lung adenocarcinoma and squamous carcinoma subtypes. Leveraging this finding, we have investigated if potentiating GABAAR in lung adenocarcinoma cells with a novel benzodiazepine analog called QH-II-066 as well as other compounds of similar structure can impair tumor growth. We find that QH-II-066 treatment induces apoptosis in patient-derived adenocarcinoma cells. We also find that QH-II-066 synergistically can potentiate the chemotherapeutic docetaxel, even at an ineffective dose. We have generated a flank xenograft mouse model using patient derived adenocarcinoma cells to evaluate the efficacy of QH-II-066 and will utilize this model to evaluate the ability of QH-II-066 to sensitize tumor cells to docetaxel such that this drugs toxicity profile is reduced while it retains its potency. Our long-term goal is to establish that the novel benzodiazepine analog QH-II-066 can function to potentiate chemotherapeutic for treatment of NSCLC, thereby increasing its effectiveness and mitigating toxic side-effects.

Invention Features Seeking Protection:

GABAAR structure-function. GABA receptors (GABAARs) form pentameric chloride (Cl-) channels, composed most commonly of two α, two β, and γ subunits encoded by GABR genes GABRA (1-6), GABRB (1-3), and GABRG (1-3), respectively (7,8) (Fig. 1a). GABAARs are fundamental in determining an excitation/inhibition balance in the central nervous system. As a receptor mediating Cl- flux, GABAARs predominantly function to hyperpolarize neural cells, following binding of its ligand GABA (Fig. 1b).

GABAAR activation. GABAARs have been an important therapeutic target since the clinical introduction of benzodiazepines in the 1960s. Benzodiazepines bind at the γ-α interface of GABAAR (Fig. 1a) and act to increase effectiveness of GABA and thus enhance Cl- flux (Fig. 1b). FDA approved benzodiazepines consist most commonly of fusion of diazepine and benzene rings (1,4-benzodiazepine) and a phenol ring (5-phenyl-1H-benzo[e]) (Fig. 1c). J. Cook and his team (Univ. Wisconsin-Milwaukee) introduced an ethinyl bond at R7 in place of a chlorine in Valium (Fig. 1c). which confers anti-cancer activity.

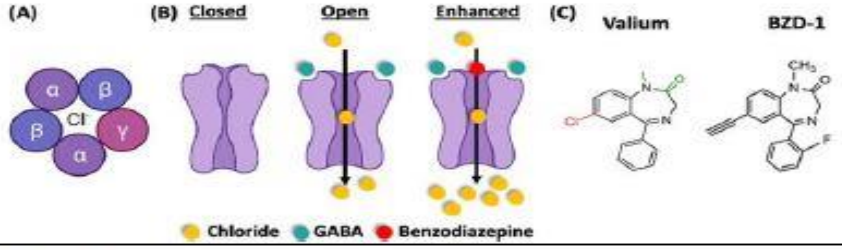


Page 1 v.14b

Potential Areas of Application:

Healthcare & Cancer tumor treatment

Inventor Provided Background Art:

1. Sengupta S., Weeraratne S.D., Sun H, Phallen J., Rallapalli S.K., Teider N., Kosaras B., Amani V., Pierre-Francois J., Tang Y., Nguyen B., Yu F., Schubert S., Balansay B., Mathios D., Lechpammer M., Archer T.C., Tran P., Reimer R.J., Cook J.M., Lim M., Jensen F.E., Pomeroy S.L., Cho Y.J. (2014). a5-GABAA receptors negatively regulate MYC-amplified medulloblastoma growth. Acta Neuropathol. 127: 593-603.
2. Jonas O., Calligaris D., Methuku K.R. Poe M.M., Francois J.P., Tranghese F., Changelian A., Sieghart W., Ernst M., Krummel D.A., Cook J.M., Pomeroy S.L., Cima M., Agar N.Y., Langer R., Sengupta S. (2016). First in vivo testing of compounds targeting Group 3 medulloblastomas using an implantable microdevice as a new paradigm for drug development. J. Biomed. Nanotech. 12(6): 1297-302.
3. Kallay L., Keskin H., Ross A., Rupji M., Moody O.A., Li G., Ahmed T., Rashid R., Stephen M.R., Cottrill K.A., Nuckols A., Zu M., Martinson D.E., Tranghese F., Wang X., Taylor M., Cook J., Kowalski J., Jenkins A., Pomeranz Krummel D., Sengupta S. (2019). Modulating native GABAA receptors in cancer cells with positive allosteric benzodiazepine-derivatives induces cell death. J. Neuro-Oncol. 142: 411-422.
4. Pomeranz Krummel D.A., Nasti T.H., Izar B., Press R.H., Xu M., Lowder L., Kallay L., Rupji M., Rosen H., Su J., Curran W., Olson J., Weinberg B., Schniederjan M., Neill S., Lawson D., Kowalski J., Khan M.K., Sengupta S. (2020). Impact of sequencing radiation therapy and immune checkpoint inhibitors in the treatment of melanoma brain metastases. International J. Radiation Oncology, Biology, Physics. 108(1): 157-163.

Debanjan Bhattacharya, Kamdem Donatien Toukam, Laura Kallay, Vaibhavkumar Gawali, Mario Medvedovic, Riccardo Barrile Daniel A Pomeranz Krummel, Soma Sengupta

## B. SOURCES AND FIELDS SEARCHED

| *Scientific Literature:* | *Patent Databases:* |
|---|---|
| Scientific and Technical Databases<br>☒ Google Scholar<br>☐ Other:<br>General Web Search<br>☒ List search engine(s): Google | Innography (All sources)<br>☐ USPTO<br>☒ Google Patents<br>☐ International Patents |

Key Phrases and Keywords Searched:

benzodiazepines + TMZ + glioblastoma
benzodiazepines + DTX + lung cancer

## C. SEARCH RESULTS AND FINDINGS

### Patents

**USES OF RADIATION AND BENZODIAZEPINE DERIVATIVES IN CANCER THERAPIES**, PCT/US2020/034169A1, EMORY UNIVERSITY, 22 May 2020 (22.05.2020)

This disclosure relates to uses of radiation and benzodiazepines optionally in combination with other anticancer agents for treating cancer. In certain embodiments, this disclosure relates to methods of using radiation, benzodiazepines, and check point inhibitors in cancer therapies.

**Mention of radiation and benzodiazepine use for cancer therapy.**

**POTENTIATION OF ANTI-CANCER ACTIVITY THROUGH COMBINATION THERAPY WITH BER PATHWAY INHIBITORS**, PCT/US2011/032762, Tracon Pharmaceuticals, Inc., 15.04.2011

The disclosure generally relates to pharmaceutical compositions and methods for the treatment of certain cancers. Provided herein are pharmaceutical compositions and methods of treating cancer wherein the cytotoxic activity of an anticancer agent or radiation therapy is potentiated by the combination with base excision repair (BER) pathway inhibitors, such as methoxyamine and PARP inhibitors.

Cancer is a worldwide problem. As such, finding compositions and methods for the treatment of cancer is of vital interest. The treatment of cancer falls into three general categories: chemotherapy, radiation therapy, and surgery. Frequently, therapies are combined since a combination of therapies often increases the probability that the cancer will be eradicated as compared to treatment strategies utilizing a single therapy. Most typically, the surgical excision of large tumor masses is followed by chemotherapy and/or radiation therapy.

Chemotherapeutic anticancer agents work in a number of ways. For example, anticancer agents work by interfering with cell cycle progression or by generating DNA strand breaks. If the cancer cell is not able to overcome the cell cycle blockage or cell injury, the cell will often die via apoptotic mechanisms. However, in certain instances cancer cells develop resistance to anticancer agents, which results either in the renewed spread of the cancer and/or the requirement for higher dosages of the anticancer agent, which in some instances is toxic to the patient.

**Mention of radiation therapy for cancer treatment.**

## Publications

> **HERRLINGER**, "Lomustine-temozolomide combination therapy versus standard temozolomide therapy in patients with newly diagnosed glioblastoma with methylated MGMT promoter (CeTeG/NOA–09): a randomised, open-label, phase 3 trial," Lancet 2019; 393: 678–88

Background There is an urgent need for more effective therapies for glioblastoma. Data from a previous unrandomised phase 2 trial suggested that lomustine-temozolomide plus radiotherapy might be superior to temozolomide chemoradiotherapy in newly diagnosed glioblastoma with methylation of the MGMT promoter. In the CeTeG/NOA-09 trial, we aimed to further investigate the effect of lomustine-temozolomide therapy in the setting of a randomised phase 3 trial.
Methods In this open-label, randomised, phase 3 trial, we enrolled patients from 17 German university hospitals who were aged 18–70 years, with newly diagnosed glioblastoma with methylated MGMT promoter, and a Karnofsky Performance Score of 70% and higher. Patients were randomly assigned (1:1) with a predefined SAS-generated randomisation list to standard temozolomide chemoradiotherapy (75 mg/m² per day concomitant to radiotherapy [59–60 Gy] followed by six courses of temozolomide 150–200 mg/m² per day on the first 5 days of the 4-week course) or to up to six courses of lomustine (100 mg/m² on day 1) plus temozolomide (100–200 mg/m² per day on days 2–6 of the 6-week course) in addition to radiotherapy (59–60 Gy). Because of the different schedules, patients and physicians were not masked to treatment groups. The primary endpoint was overall survival in the modified intention-to-treat population, comprising all randomly assigned patients who started their allocated chemotherapy. The prespecified test for overall survival differences was a log-rank test stratified for centre and recursive partitioning analysis class. The trial is registered with ClinicalTrials.gov, number NCT01149109.

**Mention of temozolomide therapy with glioblastoma.**

> **BOGGS**, "**Strategies to Prevent Brain Metastasis in High-Risk Non–Small-Cell Lung Cancer: Lessons Learned From a Randomized Study of Maintenance Temozolomide Versus Observation**," Clinical Lung Cancer, Volume 15, Issue 6, November 2014, Pages 433-440

This study investigated whether maintenance temozolomide (TMZ) after definitive therapy for locally advanced non–small-cell lung cancer (NSCLC) could decrease the incidence of brain metastasis (BM).

Eligible patients included those with stage IIIA, IIIB, or IV (for stage IV, only with malignant pleural/pericardial effusion) NSCLC with no BM at diagnosis and stable disease, partial response, or complete response after first-line chemotherapy using at least 2 agents. Patients were randomized to observation or TMZ (75 mg/m2 for 21 consecutive days followed by a 7-day rest for up to 6 cycles or progression). The primary end point was incidence of radiographically diagnosed BM within 12 months from day 1 of first-line chemotherapy. Secondary end points included overall survival (OS), time to progression, incidence of BM at first progression, and toxicity.

The study was closed early on the basis of a futility analysis; 45 of 53 enrolled patients were evaluable from an original target of 100. No difference was noted in the incidence of BM at 1 year in the TMZ and observation groups (18% and 13%, respectively), in median time to progression (11.7 and 10.7 months, respectively), or in median OS (27.1 and 22.5 months, respectively). Common Terminology Criteria for Adverse Events grade 3 or 4 adverse events were 46% in the TMZ group and 19% in the observation group.

TMZ monotherapy does not appear to decrease the incidence of BM in patients with locally advanced NSCLC. These results considered in the context of the existing literature have implications for future clinical trial design.

**Mention of temozolomide therapy for treating lung cancer.**

> **Laura Kallay, Alexandra Ross, Olivia Moody, Guanguan Li, James Cook, Tobey MacDonald, Andrew Jenkins, Daniel Pomeranz Krummel, and Soma Sengupta**, "PATH-50. UNDERSTANDING THE MECHANISM OF BENZODIAZEPINE MEDIATED CELL DEATH IN GABRA5 OVEREXPRESSING GROUP 3 MEDULLOBLASTOMAS," Winship Cancer Institute, Emory, University Hospital, Atlanta, GA, USA, 2Department of Pharmacology, Emory School of Medicine, Atlanta, GA, USA, 3Departments of Chemistry, University of Wisconsin-Milwaukee, Milwaukee, WI, USA, 4Department of Pediatrics, Children's Hospital of Atlanta, Atlanta, GA, 2017

Medulloblastoma (MB) is a common pediatric malignant primary brain tumor originating in the posterior fossa. MB is generally classified into one of four molecular subgroups: Wnt, Shh, Group 3, and Group 4. Group 3
is the most clinically aggressive of the four and exhibits a molecular signature that includes over-expression of the GABRA5 isoform of the GABAA neurotransmitter receptor. Paradoxically, we previously observed that by administration of a positive modulator of the GABAA neurotransmitter receptor, a benzodiazepine, Group 3 cells with a GABRA5 signature could

be arrested. We subsequently reported on use of a novel microdevice to screen a broad range of benzodiazepine compounds that functioned as GABRA5 positive modulators. This study identified a new benzodiazepine compound (KRM-II-08) that was particularly efficacious and thus an attractive candidate as a therapeutic against Group 3 MB. Using KRMII-08 we have examined how a benzodiazepine can effectively arrest Group 3 MB cells. We report on the mechanism underlying the cell cycle arrest.

**Mention of benzodiazepine in treating brain tumors.**

> **RIVA**, "Radiotherapy, Temozolomide, and Antiprogrammed Cell Death Protein 1 Treatments Modulate the Immune Microenvironment in Experimental High-Grade Glioma," Neurosurgery, Volume 88, Issue 2, February 2021, Pages E205–E215,

The lack of immune synergy with conventional chemoradiation could explain the failure of checkpoint inhibitors in current clinical trials for high-grade gliomas (HGGs).

To analyze the impact of radiotherapy (RT), Temozolomide (TMZ) and antiprogrammed cell death protein 1 (αPD1) (as single or combined treatments) on the immune microenvironment of experimental HGGs.

Mice harboring neurosphere /CT-2A HGGs received RT (4 Gy, single dose), TMZ (50 mg/kg, 4 doses) and αPD1 (100 μg, 3 doses) as monotherapies or combinations. The influence on survival, tumor volume, and tumor-infiltrating immune cells was analyzed.

RT increased total T cells (P = .0159) and cluster of differentiation (CD)8+ T cells (P = .0078) compared to TMZ. Lymphocyte subpopulations resulting from TMZ or αPD1 treatment were comparable with those of controls. RT reduced M2 tumor-associated macrophages/microglia (P = .0019) and monocytic myeloid derived suppressor cells (mMDSCs, P = .0003) compared to controls. The effect on mMDSC was also seen following TMZ and αPD1 treatment, although less pronounced (P = .0439 and P = .0538, respectively). Combining RT with TMZ reduced CD8+ T cells (P = .0145) compared to RT alone. Adding αPD1 partially mitigated this effect as shown by the increased CD8+ T cells/Tregs ratio, even if this result failed to reach statistical significance (P = .0973). Changing the combination sequence of RT, TMZ, and αPD1 did not alter survival nor the immune effects.

RT, TMZ, and αPD1 modify the immune microenvironment of HGG. The combination of RT with TMZ induces a strong immune suppression which cannot be effectively counteracted by αPD1.

**Keywords**: High-grade glioma, Glioblastoma, Combination therapies, Immunotherapy, PD1, Temozolomide, Stereotactic radiotherapy

**Mention of radiotherapy with TMZ as potential therapy for tumors.**

> **SUTTER**, "Peripheral benzodiazepine receptor ligands induce apoptosis and cell cycle arrest in human hepatocellular carcinoma cells and enhance chemosensitivity to paclitaxel, docetaxel, doxorubicin and the Bcl-2 inhibitor HA14-1," Journal of Hepatology, Volume 41, Issue 5, November 2004, Pages 799-807

Hepatocellular carcinoma (HCC) is one of the most common causes of cancer deaths worldwide. Thus, novel therapies are urgently needed. A promising approach is the use of peripheral benzodiazepine receptor (PBR) ligands which inhibit the proliferation of various tumors.

PBR expression both in human HCC cell lines and in tumor specimens of HCC patients was analyzed by RT-PCR and immunostaining. To evaluate PBR ligands for the treatment of HCC, we tested their effects on human HCC cells.

PBR was localized to the mitochondria both of HCC cell lines and tumor tissues of HCC patients. In contrast, normal liver did not express PBR. PBR ligands inhibited the proliferation of HCC cell lines by inducing apoptosis and cell cycle arrest. Apoptosis was characterized by a breakdown of the mitochondrial membrane potential, caspase-3 activation and nuclear degradation. Furthermore, pro-apoptotic Bax was overexpressed while anti-apoptotic Bcl-2 and Bcl-XL were suppressed. Cell cycle was arrested both at the G1/S- and G2/M-checkpoints. Synergistic anti-neoplastic effects were obtained by a combination of PBR ligands with cytostatic drugs (paclitaxel, docetaxel, doxorubicin), or with an experimental Bcl-2 inhibitor.

This is the first report on the induction of apoptosis and cell cycle arrest by PBR ligands in HCC cells. Moreover, PBR ligands sensitized HCC cells to taxans and doxorubicin.

Keywords: BaxBcl-2 Chemoresistance Chemotherapy Peripheral benzodiazepine receptor Apoptosis Cell cycle

**Mention of benzodiazepines for cancer treatment.**

> **O'MALLEY**, "Effects of Cigarette Smoking on Metabolism and Effectiveness of Systemic Therapy for Lung Cancer," Journal of Thoracic Oncology, Volume 9, Issue 7, July 2014, Pages 917-926

Cigarette smoke associated polycyclic aromatic hydrocarbons can induce key drug-metabolizing enzymes of cytochrome P450 and isoforms of the glucuronyl transferases families. These enzymes metabolize several systemic therapies for lung cancer. Induction of these enzymes may lead to accelerated clearance with resultant impact on systemic therapy efficacy

and toxicity in smokers compared with nonsmokers. This article reviews published literature regarding the influence of smoking as it relates to alteration of metabolism of systemic therapy in lung cancer.

A structured search of the National Library of Medicine's PubMed/MEDLINE identified relevant articles. Data were abstracted and analyzed to summarize the findings.

Studies that analyzed pharmacokinetic data were prospective. Smokers receiving erlotinib exhibited rapid clearance, requiring a higher dose to reach equivalent systemic exposure compared with nonsmokers. Smokers receiving irinotecan also demonstrated increased clearance and lower systemic exposure. There was no difference in clearance of paclitaxel or docetaxel in smokers. Chemotherapy-associated neutropenia was worse in nonsmokers compared with smokers in patients treated with paclitaxel, docetaxel, irinotecan, and gemcitabine.

Systemic therapy for lung cancer has a narrow therapeutic index such that small changes in plasma concentrations or exposure in smokers may result in suboptimal therapy and poor outcomes. Smoking cessation must be emphasized at each clinical visit. However, prospective trials should take into consideration the effects of smoking history on drug pharmacokinetics and efficacy. The metabolizing enzyme phenotype in smokers may require individualized dose algorithms for specific agents.

Key words: Pharmacokinetics Pharmacodynamics Smoking Chemotherapy metabolism Nicotine Response Toxicities Lung cancer

**Mention of docetaxel (DTX) for lung cancer treatment.**

> **Cheepsattayakorn**, Attapon; Cheepsattayakorn, Ruangrong, "Lung Cancer Chemotherapy, New Treatment and Related Patents," Recent Patents on Anti-Cancer Drug Discovery, Volume 9, Number 3, 2014, pp. 372-381(10)

The majority of patients with lung cancer present with advanced stage which contributes to death of more people than any other malignancy in the world. The discovery of a number of lung cancer-molecular alterations contributes to uniquely targeted therapies with specific inhibitors for non-small cell lung cancer such as erlotinib, gefitinib and crizotinib. Pemetrexed has statistically shown significantly reduced adverse side effects of drug compared with docetaxel. V1801, an analog of gefitinib may overcome gefitinib resistance in patients with non-small cell lung cancer. Thymosin α1, an immunomodulator significantly improves patient's quality of life by enhancing T-cell function, stimulation of Tcell maturation and differentiation. Various novel compounds and chemotherapeutics were introduced in 2013 patents such as taxane, quinazoline, arylamino purine, benzodiazepine, pyrrolopyrimidine, nitrobenzamide, cyclopropane amide, 4-iodo-3-nitrobenzamide, heteroaryl (alkyl) dithiocarbamate, and histone deacetylase in treating non-small-cell lung cancer and piperidine, piperazine, picoplatin, and arsenic trioxide in treating small-cell lung cancer.

Keywords: Cancer; chemotherapy; lung; lung cancer-molecular alterations; related patents; treatment

**Mention of benzodiazepine in treating small cell lung cancer.**

## D. DOCUMENTS CONSIDERED TO BE OF DIRECT RELEVANCE

| Citation of patent/ document/ classification | Comments |
|---|---|
| **USES OF RADIATION AND BENZODIAZEPINE DERIVATIVES IN CANCER THERAPIES**, PCT/US2020/034169A1, EMORY UNIVERSITY, 22 May 2020 (22.05.2020) | **Mention of radiation and benzodiazepine use for cancer therapy.** |
| **POTENTIATION OF ANTI-CANCER ACTIVITY THROUGH COMBINATION THERAPY WITH BER PATHWAY INHIBITORS**, PCT/US2011/032762, Tracon Pharmaceuticals, Inc., 15.04.2011 | |
| HERRLINGER, "**Lomustine-temozolomide combination therapy versus standard temozolomide therapy in patients with newly diagnosed glioblastoma with methylated MGMT promoter (CeTeG/NOA–09): a randomised, open-label, phase 3 trial**," Lancet 2019; 393: 678–88 | |

☒ Further documents are listed in the continuation of Box D. ☐ No further documents attached.

## E. RESULTS AND FINDINGS

Summary of Search Results:

Some references were provided by the University of Cincinnati as potential prior art. The remaining publications were found by UWMRF and should be reviewed by the inventors for any overlapping concern.

## F. OVERALL OPINION

Recommendations:

This technology was filed for a PPA by the University of Cincinnati. It is listed as Active in our system at UWM. We would like to have a conversation with both universities to discuss the potential licensing interests of the inventors' startup company before consideration of converting the PPA to a utility patent.

**UWM Research Foundation** July 6, 2021

***Commercialization REPORT***

Title: Brain Penetrant Chemosensitizer to Treat Lung Cancer & Small brain penetrant molecule to potentiate TMZ for glioblastoma

Inventor(s): James Cook, Soma Sengupta, Taukir Ahmed, Daniel Krummel, Debanjan Bhattacharya, Donatien Kamdem Toukam, Aniruddha Karve, Laura Kelly

OTT Matter: 1752 and 1753

Reviewer: Erin Puro

*This report is intended to provided a market overview, comparison of exisiting competing products, product vision and applicaitions, commercial and licensing potential for the purposes of dispositioning a disclosure technology.*

## A. SUBJECT MATTER

General Technology Description:

Non-small cell lung cancer (NSCLC) accounts for a majority (80%-85%) of lung cancer cases. The most common NSCLC histological subtype (40-50%) is lung adenocarcinoma. A great majority of NSCLC patients with advanced stage of the disease face local and/or distant recurrences, including metastasis to the brain, in the first 2 years after the completion of primary treatment. More effective therapies are needed to boost tumor control, prevent metastasis, and improve overall survival while mitigating side-effects.

We find that Type-A GABA neurotransmitter receptors (GABAARs) are expressed in not only cancers of the central nervous system, but also systemic cancers. In previous studies we reported that by activating GABAAR function and signaling with a new class of benzodiazepine analogs, tumor cells can be sensitized to radiation resulting in significant tumor regression in mouse models of medulloblastoma and melanoma (1-4). Our analysis of patient data has revealed that GABAAR expression is present in both lung adenocarcinoma and squamous carcinoma subtypes. Leveraging this finding, we have investigated if potentiating GABAAR in lung adenocarcinoma cells with a novel benzodiazepine analog called QH-II-066 as well as other compounds of similar structure can impair tumor growth. We find that QH-II-066 treatment induces apoptosis in patient-derived adenocarcinoma cells. We also find that QH-II-066 synergistically can potentiate the chemotherapeutic docetaxel, even at an ineffective dose. We have generated a flank xenograft mouse model using patient derived adenocarcinoma cells to evaluate the efficacy of QH-II-066 and will utilize this model to evaluate the ability of QH-II-066 to sensitize tumor cells to docetaxel such that this drugs toxicity profile is reduced while it retains its potency. Our long-term goal is to establish that the novel benzodiazepine analog QH-II-066 can function to potentiate chemotherapeutic for treatment of NSCLC, thereby increasing its effectiveness and mitigating toxic side-effects.

## B. MARKET OVERVIEW

Summary

http://www.futuremarketinsights.com/reports/glioblastoma-treatment-drugs-market

Brain tumors is one of the leading cause of cancer which is common among children and teenagers. Glioblastoma (GBM) is most common grade four tumor, is malignant and contains dead tumor cells. It is also called as Glioblastoma multiforme, it has variants of giant cell Glioblastoma and gliosarcoma found in cerebral hemisphere of brain. The exact cause of this tumor is not known but is also found in spinal cord and represents about 15.4% of all primary brain tumors. Glioblastoma is also difficult to treat because of number of different types of cells and thus combines various treatment plans combined. The drugs involved in treating glioblastoma are antineoplastic orcytotoxic drugs. There is significant development in chemotherapy drugs to treat the malignant tumors and each year there are new drugs in the market to overcome the blood-brain barrier.

Glioblastoma Treatment Drugs Market: Drivers & Restraints

Glioblastoma is a complicated disease and thus the treatment for it involves various approaches combining various treatments which is the major market driver for Glioblastoma treatment drugs market. Treating such tumors is a challenge which forces the researchers to look for diagnosis and newer chemotherapy drugs. Changing demography, access to healthcare facilities and financial demands are some factors which are lagging in the further developments of glioblastoma. Gaining better understanding of this disease and efficient treatment will improvise which is only possible through developments in molecular mechanisms, clinical trials leading to more promising and tailored therapeutic approaches.

Glioblastoma Treatment Drugs Market: Overview

The market for Glioblastoma treatment drugs will grow significantly as the increasing cases of glioblastoma where doctors are looking for newer drugs and treatment methods to overcome the disease. 'Quality of life' has become an essential factor in the survival of cancer patients which is driving the market for new drug development methods with different approaches. It is a leading cause of cancer in children and males it is mostly encountered in the developed economies as

U.S, U.K and Asian countries. There are various organizations which are supporting Glioblastoma patients and efforts are being taken to improvise the treatments related to it.

Glioblastoma Treatment Drugs Market: Region-wise Outlook

Worldwide, there are an estimated 240,000 cases related to brain cancer and Glioblastoma is most common and lethal disease. Every year in U.S there are about 18000 people diagnosed with GBM and in European countries 25000 cases therefore there is prime incidences of this disease. More treatments are coming forward which can be used alone or in combination with radiotherapy and chemotherapy, but there are chances of reappearance. For long term survival of in glioblastoma, there are newer combination therapies studied and various clinical trials are in order to fight against these disease.

Glioblastoma TreatmentDrugs Market: Key Players

The key players for the Glioblastoma Treatment Drugs Market are F. Hoffmann-La Roche AG, Merck & Co., Inc., Sandoz, Arbor Pharms LLC., Emcure Pharmaceuticals Ltd., Bristol-Myers Squibb Company and Sigma-Tau Pharmaceuticals, Inc.

http://www.grandviewresearch.com/industry-analysis/brain-tumor-diagnosis-and-therapeutics-market

The global brain tumor diagnosis and therapeutics market was valued at USD 354.9 million in 2015 and is expected to grow at a CAGR of 8.1% over the forecast period. Rising prevalence of such cancer and growing geriatric population are key drivers expected to nurture growth of brain tumor diagnosis market worldwide.


As per statistics published by the WHO in 2012, more than14 million new cases of cancer and about 8.2 million deaths were reported; thus alerting the healthcare fraternity to the augmenting growth of the disease. Furthermore, it stated that morbidity is expected to increase by about 70.0% over the next two decades. Similar data was published by the Global Health Observatory (GHO) in 2015, which stated that the number of premature deaths due to cancer is expected to increase by 44.0% by 2030.

As per the Central Brain Tumor Registry of the United States (CBTRUS) statistical report 2016, an estimated 79,270 new cases of primary malignant, nonmalignant, and other CNS cancers are anticipated to be diagnosed in the U.S. in 2017 (26,070 primary malignant and 53,200 nonmalignant). Increasing prevalence of brain cancer cases across the globe is expected to propel the demand of brain tumor diagnosis over the forecast period.

Population above 60 years of age forms the target demographic segment for this vertical, as this population subset is more prone to neurological conditions. Advancement of diagnostics equipment increases the lifespan of this demographic and improves the quality of life for those suffering from neurological conditions. Hence, presence of a large geriatric population pool is considered as a vital driver for this industry.

Type Insights

Computer Tomography (CT) dominated the type segment with over 38.0%of the market share in 2015 and is expected to witness lucrative growth during the forecast period. It displays higher efficiency in delivering doses of cancer tissue damaging radiation in comparison to conventional X-rays. This augments use of CT scans for diagnosing diseases.

According to an independent survey, around 3 million CT scans are carried out each year in the UK. Furthermore, this scanning rate per person is approximately five times greater than that in the U.S., which promises lucrative growth of the segment over the forecast period. In addition, initiatives taken by various governments worldwide to raise awareness regarding brain tumor prevalence and diagnosis are expected to positively impact growth.

MRI follows the CT scan segment and is expected to register profitable growth over the forecast period. These devices are utilized by numerous neurologists because of their accuracy in analysis. Furthermore, they also provide detailed images of the anatomy of the brain, thereby helping in accurately identifying the location of possible cancerous tissue. Amalgamation of CT scan with PET technology (PET-CT Scan) is used to in case of analysis of lumps while a patient is undergoing treatment. The PET-CT scan is often used for diagnosis when CT scan and MRI are unable to provide enough information.

Therapeutics Insights

Owing to the rising incidence of brain tumor and augmenting death rate, the market for its treatment is also anticipated to witness lucrative growth over the forecast period. Various government and independent organizations, such as the WHO, American Brain Tumor Association, and International Brain Tumor Alliance, are working toward supporting availability of treatment and conducting research on novel cure for the disease.

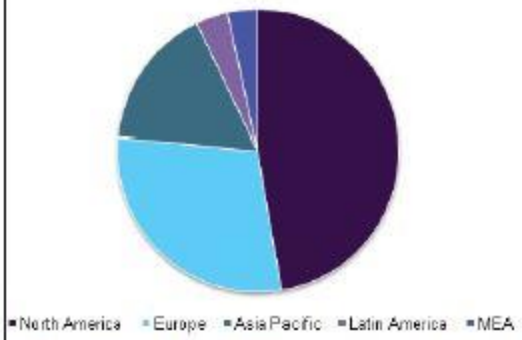


On the basis of therapeutics, the market has been segmented into radiation therapy, chemotherapy, targeted therapy, surgery, and immunotherapy. As of 2015, surgery is anticipated to contribute highest revenue to the brain tumor and therapeutics market. The low awareness levels and limited treatment options leading to aggravation of the disease to grade IV stage, are expected to boost the demand for surgeries.

Radiation therapy is anticipated to exhibit significant growth over the forecast period as this therapy kills the cancer cells by using X-rays, gamma rays, or protons and is the second best choice after surgery.

Rising preference for alkylating neoplastic agents, such as carmustine, vincristine, lomustine, procarbazine, and temozolomide, for chemotherapy is expected to contribute favorably to the growth of this vertical. For instance, various new drugs are in pipeline of leading players, such as varlilumab by Celldex Therapeutics.

Regional Insights

North America held more than 45.0% share in the global brain tumor diagnosis and therapeutics market in 2015. Developed healthcare infrastructure, greater per capita healthcare spending, and comparatively higher awareness regarding advanced technologies are certain impact rendering factors.

Europe is expected to contribute significantly to this space over the forecast period, which can be attributed to the increasing prevalence of malignant cancers in the countries like the UK. For instance, as per statistics provided by the Office for National Statistics, UK, in 2014, around 10,981 new cases were registered in the region.

Competitive Insights

Some of the key players operating in this space are GE Healthcare; Hitachi, Ltd.; Philips Healthcare; Siemens Healthineers; Toshiba Corporation; Fujifilm Corporation; Shimadzu Corporation; and Carestream Health.

New product development, geographical expansion, collaborations, mergers & acquisitions, and pricing strategies are the key undertakings of these players in this vertical. For instance, in November 2016, Toshiba Corporation launched new Vantage Galan 3T MR scan, an advanced imaging technique with improved high-quality imaging, which finds high application in neurological cancer diagnosis.

https://www.alliedmarketresearch.com/oncology-cancer-drugs-market

Oncology Drugs Market Overview:
The global oncology drugs market was valued at $128,352 million in 2019, and is projected to reach $222,380 million by 2027, registering a CAGR of 7.4%.

Cancer is a group of diseases associated with abnormal cell growth with the potential to plague or spread to other parts of the body. Major types of cancers include carcinomas, sarcomas, lymphomas, and leukemia. Sarcomas begin in the connective tissue such as muscle or bones. Soft-tissue sarcomas can begin in fatty tissues. Moreover, the treatment of cancer in patients requires the use of different drugs like hormonal therapy, immunotherapy, targeted therapy, and others. Furthermore, biological drugs on the basis of monoclonal antibodies (mAbs) have emerged as a preferred option to treat various cancer types, especially blood cancer (leukemia). Rise in incidence of various cancer conditions, increase in popularity of advance therapies (biological and targeted drug therapies), and surge in geriatric population worldwide are the key factors driving the growth of the global oncology/cancer drugs market. Furthermore, rise in cancer awareness and availability of cancer drugs are expected to boost the market growth.

The COVID-19 pandemic has disrupted virtually each aspect of healthcare provision including cancer care. The outbreak of Coronavirus disease (COVID-19) has acted as a significant restraint on the oncology/cancer drugs market in 2020 as supply chains were disrupted due to restrictions on trade of pharmaceutical ingredients and products across countries. In addition, COVID 19 is an infectious disease with flu-like symptoms including fever, cough, and difficulty in breathing. COVID-19 pandemic has impacted the most crucial areas of the oncology/cancer drugs market by disrupting clinical trials and drug supply chains. Pandemic has directly affected the supply of oncology drugs to cancer patients; it is difficult to administer chemotherapy and certain other treatments outside of a clinic. Also, the spread of coronavirus has reduced patients' willingness and ability to access not just treatments, but trials for new medicines. COVID-19's interference with the research and development of new treatments is one of the most significant blows to the cancer drugs market. According to, Centre for Drug Development (UK), the pandemic initially drew recruitment for UK clinical trials to an almost complete pause.

7/6/2021

The growth of the global oncology/cancer drugs market is majorly driven by increase in incidence of various cancer conditions, rise in popularity of advance therapies (biological and targeted drug therapies), and surge in geriatric population worldwide. Furthermore, rise in cancer awareness and availability of cancer drugs are expected to boost the market growth. However, high cost involved in new drug development coupled with threat of failure & adverse effects associated with cancer drugs therapies is expected to restrain the growth of the market. Conversely, high potential of emerging economies and increase in number of pipeline products are expected to provide new opportunities for market players in future.

The global oncology/cancer drugs market is segmented on the basis of drug class type, indication, and region. By drug class type, the market is divided into chemotherapy, targeted therapy, immunotherapy (biologic therapy), and hormonal therapy. By indication, it is categorized into lung cancer, stomach cancer, colorectal cancer, breast cancer, prostate cancer, liver cancer, esophagus cancer, cervical cancer, kidney cancer, bladder cancer, and other cancers. Region wise, the market is studied across North America (U.S., Canada, and Mexico), Europe (Germany, France, the UK, Italy, Spain, and rest of Europe), Asia-Pacific (China, Japan, Australia, India, South Korea, and rest of Asia-Pacific), and LAMEA (Brazil, South Africa, Saudi Arabia, and rest of LAMEA)

Segmental review
By drug class type, the targeted therapy segment is anticipated to grow with the largest share throughout the forecast period. This is attributed to the identification of molecular targets of cancer cells. Recent advances in cellular technology and gene therapy have contributed to improve the understanding of tumor cells and their metabolism at molecular level, thus driving the need for targeted drug therapies for cancer treatment. On the other side, the demand for immunotherapy is projected to exhibit the fastest global oncology/cancer drugs market. growth during the forecast period.

North America accounted for the largest share of revenue in 2019, and is anticipated to maintain its dominance from 2020 to 2027, owing to presence of large patient population and early adoption of advance drugs. However, Asia-Pacific is expected to grow at the highest CAGR, owing to increase in disposable income; surge in research, development, & innovation activities; and rise in awareness related to different cancers. Moreover, rise in incidence of cancer worldwide fuels the global oncology/cancer drugs market growth.

Some of the key players operating in the global oncology/cancer drugs market. include AbbVie Inc. Amgen, Astellas Pharma Inc., AstraZeneca PLC, Bristol-Myers Squibb Company, F. Hoffmann-La Roche Ltd., Johnson & Johnson (Janssen Global Services, LLC,), Merck & Co., Inc., Novartis AG, and Pfizer Inc.

https://globenewswire.com/news-release/2016/12/12/896798/0/en/Global-Cancer-Drugs-Market-expected-to-reach-USD-161-30-Billion-by-2021-Zion-Market-Research.html

Sarasota, FL, Dec. 12, 2016 (GLOBE NEWSWIRE) -- Zion Research has published a new report titled "Cancer Drugs Market by Therapy (Immunotherapy, Targeted Therapy, Chemotherapy, Hormone Therapy and Others) for Breast Cancer, Blood Cancer, Gastrointestinal Cancer, Prostate Cancer, Skin Cancer, Lung Cancer and Other Cancer: Global Industry Perspective, Comprehensive Analysis and Forecast, 2015 - 2021". According to the report, global demand for cancer drugs market was valued at approximately USD 112.90 billion in 2015 and is expected to generate revenue of around USD 161.30 billion by end of 2021, growing at a CAGR of around 7.4% between 2016 and 2021.
Global cancer drugs market is primarily driven by growing incidences of target disease such as lung cancer, breast cancer, cervical cancer, etc. across the globe. Other major driving factors are increasing research and development on biological and targeted drug therapies for the treatment of cancer coupled along with the expiration of patents. However, the high price of drug development and stringent regulatory policies coupled along with the possibility of failure are the major restraints that may limit the growth of the market. Nonetheless increasing focus on personalized medicine coupled along with huge investment in anti-cancer drugs research across the globe is likely to disclose the new avenues for cancer drugs market in the near future.

Breast cancer, blood cancer, gastrointestinal cancer, prostate cancer, skin cancer, lung cancer and others are the key cancer types of the global cancer drugs market. The blood cancer segment dominated the market in terms of revenue.

North America represents developed regional markets for cancer drugs and is expected to see the rapid growth in the years to come. The U.S. is by far the leading cancer drugs market by country in North America. The U.S. market is expected to grow at the highest CAGR during the forecast period. This growth is mainly due to the well-developed healthcare infrastructure and the increase in research and development on cancer drugs. Moreover, the disposable income and reimbursement of life-threatening diseases are very high in this region which promotes the growth of cancer drugs market.

Asia-Pacific is expected to witness noticeable growth in the near future. In Asia, China, India, and Japan will continue to be the fastest growing markets in cancer drugs market. Growth in Asia-Pacific market is expected to be driven by increasing tobacco consumption, growing population, and increasing disposable income.

Some of the key players in cancer drugs market include Bayer, GlaxoSmithKline, Novartis, Sanofi and Pfizer, Amgen, Merck, Bristol-Myers Squibb, Celgene Corporation, Ariad Pharmaceuticals, Eli Lilly, Hoffmann-La Roche Ltd, Boehringer Ingelheim GmbH, Johnson and Johnson and Teva Pharmaceuticals among others.

7/6/2021

Market Size

The global oncology/cancer drugs market size reached a value of nearly $167.9 billion in 2019, having increased at a compound annual growth rate (CAGR) of 9.8% since 2015. The oncology market size 2020 is expected to decline from $167.9 billion in 2019 to $149.9 billion in 2020 at a rate of -11%.

https://www.globenewswire.com/news-release/2020/10/06/2104100/0/en/Oncology-Market-Size-2020-Particularly-Prone-To-Disruption-During-Pandemic-In-The-Global-Oncology-Market.html#:~:text=The%20global%20oncology%2Fcancer%20drugs%20market%20size%20reached%20a,billion%20in%202020%20at%20a%20rate%20of%20-11%25.

Oncology Market Size 2020 Particularly Prone To Disruption During Pandemic In The Global Oncology Market
According to The Business Research Company's research report on the oncology drugs market, the oncology market 2020 is particularly prone to disruption from the coronavirus outbreak as patients with cancer are more susceptible to viral infections, especially after chemotherapy, stem cell transplants, or surgeries. COVID-19 has caused clinical trial delays for oncology drugs and has resulted in low usage of cancer drugs. Due to the worldwide lockdown, production is also being halted which is causing supply chain issues.

LONDON, Oct. 06, 2020 (GLOBE NEWSWIRE) -- (Oncology Drugs Companies Included: F. Hoffmann-La Roche AG, Novartis AG, Bristol-Myers Squibb Company, Merck & Co., Inc., Johnson & Johnson)

The global oncology/cancer drugs market size reached a value of nearly $167.9 billion in 2019, having increased at a compound annual growth rate (CAGR) of 9.8% since 2015. The oncology market size 2020 is expected to decline from $167.9 billion in 2019 to $149.9 billion in 2020 at a rate of -11%. The decline is mainly due to lockdown and social distancing norms imposed by various countries and economic slowdown across countries owing to the COVID-19 outbreak and the measures to contain it. The market is then expected to grow slightly from $201.1 billion in 2021 to $284.5 billion in 2023 at a CAGR of 9.7%. North America has the largest cancer drug market share, accounting for 41.2% of the total market.

The Business Research Company's report titled Oncology Drugs Market - Opportunities And Strategies - Global Forecast To 2030 covers major oncology drugs companies, oncology drugs market share by company, oncology drugs manufacturers, oncology drugs infrastructure market size, and oncology drugs market forecasts. The report also covers the global oncology drugs market and its segments. The cancer market by type is segmented into drugs for lung cancer, pancreatic cancer, breast cancer, prostate cancer, ovarian cancer, colorectal cancer, gastric cancer, kidney cancer, brain tumor, thyroid cancer, skin cancer, bladder cancer, cervical cancer, blood cancer and others, by drug class type into targeted therapy, immunotherapy (biologic therapy), chemotherapy and hormonal therapy, by distribution channel into hospital pharmacies, retail pharmacies/drug stores and others, by route of administration into oral, parental and others, by drug classification into branded drugs and generic drugs.

Request For A Sample Of The Global Oncology Drugs Market Report:

https://www.thebusinessresearchcompany.com/sample.aspx?id=3440&type=smp

Companies in the oncology drugs market are increasing their product innovation through strategic collaborations. To sustain in the increasingly competitive market, organizations are developing innovative products as well as sharing skills and expertise with other such enterprises. While oncology drug companies have long collaborated with each other as well as with academic and research institutions in this market by way of partnerships, in or out licensing deals, this trend has been increasing over the recent years.

New technologies are being implemented in the cancer drug market, such as artificial intelligence in the research and development process, as well as 3D printing devices to mimic the human body for trials and testing of the drugs developed. Companies are also investing in technologies to develop next generation biologics such as antibody drug conjugates, bispecifics, fusion proteins, cell and gene therapy that will be more effective as they are expected to have better potency against the target disease as well as have the ability to treat more than one aspect of the disease. Over the last few years, there has been a significant rise in accelerated approval of cell and gene therapies for cancer treatment by regulatory bodies across the globe. CRISPR technology can be used to discover the non-coding cancer genome. CRISPR-Cas9 genome editing reduces the processing associated with the generation of cell line and animal models of cancer and complex generations. Thus, it generates a better cancer model for target validation and drug evaluation. CRISPR–Cas9 is accelerating the different stages of oncology drug discovery including target identification, validation and deconvolution, drug synthesis, assessment of drug sensitivity and resistance.

With innovation through technology and rising focus on development of new drugs, the oncology drugs market trends ought to bring advances in cancer therapies in the forecasted period.

State or Federal Regulations

FDA approval for drugs

7/6/2021

Licensing Barriers

Understanding the freedom to operate with the combination of drugs already on the market or already described in the literature. Must look at patent landscape.

Market Location

North America represents developed regional markets for cancer drugs and is expected to see the rapid growth in the years to come. The U.S. is by far the leading cancer drugs market by country in North America. The U.S. market is expected to grow at the highest CAGR during the forecast period. This growth is mainly due to the well-developed healthcare infrastructure and the increase in research and development on cancer drugs. Moreover, the disposable income and reimbursement of life-threatening diseases are very high in this region which promotes the growth of cancer drugs market.

Asia-Pacific is expected to witness noticeable growth in the near future. In Asia, China, India, and Japan will continue to be the fastest growing markets in cancer drugs market. Growth in Asia-Pacific market is expected to be driven by increasing tobacco consumption, growing population, and increasing disposable income.

---

Regional Insights

North America held more than 45.0% share in the global brain tumor diagnosis and therapeutics market in 2015. Developed healthcare infrastructure, greater per capita healthcare spending, and comparatively higher awareness regarding advanced technologies are certain impact rendering factors.

Europe is expected to contribute significantly to this space over the forecast period, which can be attributed to the increasing prevalence of malignant cancers in the countries like the UK. For instance, as per statistics provided by the Office for National Statistics, UK, in 2014, around 10,981 new cases were registered in the region.

## C. COMPETITION

Alternative Products

http://www.abta.org/brain-tumor-information/types-of-tumors/medulloblastoma.html

https://www.cancer.gov/about-cancer/treatment/drugs/brain

http://www.webmd.com/drugs/condition-457-Malignant+Brain+Tumor+Glioblastoma.aspx?names-dropdown=DE

https://www.cancer.org/cancer/neuroblastoma/treating/chemotherapy.html

Time to Market

10-15 yrs

## D. CUSTOMERS

Potential Licensees

Some of the key players in cancer drugs market include Bayer, GlaxoSmithKline, Novartis, Sanofi and Pfizer, Amgen, Merck, Bristol-Myers Squibb, Celgene Corporation, Ariad Pharmaceuticals, Eli Lilly, Hoffmann-La Roche Ltd, Boehringer Ingelheim GmbH, Johnson and Johnson and Teva Pharmaceuticals among others.

Public Perception

Positive for cures, especially in children.

## E. MARKET OPPORTUNITY

Timing

There are a number of drug on the market for chemotherapy for brain and lung tumors. If this combination can be advantageous over other regarding toxicity, perhaps there would be a benefit over competitors. There would need to be some sort of strong advantage to compete against approved drugs.

Market Need

Similar to above, effective drugs with less side effects would be a strong need in the cancer realm. More targeting therapies are of interest to the market.

http://www.newsmax.com/Health/Cancer/ALLWWCUR-ASFEAT-BGOVALL-BGOVBILLGO/2017/06/22/id/797594/
The Food and Drug Administration will soon announce a plan to update agency policies and facilitate the approval of critically needed drugs, including so-called "tumor-agnostic" therapies that target cancer-linked DNA, according to FDA Commissioner Scott Gottlieb.

7/6/2021

"The most tangible way we're going to reduce health-care costs is by finding better treatments for a lot of costly diseases," Gottlieb told the Senate panel responsible for overseeing the agency's budget on Tuesday.

## F. OVERALL OPINION

Recommendations: Share and discuss reports and data with Emory team, both technologies have been filed as of June 2021. The disclosure is set to "Active."

## 5. 2. 2 Small brain penetrant molecule to potentiate TMZ for glioblastoma

| Electronic Acknowledgement Receipt | |
|---|---|
| **EFS ID:** | 42888945 |
| **Application Number:** | 63196459 |
| **International Application Number:** | |
| **Confirmation Number:** | 7944 |
| **Title of Invention:** | Small brain penetrant molecule to potentiate TMZ for glioblastoma |
| **First Named Inventor/Applicant Name:** | Soma Sengupta |
| **Customer Number:** | 24256 |
| **Filer:** | Jennifer Lynn Livingston/Jessica Desmarais |
| **Filer Authorized By:** | Jennifer Lynn Livingston |
| **Attorney Docket Number:** | 2021-140; CIN0342MA |
| **Receipt Date:** | 03-JUN-2021 |
| **Filing Date:** | |
| **Time Stamp:** | 16:02:26 |
| **Application Type:** | Provisional |

**Payment information:**

| | |
|---|---|
| Submitted with Payment | yes |
| Payment Type | CARD |
| Payment was successfully received in RAM | $150 |
| RAM confirmation Number | E202163G02571781 |
| Deposit Account | 041133 |
| Authorized User | Jessica Desmarais |
| The Director of the USPTO is hereby authorized to charge indicated fees and credit any overpayment as follows:<br>37 CFR 1.16 (National application filing, search, and examination fees)<br>37 CFR 1.17 (Patent application and reexamination processing fees) | |

37 CFR 1.19 (Document supply fees)

37 CFR 1.20 (Post Issuance fees)

37 CFR 1.21 (Miscellaneous fees and charges)

## File Listing:

| Document Number | Document Description | File Name | File Size(Bytes)/ Message Digest | Multi Part /.zip | Pages (if appl.) |
|---|---|---|---|---|---|
| 1 | Specification | 2021-06-03_Specification_CIN0342MA.pdf | 670466<br>5cd3642f1e4b068e67238c9f1897ba4f1743c015 | no | 9 |
| **Warnings:** | | | | | |
| **Information:** | | | | | |
| 2 | Provisional Cover Sheet (SB16) | 2021-06-03_Provisional_Coversheet_CIN0342MA.pdf | 2032481<br>208a73a11d91954d1fd382ea7e25871db79edd1f | no | 4 |
| **Warnings:** | | | | | |
| **Information:** | | | | | |
| 3 | Drawings-other than black and white line drawings | 2021-06-03_Drawings_CIN0342MA.pdf | 450162<br>672193222b50ce2d0d0484406d483ce56e0be388 | no | 2 |
| **Warnings:** | | | | | |
| **Information:** | | | | | |
| 4 | Application Data Sheet | 2021-06-03_ADS_CIN0342MA.pdf | 1256424<br>6c2c29f52f247cd7636eee41eeec8821d8aa1e2f | no | 11 |
| **Warnings:** | | | | | |
| **Information:** | | | | | |
| 5 | Fee Worksheet (SB06) | fee-info.pdf | 29873<br>964f87e76597dc0918572867b7d6be42951e1fe4 | no | 2 |
| **Warnings:** | | | | | |
| **Information:** | | | | | |
| | | **Total Files Size (in bytes):** | 4439406 | | |

**This Acknowledgement Receipt evidences receipt on the noted date by the USPTO of the indicated documents, characterized by the applicant, and including page counts, where applicable. It serves as evidence of receipt similar to a Post Card, as described in MPEP 503.**

**New Applications Under 35 U.S.C. 111**
**If a new application is being filed and the application includes the necessary components for a filing date (see 37 CFR 1.53(b)-(d) and MPEP 506), a Filing Receipt (37 CFR 1.54) will be issued in due course and the date shown on this Acknowledgement Receipt will establish the filing date of the application.**
**National Stage of an International Application under 35 U.S.C. 371**
**If a timely submission to enter the national stage of an international application is compliant with the conditions of 35 U.S.C. 371 and other applicable requirements a Form PCT/DO/EO/903 indicating acceptance of the application as a national stage submission under 35 U.S.C. 371 will be issued in addition to the Filing Receipt, in due course.**
**New International Application Filed with the USPTO as a Receiving Office**
**If a new international application is being filed and the international application includes the necessary components for an international filing date (see PCT Article 11 and MPEP 1810), a Notification of the International Application Number and of the International Filing Date (Form PCT/RO/105) will be issued in due course, subject to prescriptions concerning national security, and the date shown on this Acknowledgement Receipt will establish the international filing date of the application.**

2021-140

# SMALL BRAIN PENETRANT MOLECULE TO POTENTIATE TMZ FOR GLIOBLASTOMA

## TECHNICAL FIELD

This disclosure relates to the field of cancer therapy. Specifically, the disclosure relates to the treatment of glioblastoma with benzodiazepine analogs to potentiate temozolomide (TMZ) treatment of glioblastoma multiforme (GBM).

## BACKGROUND

Glioblastoma multiforme (GBM) is a highly malignant (Grade IV) primary brain tumor. Standard-of-care for GBM includes radiotherapy with concomitant administration of a DNA alkylator, temozolomide (TMZ). This approach shows a degree of effectiveness if GBM cells are adequately MGMT promoter methylated (~50% of GBM tumors), as reduction in MGMT protein leads to diminished ability to reverse TMZ-induced DNA damage. Histone deacetylase inhibitors have recently been employed to improve TMZ effectiveness, but unfortunately result in bone marrow toxicity without contributing to durable responses. TMZ is also not without its own debilitating and life-threatening side-effects, including leukopenia. Tragically, survival remains only 12-15 months under this treatment regimen. There is an urgent need to increase the effectiveness of TMZ for MGMT methylated GBMs, identify a treatment approach that is effective for MGMT unmethylated GBMs, and reduce TMZ side-effects.

GBM is one of the deadliest human cancers and highly challenging to treat. GBM tumor cells interact with diverse cells in a complex microenvironment. Further, the blood-brain barrier (BBB) acts to limit drug bioavailability and facilitate immune evasion. Unfortunately, GBM cells frequently subvert the physiological function of the cerebrovascular tissue and turn the BBB into an effective blood-tumor barrier (BTB) capable of protecting the cancer tissue from drugs as well as systemic immunity. Despite increasing knowledge of genetic and epigenetic changes underlying GBM tumor initiation and growth, GBM prognosis remains poor.

GABA receptors ($GABA_ARs$) form pentameric chloride ($Cl^-$) channels, composed most commonly of two α, two β, and γ subunits encoded by GABR genes GABRA, GABRB, and GABRG, respectively (Fig. 1a). $GABA_ARs$ are fundamental in determining an excitation/inhibition balance in the central nervous system. As a receptor mediating $Cl^-$ flux,

$GABA_AR$s predominantly function to hyperpolarize neural cells, following binding of its ligand GABA (Fig. 1b).

$GABA_AR$s have been an important therapeutic target since the clinical introduction of benzodiazepines in the 1960s. Benzodiazepines bind at the γ-α interface of $GABA_AR$ (Fig. 1a) and act to increase effectiveness of GABA and thus enhance $Cl^-$ flux (Fig. 1b). FDA approved benzodiazepines consist most commonly of fusion of diazepine and benzene rings (1,4-benzodiazepine) and a phenol ring (5-phenyl-1H-benzo[e]) (Fig. 1c). J. Cook and his team (Univ. Wisconsin-Milwaukee) introduced an ethinyl bond at R7 in place of a chlorine in Valium (Fig. 1c), which confers anti-cancer activity.

Nevertheless, a need exists for improved therapies to treat glioblastoma multiforme and slow disease progression.

## SUMMARY

Accordingly, provided herein are compositions and methods for the treatment of glioblastoma multiforme. The disclosed compositions and methods potentiate TMZ treatment of glioblastoma, leading to enhanced anti-cancer activity, irrespective of *MGMT* methylation status.

In one embodiment, a method of treating cancer in a subject in need thereof is provided, the method comprising administering to the subject a combination of temozolomide (TMZ) and a benzodiazepine analog.

In another embodiment, a pharmaceutical composition is provided, comprising: a therapeutic amount of a benzodiazepine analog; a therapeutic amount of temozolomide; and one or more pharmaceutically-acceptable excipients.

In another embodiment, a method of inducing apoptosis of a cancer cell is provided, the method comprising contacting the cell with an effective amount of temozolomide and an effective amount of a benzodiazepine analog.

In another embodiment, a method of inducing regression of a tumor is provided, the method comprising contacting the tumor with an effective amount of temozolomide and an effective amount of a benzodiazepine analog.

These and other objects, features, embodiments, and advantages will become apparent to those of ordinary skill in the art from a reading of the following detailed description and the appended claims.

## BRIEF DESCRIPTION OF THE DRAWINGS

**Fig. 1. $GABA_AR$s.** (A) A $GABA_AR$, looking down the chloride ion conduction pore, showing the structure of α, β, and γ subunits. (B) Binding of two GABA ligands opens the channel, binding of a benzodiazepine enhances chloride ion flux. (C) Structure of the classic benzodiazepine Valium (left) and the novel benzodiazepine analog used in proposed studies (right; QH-II-066 or BZD-1). The key difference is an ethinyl bond in place of a chlorine moiety.

**Fig. 2. Cytotoxicity of unmethylated GBM cell lines treated with BZD-1±TMZ.** Spheroids of unmethylated GBM lines BT142-GFP (A) and G43 (B) were treated with TMZ, BZD-1, or BZD-1+TMZ.

**Table** 1. Cytotoxic responses of GBM cell lines treated with BZD-1 + TMZ.

## DETAILED DESCRIPTION

The details of embodiments of the presently-disclosed subject matter are set forth in this document. Modifications to embodiments described in this document, and other embodiments, will be evident to those of ordinary skill in the art after a study of the information provided in this document.

While the following terms are believed to be well understood in the art, definitions are set forth to facilitate explanation of the presently-disclosed subject matter. Unless defined otherwise, all technical and scientific terms used herein have the same meaning as commonly understood by one of ordinary skill in the art to which the presently-disclosed subject matter belongs.

Unless otherwise indicated, all numbers expressing quantities of ingredients, properties such as reaction conditions, and so forth used in the specification and claims are to be understood as being modified in all instances by the term "about." Accordingly, unless indicated to the contrary, the numerical parameters set forth in this specification and claims are approximations that can vary depending upon the desired properties sought to be obtained by the presently-disclosed subject matter.

As used herein, the term "about," when referring to a value or to an amount of mass, weight, time, volume, concentration or percentage is meant to encompass variations of in some embodiments ±20%, in some embodiments ±10%, in some embodiments ±5%, in some embodiments ±1%, in some embodiments ±0.5%, and in some embodiments ±0.1% from the specified amount, as such variations are appropriate to perform the disclosed method.

It should be understood that every maximum numerical limitation given throughout this specification includes every lower numerical limitation, as if such lower numerical limitations were expressly written herein. Every minimum numerical limitation given throughout this specification will include every higher numerical limitation, as if such higher numerical limitations were expressly written herein. Every numerical range given throughout this specification will include every narrower numerical range that falls within such broader numerical range, as if such narrower numerical ranges were all expressly written herein.

As used in this specification and the appended claims, the singular forms "a," "an" and "the" include plural references unless the content clearly dictates otherwise.

TMZ is used to treat all GBMs. However, TMZ shows a degree of effectiveness for only half of GBMs, those that are *MGMT* methylated. Moreover, TMZ is associated with debilitating and life-threatening side-effects. The present disclosure provides a brain-penetrant benzodiazepine analog that potentiates TMZ synergistically, irrespective of GBM methylation status.

Our goal is to identify an approach capable of potentiating current GBM standard-of-care treatment irrespective of *MGMT* methylation status, as well as mitigate side effects. We have shown that by targeting a unique electrochemical vulnerability in GBMs with a non-toxic brain-penetrant small molecule, GBM tumor cells can be sensitized to TMZ irrespective of *MGMT* methylation status. While not desiring to be bound by theory, the rationale that underlies this proposal is our finding that GBM cells as well as tumor cells from a subgroup of patients of the pediatric brain cancer medulloblastoma and melanomas possess functional Type-A GABA receptors ($GABA_ARs$), chloride ion channels, that when targeted with members of a novel class of benzodiazepine analogs (BZDs), ion dynamics in these disparate cancer cells is altered and apoptotic responses elicited (1-4). We have found using medulloblastoma and melanoma mouse models that BZD on its own can induce apoptosis and regress tumor volume. In a syngeneic melanoma mouse model, we find that a particular BZD (termed QH-II-066) when combined with radiation, even at suboptimal-doses, results in complete tumor loss in most mice. In our studies on GBM, QH-II-066 can potentiate TMZ irrespective of the *MGMT* methylation status. This effect is dramatic and synergistic. The data indicates that QH-II-066 can be an effective 'add-on' therapeutic to potentiate TMZ irrespective of *MGMT* methylation status.

**Highlights**

- QH-II-066 enhances $Cl^-$ anion transport via $GABA_AR$, thereby altering ion dynamics, inhibiting the drug efflux transporter P-glycoprotein, and inducing apoptotic responses.
- QH-II-066-triggered electrochemical changes in the cancer cells potentiate TMZ significantly and synergistically, irrespective of the MGMT status of GBM cells.

## EXAMPLES

The following examples are given by way of illustration are not intended to limit the scope of the disclosure.

**Example 1. BZD-1 potentiates TMZ, irrespective of *MGMT* methylation status**.

*In vitro* cytotoxicity studies of methylated and unmethylated GBM cells treated with QH-II-066 and TMZ as single agents or in combination demonstrates that the combined therapy overcomes TMZ resistance in unmethylated GBM cell lines and is significantly more potent than TMZ alone in killing GBM cells, irrespective of methylation status (Table 1). Using the Chou-Talay Combination Index Equation for quantitative synergy determination in two-drug combinations, we find that QH-II-066 and TMZ act synergistically. We also conducted spheroid assays using two unmethylated GBM lines to qualitatively assess the effect of QH-II-066+TMZ. This assay revealed a very significant disaggregation in response to combination therapy, suggestive of a disruption in tumor-initiating activity (Fig. 2).

**Example 2. Formulated QH-II-066 is metabolically stable and rapidly penetrates and accumulates in the brain**.

We have explored different approaches to formulate QH-II-066. We identified a co-solvent based injectable formulation (already U.S. FDA approved for benzodiazepines) as satisfactory. In this co-solvent formulation, QH-II-066 is highly soluble (10 mg/mL); stable at room temperature for up to 6 months; shows no visible adverse effects in rats 12 hrs after single dose i.p. administration. We also conducted metabolic stability studies using human liver microsomes and found no breakdown products within 1 hr, in contrast to the FDA approved benzodiazepine Midazolam. Pharmacokinetics of QH-II-066 show a rapid penetration into the brain (within ~5 minutes) and significant accumulation of QH-II-066 (161.3 ng/mL) into brain extracellular fluid.

All documents cited are incorporated herein by reference in their entirety; the citation of any document is not to be construed as an admission that it is prior art with respect to the present invention.

It is to be further understood that where descriptions of various embodiments use the term "comprising," and/or "including" those skilled in the art would understand that in some specific instances, an embodiment can be alternatively described using language "consisting essentially of" or "consisting of."

The foregoing description is illustrative of particular embodiments of the invention but is not meant to be a limitation upon the practice thereof. While particular embodiments have been illustrated and described, it would be obvious to one skilled in the art that various other changes and modifications can be made without departing from the spirit and scope of the invention. It is therefore intended to cover in the appended claims all such changes and modifications that are within the scope of this invention.

What is claimed is:

## CLAIMS

1. A method of treating cancer in a subject in need thereof, the method comprising administering to the subject a combination of temozolomide (TMZ) and a benzodiazepine analog.

2. The method according to claim 1, wherein the benzodiazepine analog is BZD-1.

3. The method according to any of the preceding claims, wherein the cancer is selected from the group consisting of glioblastoma multiforme (GBM), medulloblastoma, and melanoma.

4. The method according to claim 1, wherein the TMZ and the benzodiazepine analog are administered concurrently or sequentially.

5. A pharmaceutical composition comprising:
a therapeutic amount of a benzodiazepine analog;
a therapeutic amount of temozolomide; and
one or more pharmaceutically-acceptable excipients.

6. The pharmaceutical composition according to claim 5, wherein the benzodiazepine analog is BZD-1.

7. A method of inducing apoptosis of a cancer cell, the method comprising contacting the cell with an effective amount of temozolomide and an effective amount of a benzodiazepine analog.

8. The method according to claim 7, wherein the benzodiazepine analog is BZD-1.

9. A method of inducing regression of a tumor, the method comprising contacting the tumor with an effective amount of temozolomide and an effective amount of a benzodiazepine analog.

10. The method according to claim 9, wherein the benzodiazepine analog is BZD-1.

11. The composition or methods according to any of the preceding claims, wherein the benzodiazepine analog potentiates the anti-cancer effect of TMZ, irrespective of *MGMT* methylation status of the cancer, cell, or tumor.

## REFERENCES


1. Sengupta S., Weeraratne S.D., Sun H, Phallen J., Rallapalli S.K., Teider N., Kosaras B., Amani V., Pierre-Francois J., Tang Y., Nguyen B., Yu F., Schubert S., Balansay B., Mathios D., Lechpammer M., Archer T.C., Tran P., Reimer R.J., Cook J.M., Lim M., Jensen F.E., Pomeroy S.L., Cho Y.J. (2014). a5-GABAA receptors negatively regulate MYC-amplified medulloblastoma growth. Acta Neuropathol. 127: 593-603.

2. Jonas O., Calligaris D., Methuku K.R. Poe M.M., Francois J.P., Tranghese F., Changelian A., Sieghart W., Ernst M., Krummel D.A., Cook J.M., Pomeroy S.L., Cima M., Agar N.Y., Langer R., Sengupta S. (2016). First in vivo testing of compounds targeting Group 3 medulloblastomas using an implantable microdevice as a new paradigm for drug development. J. Biomed. Nanotech. 12(6): 1297-302.

3. Kallay L., Keskin H., Ross A., Rupji M., Moody O.A., Li G., Ahmed T., Rashid R., Stephen M.R., Cottrill K.A., Nuckols A., Zu M., Martinson D.E., Tranghese F., Wang X., Taylor M., Cook J., Kowalski J., Jenkins A., Pomeranz Krummel D., Sengupta S. (2019). Modulating native GABAA receptors in cancer cells with positive allosteric benzodiazepine-derivatives induces cell death. J. Neuro-Oncol. 142: 411-422.

4. Pomeranz Krummel D.A., Nasti T.H., Izar B., Press R.H., Xu M., Lowder L., Kallay L., Rupji M., Rosen H., Su J., Curran W., Olson J., Weinberg B., Schniederjan M., Neill S., Lawson D., Kowalski J., Khan M.K., Sengupta S. (2020). Impact of sequencing radiation therapy and immune checkpoint inhibitors in the treatment of melanoma brain metastases. International J. Radiation Oncology, Biology, Physics. 108(1): 157-163.

5. Quail DF, Joyce JA. (2017). The Microenvironmental Landscape of Brain Tumors. Cancer Cell. 31(3): 326–341.

6. Chen J, Li Y, Yu T-S, McKay RM, Burns DK, Kernie SG, et al. (2012). A restricted cell population propagates glioblastoma growth after chemotherapy. Nature. 488(7412): 522–526.
7. Sigel E, Steinmann ME. (2012). Structure, function, and modulation of GABAA receptors. J. Biol. Chem. 287: 40224-40231.

8. Olsen RW, Sieghart W. (2009). GABAA receptors: subtypes provide diversity of function and pharmacology. Neuropharmacol. 56: 141-148.

# Please wait...

If this message is not eventually replaced by the proper contents of the document, your PDF viewer may not be able to display this type of document.

You can upgrade to the latest version of Adobe Reader for Windows®, Mac, or Linux® by visiting http://www.adobe.com/go/reader_download.

For more assistance with Adobe Reader visit http://www.adobe.com/go/acrreader.

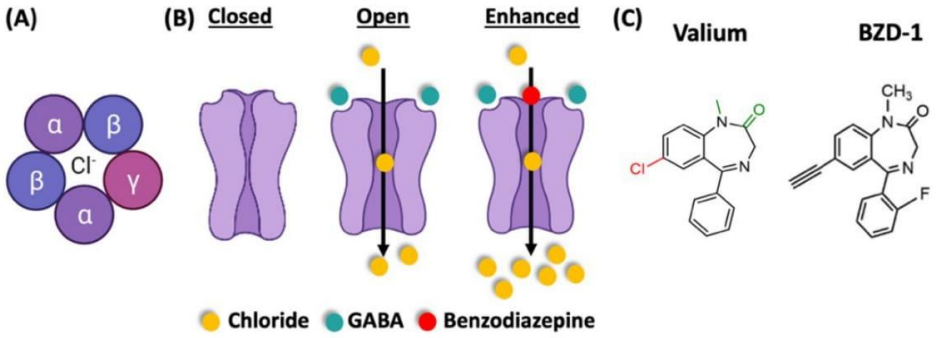
(A)
(B) Closed
Open
Enhanced
(C)
Valium
BZD-1
α
β
β
γ
α
Cl-
Chloride
GABA
Benzodiazepine

FIG. 1

**Table 1**. Cytotoxic responses of GBM cell lines treated with BZD-1±TMZ.

| Line | *MGMT* status | Recurrent or Primary | $IC_{50}$ TMZ, μM | $IC_{50}$ BZD-1, μM | $IC_{50}$ BZD-1 (0.1 μM) (non-cytotoxic conc.) + TMZ (μM) | Combination Index |
|---|---|---|---|---|---|---|
| G76 | Methylated | Recurrent | 1.31 | 0.613 | 0.103 | 0.24 |
| G75 | Unmethylated | Primary | 106.73 | 3.23 | 0.126 | 0.032 |
| G43 | Unmethylated | Primary | 165.43 | 6.67 | 0.360 | 0.018 |
| BT142 | Unmethylated (IDH1 mutant) | Primary | 15.33 | 0.443 | 0.190 | 0.235 |

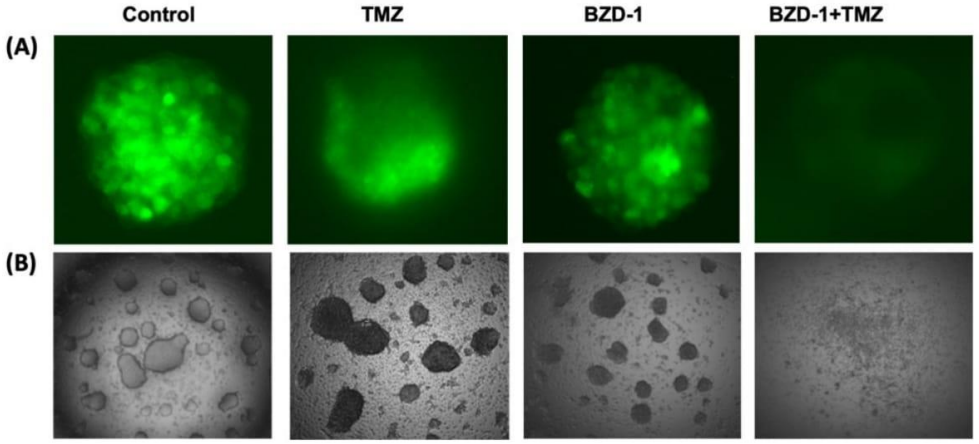


FIG. 2

PTO/AIA/14 (02-18)
Approved for use through 11/30/2020. OMB 0651-0032
U.S. Patent and Trademark Office; U.S. DEPARTMENT OF COMMERCE


| Application Data Sheet 37 CFR 1.76 | Attorney Docket Number | 2021-140; CIN0342MA |
|---|---|---|
| | Application Number | |
| Title of Invention | Small brain penetrant molecule to potentiate TMZ for glioblastoma | |

The application data sheet is part of the provisional or nonprovisional application for which it is being submitted. The following form contains the bibliographic data arranged in a format specified by the United States Patent and Trademark Office as outlined in 37 CFR 1.76.
This document may be completed electronically and submitted to the Office in electronic format using the Electronic Filing System (EFS) or the document may be printed and included in a paper filed application.

## Secrecy Order 37 CFR 5.2:

☐ Portions or all of the application associated with this Application Data Sheet may fall under a Secrecy Order pursuant to 37 CFR 5.2 (Paper filers only. Applications that fall under Secrecy Order may not be filed electronically.)

## Inventor Information:

**Inventor 1** Remove

**Legal Name**

| Prefix | Given Name | Middle Name | Family Name | Suffix |
|---|---|---|---|---|
| | Soma | | Sengupta | |

**Residence Information (Select One)** ◉ US Residency ○ Non US Residency ○ Active US Military Service

| City | Cincinnati | State/Province | OH | Country of Residence | US |
|---|---|---|---|---|---|

**Mailing Address of Inventor:**

| Address 1 | 209 Hosea Avenue | | |
|---|---|---|---|
| Address 2 | | | |
| City | Cincinnati | State/Province | OH |
| Postal Code | 45220 | Country | US |

**Inventor 2** Remove

**Legal Name**

| Prefix | Given Name | Middle Name | Family Name | Suffix |
|---|---|---|---|---|
| | Daniel | Pomeranz | Krummel | |

**Residence Information (Select One)** ◉ US Residency ○ Non US Residency ○ Active US Military Service

| City | Cincinnati | State/Province | OH | Country of Residence | US |
|---|---|---|---|---|---|

**Mailing Address of Inventor:**

| Address 1 | 209 Hosea Avenue | | |
|---|---|---|---|
| Address 2 | | | |
| City | Cincinnati | State/Province | OH |
| Postal Code | 45220 | Country | US |

**Inventor 3** Remove

**Legal Name**

| Prefix | Given Name | Middle Name | Family Name | Suffix |
|---|---|---|---|---|
| | James | | Cook | |

**Residence Information (Select One)** ◉ US Residency ○ Non US Residency ○ Active US Military Service

PTO/AIA/14 (02-18)
Approved for use through 11/30/2020. OMB 0651-0032
U.S. Patent and Trademark Office; U.S. DEPARTMENT OF COMMERCE
Under the Paperwork Reduction Act of 1995, no persons are required to respond to a collection of information unless it contains a valid OMB control number.

| Application Data Sheet 37 CFR 1.76 | Attorney Docket Number | 2021-140; CIN0342MA |
|---|---|---|
| | Application Number | |
| Title of Invention | Small brain penetrant molecule to potentiate TMZ for glioblastoma | |

| City | Whitefish Bay | State/Province | WI | Country of Residence | US |
|---|---|---|---|---|---|

**Mailing Address of Inventor:**

| Address 1 | 6139 North Lake Dr. | | |
|---|---|---|---|
| Address 2 | | | |
| City | Whitefish Bay | State/Province | WI |
| Postal Code | 53217 | Country | US |

Remove

**Inventor 4**

**Legal Name**

| Prefix | Given Name | Middle Name | Family Name | Suffix |
|---|---|---|---|---|
| | Taukir | | Ahmed | |

**Residence Information (Select One)** (•) US Residency ( ) Non US Residency ( ) Active US Military Service

| City | Milwaukee | State/Province | WI | Country of Residence | US |
|---|---|---|---|---|---|

**Mailing Address of Inventor:**

| Address 1 | 2466 N. Oakland Ave. Apt. 329 | | |
|---|---|---|---|
| Address 2 | | | |
| City | Milwaukee | State/Province | WI |
| Postal Code | 53211 | Country | US |

Remove

**Inventor 5**

**Legal Name**

| Prefix | Given Name | Middle Name | Family Name | Suffix |
|---|---|---|---|---|
| | Aniruddha | | Karve | |

**Residence Information (Select One)** (•) US Residency ( ) Non US Residency ( ) Active US Military Service

| City | Cincinnati | State/Province | OH | Country of Residence | US |
|---|---|---|---|---|---|

**Mailing Address of Inventor:**

| Address 1 | 2921 Marshall Avenue, Apt. 4 | | |
|---|---|---|---|
| Address 2 | | | |
| City | Cincinnati | State/Province | OH |
| Postal Code | 45220 | Country | US |

Remove

**Inventor 6**

**Legal Name**

| Prefix | Given Name | Middle Name | Family Name | Suffix |
|---|---|---|---|---|
| | Laura | | Kallay | |

**Residence Information (Select One)** (•) US Residency ( ) Non US Residency ( ) Active US Military Service

| City | Cincinnati | State/Province | OH | Country of Residence | US |
|---|---|---|---|---|---|

PTO/AIA/14 (02-18)
Approved for use through 11/30/2020. OMB 0651-0032
U.S. Patent and Trademark Office; U.S. DEPARTMENT OF COMMERCE


| Application Data Sheet 37 CFR 1.76 | Attorney Docket Number | 2021-140; CIN0342MA |
|---|---|---|
| | Application Number | |
| Title of Invention | Small brain penetrant molecule to potentiate TMZ for glioblastoma | |

**Mailing Address of Inventor:**

| | | | |
|---|---|---|---|
| **Address 1** | 222 Hosea Ave. Apt. 2 | | |
| **Address 2** | | | |
| **City** | Cincinnati | **State/Province** | OH |
| **Postal Code** | 45220 | **Country** i | US |

**Inventor 7** Remove

**Legal Name**

| Prefix | Given Name | Middle Name | Family Name | Suffix |
|---|---|---|---|---|
| | Pankaj | | Desai | |

**Residence Information (Select One)** (•) US Residency ( ) Non US Residency ( ) Active US Military Service

| | | | | | |
|---|---|---|---|---|---|
| **City** | Cincinnati | **State/Province** | OH | **Country of Residence** i | US |

**Mailing Address of Inventor:**

| | | | |
|---|---|---|---|
| **Address 1** | 7470 Rodney Court | | |
| **Address 2** | | | |
| **City** | Cincinnati | **State/Province** | OH |
| **Postal Code** | 45241 | **Country** i | US |

All Inventors Must Be Listed - Additional Inventor Information blocks may be generated within this form by selecting the **Add** button. Add

## Correspondence Information:

**Enter either Customer Number or complete the Correspondence Information section below.**
**For further information see 37 CFR 1.33(a).**

☐ **An Address is being provided for the correspondence Information of this application.**

| | | | |
|---|---|---|---|
| **Customer Number** | 24256 | | |
| **Email Address** | | Add Email | Remove Email |

## Application Information:

| | | | |
|---|---|---|---|
| **Title of the Invention** | Small brain penetrant molecule to potentiate TMZ for glioblastoma | | |
| **Attorney Docket Number** | 2021-140; CIN0342MA | **Small Entity Status Claimed** | ☒ |
| **Application Type** | Provisional | | |
| **Subject Matter** | Utility | | |
| **Total Number of Drawing Sheets (if any)** | 2 | **Suggested Figure for Publication (if any)** | |

PTO/AIA/14 (02-18)
Approved for use through 11/30/2020. OMB 0651-0032
U.S. Patent and Trademark Office; U.S. DEPARTMENT OF COMMERCE
Under the Paperwork Reduction Act of 1995, no persons are required to respond to a collection of information unless it contains a valid OMB control number.

| **Application Data Sheet 37 CFR 1.76** | Attorney Docket Number | 2021-140; CIN0342MA |
|---|---|---|
| | Application Number | |
| Title of Invention | Small brain penetrant molecule to potentiate TMZ for glioblastoma | |

## Filing By Reference:

Only complete this section when filing an application by reference under 35 U.S.C. 111(c) and 37 CFR 1.57(a). Do not complete this section if application papers including a specification and any drawings are being filed. Any domestic benefit or foreign priority information must be provided in the appropriate section(s) below (i.e., "Domestic Benefit/National Stage Information" and "Foreign Priority Information").

For the purposes of a filing date under 37 CFR 1.53(b), the description and any drawings of the present application are replaced by this reference to the previously filed application, subject to conditions and requirements of 37 CFR 1.57(a).

| Application number of the previously filed application | Filing date (YYYY-MM-DD) | Intellectual Property Authority or Country |
|---|---|---|
| | | |

## Publication Information:

☐ Request Early Publication (Fee required at time of Request 37 CFR 1.219)

☐ **Request Not to Publish.** I hereby request that the attached application not be published under 35 U.S.C. 122(b) and certify that the invention disclosed in the attached application **has not and will not** be the subject of an application filed in another country, or under a multilateral international agreement, that requires publication at eighteen months after filing.

## Representative Information:

Representative information should be provided for all practitioners having a power of attorney in the application. Providing this information in the Application Data Sheet does not constitute a power of attorney in the application (see 37 CFR 1.32).
Either enter Customer Number or complete the Representative Name section below. If both sections are completed the customer Number will be used for the Representative Information during processing.

| Please Select One: | ◉ Customer Number | ○ US Patent Practitioner | ○ Limited Recognition (37 CFR 11.9) |
|---|---|---|---|
| Customer Number | 24256 | | |

## Domestic Benefit/National Stage Information:

This section allows for the applicant to either claim benefit under 35 U.S.C. 119(e), 120, 121, 365(c), or 386(c) or indicate National Stage entry from a PCT application. Providing benefit claim information in the Application Data Sheet constitutes the specific reference required by 35 U.S.C. 119(e) or 120, and 37 CFR 1.78.
When referring to the current application, please leave the "Application Number" field blank.

| Prior Application Status | | | Remove |
|---|---|---|---|
| Application Number | Continuity Type | Prior Application Number | Filing or 371(c) Date (YYYY-MM-DD) |
| | | | |

Additional Domestic Benefit/National Stage Data may be generated within this form by selecting the **Add** button.

PTO/AIA/14 (02-18)
Approved for use through 11/30/2020. OMB 0651-0032
U.S. Patent and Trademark Office; U.S. DEPARTMENT OF COMMERCE


| **Application Data Sheet 37 CFR 1.76** | Attorney Docket Number | 2021-140; CIN0342MA |
|---|---|---|
| | Application Number | |
| Title of Invention | Small brain penetrant molecule to potentiate TMZ for glioblastoma | |

## Foreign Priority Information:

This section allows for the applicant to claim priority to a foreign application. Providing this information in the application data sheet constitutes the claim for priority as required by 35 U.S.C. 119(b) and 37 CFR 1.55. When priority is claimed to a foreign application that is eligible for retrieval under the priority document exchange program (PDX)[i] the information will be used by the Office to automatically attempt retrieval pursuant to 37 CFR 1.55(i)(1) and (2). Under the PDX program, applicant bears the ultimate responsibility for ensuring that a copy of the foreign application is received by the Office from the participating foreign intellectual property office, or a certified copy of the foreign priority application is filed, within the time period specified in 37 CFR 1.55(g)(1).

Remove

| Application Number | Country[i] | Filing Date (YYYY-MM-DD) | Access Code[i] (if applicable) |
|---|---|---|---|
| | | | |

Additional Foreign Priority Data may be generated within this form by selecting the **Add** button.

## Statement under 37 CFR 1.55 or 1.78 for AIA (First Inventor to File) Transition Applications

☐ This application (1) claims priority to or the benefit of an application filed before March 16, 2013 and (2) also contains, or contained at any time, a claim to a claimed invention that has an effective filing date on or after March 16, 2013.
NOTE: By providing this statement under 37 CFR 1.55 or 1.78, this application, with a filing date on or after March 16, 2013, will be examined under the first inventor to file provisions of the AIA.

PTO/AIA/14 (02-18)
Approved for use through 11/30/2020. OMB 0651-0032
U.S. Patent and Trademark Office; U.S. DEPARTMENT OF COMMERCE
Under the Paperwork Reduction Act of 1995, no persons are required to respond to a collection of information unless it contains a valid OMB control number.

| **Application Data Sheet 37 CFR 1.76** | Attorney Docket Number | 2021-140; CIN0342MA |
|---|---|---|
| | Application Number | |
| Title of Invention | Small brain penetrant molecule to potentiate TMZ for glioblastoma | |

## Authorization or Opt-Out of Authorization to Permit Access:

When this Application Data Sheet is properly signed and filed with the application, applicant has provided written authority to permit a participating foreign intellectual property (IP) office access to the instant application-as-filed (see paragraph A in subsection 1 below) and the European Patent Office (EPO) access to any search results from the instant application (see paragraph B in subsection 1 below).

Should applicant choose not to provide an authorization identified in subsection 1 below, applicant **must opt-out** of the authorization by checking the corresponding box A or B or both in subsection 2 below.

**NOTE**: This section of the Application Data Sheet is **ONLY** reviewed and processed with the **INITIAL** filing of an application. After the initial filing of an application, an Application Data Sheet cannot be used to provide or rescind authorization for access by a foreign IP office(s). Instead, Form PTO/SB/39 or PTO/SB/69 must be used as appropriate.

**1. Authorization to Permit Access by a Foreign Intellectual Property Office(s)**

**A. Priority Document Exchange (PDX)** - Unless box A in subsection 2 (opt-out of authorization) is checked, the undersigned hereby **grants the USPTO authority** to provide the European Patent Office (EPO), the Japan Patent Office (JPO), the Korean Intellectual Property Office (KIPO), the State Intellectual Property Office of the People's Republic of China (SIPO), the World Intellectual Property Organization (WIPO), and any other foreign intellectual property office participating with the USPTO in a bilateral or multilateral priority document exchange agreement in which a foreign application claiming priority to the instant patent application is filed, access to: (1) the instant patent application-as-filed and its related bibliographic data, (2) any foreign or domestic application to which priority or benefit is claimed by the instant application and its related bibliographic data, and (3) the date of filing of this Authorization. See 37 CFR 1.14(h)(1).

**B. Search Results from U.S. Application to EPO** - Unless box B in subsection 2 (opt-out of authorization) is checked, the undersigned hereby **grants the USPTO authority** to provide the EPO access to the bibliographic data and search results from the instant patent application when a European patent application claiming priority to the instant patent application is filed. See 37 CFR 1.14(h)(2).

The applicant is reminded that the EPO's Rule 141(1) EPC (European Patent Convention) requires applicants to submit a copy of search results from the instant application without delay in a European patent application that claims priority to the instant application.

**2. Opt-Out of Authorizations to Permit Access by a Foreign Intellectual Property Office(s)**

☐ A. Applicant **DOES NOT** authorize the USPTO to permit a participating foreign IP office access to the instant application-as-filed. If this box is checked, the USPTO will not be providing a participating foreign IP office with any documents and information identified in subsection 1A above.

☐ B. Applicant **DOES NOT** authorize the USPTO to transmit to the EPO any search results from the instant patent application. If this box is checked, the USPTO will not be providing the EPO with search results from the instant application.

**NOTE:** Once the application has published or is otherwise publicly available, the USPTO may provide access to the application in accordance with 37 CFR 1.14.

PTO/AIA/14 (02-18)
Approved for use through 11/30/2020. OMB 0651-0032
U.S. Patent and Trademark Office; U.S. DEPARTMENT OF COMMERCE
Under the Paperwork Reduction Act of 1995, no persons are required to respond to a collection of information unless it contains a valid OMB control number.

| **Application Data Sheet 37 CFR 1.76** | Attorney Docket Number | 2021-140; CIN0342MA |
|---|---|---|
| | Application Number | |
| Title of Invention | Small brain penetrant molecule to potentiate TMZ for glioblastoma | |

## Applicant Information:

Providing assignment information in this section does not substitute for compliance with any requirement of part 3 of Title 37 of CFR to have an assignment recorded by the Office.

**Applicant 1**

If the applicant is the inventor (or the remaining joint inventor or inventors under 37 CFR 1.45), this section should not be completed. The information to be provided in this section is the name and address of the legal representative who is the applicant under 37 CFR 1.43; or the name and address of the assignee, person to whom the inventor is under an obligation to assign the invention, or person who otherwise shows sufficient proprietary interest in the matter who is the applicant under 37 CFR 1.46. If the applicant is an applicant under 37 CFR 1.46 (assignee, person to whom the inventor is obligated to assign, or person who otherwise shows sufficient proprietary interest) together with one or more joint inventors, then the joint inventor or inventors who are also the applicant should be identified in this section.

Clear

| ◯ Assignee | ◯ Legal Representative under 35 U.S.C. 117 | ◯ Joint Inventor |
|---|---|---|
| ◉ Person to whom the inventor is obligated to assign. | ◯ Person who shows sufficient proprietary interest | |

If applicant is the legal representative, indicate the authority to file the patent application, the inventor is:

Name of the Deceased or Legally Incapacitated Inventor:

If the Applicant is an Organization check here. ☒

| Organization Name | University of Cincinnati |
|---|---|

**Mailing Address Information For Applicant:**

| **Address 1** | 2900 Reading Road | | |
|---|---|---|---|
| Address 2 | Suite 460 | | |
| **City** | Cincinnati | **State/Province** | OH |
| **Country** | US | Postal Code | 45221 |
| Phone Number | | Fax Number | |
| Email Address | | | |

Additional Applicant Data may be generated within this form by selecting the Add button.

PTO/AIA/14 (02-18)
Approved for use through 11/30/2020. OMB 0651-0032
U.S. Patent and Trademark Office; U.S. DEPARTMENT OF COMMERCE
Under the Paperwork Reduction Act of 1995, no persons are required to respond to a collection of information unless it contains a valid OMB control number.

| **Application Data Sheet 37 CFR 1.76** | Attorney Docket Number | 2021-140; CIN0342MA |
|---|---|---|
| | Application Number | |
| Title of Invention | Small brain penetrant molecule to potentiate TMZ for glioblastoma | |

**Applicant 2**

If the applicant is the inventor (or the remaining joint inventor or inventors under 37 CFR 1.45), this section should not be completed. The information to be provided in this section is the name and address of the legal representative who is the applicant under 37 CFR 1.43; or the name and address of the assignee, person to whom the inventor is under an obligation to assign the invention, or person who otherwise shows sufficient proprietary interest in the matter who is the applicant under 37 CFR 1.46. If the applicant is an applicant under 37 CFR 1.46 (assignee, person to whom the inventor is obligated to assign, or person who otherwise shows sufficient proprietary interest) together with one or more joint inventors, then the joint inventor or inventors who are also the applicant should be identified in this section.

Clear

| ◯ Assignee | ◯ Legal Representative under 35 U.S.C. 117 | ◯ Joint Inventor |
|---|---|---|
| ◉ Person to whom the inventor is obligated to assign. | ◯ Person who shows sufficient proprietary interest | |

If applicant is the legal representative, indicate the authority to file the patent application, the inventor is:

Name of the Deceased or Legally Incapacitated Inventor:

If the Applicant is an Organization check here. ☒

| Organization Name | ~~University of Wisconsin~~ UWM Research Foundation, Inc. |
|---|---|

**Mailing Address Information For Applicant:**

| **Address 1** | ~~UWM Research Foundation, Inc.~~ 1440 East North Avenue | | |
|---|---|---|---|
| Address 2 | ~~1440 East North Avenue~~ | | |
| **City** | Milwaukee | **State/Province** | WI |
| **Country** | US | Postal Code | 53202 |
| Phone Number | | Fax Number | |
| Email Address | | | |

Additional Applicant Data may be generated within this form by selecting the Add button.

## Assignee Information including Non-Applicant Assignee Information:

Providing assignment information in this section does not substitute for compliance with any requirement of part 3 of Title 37 of CFR to have an assignment recorded by the Office.

**Assignee 1**

Complete this section if assignee information, including non-applicant assignee information, is desired to be included on the patent application publication. An assignee-applicant identified in the "Applicant Information" section will appear on the patent application publication as an applicant. For an assignee-applicant, complete this section only if identification as an assignee is also desired on the patent application publication.

If the Assignee or Non-Applicant Assignee is an Organization check here. ☒

PTO/AIA/14 (02-18)
Approved for use through 11/30/2020. OMB 0651-0032
U.S. Patent and Trademark Office; U.S. DEPARTMENT OF COMMERCE
Under the Paperwork Reduction Act of 1995, no persons are required to respond to a collection of information unless it contains a valid OMB control number.

| **Application Data Sheet 37 CFR 1.76** | Attorney Docket Number | 2021-140; CIN0342MA |
|---|---|---|
| | Application Number | |
| Title of Invention | Small brain penetrant molecule to potentiate TMZ for glioblastoma | |

| Organization Name | ~~University of Cincinnati~~ | | |
|---|---|---|---|
| **Mailing Address Information For Assignee including Non-Applicant Assignee:** | | | |
| **Address 1** | ~~2900 Reading Road~~ | | |
| Address 2 | ~~Suite 460~~ | | |
| **City** | ~~Cincinnati~~ | **State/Province** | ~~OH~~ |
| **Country** [i] | ~~US~~ | Postal Code | ~~45221~~ |
| Phone Number | | Fax Number | |
| Email Address | | | |

Additional Assignee or Non-Applicant Assignee Data may be generated within this form by selecting the Add button.

**Assignee 2**

Complete this section if assignee information, including non-applicant assignee information, is desired to be included on the patent application publication. An assignee-applicant identified in the "Applicant Information" section will appear on the patent application publication as an applicant. For an assignee-applicant, complete this section only if identification as an assignee is also desired on the patent application publication.

If the Assignee or Non-Applicant Assignee is an Organization check here. ~~☒~~

| Organization Name | ~~University of Wisconsin~~ | | |
|---|---|---|---|
| **Mailing Address Information For Assignee including Non-Applicant Assignee:** | | | |
| **Address 1** | ~~UWM Research Foundation, Inc.~~ | | |
| Address 2 | ~~1440 East North Avenue~~ | | |
| **City** | ~~Milwaukee~~ | **State/Province** | ~~WI~~ |
| **Country** [i] | ~~US~~ | Postal Code | ~~53202~~ |
| Phone Number | | Fax Number | |
| Email Address | | | |

Additional Assignee or Non-Applicant Assignee Data may be generated within this form by selecting the Add button.

PTO/AIA/14 (02-18)
Approved for use through 11/30/2020. OMB 0651-0032
U.S. Patent and Trademark Office; U.S. DEPARTMENT OF COMMERCE
Under the Paperwork Reduction Act of 1995, no persons are required to respond to a collection of information unless it contains a valid OMB control number.

| **Application Data Sheet 37 CFR 1.76** | Attorney Docket Number | 2021-140; CIN0342MA |
|---|---|---|
| | Application Number | |
| Title of Invention | Small brain penetrant molecule to potentiate TMZ for glioblastoma | |

## Signature:

**NOTE:** This Application Data Sheet must be signed in accordance with 37 CFR 1.33(b). **However, if this Application Data Sheet is submitted with the INITIAL filing of the application and either box A or B is not checked in subsection 2 of the "Authorization or Opt-Out of Authorization to Permit Access" section, then this form must also be signed in accordance with 37 CFR 1.14(c).**

This Application Data Sheet **must** be signed by a patent practitioner if one or more of the applicants is a **juristic entity** (e.g., corporation or association). If the applicant is two or more joint inventors, this form must be signed by a patent practitioner, **all** joint inventors who are the applicant, or one or more joint inventor-applicants who have been given power of attorney (e.g., see USPTO Form PTO/AIA/81) on behalf of **all** joint inventor-applicants.

See 37 CFR 1.4(d) for the manner of making signatures and certifications.

| **Signature** | /Jennifer L. Livingston/ | | | Date (YYYY-MM-DD) | 2021-06-04 |
|---|---|---|---|---|---|
| First Name | Jennifer L. | Last Name | Livingston | Registration Number | 56,404 |

Additional Signature may be generated within this form by selecting the Add button.

This collection of information is required by 37 CFR 1.76. The information is required to obtain or retain a benefit by the public which is to file (and by the USPTO to process) an application. Confidentiality is governed by 35 U.S.C. 122 and 37 CFR 1.14. This collection is estimated to take 23 minutes to complete, including gathering, preparing, and submitting the completed application data sheet form to the USPTO. Time will vary depending upon the individual case. Any comments on the amount of time you require to complete this form and/or suggestions for reducing this burden, should be sent to the Chief Information Officer, U.S. Patent and Trademark Office, U.S. Department of Commerce, P.O. Box 1450, Alexandria, VA 22313-1450. DO NOT SEND FEES OR COMPLETED FORMS TO THIS ADDRESS. **SEND TO: Commissioner for Patents, P.O. Box 1450, Alexandria, VA 22313-1450.**

# Privacy Act Statement

The Privacy Act of 1974 (P.L. 93-579) requires that you be given certain information in connection with your submission of the attached form related to a patent application or patent. Accordingly, pursuant to the requirements of the Act, please be advised that: (1) the general authority for the collection of this information is 35 U.S.C. 2(b)(2); (2) furnishing of the information solicited is voluntary; and (3) the principal purpose for which the information is used by the U.S. Patent and Trademark Office is to process and/or examine your submission related to a patent application or patent. If you do not furnish the requested information, the U.S. Patent and Trademark Office may not be able to process and/or examine your submission, which may result in termination of proceedings or abandonment of the application or expiration of the patent.

The information provided by you in this form will be subject to the following routine uses:

1 The information on this form will be treated confidentially to the extent allowed under the Freedom of Information Act (5 U.S.C. 552) and the Privacy Act (5 U.S.C. 552a). Records from this system of records may be disclosed to the Department of Justice to determine whether the Freedom of Information Act requires disclosure of these records.

2. A record from this system of records may be disclosed, as a routine use, in the course of presenting evidence to a court, magistrate, or administrative tribunal, including disclosures to opposing counsel in the course of settlement negotiations.

3 A record in this system of records may be disclosed, as a routine use, to a Member of Congress submitting a request involving an individual, to whom the record pertains, when the individual has requested assistance from the Member with respect to the subject matter of the record.

4. A record in this system of records may be disclosed, as a routine use, to a contractor of the Agency having need for the information in order to perform a contract. Recipients of information shall be required to comply with the requirements of the Privacy Act of 1974, as amended, pursuant to 5 U.S.C. 552a(m).

5. A record related to an International Application filed under the Patent Cooperation Treaty in this system of records may be disclosed, as a routine use, to the International Bureau of the World Intellectual Property Organization, pursuant to the Patent CooperationTreaty.

6. A record in this system of records may be disclosed, as a routine use, to another federal agency for purposes of National Security review (35 U.S.C. 181) and for review pursuant to the Atomic Energy Act (42 U.S.C. 218(c)).

7. A record from this system of records may be disclosed, as a routine use, to the Administrator, General Services, or his/her designee, during an inspection of records conducted by GSA as part of that agency's responsibility to recommend improvements in records management practices and programs, under authority of 44 U.S.C. 2904 and 2906. Such disclosure shall be made in accordance with the GSA regulations governing inspection of records for this purpose, and any other relevant (i.e., GSA or Commerce) directive. Such disclosure shall not be used to make determinations about individuals.

8. A record from this system of records may be disclosed, as a routine use, to the public after either publication of the application pursuant to 35 U.S.C. 122(b) or issuance of a patent pursuant to 35 U.S.C. 151. Further, a record may be disclosed, subject to the limitations of 37 CFR 1.14, as a routine use, to the public if the record was filed in an application which became abandoned or in which the proceedings were terminated and which application is referenced by either a published application, an application open to public inspections or an issued patent.

9. A record from this system of records may be disclosed, as a routine use, to a Federal, State, or local law enforcement agency, if the USPTO becomes aware of a violation or potential violation of law or regulation.

EFS Web 2.2.13

**IN THE UNITED STATES PATENT AND TRADEMARK OFFICE**

Application of:

Applicants : University of Cincinnati & UWM Research Foundation, Inc.
Serial No. : 63/196,459
Filed : June 3, 2021
Title : Small brain penetrant molecule to potentiate TMZ for glioblastoma
Docket : 2021-140; CIN0342MA
Confirm. No.: 7944

Commissioner for Patents
P.O. Box 1450
Alexandria, VA 22313-1450

Commissioner:

**COMMUNICATION**

The above-identified provisional application was electronically filed with the U.S. Patent Office on June 3, 2021. In reviewing the filed documents, it was noted that certain to the Application Data Sheet and Provisional Cover Sheet are required. Accordingly, an updated Application Data Sheet and Provisional Cover Sheet are submitted herewith, wherein the following corrections are made:

Provisional Cover Sheet:

- The city of Inventor 3 is corrected to delete "Cincinnati" and recite "Whitefish Bay."

Application Data Sheet:

- The name of the second Applicant is amended to delete "University of Wisconsin" and recite "UWM Research Foundation, Inc."
- The address of the second Applicant is amended to recite "1440 East North Avenue, Milwaukee, WI 53202."
- Information for Assignees 1 and 2 is deleted.

Applicants respectfully request that the above corrections be made and reflected on the official filing receipt for this application.

Please direct any questions or comments to the undersigned attorney. It is believed that no additional fees are required to effect these corrections. However, the Director is hereby authorized to charge any required fee connected with this request to Deposit Account No. 04-1133.

Respectfully submitted,
DINSMORE & SHOHL LLP

By /Jennifer L. Livingston/
Jennifer L. Livingston
Reg. No. 56,404

Fifth Third Center
255 East Fifth Street, Suite 1900
Cincinnati, OH 45202
Telephone: 513/977-8359
Facsimile: 513/977-8141

.

## 5. 2. 3 Novel deuterated benzodiazepine analogs for cancer use

### Inventors

Daniel Krummel, University of Cincinnati College of Medicine; Soma Sengupta, University of Cincinnati College of Medicine; James Cook, University of Wisconsin-Milwaukee; Taukir Ahmed, University of Wisconsin-Milwaukee

### Background

Deuterium (D) is an isotope of hydrogen that occupies a smaller volume, is less lipophilic, and forms a shorter and thus stronger bond with Carbon. These attributes contribute to reducing the metabolization of molecules with deuterium incorporated and thus improve their pharmacokinetic profile[1]. This may serve to lower the therapeutic doses needed to achieve efficacy, thereby reducing the molecules potential side-effects or toxicity. As well as enhancing the bioavailability of molecules, deuterium may also be used for imaging in medical applications. Deuterated molecules can be imaged and quantified using magnetic resonance. For example, deuterium in vivo [$^2$H] MR spectroscopic imaging has been used to quantify metabolic differences of tumors versus healthy tissue in an animal model as well as in humans by using deuterium labeled glucose and following deuterated products of glycolysis[2]. This research has opened the way for using deuterated compounds to image tumors as well as investigate tumor biology in vivo.

Type-A GABA neurotransmitter receptors are a major inhibitory neurotransmitter receptor in the mammalian central nervous system. Type-A GABA neurotransmitter receptors are also present outside of the CNS. In addition, genes coding for subunits of Type-A GABA neurotransmitter receptors are expressed in disparate cancer cells and we have contributed to establishing that cancer cells possess intrinsic functional Type-A GABA neurotransmitter receptors[3-7].

Type-A GABA neurotransmitter receptors are significant pharmacologic targets to treat various neurological disorders, including anxiety and epilepsy. Amongst the pharmacologics that work through acting on the Type-A GABA neurotransmitter receptors are the benzodiazepines, which bind at the interface between its alpha and gamma subunits of the pentameric structure (Figure 2A). We have previously reported that a class of benzodiazepines are also effective in impairing the viability of cancer cells[3-7]. Benzodiazepines function to enhance the effectiveness (chloride anion transport) of the natural ligand Type-A GABA neurotransmitter receptors GABA (Figure 2B). In cancer cells we have found that our novel class of benzodiazepines enhance in cancer cells a chloride anion efflux which initiates a cascade of events that impairs cancer cell viability[3-7].

We have synthesized new deuterated benzodiazepine analogs for targeted binding to the Type-A GABA neurotransmitter receptor (Figure 1). We have assayed MYM-III-85 to impair viability of disparate cancer cells, using to assess efficacy an established technique (CellTiter96R Aqueous One Solution Cell Proliferation Assay, Promega). The human cell lines tested: glioma line LN18 (ATCC CRL-2610, which is mutated TP53); glioma line U87 (ATCC HTB-14); non-small cell lung cancer line H1792 (ATCC CRL-5895); medulloblastoma MB002 (available via Expasy Accession# CVCL_VU79). The growth of these lines is impaired by incubation with MYM-III-85 with IC50 values of 2-4 micromolar (Table 1; Figure 3). The novel deuterated variant MYM-III-85 is as potent as the non-deuterated variant.

### References

1. Knutson DE, Kodali R, Divović B, et al. (2018). Design and Synthesis of Novel Deuterated Ligands Functionally Selective for the γ-Aminobutyric Acid Type A Receptor (GABAAR) α6 Subtype with Improved Metabolic Stability and Enhanced Bioavailability. J Med Chem. 61: 2422-2446.
2. De Feyter HM, Behar KL, Corbin ZA, et al. (2018). Deuterium metabolic imaging (DMI) for MRI-based 3D mapping of metabolism in vivo. Sci Adv. 4: t7314.
3. Sengupta S., Weeraratne S.D., Sun H, Phallen J., Rallapalli S.K., Teider N., Kosaras B., Amani V., Pierre-Francois J., Tang Y., Nguyen B., Yu F., Schubert S., Balansay B., Mathios D., Lechpammer M., Archer T.C., Tran P., Reimer R.J., Cook J.M., Lim M., Jensen F.E., Pomeroy S.L., Cho Y-J. (2014). a5-GABAA receptors negatively regulate MYC-amplified medulloblastoma growth. Acta Neuropathol. 127: 593-603
4. Jonas O., Calligaris D., Methuku K.R., Poe M.M., Francois J.P., Tranghese F., Changelian A., Sieghart W., Ernst M., Pomeranz Krummel D.A., Cook J.M., Pomeroy S.L., Cima M., Agar N.Y., Langer R., Sengupta S. (2016). First in vivo testing of compounds targeting Group 3 medulloblastomas using an implantable microdevice as a new paradigm for drug development. J. Biomed. Nanotech. 12(6): 1297-302.
5. Kallay L., Keskin H., Ross A., Rupji M., Moody O.A., Li G., Ahmed T., Rashid R., Stephen M.R., Cottrill K.A., Nuckols A., Zu M., Martinson D.E., Tranghese F., Wang X., Taylor M., Cook J., Kowalski J., Jenkins A., Pomeranz Krummel D., Sengupta S. (2019). Modulating native GABAA receptors in cancer cells with positive allosteric benzodiazepine-derivatives induces cell death. J Neuro-Oncol. 142: 411-422.
6. Pomeranz Krummel D.A., Nasti T.H., Kaluzova M., Kallay L., Bhattacharya D., Melms J.C., Izar B., Xu M., Burnham A., Ahmed T., Li G, Lawson D., Kowalski J., Cao Y., Switchenko J.M., Ionascu D., Cook J.M., Medvedovic M., Jenkins A., Khan M.K., Sengupta S. (2021). Melanoma cell intrinsic $GABA_A$ receptor enhancement potentiates radiation and immune checkpoint response by promoting direct and T cell-mediated anti-tumor activity. International Journal of Radiation Oncology, Biology, Physics. 109(4): P1040-1053.
7. Bhattacharya D., Gawali V.S., Kallay L., Toukam D.K., Koehler A., Stambrook P., Pomeranz Krummel D.A., Sengupta S. (2021). Therapeutically leveraging $GABA_A$ receptors in cancer. Experimental Biology and Medicine. 246: 2128-2135.

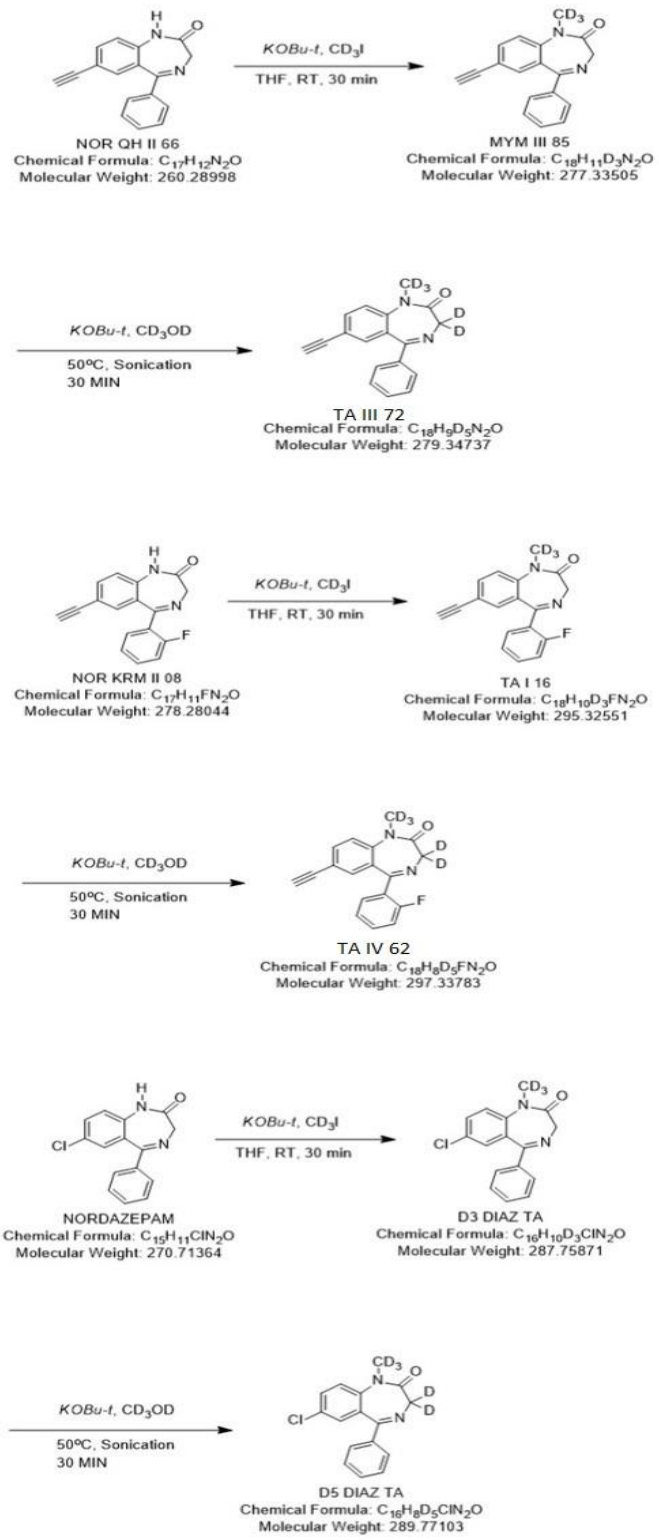


**Figure 1.** Synthesis of deuterated benzodiazepine analogues.

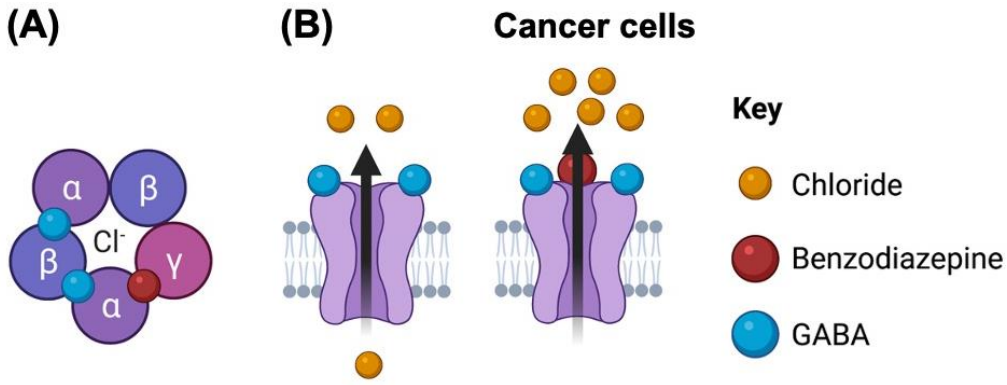


**Figure 2.** (**A**) Type-A GABA receptors are composed most commonly of two α, two β, and γ subunits. Type-A GABA receptors consists of five subunit transmembrane segments which create the chloride ($Cl^-$) conduction pore. Inter-subunit binding sites for GABA (cyan) and benzodiazepine (red) are shown, recognizing the αβαβγ subunit stoichiometry. (B) Binding of GABA (agonist) to Type-A GABA receptors leads to $Cl^-$ transport. Binding of benzodiazepine to Type-A GABA receptors enhanced $Cl^-$ transport.

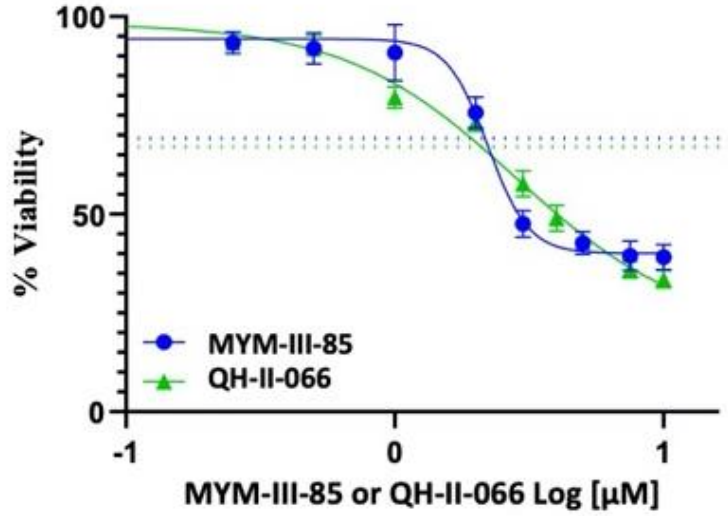


**Figure 3.** Dose response curve of MYM-III-85 and QH-II-066 in human glioma line LN18.

**Table 1**. IC50 values of benzodiazepine analogs with disparate human cancer cell lines.

| Compound | Structure | Glioblastoma (LN18) IC50 | Glioblastoma (U87) IC50 | Non-small Cell Lung Cancer (H1792) IC50 | Medulloblastoma (MB002) IC50 |
|---|---|---|---|---|---|
| QH-II-066 |  | 2.8 | - | 4.5 | - |
| NOR-QH-II-066 |  | 0.69 | - | - | - |
| MYM-III-85 | 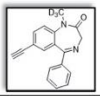 | 2.2 | 4 | 3.3 | 2.2 |

### 5. 2. 4 Small brain penetrant molecule to potentiate TMZ for glioblastoma

## OVERVIEW OF INVENTION

Glioblastoma multiforme (GBM) is a highly malignant (Grade IV) primary brain tumor. Standard-of-care for GBM includes radiotherapy with concomitant administration of a DNA alkylator, temozolomide (TMZ). This approach shows a degree of effectiveness if GBM cells are adequately *MGMT* promoter methylated (~50% of GBM tumors), as reduction in MGMT protein leads to diminished ability to reverse TMZ-induced DNA damage. Histone deacetylase inhibitors have recently been employed to improve TMZ effectiveness, but unfortunately result in bone marrow toxicity without contributing to durable responses. TMZ is also not without its own debilitating and life-threatening side-effects, including leukopenia. Tragically, survival remains only 12-15 months under this treatment regimen. There is an ***urgent need*** to increase the effectiveness of TMZ for *MGMT* methylated GBMs, identify a treatment approach that is effective for *MGMT* unmethylated GBMs, and reduce TMZ side-effects.

Our ***goal*** is to identify an approach capable of potentiating current GBM standard-of-care treatment irrespective of *MGMT* methylation status, as well as mitigate side effects. We have shown that by targeting a unique electrochemical vulnerability in GBMs with a non-toxic brain-penetrant small molecule, GBM tumor cells can be sensitized to TMZ irrespective of *MGMT* methylation status. The ***rationale*** that underlies this proposal is our finding that GBM cells as well as tumor cells from a subgroup of patients of the pediatric brain cancer medulloblastoma and melanomas possess functional Type-A GABA receptors ($GABA_ARs$), chloride ion channels, that when targeted with members of a novel class of benzodiazepine analogs (BZDs), ion dynamics in these disparate cancer cells is altered and apoptotic responses elicited (1-4). We have found using

medulloblastoma and melanoma mouse models that BZD on its own can induce apoptosis and regress tumor volume (2,4). In a syngeneic melanoma mouse model, we find that a particular BZD (termed QH-II-066) when combined with radiation, even at suboptimal-doses, results in complete tumor loss in most mice. In our studies on GBM, QH-II-066 can potentiate TMZ irrespective of the *MGMT* methylation status. This effect is dramatic and synergistic. *Our central hypothesis* is that QH-II-066 can be an effective 'add-on' therapeutic to potentiate TMZ irrespective of *MGMT* methylation status.

**Highlights**

- QH-II-066 enhances $Cl^-$ anion transport via $GABA_AR$, thereby altering ion dynamics, inhibiting the drug efflux transporter P-glycoprotein, and inducing apoptotic responses.
- QH-II-066 triggered electrochemical changes in the cancer cells potentiates TMZ significantly and synergistically, irrespective of the MGMT status of GBM cells.

## BACKGROUND

**Glioblastoma**. GBM is one of the deadliest human cancers and highly challenging to treat. GBM tumor cells interact with diverse cells in a complex microenvironment (5,6). Further, the Blood-Brain Barrier (BBB) acts to limit drug bioavailability and facilitate immune evasion. Unfortunately, GBM cells frequently subvert the physiological function of the cerebrovascular tissue and turn the BBB into an effective Blood-Tumor Barrier (BTB) capable of protecting the cancer tissue from drugs as well as systemic immunity. Despite increasing knowledge of genetic and epigenetic changes underlying GBM tumor initiation and growth, GBM prognosis remains poor.

**GABA$_A$R structure-function**. GABA receptors (GABA$_A$Rs) form pentameric chloride ($Cl^-$) channels, composed most commonly of two α, two β, and γ subunits encoded by GABR genes GABRA (1-6), GABRB (1-3), and GABRG (1-3), respectively (7,8) (Fig. 1a). GABA$_A$Rs are fundamental in determining an excitation/inhibition balance in the central nervous system. As a receptor mediating $Cl^-$ flux, GABA$_A$Rs predominantly function to hyperpolarize neural cells, following binding of its ligand GABA (Fig. 1b).

**GABA$_A$R activation**. GABA$_A$Rs have been an important therapeutic target since the clinical introduction of benzodiazepines in the 1960s. Benzodiazepines bind at the γ-α interface of GABA$_A$R (Fig. 1a) and act to increase effectiveness of GABA and thus enhance $Cl^-$ flux (Fig. 1b). FDA approved benzodiazepines consist most commonly of fusion of diazepine and benzene rings (1,4-benzodiazepine) and a phenol ring (5-phenyl-1H-benzo[e]) (Fig. 1c). J. Cook and his team (Univ. Wisconsin-Milwaukee) introduced an ethinyl bond at R7 in place of a chlorine in Valium (Fig. 1c). which confers anti-cancer activity.

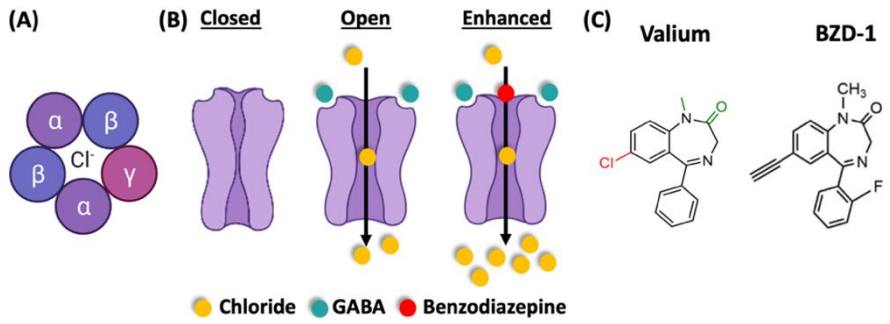


**Fig. 1. GABA$_A$Rs.** (A) A GABA$_A$R, looking down the chloride ion conduction pore. (B) Binding of two GABA ligands opens the channel, binding of a benzodiazepine enhances chloride ion flux. (C) Structure of the classic benzodiazepine Valium (left) and the novel benzodiazepine analog used in proposed studies (right; QH-II-066 or BZD-1). Key difference is an ethinyl bond in place of a chlorine

## DATA

**BZD-1 potentiates TMZ, irrespective of *MGMT* methylation status**. In vitro cytotoxicity studies of methylated and unmethylated GBM cells treated with QH-II-066 and TMZ as single agents or in combination demonstrates that the combined therapy overcomes TMZ resistance in unmethylated GBM cell lines and is significantly more potent than TMZ alone in killing GBM cells, irrespective of methylation status (Table 1). Using the Chou-Talay Combination Index Equation for quantitative synergy determination in two-drug combinations, we find that QH-II-066 and TMZ act synergistically. We also conducted spheroid assays using two unmethylated GBM lines to qualitatively assess the effect of QH-II-066+TMZ. This assay revealed a very significant disaggregation in response to combination therapy, suggestive of a disruption in tumor-initiating activity (Fig. 2).

**Table 1**. Cytotoxic responses of GBM cell lines treated with BZD-1±TMZ.

| Line | *MGMT* status | Recurrent or Primary | $IC_{50}$ TMZ, μM | $IC_{50}$ BZD-1, μM | $IC_{50}$ BZD-1 (0.1 μM) (non-cytotoxic conc.) + TMZ (μM) | Combination Index |
|---|---|---|---|---|---|---|
| G76 | Methylated | Recurrent | 1.31 | 0.613 | 0.103 | 0.24 |
| G75 | Unmethylated | Primary | 106.73 | 3.23 | 0.126 | 0.032 |
| G43 | Unmethylated | Primary | 165.43 | 6.67 | 0.360 | 0.018 |
| BT142 | Unmethylated (IDH1 mutant) | Primary | 15.33 | 0.443 | 0.190 | 0.235 |

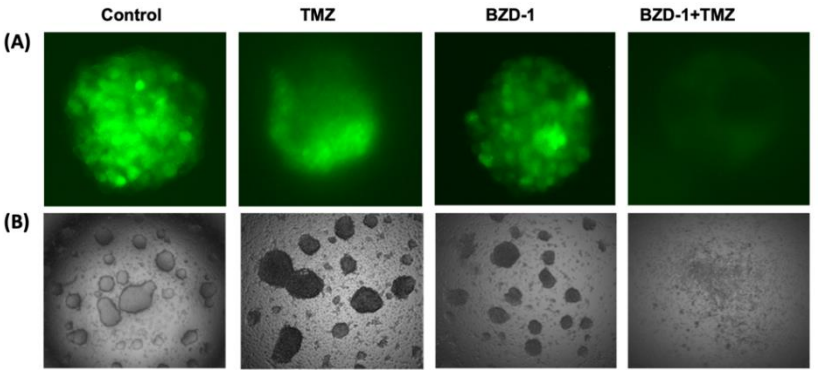


**Fig. 2. Cytotoxicity of unmethylated GBM cell lines treated with BZD-1±TMZ.** Spheroids of unmethylated GBM lines BT142-GFP (A) and G43 (B) were treated with TMZ, BZD-1, or BZD-1+TMZ.

**Formulated QH-II-066 is metabolically stable and rapidly penetrates and accumulates in the brain**. We have explored different approaches to formulate QH-II-066. We identified a co-solvent based injectable formulation (already U.S. FDA approved for benzodiazepines) as satisfactory. In this co-solvent formulation, QH-II-066 is highly soluble (10 mg/mL); stable at room temperature for up to 6 months; shows no visible adverse effects in rats 12 hrs after single dose i.p. administration. We also conducted metabolic stability studies using human liver microsomes and found no breakdown products within 1 hr, in contrast to the FDA approved benzodiazepine

Midazolam. Pharmacokinetics of QH-II-066 show a rapid penetration into the brain (within ~5 minutes) and significant accumulation of QH-II-066 (161.3 ng/mL) into brain extracellular fluid .

## SUMMARY

TMZ is used to treat all GBMs. But it shows a degree of effectiveness for only half of GBMs, those *MGMT* methylated. TMZ is associated with debilitating and life-threatening side-effects. We are advancing a brain-penetrant benzodiazepine analog that potentiates TMZ synergistically, irrespective of GBM methylation status.

## REFERENCES


1. Sengupta S., Weeraratne S.D., Sun H, Phallen J., Rallapalli S.K., Teider N., Kosaras B., Amani V., Pierre-Francois J., Tang Y., Nguyen B., Yu F., Schubert S., Balansay B., Mathios D., Lechpammer M., Archer T.C., Tran P., Reimer R.J., Cook J.M., Lim M., Jensen F.E., Pomeroy S.L., Cho Y.J. (2014). a5-GABAA receptors negatively regulate MYC-amplified medulloblastoma growth. Acta Neuropathol. 127: 593-603.
2. Jonas O., Calligaris D., Methuku K.R. Poe M.M., Francois J.P., Tranghese F., Changelian A., Sieghart W., Ernst M., Krummel D.A., Cook J.M., Pomeroy S.L., Cima M., Agar N.Y., Langer R., Sengupta S. (2016). First in vivo testing of compounds targeting Group 3 medulloblastomas using an implantable microdevice as a new paradigm for drug development. J. Biomed. Nanotech. 12(6): 1297-302.
3. Kallay L., Keskin H., Ross A., Rupji M., Moody O.A., Li G., Ahmed T., Rashid R., Stephen M.R., Cottrill K.A., Nuckols A., Zu M., Martinson D.E., Tranghese F., Wang X., Taylor M., Cook J., Kowalski J., Jenkins A., Pomeranz Krummel D., Sengupta S. (2019). Modulating native GABAA receptors in cancer cells with positive allosteric benzodiazepine-derivatives induces cell death. J. Neuro-Oncol. 142: 411-422.
4. Pomeranz Krummel D.A., Nasti T.H., Izar B., Press R.H., Xu M., Lowder L., Kallay L., Rupji M., Rosen H., Su J., Curran W., Olson J., Weinberg B., Schniederjan M., Neill S., Lawson D., Kowalski J., Khan M.K., Sengupta S. (2020). Impact of sequencing radiation therapy and immune checkpoint inhibitors in the treatment of melanoma brain metastases. International J. Radiation Oncology, Biology, Physics. 108(1): 157-163.
5. Quail DF, Joyce JA. (2017). The Microenvironmental Landscape of Brain Tumors. Cancer Cell. 31(3): 326–341.

6. Chen J, Li Y, Yu T-S, McKay RM, Burns DK, Kernie SG, et al. (2012). A restricted cell population propagates glioblastoma growth after chemotherapy. Nature. 488(7412): 522–526.
7. Sigel E, Steinmann ME. (2012). Structure, function, and modulation of GABAA receptors. J. Biol. Chem. 287: 40224-40231.
8. Olsen RW, Sieghart W. (2009). GABAA receptors: subtypes provide diversity of function and pharmacology. Neuropharmacol. 56: 141-148.

### 5. 2. 5 Brain penetrant chemosensitizer to treat lung cancer

## OVERVIEW OF INVENTION

Non-small cell lung cancer (NSCLC) accounts for a majority (80%-85%) of lung cancer cases. The most common NSCLC histological subtype (40-50%) is lung adenocarcinoma. A great majority of NSCLC patients with advanced stage of the disease face local and/or distant recurrences, including metastasis to the brain, in the first 2 years after the completion of primary treatment. More effective therapies are needed to boost tumor control, prevent metastasis, and improve overall survival while mitigating side-effects.

We find that Type-A GABA neurotransmitter receptors ($GABA_AR$s) are expressed in not only cancers of the central nervous system, but also systemic cancers. In previous studies we reported that by activating $GABA_AR$ function and signaling with a new class of benzodiazepine analogs, tumor cells can be sensitized to radiation resulting in significant tumor regression in mouse models of medulloblastoma and melanoma (**1-4).** Our analysis of patient data has revealed that $GABA_AR$ expression is present in both lung adenocarcinoma and squamous carcinoma subtypes. Leveraging this finding, we have investigated if potentiating $GABA_AR$ in lung adenocarcinoma cells with a novel benzodiazepine analog called QH-II-066 as well as other compounds of similar structure can impair tumor growth. We find that QH-II-066 treatment induces apoptosis in patient-derived adenocarcinoma cells. We also find that QH-II-066 synergistically can potentiate the chemotherapeutic docetaxel, even at an ineffective dose. We have generated a flank xenograft mouse model using patient derived adenocarcinoma cells to evaluate the efficacy of QH-II-066 and will utilize this model to evaluate the ability of QH-II-066 to sensitize tumor cells to docetaxel such that this drugs toxicity profile is reduced while it retains its potency. Our *long-term goal* is to establish that the novel benzodiazepine analog QH-II-066 can function to potentiate chemotherapeutic for treatment of NSCLC, thereby increasing its effectiveness and mitigating toxic side-effects.

## BACKGROUND

**$GABA_AR$ structure-function**. GABA receptors ($GABA_AR$s) form pentameric chloride ($Cl^-$) channels, composed most commonly of two α, two β, and γ subunits encoded by GABR genes GABRA (1-6), GABRB (1-3), and GABRG (1-3), respectively (7,8) (Fig. 1a). $GABA_AR$s are fundamental in determining an excitation/inhibition balance in the central nervous system. As a receptor mediating $Cl^-$ flux, $GABA_AR$s predominantly function to hyperpolarize neural cells, following binding of its ligand GABA (Fig. 1b).

**$GABA_AR$ activation**. $GABA_AR$s have been an important therapeutic target since the clinical introduction of benzodiazepines in the 1960s. Benzodiazepines bind at the γ-α interface of

$GABA_AR$ (Fig. 1a) and act to increase effectiveness of GABA and thus enhance $Cl^-$ flux (Fig. 1b). FDA approved benzodiazepines consist most commonly of fusion of diazepine and benzene rings (1,4-benzodiazepine) and a phenol ring (5-phenyl-1H-benzo[e]) (Fig. 1c). J. Cook and his team (Univ. Wisconsin-Milwaukee) introduced an ethinyl bond at R7 in place of a chlorine in Valium (Fig. 1c). which confers anti-cancer activity.

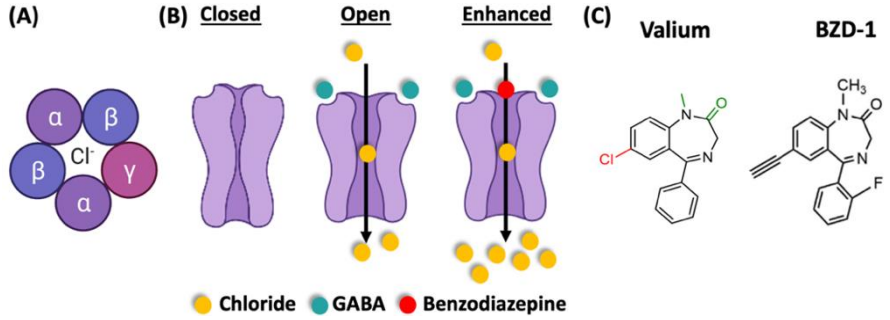


**Fig. 1. $GABA_AR$s.** (A) A $GABA_AR$, looking down the chloride ion conduction pore. (B) Binding of two GABA ligands opens the channel, binding of a benzodiazepine enhances chloride ion flux. (C) Structure of the classic benzodiazepine Valium (left) and the novel benzodiazepine analog used in proposed studies (right; QH-II-066 or BZD-1). Key difference is an ethinyl bond in place of a chlorine.

## REFERENCES


1. Sengupta S., Weeraratne S.D., Sun H, Phallen J., Rallapalli S.K., Teider N., Kosaras B., Amani V., Pierre-Francois J., Tang Y., Nguyen B., Yu F., Schubert S., Balansay B., Mathios D., Lechpammer M., Archer T.C., Tran P., Reimer R.J., Cook J.M., Lim M., Jensen F.E., Pomeroy S.L., Cho Y.J. (2014). a5-GABAA receptors negatively regulate MYC-amplified medulloblastoma growth. Acta Neuropathol. 127: 593-603.

2. Jonas O., Calligaris D., Methuku K.R. Poe M.M., Francois J.P., Tranghese F., Changelian A., Sieghart W., Ernst M., Krummel D.A., Cook J.M., Pomeroy S.L., Cima M., Agar N.Y., Langer R., Sengupta S. (2016). First in vivo testing of compounds targeting Group 3 medulloblastomas using an implantable microdevice as a new paradigm for drug development. J. Biomed. Nanotech. 12(6): 1297-302.

3. Kallay L., Keskin H., Ross A., Rupji M., Moody O.A., Li G., Ahmed T., Rashid R., Stephen M.R., Cottrill K.A., Nuckols A., Zu M., Martinson D.E., Tranghese F., Wang X., Taylor M., Cook J., Kowalski J., Jenkins A., Pomeranz Krummel D., Sengupta S. (2019). Modulating native GABAA receptors in cancer cells with positive allosteric benzodiazepine-derivatives induces cell death. J. Neuro-Oncol. 142: 411-422.

4. Pomeranz Krummel D.A., Nasti T.H., Izar B., Press R.H., Xu M., Lowder L., Kallay L., Rupji M., Rosen H., Su J., Curran W., Olson J., Weinberg B., Schniederjan M., Neill S., Lawson D., Kowalski J., Khan M.K., Sengupta S. (2020). Impact of sequencing radiation therapy and immune checkpoint inhibitors in the treatment of melanoma brain metastases. International J. Radiation Oncology, Biology, Physics. 108(1): 157-163.



Debanjan Bhattacharya, Kamdem Donatien Toukam, Laura Kallay, Vaibhavkumar Gawali, Mario Medvedovic, Riccardo Barrile Daniel A Pomeranz Krummel, Soma Sengupta

# 5. 3 Paper published on QH II 66

## 5. 3. 1 Paper 1: Modulation of a5 Subunit-Containing GABAA Receptors Alters Alcohol Drinking by Rhesus Monkeys.

ALCOHOLISM: CLINICAL AND EXPERIMENTAL RESEARCH

Vol. 37, No. 4
April 2013

# Modulation of α5 Subunit-Containing $GABA_A$ Receptors Alters Alcohol Drinking by Rhesus Monkeys

Daniela Rüedi-Bettschen, James K. Rowlett, Sundari Rallapalli, Terry Clayton, James M. Cook, and Donna M. Platt

**Background:** Alcohol's ability to potentiate the activity of γ-aminobutyric acid (GABA) at $GABA_A$ receptors has been implicated as a key mechanism underlying the behavioral effects of alcohol. The complex molecular biology of these receptors raises the possibility that particular receptor subtypes may play unique roles in alcohol's abuse-related effects and that subtype-selective ligands with therapeutic specificity against alcohol might be developed. This study evaluated the capacity of α5$GABA_A$ receptor ligands to alter selectively the reinforcing effects of alcohol.

**Methods:** Two groups of rhesus monkeys were trained to orally self-administer alcohol or sucrose under fixed-ratio schedules and limited daily access conditions. In addition, following daily self-administration sessions, the behavior of each monkey was scored for both species-typical and drug-induced behaviors.

**Results:** Concentrations of 1 to 6% alcohol maintained self-administration above water levels, engendered pharmacologically relevant blood alcohol levels ranging from 90 to 160 mg/dl, and produced changes in behavior typical of alcohol intoxication. Concentrations of 0.3 to 3% sucrose also reliably maintained self-administration. The α5$GABA_A$ receptor agonist QH-ii-066 enhanced and the α5$GABA_A$ receptor inverse agonist L-655,708 inhibited alcohol, but not sucrose drinking. The changes in alcohol drinking could be reversed with the α5$GABA_A$ receptor antagonist XLi-093. However, L-655,708 increased yawning in both alcohol and sucrose drinkers, possibly indicative of an anxiogenic effect.

**Conclusions:** These findings suggest a prominent and specific role for α5$GABA_A$ receptor mechanisms in the reinforcing effects of alcohol. Moreover, these results suggest that α5$GABA_A$ receptors may represent a novel pharmacological target for the development of medications to reduce drinking. Of ligands modulating this receptor, α5$GABA_A$ receptor inverse agonists may hold the most promise as alcohol pharmacotherapies.

**Key Words:** $GABA_A$ Receptors, Alcohol Self-Administration, Monkey, Pharmacotherapy, QH-ii-066, L-655,708, XLi-093, Naltrexone.

ALCOHOL's ability to potentiate the activity of γ-aminobutyric acid (GABA) at $GABA_A$ receptors has been implicated as a key mechanism underlying the abuse-related effects of alcohol in both human and nonhuman subjects (e.g., Hyytiä and Koob, 1995; June et al., 1995, 1998; Korpi, 1994; Söderpalm and Hansen, 1998). Molecular biological studies have shown that the mammalian $GABA_A$ receptor is a pentamer consisting of subunits from at least 5 different families, including the α, β, and γ subunits (McKernan and Whiting, 1996; Pritchett et al., 1989; Rudolph et al., 2001). In addition, most of these subunits have a number of different isoforms (e.g., α1 to α6, β1 to β3, γ1 to γ3; Olsen and Sieghart, 2008). The complex molecular biology of $GABA_A$ receptors raises the possibility that subtype-selective agents with therapeutic specificity against alcohol might be developed.

$GABA_A$ receptors expressing the α5 subunit (α5$GABA_A$ receptors) comprise only a small proportion of native $GABA_A$ receptors and are found primarily in the hippocampus (Sur et al., 1999; Uusi-Oukari and Korpi, 2010). Projections from the CA1 and CA3 hippocampal fields have been shown to innervate brain regions implicated in the reinforcing effects of alcohol (e.g., Sesack and Grace, 2010). Several lines of evidence support a potential role for α5$GABA_A$ receptor mechanisms in the abuse-related effects of alcohol. In this regard, using data from the Collaborative Study on the Genetics of Alcoholism, Song and colleagues (2003) reported a significant association between *GABRA5* (the gene encoding the α5 subunit of the $GABA_A$ receptor) and alcohol

*From the Harvard Medical School (DR-B, JKR, DMP), New England Primate Research Center, Southborough, Massachusetts; and Department of Chemistry (SR, TC, JMC), University of Wisconsin-Milwaukee, Milwaukee, Wisconsin.*

*Received for publication November 28, 2011; accepted August 22, 2012.*

*Reprint requests: Donna M. Platt, PhD, Harvard Medical School, New England Primate Research Center, One Pine Hill Drive, PO Box 9102, Southborough, MA 01772-9102; Tel.: 508-624-8090; Fax: 508-624-8197; E-mail: donna_platt@hms.harvard.edu*

*Present address: Daniela Rüedi-Bettschen, Department of Pharmacology and Toxicology, College of Medicine, University of Arkansas for Medical Sciences, 4301 W. Markham, #611, Little Rock, AR, 72205*



**DOI: 10.1111/acer.12018**

## 5. 3. 2 Paper 2: [$^3$H] RY- 80: A High-Affinity, Selective Ligand for *g*-Aminobutyric AcidA Receptors Containing *Alpha*-5 Subunits

0022-3565/97/2832-0488$00.00/0
THE JOURNAL OF PHARMACOLOGY AND EXPERIMENTAL THERAPEUTICS
Copyright © 1997 by The American Society for Pharmacology and Experimental Therapeutics
JPET 283:488–493, 1997

Vol. 283, No. 2
*Printed in U.S.A.*



# [$^3$H]RY 80: A High-Affinity, Selective Ligand for γ-Aminobutyric Acid$_A$ Receptors Containing *Alpha*-5 Subunits[1, 2]

PHIL SKOLNICK, RONA J. HU, CHRISTINE M. COOK, STEPHEN D. HURT, JOSEPH D. TROMETER, RUIYAN LIU, QI HUANG and JAMES M. COOK

*Laboratory of Neuroscience, National Institute of Diabetes and Digestive and Kidney Diseases, National Institutes of Health, Bethesda, Maryland (R.J.H., C.M.C., P.S.), New England Nuclear, Boston, Massachusetts (S.D.H., J.D.T.), and Department of Chemistry, University of Wisconsin-Milwaukee, Milwaukee, Wisconsin (R.L., Q.H., J.M.C.)*

Accepted for publication July 29, 1997

**ABSTRACT**

The radiochemical synthesis and pharmacological properties are described of [$^3$H]RY 80 (ethyl-8-acetylene-5,6-dihydro-5-methyl-6-oxo-4H-imidazo[1,5*a*][1,4]benzodiazepine-3-carboxylate, [*ethyl*-$^3$H]). This compound is one of a series of 8-substituted imidazobenzodiazepines that exhibits both high affinity and selectivity for γ-aminobutyric acid (GABA)$_A$ receptors containing *alpha*-5 subunits. Saturable, high-affinity ($K_d$ ~0.7 nM) binding of [$^3$H]RY 80 was observed in hippocampal membranes. The maximum number ($B_{max}$) of [$^3$H]RY 80 binding sites was ~18% of that obtained with [$^3$H]flunitrazepam, a radioligand that labels all "diazepam-sensitive" GABA$_A$ receptors. This value is consistent with previous estimates (10–20%) of the proportion of rat hippocampal GABA$_A$ receptors containing *alpha*-5 subunits determined by immunoprecipitation with selective antibodies and competition experiments using an *alpha*-5-selective ligand. In recombinant GABA$_A$ receptors composed of *alpha*-5 *beta*-3 *gamma*-2 subunits, the $K_d$ of [$^3$H]RY 80 (~0.5 nM) was consistent with the value obtained in hippocampus, whereas the $B_{max}$ value was not significantly different from that obtained with [$^3$H]flunitrazepam. The potencies of several benzodiazepine site ligands to inhibit [$^3$H]RY 80 binding to hippocampal membranes were in agreement with the values obtained in recombinant (*alpha*-5 *beta*-3 *gamma*-2) GABA$_A$ receptors. [$^3$H]RY 80 was used both in a "GABA shift" assay to correctly predict the *in vivo* actions of a novel, *alpha*-5-selective ligand and to characterize a population of GABA$_A$ receptors containing *alpha*-5 subunits in neonatal rat cortex. These findings demonstrate that [$^3$H]RY 80 can be used as a radioligand to examine the properties of GABA$_A$ receptors containing *alpha*-5 subunits.



GABA$_A$ receptors possess multiple, allosterically linked modulatory sites that are loci for drug action (reviewed in Skolnick and Paul, 1988; Johnston, 1996). However, from a therapeutic and drug development perspective, benzodiazepine binding sites are perhaps the most important. Thus, benzodiazepine binding sites mediate the principal therapeutic actions of 1,4-benzodiazepines (*e.g.,* diazepam and flurazepam) as well as a large group of structurally unrelated molecules including imidazopyridines (*e.g.,* zolpidem), cyclopyrrolones (*e.g.,* zopiclone) and β-carbolines (*e.g.,* abecarnil).

GABA$_A$ receptors are a heterogeneous family of ligand-gated ion channels that may be assembled from at least 15 structurally related subunits (*alpha*, *beta*, *gamma*, *delta* and *rho*) (reviewed in Stephenson, 1995). Immunochemical studies have demonstrated that GABA$_A$ receptors most often exist as ternary complexes composed of *alpha*, *beta*, and *gamma* subunits (; DeBlas, 1996; Fritschy and Mohler, 1993) arranged as pentamers (Nayeem *et al.*, 1994). Although GABA$_A$ receptor subunit stoichiometry remains controversial (Backus *et al.*, 1993; Chang *et al.*, 1996; Tretter *et al.*, 1997), both the affinities and efficacies of drugs acting at this family of ligand-gated ion channels (including benzodiazepine site ligands) appear to be defined by subunit composition. For example, studies in recombinant GABA$_A$ receptors have shown that the *alpha* subunit is a primary determinant of ligand affinity at benzodiazepine binding sites (Hadingham *et al.*, 1993; Lüddens *et al.*, 1990; Pritchett and Seeburg, 1990), with the *gamma* subunit playing a smaller, albeit significant role for some ligands (Benke *et al.*, 1996; Lüddens *et al.*, 1994). Ligand efficacy at benzodiazepine binding sites appears to be determined primarily by the *gamma* subunit (Ducic *et al.*, 1993; von Blankenfeld *et al.*, 1990; Wafford *et al.*, 1993). These studies in recombinant receptors have provided valuable insights that explain many aspects of the

Received for publication March 19, 1997.
[1] Portions of this work were presented at the 35th Annual Meeting of the American College of Neuropsychpharmacology, December 9–13, 1996, San Juan, PR.
[2] This work was supported in part by a predoctoral fellowship from the American Society for Pharmacology and Experimental Therapeutics (C.M.C.) and NIMH Grant MH-46851 (J.M.C.). R.J.S. is a PRAT Fellow, NIGMS.

**ABBREVIATIONS:** GABA, γ-aminobutyric acid; DMCM, methyl-6,7-dimethoxy-4-ethyl-β-carboline-3-carboxylate; HEK, human embryonic kidney.

## 5. 3. 3 Paper 3: Glutamatergic and GABAergic modulations of ultrasonic vocalizations during maternal separation distress in mouse pups.

Psychopharmacology (2009) 204:61–71
DOI 10.1007/s00213-008-1437-8

ORIGINAL INVESTIGATION

# Glutamatergic and GABAergic modulations of ultrasonic vocalizations during maternal separation distress in mouse pups

**Aki Takahashi · Jasmine J. Yap · Dawnya Zitzman Bohager · Sara Faccidomo · Terry Clayton · James M. Cook · Klaus A. Miczek**

Received: 1 October 2008 / Accepted: 5 December 2008 / Published online: 20 December 2008


**Abstract**
*Introduction* Dysregulation of GABAergic inhibition and glutamatergic excitation has been implicated in exaggerated anxiety. Mouse pups emit distress-like ultrasonic vocalizations (USVs) when they are separated from their dam/siblings, and this behavior is reduced by benzodiazepines (BZs) which modulate GABAergic inhibition. The roles of glutamate receptors on USVs remain to be investigated.
*Materials and methods* We examined the roles of glutamate receptor subtypes on mouse pup USVs using *N*-methyl-D-aspartate (NMDA) receptor antagonists with different affinities [dizocilpine (MK-801), memantine, and neramexane] and group II metabotropic glutamate receptor agonist (LY-379268) and antagonist (LY-341495). These effects were compared with classic BZs: flunitrazepam, bromazepam, and chlordiazepoxide. To assess the role of $GABA_A$ receptor subunits on USVs, drugs that have preferential actions at different $GABA_A$-α subunits (L-838417 and QH-ii-066) were tested. Seven-day-old CFW mouse pups were separated from their dam and littermates and placed individually on a 19°C test platform for 4 min. Grid crossings and body rolls were measured in addition to USVs.
*Results* Dizocilpine dose-dependently reduced USVs, whereas memantine and neramexane showed biphasic effects and enhanced USVs at low to moderate doses. The NMDA receptor antagonists increased locomotion. LY-379268 reduced USVs but also suppressed locomotion. All BZs reduced USVs and increased motor incoordination. Neither L-838417 nor QH-ii-066 changed USVs, but both induced motor incoordination.
*Conclusion* Low-affinity NMDA receptor antagonists, but not the high-affinity antagonist, enhanced mouse pup distress calls, which may be reflective of an anxiety-like state. BZs reduced USVs but also induced motor incoordination, possibly mediated by the α5 subunit containing $GABA_A$ receptors.

**Keywords** Anxiety · Ultrasonic vocalizations · Mouse pups · NMDA receptor · mGluR2/3 · $GABA_A$ receptor subtypes · Motor activity · Motor incoordination

**Electronic supplementary material** The online version of this article (doi:10.1007/s00213-008-1437-8) contains supplementary material, which is available to authorized users.

A. Takahashi · J. J. Yap · D. Z. Bohager · S. Faccidomo · K. A. Miczek (✉)
Department of Psychology, Tufts University,
530 Boston Ave. (Bacon Hall),
Medford, MA 02155, USA
e-mail: klaus.miczek@tufts.edu

K. A. Miczek
Departments of Psychiatry, Pharmacology and Neuroscience,
Tufts University,
Medford, MA, USA

T. Clayton · J. M. Cook
Department of Chemistry and Biochemistry,
University of Wisconsin–Milwaukee,
Milwaukee, WI, USA

*Present address:*
D. Z. Bohager · S. Faccidomo
Bowles Center for Alcohol Studies,
University of North Carolina at Chapel Hill,
Chapel Hill, NC, USA

## Introduction

Rodent pups that are separated from their dam and/or siblings emit distress calls (ultrasonic vocalizations, USVs) that prompt retrieval by their dam (Noirot 1972; Brunelli et al. 1994). This behavior may represent an expression of affect by the pup, and separation-induced USVs have been

## 5. 3. 4 Paper 4: Contribution of ⟨1GABAA and ⟨5GABAA Receptor Subtypes to the Discriminative Stimulus Effects of Ethanol in Squirrel Monkeys

JPET Fast Forward. Published on January 13, 2005 as DOI: 10.1124/jpet.104.080275
JPET Fast Forward. Published on January 13, 2005 as DOI: 10.1124/jpet.104.080275

JPET #80275

**Contribution of $\alpha_1$GABA$_A$ and $\alpha_5$GABA$_A$ Receptor Subtypes to the Discriminative Stimulus Effects of Ethanol in Squirrel Monkeys**

Donna M. Platt, Annemarie Duggan, Roger D. Spealman, James M. Cook, Xiaoyan Li, Wenyuan Yin and James K. Rowlett

Harvard Medical School (DMP, AD, RDS, JKR)

New England Primate Research Center

One Pine Hill Drive, Box 9102

Southborough, MA 01772-9102

USA

and

Department of Chemistry (JMC, XL, WY)

University of Wisconsin-Milwaukee

3210 N. Cramer Street

Milwaukee, WI 53211

USA

JPET Fast Forward. Published on January 13, 2005 as DOI: 10.1124/jpet.104.080275
This article has not been copyedited and formatted. The final version may differ from this version.



Running title: alpha1 and alpha5 GABA-A receptor mechanisms and ethanol

Corresponding author: Donna M. Platt, Ph.D.

Harvard Medical School/New England Primate Research Center

One Pine Hill Drive, Box 9102

Southborough, MA 01772-9102

Phone: (508) 624-8090

Fax: (508) 624-8172

Email: donna_platt@hms.harvard.edu

Number of text pages: 18 (Introduction through Discussion)

Number of tables: 0

Number of figures: 8

Number of references: 43

Words in Abstract: 233

Words in Introduction: 759

Words in Discussion: 1096

Abbreviations: GABA, γ-aminobutyric acid; β-CCt, β-carboline-*t*-butyl ester; RY-23, tert-butyl 8-[(trimethylsilyl) ethynyl]-5,6-dihydro-5-methyl-6-oxo-*4H*-imidazo [1,5*a*] [1,4]benzodiazepine-3-carboxylate; DS, discriminative stimulus; CL218872, 3-methyl-6-[3-(trifluoromethyl) phenyl]-1,2,4-triazolo[4,3-*b*]pyridazine; QH-ii-066, 1-methyl-7-acetyleno-5-phenyl-1,3-dihydro-benzo [e]-1,4-diazepin-2-one; panadiplon, 3-(5-cyclopropyl-1,2,4-oxadiazol-3-yl)-5-(1-methylethyl) imidazo(1,5-*a*)quinoxalin-4(*5H*)-o-ne; L-655,708, ethyl [*S*]-11,12,13,13*a*-tetrahydro-7-methoxy-9-oxo-9*H*-imidazo[1,5-*a*]pyrrolo[2,1-*c*][1,4]benzodiazepine-1-carboxlate; FR, fixed-ratio

Section assignment: Behavioral Pharmacology

JPET Fast Forward. Published on January 13, 2005 as DOI: 10.1124/jpet.104.080275
This article has not been copyedited and formatted. The final version may differ from this version.



Abstract

Ethanol's ability to enhance γ-aminobutyric acid (GABA) neurotransmission via $GABA_A$ receptors has been implicated as an important mechanism underlying its discriminative stimulus (DS) effects in animals and subjective effects in humans. The present study assessed the contribution of $\alpha_1GABA_A$ and $\alpha_5GABA_A$ receptors to the DS effects of ethanol. Squirrel monkeys were trained to discriminate i.v. ethanol from saline under a fixed-ratio schedule of food delivery. Under test conditions, ethanol engendered a dose-dependent increase in drug-lever responding, reaching an average maximum of >80%. In substitution experiments, the $\alpha_1GABA_A$ agonists zolpidem, zaleplon and CL 218,872, the $\alpha_5GABA_A$ agonists QH-ii-066 and panadiplon, and representative nonselective agonists partially-to-fully reproduced the ethanol DS. In antagonism studies, the $\alpha_1GABA_A$ antagonist β-CCt did not attenuate the DS effects of ethanol or the ethanol-like effects of zolpidem and zaleplon. In contrast, pretreatment with the $\alpha_5GABA_A$ inverse agonist L-655,708 dose-dependently attenuated the DS effects of ethanol and the ethanol-like effects of QH-ii-066. RY-23, another $\alpha_5GABA_A$ inverse agonist, similarly attenuated the ethanol-like DS effects of QH-ii-066. Antagonism of both QH-ii-066 and ethanol by the $\alpha_5GABA_A$ inverse agonists occurred at doses that did not alter the rate of responding suggesting that this blockade was pharmacologically specific and not the result of a nonspecific disruption of operant behavior. These findings suggest a key role for $\alpha_5GABA_A$, but not $\alpha_1GABA_A$, receptor mechanisms in the DS effects of ethanol and the ethanol-like DS effects of benzodiazepine agonists.

## 5. 3. 5 Paper 5: Modulating native GABAA receptors in medulloblastoma with positive allosteric benzodiazepine-derivatives induces cell death.

Journal of Neuro-Oncology (2019) 142:411–422
https://doi.org/10.1007/s11060-019-03115-0

LABORATORY INVESTIGATION

# Modulating native $GABA_A$ receptors in medulloblastoma with positive allosteric benzodiazepine-derivatives induces cell death

Laura Kallay[1] · Havva Keskin[1] · Alexandra Ross[1] · Manali Rupji[2] · Olivia A. Moody[3] · Xin Wang[4,5] · Guanguan Li[6] · Taukir Ahmed[6] · Farjana Rashid[6] · Michael Rajesh Stephen[6] · Kirsten A. Cottrill[7] · T. Austin Nuckols[7] · Maxwell Xu[8] · Deborah E. Martinson[2] · Frank Tranghese[9] · Yanxin Pei[10] · James M. Cook[6] · Jeanne Kowalski[2,11] · Michael D. Taylor[4,5,12] · Andrew Jenkins[13] · Daniel A. Pomeranz Krummel[1,2,16] · Soma Sengupta[1,2,14,15,16]

Received: 2 November 2018 / Accepted: 31 January 2019 / Published online: 6 February 2019


**Abstract**

**Purpose** Pediatric brain cancer medulloblastoma (MB) standard-of-care results in numerous comorbidities. MB is comprised of distinct molecular subgroups. Group 3 molecular subgroup patients have the highest relapse rates and after standard-of-care have a 20% survival. Group 3 tumors have high expression of *GABRA5*, which codes for the α5 subunit of the γ-aminobutyric acid type A receptor ($GABA_AR$). We are advancing a therapeutic approach for group 3 based on $GABA_AR$ modulation using benzodiazepine-derivatives.

**Methods** We performed analysis of *GABR* and *MYC* expression in MB tumors and used molecular, cell biological, and whole-cell electrophysiology approaches to establish presence of a functional 'druggable' $GABA_AR$ in group 3 cells.

**Results** Analysis of expression of 763 MB tumors reveals that group 3 tumors share high subgroup-specific and correlative expression of *GABR* genes, which code for $GABA_AR$ subunits α5, β3 and γ2 and 3. There are ~1000 functional α5-$GABA_ARs$ per group 3 patient-derived cell that mediate a basal chloride-anion efflux of $2 \times 10^9$ ions/s. Benzodiazepines, designed to prefer α5-$GABA_AR$, impair group 3 cell viability by enhancing chloride-anion efflux with subtle changes in their structure having significant impact on potency. A potent, non-toxic benzodiazepine ('KRM-II-08') binds to the α5-$GABA_AR$ (0.8 μM $EC_{50}$) enhancing a chloride-anion efflux that induces mitochondrial membrane depolarization and in response, *TP53* upregulation and p53, constitutively phosphorylated at S392, cytoplasmic localization. This correlates with pro-apoptotic Bcl-2-associated death promoter protein localization.

**Conclusion** *GABRA5* expression can serve as a diagnostic biomarker for group 3 tumors, while α5-$GABA_AR$ is a therapeutic target for benzodiazepine binding, enhancing an ion imbalance that induces apoptosis.

**Keywords** Benzodiazepine · Medulloblastoma · $GABA_A$ receptor · Apoptosis · *TP53*

## Introduction

Medulloblastoma is a significant cause of cancer-related morbidity and mortality in children [1]. Its standard-of-care consists of surgical resection, followed by radiotherapy and chemotherapy, which cause neurocognitive side effects [2–4]. Medulloblastoma molecular profiling delineated four subgroups, by consensus termed wingless (WNT), sonic hedgehog (SHH), group 3, and group 4 [5–7]. WNT and SHH exhibit anomalous expression of genes associated with the Wnt and Shh pathways, consistent with genomic alterations [8–10]. Groups 3 and 4, which account for ~60% of medulloblastomas and include those with poorest prognosis, do not have shared subgroup-specific genomic alterations

Havva Keskin and Alexandra Ross have contributed equally to this work.

**Electronic supplementary material** The online version of this article (https://doi.org/10.1007/s11060-019-03115-0) contains supplementary material, which is available to authorized users.

✉ Daniel A. Pomeranz Krummel
pomeranz.krummel@emory.edu

✉ Soma Sengupta
soma.sengupta@emory.edu

Extended author information available on the last page of the article

**Title:** Melanoma cell intrinsic $GABA_A$ receptor enhancement potentiates radiation and immune checkpoint inhibitor response by promoting direct and T cell-mediated anti-tumor activity

**Running title:** Benzodiazepine potentiates radioimmunotherapy

Daniel A. Pomeranz Krummel, PhD,[1‡] Tahseen H. Nasti, PhD,[2‡] Milota Kaluzova, PhD,[3] Laura Kallay, PhD,[1] Debanjan Bhattacharya, PhD,[1] Johannes C. Melms, MD,[4] Benjamin Izar, MD, PhD,[4] Maxwell Xu, BS,[5] Andre Burnham, PhD,[3] Taukir Ahmed, PhD,[6] Guanguan Li, PhD,[6] David Lawson, MD,[7] Jeanne Kowalski, PhD,[8] Yichun Cao, MPH,[9] Jeffrey M. Switchenko, Ph.D., [9,10] Dan Ionascu, PhD,[11] James M. Cook, PhD,[6] Mario Medvedovic, PhD,[12] Andrew Jenkins, PhD,[13] Mohammad K. Khan, MD, PhD,[14] and Soma Sengupta, MD, PhD[1]

[‡]Co-first authors

[1]Department of Neurology & Rehabilitation Medicine, University of Cincinnati College of Medicine, Cincinnati, OH, USA. [2]Department of Microbiology & Immunology, Emory Univ. School of Medicine, Atlanta, GA, USA. [3]Emory Univ. School of Medicine, Atlanta, GA, USA. [4]Columbia Center for Translational Immunology, Columbia University College of Physicians and Surgeons, New York, NY, USA. [5]Johns Hopkins University, Baltimore, MD, USA. [6]Department of Chemistry & Biochemistry, Univ. of Wisconsin-Milwaukee, Milwaukee, WI, USA. [7]Department of Hematology & Medical Oncology,

Winship Cancer Institute of Emory University, Atlanta, GA, USA. [8]Department of Oncology, LIVESTRONG Cancer Institutes, Dell Medical School, Univ. of Texas, Austin, TX, USA. [9]Biostatistics Shared Resource, Winship Cancer Institute of Emory University, Atlanta, GA, USA. [10]Department of Biostatistics & Bioinformatics, Rollins School of Public Health, Emory University, Atlanta, GA, USA. [11]Department of Radiation Oncology, University of Cincinnati College of Medicine, Cincinnati, OH, USA. [12]Department of Environmental Health, University of Cincinnati College of Medicine, Cincinnati, OH, USA. [13]Departments of Anesthesiology, Pharmacology & Chemical Biology, Emory Univ. School of Medicine, Atlanta, GA, USA. [14]Department of Radiation Oncology, Winship Cancer Institute of Emory University, Atlanta, GA, USA.

**Corresponding authors:**

Soma Sengupta, University of Cincinnati College of Medicine, The Vontz Center for Molecular Studies, ML: 0521; 3125 Eden Avenue, Cincinnati, OH, USA 45267; E-mail: sengupsm@ucmail.uc.edu; Phone: (513) 558-0119

Mohammad K. Khan, Emory University School of Medicine, 1365C Clifton Rd., Atlanta, GA, USA 30322; E-mail: drkhurram2000@gmail.com; Phone: (404) 778-5000

**Author of Statistical Analysis:** Mario Medvedovic, University of Cincinnati College of Medicine, Kettering Laboratory, 160 Panzeca Way, Cincinnati, OH, USA 45267;E-mail: medvedm@ucmail.uc.edu; Phone: (513) 281-2513

**Disclosure:** Grant from Merck Pharmaceuticals (M.K.K.), outside the submitted work. Advisory role for NovoCure Ltd. (S.S.). Personal fees from Merck and Volastra Therapeutics (B.I.), outside the submitted work. Co-founders of Amlal Pharmaceutics Inc. and serve on its Board of Directors (D.A.P.K., J.M.C., S.S.). Patent Benzodiazepine Mediated Radiosensitization of Metastatic Melanoma pending (T.N.). Patent International PCT Application No. PCT/US2020/034169 pending (J.C.). Patent Emory 19109 PCT pending (S.S.). Applied for provision patent pending (M.K.).

**Funding:** NIH-NINDS under award number K08-NS083626 to S.S.; Thomas E. & Pamela M. Mischell Family Foundation to S.S.; Harold C. Schott Foundation funding of the Harold C. Schott Endowed Chair, UC College of Medicine, to S.S.; Winship Cancer Institute Melanoma Philanthropic Funds to S.S. and M.K.K.; NIH-NINDS under award number NS089719 to A.J.; NIH under award numbers DA043204, NS076517 to J.M.C; NSF Division of Chemistry (CHE1625735) to J.M.C.; Milwaukee Institute for Drug Discovery to J.M.C.; American Cancer Society Institutional Research Grant to M.K.K; Department of Radiation Oncology, Emory Univ. Research Funds to M.K.K.; Merck Sharp & Dohme Corp. to M.K.K.; NIH-NCI K08-CA222663 and NIH-NCI U54-CA225088 to B.I.; SITC-BMS Cancer Immunotherapy Translational Fellowship to B.I.; Burroughs Wellcome Fund Career Award for Medical Scientists to B.I.; Department of Oncology, LIVESTRONG Cancer Institutes, Dell Medical School, University of Texas at Austin, TX, Research Funds to J.K.; CPRIT Scholar Award #RR160093 to S. Gail Eckhardt; J.M.C. received support for use of analytical instrumentation provided by UW-Milwaukee's Shimadzu Laboratory for Advanced Applied and Analytical Chemistry. Research was

also supported in part by the Biostatistics & Bioinformatics and the Integrated Cellular Imaging Shared Resources of the Winship Cancer Institute of Emory University and NIH/NCI under award number P30CA138292. The content is solely the responsibility of the authors and does not necessarily represent the official views of the NIH.

**Acknowledgments**: Authors thank Drs. Peter Stambrook, Martha Neagu, and Jess Guarnaschelli for helpful comments on the manuscript. We thank Dr. Zalfa Abdel-Malek for providing a primary melanocyte cell line and technical advice for its use in our studies.

**Data sharing**: Research data are stored in an institutional repository and will be shared upon request to the corresponding author(s). RNA-seq ".fastq files" have been deposited to the Gene Expression Omnibus (GEO).

# Melanoma Cell Intrinsic $GABA_A$ Receptor Enhancement Potentiates Radiation and Immune Checkpoint Inhibitor Response by Promoting Direct and T Cell-Mediated Anti-Tumor Activity


## Abstract

**Purpose**: Most metastatic melanoma patients show variable responses to radiotherapy and do not benefit from immune checkpoint inhibitors (ICIs). Improved strategies for combination therapy that leverage potential benefits from radiotherapy and ICI are critical.

**Methods and Materials**: We analyzed metastatic melanoma tumors in the TCGA cohort for expression of genes coding for subunits of Type-A γ-aminobutyric acid (GABA) receptor ($GABA_AR$), a chloride ion channel and major inhibitory neurotransmitter receptor. Electrophysiology was used to determine if melanoma cells possess intrinsic $GABA_AR$ activity. Melanoma cell viability studies were conducted to test if enhancing $GABA_AR$ mediated chloride transport using a benzodiazepine impaired viability. While a syngeneic melanoma mouse model was used to assay the effect of benzodiazepine on tumor volume and its ability to potentiate radiation and/or immunotherapy. Treated tumors were analyzed for changes in gene expression by RNA sequencing and presence of tumor infilitrating lymphocytes by flow cytometry.

**Results**: Genes coding for subunits of $GABA_ARs$ express functional $GABA_ARs$ in melanoma cells. By enhancing $GABA_AR$ mediated anion transport, benzodiazepines depolarize melanoma cells and impair their viability. *In vivo*,

## 5. 3. 6 Paper 6: α5-GABAA receptors negatively regulate *MYC*-amplified medulloblastoma growth.

Acta Neuropathol
DOI 10.1007/s00401-013-1205-7

ORIGINAL PAPER

# α5-GABAA receptors negatively regulate *MYC*-amplified medulloblastoma growth

**Soma Sengupta · Shyamal Dilhan Weeraratne · Hongyu Sun · Jillian Phallen · Sundari K. Rallapalli · Natalia Teider · Bela Kosaras · Vladimir Amani · Jessica Pierre-Francois · Yujie Tang · Brian Nguyen · Furong Yu · Simone Schubert · Brianna Balansay · Dimitris Mathios · Mirna Lechpammer · Tenley C. Archer · Phuoc Tran · Richard J. Reimer · James M. Cook · Michael Lim · Frances E. Jensen · Scott L. Pomeroy · Yoon-Jae Cho**

Received: 3 September 2013 / Accepted: 28 October 2013


**Abstract** Neural tumors often express neurotransmitter receptors as markers of their developmental lineage. Although these receptors have been well characterized in electrophysiological, developmental and pharmacological settings, their importance in the maintenance and progression of brain tumors and, importantly, the effect of their targeting in brain cancers remains obscure. Here, we demonstrate high levels of *GABRA5,* which encodes the α5-subunit of the GABAA receptor complex, in aggressive MYC-driven, "Group 3" medulloblastomas. We hypothesized that modulation of α5-GABAA receptors alters medulloblastoma cell survival and monitored biological and electrophysiological responses of GABRA5-expressing medulloblastoma cells upon pharmacological targeting of the GABAA receptor. While antagonists, inverse agonists and non-specific positive allosteric modulators had limited effects on medulloblastoma cells, a highly specific and potent α5-GABAA receptor agonist, QHii066, resulted in marked membrane depolarization and a significant decrease in cell survival. This effect was GABRA5 dependent and mediated through the induction of apoptosis as well as accumulation of cells in S and G2 phases of the cell cycle. Chemical genomic profiling of QHii066-treated medulloblastoma cells confirmed inhibition of MYC-related transcriptional activity and revealed an enrichment of HOXA5 target gene expression. siRNA-mediated knockdown of HOXA5 markedly blunted the response of medulloblastoma cells to QHii066. Furthermore, QHii066

S. Sengupta and S. D. Weeraratne contributed equally.
F. E. Jensen, S. L. Pomeroy and Y.-J. Cho are co-senior authors.

**Electronic supplementary material** The online version of this article (doi:10.1007/s00401-013-1205-7) contains supplementary material, which is available to authorized users.

S. Sengupta · S. D. Weeraratne · H. Sun · N. Teider · B. Kosaras · V. Amani · J. Pierre-Francois · M. Lechpammer · T. C. Archer · F. E. Jensen · S. L. Pomeroy
Department of Neurology, Boston Children's Hospital, Boston, MA, USA

S. Sengupta
Department of Neurology, BIDMC, Boston, MA, USA

H. Sun · F. E. Jensen
Department of Neurology, University of Pennsylvania, Philadelphia, PA, USA

J. Phallen · D. Mathios · M. Lim
Department of Neurosurgery, Johns Hopkins School of Medicine, Baltimore, MD, USA

S. K. Rallapalli · J. M. Cook
Department of Chemistry and Biochemistry, University of Wisconsin, Milwaukee, Milwaukee, WI, USA

Y. Tang · B. Nguyen · F. Yu · S. Schubert · B. Balansay · R. J. Reimer · Y.-J. Cho
Department of Neurology and Neurological Sciences, Stanford University School of Medicine, Stanford, CA, USA

M. Lechpammer
Department of Pathology, UC Davis, Sacramento, CA, USA

P. Tran
Department of Radiation Oncology and Molecular Radiation Sciences, Johns Hopkins School of Medicine, Baltimore, MD, USA

Y.-J. Cho (✉)
Department of Neurology and Neurological Sciences, Stanford University School of Medicine, 1201 Welch Road, MSLS Bldg, Room P213, Stanford, CA 94305, USA
e-mail: yjcho1@stanford.edu

Published online: 07 November 2013

## 5. 4 Posters and other publications

### 5. 4. 1 Melanoma cell intrinsic gabaa receptor enhancement potentiates radiation and immune checkpoint inhibitor response by promoting direct and t cell-mediated anti-tumor activity

versus 7.0 months [95%CI: 6.1–8.3]; p=0.0003) and patients with <5 BM versus ≥5 BM (12.49 months [95%CI: 10.52–16.03] versus 5.48 months [95%CI: 4.2–6.8]; p<0.0001). Prognostic multivariable modeling significantly associated shortened OS independently with leptomeningeal dissemination (p<0.0001), >5 BM at diagnosis (p<0.0001), MBM diagnosis year 2010–2014 (p=0.0007), immunotherapy treatment prior to BM diagnosis (p=0.02), and extracranial disease presence (p=0.03). CNS-directed treatment modalities associated with BM number, dominant BM size, presenting symptoms, diagnosis year, and extracranial disease presence. Multivariable analysis demonstrated improved survival for patients that underwent craniotomy (p=0.01). CONCLUSIONS: MBM prognosis has improved in the period following targeted and immunotherapy introduction, and even within the last 5 years of this study. Improving survival reflects and may influence the willingness to use aggressive multimodality treatment for MBM.

#### 19. PLEKHA5 REGULATES TUMOR GROWTH IN METASTATIC MELANOMA

Victor Oria[1], Hongyi Zhang[1,2], Huifang Zhu[1,2], Gang Deng[4,5], Christopher Zito[1,6], Chetan Rane[1], Shenqi Zhang[4], Sarah Weiss[1], Thuy Tran[1], Adebowale Adeniran[7], Fanfan Zhang[1], Jiangbing Zhou[4], Yuval Kluger[7], Marcus Bosenberg[8], Harriet Kluger[3], and Lucia Jilaveanu[1]; [1]Dept of Medical Oncology, Yale University, New Haven, CT, USA, [2]Dept of Microbiology and Immunology, Jinan University, Guangzhou, Guangdong, China, [3]Cancer Research Center, Chongqing Medical University, Chongqing, China, [4]Dept of Neurosurgery, Yale University, New Haven, CT, USA, [5]Dept of Neurosurgery, Renmin Hospital of Wuhan University, Wuhan, Hubei, China, [6]Dept of Biology, University of Saint Joseph, West Hartford, CT, USA, [7]Dept of Pathology, Yale University, New Haven, CT, USA, [8]Dept of Dermatology, Yale University, New Haven, CT, USA

Understanding the mechanisms behind melanoma brain metastasis, a disease that continues to portend a poor prognosis, will lead to the identification and development of novel drug targets. We previously identified PLEKHA5, a gene involved in brain development, as a novel molecule implicated in melanoma brain metastasis. Our aim was to further characterize the function of this protein in brain-tropic melanoma. We established stable loss- and gain-of-function cell lines to explore the underlying mechanisms of PLEKHA5-mediated tumor growth. The effect of PLEKHA5 expression silencing on proliferation and tumor growth was assessed using both in vitro systems and xenograft models of brain-tropic melanomas, respectively. The clinical relevance of PLEKHA5 dysregulation in brain metastasis was also investigated in two unique cohorts of melanoma patients with cerebrotropic disease and included analysis of matched cranial and extra-cranial specimens. Knock-down of PLEKHA5 in brain-tropic melanoma cells negatively regulated cell proliferation by inhibiting G1 to S cell cycle transition. This coincided with up-regulation of PDCD4, p21, and p27, as well as the downregulation of pRb protein, involved in the regulation of cell cycle. Conversely, the ectopic re-expression of PLEKHA5 had an inverse effect. Subcutaneous and direct cranial injections of PLEKHA5 knock-down cells in nude mice significantly inhibited tumor growth, while its overexpression upregulated the growth of tumors. This reduction in tumor growth in vivo might be attributed to decreased phosphorylation of Akt (S473) and mTOR (S2448), key mediators for tumor growth and survival. Our results demonstrate the role of PLEKHA5 as a mediator of melanoma brain metastasis. Our findings highlight the significance of PLEKHA5 as a possible regulator of cell cycle transition via crosstalk with the ubiquitin-proteasome and PI3K/AKT/mTOR signaling pathways, driving the proliferation and growth of brain-tropic melanomas. Our studies suggest that PLEKHA5 targeting should be further investigated for melanoma brain metastasis patient population.

#### 20. MELANOMA CELL INTRINSIC GABAA RECEPTOR ENHANCEMENT POTENTIATES RADIATION AND IMMUNE CHECKPOINT INHIBITOR RESPONSE BY PROMOTING DIRECT AND T CELL-MEDIATED ANTI-TUMOR ACTIVITY

Soma Sengupta[1], Tahseen Nasti[2], Milota Kaluzova[2], Laura Kallay[3], Johannes Melms[4], Benjamin Izar[4], Maxwell Xu[5], Debanjan Bhattacharya[1], Andre Burnham[1], Guangtaan Li[6], Taukir Ahmed[6], David Lawson[2], Jeanne Kowalski[7], James Cook[6], Mario Medvedovic[1], Andrew Jenkins[2], Mohammad Khan[2], and Daniel Pomeranz Krummel[3]; [1]University of Cincinnati, Cincinnati, OH, USA, [2]Emory University, Atlanta, GA, USA, [3]University of Cincinnati, Cincinnati, OH, USA, [4]Columbia University, New York, NY, USA, [5]Johns Hopkins, Baltimore, MD, USA, [6]University of Wisconsin, Milwaukee, WI, USA, [7]University of Texas, Austin, TX, USA

Most metastatic melanoma patients exhibit poor and variable response to radiotherapy and targeted therapies, including immune checkpoint inhibitors. There is a need for therapeutics that can potentiate existing treatments to positively impact clinical outcomes of metastatic melanoma patients. We reanalyzed melanoma TCGA transcriptomes and identified, as linked to previously defined molecular subgroups, enhanced expression of genes coding for subunits of the Type A GABA receptor ($GABA_AR$), a chloride ion channel and major inhibitory neurotransmitter receptor. Using whole-cell patch clamp electrophysiology, we find that melanoma cells possess $GABA_ARs$ that control membrane permeability to anions. Select benzodiazepines, by enhancing $GABA_AR$ mediated anion transport, depolarize melanoma cell mitochondrial membrane potential and impair cell viability *in vitro*. Using a syngeneic melanoma mouse model, we find that a benzodiazepine promotes reduction in tumor volume when administered alone and potentiated radiation or immune checkpoint inhibitor α-PD-L1. When a benzodiazepine is combined with concurrent α-PD-L1 and a sub-lethal radiation dose, there is near complete loss of tumor, beyond what is observed for benzodiazepine with radiation or α-PD-L1. Mechanistically, benzodiazepine with radiation or α-PD-L1 results in ipsilateral and an abscopal tumor volume reduction commensurate with enhanced infiltration into the tumor milieu of polyfunctional CD8 T-cells. There is also an increased expression of genes with roles in the cytokine-cytokine receptor and p53 signaling pathways. This study provides evidence for melanoma cell $GABA_ARs$ as a therapeutic vulnerability with benzodiazepines promoting both direct and immune-mediated anti-tumor activity.

#### 21. A PHASE II TRIAL OF COMPREHENSIVE TREATMENT BASED ON RADIOTHERAPY IN LEPTOMENINGEAL METASTASIS

Siran Yang, Qingfeng Liu, Jianping Xiao, Hongmei Zhang, Nan Bi, Ye Zhang, Yuchao Ma, Kai Wang, Xuesong Chen, Ruizhi Zhao, Xi Wu, Junling Li, Junlin Yi, Shulian Wang, and Yexiong Wang; National Cancer Center/National Clinical Research Center for Cancer/Cancer Hospital, Chinese Academy of Medical Sciences and Peking Union Medical College, Beijing, China

OBJECTIVES: To investigate the efficacy and security prospectively for patients with leptomeningeal metastases (LM) of comprehensive treatment based on radiotherapy. METHODS: From 2014 to 2017, 93 patients diagnosed with LM admitted to our hospital who underwent whole brain radiotherapy (WBRT) or craniospinal irradiation (CSI) with or without simultaneously boost were enrolled. The dynamic changes of enhanced magnetic resonance imaging, clinical signs and symptoms, cerebrospinal fluid cytology and liquid biopsy detection were recorded. The primary endpoint was overall survival (OS), the secondary endpoints were local control (LC), intracranial progress-free survival (IPFS), brain metastasis specific survival (BMSS) and toxicity. RESULTS: The major primary diagnosis was non-small cell lung cancer. Subjects received WBRT with boost (40 Gy in 20 fractions (f) for WBRT and 60Gy in 20 f for boost), focal radiation to LM, WBRT and CSI (40 Gy in 20 f or 50Gy in 25 f for WBRT and 36 Gy in 20 f for CSI). 20 patients were found tumor cells and were administrated intrathecal chemotherapy. 63 patients used target therapy. The median follow-up time was 33.8 months. OS/LC/IPFS at 1 year were 62.4%/77.2% and 52.6%, respectively. The median survival time was 15.9 months, and the median brain metastasis-specific survival was 42.2 months. Treatment-related grade 3-4 adverse events were rare and included eight grade 3 hematological toxicity. CONCLUSION: Reasonable comprehensive treatment including precise radiotherapy, intrathecal chemotherapy and targeted agents were well tolerated and could extend the survival time of LM patients compared with historical controls.

KEY WORDS: Leptomeningeal Metastasis; Tomotherapy; Comprehensive treatment

#### 22. COMPARATIVE EFFICACY OF ALK-INHIBITORS IN ALK INHIBITOR-NAIVE ALK+ LUNG CANCER BRAIN METASTASES: A NETWORK META-ANALYSIS

Philip Haddad, Dalia Hammoud, and Kevin Gallagher; LSUHSC-S/Overton Brooks VAMC, Shreveport, LA, USA

BACKGROUND: Lung cancer has been the leading cause of cancer death for both men and women worldwide. Non-small-cell lung cancer (NSCLC) displays an array of molecular abnormalities most commonly involving ALK and EGFR pathways. NSCLC with ALK rearrangements comprises around 5% of cases. Over the years, several ALK inhibitors (ALKI) have been approved with notable activity in brain metastases. However, there have been limited comparative studies exploring their relative efficacies. This analysis was conducted to compare the relative efficacy of ALKIs against ALKI-naive ALK+ lung cancer brain metastases. METHODOLOGY: A review of the medical literature was conducted using online databases. Inclusion criteria consisted of English language; diagnosis of ALKI-naive ALK+ lung cancer trials with brain metastases; treatment with Crizotinib (CRZ), Alectinib (ALC), Brigatinib (BRG), and Ceritinib (CER); and comparative studies reporting brain metastases specific responses/events. A Bayesian and a frequentists network meta-analysis were conducted using netmeta package and the random-effects model. RESULTS: Eight studies

**5. 4. 2 Targeting a unique electrochemical vulnerability in a pediatric brain tumor to potentiate proton beam radiotherapy.**

**AACR Virtual Special Conference on Radiation Science and Medicine**

**March 2-3, 2021 • Virtual Meeting**

**Targeting a unique electrochemical vulnerability in a pediatric brain tumor to potentiate proton beam radiotherapy**

Daniel A. Pomeranz Krummel[1], Laura Kallay[1], Debanjan Bhattacharya[1], Vaibhavkumar Gawali[1], Kamdem T. Donatien[1], **Taukir Ahmed[2]**, James M. Cook[2], Michael Lamba[3], Susanne Wells[4], Ralph E. Vatner[4], Mathieu Sertorio[4], Dan Ionascu[3], and Soma Sengupta[1]

[1]Department of Neurology & Rehabilitation Medicine, University of Cincinnati College of Medicine, Cincinnati, OH, USA. [2]Department of Chemistry & Biochemistry, Univ. of Wisconsin-Milwaukee, Milwaukee, WI, USA. [3]Department of Radiation Oncology, University of Cincinnati College of Medicine, Cincinnati, OH, USA. [4]Department of Pediatrics, University of Cincinnati College of Medicine, Cincinnati, OH, USA.

Medulloblastoma (MB) is the most common malignant (WHO Grade IV) primary brain cancer in children, adolescents, and young adults. Radiotherapy (RT) is a mainstay of MB treatment, as it is for most childhood and adult cancers. RT dose and frequency needed to achieve efficacy in MB patients severely impacts survival outcomes and is the cause of long-term cognitive deficits. To

improve on short-term side effects and long-term complications, scanning beam proton therapy is employed, when available. While this recent technological advance significantly reduces damage to surrounding healthy brain tissue, survivors continue to experience induced radiation damage, including neurocognitive sequelae. To impact survivors' health-related quality of life and caregivers' emotional and financial burden, it is critical to identify approaches that reduce RT dose to mitigate side-effects without impacting RT effectiveness.

We are investigating targeting a unique MB electrochemical vulnerability as a means to sensitize MB tumor cells to RT. There are four MB molecular subgroups: wingless, sonic-hedgehog, Group 3, and Group 4. Our analysis of 763 MB tumor transcriptomes reveals that all Group 3 MB tumors share an enhanced expression of genes-coding for subunits of the Type-A GABA receptor ($GABA_AR$), a chloride channel. Using patch-clamp electrophysiology, we found that $GABA_ARs$ conduct $Cl^-$ in MB cells and that a brain-penetrant benzodiazepine (BZ) enhances this effect and triggers cytotoxic responses commensurate with mitochondrial depolarization. We find that BZ combined with RT, even at a sub-lethal dose, is highly effective in impairing the viability of MB tumor cells, greater than RT alone. Our BZ is capable of penetrating the blood-brain barrier in minutes, is metabolically stable, and showed no toxicity in a primate model. We are investigating its suitability to be used concomitant with proton beam radiotherapy, replacing standard of care vincristine, to reduce radiation-induced brain toxicity experienced by MB patients and survivors while not decreasing RT effectiveness.

### 5. 4. 3 Modulating native GABAA receptors in medulloblastoma with positive allosteric benzodiazepine-derivatives induces cell death

Modulating native GABAA receptors in medulloblastoma with positive allosteric benzodiazepine-derivatives induces cell death

*J. Neuro-Oncol.* **2019**, *142*, 411. DOI: https://doi.org/10.1007/s11060-019-03115-0

Laura Kallay; Havva Keskin; Alexandra Ross; Manali Rupji; Olivia A. Moody; Xin Wang; Guanguan Li; Taukir Ahmed; Farjana Rashid; Michael Rajesh Stephen; Kirsten A. Cottril; T. Austin Nuckols; Maxwell Xu; Deborah E. Martinson; Frank Tranghese; Yanxin Pei; James M. Cook; Jeanne Kowalski; Michael D. Taylor; Andrew Jenkins; Daniel A. Pomeranz Krummel; Soma Sengupta.

Email: soma.sengupta@emory.edu;
pomeranz.krummel@emory.edu;
capncook@uwm.edu;

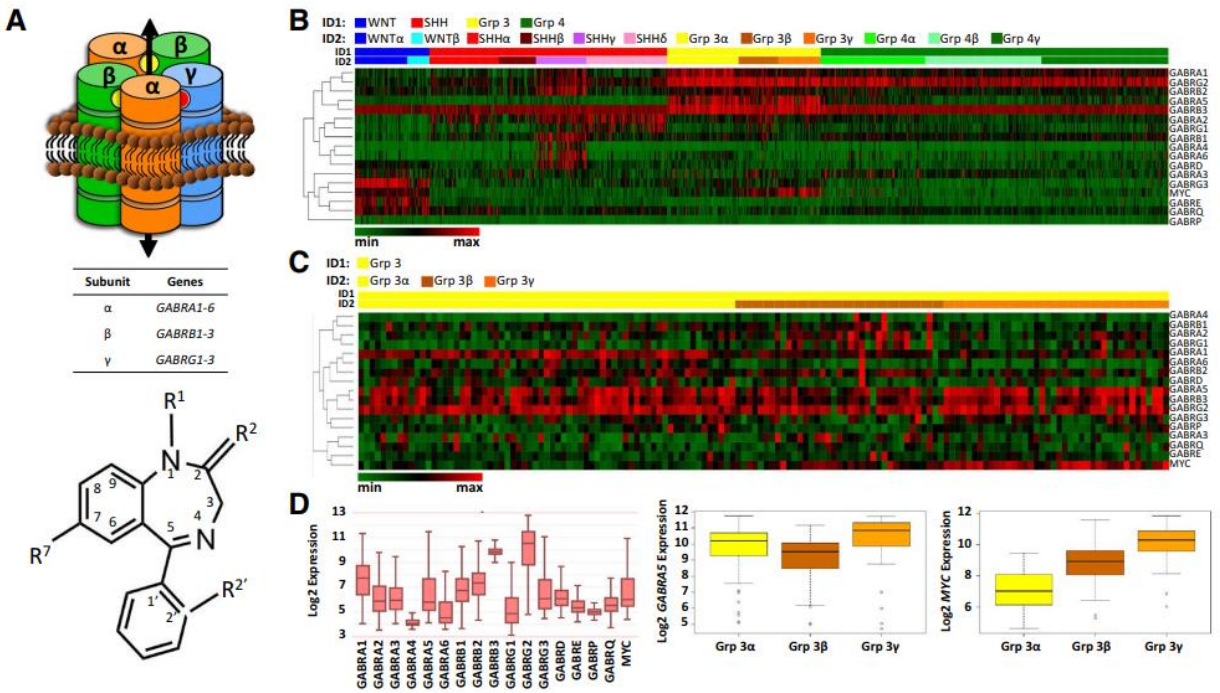



**Abstract:**

**Purpose** Pediatric brain cancer medulloblastoma (MB) standard-of-care results in numerous comorbidities. MB is comprised of distinct molecular subgroups. Group 3 molecular subgroup patients have the highest relapse rates and after standard-of-care have a 20% survival. Group 3 tumors have high expression of GABRA5, which codes for the α5 subunit of the γ-aminobutyric acid type A receptor (GABAAR). We are advancing a therapeutic approach for group 3 based on GABAAR modulation using benzodiazepine-derivatives.

Methods We performed analysis of GABR and MYC expression in MB tumors and used molecular, cell biological, and whole-cell electrophysiology approaches to establish presence of a functional 'druggable' GABAAR in group 3 cells.

**Results** Analysis of expression of 763 MB tumors reveals that group 3 tumors share high subgroup-specifc and correlative expression of GABR genes, which code for GABAAR subunits α5, β3 and γ2 and 3. There are ~1000 functional α5-GABAARs per group 3 patient-derived cell that mediate a basal chloride-anion efux of 2 × 109 ions/s. Benzodiazepines, designed to prefer α5-GABAAR, impair group 3 cell viability by enhancing chloride-anion efux with subtle changes in their structure having signifcant impact on potency. A potent, non-toxic benzodiazepine ('KRM-II-08') binds to the α5-GABAAR (0.8 μM EC50) enhancing a chloride-anion efux that induces mitochondrial membrane depolarization and in response, TP53 upregulation and p53, constitutively phosphorylated at S392, cytoplasmic localization. This correlates with pro-apoptotic Bcl-2-associated death promoter protein localization.

**Conclusion** GABRA5 expression can serve as a diagnostic biomarker for group 3 tumors, while α5-GABAAR is a therapeutic target for benzodiazepine binding, enhancing an ion imbalance that induces apoptosis.

**Keywords** Benzodiazepine · Medulloblastoma · GABAA receptor · Apoptosis · TP53

# 5. 4. 4 PDTM-45. POSITIVE MODULATION OF NATIVE GABAA RECEPTORS IN MEDULLOBLASTOMA CANCER CELLS WITH BENZODIAZEPINES INDUCES RAPID MITOCHONDRIAL FRAGMENTATION AND TP53-DEPENDENT, CELL CYCLE-INDEPENDENT APOPTOSIS.



of JQ1 + GSKJ4 will be measured by bioluminescence imaging and animal survival studies in our human DIPG xenograft model.

PDTM-43. THE ROLE OF TUMOR ASSOCIATED MACROPHAGES IN PEDIATRIC HIGH-GRADE GLIOMA

James Ross[1], Zhibong Chen[1], Frank Szulzewsky[2], Matthew Schniederjan[3], Oren Becher[4] and Dolores Hambardzumyan[5]; [1]Emory University, Department of Pediatrics, Atlanta, GA, USA, [2]Fred Hutch Cancer Center, Department of Human Biology, Seattle, WA, USA, [3]Emory University, Department of Pathology and Laboratory Medicine, Atlanta, GA, USA, [4]Northwestern University, Department of Pediatrics, Chicago, IL, USA

Pediatric high-grade gliomas (pHGG) account for the most cancer-related deaths in children under the age of 19 years old. Recent advances have demonstrated that pHGGs drastically differ from their adult counterparts in terms of genetic and epigenetic alterations, suggesting they may also differ in the constituency of their tumor microenvironment. It is now known tumor associated macrophages (TAMs) can make up 30–40% of the total tumor cell mass in adult high-grade gliomas and play important roles in immune suppression and tumor promotion. This raises the question of whether pHGGs possess a distinct constituency of TAMs due to their unique genetic and epigenetic landscapes. To uncover the composition and behavior of TAMs in pHGG we utilize RCAS/tva, a somatic cell-type specific gene transfer system in which we administer RCAS-PDGFA or RCAS-PDGFB to simulate PDGF receptor activation in immune-competent new-born mice. We found that PDGFB-driven tumors have a significantly lower median survival compared to PDGFA-driven tumors. PDGFB-driven tumors also have increased infiltration of TAMs, made evident by immunohistochemical staining for IBA1. Flow cytometry analysis indicates the increased number of TAMs is due to an increased inflammatory monocyte population, but not due to the microglial population. We hypothesize these findings are attributable to the additional activation of the stromal population by PDGFB, as it can activate both PDGFRα and PDGFRβ while PDGFA only activates PDGFRα. Gene expression analysis indicates that several chemokines, chemokine receptors, macrophage, and immune markers are differentially expressed between PDGFB and -A tumor types. To establish correlations between PDGF signaling and TAM infiltration in human pediatric tumor samples, we stained 37 tumors for IBA1, PDGF-receptors, and PDGF-ligands. A positive correlation exists between high PDGFRb and PDGFB staining with high IBA1. Further studies will be done to discern the effects of increased TAM infiltration and the mechanisms driving enhanced tumor malignancy.

PDTM-44. INTRACRANIAL EPENDYMOMA: DEVELOPING PRECLINICAL MODELS AND IDENTIFYING NOVEL TREATMENTS

Ashleigh Lester, Sylvia Chung, Shane Whittaker, Robert Rapkins and Kerrie McDonald; University of New South Wales, Sydney, NSW, Australia

INTRODUCTION: Clinical trials have not identified any effective chemotherapeutic treatments for intracranial ependymomas. This failure is partially explained by the recent identification of 6 molecularly distinct intracranial subgroups. Whilst subgroup specific preclinical investigations and treatments are required, these investigations have been hampered by the rarity of the tumours, failure to identify driver mutations for 5 of the subgroups, and difficulties establishing appropriate models. This study aims to establish patient derived cell lines, brain slice co-culture models and patient derived mouse models of intracranial ependymomas and utilise these models to identify and test novel subgroup specific drug treatments. METHODS/RESULTS: Two patient-derived intracranial ependymoma cultures have been successfully established in neurobasal and serum free media, as adherent cells and neurospheres. Whole genome methylation sequencing and immunohistochemistry are being used to characterise the cultures. Brain slice co-culture models have been successfully created, with tumour cells growing on 200μM slices of brain from neo-natal mice. Cells dissociated from patient tumour tissue and matched low passage cultures have been injected intracranially into 25 mice, with evidence of tumours in three of the mice induced with cells from the first patient tumour. A screen of 111 approved drugs on ependymoma suspension cultures, has identified 4 drugs, including Bortezomib and Ponatinib, for further investigation in the established models. CONCLUSION: Patient-derived ependymoma cells can be successfully cultured as adherent cells, neurospheres, and in co-culture models. Subgrouping the samples, screening them against approved drugs, and testing potential drugs in patient-derived models is an effective mechanism for identifying candidate drugs for subgroups of these rare tumours.

PDTM-45. POSITIVE MODULATION OF NATIVE $GABA_A$ RECEPTORS IN MEDULLOBLASTOMA CANCER CELLS WITH BENZODIAZEPINES INDUCES RAPID MITOCHONDRIAL FRAGMENTATION AND TP53-DEPENDENT, CELL CYCLE-INDEPENDENT APOPTOSIS

Laura Kallay[1], Havva Keskin[1], Alexandra Ross[1], Olivia Moody[2], Kirsten Cottrill[1], Austin Nuckols[1], Guanguan Li[3], Taukir Ahmed[4], Farjana Rashid[3], Michael Stephen[2], Maxwell Xu[4], Deborah Martinson[1], Tobey Macdonald[1], Jeanne Kowalski[1], Xin Wang[3], Michael Taylor[5], James Cook[3], Andrew Jenkins[1], Daniel Pomeranz Krummel[3] and Soma Sengupta[1]; [1]Emory University, Atlanta, GA, USA, [2]VA Medical Center, Atlanta, GA, USA, [3]University of Wisconsin, Milwaukee, WI, USA, [4]Johns Hopkins University, Atlanta, GA, USA, [5]Hospital for Sick Children, Toronto, ON, Canada

Medulloblastoma is the most common childhood malignant brain tumor. Children with highest morbidity have tumors that are *TP53* wild-type and express high levels of *MYC* and *GABRA5*, which codes for the α-5 subunit of the ligand (chloride) gated $GABA_A$ receptor. Previously, we have established that the α-5 subunit of the $GABA_A$ receptor contributes to the assembly of a functional receptor in a subset of medulloblastoma cells and benzodiazepines, synthesized to function as α-5 selective ligands with psychotropic activity, impair viability[1,2]. Utilizing a *TP53* wild-type medulloblastoma cell line with amplified *MYC*, high *GABRA5* expression, and a functional α-5 $GABA_A$ receptor, we provide insight into how benzodiazepines impair cell viability by positively modulating the native $GABA_A$ receptors. We screened benzodiazepines to assess impact of varying chemical group identity on cell viability. The most potent benzodiazepine binds with specificity to ~1000 native receptors per cell with EC50 and IC50 values of ~0.8 micromolar. This binding evokes a $2 \times 10^9$ ions.sec-1 chloride flux, which morphologically elicits mitochondrial fragmentation, nuclei distention, and cellular blebbing. The cascade of events culminates in a caspase-mediated activation of apoptosis through the intrinsic pathway and a localization of pro-apoptotic Bcl-2-associated death promoter (BAD) protein. Benzodiazepines may be efficacious as anti-cancer therapeutics for medulloblastoma patients exhibiting a $GABA_A$ receptor expression signature by driving a chloride imbalance that leads to cell apoptosis. References: [1]Sengupta, et al. α5-GABAA receptors negatively regulate MYC-amplified medulloblastoma growth. Acta Neuropathol. 2014; 127(4): 593–603. [2]Jonas, et al. First in vivo testing of compounds targeting Group 3 medulloblastomas using an implantable microdevice as a new paradigm for drug development. J. Biomed. Nanotechnol. 2016; 12(6): 1297–1302.

PDTM-46. POLIOVIRUS RECEPTOR (CD155) EXPRESSION IN PEDIATRIC BRAIN TUMORS MEDIATES ONCOLYSIS OF MEDULLOBLASTOMA AND PLEOMORPHIC XANTHOASTROCYTOMA

Eric Thompson[1], Michael Brown[2], Elena Dobrikova[2], Vijay Ramaswamy[3], Michael Taylor[4], Roger McLendon[2], Vidya Chandramohan[1], Darell Bigner[1] and Matthias Gromeier[2]; [1]Duke University Medical Center, Durham, NC, USA, [2]Duke University, Durham, NC, USA, [3]Division of Haematology/Oncology, Hospital for Sick Children, Toronto, ON, Canada, [4]Hospital for Sick Children, Toronto, ON, Canada

INTRODUCTION: Poliovirus oncolytic viral immunotherapy is a putatively novel approach to treat both low grade and malignant pediatric brain tumors. However, the expression of the poliovirus receptor (PVR), CD155, on a variety of pediatric brain tumors and its ability to infect, propagate, and lyse pediatric brain tumor cells is unknown. METHODS: CD155 expression in a variety of pediatric tumor specimens including pleomorphic xanthoastrocytoma (PXA), medulloblastoma, atypical teratoid rhabdoid tumor, embryonal tumor, and anaplastic ependymoma was assessed using a validated rabbit monoclonal antibody. The ability of poliovirus:rhinovirus genetic recombinant, PVSRIPO, to infect PXA (645 [BRAF V600E mutation] and 2363) and medulloblastoma (D283, D341) cell lines was determined by measurement of viral propagation and cell killing. Gene expression data from a medulloblastoma patient cohort of 763 patients was used to determine differential *PVR* mRNA expression and compared using analysis of variance. RESULTS: CD155 expression was present in 53 of 57 patient specimens analyzed in all PXA and medulloblastoma cell lines. One-step growth curves of PVSRIPO at a multiplicity of infection of 10 demonstrated productive infection and peak plaque formation units at 5–10 hours. PVSRIPO infection of all four cell lines demonstrated decreased proliferation in 2363, 645, and D341 cell lines at 48 hours ($p<0.001$) and resulted in cell death. *PVR* expression was significantly highest in Group 3γ, WNTα, and WNT (subgroups with c-myc overexpression) compared to the other medulloblastoma subtypes ($p<0.001$). CONCLUSIONS: Poliovirus receptor, CD155, is widely expressed in a variety of brain tumor specimens. This proof-of-concept *in vitro* study demonstrated that PVSRIPO was capable of infecting, propagating, and prohibiting cell proliferation in PXA with and without BRAF V300E mutations and Group 3 medulloblastoma. Future studies will evaluate PVSRIPO to treat pediatric brain tumors and the possible link between c-myc and PVR expression.

PDTM-47. REAL TIME IN VIVO MONITORING OF 18F-LABELED PANOBINOSTAT PHARMAKOKINETICS FOR TREATMENT OF DIFFUSE INTRINSIC PONTINE GLIOMA (DIPG) VIA CONVECTION ENHANCED DELIVERY (CED)

Umberto Tosi[1], Harikrishna Kommidi[2], Uday Bhanu Maachani[1], Christopher Marnell[1], Hua Guo[2], Melanie Schweitzer[1], Richard Ting[3] and Mark Souweidane[1]; [1]Department of Neurosurgery, Weill Cornell Medicine, New York, NY, USA, [2]Department of Radiology, Weill Cornell Medicine, New York, NY, USA, [3]Weill Cornell Medicine, New York, NY, USA

## 5. 4. 5 QH-II-66, a potential drug candidate for the treatment of Melanoma.

MILWAUKEE INSTITUTE FOR DRUG DISCOVERY
UNIVERSITY OF WISCONSIN-MILWAUKEE

# QH-II-66, a potential drug candidate for the treatment of Melanoma.

UNIVERSITY of WISCONSIN UWMILWAUKEE

**Taukir Ahmed**[1], Laura Kallay[2], Soma Sengupta[2], Daniel Krummel[2] and James Cook[1]

[1] Department of Chemistry & Biochemistry, University of Wisconsin-Milwaukee, Milwaukee, WI 53211; [2] Department of Neurology and Rehabilitation Medicine, University of Cincinnati College of Medicine, Cincinnati, Ohio

## Abstract

Melanoma is the deadliest form of skin cancer. More than 100,000 people are expected to be diagnosed in the USA in 2021. Current treatment with radiotherapy and immune checkpoint inhibitors do not show significant improvement in patients. Therapy combined with QH-II-66, radiation, and an immune checkpoint inhibitor shows improved results in controlling the metastasis by lowering the mass of the tumor. By gene expression analysis it was seen that these cancer cells show high expression of $GABA_A$ receptors. Electrophysiology shows these receptors are functional. This sensitization to melanoma cells is benzodiazepine exclusive and does not impair normal cells. In a syngeneic mouse model of melanoma shows QH-II-66 increases the depolarization in mitochondria which initiates programmed cell death of cancer cells. Combined therapy with QH II 66 and radiation show even better results. Lymphocyte and CD8+T cell counts were also increased after the treatment. Large-scale synthesis was developed for QH II 66. Thus, this potent, non-toxic benzodiazepine may serve as an efficient anti-cancer drug for melanoma.

## GABA/BzR Chloride Ion Complex

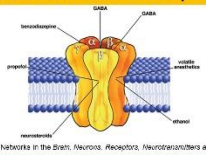


Modified form Lovinger, Comm. Networks in the Brain. Neurons, Receptors, Neurotransmitters and Alcohol, NIAAA Publications.

## Action at $\alpha_{1\text{-}6}\beta_{2/3}\gamma_2$ $GABA_AR$ Subtypes

| Subtype | Associated effect |
|---|---|
| α1 | Anxiolytic, sedation, anterograde amnesia, ataxia, some anticonvulsant action, addiction, dependance, as well as involved in the development of tolerance and muscle relaxation |
| α2 | Anxiolytic, anticonvulsant action, antihyperalgesic effects |
| α3 | Some anxiolytic action, some antinociceptive effects, anticonvulsant actions at higher doses, some muscle relaxation at higher doses. |
| α4 | Diazepam-insensitive (DI) site, important in lung disorders in the periphery. |
| α5 | Cognition, learning, temporal, and spatial memory (may be memory component of anxiety), schizophrenia, depression and in the peripheral asthma. |
| α6 | Diazepam-insensitive (DI) site, important in Tic disorders, Tourette's syndrome, migraine, trigeminal orofacial pain and perhaps schizophrenia. |

Mohler, Mckernan, Walford, Rudolph, Rowlett, et al

## How $GABA_AR$ works

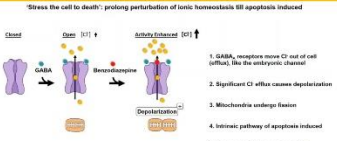


Krummel et al, Int J Radiat Oncol Biol Phys. 2021 Mar 15;109(4):1040-1053.

## Bz/GABAAR in vitro binding data of diazepam and QH-II-066

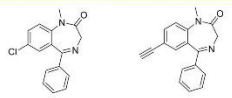


Bz/$GABA_A$ receptor binding data ($K_i$ = nM)

| | α1 | α2 | α3 | α5 | α1/α5 | Change in Selectivity |
|---|---|---|---|---|---|---|
| diazepam | 14 | 20 | 15 | 11 | 1.27 | 8.83 |
| QH-II-066 | 76.3 | 42.1 | 47.4 | 6.8 | 11.22 | |

*He et al. Drug Dev. Discov.* **2000**, *17*, 131 - 171.

## In Vitro Data of QH II 66

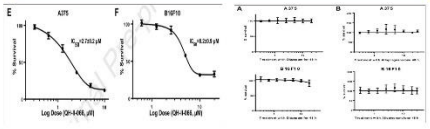

Krummel et al. Int J Radiat Oncol Biol Phys. 2021 Mar 15;109(4):1040-1053.

## Reduction of tumor size in mouse model

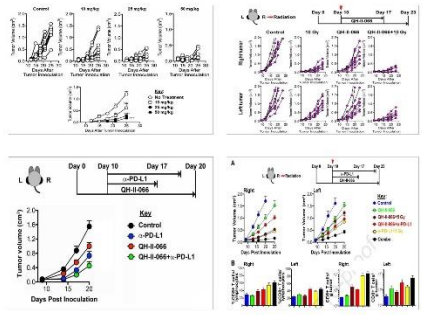


Krummel et al. Int J Radiat Oncol Biol Phys. 2021 Mar 15;109(4):1040-1053.

## Large scale synthesis of QH II 66

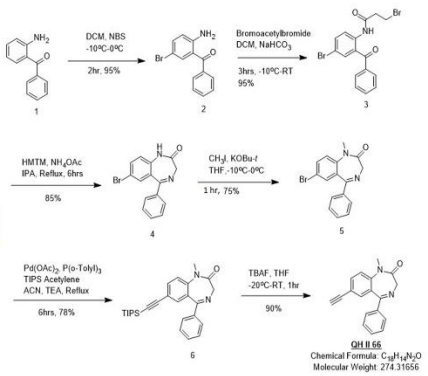


**Largest scale done: 100 gm** **Product recovered: 55 gm**

**Overall yield: 40%**

## Results and Conclusion

Results shown here indicates that QH II 66 can be potential candidate as an anti-cancer agent for the treatment of melanoma. By enhancing $GABA_AR$-mediated anion transport, benzodiazepines depolarize melanoma cells and impair their viability. In vivo, benzodiazepine alone reduces tumor growth and potentiates radiation therapy and α-PD-L1 antitumor activity. The combined treatment with benzodiazepine, radiation therapy, and α-PD-L1 results in near complete regression of treated tumors and a potent abscopal effect, mediated by increased infiltration of polyfunctional $CD8^+$ T cells. A large-scale synthesis method for QH II 66 was also developed with improved percent yield where the overall yield is 40%.

## Acknowledgments

We thank the NIH (K08-NS083626) for financial support. We also thank the Shimadzu Laboratory for Advanced Applied and Analytical Chemistry, and the Milwaukee Institute of Drug Discovery (MIDD) for spectroscopy.

## References

1.Mohler, Mckernan, Walford, Rudolph, Rowlett, et al.
2. *He et al. Drug Dev. Discov.* **2000**, *17*, 131 - 171
3. Krummel et al, Int J Radiat Oncol Biol Phys. 2021 Mar 15;109(4):1040-1053

## 5. 5 Curriculum Vitae

### 5. 5. 1 Profile

Experienced chemist with a demonstrated history of working in analytical chemistry sector. Currently pursuing PhD in Organic and Medicinal Chemistry. Skilled in Organic Chemistry, Organic Synthesis, Molecule characterization (NMRs, GC-MS, GC-ECD, Liquid Chromatography-Mass Spectrometry (LC-MS), HPLC, FTIR, UV-Vis, ICP-MS, ICP-OES, AAS), Process Development and Purification.

### 5. 5. 2 Education

**PhD candidate in Organic Chemistry.**

University of Wisconsin – Milwaukee - Milwaukee, WI

August 2015 to May 2022 (expected)

**Master's in applied chemistry and Chemical Engineering.**

University of Dhaka - Dhaka, Bangladesh.

January 2011 to June 2012

**Bachelor's in applied chemistry and Chemical Engineering.**

University of Dhaka - Dhaka, Bangladesh.

April 2006 to December 2010

### 5. 5. 3 Experience

**Graduate Research Assistant (GRA)** | University of Wisconsin-Milwaukee - Milwaukee, WI

August 2015 to Present

- Synthesizes new benzodiazepine analogues to treat medulloblastoma, melanoma and lung cancer.
- Synthesizes alpha5 subtype selective GABA(A) receptor agonists, antagonists as well as inverse agonists to find a suitable drug to treat schizophrenia and depression.
- Develops and optimizes synthetic routes to synthesize lead compound analogues by using conventional and microwave reaction techniques.
- Performs multistep synthesis of chiral and non-chiral compounds by using required metal catalysts.
- Performs purification by using appropriate chromatography (such as TLC, Column Chromatography), crystallization and distillation techniques
- Performs characterization of intermediates and products of a reaction by using NMR, IR spectroscopy, Mass spectrometry and Elemental analysis.
- Demonstrates excellent writing skills and performs literature searches using scifinder.com, reaxys.com, pubmed.com etc.

**Senior Officer – Analytical Laboratory** | TUV – SUD Bangladesh Pvt. Ltd. - Dhaka, Bangladesh
August 2013 to July 2015

- Detection and quantification of 26 banned disperse dyes by using Agilent UPLC-MS
- Detection and quantification of Alkyl phenol ethoxylates (APEOs) by using UPLC-MS/MS, Waters Technologies with Photodiode Array Detector (PDA).
- Preparation of proper documentation to release test results.
- Performed routine maintenance and troubleshooting of analytical equipment.

**Executive – Lab analyst, RSTS Laboratory** | SGS Bangladesh Pvt. Ltd. - Dhaka, Bangladesh.
August 2012 to July 2013

- Detection and analysis of restricted azo dye compounds by using Agilent 6890 GC with Agilent 5973 Mass Spectrometer.
- Confirmation of the spectrum of azo dye compound by using Agilent UPLC 1290 (DAD).
- Quantification of Formaldehyde and Chromium hexavalent compounds by using Shimadzu UV-VIS Spectrophotometer UV-3600.
- Performed routine maintenance and troubleshooting of analytical equipment.

**Assistant Executive – Lab analyst, RSTS Laboratory** | SGS Bangladesh Pvt. Ltd. - Dhaka, Bangladesh.
August 2011 to July 2012

- Conducted routine analytical studies of samples, preparation and extraction following laboratory Standard Operating Procedures (SOPs) and protocols.
- Preparation of sample (including extraction) for the detection of carcinogenic Azo dyes, Disperse dyes, pthalates, APEOs, NPEOs Formaldehyde in finished garments products.
- Preparation of stock solutions in different concentrations for instruments like GCMS, UPLC, ICP-OES, AAS etc.
- Preparation of different buffer solutions for HPLC and UPLC for different experiments.
- Maintained logbook for sample preparation. Maintenance and calibration of instruments like UV-Vis, pH meter, mechanical shaker, rotary evaporators etc.

## 5. 5. 4 Awards & Affiliations

- Chancellor's Graduate Student Award (fall'15 to spring'20)
- Member of American Chemical society (ACS) since 2016.

### 5. 5. 5 Publications

- **Modulating native $GABA_A$ receptors in medulloblastoma with positive allosteric benzodiazepine-derivatives induces cell death.** J Neurooncol. 2019 May;142(3):411-422. doi: 10.1007/s11060-019-03115-0. Epub 2019 Feb 6. PMID: 30725256; PMCID: PMC6478651.Kallay L, Keskin H, Ross A, Rupji M, Moody OA, Wang X, Li G, **Ahmed T**, Rashid F, Stephen MR, Cottrill KA, Nuckols TA, Xu M, Martinson DE, Tranghese F, Pei Y, Cook JM, Kowalski J, Taylor MD, Jenkins A, Pomeranz Krummel DA, Sengupta S.

- **Melanoma Cell Intrinsic $GABA_A$ Receptor Enhancement Potentiates Radiation and Immune Checkpoint Inhibitor Response by Promoting Direct and T Cell-Mediated Antitumor Activity.** Int J Radiat Oncol Biol Phys. 2021 Mar 15;109(4):1040-1053. doi: 10.1016/j.ijrobp.2020.10.025. Epub 2020 Oct 24. PMID: 33289666; PMCID: PMC8329598. Pomeranz Krummel DA, Nasti TH, Kaluzova M, Kallay L, Bhattacharya D, Melms JC, Izar B, Xu M, Burnham A, **Ahmed T,** Li G, Lawson D, Kowalski J, Cao Y, Switchenko JM, Ionascu D, Cook JM, Medvedovic M, Jenkins A, Khan MK, Sengupta S.

- **Design, synthesis and characterization of novel gamma-aminobutyric acid type A receptor ligands.** ARKIVOC. 2020;2020(Pt 7):242-256. doi: 10.24820/ark.5550190.p011.398. Epub 2020 Dec 2. PMID: 33642954; PMCID: PMC7909486. Pandey KP, Khan ZA, Golani LK, Mondal P, Mian Y, Rashid F, Tiruveedhula VVNPB, Knutson DE, Sharmin D, **Ahmed T**, Rezvanian S, Zahn NM, Arnold LA, Witkin JM, Cook JM.

- **Rationalizing the binding and α subtype selectivity of synthesized imidazodiazepines and benzodiazepines at GABAA receptors by using molecular docking studies.** Bioorganic & Medicinal Chemistry Letters, Volume 62, 2022,128637, ISSN 0960-894X, https://doi.org/10.1016/j.bmcl.2022.128637. Lalit K Golani, Md Yeunus Mian, **Taukir Ahmed**, Kamal P Pandey, Prithu Mondal, Dishary Sharmin, Sepideh Rezvanian, Jeffrey M Witkin, James M Cook,

### 5. 5. 6 Patents

- Cook, J. M.; **Ahmed, T**.; Tiruveedhula, V. V. N. P. B.; Jahan, R.; Golani, L. K.; Li, G.; Rashid, F.; GABA(A)ergic Subtype Selective Ligands as Anxiolytic, Antinociceptive, Anticonvulsant and Antidepressant Agents *via* Deuterium Exchange. PCT Patent filed on January 3, 2019.

- Sengupta, S.; Krummel, D. P.; Cook, J. M.; **Ahmed, T.;** Karve, A.; Kallay, L.; Desai, P. US Provision patent filing 2021 for Glioblastoma combination therapy. PCT Patent filed on June 3, 2021.
- Brain penetrant chemosensitizer to treat lung cancer.
- Novel deuterated benzodiazepine analogs for cancer use.
- Development of a new class of small molecule autophagy modulators for treatment of cancers.